SYNTHESIS OF HETEROATOM-SUBSTITUTED CARBENE COMPLEXES OF RHODIUM(I) AND IRIDIUM(I) FOR APPLICATION IN 1-OCTENE HYDROFORMYLATION

By

Tshegofatso Lydia Mashabane

A thesis submitted to the

Faculty of Science

University of the Witwatersrand

Johannesburg

in fulfilment of the requirements for the degree

Doctor of Philosophy

Chemistry

Supervisor: Prof. Daniela I Bezuidenhout

October 2020 in Johannesburg

Declaration

I, Tshegofatso Lydia Mashabane declare that the thesis which I hereby submit for the degree Ph.D. Chemistry at the University of the Witwatersrand is my own work and has not been previously submitted by me for a degree at this or any other university.

_____

(Signature of the candidate)

On the 21st day of October 2020

Abstract

In this project, different mono-heteroatom stabilized carbene complexes of rhodium(I) and iridium(I) were prepared as catalyst precursors for the hydroformylation of the 1-octene as a model reaction. The variation of the electronic properties of the carbene ligands were achieved by utilising either electrophilic, π-acceptor Fischer carbenes or σ-donor, basic 1,2,3-triazol-5-ylidenes. The modulation of molecular catalyst electronic and steric properties arguably play the greatest role in optimisation of (homogeneous) catalyst performance.

Rhodium(I) Fischer carbene complexes were prepared using a transmetalation method from the group 6 transition metal precursor, $[W(CO)_5\{C(OEt)(p\text{-DMA})\}]$. The formation of the Rh–C bond is confirmed by the presence of the carbene carbon atom resonance as a downfield doublet in the corresponding ^{13}C NMR spectrum. Aminolysis was confirmed by an upfield shift of the carbene doublet, corroborating a decrease electronegativity of the carbene complex **2** (70%). Furthermore, a decrease in π-character of this bond is substantiated by SC XRD molecular structure where an increase in the Rh-C bond length of complex **2** is observed, in comparison to **1**. The labile bidentate 1,5-cyclooctadiene (cod) co-ligand is replaced by a pair of π-acidic carbonyl ligands to afford **3** with a 90% yield, circumstantiated by the appearance of a pair of doublets at 186.9 ppm and 184.2 ppm. To determine the donor strength of the *NN*-dimethylaniline ligand, the TEP of **3** was calculated to be 2043 cm^{-1}.

The triazolylidene complexes were prepared from the metalation of the corresponding triazolium salts. The preparation of the N3-alkylated 1,2,3-triazolium salt, **L2** (63%) proceeded via the "click" reaction, and subsequent alkylation at position 3. The 1,3-diarylated 1,2,3-triazolium salt **L3** (69%) was accessed by the copper-free 1,3-dipolar cycloaddition of a 1,3-diaza-2-azoniaallene salt with an aryl-alkyne. Both were deprotonated independently in the presence of $[Rh(cod)Cl]_2$, resulting in rhodium(I) 1,2,3-triazol-5-ylidene complexes, **5** (48%) and **9** (62%) from **L2** and **L3** respectively. Once again, the ^{13}C NMR was employed to confirm metalation by the appearance of a downfield doublet signal for **5** and **9**, representing the respective carbene carbon atoms. The upfield carbene carbon resonances are in stark contrast to the low field chemical shifts observed for the electrophilic withdrawing Fischer carbene carbons. Moreover, a longer Rh -C bond was observed in the molecular crystal structures of **5** (2.029(4) Å) and **9** (2.053(4) Å), compared to the 2.006(16) Å observed for **2**. This is indicative of negligible π-character between Rh–C bonds of **5** and **9** Complexes **5** and **9** were subjected to ligand exchange reactions resulting in dicarbonyl complexes **6** and **10** respectively. The presence of the carbonyl ligands allowed for the measurement of TEP values from the FT-IR measurements of the carbonyl stretching frequencies. The TEP values of **6** (2047 cm^{-1}) and **10** (2049 cm^{-1}) confirmed the superior donor ability of the 1,2,3-triazol-5-ylidene ligands compared to the Fischer carbene ligand.

The salts **L2** and **L3** also underwent direct metalation with AgO_2, affording the isolated intermediates **S2** (52%) and **S3** (43%), before transmetalation to $[Ir(cod)Cl]_2$ resulting in the corresponding complexes **7** (63%) and **11** (67%). The successful transmetalation was signalled by the disappearance of a doublet of doublets signal in the ^{13}C NMR spectra, and the appearance of new characteristic carbene carbon atom singlets at *ca.*173 ppm in both cases. Following ligand exchange of the coordinated cod ligands with carbonyls, new complexes **8** (from **7**) and **12** (from **11**) could be isolated. Analogous with what was observed for their rhodium(I) counterparts, deshielding of the carbene chemical shifts as a consequence of the π-accepting character of the carbonyl co-ligands was observed.

The click reaction was employed to obtain the 4,4'-bis(1,2,3-triazole) (**L4** (24%)), followed by alkylation (**L5** (69 %)) and coordination to rhodium. The envisaged chelated complex (**14** (42%)) and an unanticipated μ^2-bridged complex (**13** (49%)) were isolated The differing coupling constants displayed in the NMR spectra of these complexes are indicative of a difference in coordination to the metal centre. To corroborate this, the SC XRD structure of **13** was obtained.

It was aimed to prepare a 'mixed' biscarbene complex containing both a σ-donor and π-acceptor carbene ligand to exploit the 'push-pull' electronic effects of the combination of the two different types of carbene ligands. Attempts to isolate a complex bearing the electron withdrawing Fischer carbene ligand and the electron donating 1,2,3-triazol-5-ylidene proved unsuccessful. A range of transmetalation reactions were performed, including transmetalation of a Fischer carbene ligand to a rhodium(I) 1,2,3-triazol-5-ylidene complex and the transmetalation of a 1,2,3-triazol-5-ylidene ligand to a rhodium(I) Fischer carbene complex.

The modulation of molecular catalyst electronic and steric properties play a big role in the (homogeneous) catalyst performance. The isolated rhodium and iridium complexes were screened for activity in hydroformylation reactions, and the most active were the rhodium Fischer carbene complexes. These complexes displayed conversions of up to >99%, with TOFs ranging between 386 h^{-1} and 543 h^{-1}. The bulkier rhodium 1,2,3-triazol-5-ylidene complexes were significantly more regioselective under the same conditions employed for the rhodium Fischer carbene complexes, with *n/iso* ratios of up to 2.67 . The iridium complexes displayed limited activity with TOFs below 45 h^{-1} under the same conditions as their rhodium counterparts, consolidating the considerable role of the metal centre.

I dedicate this to my dad

Maile, *swifi la Boroka. La fifala pula e yana.*

Samuel “Benjamin” Mashabane

Acknowledgements

Firstly, I would like to thank the Creator, my Heavenly Father without whom none of this would have been possible. Thank you for strength, discipline and peace throughout this project.

I would like to thank my supervisor, Prof Daniela Bezuidenhout for the immeasurable support and guidance. Thank you for your continuous motivation, for your top tier dedication to teaching and mentoring me regardless of where you are in the world.

Prof Gregory Smith, thank you for the warm welcome into your lab during both my research visits, and making me feel like one of your students. Thank you for your support, guidance and advice.

I would like to thank my lab mates at Wits University and at UCT and for the valuable input and advice throughout my project, and most importantly for your companionship.

I would like to thank my dad, Maile Mashabane. Papa, thank you for your never-ending love and support not only through this Ph.D. but throughout my life. I cannot recall a single moment where you were not there, taking on the role of two parents time and time again. The sacrifices you have made for me to finish studying to my heart's content will never be forgotten. Words cannot explain how fortunate and grateful I am to have you as my dad.

I would like to thank my mom Sarah Mashabane and my grandmother Annah Mokonyane for the endless prayers and support; my cousin Rebecca Yam and her husband for accommodating me on both my research visits; my uncle David Mashabane for helping me kickstart my university career; my baby brother Khutso Mashabane just for being alive and the rest of my family for support and encouragement.

Lastly, I would like to thank my friends for listening, for your love, support and encouragement throughout the longest, hardest journey of my life.

Contributions to this thesis are hereby acknowledged:

The collection and refinement of the crystal structure data presented in this thesis was done by Prof Manuel A. Fernandes at the University of the Witwatersrand.

The hydroformylation catalytic studies were carried out by myself, with the exception of complexes **13** and **14,** which were done by Shepherd Siangwata and Stephen De Doncker under the supervision of Prof Gregory S. Smith at the University of Cape Town.

Complexes **1** and **4** (Chapter 2) were prepared by Kabelo Ramollo as part of her Ph.D. project but the syntheses repeated by the author for comparative catalytic purposes in this thesis. The reference citation to the publication of these compounds are included in this thesis.

I hereby acknowledge the National Research Foundation (NRF) and Sasol Technology R&D Pty. Ltd. South Africa for financial assistance. The conclusions arrived at are those of the author and are not to be attributed to the NRF or Sasol Technology R&D Pty. Ltd. South Africa.

Preface

The layout of the thesis is such that it is divided into 8 chapters. The first chapter contains an introduction detailing the background literature review, as well as the aims and objectives of this overall study. Chapter 2 involves the preparation and characterisation of two new rhodium(I) Fischer carbene complexes, each bearing an *N,N*-dimethylaniline substituent. In this chapter, two previously reported rhodium(I) Fischer carbene complexes are included for comparative studies, however one of these complexes serves as the precursor for the reported new complexes. Chapter 3 features the synthesis and characterisation of four 1,2,3-triazol-5-ylidene rhodium(I) and iridium(I) complexes, alkylated at the N3 position. The rhodium complexes are prepared directly from the analogous triazolium salt, while the iridium complexes are prepared from a new isolated bis(N3-alkylated-1,2,3-triazol-5-ylidene) silver(I) complex, a carbene transfer agent. Pertinently, the diarylated 1,2,3-triazol-5-ylidene complexes of rhodium are reported in Chapter 4, highlighting the variation in the preparation of the preceding triazolium salt, in contrast to that reported in Chapter 3. Once again a new bis(1,3-diarylated-1,2,3-triazol-5-ylidene) silver(I) complex is prepared and isolated as an intermediate to the corresponding iridium(I) carbene complex. Lastly, a chromium 1,2,3-triazol-5-ylidene is reported in this chapter, as a precursor to a transmetalation reaction reported in the following chapter. Chapter 5 reports a bis(1,2,3-triazol-5-ylidene) or *i*bitz ligand, which is coordinated to a rhodium(I) metal in a bidentate fashion, as a mononuclear complex; as well as a dinuclear complex with a bridging chlorido ligand. Furthermore, a range of synthetic approaches to access the mixed biscarbene rhodium complex, are explored and reported in this chapter. These complexes prepared throughout Chapters 2 – 5 are employed as catalyst precursors for the hydroformylation of 1-octene, and the outcomes are recorded and discussed in Chapter 6. Chapter 7 summarises the findings of Chapters 2 – 6, along with the future considerations; and the experimental techniques are detailed in Chapter 8.

The results presented in this thesis was published in:

Tunable Rh(I) Fischer Carbene Complexes For Application in the Hydroformylation of 1-octene.

T. L. Mashabane, G. K. Ramollo, G. Kleinhans, S. De Doncker, S. Siangwata, M. A. Fernandes, A. Lemmerer, G. S. Smith and D. I. Bezuidenhout, *Journal of Organometallic Chemistry*, 2020, **920**, 121341. DOI:10.1016/j.jorganchem.2020.121341.

Contents

List of Figures

List of Schemes

List of Tables

List of Compounds

Chapter 2

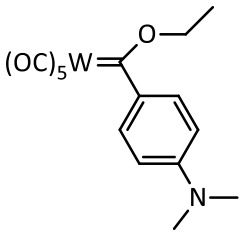

S1

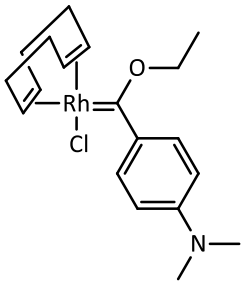

1

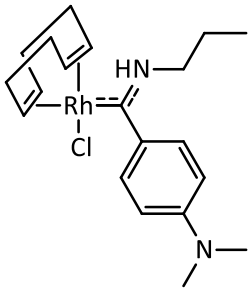

2

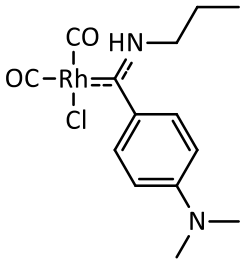

3

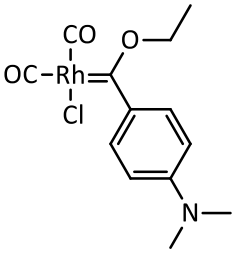

4

Chapter 3

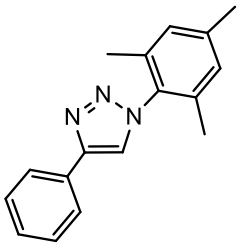

L1

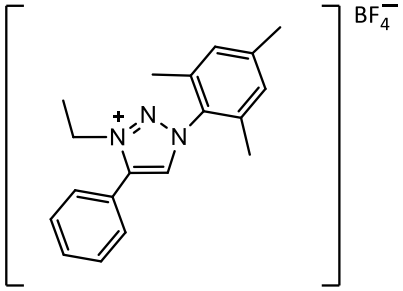

L2

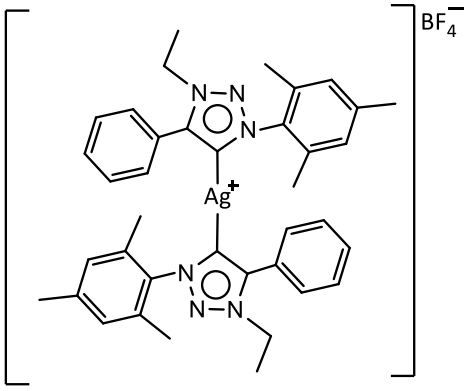

S2

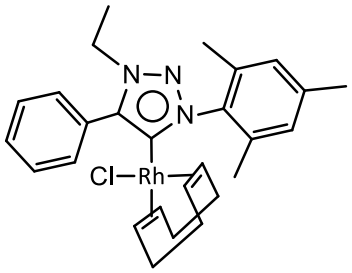

5

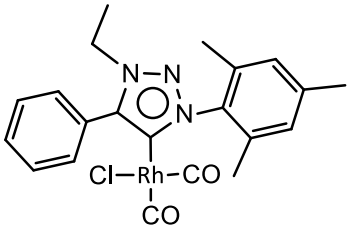

6

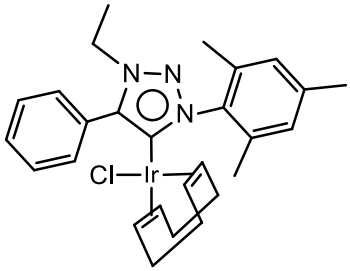

7

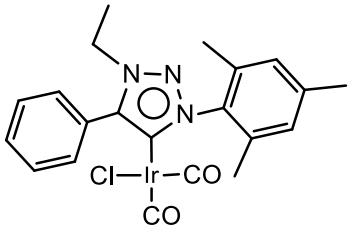

8

Chapter 4

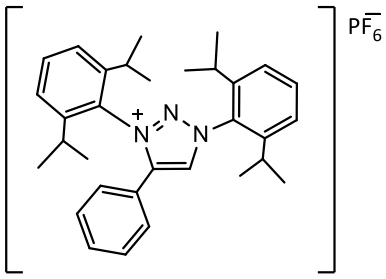

L3

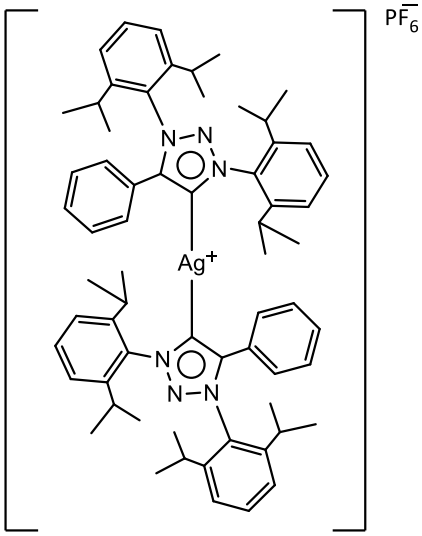

S3

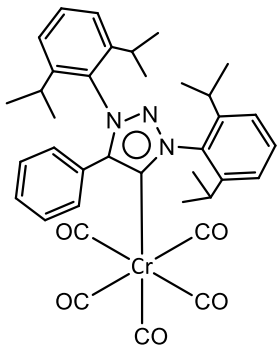

S4

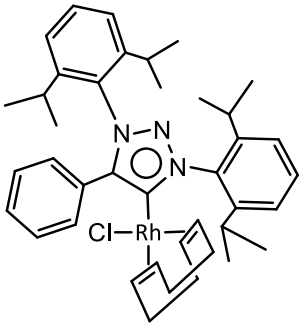

9

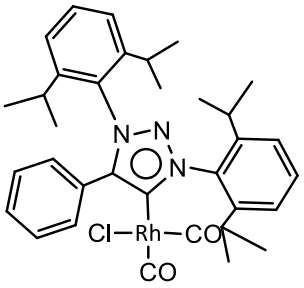

10

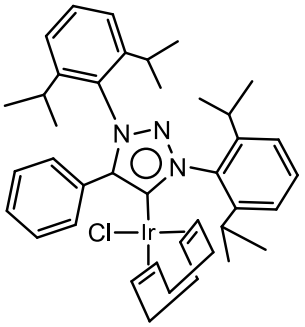

11

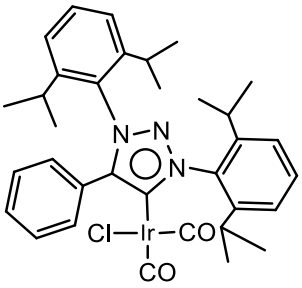

12

Chapter 5

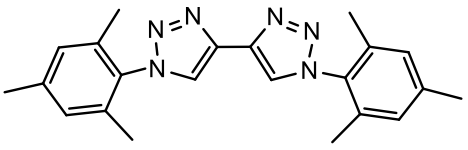

L4

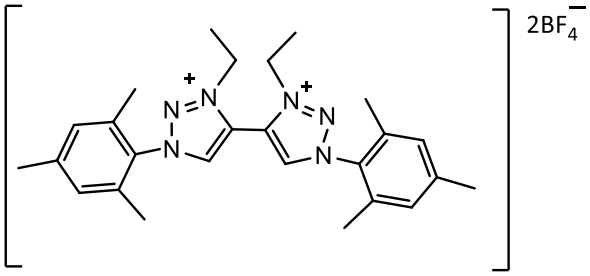

L5

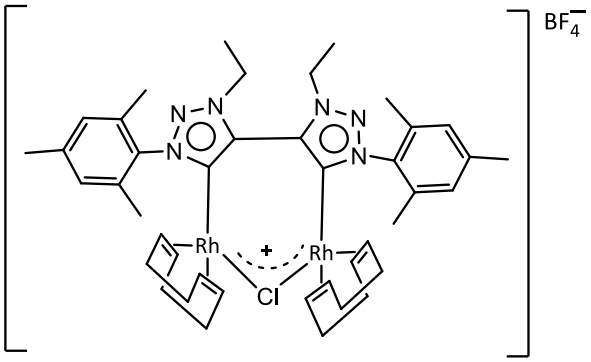

13

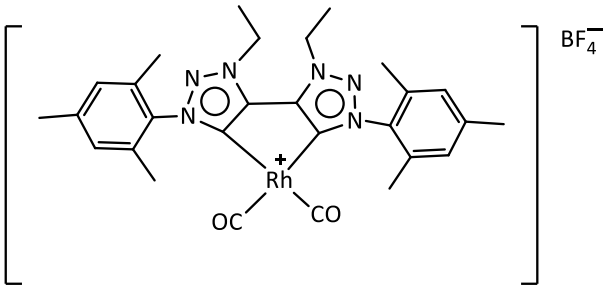

14

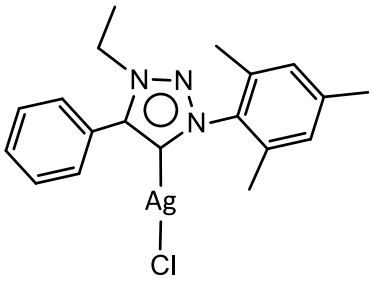

15

List of Abbreviations

*a*NHC	*abnormal* N-heterocyclic carbene
Ar	aryl
bitz	4,4'-bis(1,2,4-triazol-5-ylidene)
br s	broad singlet
cod	1,5-cyclooctadiene
d	doublet
DCM	dichloromethane
dd	doublet of doublets
DFT	density functional theory
Dipp	diisopropylphenyl
dq	doublet of quartets
dt	doublet of triplets
ESI-MS	electron spray ionisation mass spectroscopy
Fc	ferrocenyl
FCC	Fischer carbene complex
FT-IR	Fourier transform Infrared
HOMO	highest occupied molecular orbital
hrs	hours
i-bitz	4,4'-bis(1,2,3-triazol-5-ylidene)
^{i}Pr	Isopropyl
J	coupling constant
KHMDS	potassium bis(trimethylsilyl)amide
LUMO	lowest unoccupied molecular orbital
m	multiplet
M.P.	melting point
Mes	mesityl (2,4,6-trimethylphenyl)
MIC	mesoionic carbene
NHC	N-heterocyclic carbene
NMR	nuclear magnetic resonance
p-DMA	*N,N*-dimethylaniline
PGM	precious group metal

ppm	parts per million
Pr	propyl
py	pyridine
q	quartet
rt	room temperature
s	singlet
SC-XRD	single crystal X-ray diffraction
sept	septet
td	triplet of doublets
TEP	Tolman electronic parameter
THF	tetrahydrofuran
TLC	thin layer chromatography
TOF	turnover frequency
trz	1,2,3-triazol-5-ylidene
tt	triplet of triplets

Chapter 1: Introduction

1.1. Carbenes: A general overview

The advancement of carbene ligands over the years has rendered them ubiquitous in the field of organometallic chemistry.[1] These ligands have developed commercial relevance in catalysis,[1b] photochemistry[1c] and drug design.[1d-e] In this introductory chapter, a literature background of the general structure, bonding and reactivity of the different topical carbenes are presented, as well as a general overview of the catalytic hydroformylation reaction. A critical evaluation of the state-of-the art of each specific carbene relevant to this study, is presented in each subsequent reaction.

A carbene is a highly reactive derivative of a divalent, neutral carbon with six valence electrons typically stabilized by a transition metal.[1] There are three categories describing the electronic properties of the metal-carbene bond as well as the structural properties of carbene complexes, namely: Fischer carbene (Figure 1.1, **a**); Schrock carbene (Figure 1.1, **b**) and N-heterocyclic carbene (NHC) complexes (Figure 1.1, **c**).[2]

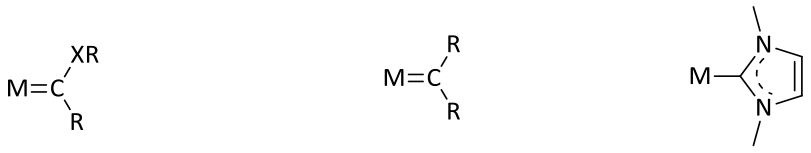

a **b** **c**

Figure 1. 1: Illustration of a Fischer carbene complex (a), a Schrock carbene complex (b) and an NHC metal complex (c)

Fischer carbenes are electrophilic singlet state carbenes stabilized by an adjacent electronegative heteroatom. The singlet state of these carbenes implies the sp^2 hybridize*d* orbital contains spin paired electrons for donation to the metal forging a σ-bond,[1] while the empty p-orbital, allows the coordinated low oxidation state transition metal to donate π-electrons.[2] Conversely, Schrock carbenes are diradical in nature. These are referred to as triplet state carbenes with no heteroatom stabilization, bearing a δ^- charge on the carbene carbon resulting in a covalent bond with high oxidation state metals, thus making them nucleophilic.[1] N-heterocyclic carbenes (NHCs), a sub-class of the Fischer-type diaminocarbenes are singlet carbenes. However instead of a single heteroatom, these carbenes are stabilized by two or more heteroatoms in a cyclic scaffold.[3] These nucleophilic carbenes experience negligible π-backdonation from the coordinated metal, justifying a single bond interaction between the metal and the carbene carbon.[1,3]

1.1.1. Fischer carbene complexes

1.1.1.1. Developments in the preparation of the Fischer carbene

The first Fischer carbene complex was isolated in 1964 following the reaction between $W(CO)_6$ and R-Li (where R = CH_3, C_6H_5) in diethyl ether under inert conditions. In an experiment performed by E.O Fischer, the resulting complex **d** was protonated, Scheme 1.1, and subsequently treated with diazomethane resulting in **f** after recrystallisation.[4] Later, Meerwein's salts were found to be better alkylating agents, circumventing the protonation step prior to alkylation.[5]

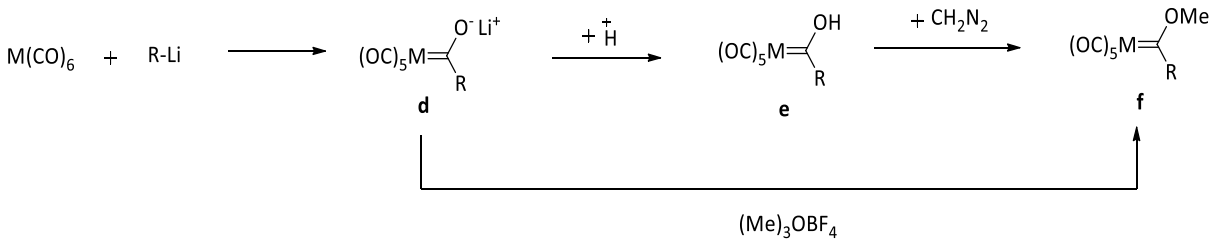

Scheme 1. 1: Preparation and isolation of the first Fischer carbene complex.[4]

1.1.1.2. HOMO-LUMO interactions between the metal and the carbene ligand

The confirmation of this metal-carbene bond is found by the inspection of the molecular orbital interactions, where the HOMO (highest occupied molecular orbital) and the LUMO (lowest unoccupied molecular orbital) of the carbene result in a double bond interaction with the d-orbitals of the metal. Electrons are donated from the carbene's HOMO to the metal's d-orbitals, and conversely, electrons from the metal's d-orbitals are donated into the LUMO of the carbene carbon.[1e] Furthermore, from these interactions it was postulated that the polarisation of the σ-bond lies towards the carbene, while that of the π-bond lies towards the metal.[1e] The energy of the HOMO and LUMO orbitals of the carbene carbon are influenced by the carbene's heteroatom α-substituents. The reduced inductive effect of an amino compared to an ethoxy substituent results in an increase in energy of the HOMO and LUMO orbitals of the carbene, resulting in increased carbene nucleophilicity.[1e] This in turn induces a strong σ-bond between the metal and the carbene, and lessens the π-acidity of the of the carbene ligand and consequently π-backdonation from the metal resulting in a reduction in double bond character of this metal-carbene bond.[1e,6,7]

1.1.1.3. The electronic influence of the substituents on the Fischer carbene ligand

To study the effect of the R substituent on the carbene carbon, Fischer prepared a range group 6 transition metal Fischer carbenes $[(CO)_5M\{C(OCH_3)R\}]$, (Scheme 1.2). Carbene **g** was treated with deuterated methanol (Scheme 1.2, Part A), resulting in **h** and leading to the conclusion that the $-CH_3$ protons are acidic, a consequence of electron donation from the carbene to the central metal.[7] This behaviour is further corroborated by Part B of Scheme 1.2. Thus, complexes **k** and **l** were prepared to demonstrate the transfer of electron density from the R-group to the carbene, and the effect this would have on the π-basic *trans* carbonyl ligand. Although not of great magnitude, the phenyl substituent displays the delocalisation of π-density across the empty *p*-orbital of the carbene which is transferred through the central metal to the CO ligand resulting in a decrease in stretching frequency compared to the less π-acidic $-CH_3$.[7] The enhancement of this mesomeric effect can be seen when the *para* position of the phenyl is substituted with $-N(CH_3)_2$, further decreasing the stretching frequency of the *trans* carbonyl.[7,8]

Part A

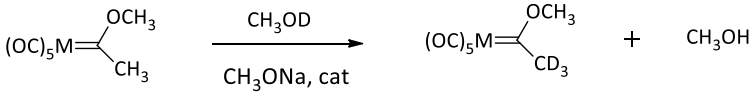

g **h**

Part B

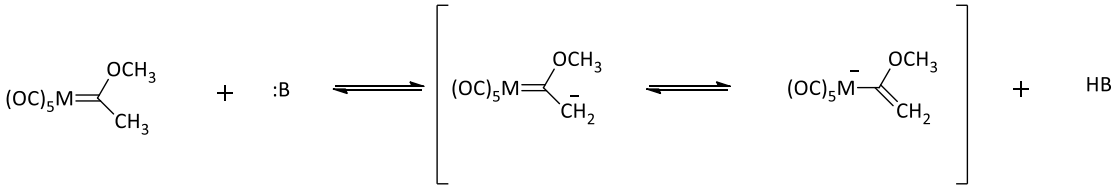

g **i** **j**

Part C

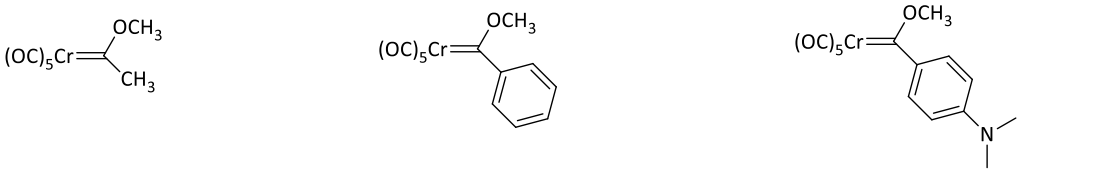

g: $A_1^{(1)}$ = 2068 cm^{-1} **k:** $A_1^{(1)}$ = 2064 cm^{-1} **l:** $A_1^{(1)}$ = 2052 cm^{-1}

M = Cr, Mo, W

Scheme 1. 2: The effect of varied R-substituents on the electronic properties of the carbene.[7]

1.1.1.4. Rationale for transmetalation to late group transition metals

Group 6 Fischer carbene complexes are useful as precursors in a range of stoichiometric and catalytic transformations including olefin metathesis reactions, olefin cyclopropanation reactions, Fischer-Tropsch reactions, C-H insertion and dimerization reactions.[9,10] However, in most instances these transformations require the addition of a catalytic amount of a late group transition metal salt to the reaction.[9] Sierra and co-workers studied the reaction pathways of different catalytic transformations such as dimerizations reactions, β-elimination and C-H insertion (Scheme 1.3), to better understand the role of the late group transition metal. It was found that the *in-situ* formation of the late-group transition metal Fischer carbene complex increased activity at lower temperatures. Furthermore,

improved selectivity and reaction rates were observed following the addition of this secondary transition metal to the dimerization reactions.[9,11]

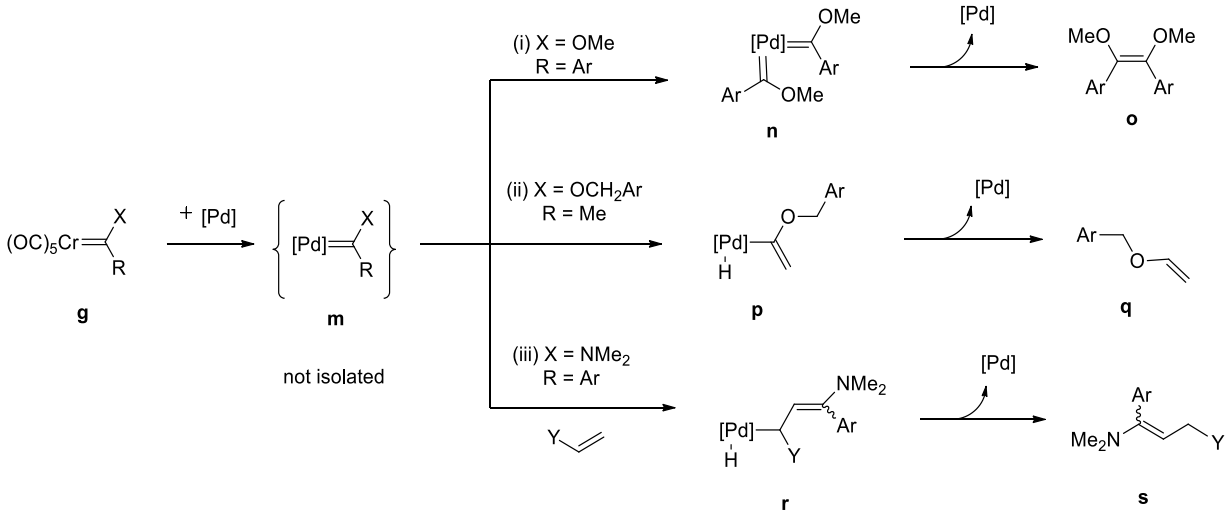

Scheme 1. 3:Proposed reaction pathways for palladium(0) catalysed (i) dimerization, (ii) β-elimination and (iii) C-H insertion.

Although late-group transition metal Fischer carbene complexes displayed better activity under milder conditions in a range of catalytic reactions, carbonyl or isonitrile late group transition metal precursors without halide co-ligands are rare, and not compatible with organolithium reagents. Consequently, these complexes could not be accessed by treating the metal precursor with an organolithium.[12] Based on the premise that the nucleophilic attack of a carbonyl group coordinated to a transition metal gives access to the corresponding Fischer carbene complex, Fischer treated $Fe(CO)_5$ with R-Li (where R = CH_3 of C_6H_5). Instead of alkylation at the metal acylate O-atom, metal alkylation of complex **t** occurred, resulting in the formation of the ketone dimer **u**. This prompted Fischer to search for alternative methods to access the Fischer carbene complex of iron(0). In 1970, the iron(0) Fischer carbene complex was obtained by carbene transfer from a group 6 Fischer carbene complex to the UV irradiated $Fe(CO)_5$.[12] The isolation of the nickel(0) Fischer carbene complex without irradiation, corroborated Sierra's postulation of the *in situ* formation of a late-group transition metal Fischer carbene complex.[9,11] This expanded the scope of synthetic reactions with catalyst precursors of late-group transition metals featuring Fischer carbene ligands.

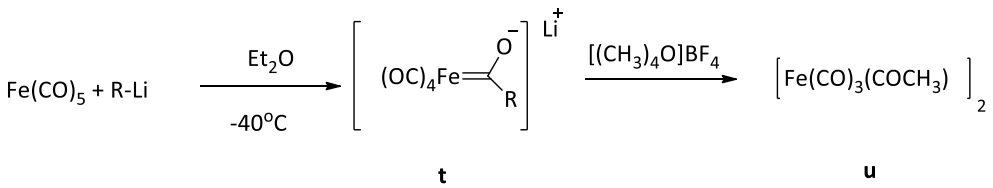

*Scheme 1. 4: Classical Fischer approach applied for the preparation of an iron(0) Fischer carbene complex, results in dimer **u**.[7]*

Part A

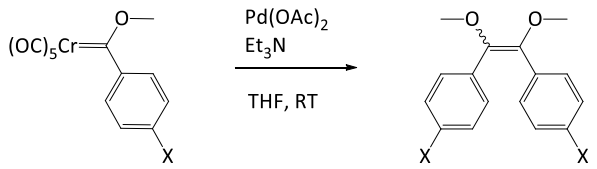

v X = H, Br

w E/Z 2:1

Part B

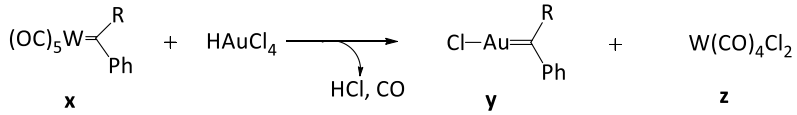

x **y** **z**

R = OMe, NH_2

Part C

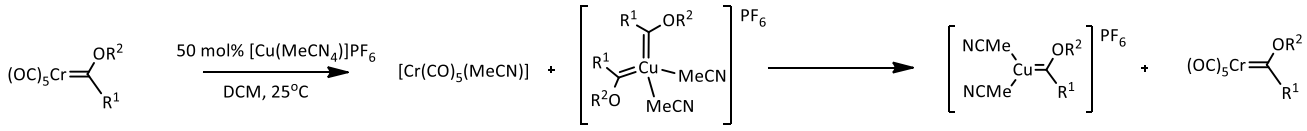

aa **ab** **ac** **ad**

R^1 = CHCH-2-furyl, R^2 = menthyl

Part D

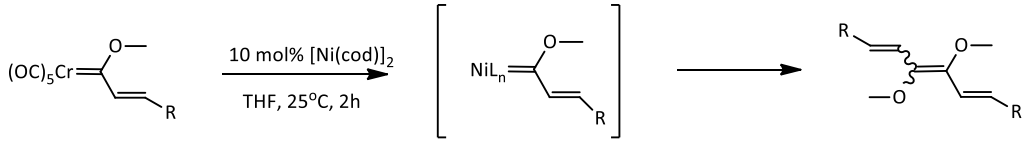

ae R = Ph

af

in situ

ag

cod = 1,5-cyclooctadiene

Scheme 1. 5: Part A: The palladium-catalysed carbene self-dimerization reaction.[9] Part B: Synthesis of the first Au(I) alkoxy Fischer carbene complex via the transmetalation route. Part C: Preparation of the first Cu(I) Fischer carbene complex by transmetalation from a group 6 metal.[16] Part D: Nickel catalysed alkoxycarbene self-dimerisation[18]

In the 1980s, more stoichiometric transfers of carbene ligands from group 6 to group 10 transition metals (platinum, palladium and nickel) were reported.[13] Sierra and co-workers used this knowledge to justify the intermediate formation of the transient palladium Fischer carbene complex in palladium-catalysed carbene dimerization reactions. The chromium(0) carbene complexes were reacted with Et_3N and catalytic amounts of $Pd(OAc)_2$ in THF to facilitate the intermolecular carbene transfer. Thus resulting in a 2:1 ratio mixture of *E/Z* isomers (Scheme 1.5, part A) of the olefinic product and $Cr(CO)_6$.[9]

With the focus on carbene ligand dimerization, Sierra proceeded to study reaction pathways that would result in the intermediate formation of these highly unstable late transition group carbene complexes to facilitate a thermal-free reaction pathway to the formation of these olefins. It was argued that these *in situ* generated late transition metal Fischer carbene complexes would dimerize more readily than the group 6 complexes essentially making them better catalysts in these dimerization reactions.[11] To this effect, three important observations and subsequent conclusions were made. Firstly, palladium was the best catalyst, requiring mild conditions to enable the dimerization reaction rendering it one of the least stable late group transition metal Fischer carbene complex to be generated *in situ*. Secondly, amino Fischer carbene complexes required harsher reaction conditions than their alkoxy counterparts making them relatively unreactive; and lastly rhodium-catalysed carbene transfer reactions required higher temperatures and longer reaction times suggesting that even if the transmetalation from chromium to rhodium is generated *in situ,* the rhodium Fischer carbene is relatively stable at temperatures below 100°C.[11]

Soon after Sierra's findings, Barluenga and co-workers prepared copper-catalysed carbene olefins, rationalized by the successful isolation of gold Fischer carbene complexes (Scheme 1.5, Part B).[14] The same theory of the intermediate generation of the corresponding late group transition metal Fischer carbene complexes was used to support their competitive yields. Barluenga observed that 0.5 equivalents of the copper catalyst $[Cu(MeCN)_4][PF_6]$ was consumed in a reaction with the chromium methoxy carbene complex. When characterised, it was found that the crude mixture contained the first isolated example of a copper Fischer carbene complex (Scheme 1.5, Part C).[15] Moreover, once dissolved in a Et_2O: dichloromethane (DCM) 1:5 mixture, one of the MeCN ligands were substituted with the weakly coordinating Et_2O.

Highlighting the catalytic relevance of these late transition metal Fischer complexes, Barluenga postulated that nickel-catalysed dimerization from chromium Fischer carbene complexes, generates a nickel(0) Fischer carbene *complex in situ* based on Sierra's earlier findings. To substantiate this hypothesis, prompted by the severe limitations in cyclisation reactions of electrophilic alkynes with group 6 Fischer carbene complexes, Barluenga went on to perform the reaction in the absence of the nickel catalyst, and the reactions were unsuccessful.[16]

1.1.1.5. Rhodium Fischer carbene complexes and their catalytic applications

Rhodium Fischer carbene complexes have played an important role as intermediates in catalysing organic transformations such as cyclisation reactions of the allenyl carbene ligands of group 6 metal precursors.[17] Ambient temperatures were reported for cyclisation of tungstaoctatetraenes, along with improved activities when catalytic quantities of a rhodium catalyst were added to the reaction. Aumann *et al* also observed the formation of these isolable intermediates, and substantiated their formation with the inactivity observed in the absence of the rhodium catalyst.[22b] Some years later,

Barluenga and co-workers prepared cationic α-β unsaturated rhodium(I) Fischer carbene complexes for cyclisation reactions, highlighting the inertness of the group 6 aminocarbene complex in the preceding transmetalation reactions. Additionally, the simultaneous transfer of both the Fischer carbene and the carbonyl ligands was observed, resulting in the highly active cationic rhodium(I) Fischer carbene complexes.[20a] Selectivities of 50%-58% were observed when **ai** was isolated prior to the cyclisation reaction, however pronounced selectivity increases (68%-89%) was observed for the corresponding one-pot reactions.[20a]

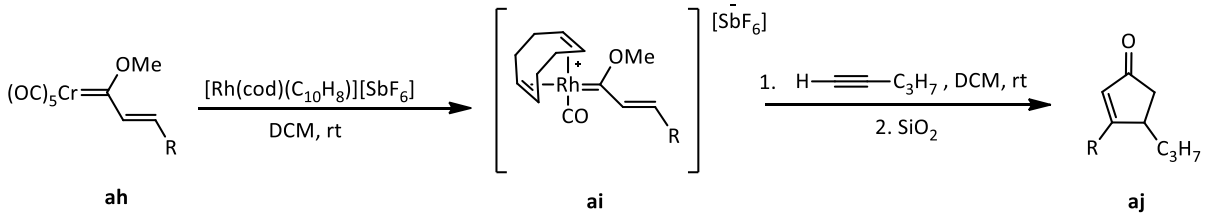

ah **ai** **aj**

Scheme 1. 6: Preparation of the cationic α-β unsaturated rhodium(I) Fischer carbene complexes for cyclization reactions.[20a]

Following this, Barluenga *et al* performed the same transmetalation reaction on a rhodium(I) NHC precursor in a bid to merge the electronic push-pull effects of a Fischer carbene and an NHC ligand on the same rhodium centre (*vide infra* Chapter 2, Scheme 2.2).[18] Surprisingly, marginal activity was observed, and was subsequently improved by a chloride abstractor additive, leading to the conclusion that the cationic species is the catalytically active species. It was noted that upon heating in toluene to 60°C, the transmetalation product undergoes dimerization, resulting in a methoxy dimer and $[Rh(NHC)(CO)Cl]_2$, a then novel rhodium(I) NHC dimeric complex.[18]

1.1.2. N-Heterocyclic carbene complexes

An N-heterocyclic carbene (NHC) is tantamount to a Fischer carbene, in that both are heteroatom stabilized singlet carbenes. However, unlike the Fischer carbene,[19] the inductive effect of the two flanking nitrogen atoms results in a stabilized σ-orbital, while the electron deficiency of the carbene carbon is decreased by a four-electron three-orbital π-system, delocalised through the empty *p*-orbital of the carbene (Figure 1.2).[20]

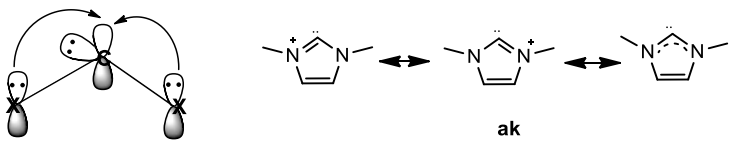

ak

Figure 1. 2: N-heterocyclic carbene resonance structures as a result of the delocalisation of π-electrons.[23]

The established stability of diaminocarbenes as opposed to mono-heteroatom stabilized carbenes prompted Wanzlick to attempt the isolation of the free NHC of **al** by thermolysis, however this yielded the dimer **am** (Scheme 1.7, Part A).[15] Subsequently, Wanzlick used a non-nucleophilic base to deprotonate the tetraphenyl imidazolium salt, **ac** to obtain the free NHC **ad** (Scheme 1.6, Part B)**,**

however this imidazol-2-ylidene was not isolated. Instead it was exposed to water and oxygen initiating the immediate decomposition of the NHC.[21] Following this, in 1968 both Wanzlick and Öfele independently isolated the first NHC metal complexes (Scheme 1.6, Part C).[22]

Further developments in the attempts to isolate the free NHC became dormant, until Arduengo revisited the concept in 1991.[23] 1,3-diadamantyl imidazol-2-ylidene was isolated from the corresponding salt following its deprotonation with dimsyl anion. It was noted that the same product can be obtained using ^{t}BuOK as a base. The imidazol-2-ylidene is stable for a notable amount of time and decomposed at a temperature of 240°C.[24,81] The stability of this free NHC was attributed to the collaborative effect of the electronic factors, the σ-pull π-push system; as well as the steric bulk of the wingtip substituents.[25]

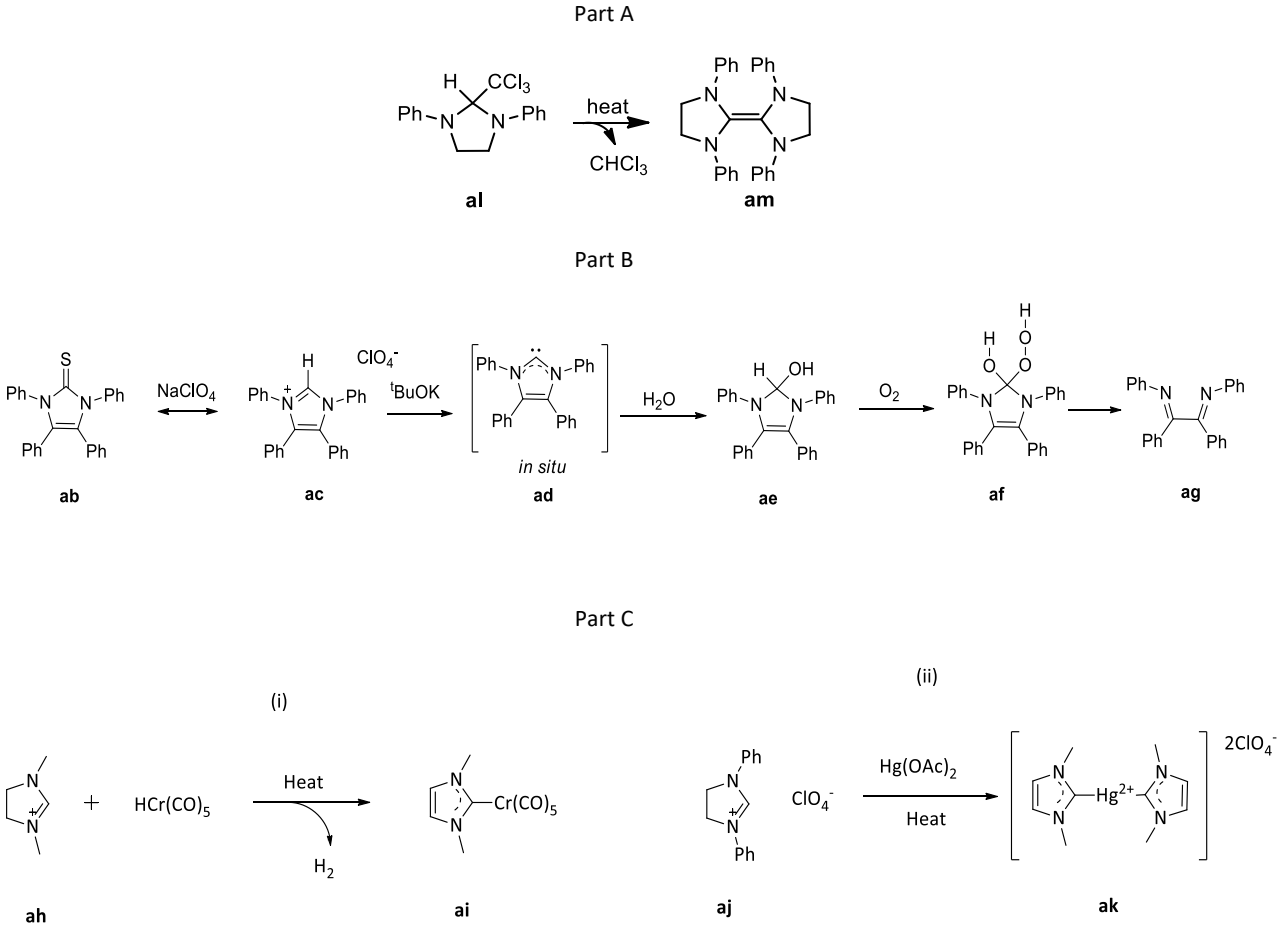

*Scheme 1. 7: (a) Thermal elimination of chloroform from **z**, (b) Deprotonation of **ac** by a non-nucleophilic base. (c) Preparation of the first NHC metal complexes by (i) Ofele and (ii) Wanzlick.*

Following the isolation of the first NHC, Arduengo patented a facile one pot synthetic procedure to access a range of 1,3-disubstituted imidazolium salts (Scheme 1.7).[26] The preparation is carried out under inert conditions and involves a primary amine, an aldehyde, an acid and an α-dicarbonyl with a molar ratio of 2:1:1:1. The acid used is often a strong acid with a pK_a of 6 or less, as the conjugate base is the stabilizing anion for the envisaged imidazolium salt. Two different primary amines may be employed provided the overall molar ratio is 2, as well as an α-dicarbonyl with non-equivalent R-

groups depending on one's steric needs, however this may result in a mixture of isomers. This reaction is highly exothermic, thus cooling to maintain the optimum temperature (20°C-100°C) will be required throughout the duration of the reaction which is typically 0.5-24 hours. For the reaction to reach completion, the removal of the water produced during the reaction is required.[20]

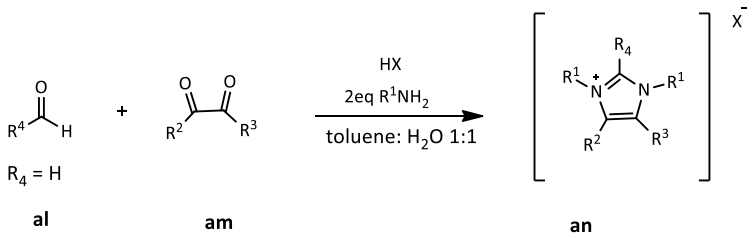

R^1- R^3 = independantly hydrocarbyl group, or a substituted hydrocarbyl group

Scheme 1. 8: One pot preparation of a 1-3 disubstituted imidazolium salt.[20]

Given the stability and tunability of the free NHC, Herrmann proposed coordinating these accessible ligands to transition group metals for use in catalytic reactions as replacements for phosphines due to the inferior strength of the P-metal bond as opposed to the C-metal bond of the carbene.[27] The resulting palladium catalyst was found to be robust and active in Heck coupling reactions.[20] This incited a considerable amount of work around homogeneous catalysis where NHC-metal complexes catalysed a range of organic transformations.[28]

1.1.2.1. Abnormal N-Heterocyclic carbene complexes

Electronic factors, such as the inductive effect of the two nitrogen atoms on C2 as well as density function theory calculations advocate for deprotonation and metalation to occur at the C2 proton of imidazolium salts.[29] However, during the metalation of **ao** in 2001**,** Crabtree isolated and characterised complex **aq**, an *abnormal* NHC (*a*NHC) complex, instead of the anticipated **ap**.[29] The ^{13}C NMR spectrum showed a downfield shift of the carbene signal at 141.1 ppm instead of the expected 129.6 ppm, and the structure of **aq** was confirmed by X-ray diffraction (XRD) crystallography.[29] It was later established that the direct metalation of **ao** results in an inseparable mixture of **ap** and **aq**. Furthermore, due to similar densities these complexes cannot be separated.[30] Once coordinated, neither of these complexes convert to the other, even under temperatures as high as 100°C for up to 3 days. Only the decomposition products are observed.[30] Thus Crabtree concluded that metalation and protonation can occur at C2 or C5, where C2 coordination is favoured by longer linkers, while shorter linkers favour C5 coordination in the case of bidentate ligands. It was further concluded that steric bulk of the R substituent promotes C5 coordination.[30]

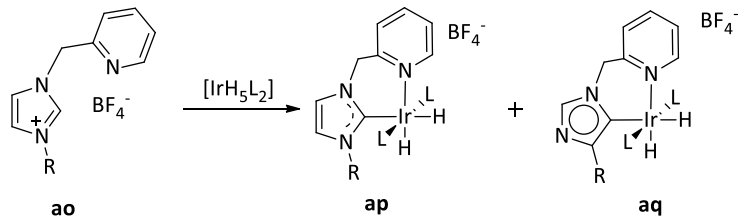

*Scheme 1. 9: The two possible coordination modes of **ao,** where **ap** is the normal mode of coordination and **aq** is the unexpected abnormal mode of coordination to the central metal iridium (I).*[29]

In 2004, Crabtree synthesised monodentate iridium(I) carbene complexes to establish whether or not the stability of *a*NHC complexes are governed by chelation. It was reported that bidentate *a*NHC complexes exhibit superior stability compared to their monodentate counterparts, as intuitively expected.[30] To enhance stability, a phenyl group was appended to the C4 position and the donor properties of the *a*NHC monodentate ligand were examined following the substitution of the 1,5-cyclooctadiene (cod) co-ligand with carbonyls.[30] The *a*NHC ligand is flanked by a single nitrogen atom, consequently, it was reported to be markedly more donating than the NHC due to the reduced inductive effect on the carbene carbon.[30] The counterion effect was investigated. It was revealed that **ap** and **aq** do not interconvert when heated, however the opposite is true when a counterion exchange reaction is performed on **aq**. Therefore, it was deduced that **ap** is the thermodynamically stable product, while **aq** is the kinetically favoured product. The more sterically demanding the counterion, the higher the probability of obtaining an abnormally bound product.[31]

In 2008, Albrecht highlighted that the lack of dual heteroatom stabilization as *a*NHCs,[5] compromises the overall stability of these free carbenes,[32] based on the DFT calculations performed by Tonner *et al*. in 2007 on normal and *abnormal* NHCs. [33] These findings concluded that NHCs are lower in energy than *a*NHCs by ~17 kcal/mol. Furthermore, the acid dissociation constants (pK_a values) are 24.9 and 33.0 for the corresponding imidazolium salts of NHCs and *a*NHCs, respectively. This suggests a higher energy barrier for the activation of the C-H bond in direct metalation reactions of aNHCs than of NHCs.[34] Facile deprotonation and thus metalation at the C2 carbon is thus implied to afford a normal NHC. To access the *a*NHC, the C2 position would have to be protected with an alkyl or an aryl group. Albrecht also cautioned that other side reactions may occur in an attempt to alkylate the C2 carbon under certain conditions i.e. metalation with AgO_2,[34,35] however it was concluded that all experimental and theoretical data suggests the mesoionic nature of *a*NHCs enables the formation of a considerably stronger metal–carbene bond than its normal counterpart.

Until 2009, the only reported routes to access *a*NHC complexes was *in situ* deprotonation, direct metalation, transmetalation and oxidative addition.[36] To access the free *a*NHC, every position was substituted with an aryl group excluding the C5 position which was deprotonated with a non-nucleophilic base. This marked the isolation of the first free *a*NHC, consolidating its stability despite only having one α-heteroatom, much like the Fischer carbene.[37]

1.1.2.2. 1,2,3-Triazol-5-ylidene complexes

1,2,3-Triazol-5-ylidenes are a class of *a*NHCs where the carbon at position 2 is replaced by a third nitrogen atom. This augments the inductive effect on the carbene carbon by further withdrawing electron density from the σ-orbital of the carbene carbon thus weakening its σ-donor ability to the central metal.[13] However, this in turn intensifies π-electron delocalisation enhancing the stability of the carbene. Compared to imidazol-4-ylidenes, 1,2,3-triazol-5-ylidenes are weaker σ-donors but are still better donors when compared to imidazol-2-ylidenes. The electronic and steric properties of these ligands can be altered by varying the substituents on the heterocycle.

1.1.2.2.1. The copper-catalysed azide alkyne cycloaddition mechanism

N-alkylated 1,2,3-triazolium salts are accessed from the corresponding 1,2,3-triazole, a heterocycle synthesized from the copper-catalysed 1,3-dipolar cycloaddition reaction of azides and alkynes, commonly referred to as the "click chemistry".[38] This high yielding method is preferred due to its selectivity and unlimited versatility, giving access to a wide range of 1,4-disubstituted 1,2,3-triazoles.[34]

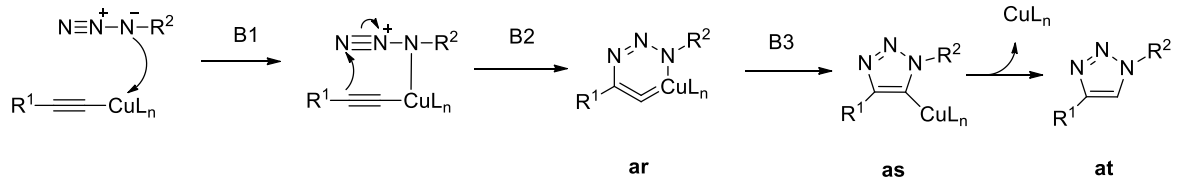

Scheme 1. 10: Mechanism proposed by Fokin detailing the ligation of the 1,2,3-triazol.[31]

Although this reaction has been widely used for [3+2] cycloaddition reactions, the mechanism is not completely understood.[39] In 2002, Fokin and co-workers proposed a mechanism where a six membered copper containing intermediate forms during the reaction. The reaction between the catalyst and the R^1-substituted alkyne results in the formation of a copper acetylide, eliminating HX. Consequently, a bond is established between copper and the R^2-substituted nitrogen, which induces bond formation between the terminal nitrogen of the azide, and the sp hybridised carbon resulting in **ar** (Scheme 1.10).[40] Bertrand and co-workers showed that the formation of binuclear copper intermediates follows the kinetically favoured pathway (Scheme 1.11), and the limiting step is the formation of the copper acetylide.[30]

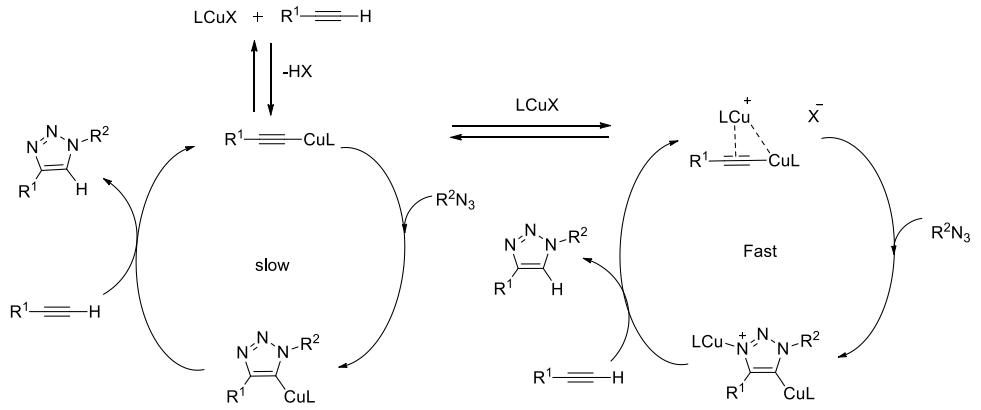

Scheme 1. 11: Bertrand's proposed mechanism of the catalytic cycle for the copper catalysed "click" reaction.[30]

1.1.2.2.2. Early 1,2,3-triazol-5-ylidene metal complexes

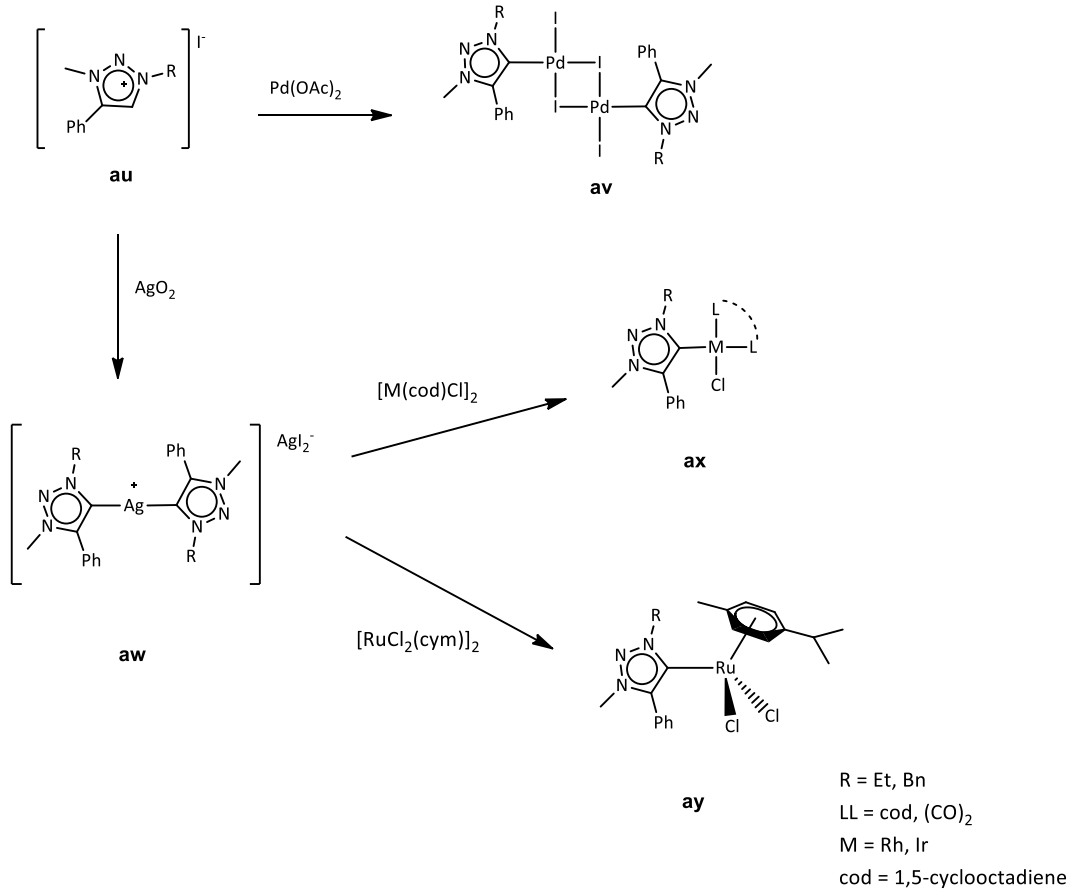

Scheme 1. 12: Preparation of the first 1,2,3-triazolylidene metal complexes ***au-ay.***[44]

Prior to the isolation of the first free 1,2,3-triazol-5-ylidene, it was considered that they tend to decompose. However, Albrecht and co-workers confirmed their metalation by preparing the

corresponding palladium(II) complex using metal precursor containing an internal base, or following a transmetalation route from the silver(I) complex which further opened up a new range of metal complexes such as ruthenium, rhodium, and iridium (Scheme 1.12).[41] Albrecht and co-workers went on to study the donor properties of this ligand using the IR stretching vibrations of the CO co-ligands on the iridium(I) complex, **I** as a direct probe to determine its electronic parameters. An earlier study by Crabtree revealed the presence of a linear correlation between Tolman's Electronic Parameter(TEP) and the average stretching frequency of the coordinated CO ligands, which he applied to complexes of type $[(L)Ir(CO)_2Cl]$, where L is an NHC.[42] From these, Albrecht concluded that substituents on the heterocycle play a role in the donor properties of the ring. Furthermore, triazolylidene metal complexes were predicted to have significant potential as exceptional catalyst precursors.

Shortly after this, Bertrand isolated the first free *N*-alkylated 1,2,3-triazol-5-ylidene, and found that this carbene undergoes intermolecular alkyl rearrangement when heated to 50°C.[43] This prompted studies into the synthesis of N3-arylated 1,2,3-triazolium salts, which could not be prepared using "click" chemistry.

To prepare *N*3-arylated 1,3,4-trisubstituted 1,2,3-triazolium salts, Bertrand and co-workers followed a modified copper-free formal cycloaddition reaction proposed by Wirschun and Jochims (Scheme 1.12).[44,45] Previously, a cycloaddition reaction between 1,3-diaza-2-azoniaallene salts and alkynes was successfully developed, preparing a range of 1,3-diarylated triazolium salts.[45] The triazene was treated with ^{t}BuOCl, and a Lewis acid $SbCl_5$ or KPF_6 at -78°C in the presence of an alkyne. It was cautioned that at temperatures above -25°C, the intermediate triazene salt disintegrates into diazonium salts and azo compounds. Additionally, it was concluded that successful cycloaddition occurs in the presence of ^{t}BuOCl and a Lewis acid at -78°C to yield the desired 1,3-diarylated-1,2,3-triazolium salt.[45] This was followed by the isolation of the free 1,3,4-triarylated 1,2,3-triazol-5-ylidene which was reported to be robust for extended periods of time even under thermally elevated conditions. The salt was successively coordinated to ruthenium for application as an olefin metathesis precatalyst, as well as to iridium to study the ligand's donor properties.[43]

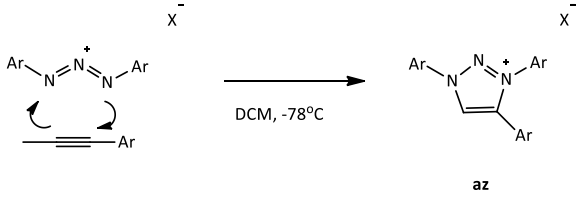

Scheme 1. 13: Formal cycloaddition reaction of 1,3-diaryl-2-azoniaallene salt with an alkyne.[45]

1.1.2.2. Bidentate N-heterocyclic carbene ligands

Thus, Herrmann and co-workers published a range of late transition metal chelating NHC complexes in the mid-late 1990s, starting with the chelation of **ba** to palladium.[46] This resulted in a square planer complex (**bb**) stable at temperatures of up to 70°C in solution and 280°C in solid state (Scheme 1.14).[46] Furthermore, carbene complexes were reported to increase catalytic activity over a spectrum of catalytic reactions.[47] These were found to minimize steric demand, and therefore steric repulsions due to the planar geometry of the heterocyclic ring, compared to the bulkier phosphine ligands.[51a]

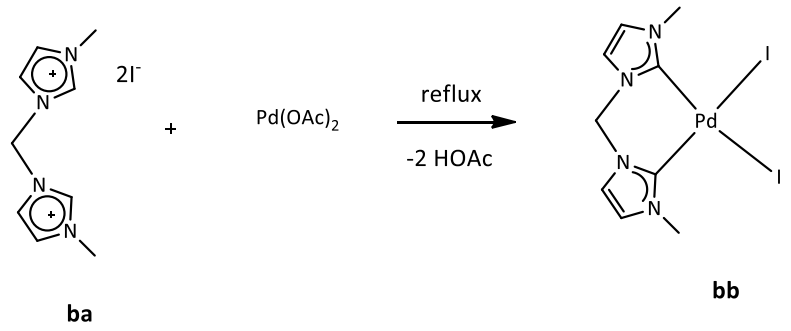

*Scheme 1. 14: The preparation of the chelated Pd(II) biscarbene complex **bb**.[51a]*

Bidentate NHCs have been observed to coordinate to the metal centre by chelation or by bridging. Crabtree and co-workers studied the factors affecting the outcome of coordination once the ligand had been activated at position C2.[48] The length of the linker between the rings is one such factor. Due to the negligible π backdonation from the metal of the metal-carbene bond in monodentate NHC complexes, these planar rings experience free rotation about this bond in contrast to chelate bidentate NHC complexes.[53] When chelated to a square planar metal centre, NHCs bearing wingtip-substituents with reduced steric bulk and short linkers i.e n = 1-2 (Figure 1.3, **bc**), orientate themselves along the *xy* plane, while longer linkers allow the rings to rotate into the *z* plane(Figure 1.3, **be**).[49] Bulkier co-ligands such as 1,5-cyclooctadiene (cod), force the rings to rotate, placing the wing-tip substituents in the *z* plane to reduce steric repulsion in the already occupied *xy* planes. This is unfavourable for short linkers with bulky wingtip groups and co-ligands. So, to ease this strain on the square planar metal centre, the bridged orientation is favoured, affording a dinuclear complex, **bd**.[54]

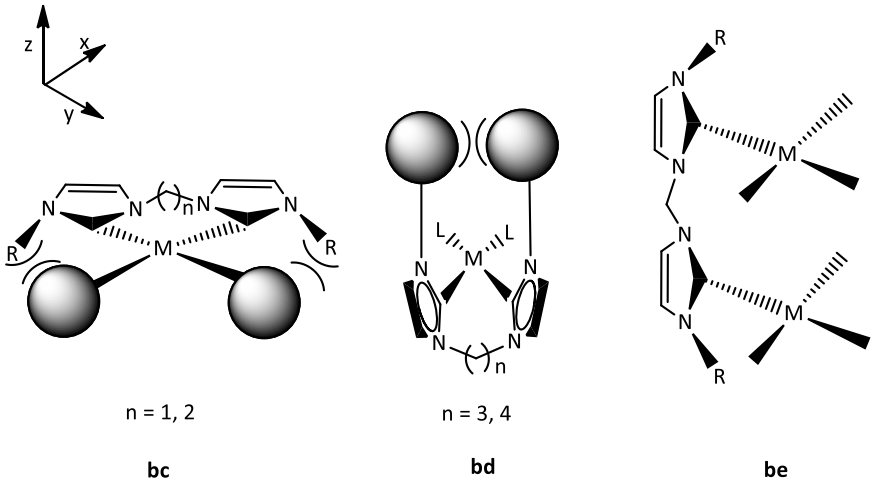

Figure 1. 3: Spatial arrangements of the bidentate NHC ligand coordinated to square planar metal centres[53,54]

Contrary to what Crabtree *et al*. had previously reported,[54] Field and co-workers isolated the mononuclear chelating rhodium N-heterocyclic biscarbene complex **bf** from the corresponding precursor imidazolium salt and $[Rh(cod)(OEt)]_2$ (Figure 1.4).[52] Following this, Slaughter and co-workers reported chelating rhodium complexes with bulky wingtip groups, and a short linker obtained from a transmetalation reaction with a dinuclear silver N-heterocyclic biscarbene.[50] According to Crabtree's

earlier predictions, bridged complexes were to be expected in both cases. This prompted further investigations and ultimately the conclusion that the counterion plays a significant role in whether chelation or bridging would occur. Crabtree reported that the presence of a halide in the reaction medium results in a dinuclear rhodium(I) complex for linkers of lengths n = 1-4, where the R-substituents (Figure 1.3) are bulky. Where the R-substituents are less sterically hindering, bulky co-ligands with a short linker ie. n = 1 in the presence of a halide will also result in a dinuclear complex. Mononuclear complexes were reported to be obtained from wingtip groups and co-ligands with limited steric bulk, regardless of the length of the linker; as well as from sterically hindered R-groups with short linkers in the absence of a halide.[51]

bf **bg**

X = PF_6, BPh_4 Mes = mesityl

*Figure 1. 4: Chelating mononuclear rhodium(I) N-heterocyclic biscrabene complexes **bf** and **bg***

Crabtree began working on bitriazole (bitz) NHC ligands that he found to be easily accessible, and significantly versatile. However, after isolation the free carbene ligand rearranges to the corresponding bitriazole spontaneously.[52] This ligand salt precursor (**bh**-$2I^-$, Scheme 1.15) was found to deprotonate with ease under mild conditions. The acidity of the carbene carbon C2 is speculated to be a direct influence of the high inductive effect on the carbene carbon from the two flanking heteroatoms.[58] The direct N-N bond linking the two heteroarenes was said to eliminate unwanted by-products due to the lack of a linker. Furthermore, the planarity of this ligand encourages square planar coordination about the metal centre. The metalation of this complex with a rhodium(I) precursor containing a halide, resulted in the formation of the octahedral rhodium(III) complexes **bi** and **bj** (Scheme 1.15).[53] In an attempt to study the donor strength of the ligand, **bh**-$2BF_4^-$ was treated with $[Rh(CO)_2(OAc)]$ with the prospect of isolating the square planar cationic $[Rh(CO)_2(bitz)]$ complex. Instead, the dinuclear complex **bk** resulted. Only complexes **bi** and **bj** were found to be catalytically active in base mediated transfer hydrogenation reactions, with similar reaction rates.[57]

The pioneering work by Crabtree on 4,4'-bis(1,2,4-triazol-5-ylidene) or the bitz ligand, was followed by the preparation of the first free 4,4'-bis(1,2,3-triazol-5-ylidene) or the i-bitz ligand, similar in topology to the existing 2,2'-bipyridine.[54] The preparation of the i-bitz by Bertrand *et al*. followed an adaptation of the "click" method, however the coordination of this bidentate ligand to rhodium proceeded by deprotonation with NaOEt to promote chelation. Bidentate ligands classically coordinate by chelating to a single metal centre, or by bridging between two metal centres. Factors

such as linker-length, choice of counterion, steric bulk of the co-ligands and the heterocycle's substituents allow for the prediction of the ligand's mode of coordination to the metal centre (*vide infra*).[53,54]

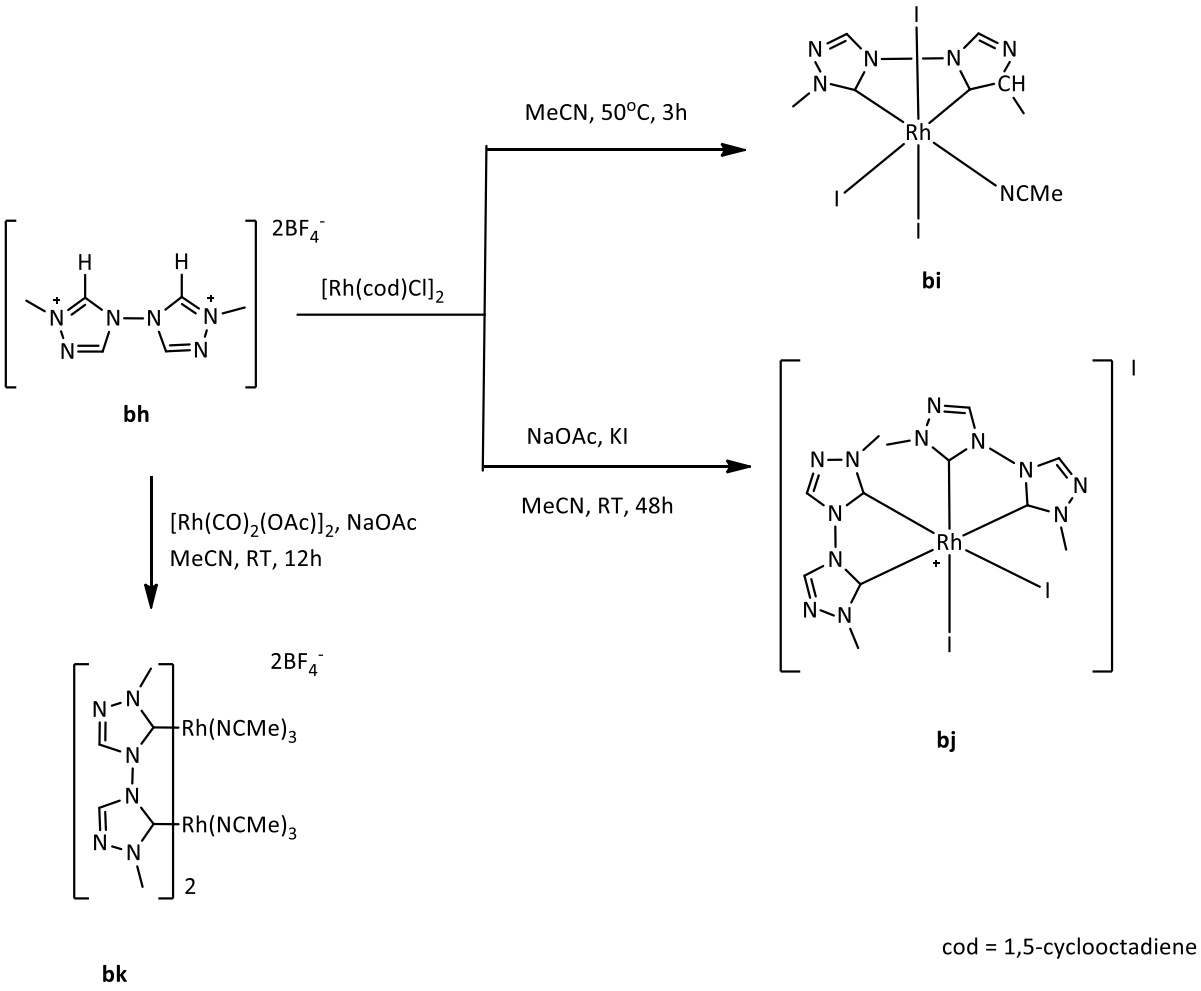

*Scheme 1. 15: The coordination of the bitz ligand **bh** to rhodium using MeCN as a solvent.*

In 2014, Elsevier and Sluijter prepared chelated heterodicarbene complexes of rhodium(I) from a range of bidentate ligands. These ligands contained a normal NHC linked to a 1,2,3-triazolylidene by a CH_2 linker (Scheme 1.16), following their previous work on the heteroditopic triazolyl-functionalised NHC. The preparation of these imidazolium-triazolium salt precursors involved the classical "click" reaction on an alkynyl substituted NHC, followed by alkylation of the triazolyl ligand to afford **bm.** $[M(cod)(OMe)]_2$ was prepared *in situ* before the addition of the salt, yielding only the pseudo-square planar mononuclear product **bl**. These electron-rich mixed carbene complexes were notably unstable and had to be prepared just prior to their use in hydrogenation reactions. From the obtained data, varying the substituents on the triazolylidene moiety seemed to have no significant effect on the activity of the precatalyst. However, better conversion rates were observed for **bm** in contrast to similar bidentate NHC-NHC complexes.[55]

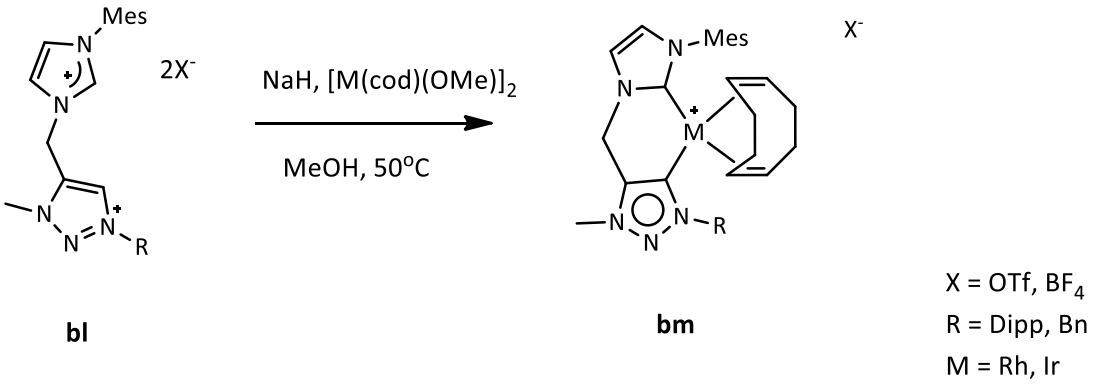

bl **bm**

*Scheme 1. 16: Chelation of the bidentate heterodicarbene **bl** to a square planar metal centre.[60]*

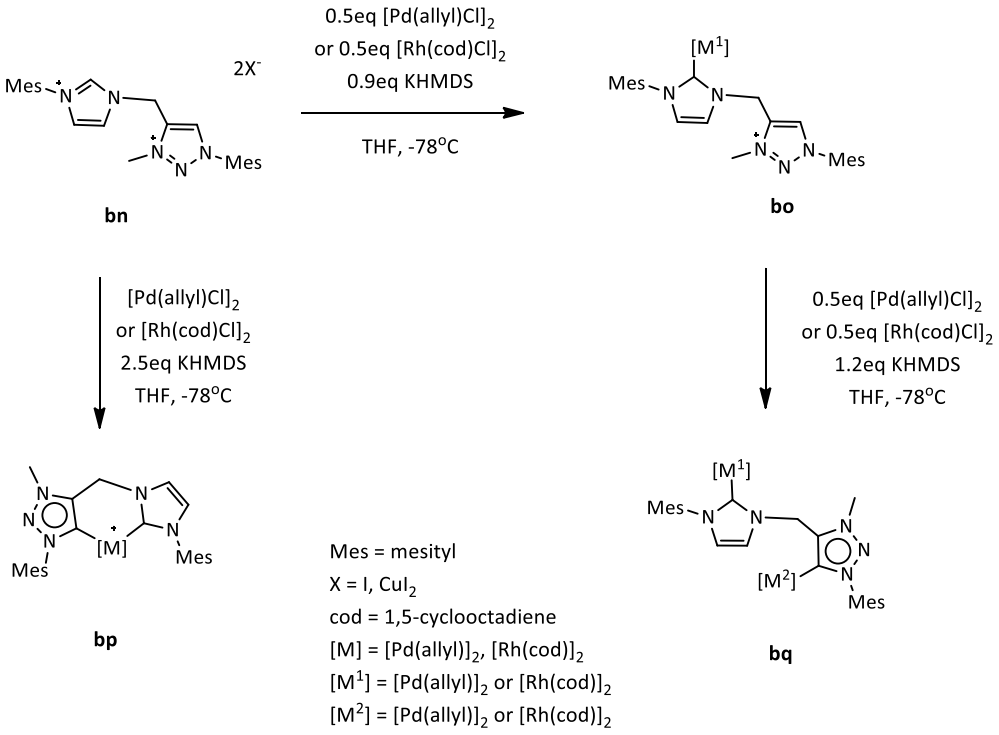

bn **bo** **bp** **bq**

*Scheme 1. 17: The preparation of chelated heterodicarbene complexes **bp**, as well as bridged heterobimetallic heterodicarbene complexes **bq**.[61]*

Taking advantage of the bidentate-type ligand, Mendoza-Espinoza and co-workers prepared bidentate palladium and rhodium complexes where the ligand chelates to the metal (**bp**, Scheme 1.17); where the NHC bound complex consists of the triazolium functionality (**bo**, Scheme 1.17); as well as where the bridged bimetallic complex contains both the rhodium and the palladium metal on each carbene (**bq**, Scheme 1.17).[60] To prepare **bp**, **bi** was treated with 2.5 equivalents of KHMDS in the presence of 1 equivalent of the metal. Complex **bo** was prepared by treating **bi** with 1 equivalent of base and 0.5 equivalent of metal to yield a palladium or a rhodium complex. To obtain the heterobimetallic complex **bq**, complex **bo** (bearing one of the metals) was deprotonated with 1.2 equivalence of base and treated with 0.5 equivalent of the other metal.[60] Although no catalytic data has been reported for these complexes to date, the aim was to combine and study the effect of the varied donor ability of the respective carbene groups in a hybrid ligand .[56]

1.2. Hydroformylation

In this thesis, the catalytic transformation investigated for the applicability of the prepared ligands and coordination compounds, is the alkene hydroformylation reaction. Hydroformylation is an atom economical, catalytic insertion of an aldehyde or a formyl group to an olefin using synthesis gas (syngas), a mixture of carbon monoxide (CO) and molecular hydrogen (H_2).[57,58] The hydroformylation process primarily produces aldehydes. With the exception of ethylene, alkene substrates may undergo isomerisation followed by hydroformylation resulting in branched alkenes.[57] Additionally, without removal of the catalyst, the produced aldehydes undergo reduction at elevated temperatures and pressures for extended time periods causing the formation of alcohols (Scheme 1.12). The factors influencing the outcome of hydroformylation are reactions conditions such as syngas pressures, reaction temperature, rate of reaction, and the electronic and steric properties of the catalyst precursor.[58]

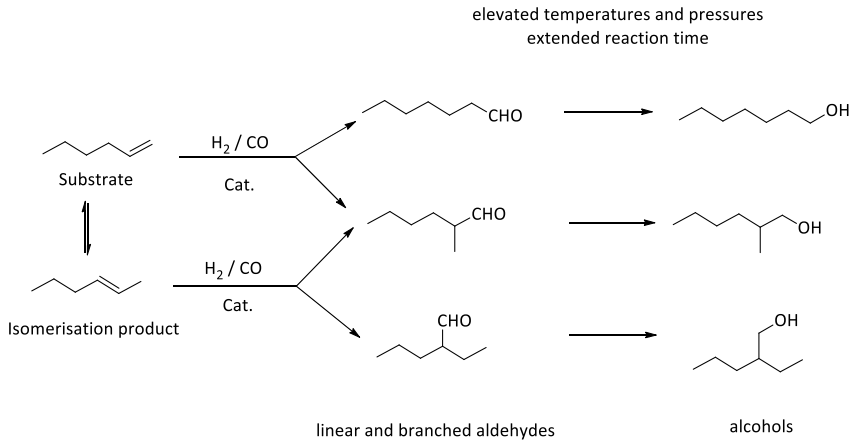

Scheme 1. 18: Olefin hydroformylation reaction products.[57]

The development of these hydroformylation catalyst precursors gained traction over the years since the first discovery in 1938, during a Fischer-Tropsch reaction.[57] The original catalyst precursor [$Co_2(CO)_8$] required harsher conditions with temperatures of up to 300°C and pressures of up to 200 bar.[59] The active species, usually formed *in situ,* [$HCo(CO)_4$] follows the Heck and Breslow mechanism (Scheme 1.13).[60,61] The equatorial CO is dissociated from the active species forming a 16 electron species [$HCo(CO)_3$], creating a vacancy for the alkene to coordinate. The alkene coordination can either occur perpendicular to the Co–H bond, which is lower in energy due to reduced steric orbital interaction, or parallel to the Co–H bond.[60] The alkene undergoes migratory insertion between the Co–H resulting in an alkyl complex followed by the addition of CO at the vacant equatorial position. The CO inserts between the central metal and the alkyl group resulting in an acyl complex. The formation of the linear product (*anti*-Markovnikov insertion) is thermodynamically favoured, however, this does not rule out the possibility of the Markovnikov product (branched aldehyde). The oxidative addition of H_2 leads to a rate determining agostic interaction of the H_2 with the acyl Co–C(=O).[60] The aldehyde undergoes reductive elimination, regenerating the catalyst thus marking the end of the cycle, and initiating the next.[60]

The first generation of hydroformylation catalyst precursors were cobalt salts, where the reactions proceeded with a turnover of less than 10 kt of aldehydes per year.[57] Roelen postulated that the active species was [$HCo(CO)_4$], a complex isolated four years prior.[68] Although hydroformylation was known to produce aldehydes, alcohols and iso-alkenes from the corresponding olefins (Scheme 6.1), this reaction could not proceed in the absence of a catalyst.[62] Moreover, for these reactions to proceed, temperatures of between 100°C and 300°C were required along with pressures ranging from 100 bars to 200 bar.[62] A drawback of this process was the inability to produce substantial quantities of the alcohol product, so therefore if the desired product is an alcohol, the obtained aldehydes would be required to undergo an additional hydrogenation step.[63] This implied that the hydroformylation process is chemoselective towards aldehydes, however challenges in obtaining high ratios of linear to branched aldehydes were recorded as a disadvantage of this process. To improve the chemo- and regioselectivity of the reaction, the olefin was to be reacted with CO and H_2 (syngas) in the presence of an improved catalyst, requiring lower reaction pressures.[63] Therefore, rhodium and ruthenium based catalysts containing phosphine with a range of steric demands, as well as carbonyl ligands were explored, where lower temperatures were employed with 195°C being the optimal.[63]

Slaugh and Mullineaux modified the cobalt catalyst precursor by substituting one of the carbonyl ligands on each metal centre with a phosphite or tertiary phosphine ligand, to increase selectivity. It was observed that the more phosphines were present in the reaction mixture the better the selectivity towards linear aldehydes. However, phosphines are easily replaced by carbonyls, therefore to counter this, excess phosphines are added to the reaction.[29] Reduced reaction rates and pressures were observed, along with better selectivity towards alcohols.[64] Thus began the modification of the cobalt precatalyst by substituting carbonyls for phosphines with a range of steric and electronic properties to increase selectivity. Wilkinson and co-workers evoked an interest in the use of rhodium as a central metal instead of cobalt in 1968.[65] With the assumption that the active species is [$HRh(CO)_4$] similar to the cobalt active species, the rhodium counterpart exhibits better activity under milder conditions in stark contrast to cobalt. [65]

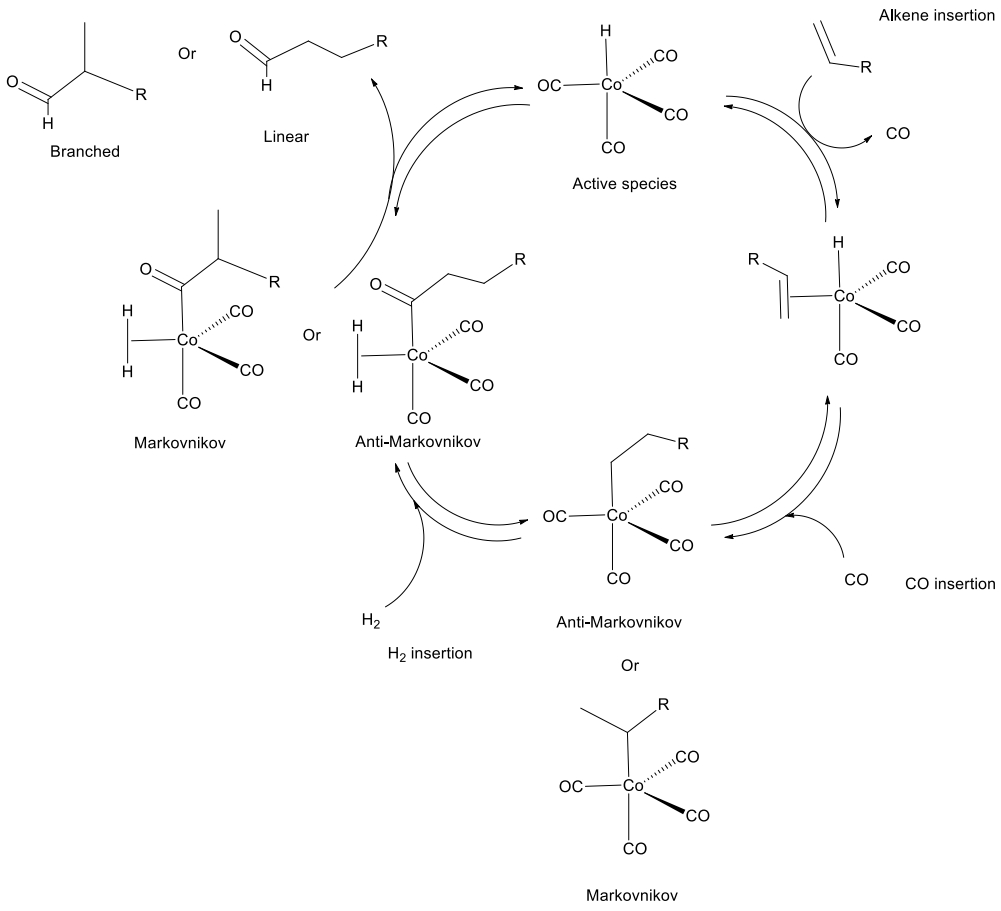

Scheme 1. 19: The mechanism proposed by Heck and Breslow of the hydroformylation reaction of an olefin with catalyst $[HCo(CO)_4]$.[60,61]

In 1965, Wlkinson and co-workers reported hydroformylation reactions under milder conditions with a syngas (1:1 CO/H_2) pressure of 90 atm and a temperature of 55°C. After 12 hours in a solution of benzene/ethanol (1:1), hexene was converted into ~70% 1-heptanal and ~20% 2-heptanal in the presence of 1 mol% of the catalyst $[Rh(PPh_3)_3Cl_3]$.[66] Under the same conditions, comparable conversions were observed when $[Rh(py)_3Cl_3]$ and $Rh_2Cl_2(Sn_2Cl_2.EtOH)_4$ were employed as catalysts.[66] It was therefore speculated that the active species is $[HRh(CO)_4]$, analogous with the previously reported active species of cobalt.[67] Furthermore, it was found that this rhodium catalyst is effective at temperatures less than 55°C and syngas pressures less than 10 atm.[65] This is a direct consequence of the ease of oxidative addition of the hydride to the rhodium catalyst (an intermediate step during the hydroformylation reaction) in comparison to cobalt. Therefore, in order to induce oxidative addition in cobalt catalysts, harsher conditions (i.e. temperature and pressure) are necessary.[65,68] Moreover, the dissociation of the aldehyde product from the catalyst in the cycle occurs more readily for rhodium catalysts, necessitating milder reaction conditions and thus making rhodium-based catalysts markedly more active than cobalt based catalysts.[65,68]

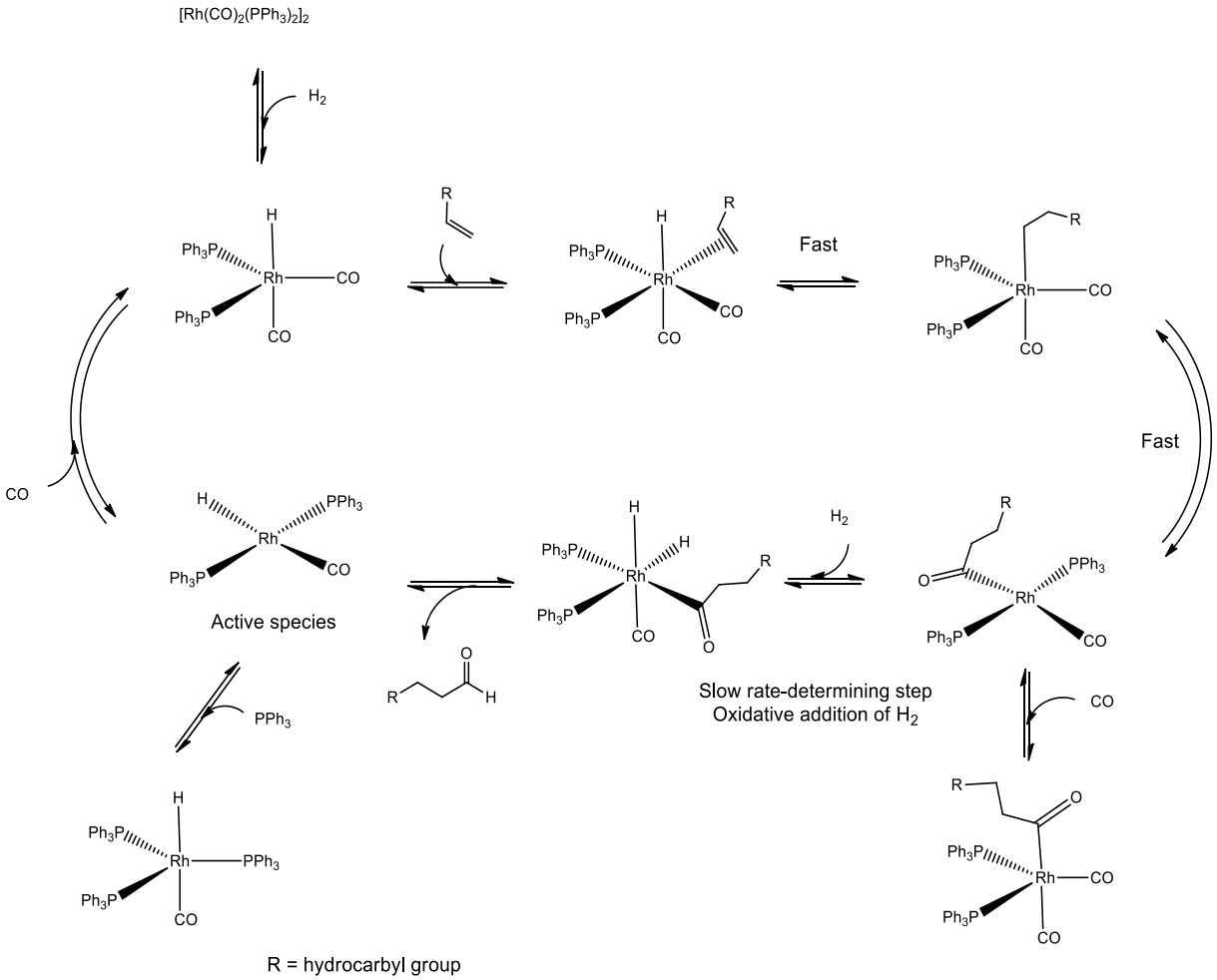

Scheme 1. 20: Modified Heck and Breslow hydroformylation mechanism of rhodium complexes suggested by Wilkinson and co-workers.[65]

Wilkinson and co-workers found that [$RhCl(PPh_3)_3$] adopts a modified version of the Heck and Breslow mechanism during hydroformylation reactions. When exposed to carbon monoxide, one of the PPh_3 groups is substituted by a CO to form [$RhCl(CO)(PPh_3)_2$], the same product formed when rhodium(III) complexes are exposed to syngas.[65] This chlorinated precatalyst undergoes hydrogenolysis to replace the chloride with a hydride forming the catalytically active species [$HRh(CO)(PPh_3)_2$)] (Scheme 1.15), eliminating the inhibition period induced by chlorido complexes during the reaction.[65] CO is inserted rapidly *cis* to the existing CO, forming a pentacoordinated rhodium(I) species. Alkene coordination occurs resulting in an octahedral complex followed by a fast migration step between the metal centre and the hydride complex which will proceed in the Markovnikov or *anti*-Markovnikov fashion. The intramolecular swift insertion of CO results in a square planar acyl complex. The slow *cis* oxidative addition of molecular hydrogen occurs, resulting in the change in oxidation state thus leading to the deduction that this step is rate determining. The simultaneous loss of the acyl and hydride group affords the aldehyde and the starting active catalyst.[65]

Over and above catalytic activity, the chemo- and regioselectivity of a catalyst is an imperative function in catalyst design. Phosphorous ligands of type PR_3 gained popularity as modifying ligands in hydroformylation reactions due to their ability to increase reaction rates under mild conditions.[69] The

electronic and steric properties of phosphorous modified ligands play a significant role in the increase of reaction rates, due to their ability to stabilize the intermediate unsaturated rhodium complexes.[70] Bulkier phosphine ligands which tend to be poor σ-donors and good π-accepters, allow for the insertion of the olefin in anti-Markovnikov fashion resulting in the formation of linear aldehydes and thus increasing regioselectivity.[71] Therefore it was concluded that the more electron withdrawing the PR_3 ligand, the better the selectivity and overall activity of the catalyst towards formation of the linear product.[72] To classify the steric interactions of these phosphorous ligands, Tolman developed the cone angle concept measured at 2.28 Å from the phosphorous atom to the metal centre.[73] The infrared (IR) CO stretching frequencies (measured in wavenumbers) of the complex $[(L)Ni(CO)_3]$ define the electronic parameter X (later named the Tolman Electronic Parameter or TEP), which is a measure of the donor ability of the ligand L.[73,74]

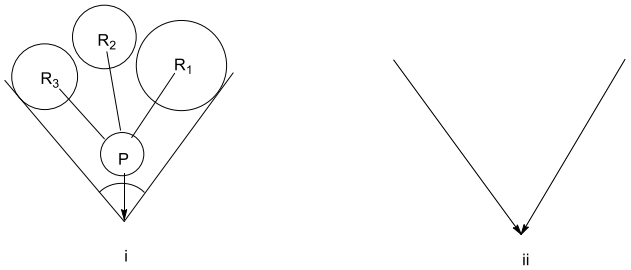

Figure 1. 5: Graphical representation of Tolman's (i) cone angle concept defining steric effects and (ii) electronic parameter X.[72,73]

However, in 1995, Herrmann and co-workers highlighted the disadvantages of phosphines as ligands of homogenous catalysts, accentuating the instability of the catalyst upon exposure to air and moisture. Additionally, the P–C bond undergoes cleavage resulting in the degradation of the catalyst precursor therefore to circumvent these factors, excess ligand is typically added to the reaction.[29] Also necessitating excess ligand is the similarity in rhodium binding constants of phosphines and carbonyls where the phosphines can be replaced by the carbonyl at elevated gas pressures, therefore to improve regioselectivity maintaining steric bulk around the metal centre is a requirement.[75] Using N-Heterocyclic carbene (NHC) ligands as phosphine mimics,[76] Herrmann demonstrated the superiority of the NHC as a ligand on a catalyst precursor emphasizing the thermal stability of these types of complexes. Furthermore, no excess ligand was required to maintain equilibrium in the activation steps of the catalytic process.[29] NHCs are easily accessible and better donors than phosphines according to TEP calculations validating their stability.[72] NHC ligands are easily tunable. By varying the substituents on the ring, the electronic and steric properties of the ligand can be altered depending on one's catalytic needs.[72] Surprisingly, due to increased electron density at the metal centre according to speculations by Herrmann in 1997, rhodium NHC complexes display reduced activity in hydroformylation reactions.[77] However, the activity improved significantly when a phosphine co-ligand is coordinated to the rhodium NHC complex.[77]

In 2015 our group prepared the first rhodium(I) Fischer carbene complexes (Figure 1.6, **bs**) with donor properties comparable to those of NHCs. This prompted the investigation into the activity of a Fischer

carbene ligand in hydroformylation reactions.[80] Shortly after this in 2016, 1,2,3-triazol-5-ylidene bearing rhodium(I) complexes (Figure 1.5, **br**) were employed as catalyst precursors for the hydroformylation of 1-octene although these ligands presented high selectivity, lower conversions were observed for these ligands in contrast to Fischer carbene ligands.[81]

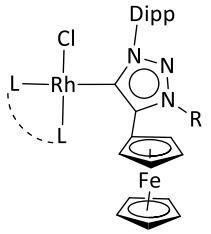

br

R = Dipp, Ethyl
LL = cod, CO
Dipp = 2,6-diisopropylphenyl

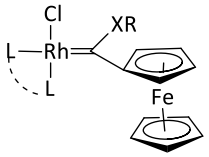

bs

XR = OEt; ^{n}PrNH
LL= cod; $(CO)_2$; CO,PR_3; CO, $AsPh_3$

cod = 1,5-cyclooctadiene

Figure 1. 6: Previously prepared hydroformylation catalyst precursors.

As mentioned earlier, the insertion of the alkene across the rhodium and hydride bond occurs in the *anti* Markovnikov or Markovnikov fashion. This is speculated to be influenced by the ligand coordinated *trans* to the M–H bond which polarises this bond. In this particular instance, the π-accepting CO induces a δ^+ charge on the hydrido ligand favouring Markovnikov addition, which stimulates alkene isomerisation.[65] Other more pronounced effects include the steric bulk of the ligands *cis* to the hydrido, where the steric repulsion of the PPh_3 co-ligand directs the insertion of the alkene towards *anti* Markovnikov addition which is less likely to isomerise, favouring linear aldehyde formation.[65]

The insertion of the CO to form the acyl complex is a fast reaction when the metal centre is rhodium, however in the case of iridium this complex is stable and requires elevated temperatures and pressures to coerce CO insertion.[65] At lower temperatures and pressure, this process does not occur fast enough allowing the competing hydrogenation reaction to proceed ahead of CO insertion thus making the iridium metal centre an excellent hydrogenation catalyst. Furthermore, the oxidative addition of hydrogen results in a stable iridium(III) complex, which does not undergo elimination efficiently compared to the corresponding rhodium(III). This contributes to the poor activity of the iridium catalyst precursor in hydroformylation transformations.[65]

In an effort to suppress competing hydrogenation reactions, a salt promoter was added to the iridium-catalysed hydroformylation reaction.[78] For the catalyst $[Ir_4(CO)_{12}]$, the addition of a chloride salt resulted in better aldehyde yields were obtained compared to the when Li_2CO_3 was used implying that the presence of a chloride in the reaction mixture promotes hydroformylation. Furthermore, the homogeneity of the precatalyst was increased due to its improved solubility in the presence of a chloride salt.[79] Similar results were reported for $IrCl_3$, regarding the hydroformylation products when

LiCl was added. Contrary to what was observed for $[Ir_4(CO)_{12}]$ in the presence of Li_2CO_3, more alcohol products were obtained when Li_2CO_3 was added to an $IrCl_3$. Thus, it was concluded that LiCl is the better promoter, based on the atomic radius of both the anion and the cation. Salts containing larger cations and anions do not suppress hydrogenation reactions as effectively as LiCl. It was further postulated that the role of the promoter is to stimulate the formation of the active species by coordination of the chloride to the central metal, while the complex is stabilized by the anion.[78,79]

1.3. Aims and Objectives

1.3.1. Problem statement and rationale

Hydroformylation is one of the largest most valuable industrial homogenous processes, producing aldehydes and alcohols as intermediates for the productions of plasticizers, fragrances, detergents and flavourants to name but a few.[57] Therefore the optimisation of this process is of utmost importance, establishing the foundation and central theme of this project.

Up to this point, the performance of hydroformylation catalyst precursors has been measured according to selectivity towards the desired product, linear aldehydes. In the past our group has prepared ferrocenyl-substituted rhodium (I) Fischer carbene complexes as well as ferreocenyl-substituted rhodium(I) 1,2,3-triazol-5-ylidene complexes as precursors for this transformation, to address the scarcity of the use of these types of complexes in such transformations. The rhodium Fischer carbene complexes displayed 90-100% conversions, with chemoselectivities of between 85% and 100% towards aldehydes and TOFs of 204 h^{-1}-483 h^{-1}. Conversely, lower regioselectivities towards the desired linear aldehydes were observed, with n/iso ratios of 0.70-1.25.[86] The rhodium 1,2,3-triazol-5-ylidene complexes exhibited conversions comparable to those of the Fischer carbene complexes, with reactions times twice as long as those employed for the Fischer carbene complexes. Chemoselectivity was lower than that of the Fischer carbene complexes ranging from 67%-80%. Furthermore, TOFs were observed to between 100 h^{-1} and 125 h^{-1}. However, compared to the Fischer carbene complexes, the 1,2,3-triazol-5-ylidene complexes displayed relatively high regioselectivity towards linear aldehydes with n/iso ratio of 1.60-2.43.[87]

As aforementioned, the steric and the electronic properties play a role in the performance of the catalyst precursor. Thus far, rhodium(I) 1,2,3-triazol-5-ylidene complexes and rhodium (I) carbene complexes are still under explored as catalyst precursors for hydroformylation reactions. Furthermore, the existing catalyst precursors of this sort are each have their own limitations such as regioselectivity in the case of rhodium Fischer carbenes and chemoselectivity in the case of rhodium(I) 1,2,3-triazol-5-ylidene complexes. This is regardless of the secondary transition metal as a substituent to the carbene ligands. Therefore, this thesis will address these limitations by preparing more rhodium(I) 1,2,3-triazol-5-ylidene and rhodium(I) Fischer carbene complexes, devoid of an ancillary transition metal. This will be done in order to increase the performance of each type of catalyst precursor focussing on improving the chemoselectivity of the rhodium(I) 1,2,3-triazol-5-ylidene complexes, and bettering the regioselectivity of the Fischer carbene complexes in hydroformylation reactions.

1.3.2. Aims and hypotheses

Formerly, our group prepared rhodium(I) Fischer carbene complexes by transmetalation from ferrocenyl substituted group 6 Fischer carbene complexes, following an altered version of Barluenga's facile method to prepare rhodium(I) Fischer carbene complexes.[80] These complexes addressed the dearth of Fischer carbenes as ligands for catalyst precursors in hydroformylation reactions, performing well with conversions of up to 100% in 4 hours.[86] As an augmentation, rhodium(I) Fischer carbene complexes without a secondary oxidizable metal will be prepared and characterised for their application as precatalysts in hydroformylation reactions, to examine the effect of the absence of iron on the conversion and selectivity of these transformations. It is therefore postulated that by decreasing electron density at the metal centre with the less donating *N,N*-dimethylaniline substituent better TOFs will be observed. Furthermore, the substitution of the less bulky ethoxy group with the bulkier amino group will increase the regioselectivity of the catalyst precursor.

The use of NHC ligands as catalyst precursors for hydroformylation reactions is not unheard of, yet the rarity 1,2,3-triazol-5-ylidenes as ligands of precatalysts to this reaction prompted the preparation of these complexes. As aforementioned, 1,2,3-triazol-5-ylidenes – like Fischer carbenes – are stabilized by one heteroatom; however, they are cyclic and nucleophilic dissimilar to Fischer carbenes. Previously, ferrocenyl substituted 1,2,3-triazol-5-ylidene complexes of rhodium were prepared and applied in hydroformylation reactions. Excellent regioselectivity was observed with *n*/iso ratios of up to 2.63.[81] Rhodium(I) *N*-alkylated and diarylated 1,2,3-triazol-5-ylidene complexes will be prepared, along with bidentate chelated and bridged i-bitz rhodium complexes to study their activity in hydroformylation reactions. The *N*-alkylated rhodium(I) 1,2,3-triazol-5-ylidene complexes are less sterically demanding than their diarylated counterparts, which is presumed to have a positive effect on their behaviour as catalyst precursors. Too much steric repulsion compromises the substrate's ease of access to the metal centre, resulting in a decline in the amount of aldehydes produced per hour or the TOF. To verify this, the behaviour of the N-alkylated carbene complexes will be compared to that of the diarylated carbene complexes, as well as to the rhodium(I) ibitz. Furthermore, the electronic differences between monodentate ligands, bidentate chelated and bridged ligands will have an effect on the substrate %conversion. The more donating chelated rhodium complex is speculated to result in less conversion than the bridged counterpart. However, the bridged rhodium complex is speculated to have a lower TOF than the chelated rhodium(I) ibitz complex due to its extensive steric bulk.

Rhodium resources are gradually depleting, leading to the overpricing of this precious group metal (PGM). To alleviate the strain on this resource, investigations of alternative PGMs as the central metal in hydroformylation precatalysts has begun.[82] Examples of iridium centred hydroformylation catalyst precursors are limited despite reports of simple salts as additives to supress the side reactions which are typically favoured by iridium catalyst precursors.[82] Therefore, *N*-alkylated and diarylated 1,2,3-triazol-5-ylidene iridium complexes will be prepared and examined for activity in hydroformylation reactions. Reactions will be carried out under the same reaction conditions used for their rhodium counterparts with the addition of a hydrogenation suppressant (a salt) and without. It is hypothesised that the addition of the salt will promote hydroformylation, resulting in conversions comparable to those obtained for their rhodium counterparts, mentioned above.

The pioneering work of Barluenga to study the effect of two ligand systems with opposite electronic properties on the same central rhodium metal is still underexplored.[18] The electron withdrawing Fischer carbene and the electron donating 1,2,3-triazol-5-ylidene will be appended to the same metal centre, to evaluate the activity of this hybrid complex in hydroformylation reactions. This complex is expected to maintain the excellent chemoselectivity obtained from rhodium (I) Fischer carbene complexes, as well as the competitive regioselectivity the rhodium(I) 1,2,3-triazol-5-ylidene complexes have exhibited in the past, without any compromises in TOFs. This is hypothesised to be a super catalyst addressing all of the aforementioned drawbacks of the Fischer carbene and the 1,2,3-triazol-5-ylidene ligands in hydroformylation reactions.

1.3.3. Specific objectives

The first objective, covered in Chapter 2 of this thesis, is to prepare *NN*-dimethylaniline rhodium(I) amino Fischer carbene complexes by transmetalation from the corresponding tungsten ethoxy Fischer carbene complex. This reaction results in the rhodium(I) ethoxy Fischer carbene complex (Complex **1**) which will be aminolyzed to alter the electronic and steric properties of this complex, resulting in complex **2**. Furthermore, complex **2** will undergo a ligand substitution reaction to alter the electronics around the coordination sphere to afford complex **3**. Differences and similarities between the previously reported ferrocenyl-substituted rhodium Fischer carbene complexes will be evaluated and scrutinized, paying attention to the resultant spectroscopic and structural data. Complex 4 wil not be prepared, however its spectroscopic and structural data will be included for comparative studies. This transmetalation method was adopted from Barluenga et al, and modified by us.

Chapter 3 will focus on the preparation of N-alkylated 1,2,3-triazol-5-ylidene rhodium (I) and iridium (I) complexes. The ligand will be synthesised using click chemistry, followed by alkylation of the N3 position to increase the acidity of the proton on the C5 position of the triazol. Three different metalation techniques will be employed to coordinate this ligand. The first is the *in situ* deprotonation of the salt by a non-nucleophilic base in the presence of rhodium. The second is CH activation by direct metalation to silver, and the last is by transmetalation from silver to iridium. Both the rhodium and the iridium complexes will undergo ligand substitution to alter the electronic properties about the coordination sphere of the central metal. Once more the spectroscopic and the structural data will be discussed and compared to previously reported N-alkylated ferrocenyl substituted 1,2,3-triazol-5-ylidene complexes of rhodium.

Diarylated rhodium(I) 1,2,3-triazol-5-ylidene complexes will be explored in Chapter 4, starting with the preparation of the precursor salt, which follows a modified version of the click reaction previously employed by Bertrand *et al* and by our group. The purpose of this type of ligand was to introduce more steric bulk to the 1,2,3-triazol-5-ylidene ligand, to study the effect this will have on hydroformylation reactions compared to the N-alkylated ligand. Once isolated this ligand will be coordinated to rhodium, silver, iridium and chromium where the silver 1,2,3-triazol-5-ylidene complex will act as an intermediate for the transmetalation to iridium. The chromium 1,2,3-triazolylidene will be isolated as a precursor for the ensuing hybrid biscarbene complex to be prepared in Chapter 5. The obtained spectroscopic and structural data will be evaluated, focusing on the steric and electronic properties of these complexes, for their ultimate application as catalyst precursors.

In Chapter 5, utilization of either bidentate biscarbene ligands are explored in the preparation of either mononuclear or dinuclear biscarbene complexes. A bitriazol-5-ylidene ligand will be coordinated to a rhodium (I) metal centre in one of two ways, by bridging and by chelation. As in the previous chapters, emphasis will be placed on the electronic and steric properties of these two coordination modes leading to their comparisons with monodentate complexes as well as with previously reported ibitz complexes. Additionally, attempts at isolating the hybrid biscarbene complex where a 1,2,3-triazol-5-ylidene and a Fischer carbene ligand will be coordinated to the same rhodium(I) metal centre will be reported here.

Chapter 6 reports the application of the complexes prepared in Chapters 2-5 in the hydroformylation of 1-octene, to afford linear aldehydes. Taking into account the varied steric and electronic properties of complexes **1-14** as catalyst precursors, their performance will be monitored and reported in tabular form, focusing on the TOFs and the % conversion of the substrate along with the % aldehydes from the converted products. Of the produced aldehydes, the percentage of linear aldehydes compared to the branched will also be recorded. From this data, conclusions will be made regarding the effect of the central metal, the electronics of the coordinated ligands as well as the steric bulk of the ligand on the outcome of the hydroformylation reactions.

1.4. References

[1] (a) P. de Frémont, N. Marion and S. P. Nolan, *Coord. Chem. Rev.*, 2009, **253**, 862–892. (b) Wolfgang A. Herrmann, *Angew. Chem. Int. Ed.* 2002, **41**, 1290 ± 1309 (c) I. Fernández, F. P. Cossío and M. A. Sierra., *Acc. Chem. Res.*, 2011, **44**, 479–490. (d) W. Liu and R. Gust,. *Chem. Soc. Rev*., 2013, **42**, 755–773. (e) D. Munz, *Organometallics*, 2018, **37**, 275–289. (f) Caterina Damiano, Paolo Sonzini and Emma Gallo. *Chem. Soc. Rev.*, 2020,**49**, 4867-4905. (g) E. Rufino-Felipe, H. Valdés, J.M. Germán-Acacio, V. Reyes-Márquez, D. Morales-Morales, *J. Organomet. Chem.,* 2020, doi: https://doi.org/10.1016/j.jorganchem.2020.121364. (h) S. Ibáñez, M. Poyatos and E. Peris, *Acc. Chem. Res.*, 2020, **53**, 1401–1413. (i) Victor M. Chernyshev, Ekaterina A. Denisova, Dmitry B. Eremin and Valentine P. Ananikov*., Chem. Sci*., 2020,**11**, 6957-6977. (j) Q. Liang and D. Song, *Chem. Soc. Rev.*, 2020, **49**, 1209–1232. (k) 1 X. Zhao, M. Rudolph, A. M. Asiri and A. S. K. Hashmi, *Front. Chem. Sci. Eng.*, 2020, **14**, 317–349. (l) S. Kaufhold, L. Petermann, R. Staehle and S. Rau, *Coord. Chem. Rev.*, 2015, **304**–**305**, 73–87. (m) C. Copéret, A. Fedorov and P. A. Zhizhko, *Catal. Letters*, 2017, **147**, 2247–2259. (n) Sebastian J. Hock, Lars-Arne Schaper, Wolfgang A. Herrmann and Fritz E. Kuhn. *Chem. Soc. Rev*., 2013, **42**, 5073-5089. (o) Dao Zhang and Guofu Zi. *Chem. Soc. Rev*., 2015, **44,**1898-1921. (p) Srinivasa Budagumpi and Salasiah Endud. *Organometallics*, 2013, **32**, 1537−1562. (q) Heriberto Diaz Velazquez and Francis Verpoort., *Chem. Soc. Rev.,* 2012, **41**, 7032–7060. (r) Rosa Corberán, Elena Mas-Marzá, and Eduardo Peris. *Eur. J. Inorg. Chem*. 2009, 1700–1716.

[2] I. Hoskovcová and J. Ludvík, *Curr. Opin. Electrochem.*, 2019, **15**, 165–174.

[3] V. Nesterov, D. Reiter, P. Bag, P. Frisch, R. Holzner, A. Porzelt and S. Inoue, *Chem. Rev*, 2018, **118**, 9678–9842.

[4] E. O. Fischer; A. Maasbol, *Angew. Chemie - Int. Ed.*, 1964, **3**, 580–581.

[5] D. J. Cardin, B. Cetinkaya and M. F. Lappert, *Chem. Rev., 1972, **5**, 545–575.*

[6] V. Lavallo, J. Mafhouz, Y. Canac, B. Donnadieu, W. W. Schoeller and G. Bertrand, *J. Am. Chem. Soc.*, 2004, **126**, 8670–8671.

[7] E. O Fischer, *Rec. Pure Appl. Chem.,* 1970, **24,** 407–422

[8] S. Lotz, M. van den Berg and J. L. Dillen, *Trans. Met. Chem.*, 1988, **13**, 170-175

[9] M. A. Sierra, M. J. Mancheño, E. Saez, J. C. Amo, *J. Am. Chem. Soc.* 1998, **120**, 6812-6813.

[10] M. Brookhart And W. B. Studabaker, *Chem. Rev.,* 1987, ***87,*** 411-432 .

[11] M. A. Sierra, J. C. del Amo, M. J. Mancheno and M. Gomez-Gallego, *J. Am. Chem. Soc.*, 2001, **123**, 851-861.

[12] E. Fischer and H. J. Beck, *Angew. Chem. Int. Ed. Engl.*, 1970, **9**, 72-73.

[13] T. Ashworth and J. Howard, *Dalton Trans.*, 1980, **1593**, 0276-7333.

[14] A. Nagy, A. V. Schally, P. Armatis, K. Szepeshazi, G. Halmos, M. Kovacs, M. Zarandi, K. Groot, M. Miyazaki and A. Jungwirth, *Proc. Natl. Acad. Sci.*, 1996, **93**, 7269-7273.

[15] L. A. L. p. Jose Â Barluenga, Oliver Löber,, S. G.-G. Miguel TomaÂ s and a. J. B. Carmen Alvarez-RuÂ a, *Angew. Chem. Int. Ed*, 2001, **40**, 3392-3394.

[16] J. Barluenga, P. Barrio, L. A. Lopez, M. Tomas, S. Garcia-Granda and C. Alvarez-Rua, *Angew. Chem. Int. Ed. Engl.*, 2003, **42**, 3008-3011.

[17] (a) J. Barluenga, R. Vicente, L. A. López, E. Rubio, M. Tomás and C. Álvarez-Rúa, *J. Am. Chem. Soc.*, 2004, **126**, 470–471. (b) I. Göttker-Schnetmann, R. Aumann and K. Bergander, *Organometallics*, 2001, **20**, 3574–3581. (c) R. Aumann, I. Göttker-Schnetmann, R. Fröhlich and O. Meyer, *Eur. J. Org. Chem.,* 1999, **2**, 2545–2561.

[18] J. Barluenga, R. Vicente, L. A. López and M. Tomás, *J. Organomet. Chem.*, 2006, **691**, 5642–5647.

[19] D. Bourissou, O. Guerret, F. P. Gabbaï and G. Bertrand, *Chem. Rev.*, 2000, **100**, 39–91.

[20] G. Kleinhans, MSc Chemistry Dissertation, University of Pretoria, 2014.

[21] Wanzlick, H. W.; Scho¨nherr, H. J. *Liebigs Ann. Chem.* 1970, ***731***, 176–178.

[22] (a) H. W. Wanzlick, H. J. Schönherr, *Angew. Chem. Int. Ed. Engl.*, 1968, **7**, 141 – 142. (b) K. Öfele, *J. Organomet. Chem.*, 1968, **12**, 42 – 43.

[23] A. J. Arduengo, M. Kline, J. C. Calabrese, F. Davidson and N. M. R. Hi, *J. Am. Chem. Soc.*, 1991, **113**, 361–363.

[24] (a) Vernin, G.; Siv, C.; Metzger, *J. Synthesis* 1977, 691–693.(b) Nimitsiriwat, N.; Gibson, V. C.; Marshall, E. L.; Takolpockdee, P.; Tomov, A. K.; White, A. J. P.; Williams, D. J.; Elsegood, M. R. J.; Dale, S. H. *Inorg. Chem*. 2007, **46**, 9988–9997. (c) Barrett, A. G.; Crimmin, M. R.; Hill, M. S.; Hitchcock, P. B.; Kociok-K€ohn, G.; Procopiou, P. A. *Inorg. Chem*. 2008, 47, 7366–7376. (d) Hartman, W. W.; Dickey, J. B. *Org. Synth*. 1934, **14**, 163. (e) Hauber, S.-O.; Lissner, F.;Deacon,G. B.;Niemeyer,M. *Angew. Chem., Int. Ed*. 2005, **44**, 5871–5875. (f) Alexander, S. G.; Cole, M. L.; Forsyth, C. M.; Furfari, S.; Konstas, K. *Dalton Trans*. 2009, 2326–2336

[25] D. R. Tolentino, L. Jin, M. Melaimi and G. Bertrand, *Chem.: Asian J.*, 2015, **10**, 2139–2142.

[26] A. J. Arduengo, D. E. I Du and J. Liebigs Ann, *United States Patent (19) Arduengo, III (54) Preparation Of 1,3-Disubstituted Midazolum Salts*, 1986, vol. 64.

[27] W. Herrmann, M. Elison, J. Fischer, C. Kocher and G. R. Artus, *Angew. Chem. Int. Ed*, 1995, **34**, 2371–2375.
[28] A. R. Chianese, A. Kovacevic, B. M. Zeglis, J. W. Faller and R. H. Crabtree, *Organometallics,* 2004**, *23,*** 2461-2468.
[29] S. Grüdemann, A. Kovacevic, M. Albrecht, J. W. Faller and R. H. Crabtree, *Chem. Commun.*, 2001, 2274–2275.
[30] S. Gründemann, A. Kovacevic, M. Albrecht, J. W. Faller and R. H. Crabtree, *J. Am. Chem. Soc.*, 2002, **124**, 10473–10481.
[31] L. N. Appelhans, D. Zuccaccia, A. Kovacevic, A. R. Chianese, J. R. Miecznikowski, A. Macchioni, E. Clot, O. Eisenstein and R. H. Crabtree, *J. Am. Chem. Soc.*, 2005, **127**, 16299–16311.
[32] S. Sole, H. Gornitzka, W. W. Schoeller and G. Bertrand, 2001, **292**, 1901–1903.
[33] R. Tonner, G. Heydenrych and G. Frenking, *Chem.: Asian J.*, 2007, **2**, 1555–1567.
[34] P. Mathew, A. Neels and M. Albrecht, *J. Am. Chem. Soc.*, 2008, **130**, 13534–13535.
[35] A. R. Chianese, A. Kovacevic, B. M. Zeglis, J. W. Faller and R. H. Crabtree, 2004, 2461–2468.
[36] P. L. Arnold and S. Pearson, *Coord. Chem. Rev.*, 2007, **251**, 596–609.
[37] Aldeco-Perez, A. J. Rosenthal, B. Donnadieu, P. Parameswaran, G. Frenking and G. Bertrand, *Science*, 2009, **326**, 556–559.
[38] K. Barral, A. D. Moorhouse and J. E. Moses, *Org. Lett.*, 2007, **9**, 1809–1811.
[39] D. R. Tolentino, L. Jin, M. Melaimi and G. Bertrand, *Chem.: Asian J.*, 2015, **10**, 2139–2142.
[40] V. V Rostovtsev, L. G. Green, V. V Fokin, K. Barry Sharpless, H. K. A C Coolen, P. W. N M van Leeuwen and R. J. M Nolte, *J. Am. Chem. Soc.*, 2002, **1**, 210–216.
[41] J. D. Crowley, A. L. Lee and K. J. Kilpin, *Aust. J. of Chem*., 2011, 64, 1118–1132.
[42] (a) A. R. Chianese, X. Li, M. C. Janzen, J. W. Faller, R. H. Crabtree and W. A. *J. Organomet*., 2003, 1663–1667. (b) R. A. K. Iii, H. Clavier, S. Giudice, N. M. Scott, E. D. Stevens, J. Bordner, I. Samardjiev, C. D. Hoff, L. Cavallo and S. P. Nolan, *Organometallics*., 2008, 202–210.
[43] G. Guisado-barrios, J. Bouffard, B. Donnadieu and G. Bertrand, *Angew. Chem. Int. Ed*. 2010, **49**, 4759 –4762.
[44] J. Bouffard, B. K. Keitz, R. Tonner, G. Guisado-Barrios, G. Frenking, R. H. Grubbs and G. Bertrand, *Organometallics*, 2011, **30**, 2617–2627.
[45] W. Wirschun, M. Winkler, K. Lutz and J. C. Jochims, *J. Chem. Soc., Perkin Trans. **1***,1998, 1755-1762.
[46] (a)W. A. Herrmann, C.-P. Reisinger and M. Spiegler, *Chelating N-heterocyclic carbene ligands in palladium-catalyzed heck-type reactions 1*, 1998, vol. 557. (b) W. A. Herrmann, J. Rgen Schwarz, M. G. Gardiner and M. Spiegler, *Homoleptic chelating N-heterocyclic carbene complexes of palladium and nickel*, 1999, vol. 575. (c) M. Muehlhofer, T. Strassner and W. A. Herrmann, *New Catalyst Systems for the Catalytic Conversion of Methane into Methanol***, 2002, vol. 41.
[47] S. Burling, L. D. Field, H. L. Li, B. A. Messerle and P. Turner, *Eur. J.Inorg. Chem.*, 2003, 3179–3184.
[48] M. Poyatos, J. A. Mata and E. Peris, *Chem. Rev.*, 2009.
[49] A. Mata, A. R. Chianese, J. R. Miecznikowski, M. Poyatos, E. Peris, J. W. Faller and R. H. Crabtree, 2004, 1253–1263.
[50] Y. A. Wanniarachchi, M. A. Khan and L. G. M. Slaughter, *Organometallics*, 2004, **23**, 5881–5884.
[51] C. H. Leung, C. D. Incarvito and R. H. Crabtree, *Organometallics.* 2006. **25**. 6099–6107.
[52] G. Guisado-Barrios, M. Soleilhavoup and G. Bertrand, *Accounts of Chemical Research*, 2018, **51**, 3236–3244.
[53] M. Poyatos, W. McNamara, C. Incarvito, E. Peris and R. H. Crabtree, *Chem. Commun.*, 2007, 2267–2269.
[54] G. Guisado-Barrios, J. Bouffard, B. Donnadieu and G. Bertrand, *Organometallics*, 2011, **30**, 6017–6021.
[55] S. N. Sluijter and C. J. Elsevier, *Organometallics*, 2014, **33**, 6389–6397.
[56] D. Mendoza-Espinosa, A. Alvarez-Hernández, D. Angeles-Beltrán, G. E. Negrón-Silva, O. R. Suárez-Castillo and J. M. Vásquez-Pérez, *Inorg. Chem.*, 2017, **56**, 2092–2099.
[57] R. Franke, D. Selent and A. Börner, *Chem. Rev.*, 2012, **112**, 5675–5732.
[58] I. Piras, R. Jennerjahn, R. Jackstell, A. Spannenberg, R. Franke and M. Beller, *Angew. Chem. Int. Ed.*, 2011, **50**, 280–284.
[59] A. Volker Grenacher, F. Sauer, H. Schwahn, W. Schönmann and M. Röper, *(12) United States Patent (30) Foreign Application Priority Data*, 2001.
[60] C. F. Huo, Y. W. Li, M. Beller and H. Jiao, *Organometallics*, 2003, **22**, 4665–4677.
[61] Heck, R. F., Breslow, D. S., *J. Am. Chem. Soc.* 1961, **83**, 4023.
[62] A. Volker Grenacher, F. Sauer, H. Schwahn, W. Schönmann and M. Röper, *(12) United States Patent (30) Foreign Application Priority Data*, 2001.
[63] L. H. Slaugh and R. D. Mui, *United States Patent Office HYDROFORMYLATION OF OLEFENS*, 1966.
[64] L. H. Slaugh and R. D. Mullineaux, *J. Organomet. Chem.,* 1968, **13**, 469-477.
[65] B. D. Evans, J. A. Osborn and G. Wilkinson, *J. Am. Chem. Soc.*, 1968, **62**, 3133-3142.

[66] B. J. A Osborn, G. Wilkinson, J. F. Young, R. D. Gillard, J. A. Osborn, P. B. Stockwell and P. Chem, *Chem. Commun.*, 1964, **62**, 17-17.
[67] G. D. Frey, *J. Organomet. Chem.*, 2014, **754,** 5–7.
[68] D. Evans, G. Yagupsky and G. Wilkinson, *J. Am. Chem. Soc.*, 1968, **62**, 2660-2665
[69] L. A. Van Der Veen, P. C. J. Kamer and P. W. N. M. Van Leeuwen, *Organometallics*, 1999, **18**, 4765–4777.
[70] P. W. N. M. Van Leeuwen and C. F. Roobeek, *Hydroformylation of less reactive olefins with modified rhodium catalysts*, Elsevier Sequoia S.A, 1983, vol. 258.
[71] A. M. Trzeciak, T. Głowiak, R. Grzybek and J. J. Ziółkowski, *J. Chem. Soc*., *Dalton Trans*., 1997, 1831–1837 .
[72]W. Gil and A. M. Trzeciak, *Coord. Chem. Rev.*, 2011, **255**, 473–483.
[73] L. A. Van Der Veen, *New ligands for selective hydroformylation Unraveling the bite angle effect*, 1999.
[74] C. A. Tolman, *Chem. Rev.* 1977, **77**, 313-348.
[75] M. Bortenschlager, M. Mayr, O. Nuyken and M. R. Buchmeiser, *J. Mol. Catal. A-Chem.*, 2005, **233**, 67–71.
[76] D. Aucamp, MSc Chemistry, University of Pretoria, 2016.
[77] W. A. Herrmann and C. Kocher. *Angen. Chem. Int. Ed. Engi.* 1997,**36**, 2162-2187.
[78] M. A. Moreno, M. Haukka and T. A. Pakkanen, *J. Catal.*, 2003, **215**, 326–331
[79] I. Piras, R. Jennerjahn, R. Jackstell, A. Spannenberg, R. Franke and M. Beller, *Angew. Chem. Int. Ed.*, 2011, **50**, 280–284
[80] G. K. Ramollo, M. J. López-Gómez, D. C. Liles, L. C. Matsinha, G. S. Smith and D. I. Bezuidenhout, *Organometallics*, 2015, **34**, 5745-5753.
[81] D. Aucamp, T. Witteler, F. Dielmann, S. Siangwata, D. C. Liles, G. S. Smith and D. I. Bezuidenhout, *Eur. J. Inorg. Chem.*, 2017, **2017**, 1227–1236.
[82] (a) A. Kämper, S. J. Warrelmann, K. Reiswich, R. Kuhlmann, R. Franke and A. Behr, *Chem. Eng. Sci.*, 2016, **144**, 346-371. (b) Behr A, Kämper A, Nickel M, Franke R. *Appl. Catal. A-Gen*., 2015, **505**, 243-248.

Chapter 2: The syntheses and characterisation of NN-dimethylaniline substituted Rh(I) Fischer carbene complexes

2.1. Background

In 1964, E.O. Fisher and co-workers successfully isolated the first group 6 transition metal Fischer carbene complex.[1] Thereafter, they went on to transfer the carbene ligand from molybdenum(0) to a UV-activated iron(0) pentacarbonyl for the first time in 1970.[2] In addition, they isolated the nickel(0) Fischer carbene complex using the same approach, however without requiring the photoactivating carbonyl labilisation of the nickel tetracarbonyl precursor. These then-novel, diamagnetic complexes were found to be readily volatile and thus highly unstable upon exposure to air. Fischer also highlighted how the late group Fischer carbene complexes could not be prepared by the nucleophilic attack of an organolithium on a carbonyl ligand coordinated to the metal, as these late group transition metals are less π-basic than their group 6 counterparts.[2]

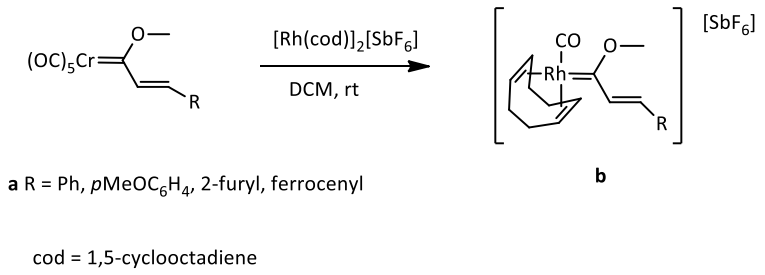

Scheme 2. 1: Synthesis of cationic rhodium(I) Fischer carbene complexes via the transmetalation approach.[3]

Although the transfer of Fischer carbene ligands to late transitions group metals became of high interest, still not many rhodium(I) Fischer carbene complexes had been isolated. This is in stark contrast to the regular reports of prepared rhodium(I) NHC complexes. Barluenga addressed this dearth in the field, by transmetalating a Fischer carbene ligand to a rhodium dimer (Scheme 2.1),[3] and later to a rhodium(I) NHC complex (Scheme 2.2).[4] The transmetalation of one carbene ligand to an existing carbene complex, was not unheard of, in fact the isolation of the tungsten Fischer carbene-NHC complex was reported in 2005,[5] however the transfer of the Fischer carbene to a rhodium(I) had not been adequately explored.

Fischer carbene complexes **c** (where X = OMe) were prepared and reacted with the rhodium(I) NHC in Scheme 2.2.[4] In this case, both the Fischer carbene and a carbonyl group were transferred simultaneously from the chromium to the rhodium NHC complex, resulting in the isolation of complexes **d** (where X = OMe). This report also recorded the formation of complexes **e** (where X = NMe_2) from the aminocarbene complexes **c** (where X = NMe_2) , although extended reaction times were required to obtain yields similar to those obtained for **d** (where X = OMe).[4] Upon heating to 60°C in toluene, complex **c** yielded two dimerised products; the corresponding methoxy carbene dimer (*E/Z* isomers 1:1) as well as the rhodium NHC dimer which had not been previously reported. The catalytic activity towards cyclisation reactions of alkenes and allenes of the complexes **b** was examined and it

was found that they have limited activity. However, chlorido ligand abstraction resulted in improved activity.[4]

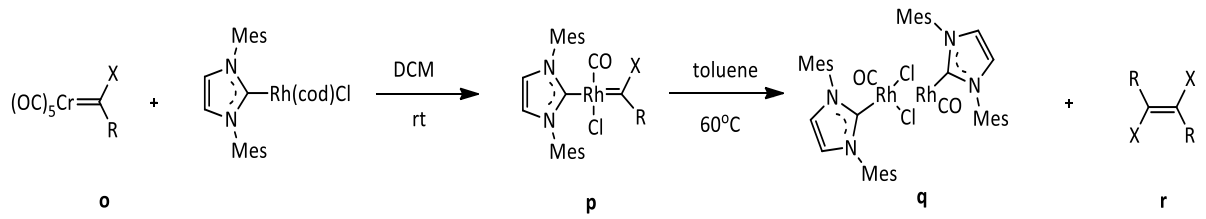

X = OMe, R = (*E*)-CH=CH-C_6H_5, (*E*)-CH=CH-*p*-MeO-C_6H_4, (*E*)-CH=CH-2-furyl, (*E*)-CH=CH-ferrocenyl, C_6H_5, *p*-MeO-C_6H_4

X = NMe, R = (*E*)-CH=CH-C_6H_5, (*E*)-CH=CH-*p*-MeO-C_6H_4

cod = 1,5-cyclooctadiene

Scheme 2. 2: The transmetalation reaction is performed by Barluenga et al.[4]

Rhodium(I) NHC complexes have gained popularity as catalysts for the hydroformylation reactions over the years, with conversions higher than 90% reported regularly.[3] With access to this transmetalation pathway reported by Barluenga and co-workers, work in our laboratory focused on the transmetalation of Fischer carbene ligands to rhodium(I) for the use as catalyst precursors in hydroformylation reactions.[6] In the first report from our group, it was found that group 6 Fischer carbene complexes containing 2-furyl- or 2-thienyl-carbene substituents, yielded self-dimerization products from the reaction between the corresponding chromium(0) Fischer carbene complexes and rhodium dimer. This challenge was overcome by preparing a chromium(0) Fischer carbene complex with a more donating ferrocenyl substituent and performing ligand exchange reactions to study the catalytic activity of this complex. Not only was this catalyst stable under hydroformylation conditions, it demonstrated catalytic performance comparable to that reported for Rh NHC complexes, with conversions of above 90% and competitive selectivity towards linear aldehydes. Surprisingly, the donating ability of the ferrocenyl carbene ligand[7] was found to be comparable to that of commonly used imidazolylidene-based NHCs. This observation, was coupled with the added advantage of an additional transition metal to the system for potential heterobimetallic synergistic effects.[6]

The above study concluded that the more electrophilic carbene ligands that did not contain a ferrocenyl carbene substituent, but rather a heteroaryl (2-furyl or 2-thienyl), precludes carbene transfer reactions and therefore prohibits the isolation of Fischer carbene complexes of late transition metals via transmetalation due to self-dimerisation.[4] This prompted the investigation for more stabilizing aryl carbene substituents that did not include a secondary transition metal as an organometallic carbene ligand substituent, for application of new rhodium(I) Fischer carbene complexes in hydroformylation reactions without any assistance from an additional metal. N,N-dimethylaniline (*p*-DMA) was reported to be highly electron donating as a result of the dipole moments directed towards the ring, thus stabilizing the Fischer carbene through π-conjugation, and making this aryl group an attractive choice for the preparation of the intended rhodium(I) Fischer carbene complexes.[8]

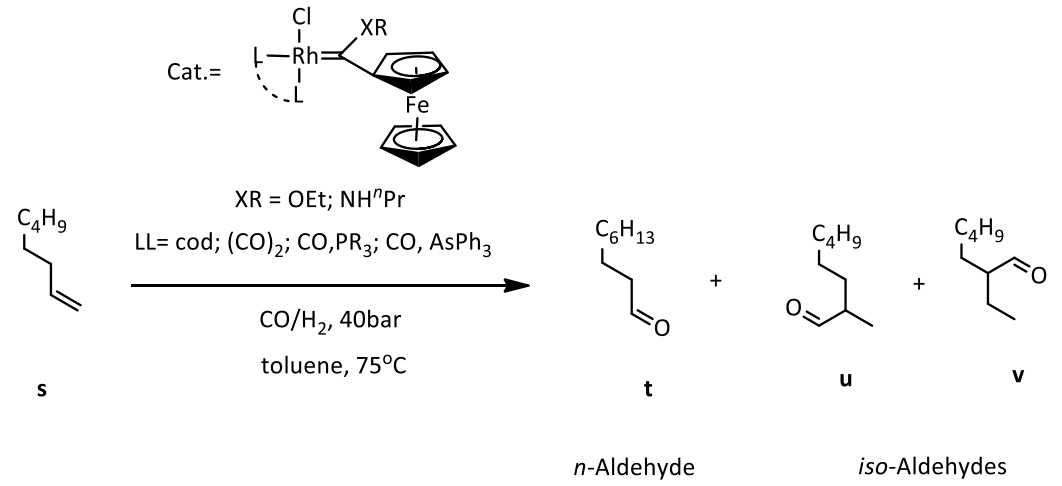

cod = 1,5-cyclooctadiene

Scheme 2. 3: Hydroformylation reaction performed using the rhodium(I) catalyst precursors prepared by Ramollo et al.[6]

2.2. Aim and objectives

2.2.1. Aim

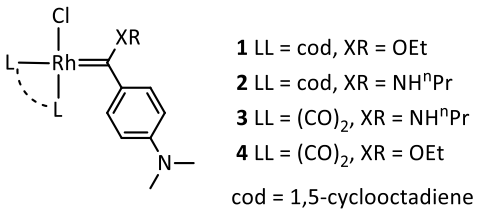

*Figure 2. 1: Targeted rhodium (I) Fischer carbene complexes **1-4***

This chapter aims to address the scarcity of rhodium (I) Fischer carbene complexes particularly in their application as catalyst precursors for hydroformylation reactions. It has been previously reported that these complexes are highly active,[6] however it is unclear whether their activity can be attributed to the presence of a secondary transition metal. To investigate this, monometallic rhodium (I) Fischer carbene complexes will be prepared taking into account the donor properties of the metal-free carbene ligand. This *p*-DMA substituted Fischer carbene ligand is expected to be far less donating than its ferrocenyl counterpart, which should in turn increase the activity of the precatalyst.

2.2.2. Objectives

Herein, complexes **1-4** (Figure 2.1) will be prepared commencing with a modified route based on the methodology reported by Barluenga, involving the transfer of the Fischer carbene ligand from a group 6 transition metal to a group 9 transition metal precursor complex, specifically the 1,5-cyclooctadienyl chloride rhodium(I) dimer.[3,4] This transmetalation approach has been seen to be successful in a case

where the carbene ligand was stabilized by a strongly electron donating aryl substituent such as the ferrocenyl as reported by Ramollo and co-workers.[6] Taking advantage of the same property in N,N-dimethylaniline,[8] $W(CO)_5${C(OEt)*p*-DMA} will be prepared as a precursor for the transmetalation reaction to afford **1**.[9] In an effort to reduce the electrophillicity, **1** will undergo an aminolysis reaction where the ethoxycarbene substituent will be replaced with the less electronegative aminocarbene to afford **2**.[10] Both **1** and **2** will undergo ligand substitution reactions where the bidentate 1,5-cyclooctadiene (cod) ligand will be replaced with two monodentate, π-accepting carbonyl ligands (Figure 2.5). The ethoxycarbene complexes **1** and **4** have been previously prepared in our group[9] and will be prepared and reported in this thesis as precursors for the amino-analogues as well for the comparison of their spectroscopic properties to the novel complexes.

2.3. Results and discussion

The preparation and spectroscopic characterisation of rhodium(I) Fischer carbene complexes **1-4** will be discussed. Comparisons will be made highlighting the implications of the change in the auxiliary co-ligands in the coordination sphere, and the effect of the variation of the carbene heteroatom substituents on the σ- and π-bonding characteristics of the carbene ligand. The spectroscopic characterisation of the complexes will be augmented by a comparison of the molecular structures of complexes **2** and **3** on the structural properties of **1** and **4**.

2.3.1. Syntheses of complexes 1, 2 and 3

For the synthesis of **1**,[9] the transmetalation approach is suggested to be the most effective route to access group 9 Fischer carbene complexes from their group 6 counterparts. The preparation of the precursor **A** [$W(CO)_5${C(OEt)*p*-DMA}] has been previously reported, and follows the classical Fischer method.[11] The precursor complex was prepared and purified in accordance with literature,[11] and added to a stoichiometric amount of $[Rh(cod)Cl]_2$ (where cod = 1,5-cyclooctadiene) in a Schlenk tube, before dissolving in dried dichloromethane (DCM), Scheme 2.5. The Schlenk tube was sealed and the reaction mixture stirred at room temperature and monitored by thin layer chromatography (TLC). Reaction completion was only observed after 72 hours. Attempts to decrease reaction time by increasing the reaction temperature were not successful, resulting in the self-dimerisation of the carbene ligand. This implies the *in situ* formation of the rhodium(I) Fischer carbene complex is short-lived at higher temperatures.[4,12] Once the reaction was complete, an aluminium oxide resin was used in the purification of **1** via column chromatography, with DCM as the eluent. The bright orange solution was concentrated under reduced pressure and layered with hexanes to afford an orange crystalline solid of 62% yield.

To obtain the aminolyzed moiety, the ethoxycarbene complex, **1** was subsequently treated with $^{n}PrNH_2$ in tetrahydrofuran (THF) and allowed to stir continuously for 1 hour before removing the solvent in *vacuo* (Scheme 2.4). The residue was washed with hexanes and **2** was extracted in DCM then recrystalized by slow diffusion resulting in a good yield of 70%.

Both **1** and **2** were subjected to ligand substitution reactions, where the cod ligand was replaced with two CO ligands. This was done by means of purging the individual DCM solutions of **1** and **2** with CO (g) for 15 minutes while stirring incessantly. The reaction mixtures were left to stir for a further 1 hour in the CO (g) atmosphere, and the solvent removed to afford **3** from **2** with a yield of 90 %, and **4** from **1** with a previously reported yield of 86%.

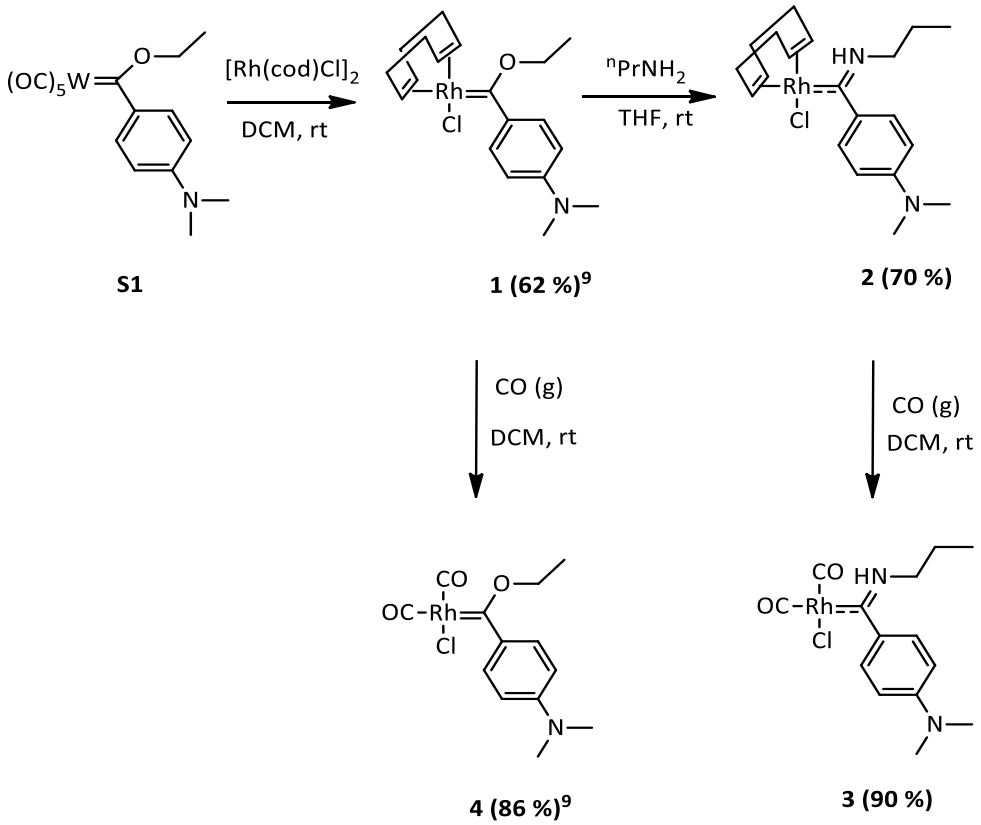

Scheme 2. 4: Synthesis of complexes **1**-**4**

2.3.2. Spectroscopic characterisation of complexes 1-3

2.3.2.1. Discussion of the ^{1}H NMR spectra of complexes 1-3

The ^{1}H NMR spectrum for **1** provides evidence of the coordination of the Fischer carbene ligand to the rhodium(I) metal, i.e. the two doublets of quartets integrating for 1 proton each at 5.94 and 5.67 ppm (for O$\underline{CH_2}$CH$_3$), instead of the expected quartet integrating for two protons, as observed for [W(CO)$_5${C(OEt)*p*-DMA}][11]. This splitting pattern is presumably due to the asymmetry of the square planar rhodium coordination sphere with the 1,5-cyclooctadiene (cod) ligand, compared to the octahedral pentacarbonyl tungsten carbene precursor. The same behaviour is seen for complexes **2** and **3**. The corresponding two signals in **2** are seen to overlap, resonating upfield between 5.04 – 4.86 ppm as a single multiplet; a direct consequence of the exchange from a more electronegative O atom, to the more stabilising N-atom. This stabilisation results from the greater donating ability of the N-atom lone pair into the electrophilic carbene carbon unoccupied *p*-orbital.[13] The upfield shift can be

attributed to the δ- charge on the corresponding carbon as a direct consequence of the increase in bond order between the amine N and the carbene carbon resulting in the δ+ charge on the amine N. This aminocarbene carbon is now less electrophilic than the alkoxy-substituted moiety.

Two characteristic N,N-dimethylaniline doublets are observed in the aromatic region of the ^{1}H NMR spectrum for **1** at 8.41 (*J*= 8.7 Hz) and 6.41 (*J*= 9.4 Hz) ppm; and for **2** at 7.99 (*J* = 9.0 Hz) and 6.71 (*J* = 9.0 Hz); clearly signifying an alteration in the electronic properties of the complexes. The reduced electrophilicity of the carbene carbon in **2** results in increased shielding of the DMA-$\underline{H_{\alpha,\alpha'}}$ manifesting in the upfield shift of these protons due to their proximity to the carbene carbon. A broad singlet is observed downfield at 8.19 ppm in **2** that does not appear in the 1H NMR spectrum for **1** , signifying the presence of NH proton, similar what is observed in the previously prepared ferrocenyl (Fc) analogue.[14] This proton resonance is shifted downfield to 8.53 ppm, when the cod ligand is substituted for two CO ligands as seen for **3**.

Furthermore, a poorly resolved triplet is observed for NH$\underline{CH_2}CH_2CH_3$ in the ^{1}H NMR spectrum of **2** (Figure 2.7) at 4.53 ppm, instead of the expected splitting pattern (doublets of quartets) observed for **1** at 5.90 ($^{2}J_{HH}$= 14.1, $^{3}J_{HH}$= 7.4 Hz) and 5.66 ($^{2}J_{HH}$ = 13.9, $^{3}J_{HH}$= 7.5 Hz) for the O$\underline{CH_2}CH_3$ protons. The triplet observed in **2** is speculated to be a pair of overlapping broad singlets similar to those observed for complex **3** at 4.29 and 4.10 ppm. Analogously, the conversion from **1** to **4** ensues with the merge of the aforementioned doublet of quartets signals of complex **1**, resulting in a multiplet (5.40 – 5.35 ppm). The downfield shift of the NH$\underline{CH_2}CH_2CH_3$ protons in both complexes **2** and **3** compared to complexes **1** and **4**, is a direct consequence of the less electronegative aminocarbene deshielding the protons on the adjacent carbon.

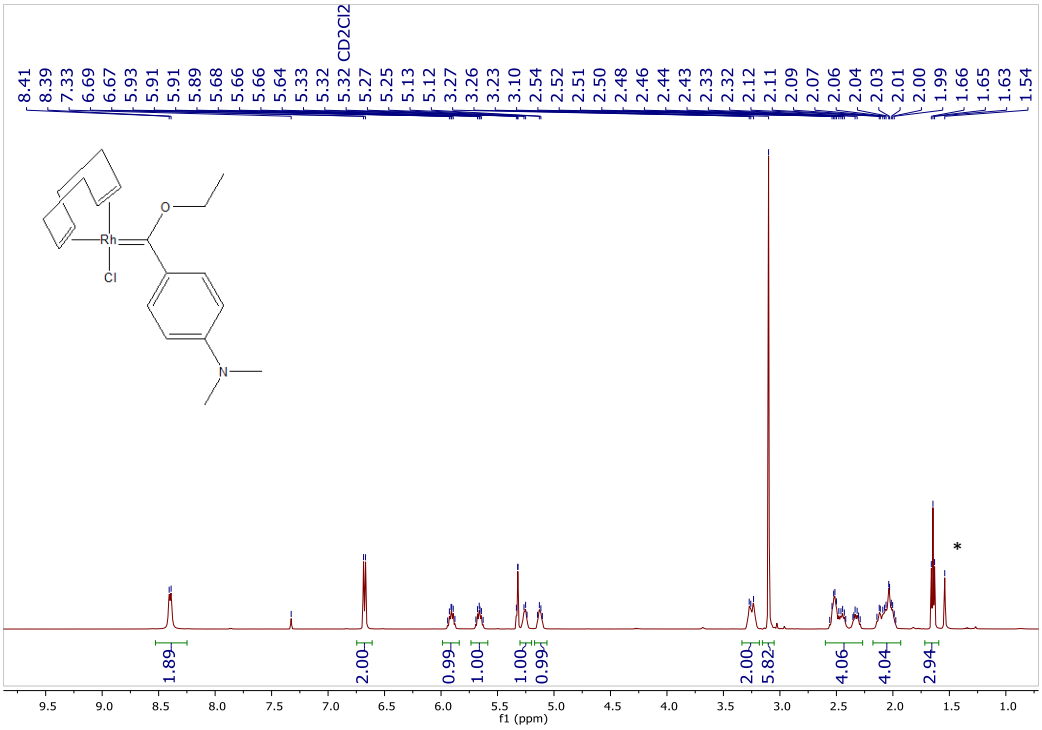

*H_2O contaminant

*Figure 2. 2: ^{1}H NMR spectrum of **1** in solvent CD_2Cl_2*

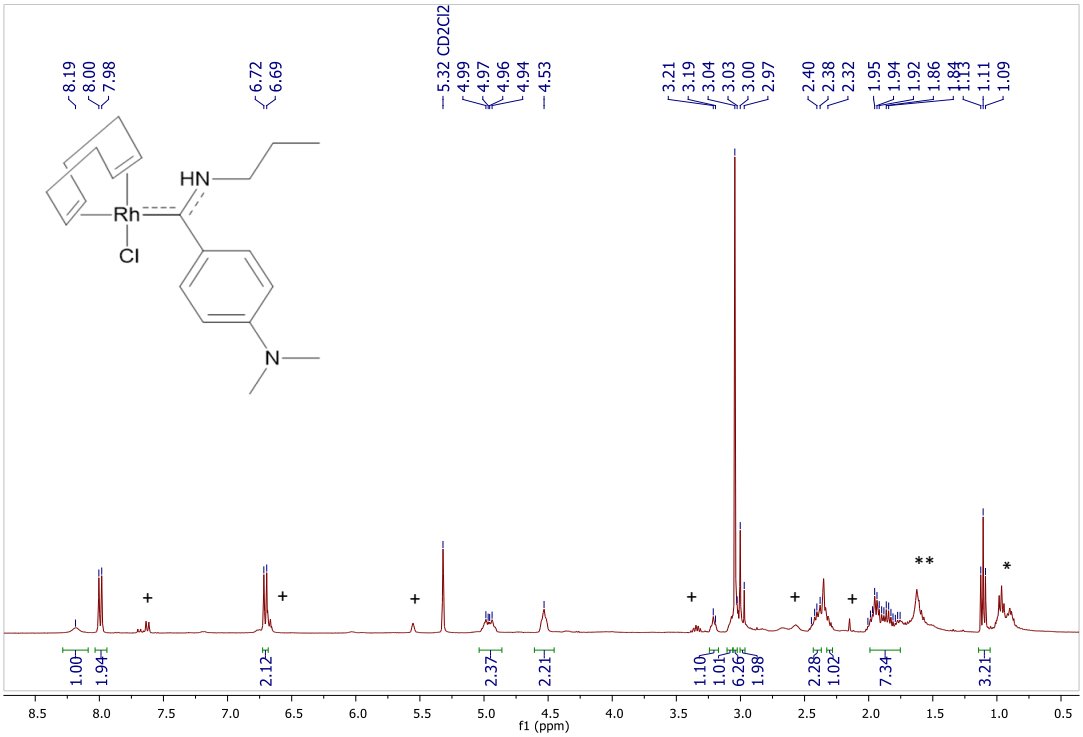

* *n*-hexane contaminant
** H_2O contaminant
\+ dimerization product contaminant

*Figure 2. 3: ^1H NMR spectrum of **2** in solvent CD_2Cl_2*

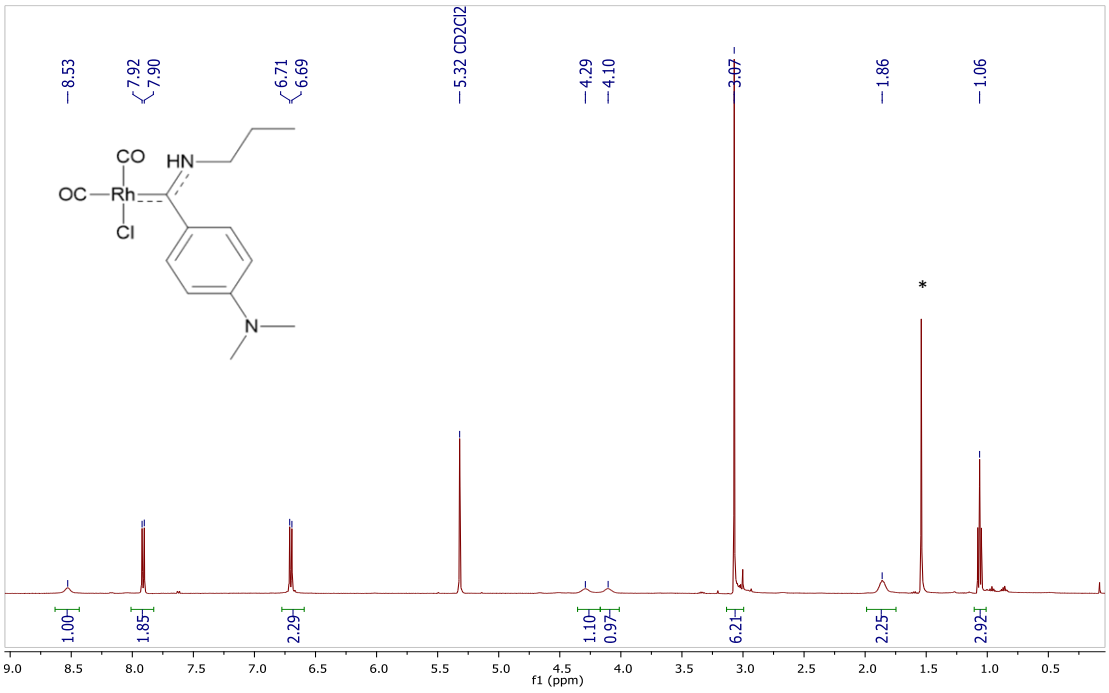

* H_2O contaminant

*Figure 2. 4: ^1H NMR spectrum of **3** in solvent CD_2Cl_2*

2.3.2.2. Discussion of the ^{13}C NMR spectra of complexes 1-3

Confirmation of this is provided by the carbene doublets in the ^{13}C NMR spectrum of **1** (297.6 ppm, *J* = 42.9 Hz) and **2** (252.2 ppm, *J* = 40.0 Hz) where the carbene carbon of **2** experiences π-electron donation from the adjacent amino group, resulting in an increase in bond order between the carbenic carbon and the amino nitrogen and therefore resonating more upfield. Congruently, the Fc analogue displayed synonymous characteristics upon undergoing aminolysis. The coupling constant of the carbene carbon in **2** (*J* = 40.0 Hz) is also smaller than what is observed for **1** (*J* = 42.9 Hz), although this difference is not pronounced, it serves as indication of an increase in electron density around the carbene carbon of complex **2**.

Carbonyls are known for their better π-accepting ability compared to the cod, affecting the electronic properties of the carbene carbon coordinated trans. Typically, this results in less π-back donation from the central metal to the carbene carbon rendering it more electrophilic and thus requiring more stabilization from its substituents through π-conjugation. Correspondingly, a considerable upfield shift of the carbene carbon atom doublet from 252.2 ppm in the ^{13}C NMR spectrum of **2** to 233.8 ppm in **3** is observed.

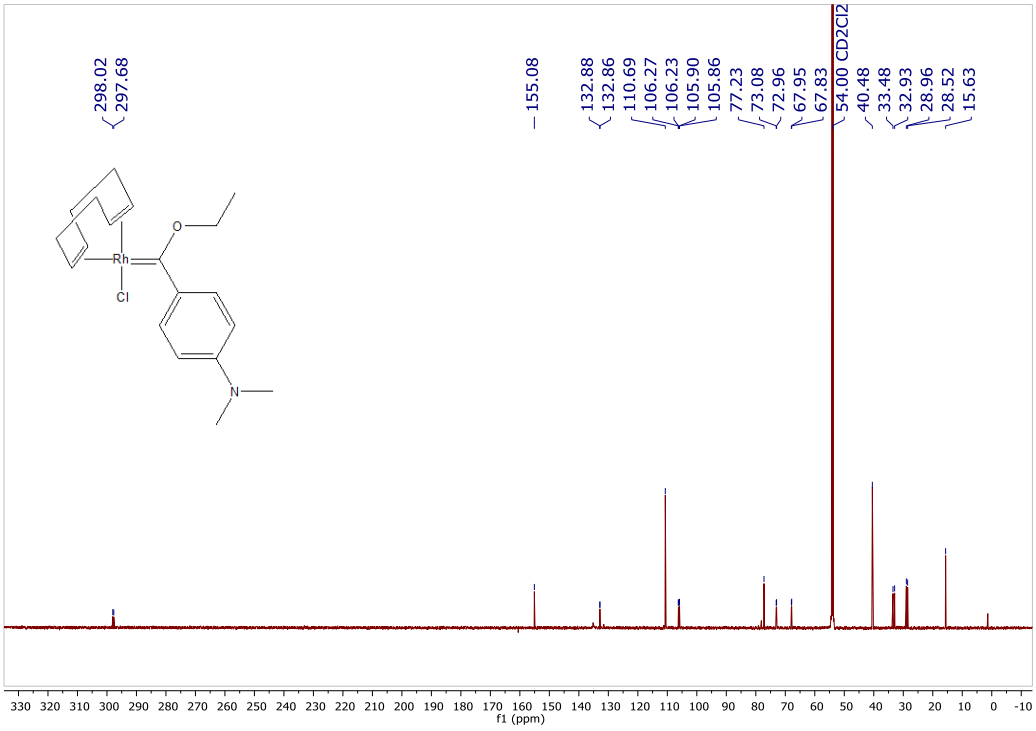

*Figure 2. 5: ^{13}C NMR spectrum of **1** in solvent CD_2Cl_2*

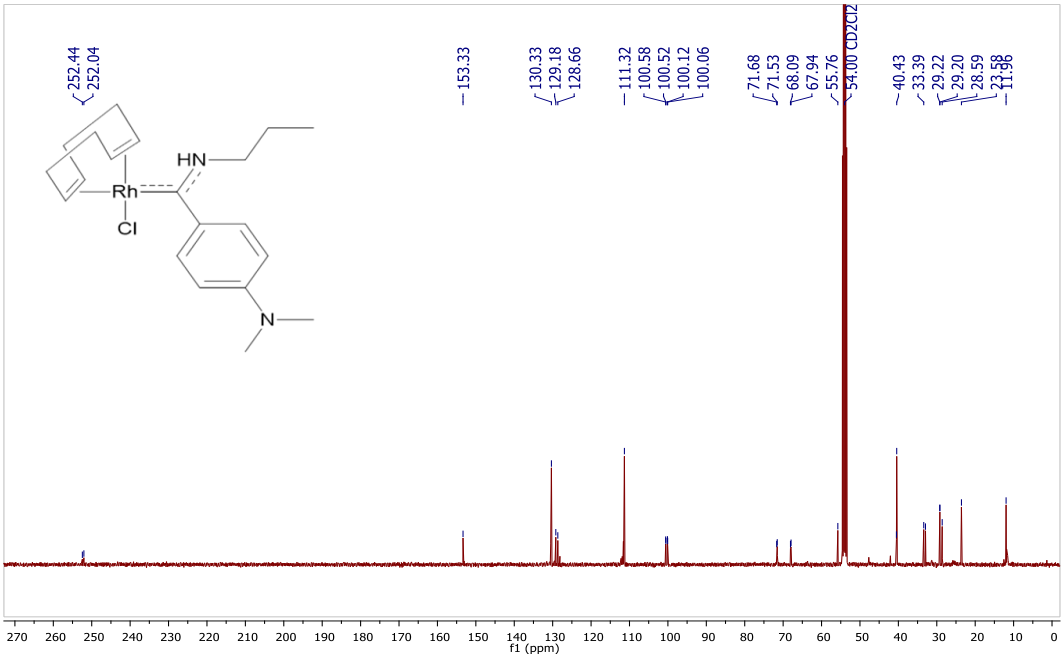

*Figure 2. 6: ^{13}C NMR spectrum of **2** in solvent CD_2Cl_2*

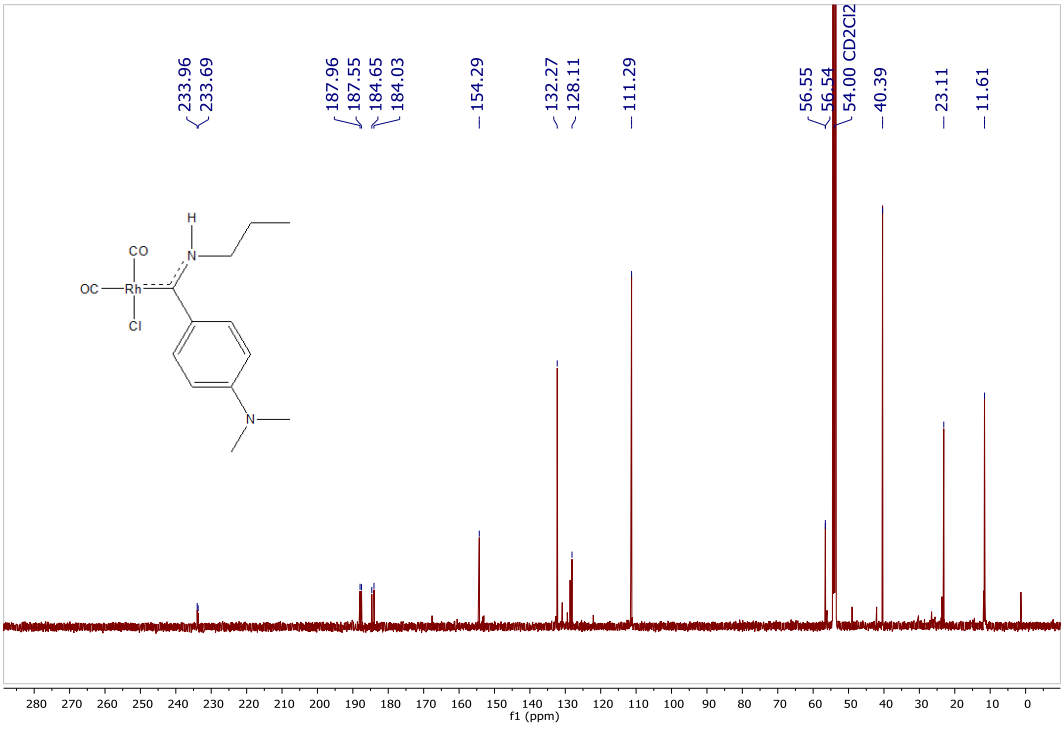

*Figure 2. 7: ^{13}C NMR spectrum of **3** in solvent CD_2Cl_2*

*Table 2.1: Spectroscopic data of complexes **1-4***

Complex	^{13}C δ($C_{carbene}$), (ppm); (^{1}J(RhC)), (Hz)	^{13}C δ(CO), (ppm); (^{1}J(RhC)), (Hz)	IR[a] ν(CO), (cm^{-1})	IR[a] ν_{av}(CO), TEP[d] (cm^{-1})
1[9]	297.9 (d, 43)	-	-	
2	252.2 (d, 40)	-	-	
3	233.8 (d, 34)	186.9 (d, 52)[b] 184.2 (d, 78)[c]	2000[c] 2055[b]	2028 2043[d]
4[9]	277.1 (d, 37)	187.7 (d, 50)[b] 183.9 (d, 78)[c]	1995[c] 2078[b]	2037 2049[d]

[a]Recorded in CH_2Cl_2. [b]CO-ligand trans to carbene. [c]CO-ligand trans to Cl. [d]Calculated using the linear regression model TEP = 0.8001ν_{av}(CO)**Rh** + 420 cm^{-1}.

2.3.2.3. Examination of the Fourier Transform Infrared spectroscopic data

The FT-IR spectra of **2, 3** and **4** were obtained, displaying the NH stretching frequency at 3303 cm^{-1} and 3288 cm^{-1} for **3** and **2** respectively, comparable to what was observed for the Fc analogue.[14] Complexes **3** and **4**, the products of the ligand substitution reactions where their respective cod ligands were replaced with CO ligands, displayed the presence of carbonyl groups with bands between 1995 and 2078 cm^{-1} on their respective IR spectra (Table 2.1). These carbonyl groups act as IR probes to facilitate the calculation of Tolman's electronic parameter (TEP) values, which help determine the donor strength of the substituents on the carbene ligand.[15] These TEP values were calculated using the simple linear regression model TEP = 0.8001ν_{av}(CO)**Rh** + 420 cm^{-1}, developed by Nolan and co-workers.[16]

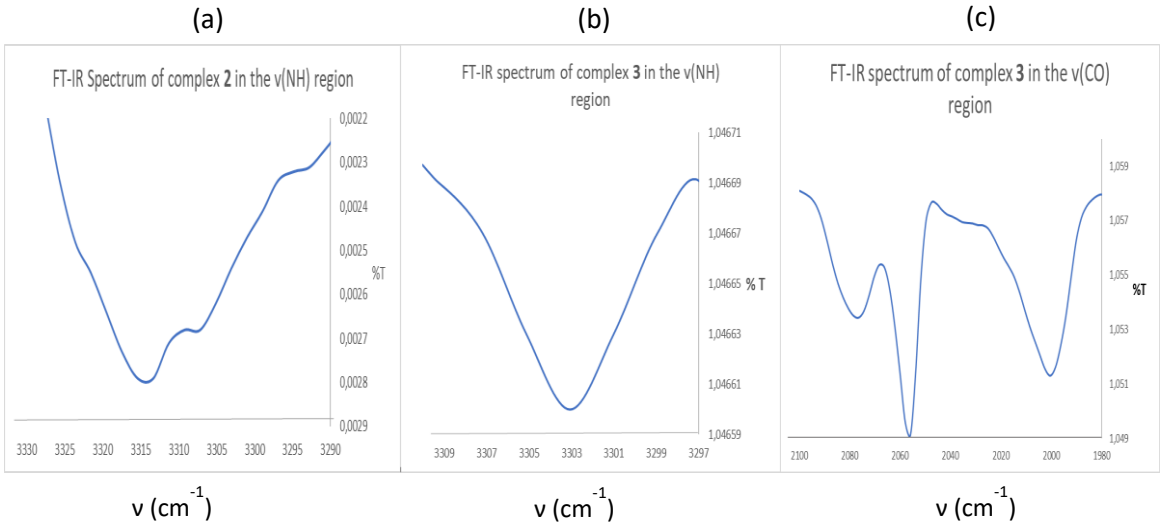

*Figure 2. 8: FT-IR spectrum of rhodium(I) amino Fischer carbene complexes **2** and **3.** (a) and (b) showing the ν(NH) band of **2** and **3** respectively, and (c) showing the ν(CO) bands of complex **3**.*

As per Table 2.1, the TEP value of the aminocarbene complex **3** (2043 cm^{-1}), is significantly smaller than that of the ethoxy carbene **4** (2049 cm^{-1}). A difference of 6 cm^{-1} is detected between these carbene complexes, identical to the observed difference between the ferrocenyl aminocarbene (2049 cm^{-1}) and the corresponding ethoxycarbene (2054 cm^{-1}) complexes.[6] Furthermore, the difference in TEP values between **3** and the corresponding ferrocenyl aminocarbene is 6 cm^{-1}, analogous to that observed between **4** and the ferrocenyl ethoxycarbene complexes. Therefore, it can be deduced that the DMA Fischer carbenes are better σ-donors/weaker π-acceptors than their ferrocenyl counterparts, since their TEP values are lesser in magnitude compared to the TEP values of the ferrocenyl carbene ligands. Moreover, it can be confirmed that the aminocarbene ligands are more donating than the ethoxy analogues, as also demonstrated in the NMR spectroscopy characterisation.

2.3.3. Molecular structures of complexes 2 and 3

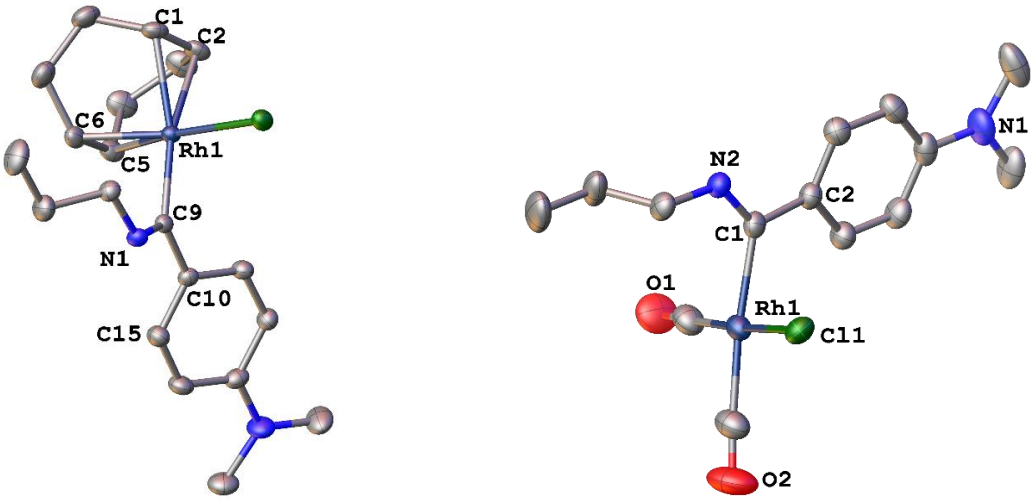

(b) **2** (a) **3**

*Figure 2. 9: Molecular structures of complexes **2** and **3** showing thermal ellipsoids at 50 % probability. Hydrogen atoms are omitted for clarity and a partial atom numbering scheme included.*

The solid state molecular structures of complexes **2** and **3** were obtained by X-ray diffraction of suitable single crystals grown from layering the DCM solution of **2** and **3** respectively with hexanes, and stored at 4°C overnight. Selected bond lengths and bond angles are reported in table 2.2, while the solid-state molecular structures are pictured in figure 2.6.

The observed bond angles around the rhodium(I) metal centre (Table 2.2) of complexes **1**-**4** are indicative of square planar geometry (Figure 2.6), comparable to their ferrocenyl counterparts.[6] The N–$C_{carbene}$–C_{ipso} bond angles of the aminocarbene complexes, **2** (116.40(14)°) and **3** (118.42(16)°) are greater than the O–$C_{carbene}$–C_{ipso} bond angles of **1** (111.7(2)°) and **4** (112.8(2)°), the ethoxycarbene complexes. It is also noted that the N–$C_{carbene}$ bond lengths of **2** and **3** are 1.307(2) Å and 1.304(2) Å respectively, indicating greater sp^2-character compared to the longer O–$C_{carbene}$ bond lengths observed

for **1** (1.436(4) Å) and **4** (1.421(4) Å), with reduced sp^2-character. To further corroborate this, Rh–$C_{carbene}$ bond lengths of **2** (2.006(16) Å) and **3** (2.0608(18) Å) are larger than what was observed for the ethoxycarbenes **1** (1.970(3) Å) and **4** (2.046(3) Å), indicating that less π-back donation from the central rhodium (I) metal is required to stabilize the empty p-orbital of the aminocarbene carbon as a direct consequence of the less electrophilic nature of this carbene. Similarly, the ferrocenyl ethoxycarbene complexes displayed noticeably shorter Rh–$C_{carbene}$ bond lengths (1.958(2) Å and 2.032(2) Å for the cod and the CO substituted complexes respectively) than their aminocarbene counterparts (2.018(1) Å and 2.06(1) Å for the cod and the CO substituted complexes respectively).[6]

Substitution of the cod ligands with the more π-acidic CO ligands results in an increase in Rh–$C_{carbene}$ bond length as observed from **1** (1.970(3) Å) to **4** (2.046(3) Å), and from **2** (2.006(16) Å) to **3** (2.0608(18) Å) with similar trends observed in the ferrocenyl analogues. This is presumably a direct consequence of the reduced metal π-backdonation to the carbene carbon, as a result of the *trans* CO ligand.

Table 2.2: Selected bond lengths and bond angles of rhodium complexes

Complex	1[17]	2	3	4[17]
Bond Lengths (Å)				
Rh-$C_{carbene}$	1.970(3)	2.006(16)	2.0608(18)	2.046(3)
$C_{carbene}$-C_q	1.332(3)	1.470(2)	1.461(2)	1.318(3)
$C_{carbene}$-O/N_1	1.436(4)	1.307(2)	1.304(2)	1.421(4)
Rh-Cl	2.383(8)	2.402(4)	2.3674(5)	2.353(8)
Rh-$Y^{a,b}$ or Rh-CO_{trans}	2.118(3)[a]	2.219(16)	1.924(2)	1.929(3)
Rh-$Y^{c,d}$ or Rh-CO_{cis}	1.990(3)[c]	2.106(17)	1.819(2)	1.833(3)
Bond Angles (°)				
$C_{carbene}$-Rh-Cl	88.09(8)	89.23(5)	87.35(5)	86.02(8)
O/N-$C_{carbene}$-C_{ipso}	111.7(2)	116.40(14)	118.42(16)	112.8(2)
Torsion Angles(°)				
$C_α$-C_{ipso}-$C_{carbene}$-O/N	7.79(4)	35.3(3)	12.5(3)	4.1(4)

[a]Y = midpoint of C(1)-C(2). [b]Y = midpoint of C(2)-C(3). [c]Y = midpoint of C(5)-C(6). [d]Y = midpoint of C(6)-C(7).

2.4. Conclusion

The synthesis of the complex **1** was achieved according to reported methodology, and the complex was used in an aminolysis reaction to afford complex **2** in good yields. Substitution of the cod-ligand in complexes **1** and **2**, to yield the corresponding analogous dicarbonyl complexes **3** and **4** was effected to introduce the carbonyl ligands in order to prepare (pre)catalysts for the hydroformylation reactions that bypass the initial cod-substitution step in the catalyst activation, according to the mechanism underlying the hydroformylation reaction.[17] In addition, the availability of complexes of the formula [$Rh(CO)_2Cl$(carbene)] presents the opportunity to determine the TEPs of the new carbene ligands. Both spectroscopic and structural evidence corroborates increased electrophilicity of the dicarbonyl complexes **3** and **4**, compared to the cod-complexes **1** and **2**; as well as the expected increase in $C_{carbene}$–N bond strength and a corresponding bond length, compared to $C_{carbene}$–O, for the

aminocarbene complexes **2** and **3**, compared to **1** and **4**, respectively. Specifically, the TEP value of the carbene ligand :C(OEt)*p*-DMA (2049 cm^{-1}) and that of :C(NH^{n}Pr)*p*-DMA (2043 cm^{-1}) supports this statement. In addition, the calculated TEP values are indicative of the even stronger donating ability of the *p*-DMA aryl carbene substituent and resulting unexpected superior stabilisation of the electrophilic carbene carbon, compared to the known ferrocenylcarbene rhodium(I) complexes.[6] This paves the way to the utilisation of these complexes as homogeneous catalysts that are thermally stable.

2.5. Experimental

2.5.1. Comprehensive synthetic methods for complexes 1-3

2.5.1.1. Synthesis of [Rh(cod)Cl{C(OEt)*p*-DMA}], **1**.[9]

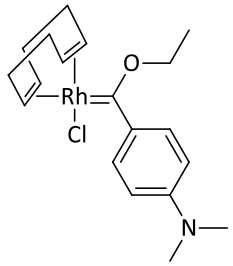

A $[W(CO)_5\{C(OEt)p\text{-DMA}\}]$ (0.32 g, 0.64 mmol) and $[Rh(cod)Cl]_2$ (0.19 g, 0.38 mmol) were transferred to a flame dried, $Ar_{(g)}$ purged Schlenk tube; and dissolved in degassed DCM. The reaction was allowed to stir for 72hrs, and the volatiles subsequently removed under reduced pressure. The crude was purified via column chromatography, and the product was concentrated under reduced pressure, yielding an orange solid. Yield: 62%.^{1}H NMR (500 MHz, CD_2Cl_2) δ 8.40 (d, br, ^3J(HH) = 8.6 Hz, 2H, DMA-$\underline{H}_{\alpha,\alpha'}$), 6.68 (d, ^3J(HH) = 8.8 Hz, 2H, DMA-$\underline{H}_{\beta,\beta'}$), 5.90 (dq, ^2J(HH)= 14.1, ^3J(HH)= 7.4 Hz, 1H, O$\underline{CH_2}CH_3$), 5.66 (dq, ^2J(HH)= 13.9, ^3J(HH)= 7.5 Hz, 1H, O$\underline{CH_2}CH_3$), 5.27 – 5.24 (m, 1H, cod-$\underline{CH}$), 5.15 – 5.10 (m, 1H, cod-$\underline{CH}$), 3.27 – 3.23 (m, 2H, cod-$\underline{CH}$), 3.10 (s, 6H, N$\underline{(CH_3)_2}$), 2.56 – 2.29 (m, 4H, cod-$\underline{CH_2}$), 2.14 – 1.97 (m, 4H, cod-$\underline{CH_2}$), 1.65 (t, ^3J(HH)= 7.2 Hz, 3H, OCH$_2\underline{CH_3}$). ^{13}C NMR (126 MHz,CD_2Cl_2) δ 297.9 (d, ^1J(RhC) = 43.0 Hz, $C_{carbene}$), 155.1 (C_q) , 132.9 (d, ^2J(RhC) = 2.2 Hz, C_{ipso}), n.o. (DMA-$\underline{C}_{\alpha,\alpha'}$), 110.7 (DMA-$\underline{C}_{\beta,\beta'}$) , 106.3 (d, ^1J(RhC) = 4.9 Hz, cod-$\underline{CH}$), 105.9 (d, ^1J(RhC) = 4.6 Hz, cod-$\underline{CH}$), 77.2 (O$\underline{CH_2}CH_3$) , 73.0 (d, ^1J(RhC) = 15.0 Hz, cod-$\underline{CH}$), 67.9 (d, ^1J(RhC) = 14.8 Hz, cod-$\underline{CH}$), 40.5 (N$\underline{(CH_3)_2}$), 33.5 (cod-$\underline{CH_2}$), 32.9 (cod-$\underline{CH_2}$), 29.0 (cod-$\underline{CH_2}$), 28.5, (cod-$\underline{CH_2}$), 15.6 (OCH$_2\underline{CH_3}$).

2.5.1.2. Synthesis of [Rh(cod)Cl{C(NH^{n}Pr)*p*-DMA}], **2.**[6]

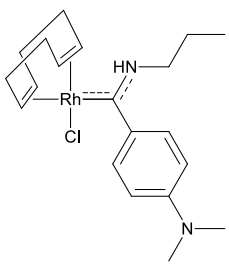

1 (0.20 g, 0.52 mmol) was dissolved in degassed DCM. $NH_2{}^nPr$ (0.17 mL, 2.08 mmol) was added dropwise and the solution stirred for 1hr. The volatiles were removed under reduced pressure and the product was washed with *n*-hexane, extracted in DCM, and the solvent removed under reduced pressure before drying under vacuum overnight. The residue was dissolved in minimum DCM for slow diffusion with *n*-hexane, to afford an orange powder. Yield = 0.145g ,70%. M.P. (,decomp): 163-165 °C ^{1}H NMR (400 MHz, CD_2Cl_2) δ 8.19 (s, br, 1H, $\underline{NH}CH_2CH_2CH_3$), 7.99 (d, ^3J(HH) = 9.0 Hz, 2H, DMA-$\underline{H}_{\alpha,\alpha'}$), 6.71 (d, ^3J(HH) = 9.0 Hz, 2H, DMA-$\underline{H}_{\beta,\beta'}$), 5.06 – 4.84 (m, 2H, cod-$\underline{CH}$), 4.53 (t, ^3J(HH) = 6.0 Hz, 2H, NH$\underline{CH_2}CH_2CH_3$), 3.25-3.27 (m,

1H, cod-CH), 3.11-3.05 (m, 1H, cod-CH), 3.04 (s, 6H, N(CH$_3$)$_2$), 2.44 – 2.37 (m, 2H, cod-CH), 2.33 – 2.28 (m, 1H, cod-CH), 1.94-1.65 (m, 4H, cod-CH$_2$, NHCH$_2$CH$_2$CH$_3$), 1.11 (t, ^3J(HH)= 7.4 Hz, 3H, NHCH$_2$CH$_2$CH$_3$). ^{13}C NMR (101 MHz, CD_2Cl_2) δ 252.2 (d, ^1J(RhC) = 40.0 Hz, $C_{carbene}$), 153.3 (C_q), 130.3 (DMA-$C_{\alpha,\alpha'}$), 128.9 (C_{ipso}), 111.3 (DMA-$C_{\beta,\beta'}$), 100.6 (d, ^1J(RhC) = 6.0 Hz, cod-CH), 100.1 (d, ^1J(RhC) = 5.8 Hz, cod-CH), 71.6 (d, ^1J(RhC) = 15.2, cod-CH), 68.1 (d, ^1J(RhC) = 15.0, cod-CH), 55.8 (NHCH$_2$CH$_2$CH$_3$), 40.4 (N(CH$_3$)$_2$), 33.4 (cod-CH$_2$), 32.9 (cod-CH$_2$), 29.2 (cod-CH$_2$), 28.6 (cod-CH$_2$), 23.6 (NHCH$_2$CH$_2$CH$_3$), 11.9 (NHCH$_2$CH$_2$CH$_3$). IR (DCM, ν(NH), cm^{-1}): 3288. ESI-HRMS (15 V, positive mode, m/ z): calcd for [M – Cl]$^+$ 401.1463; found 401.1566.

2.5.1.3. Synthesis of [Rh(CO)$_2$Cl{C(NH^{n}Pr)*p*-DMA}], **3.**[6]

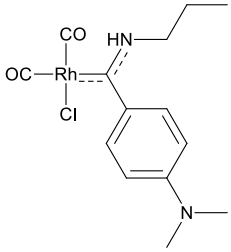

2 (0.10 g, 0.25 mmol) was dissolved in degassed DCM. The solution was purgerd with CO (g) for 15 min, in the absence of light, while stirring continuously. The reaction was allowed to stir for 1hr further, before removing volatiles under reduced pressure. The product was washed with hexanes, and subsequently dried overnight under vacuum. Yield = 0.085 g, 0.22 mmol. M.P. (decomp): 119-121°C. ^{1}H NMR (500 MHz, CD_2Cl_2) δ 8.53 (s, br, 1H, NHCH$_2$CH$_2$CH$_3$), 7.91 (d, ^3J(HH) = 9.1 Hz, 2H, DMA-H$_{\alpha,\alpha'}$), 6.70 (d, ^3J(HH) = 9.1 Hz, 2H, DMA-H$_{\beta,\beta'}$), 4.29 (br s, 1H, NHCH$_2$CH$_2$CH$_3$), 4.10 (br s, 1H, NHCH$_2$CH$_2$CH$_3$), 3.07 (s, 6H, N(CH$_3$)$_2$), 1.86 (br s, 2H, NHCH$_2$CH$_2$CH$_3$), 1.06 (t, ^3J(HH)= 7.4 Hz, 3H, NHCH$_2$CH$_2$CH$_3$). ^{13}C-NMR (126 MHz, CD_2Cl_2) δ 233.8 (d, $^1J_{RhC}$ = 34.3 Hz, $C_{carbene}$), 187.8 (d, $^1J_{RhC}$ = 51.5 Hz, CO$_{trans}$), 184.3 (d, $^1J_{RhC}$ = 77.9 Hz, CO$_{cis}$), 154.3 (C_q), 132.3 (DMA-$C_{\alpha,\alpha'}$), 128.1 (C_{ipso}), 111.3 (DMA-$C_{\beta,\beta'}$), 56.6 (d, $^3J_{RhC}$ = 1.7 Hz, NHCH$_2$CH$_2$CH$_3$), 40.4 (N(CH$_3$)$_2$), 23.1 (NHCH$_2$CH$_2$CH$_3$), 11.6 (NHCH$_2$CH$_2$CH$_3$). IR (CH_2Cl_2, ν(CO) cm^{-1}): 2000, 2055 and ν(NH), cm^{-1}): 3303. ESI-HRMS: (m/z) calcd for $C_{13}H_{18}ON_2Rh^+$:321.0474 [M – Cl - CO]$^+$; found 321.0235.

2.5.2. Molecular structural data of complexes 2 and 3

Crystal Data for **2**: $C_{21}H_{32}Cl_3N_2Rh$ (*M* =521.74 g/mol): monoclinic, space group P2$_1$/n (no. 14), *a* = 12.0275(3) Å, *b* = 11.6854(3) Å, *c* = 16.7976(4) Å, *β* = 99.2027(11)°, *V* = 2330.45(10) Å^3, *Z* = 4, *T* = 173.15 K, μ(MoKα) = 1.086 mm^{-1}, *Dcalc* = 1.487 g/cm^3, 59021 reflections measured (3.886° ≤ 2Θ ≤ 61.146°), 7133 unique (R_{int} = 0.0423, R_{sigma} = 0.0261) which were used in all calculations. The final R_1 was 0.0259 (I > 2σ(I)) and wR_2 was 0.0616 (all data).

Crystal Data for **3:** $C_{14}H_{18}ClN_2O_2Rh$ (*M* =384.66 g/mol): triclinic, space group P-1 (no. 2), *a* = 8.5569(5) Å, *b* = 10.4188(6) Å, *c* = 10.5705(6) Å, *α* = 71.6988(18)°, *β* = 66.4054(18)°, *γ* = 77.0938(19)°, *V* = 814.74(8) Å^3, *Z* = 2, *T* = 173.15 K, μ(MoKα) = 1.214 mm^{-1}, *Dcalc* = 1.568 g/cm^3, 28474 reflections measured (6.298° ≤ 2Θ ≤ 56.684°), 4026 unique (R_{int} = 0.0328, R_{sigma} = 0.0219) which were used in all calculations. The final R_1 was 0.0236 (I > 2σ(I)) and wR_2 was 0.0519 (all data).

2.6. References

[1] E. Fischer and A. Maasböl, *Angew. Chem. Int. Ed. in Engl.*, 1964, **3**, 580-581

[2] E. Fischer and H. J. Beck, *Angew. Chem. Int. Ed. Engl.,* 1970, **9**, 72-73.

[3] J. Barluenga, R. Vicente, L. A. López, E. Rubio, M. Tomás and C. Álvarez-Rúa, *J. Am. Chem. Soc.*, 2004, **126**, 470–471.

[4] J. Barluenga, R. Vicente, L. A. López and M. Tomás, *J. Organomet. Chem.*, 2006, **691**, 5642-5647.

[5] M. F. Lappert, *J. Organomet. chem.*, 2005, **690**, 5467-5473.

[6] G. K. Ramollo, M. J. López-Gómez, D. C. Liles, L. C. Matsinha, G. S. Smith and D. I. Bezuidenhout, *Organometallics*, 2015, **34**, 5745-5753.

[7] I. Hoskovcová and J. Ludvík, *Curr. Opin. Electrochem.*, 2019, **15**, 165-174.

[8] N.-a. Weststrate, S. Bouwer, C. Hassenrück, N. A. van Jaarsveld, D. C. Liles, R. F. Winter and S. Lotz, *J. Organomet. Chem.*, 2018, **869**, 54-66.

[9] T. L. Mashabane, G. K. Ramollo, G. Kleinhans, S. De Doncker, S. Siangwata, M. A. Fernandes, A. Lemmerer, G. S. Smith and D. I. Bezuidenhout, *J. Organomet. Chem.*, DOI:10.1016/j.jorganchem.2020.121341.

[10] D. Munz, *Organometallics*, 2018, **37**, 275-289.

[11] S. Lotz, M. van den Berg and J. L. Dillen, *Transition Metal Chemistry*, 1988, **13**, 170-175.

[12] (a) M. A. Sierra, M. J. Mancheño, E. Saez, J. C. Amo, *J. Am. Chem. Soc.* 1998, **120**, 6812-6813. (b) M. A. Sierra, J. C. del Amo, M. J. Mancheno and M. Gomez-Gallego, *J. Am. Chem. Soc.*, 2001, **123**, 851-861. (c) A. Nagy, A. V. Schally, P. Armatis, K. Szepeshazi, G. Halmos, M. Kovacs, M. Zarandi, K. Groot, M. Miyazaki and A. Jungwirth, *Proc. Natl. Acad. Sci.*, 1996, **93**, 7269-7273. (d) J. Barluenga, P. Barrio, L. A. Lopez, M. Tomas, S. Garcia-Granda and C. Alvarez-Rua, Angew. *Chem. Int. Ed. Engl*., 2003, **42**, 3008-3011.

[13] R. A. Kelly III, H. Clavier, S. Giudice, N. M. Scott, E. D. Stevens, J. Bordner, I. Samardjiev, C. D. Hoff, L. Cavallo, S. P. Nolan, *Organometallics* 2008, ***27***, 202-210.

[14] G. K. Ramollo, MSc Chemistry, University of Pretoria, 2016.

[15] J. K. Huang, E. D. Stevens, S. P. Nolan, *Organometallics,* 2000, ***19***, 1194-1197.

[16] R. A. K. Iii, H. Clavier, S. Giudice, N. M. Scott, E. D. Stevens, J. Bordner, I. Samardjiev, C. D. Hoff, L. Cavallo and S. P. Nolan*, Organometallics*, 2008, **27**, 202–210.

[17] B. D. Evans, J. A. Osborn and G. Wilkinson, *J. Am. Chem. Soc.*, 1968, **62**, 3133-3142.

Chapter 3: Rh(I) and Ir(I) *N3*-alkylated "click" mesoionic carbene complexes

3.1. Background

The serendipitous discovery of the *abnormal* N-heterocyclic carbene (*a*NHC) in 2001,[1] gave rise to their application in a variety of catalytic reactions as a result of the robust nature of the bond between the catalytically active central metal and the carbene carbon.[2,3] Due to their lineage, these carbenes were termed *abnormal* as the N-heterocyclic carbene was bound "incorrectly" by the C5 carbon (types III and V, Figure 3.1), where the heteroatoms are located at the α,β^{l} positions instead of the more conventional α,α^{l} positions (like types I and II, Figure 3.1).[1] Furthermore, the work by Hyunh in 2007,[4] and Albrecht in 2008[5] where carbenes of type IV and type V were coordinated to palladium, prompted Bertrand and co-workers to isolate this class of "mesoionic" carbenes (MICs) in 2010 after the isolation of the first free carbene of type III.[6] The IUPAC term mesoionic refers to the inability to represent the free carbenes of types III-IV without additional charges.[7]

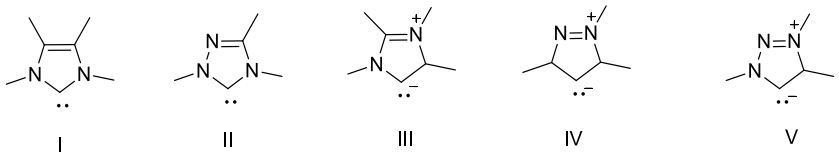

Figure 3. 1: Classical NHCs (types I-II) as well as aNHCs displaying their mesoionic character (types III-V).[6]

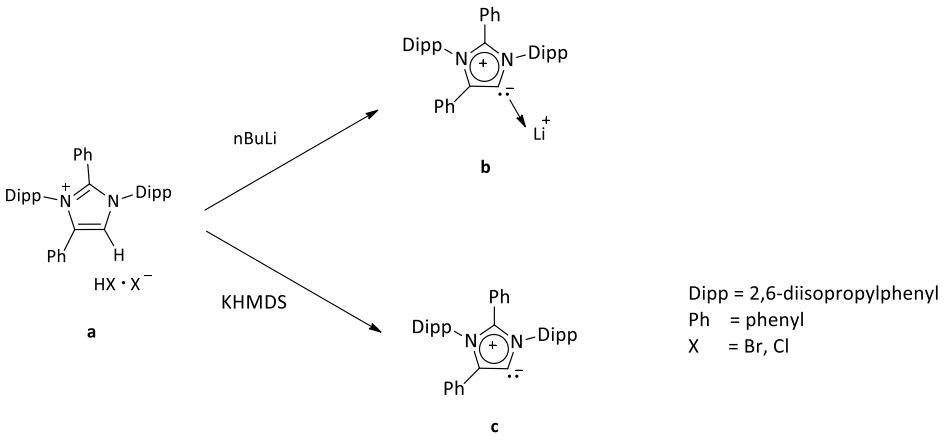

*Scheme 3. 1: Preparation of the MIC lithium adduct, **b** from **a** using nBuLi as a deprotonating agent; preparation of the first free MIC **c** from **a** using KHMDS as a deprotonating agent.[6]*

In 2008, Albrecht *et al* isolated the first 1,2,3-triazol-5-ylidene metal complexes.[5] The ligand was prepared using "click" chemistry, and the N3 position was subsequently alkylated with MeI. The salt was reacted with $Pd(OAc)_2$, followed by Ag_2O to be transmetalated to rhodium, iridium and ruthenium.[5] Thereafter, studies into the isolation of the first type V free carbene began in 2009. The rationale behind this, was the calculated difference in pK_a values of 9 units between the loss of C5 (pK_a

= 33) and the C2 (pK_a = 24) protons of the corresponding imidazolium salt. Thus, to ensure the deprotonation occurs at C5, the C2 proton was substituted by a phenyl group. Additionally, to circumvent the kinetic instability of the type III carbene, Bertrand and co-workers appended bulky aryl (2,6-diisopropylphenyl) groups on both the heteroatoms, followed by the substitution of the C4 proton with a phenyl group (**a**, Scheme 3.1).[6] Deprotonation with a strong lithium base such as *n*BuLi proved unfavourable due to the formation of the relatively stable carbene lithium adduct,[6,7] which later results in an intramolecular nucleophilic addition reaction with the C2 carbon. It was therefore concluded that non-nucleophilic bases are better suited for the preparation of free MICs for the coordination to a central metal.[6]

Bertrand *et al*. used the magnitude of the singlet-triplet band gap (56 kcal/mol) to predict the stability of the type V free carbene.[6] To validate these findings, Bertrand prepared two triazolium salts and deprotonated the C5 position, as protection of position 2 would be redundant due to the absence of a C2 proton. A bulky aryl substituent, was placed on the N1 position, and another on the C4 position to provide kinetic stability to the resultant free carbene.[8] To access the desired 1,4-diaryl-triazole, a modified method of Moses *et al*. was employed, where the aryl azide was generated *in situ* to facilitate the copper-catalysed azide alkyne cycloaddition reaction (CuAAC).[9] Position 3 was then alkylated with a methyl or an isopropyl group, and subsequently deprotonated at position C5 to afford the free 1,3,4-trisubstituted 1,2,3-triazol-5-ylidene **g**, the first of its kind to be successfully isolated in 2010. The molecular structure of compound **g** confirmed the delocalization of the charge within the triazolylidene ring. The superior donor properties of **g** compared to type I carbene ligands were corroborated by its coordination to iridium(I) and subsequent exposure to excess CO.[6]

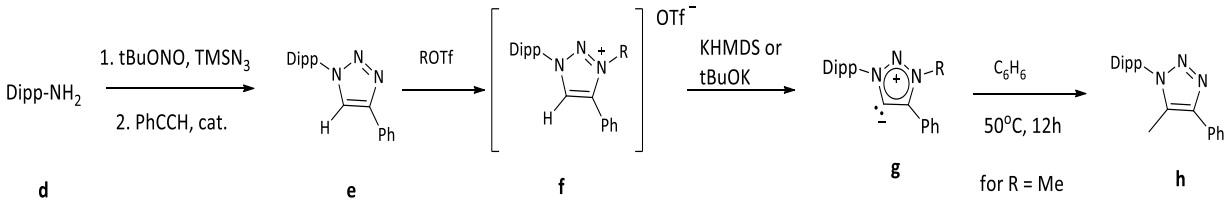

Dipp = 2,6-diisopropylphenyl
R = Me, *i*Pr

*Scheme 3. 2: The preparation of the 1,4-disubstituted triazole **e**, followed by the alkylation of position 3 (**f**) and the deprotonation of position 5 to afford **g**.*[7]

Prior to this first isolation, type V carbenes were known to readily decompose[6] by isomerizing to diazo nitriles under thermal conditions in the presence of benzene.[10] Bertrand and co-workers performed thermolysis reactions in benzene on **g** (where R = Me, ^{i}Pr) and found that when R = Me, **g** undergoes what is postulated to be an intermolecular nucleophilic attack on the methyl substituted heteroatom resulting the triazole **h**.[7] This was not observed for the isopropyl analogue. Furthermore, the isopropyl analogue remained stable significantly longer than the methyl analogue in solid state under air and moisture free conditions at temperatures ranging from -30°C to room temperature.[7] Therefore our group predicted that a range of 1,4-disubstituted triazoles could prepared and alkylated, before deprotonation and coordination to the desired metal.

3.2. Aim and objectives

3.2.1. Aim

The donor strength of this particular ligand, coupled with its notable stability once coordinated to a metal, made this ligand an attractive choice for hydroformylation catalyst precursor. The ligand is designed, keeping in mind the kinetic stability afforded by appending aryl groups at positions 1 and 4 to ensure steric bulk to circumvent decomposition of the free carbene once deprotonated. This can be achieved by taking advantage of the high yielding "click" reaction.[6] Furthermore, alkylation of the triazole increases the acidity of the proton at position 5, making it susceptible to nucleophilic attack.

3.2.2. Objectives

To date, the most efficient synthetic route to access N3-alkylated triazolium salts is by preparing 1,4-disubstituted triazoles using the CuAAC method.[7,9] Once alkylated, the triazolium salt can be metalated using a variety of late transition group metals, for application as catalyst precursors.[11] Applying the same approach and motivation used during the isolation of the first free triazolylidene, a sterically hindered aryl azide will be reacted with an aryl alkyne in the synthesis of a triazole to offer kinetic stability to the ensuing free carbene following proton abstraction. An anion-containing alkylating agent will be used to facilitate directing metalation reactions to the C4 position,[12] to achieve an N3-alkylated 1,2,3-triazolium salt with a BF_4^- counterion similar to that prepared by Sarkar *et al*.[13]

The first account of the catalytic activity of a metal complex bearing a "click" 1,2,3-triazol-5-ylidene ligand was reported by Sankararaman in 2009, following the unanticipated synthesis of the corresponding silver carbene complex.[14] Since then, palladium,[15] gold,[16] copper,[17] ruthenium,[18] iridium,[19] rhodium,[20] cobalt,[21] titanium, niobium and molibenum[22] triazolylidene complexes have been reported to have displayed catalytic activities in a variety of reactions. As such, *N3*-alkylated 1,2,3-triazol-5-ylidene metal complexes will be prepared as catalyst precursors hydroformylation reactions.

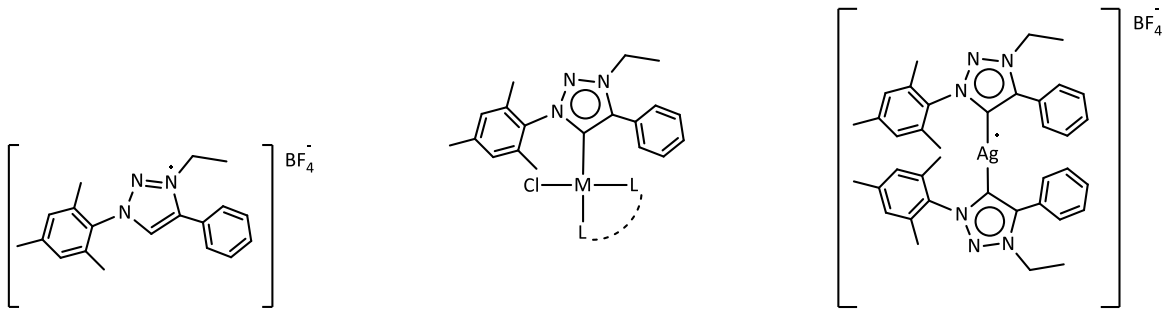

L2

5 M = Rh, LL = cod
6 M = Rh, LL = $(CO)_2$
7 M = Ir, LL = cod
8 M = Ir, LL = $(CO)_2$

S2

*Figure 3. 2: Target triazolium salt **L2**, complexes **5**-**8**, and the intermediate complex **S2**.*

A wide range of metalation techniques are available, as the deprotonation route has proven to be accessible for metalation reactions to proceed with ease. In a review article, Pearson and Arnold highlighted three main routes for the metalation of *abnormal* NHC salts:[23] deprotonation (*in situ* as well as through the isolation of the free carbene);[7] direct metalation through CH bond activation by a metal;[24] as well as through transmetalation from silver, as silver is a known carbene transfer agent.[25] In this chapter, complex **6** will be metalated with rhodium(I) after its *in situ* deprotonation with KHMDS, a non-nucleophilic base to access the rhodium complexes **5** and **6**. **L2** will also be employed in a direct metalation reaction with AgO_2, and the resulting intermediate, complex **S2,** will be used as the precursor in a transmetalation reaction with iridium(I) to afford complexes **7** and **8** (Figure 3.2).

3.3. Results and discussion

Herein, the known triazole **L1** will be prepared by Albrecht's method, and alkylated to afford the ethyl analogue of the triazolium salt **L2** reported by Sarkar. Mesityl complexes **5** and **6** will also be described, analogues of the 2,6-diisopropylphenyl rhodium complexes previously described by our group;[29] as well as silver (**S2**) and iridium (**7** - **8**) complexes of ligand precursor **L2**[I]. The analysis of the spectroscopic data obtained for these complexes, as well as the molecular structures of **L2**, **5** and **S2** will be examined and compared to previously reported findings, to allow for insight into the steric and electronic properties of each complex as well as the effect of the central metal and the ancillary coordination sphere on the 1,2,3-triazol-5-ylidene ligand.

3.3.1. Preparation of compounds L1-L2, S2, 5-8.

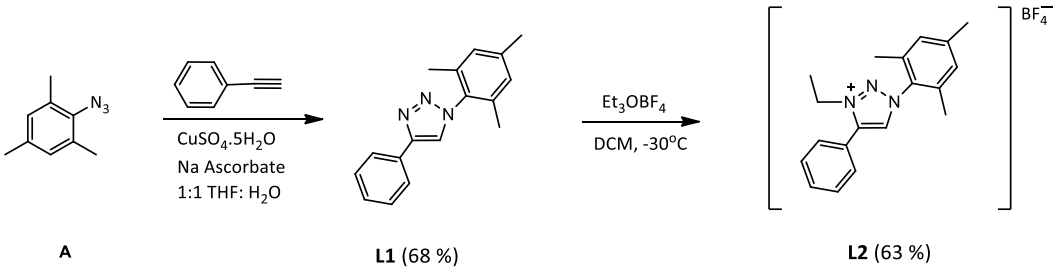

*Scheme 3. 3: Synthesis of compounds **L1** and **L2**.*[18,28,29]

The versatility of the high yielding one-pot copper catalysed azide-acetylene cycloaddition (CuAAC) method gives access to functionalized triazoles, that can be alkylated to obtain virtually any desired heterocyclic carbene ligand.[9] Compound **A** (azide) was prepared by Wei Zhua and Dawei Ma according to literature procedures,[26] and was reproduced and verified by NMR. The preparation of compound **5** was achieved following the CuAAC also termed "click" reaction, where the mesityl azide was reacted with phenylacetylene in a 1:1 THF:H_2O solution of $CuSO_4.5H_2O$ and sodium ascorbate overnight affording the 1-mesityl-4-phenyl-1,2,3-triazole reported by Albrecht in 2012.[27] The triazole was then alkylated under inert conditions at position 3 of the triazole ring, to achieve formation of **L2** (Scheme

3.4).[7,8] Subsequently, a variety of metalation techniques were employed to obtain the complexes **S2** and **5-8** from **L2** (Scheme 3.5).

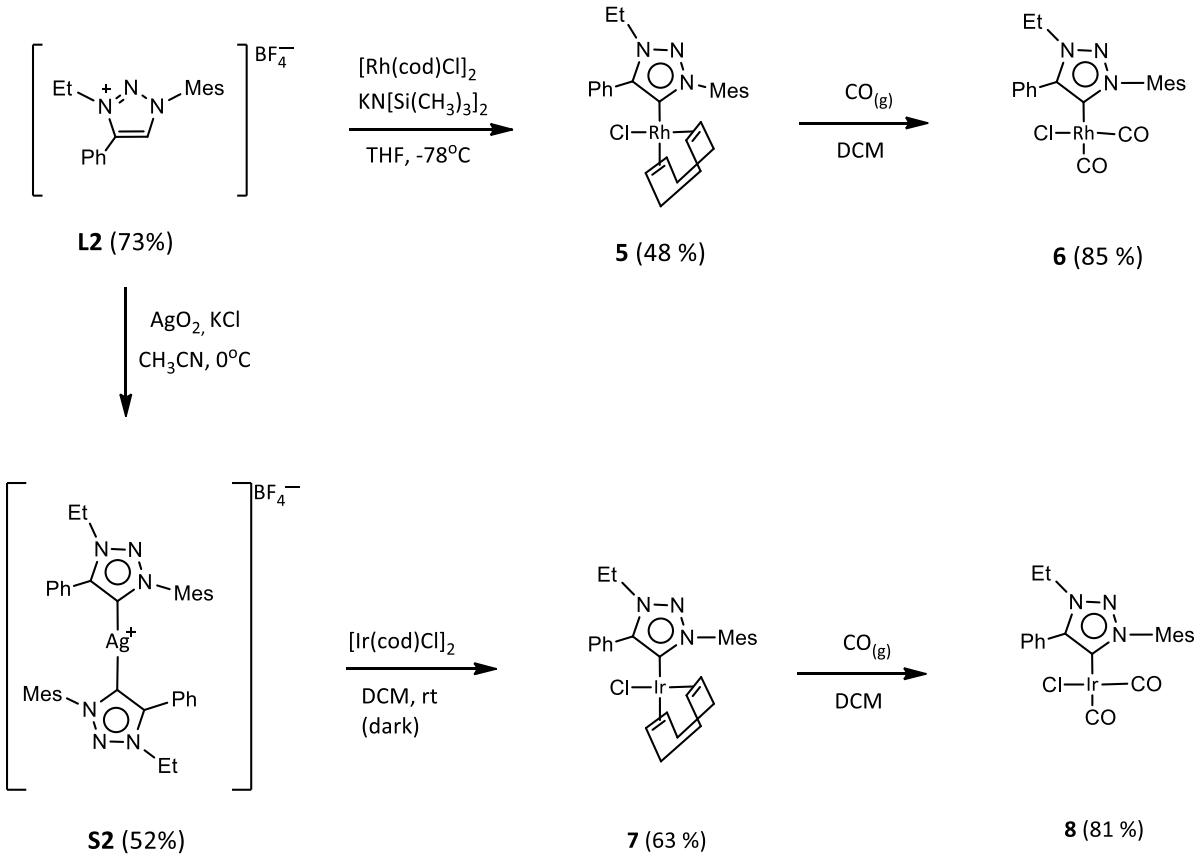

cod = 1,5-cyclooctadiene
Mes = mesityl

*Scheme 3. 4: The synthesis of complexes **S2, 5-8** from the functionalized triazolium salt **L2**.*

Triazolium salt **L2** was deprotonated with a non-nucleophilic base at position 5 under inert conditions at low temperature and the free carbene was metalated *in situ* with $[Rh(cod)Cl]_2$. The residue was washed with hexanes, followed by the extraction of complex **5** in toluene before washing further with hexanes and drying under reduced pressure over night. Complex **5** was isolated with an average yield of 48%,[28] improving on the yield reported previously for the 2,6-diisopropylphenyl (Dipp) analogue (30 %). A DCM solution of complex **5** was purged with CO gas, to substitute the labile 1,5-cyclooctadiene (cod) ligand with a pair of π-accepting CO ligands resulting in complex **6** at 85% yield, significantly higher than the previously recorded Dipp analogue (22%).[7,15]

To prepare complex **S2**, the 1,3,4-trisubstituted 1,2,3-triazolium salt, **L2** underwent treatment with excess AgO_2 in the presence of an anion donor (KCl) dissolved in MeCN[29] which produced AgCl, a thermodynamically favoured by-product, and H_2O as reported by Crudden *et al*. The metalation reaction was concentrated under reduced pressure and washed with Et_2O to afford **S2**, an intermediate 1,2,3-triazol-5-ylidene silver (I) complex, extracted in DCM and isolated in a yield of 52%.[30] Complex **S2** was isolated to ensure a more facile work-up in the ensuing transmetalation reaction.[31] Complex **7** was prepared by reacting **S2** with $[Ir(cod)Cl]_2$ in the absence of light, following

a modified version of a previously described route.[7] Complex **7** was extracted in hexane from the crude reaction mixture, and isolated in a yield of 63% (Scheme 3.5), 36% less than what Albrecht reported for the first iridium(I) triazolylidene complex (99%).[7] Complex **8** was prepared by passing gaseous CO through a DCM solution of **8**.[7]

3.3.2. Spectroscopic analyses of compounds L1-L2, S2, 5-8

3.3.2.1. Inspection and discussion of the ^{1}H NMR spectra

The alkylation of **5** is spectroscopically confirmed by the upfield shift of the triazole-CH from 7.84 ppm in the ^{1}H NMR spectrum of **5** to 8.39 ppm in **L2** (Figure 3.4);[8] as well as the presence of a BF_4^- counterion as indicated by the fluoride resonance in the corresponding ^{19}F NMR spectrum (Figure 3.5). This spectrum, shows a pair of isotopologue signals emanating from the two naturally occurring, and NMR active nuclei of ^{10}B (19.9% abundant) and ^{11}B (80.1% abundant) each coupling to the four equivalent fluorine nuclei with a single naturally occurring isotope.[32] Similarly, these isotopologue signals are observed on the ^{19}F NMR spectrum of complex **S2** (Figure 3.9)**.** The ^{1}H NMR spectrum of **S2** includes an impurity of the unreacted precursor salt which was difficult to separate from the target complex as both are cationic (Figure 3.8). The ethyl group bound to the N-atom is confirmed by the appearance of a quartet integrating for 2 protons at 4.75 ppm, and its corresponding triplet integrating for 3 protons at 1.59 ppm. The disappearance of the acidic proton at 8.39 ppm, signals the coordination of the triazolylidene carbene carbon atom to the transition metal as observed in the ^{1}H NMR spectrum of **5** and **S2** (Figures 3.6 and 3.8 respectively).[6,7] Additionally, it can be assumed that the high π-density that was previously delocalised in the triazole ring, is now being directed towards the central metal in both **5** and **S2**, forging a strong σ-bond with rhodium(I) and silver(I).

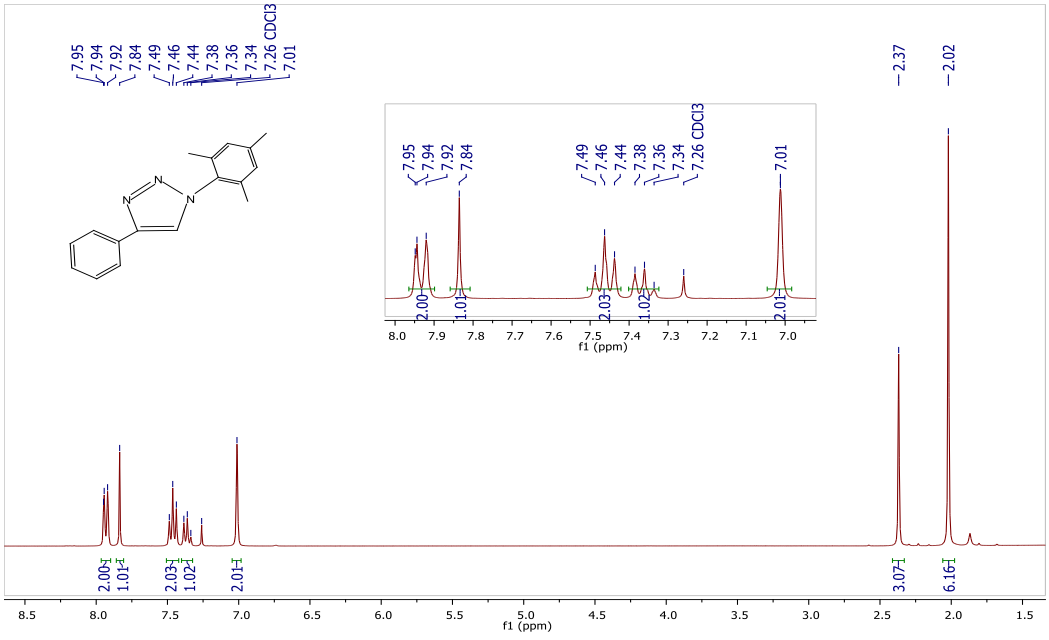

*Figure 3. 3:^{1}H NMR spectrum of **L1** in solvent: $CDCl_3$*

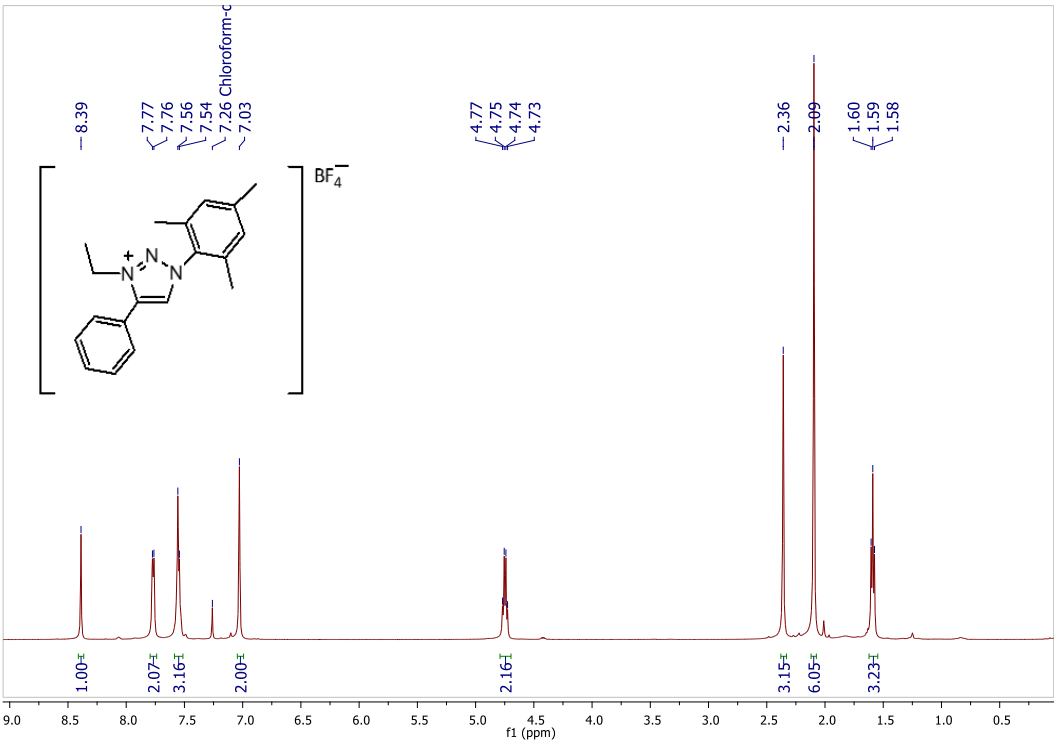

*Figure 3. 4: ^{1}H NMR spectrum of **L2** in solvent $CDCl_3$*

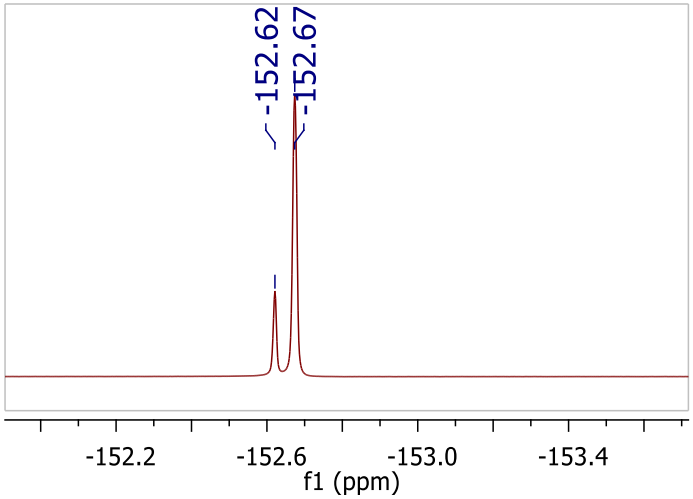

*Figure 3. 5: ^{19}F NMR spectrum of **L2** in $CDCl_3$*

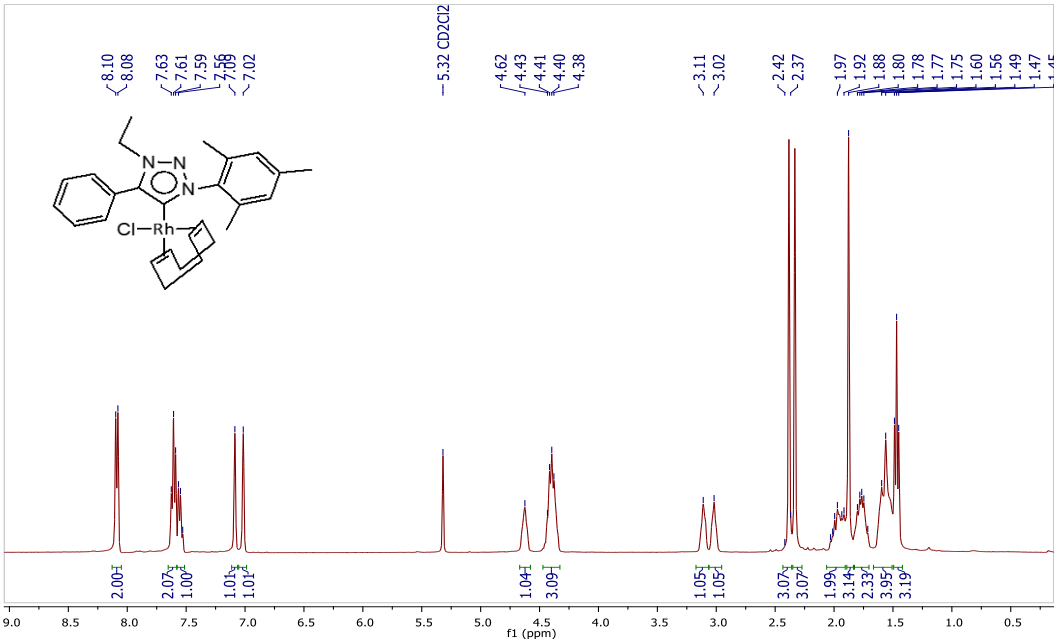

Figure 3. 6: ^{1}H NMR spectrum of **5** in solvent CD_2Cl_2

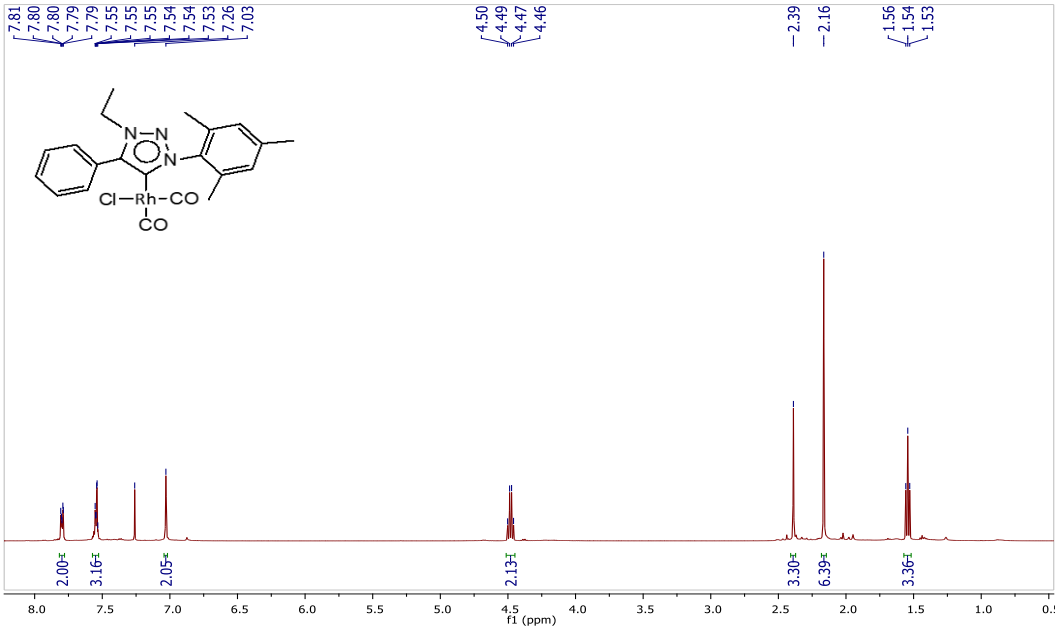

*Figure 3. 7: ^{1}H NMR spectrum of **6** in solvent $CDCl_3$*

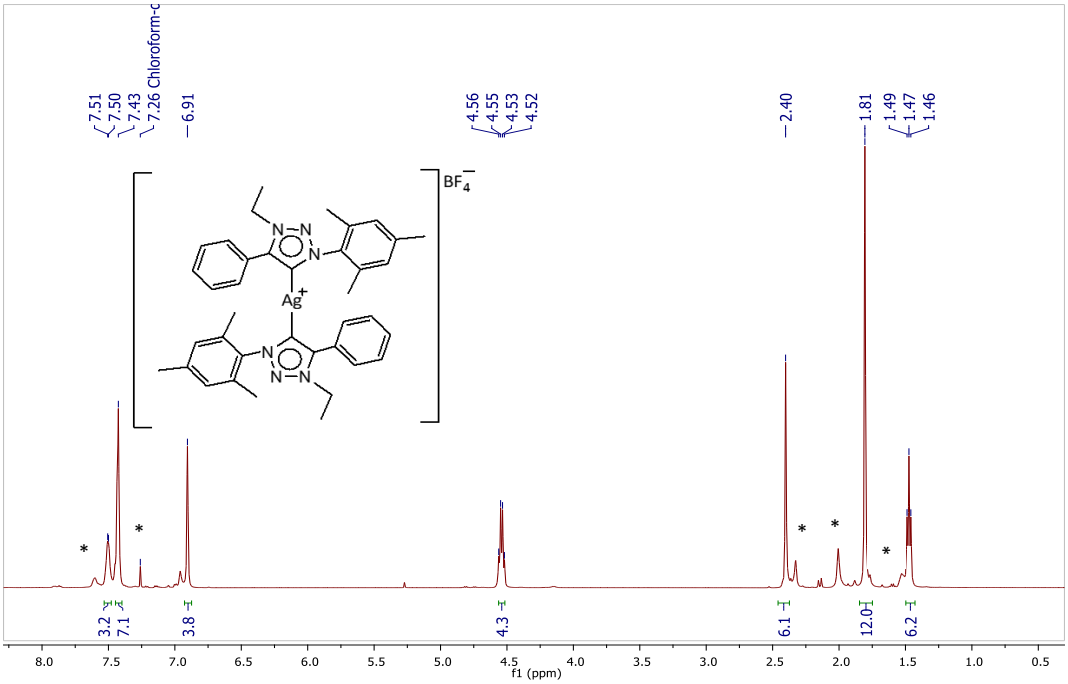

*Unreacted precursor salt

Figure 3. 8: ^{1}H NMR of **S2** in solvent $CDCl_3$

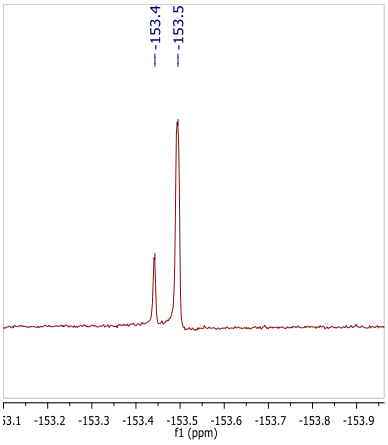

*Figure 3. 9: ^{19}F NMR spectrum of **S2** in solvent $CDCl_3$*

The differences in the coordination of the carbene (from precursor salt **L2**) to the metal centre, between complex **5** and **7** are noticeable in the aromatic region of the respective ^{1}H NMR spectra. Complex **5** falls in the range of 7.20 – 8.10 ppm while for **7**, the aromatic chemical shifts range from 6.71 ppm – 7.97 ppm. A similar trend is reported by Albrecht, where the aromatic region of the rhodium complex spans over a larger range (8.06 – 7.53 ppm) than the iridium analogue which ranges from 7.92 – 7.49 ppm.[5] However, the aliphatic regions remain comparable, along with the carbene signals with a marginal difference of 1.7 ppm (Table 3.1). The spectrum of **7** (Figure 3.10), shows organic impurities, that were extracted from the hexane fraction along with the target complex **7**. A range of solvents were employed in an attempt to purify the complex by crystallization, however this

proved to be futile. As this NMR spectrum results from the hexane fraction, presumably the impurity are organic triazole-side products and not iridium salts that would influence the catalytic activity. However, this assumption cannot be proven due to the difficulty in purifying this complex. The splitting of signals in the ^{1}H NMR spectra of **5** and **7** (Figures 3.6 and 3.10, respectively), compared to that of the uncoordinated precursor **L2** (Figure 3.4) indicates a loss of symmetry about the coordination sphere of the square planar metal centre. Similarly, the ^{13}C NMR spectra of **5** and **7** (vide infra Figures 3.14 and 3.17, respectively) display this asymmetry, a phenomenon not observed for complex **L2**.[31] This is in accordance with the data reported by our group for the 2,6-diisopropylphenyl (Dipp)-substituted rhodium complex, as well as what Albrecht and co-workers reported for their rhodium and iridium triazolylidene complexes.[7,29]

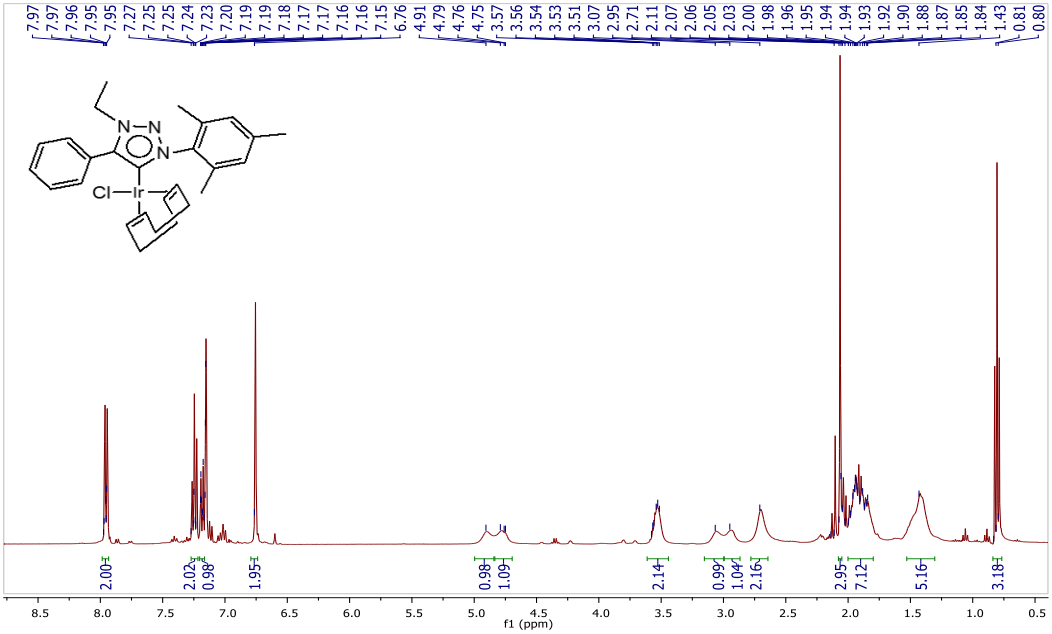

Figure 3. 10: ^{1}H NMR spectrum of **7** in solvent: C_6D_6

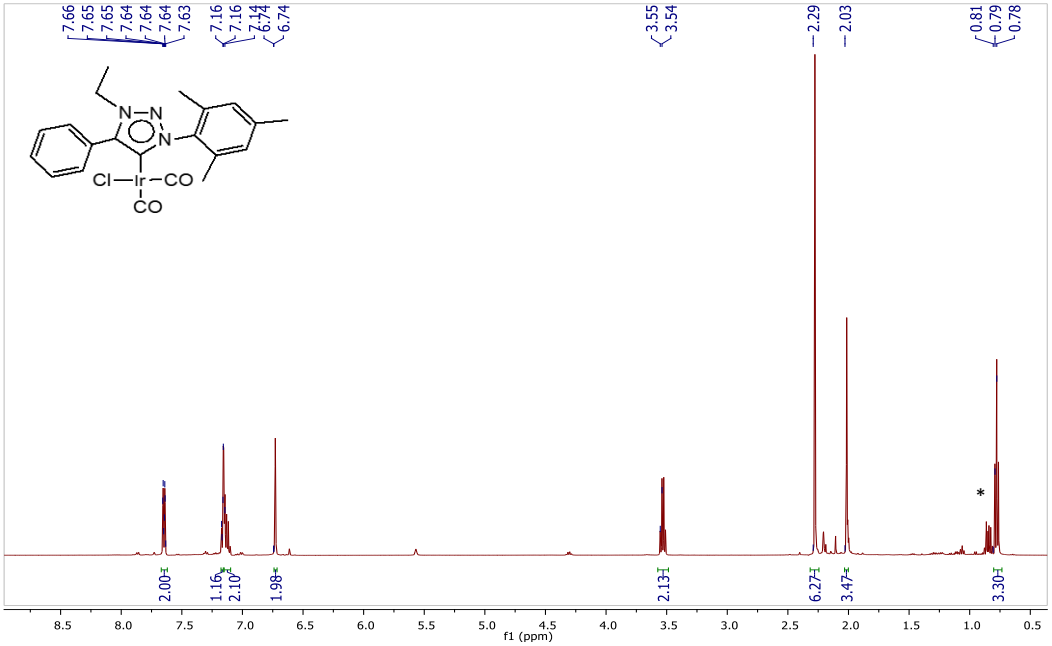

** n-hexane*

Figure 3. 11: ^{1}H NMR spectrum of **8** in solvent C_6D_6

*Table 3. 1: Spectroscopic data of complexes **S2**, **5**-**8***

Complex	^{13}Cδ($C_{carbene}$), (^{1}J($M^{g}C$))	^{13}C δ(CO), (^{1}J(RhC))	IR^{a} ν(CO), (cm^{-1})	IR^{a}ν_{av}(CO), TEP^{d} (cm^{-1})
5	171.6 (d, 47.4)	-	-	-
6	165.6 (d, 40.1)	185.6 (d, 54.5)^{b} 183.5 (d, 75.4)^{c}	1994^{c} 2074^{b}	2034 2047^{d}
S2	167.7 (dd, 177.6, 12.7)	-	-	-
7	173.3	-	-	-
8	166.8	182.3^{b} 170.3^{c}	1978^{c} 2062^{b}	2020 2048^{e}

^{a}Recorded in CH_2Cl_2. ^{b}CO-ligand trans to carbene. ^{c}CO-ligand trans to Cl. ^{d}Calculated using the linear regression model TEP = 0.8001ν_{av}(CO)Rh + 420 cm^{-1}.[15] ^{e}Calculated using the linear regression model TEP = 0.8475ν_{av}(CO)**Ir** + 336.2 cm^{-1}.[15] ^{f}CO-ligand trans to CO. ^{g}M = Rh, Ir, Ag.

3.3.2.2. Evaluation of the obtained ^{13}C NMR spectra

The ^{13}C NMR spectra of **5** and **S2** show the disappearance of the triazole-CH peak. The appearance of a downfield carbene carbon doublet resonance at 171.6 ppm (J = 47.4 Hz) is seen for **5** (Figure 3.14). This was observed to be the norm for rhodium triazolylidene complexes with aryl substituents at positions 1 and 4 of the heterocycle.[33] A low-field doublet of doublets is observed in the ^{13}C NMR spectrum of **S2** corresponding to the silver carbene carbon (Figure 3.16, 167.7 ppm (J = 177.6, 12.7 Hz), conventional for silver 1,2,3-triazol-5-ylidene complexes. The success of the transmetalation

reaction from the carbene transfer agent, **S2**, to iridium(I) in complex **7**, is substantiated by the disappearance of the doublet of doublets at 167.7 ppm and the appearance of a singlet at 173.3 ppm in the ^{13}C NMR spectrum of **7** (Figure 3.17), in the range of a characteristic iridium triazolylidene carbene carbon peak.[7] No acidic proton is observed in the ^{1}H NMR spectrum of **7**, corroborating carbene transfer without re-protonation.[27]

The splitting patterns observed for the rhodium carbene carbon atom resonance in complex **5** (doublet), and the silver carbene resonance in complex **S2** (doublet of doublets), can be attributed to the NMR-active metal coupling with the ^{13}C nuclei, in contrast to the NMR-inactive .Ir(I) metal centre where a singlet is observed for the carbene carbon atom in **7** (Figure 3.17).The ^{103}Rh nuclei couples to the ^{13}C resulting in a doublet splitting pattern for the carbene peak in Figure 3.11. Figure 3.15 displays a doublet of doublets for the silver carbene peak, a consequence of both ^{107}Ag and ^{109}Ag isotopes (with a natural abundance of 51.8% and 48.2% respectively) each coupling to the carbene carbon atom with coupling constants of 12.7 and 177.6 Hz respectively.[32]

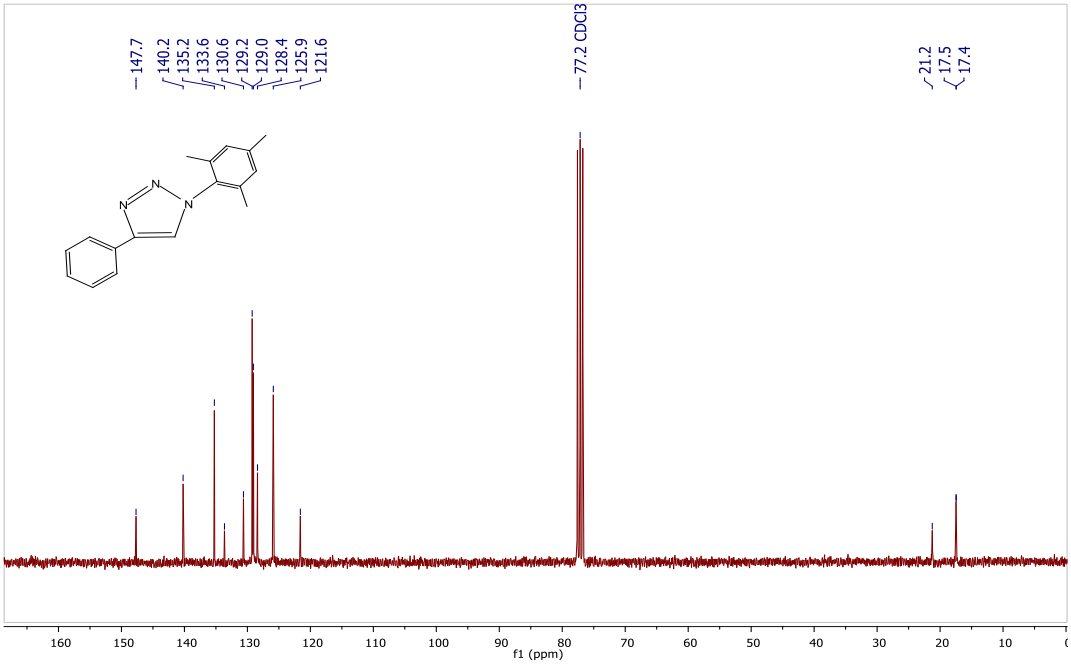

*Figure 3. 12: ^{13}C NMR spectrum of **L1** in solvent $CDCl_3$*

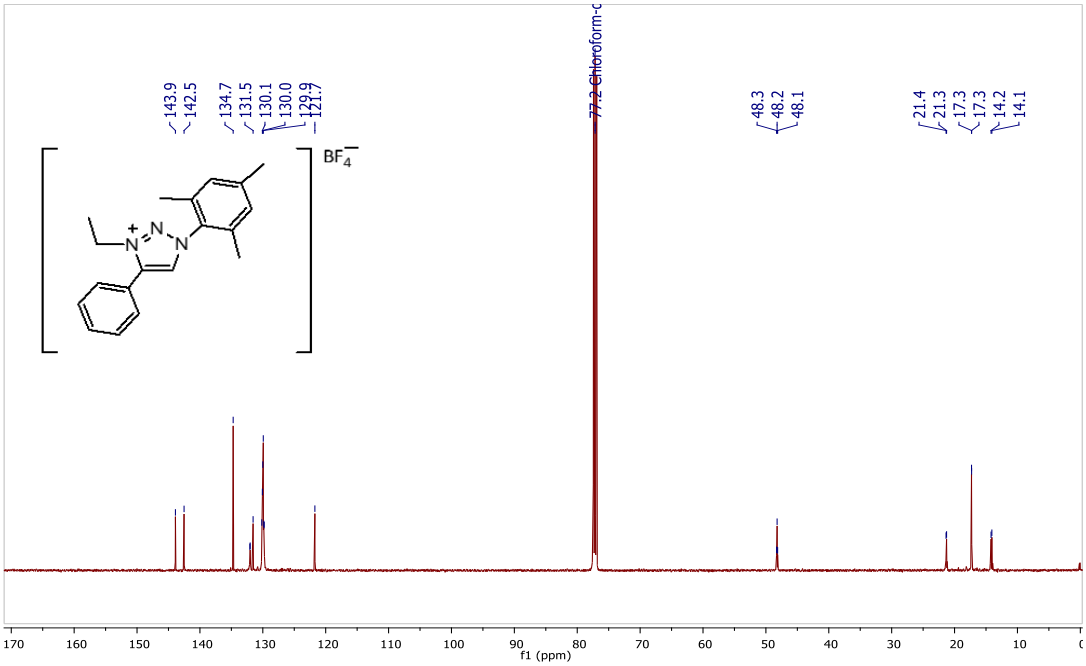

*Figure 3. 13: ^{13}C NMR spectrum of **L2** in solvent $CDCl_3$*

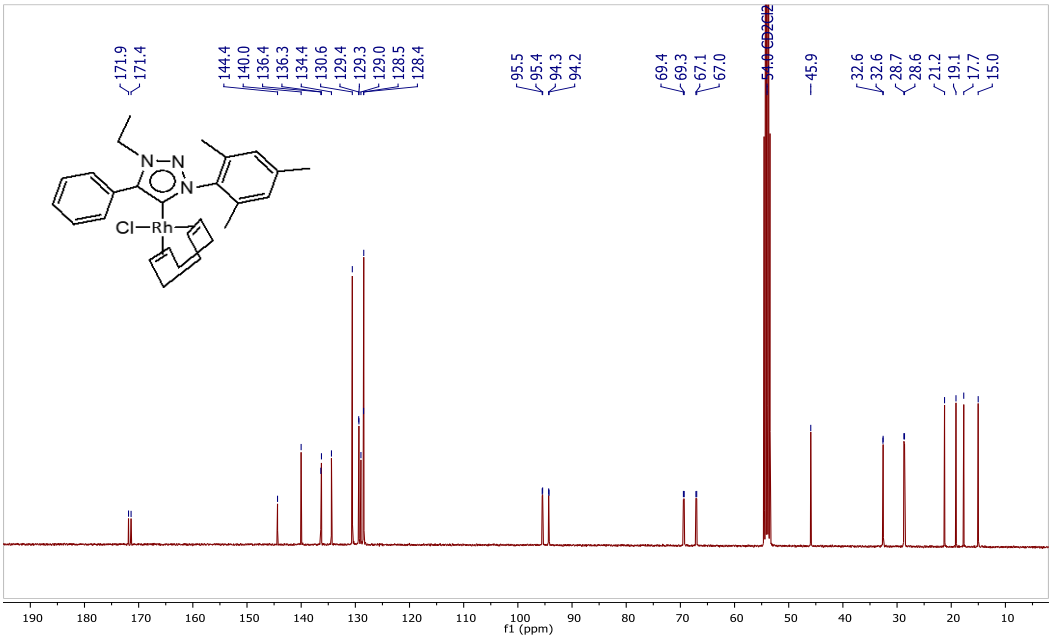

*Figure 3. 14: ^{13}C NMR of **5** in solvent CD_2Cl_2*

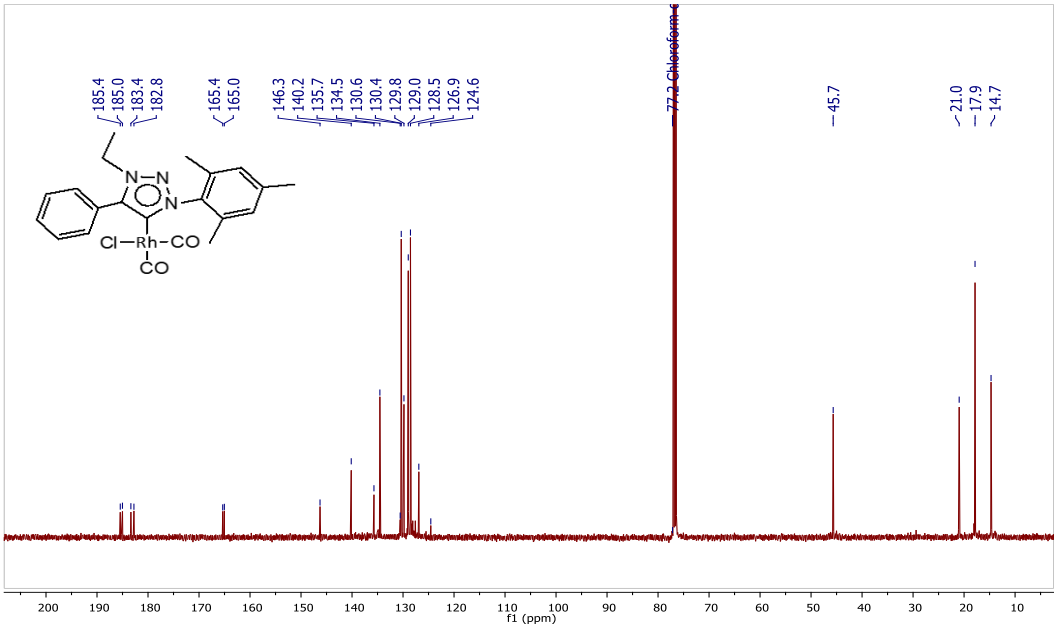

*Figure 3. 15: ^{13}C NMR spectrum of **6** in solvent $CDCl_3$*

Complex **6** displays characteristic doublets in the ^{13}C NMR at 185.6 ppm (J(RhC) = 54.5 Hz) and 183.5 ppm (J(RhC) = 75.4 Hz), where the CO *trans* to the carbene is further downfield with a smaller coupling constant due to the lesser donating ability of the carbene compared to the Cl ligand (a σ,π-donor). Furthermore, the carbene carbon resonance is shifted upfield as a result of the better π-accepting CO ligand compared to the cod. This corroborates the trends observed in our group for the Dipp analogue 185.9 ppm (J(RhC) = 54.1 Hz) for the CO trans to the carbene and 183.7 ppm (J(RhC) = 75.2 Hz) for the CO *cis* to the carbene.[15] The carbene signal of the dipp analogue was reported to be 165.2 ppm comparable to that obtained for **6** (165.6 ppm). An upfield $C_{carbene}$ signal shift is observed upon ligand exchange from cod to CO regardless of the metal as seen for complex **5** (171.6 Hz) and complex **6** (165.6 Hz); as well as for complex **7** (173.3 Hz) and complex **8** (166.8 Hz). This phenomenon is unusual considering the superior π-acidic nature of the CO ligand compared to the cod. However, the stronger σ-donor, π-acceptor CO ligands influence the $C_{carbene}$ to resonate more upfield than the cod which possesses a weaker π-donor olefinic bonding, compensated for by π-backdonation from the central metal.

Instead of doublets, complex **8** displays singlets 182.3 and 170.3 ppm representing the CO ligand *trans* to the carbene and the CO ligand trans to the Cl respectively. These are comparable to the signals reported by Albrecht (181.6 ppm for the CO trans to the carbene, 168.3 ppm for the CO *cis* to the carbene and 162.0 ppm for the carbene signal).[7] Although a significant difference is observed between the CO trans to the chloride ligand of **6** compared to **8**, similarities between the chemical shifts of the respective carbene signals (**6:** 165.6 ppm, **8**: 166.8 ppm) and the *trans* CO chemical shifts (**6:** 185.6 ppm, **8**: 182.3 ppm), show that the ligand effects are similar on metals of the same group.

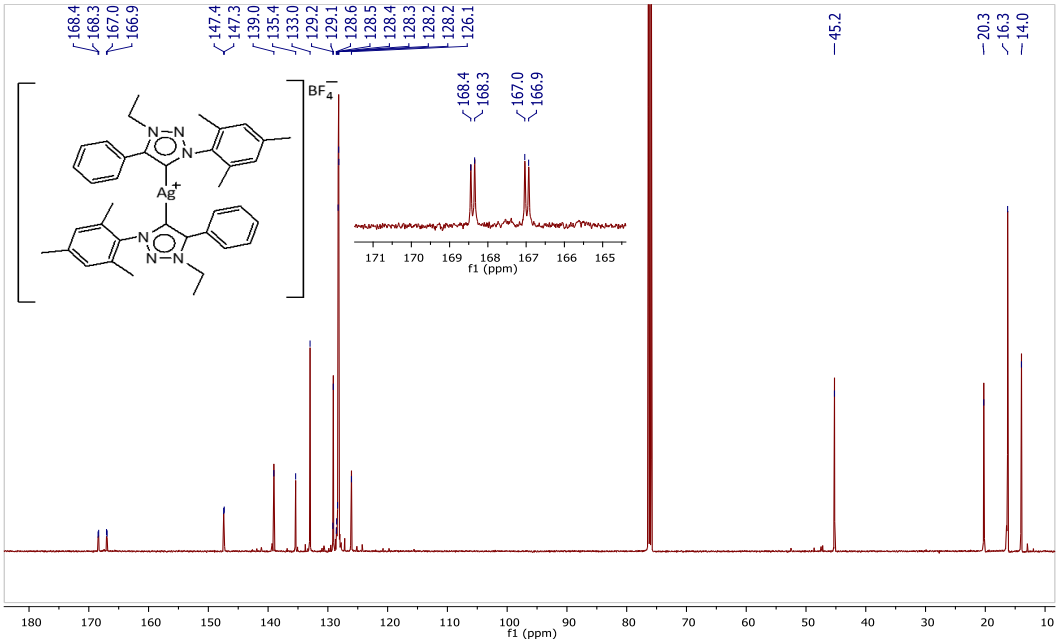

*Figure 3. 16: ^{13}C NMR spectrum of **S2** in solvent $CDCl_3$*

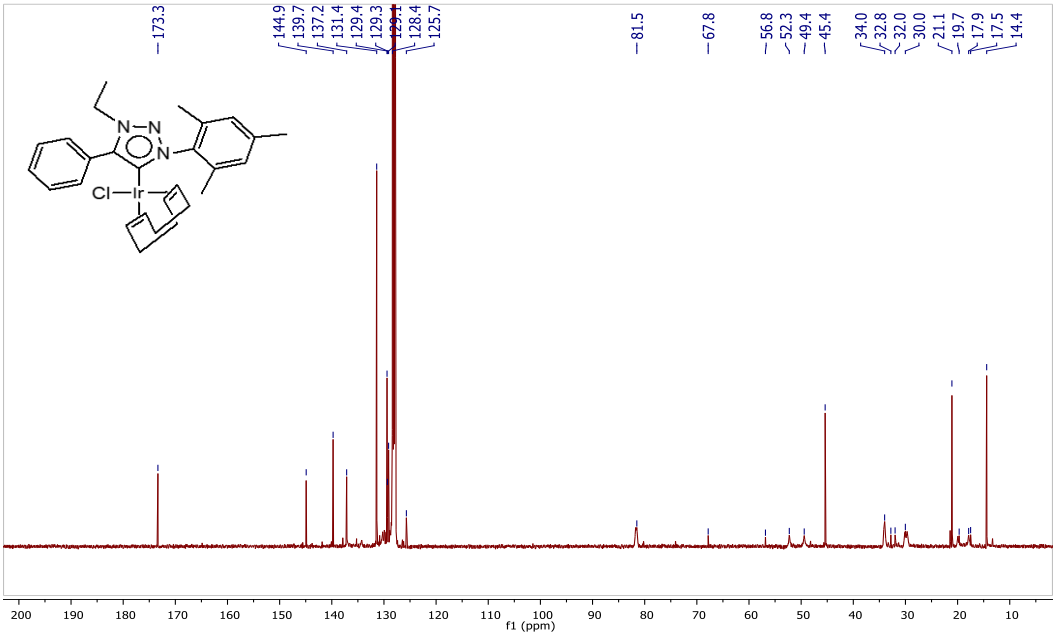

*Figure 3. 17: ^{13}C NMR spectrum of **7** in solvent:C_6D_6*

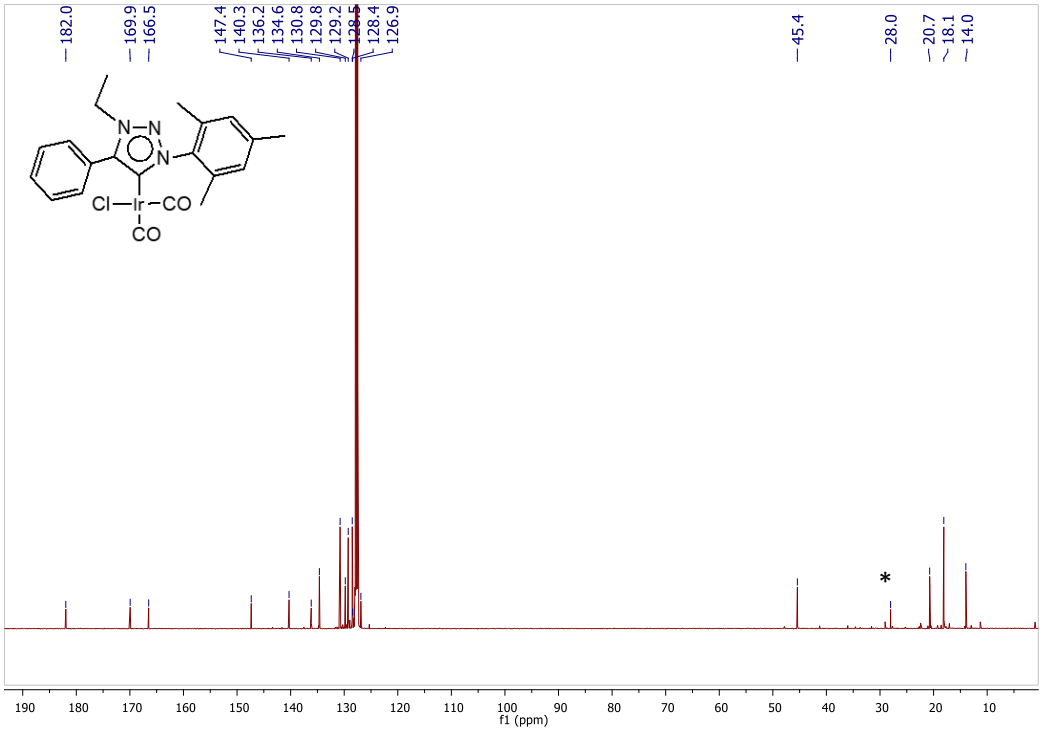

** toluene*

*Figure 3. 18: ^{13}C NMR spectrum of **8** in solvent C_6D_6*

3.3.2.3. Donor properties of the ligand L2[I]

(a) (b)

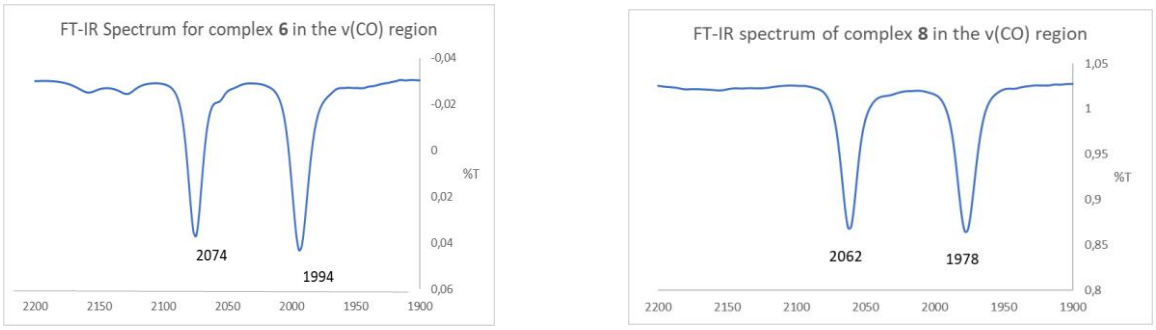

ν(cm^{-1}) ν(cm^{-1})

*Figure 3. 19: FT-IR spectra of complexes (a) **6** and (b) **8** obtained from the DCM solutions of **6** and **8**, respectively showing the ν(CO) region.*

The degree of electronic effects of the triazolylidene ligand was determined by the substitution of the labile diene ligand (cod) with a pair of CO ligands to obtain **6** from **5** and **8** from **7**.[34] The stretching frequencies of each of the CO ligands were obtained using infrared (FT-IR) spectroscopy (vide infra Figure 3.20). The average of the two CO infrared bands' wavenumbers was calculated and the linear regression model TEP = 0.8001ν_{av}(CO)Rh + 420 cm^{-1} was used to compute the TEP value of **6**, while TEP = 0.8475ν_{av}(CO)**Ir** + 336.2 cm^{-1} was used to compute the TEP of **8** (Table 3.1). The obtained TEP values of **6** (2047 cm^{-1}) and **8** (2048 cm^{-1}) are comparable. Furthermore, the TEP for **8** is comparable to what was obtained by Bertrand (L = 1-(2,6-diisopropylphenyl)-3-methyl-4-phenyl-1,2,3-triazol-5-ylidene), as well as by Albrecht (L = 1-ethyl-3-methyl-4-phenyl-1,2,3-triazol-5-ylidene) for [(L)Ir(CO)$_2$Cl].[6,7] The TEP obtained for **6** is also analogous with what has been previously reported by us for 1,2,3-triazolylidene ligands coordinated to rhodium (2047 cm^{-1}).[15] Therefore, the donor abilities of the triazolylidene ligand obtained from **L2** can be estimated by inspection of the TEPs calculated from either **6** or **8.** In addition, the ν_{av} obtained (Table 3.1) indicate enhanced donor ability compared to what has been previously reported for normal NHCs of type I (imadazol-2-ylidenes) and II (1,2,4-triazol-5-ylidenes) (Figure 3.3) ligands (2022-2031 cm^{-1}). Conversely, the donor strength of ligands of type III (imidazole-4-ylidenes) and IV (remote NHCs) (2002-2006 cm^{-1}) are superior to 1,2,3-triazol-5-ylidenes (type V).[6]

These observed trends are a consequence of the inductive effect of the heteroatoms flanking the carbene carbon. Furthermore, an increasing number of nitrogen atoms comprising the heterocycle results in decreasing donating ability of the carbene ligand. The type I and II carbenes are flanked by two nitrogen atoms, so therefore they are less donating than the aNHCs, with the type II carbene as the least donating of the two due to an increase in the inductive effect as a result of the additional heteroatom. The type V carbene is the least donating of the aNHCs, with the remote NHC being the best σ-donor as a result of the absence of an adjacent heteroatom.[6]

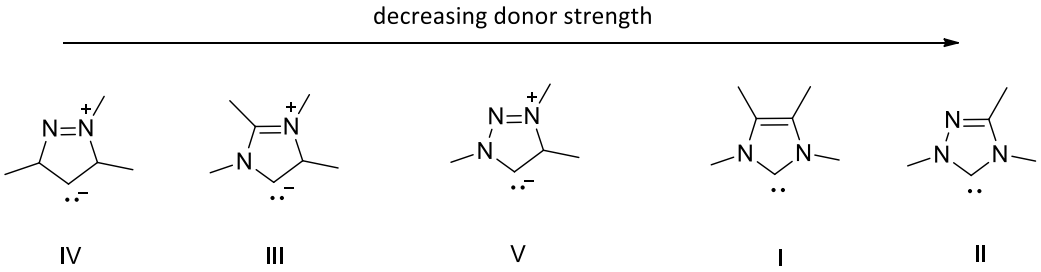

Figure 3. 20: Trends in the donor strength of normal NHCs (types I and II) and abnormal NHCs (type III-V).

3.3.3. Molecular structures of compounds L2, 5, and S2

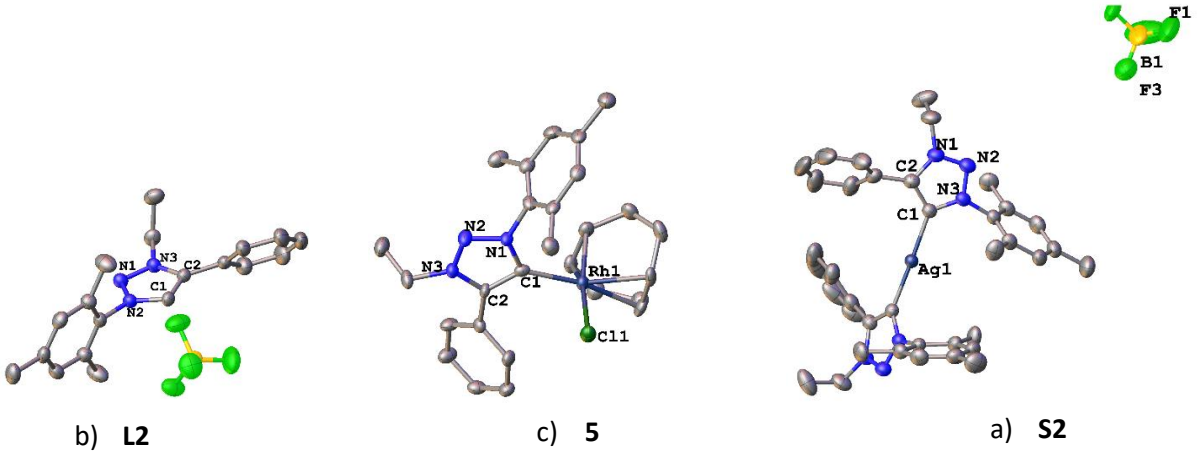

b) **L2** c) **5** a) **S2**

*Figure 3. 21: Molecular structures of compound **L2** and complexes **5** and **S2** showing thermal ellipsoids at 50 % probability. Hydrogen atoms are omitted for clarity, and a partial atom numbering scheme is included.*

The molecular structures of **L2**, **5** and **S2** were obtained from *n*-hexane layered DCM solutions of each compound. In the solid state, a planar arrangement of the heterocycle is deduced, confirmed by bond lengths that indicate delocalisation by their intermediary bond lengths (between single and double bond lengths), as observed for **L2**, **5** and **S2** (Table 3.2).[6] Although the aromatic substituents at N1 and C4 of the heterocycle also display planarity in compounds **L2**, **5** and **S2,** they are oriented perpendicular to the ring to reduce steric strain (Figure 3.21).[16,35] Upon coordination, a slight increase in the bond lengths of the heterocycle is observed from **L2** to **5** and from **L2** to **S2** (Table 3.2). This is an indication of the electron density being directed towards the metal centre from the heterocycle to forge a strong σ-bond. Prior to coordination, **L2** has a N–C_1–C_q bond angle of 105.6(2) ° becoming more acute upon co-ordination to a metal (**5,** 100.6(4)° and **S2**, 102.3(2)°), This is characteristic for type III-V carbenes,[5] and signifies the increase in σ-character of the carbene metal bond, compared to what is typically seen for the cationic triazolium salt precursor C–H bond.[24]

The rhodium – carbene carbon atom bond length of complex **5** is 2.029(4) Å, which is in agreement with what Albrecht observed for the first rhodium(I) 1,2,3-triazolylidene complex (2.027(6) Å).[5] Similar

trends are seen for other rhodium(I) 1,2,3-triazol-5-ylidene complexes reported by our group, with rhodium – carbene carbon bond lengths ranging from 2.017(2) to 2.079(4) Å.[15,36] Furthermore, a pseudo-square planar geometry is observed around the rhodium(I) metal centre of these aforementioned complexes[5,29,34] to yield a $C_{carbene}$–Rh–Cl bond angle of 91.72(12)° for **5**.

The $C_{carbene}$–Ag–$C_{carbene}$ (**S2**) displays linear coordination geometry with a characteristic bond angle of 178.13(14)°, comparable to the expected 180° for a linear complex. The slight deviation from linearity is presumed to be a direct consequence of the intramolecular steric hindrance of the mesityl groups, as seen in Figure 3.21c. Although no molecular structure data of the monodentate silver(I) 1,2,3-triazol-ylidene complex was reported by Crudden *et al*., the bidentate structure displayed comparable bond angles around each metal centre (173.9(3)°).[28] Ag–$C_{carbene}$ bond lengths were observed to be 2.076(3) Å for complex **S2**, tantamount to those obtained by Crudden 2.075(7) Å,[28] and to other silver(I) NHCs.[13]

*Table 3. 2: Selected bond lengths and bond angles obtained from the crystal structure data of **L2**, **5** and **S2**.*

Complex/compound	**L2**	**5**	**S2**
Bond Lengths (Å)			
^{c}M–$C_{carbene}$	–	2.029(4)	2.076(3)
(C1)Ccarbene–N1/3	1.356(3)	1.380(5)	1.369(3)
(C1) $C_{carbene}$–C_q	1.369(3)	1.396(6)	1.384(4)
N1–N2	1.320(2)	1.338(5)	1.335(3)
N2–N3	1.327(5)	1.328(5)	1.309(4)
N1/3–C_q	1.361(3)	1.363(5)	1.370(4)
^{c}M–Cl ($C1^{I}$)	–	2.3919(12)	2.076(3)
^{c}M–Y^{a}	–	2.088(4)	-
^{c}M–Y^{b}	–	2.2.85(4)	-
Bond Angles(°)			
$C_{carbene}$–^{c}M–Cl ($C_{carbene}$)	–	91.72(12)	178.13(14)
N–$C_{carbene}$–C_q	105.6(2)	100.6(4)	102.3(2)

^{a}Y = midpoint of C(20)-C(21). ^{b}Y = midpoint of C(24)-C(25). ^{c}M = Rh, Ag.

3.4. Conclusion

In summary, the CuAAC "click" reactions proved to be an efficient route to the preparation of the precursor triazole, as reasonable yields (up to 68%) of the 1-mesityl-4-phenyl-1,2,3-triazol were obtained. Subsequent alkylation yielded the cationic **L2**, with a bulky BF_4^- anion. The versatility of this ligand was examined by coordination to a range of transition metals i.e rhodium, silver and iridium. A variety of metalation techniques were applied to prepare complexes **5**-**8** from precursor **L2**. *In situ* deprotonation in the presence if $[Rh(cod)Cl]_2$ resulted in complex **5**, while direct metalation afforded **S2** both signalled by the disappearance of the acidic proton. **S2** was evidenced to be an exceptional carbene transfer agent during the transmetalation reaction to $[Ir(cod)Cl]_2$ to yield **7**. **5** and **7** were exposed to excess CO in a ligand substitution reaction to displace the cod-ligand, to afford the complexes with general formula $[(L)M(CO)_2Cl]$ (where M = Rh, Ir; L = 1,2,3-triazolylidene) which can be used to study the stretching frequencies of the carbonyl ligands and thus the donor properties of the ligand, L. The TEPs calculated from the modified formulae (dependent on the central metal in question) yielded, as expected, similar values for **5** and **8**, which are in line with that previously reported for other 1,2,3-triazol-5-ylidenes. All metal complexes **S2**, **5-8** are stable towards atmospheric conditions, and elevated temperatures (up to 80 °C, see experimental section). The single crystal X-ray diffraction studies of compounds **L2**, **5** and **S2** confirmed the molecular structure of these compounds.

3.5. Experimental data

3.5.1. Synthetic methods for the preparation of compounds L1-L2, S2, 5-8

3.5.1.1. Synthesis of 1-(2,4,6-trimethylphenyl)-4phenyl-triazole, **L1.**[9]

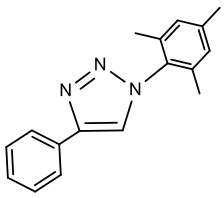

A 250 mL round bottomed flask was charged with mesityl-azide (2.34 g, 13.27 mmol) dissolved in THF (10 mL), then cooled to 0°C. Solutions of $CuSO_4.H_2O$ (3.32 g, 13.27 mmol) and sodium ascorbate (5.26 g, 26.54 mmol) in ^dH_2O (50 mL) were added respectively. The reaction mixture was left to stir overnight, while warming up to room temperature. The THF was evaporated, and the remaining solution was extracted in DCM:NH_4OH 1:1. The aqueous layer was washed with DCM (20 mL) and the organic layer was dried over $MgSO_4$ before gravity filtration, followed by concentration under vacuo to yield a pale yellow powder. The product was washed with cold *n*-hexane until off white, and dried overnight at 80°C under reduced pressure. Yield: 68%. M.P. 113-117°C. ^{1}H NMR (300 MHz, $CDCl_3$): δ 7.94 (dt, ^3J(HH) = 3.6 Hz, ^3J(HH) = 1.5 Hz, ^3J(HH) = 1.1 Hz, 2H, Ph-CH), 7.84 (s, 1H, trz-CH), 7.46 (dd, ^3J(HH) = 8.3 Hz, ^3J(HH) = 6.6 Hz, 2H, Ph-CH), 7.36 (dd, ^3J(HH) = 6.3 Hz, ^3J(HH) = 1.3 Hz, 1H, Ph-CH), 7.01 (s, 2H, Mes-CH), 2.37 (s, 3H, Mes-CH_3), 2.02(s, 6H, Mes-CH_3). ^{13}C NMR (75MHz, $CDCl_3$)δ 147.7 (Mes-C_q), 140.2 (Mes-C_q), 135.2 (Mes-C_q), 133.6 (Ph-C_q), 130.6 (trz-C_q), 129.2 (Mes-CH),129.0 (Ph-CH), 128.4 (Ph-CH), 125.9 (Ph-CH), 121.6 (trz-CH), 21.3 (Mes-CH_3), 17.5 (Mes-CH_3), 17.4 (Mes-CH_3). ESI-HRMS (15 V, positive mode, m/z): calcd for $[M]^+$: 574.2884. Found: 574.2893.

3.5.1.2. Synthesis of 3-ethyl-1-(2,4,6-trimethylphenyl)-4-phenyl-triazolium tetrafluoroborate, **L2.**[8]

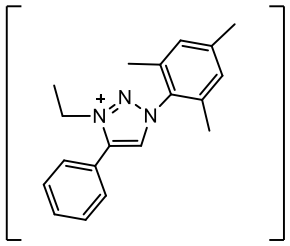

An oven dried Schlenk tube was purged with $N_{2(g)}$ before charging with **L1** (3.85 g, 14.64 mmol). Dried DCM (15 mL) was transferred to the vessel while stirring continuously and cooled to -30°C. Triethyloxonium tetrafluoroborate dissolved in DCM was then transferred to the solution of **L1**, then left to stir overnight while warming up to room temperature. The reaction mixture was then quenched with cold methanol, followed by the removal of solvent. The residue was filtered through an alumina plug, eluted with DCM:CH_3CN 1:1. Excess solvent was removed, and the residue was dissolved in ethyl acetate to yield clear crystals. The crystals were washed with cold diethyl ether, followed by *n*-hexane then dried overnight at 80°C under reduced pressure to yield an off-white powder. Yield:73% . M.P.(decomp): 114-116. ^{1}H NMR ^{1}H NMR (500 MHz, $CDCl_3$) δ 8.39 (s, 1H, trz-CH), 7.77 (d, ^3J(HH) = 6.4 Hz, 2H, Ph-CH), 7.63 – 7.48 (m, 3H, Ph-CH), 7.03 (s, 2H, mes-CH), 4.75 (q, ^3J(HH) = 7.2 Hz, 2H, NCH_2CH_3), 2.36 (s, 3H, mes-CH_3), 2.09 (s, 6H, mes-CH_3), 1.59 (t, ^3J(HH) = 7.2 Hz, 3H, NCH_2CH_3). ^{13}C NMR (75MHz, $CDCl_3$): δ 143.9(mes-C_q), 142.6(mes-C_q), 134.7(mes-C_q), 132.0(trz-CH), 131.6(trz-C_q), 130.1(Ph-CH), 130.0(Ph-CH) , 129.9(mes-CH), 121.7(Ph-C_q), 48.2(NCH_2CH_3) 21.3(mes-CH_3), 17.5 (mes-CH_3), 17.4 (mes-CH_3), 14.2(NCH_2CH_3). ^{19}F NMR (376 MHz, $CDCl_3$) δ 152.7 (d, ^1J(BF) = 19.8 Hz). ESI-HRMS (15 V, positive mode, m/z): calcd for [M-H_2O-H]+: 360.1844. Found: 360.142. ESI-HRMS (15 V, positive mode, m/z): calcd for [M]+: 292.1814. Found 292.180

3.5.1.3. Synthesis of 3-ethyl-1-mesityl-4-phenyl-1,2,3-triazol-5-ylidene chlorido-η^4-1,5-cyclooctadienerhodium(I), **5.**[11]

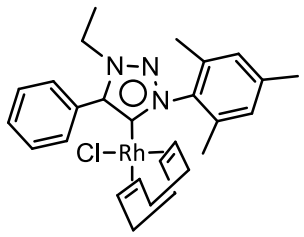

L2 (0.50 g, 1.32 mmol), $KN[Si(CH_3)_3]_2$ (0.31g, 1.58 mmol), and $[Rh(C_8H_{12})Cl]_2$ (0.33 g, 0.66 mmol) were transferred to an $Ar_{(g)}$ purged Schlenk tube, cooled to -78°C and dissolved in THF (40mL) while stirring incessantly. After an hour, the solution was allowed to warm up to room temperature and left to stir overnight. The volatiles were removed, and the residue washed with hexane and the product was extracted with toluene. The solvent was evaporated under reduced pressure, yielding a bright yellow solid which was dried overnight at 80°C under reduced pressure. Yield: 48%. MP(decomp): 187-192 °C ^{1}H NMR (400 MHz, CD_2Cl_2, -20°C): δ 8.09(d, ^3J(HH) = 7.4 Hz, 2H, Ph-CH), 7.58(m, 3H, Ph-CH), 7.09(s, 1H, mes-CH), 7.02(s, 1H, mes-CH), 4.64 (m, 1H, cod-CH), 4.40(m, 3H, cod-CH, NCH_2CH_3), 3.10(d, ^2J(HH) = 7.7 Hz, 1H, cod-CH), 3.03(d, ^2J(HH) = 7.5 Hz, 1H, cod-CH), 2.38(s, 3H, mes-CH_3), 2.33(s, 3H, mes-CH_3), 2.00(m, 2H, cod-CH_2), 1.88(s, 3H, mes-CH_3), 1.76(m, 2H, cod-CH_2), 1.56(m, 4H, cod-CH_2), 1.47(td, ^3J(HH) = 7.3, 1.8 Hz, NCH_2CH_3). ^{13}C NMR (100 MHz, CD_2Cl_2)δ 171.6 (d, ^1J(RhC) = 47.4 Hz, $C_{carbene}$), 144.4(trz-C_q), 140.0 (mes-C_q), 136.4 (mes-C_q), 136.3 (mes-C_q), 134.4(mes-C_q), 130.6(Ph-CH), 129.4(mes-CH), 129.3(mes-CH), 129.0(Ph-CH), 128.5(Ph-C_q), 128.4(Ph-CH),95.5(d, ^1J(RhC) = 7.5 Hz, cod-CH), 94.3(d, ^1J(RhC) = 7.2 Hz, cod-CH), 69.4(d, ^1J(RhC) = 14.5 Hz, cod-CH), 67.1(d, ^1J(RhC) = 14.5 Hz, cod-CH), 45.9(NCH_2CH_3), 32.6(d, ^1J(CC) =3.6 Hz, cod-CH_2), 28.7(d, ^1J(CC) = 11.8 Hz, cod-CH_2), 21.2(mes-CH_3), 19.1(mes-CH_3),17.7(mes-CH_3)

15.0($NCH_2\underline{CH_3}$). ESI-HRMS (15 V, positive mode, m/z): calcd for $[M\text{-}Cl+K]^+$: 541.4397 Found: 541.1260.). ESI-HRMS (15 V, positive mode, m/z): calcd for $[M\text{-}Cl]^+$: 502.1729. Found 502.1743.

3.5.1.4. Synthesis of 3-ethyl-1-mesityl-4-phenyl-1,2,3-triazol-5-ylidene chloridodicarbonyl rhodium(I), **6.**[5]

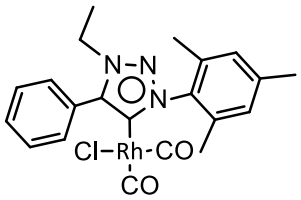

5 was dissolved in DCM (40mL) in an oven dried Schlenk tube. The solution was purged with $CO_{(g)}$ for 15 minutes, followed by the removal of DCM under reduced pressure. The resulting residue was washed with hexane, and dried overnight at 80°C under reduced pressure, yielding a dark yellow solid. Yield: 85%. MP(decomp): 183-185 °C. ^{1}H NMR (500 MHz, $CDCl_3$): δ 7.80(dd, ^3J(HH) = 7.5, 2.1 Hz, 2H, Ph-$\underline{CH}$), 7.55(dd, ^3J(HH) = 5.4, 1.9 Hz, 3H, Ph-$\underline{CH}$),7.03 (s, 2H, mes-$\underline{CH}$), 4.48(q, ^3J(HH) = 7.3 Hz, 2H, $N\underline{CH_2}CH_3$), 2.39(s, 3H, Mes-$\underline{CH_3}$), 2.16(s, 6H, mes-$\underline{CH_3}$), 1.54 (t, ^3J(HH) = 7.3 Hz, 3H, $NCH_2\underline{CH_3}$) . ^{13}C NMR (125 MHz, $CDCl_3$): δ 185.6(d, ^1J(RhC) = 54.5 Hz, CO), 183.5(d, ^1J(RhC) = 75.4 Hz, CO), 165.6 (d, ^1J(RhC) =40.1 Hz, $\underline{C_{carbene}}$), 146.7(d, ^2J(RhC) = 2.7 Hz, trz-$\underline{C_q}$), 140.6 (mes-$\underline{C_q}$), 136.1(mes-$\underline{C_q}$), 135.0(mes-$\underline{C_q}$), 130.8(Ph-$\underline{CH}$), 130.3(Ph-$\underline{C_q}$), 129.4(mes-$\underline{CH}$), 129.0(Ph-$\underline{CH}$), 127.3(Ph-$\underline{CH}$), 46.1 ($N\underline{CH_2}CH_3$), 21.4(mes-$\underline{CH_3}$), 18.3(mes-$\underline{CH_3}$), 15.2($NCH_2\underline{CH_3}$). IR (CH_2Cl_2, ν(CO), cm^{-1}):1994, 2074. ESI-HRMS (15 V, positive mode, m/z): calcd for [M+Na-2H]+: 506.7433 Found: 506.2530. ESI-HRMS (15 V, positive mode, m/z): calcd for $[M\text{-}Cl+H]^+$: 451.0762 Found: 451.0580.

3.5.1.5. Synthesis of bis(3-ethyl-1-mesityl-4-phenyl-1,2,3-triazol-5-ylidene) silver(I) tetrafluoroborate **S2**[5]

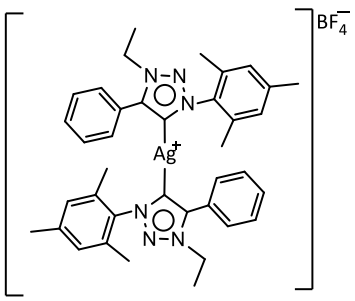

An $Ar_{(g)}$ purged Schlenk tube was charged with **L2** (0.50 g, 1.32 mmol), Ag_2O (1.22 g, 5.27 mmol), and KCl (0.59 g, 7.91 mmol) before being cooled to 0°C in the absence of light. Degassed CH_3CN (40 mL) was transferred into the vessel and the reaction mixture allowed to stir overnight, while warming up to room temperature. The volatiles were removed under reduced pressure, and the residue was washed with hexanes. The product was extracted in DCM, before the solvent was evaporated to yield a white solid, dried overnight under reduced pressure at 80°C. Yield 54%. MP(decomp): 185-189°C. ^{1}H NMR 500 MHz, $CDCl_3$ δ7.59 (p, ^3J(HH) = 3.8, 3.4 Hz, 4H, Ph-$\underline{CH}$), 7.54 (q, ^3J(HH) = 3.5 Hz, 6H, Ph-$\underline{CH}$), 6.99 (s, 4H,mes-$\underline{CH}$),4.53 (q, ^3J(HH) = 7.3 Hz, 4H, $\underline{NCH_2}CH_3$), 2.36 (s, 6H, mes-$\underline{CH_3}$), 2.02(s, 12H, mes-$\underline{CH_3}$). 1.56 (t, ^3J(HH) =7.4 Hz, 6H, $NCH_2\underline{CH_3}$). ^{13}C NMR (75MHz, $CDCl_3$) δ 167.7(dd, ^1J(AgC) = 177.6, 12.7 Hz, $\underline{C_{carbene}}$), 147.4(d, ^2J(AgC) = 12.9 Hz, trz-$\underline{C_q}$), 139.0 (mes-$\underline{C_q}$), 135.4(mes-$\underline{C_q}$), 133.0(mes-$\underline{C_q}$), 129.2(Ph-$\underline{C_q}$), 128.3 (Ph-$\underline{CH}$), 128.2(mes-$\underline{CH}$), 128.1(Ph-$\underline{CH}$), 126.0(Ph-$\underline{CH}$), 45.2($N\underline{CH_2}CH_3$), 20.3(mes-$\underline{CH_3}$), 16.3(mes-$\underline{CH_3}$), 14.0($NCH_2\underline{CH_3}$). 19F NMR: δ_F (CDCl3, 470.59 MHz): -153.5. ^{19}F NMR (376 MHz, $CDCl_3$) δ -153.47 (d, ^1J(BF) = 19.7 Hz). ESI-HRMS (15 V, positive mode, m/z): calcd for $[M+H]^+$: 803.2860 Found: 803.5470.

3.5.1.6. Synthesis of 3-ethyl-1-mesityl-4-phenyl-1,2,3-triazol-5-ylidene chlorido-η⁴-1,5-cyclooctadieneiridium(I), **7.**[5]

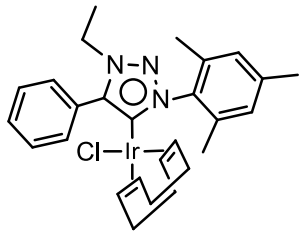

S2 (0.15 g, 0.19 mmol) and $[Ir(C_8H_{12})Cl]_2$ were transferred to an oven dried, Ar (g) purged Schlenk tube in the absence of light. DCM (40mL) was degassed and transferred into the reaction vessel, and the solution was left to stir for 4 days or until a precipitate was observed. After the removal of the solvent under reduced pressure, the product was extracted in *n*-hexane. The volatiles were evaporated, yielding a bright yellow solid. M.P.(decomp): 193-198°C. Yield 63%.^{1}H NMR (400 MHz, C_6D_6) δ 7.97 – 7.93 (m, 2H, Ph-C<u>H</u>), 7.28 – 7.21 (m, 2H, Ph-<u>CH</u>), 7.18 (dt, ^3J(HH) = 4.8, 1.9 Hz, 1H, Ph-<u>CH</u>), 6.76 (s, 2H, mes-<u>CH</u>), 4.91 (br s, 1H, cod-<u>CH</u>), 4.82 – 4.69 (br s, 1H, cod-<u>CH</u>), 3.60 – 3.46 (m, 2H, N<u>CH$_2$</u>CH$_3$), 3.07 (br s, 1H, cod-<u>CH</u>), 2.95 (br s, 1H, cod-<u>CH</u>), 2.71 (s, 2H, cod-<u>CH$_2$</u>), 2.06 (s, 3H, mes-<u>CH$_3$</u>), 2.00 – 1.79 (m, 7H, Mes-C<u>H$_3$</u>, cod-C<u>H$_2$</u>), 1.55-1.31 (m, 5H, cod-<u>CH$_2$</u>), 0.81 (t, ^2J = 7.3 Hz, 3H, NCH$_2$<u>CH$_3$</u>). ^{13}C NMR (101 MHz, C_6D_6)δ 173.3 (<u>C$_{carbene}$</u>), 144.9(trz-<u>C$_q$</u>), 139.7(mes-<u>C$_q$</u>), 137.1(mes-<u>C$_q$</u>), 131.4(Ph-<u>CH</u>), 129.4(mes-<u>CH</u>), 129.3(Ph-<u>CH</u>), 129.1(Ph-<u>CH</u>), 128.4(mes-<u>C$_q$</u>), 125.7(Ph-<u>C$_q$</u>), 81.3(cod-<u>CH$_2$</u>), 81.2(cod-<u>CH$_2$</u>), 52.0(cod-<u>CH</u>), 49.0(cod-<u>CH</u>), 45.0(N<u>CH$_2$</u>CH$_3$), 33.6(cod-<u>CH</u>), 30.0(cod-<u>CH</u>), 29.7(cod-<u>CH</u>), 21.1(mes-<u>CH$_3$</u>), 17.1(mes-<u>CH$_3$</u>),14.0(NCH$_2$<u>CH$_3$</u>). ESI-HRMS (15 V, positive mode, m/z): calcd for $[M+K]^+$: 642.1450 Found: 642.1623.

8.4.2. Synthesis of 3-ethyl-1-mesityl-4-phenyl-1,2,3-triazol-5-ylidene chloridodicarbonyl iridium(I), **8.**[5]

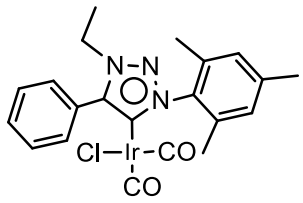

7 was dissolved in DCM (40mL) in an oven dried Schlenk tube. The solution was purged with CO (g) for 15 minutes, followed by the removal of DCM under reduced pressure. The resulting residue was washed with hexane, and dried overnight at 80°C under reduced pressure, yielding a yellow solid. Yield: 81%. M.P.(decomp): 184-186°C. ^{1}H NMR (400 MHz, C_6D_6): δ 7.66(dt, ^3J(HH) = 2.8, 1.5, 1.3 Hz, 2H, Ph-<u>CH</u>), 7.17(t, ^3J(HH) = 1.8 Hz, 1H, Ph-<u>CH</u>), 7.15-7.10 (m, 2H, Ph-<u>CH</u>), 6.73(s, 2H, Mes-<u>CH</u>), 3.54(q, ^3J(HH) = 7.3 Hz, 2H, N<u>CH$_2$</u>CH$_3$), 2.28(s, 6H, mes-<u>CH$_3$</u>), 2.02(s, 3H, mes-<u>CH$_3$</u>). ^{13}C NMR (75MHz, C_6D_6)δ 182.3(CO), 170.3(<u>CO</u>), 166.8 (<u>C$_{carbene}$</u>), 147.7(trz-<u>C$_q$</u>), 140.6(mes-<u>C$_q$</u>), 136.5(mes-<u>C$_q$</u>), 135.0(mes-<u>C$_q$</u>), 130.2(Ph-<u>C$_q$</u>), 129.6(mes-<u>CH$_3$</u>), 128.9(Ph-<u>CH</u>), 127.3(Ph-<u>CH</u>), 45.8(N<u>CH$_2$</u>CH$_3$), 21.1(mes-<u>CH$_3$</u>), 18.5(mes-<u>CH$_3$</u>), 14.4(NCH$_2$<u>CH$_3$</u>). (CH_2Cl_2, ν(CO), cm^{-1}):1978, 2062. ESI-HRMS (15 V, positive mode, m/z): calcd for $[M+Na]^+$: 556.0751 Found: 556.1020.

3.5.4 Molecular structural data of compounds L2, 5 and S2

Crystal Data for **L2**: $C_{19}H_{22}BF_4N_3$ (*M* =379.20 g/mol): monoclinic, space group $P2_1/c$ (no. 14), *a* = 20.3243(6) Å, *b* = 7.0742(3) Å, *c* = 13.9627(5) Å, *β* = 104.390(2)°, *V* = 1944.55(12) Å^3, *Z* = 4, *T* = 173.15 K, μ(MoKα) = 0.104 mm^{-1}, *Dcalc* = 1.295 g/cm^3, 15193 reflections measured (2.068° ≤ 2Θ ≤ 51.998°), 3823 unique (R_{int} = 0.0634, R_{sigma} = 0.0692) which were used in all calculations. The final R_1 was 0.0488 (I > 2σ(I)) and wR_2 was 0.1225 (all data).

Crystal Data for **5**: $C_{27}H_{33}ClN_3Rh$ (*M* =537.92 g/mol): monoclinic, space group $P2_1/c$ (no. 14), *a* = 7.8416(7) Å, *b* = 15.8217(13) Å, *c* = 19.8844(18) Å, *β* = 94.644(3)°, *V* = 2458.9(4) Å^3, *Z* = 4, *T* = 173.15 K, μ(MoKα) = 0.823 mm^{-1}, *Dcalc* = 1.453 g/cm^3, 23085 reflections measured (3.294° ≤ 2Θ ≤ 52°), 4841 unique (R_{int} = 0.1029, R_{sigma} = 0.0916) which were used in all calculations. The final R_1 was 0.0464 (I > 2σ(I)) and wR_2 was 0.0997 (all data).

Crystal Data for **S2:** for $C_{40}H_{46}AgBCl_4F_4N_6$ (*M* =947.31 g/mol): monoclinic, space group C2/c (no. 15), *a* = 17.6372(4) Å, *b* = 15.8542(4) Å, *c* = 15.9115(3) Å, *β* = 91.4780(10)°, *V* = 4447.75(17) Å^3, *Z* = 4, *T* = 173(2) K, μ(MoKα) = 0.746 mm^{-1}, *Dcalc* = 1.415 g/cm^3, 29630 reflections measured (3.454° ≤ 2Θ ≤ 56.822°), 5572 unique (R_{int} = 0.0387, R_{sigma} = 0.0283) which were used in all calculations. The final R_1 was 0.0471 (I > 2σ(I)) and wR_2 was 0.1390 (all data).

3.6. References

[1] S. Grüdemann, A. Kovacevic, M. Albrecht, J. W. Faller and R. H. Crabtree, *Chem. Commun.*, 2001, 2274–2275.
[2] T. Dröge and F. Glorius, *Angew. Chem. Intl. Ed.*, 2010, **49**, 6940–6952.
[3] A. Krüger and M. Albrecht, *Aust. J. of Chem.*, 2011, **64**, 1113–1117.
[4]Y. Han and H. V. Huynh, *Chem. Commun.*, 2007, 1089–1091.
[5] P. Mathew, A. Neels and M. Albrecht, *J.Am.Chem.Soc.*, 2008, **130**, 13534-13535.
[6] (a) E. Aldeco-Perez, A. J. Rosenthal, B. Donnadieu, P. Parameswaran, G. Frenking and G. Bertrand, *Science*, 2009, **326**, 556–559. (b) 1 J. D. Crowley, D. A. Lee and K. J. K. A, *Aust. J. Chem*., 2011, **64**, 1118–1132.
[7] G. Guisado-Barrios, J. Bouffard, B. Donnadieu and G. Bertrand, *Angew. Chem. Intl. Ed.*, 2010, **49**, 4759–4762.
[8] G. Guisado-Barrios, M. Soleilhavoup and G. Bertrand, *Acc. Chem. Res.*, 2018, **51**, 3236–3244.
[9] (a)K. Barral, A. D. Moorhouse and J. E. Moses, *Org*. 2007, 3567–3569. (b) Tornøe, C. W.; Christensen, C.; Meldal, M. *J. Org. Chem.* 2002, ***67*,** 3057-3064. (c) Rostovtsev, V. V.; Green, L. G.; Fokin, V. V.; Sharpless, K. B. *Angew. Chem.*, *Int. Ed*. 2002, ***41***, 2596-2599.
[10] H. K.-W. Hul and H. Shechter, *Thermolysis and photolysis of 4-diazo-1,2,3-triazoles in benzenoid solvents, systems which reveal decomposition of diazo compounds to carbenes to diazo compounds to carbenes*, 1982, vol. 23.
[11] K. J. Kilpin, U. S. D. Paul, A. L. Lee and J. D. Crowley, *Chem. Commun.*, 2011, **47**, 328–330.
[12] L. N. Appelhans, D. Zuccaccia, A. Kovacevic, A. R. Chianese, J. R. Miecznikowski, A. Macchioni, E. Clot, O. Eisenstein and R. H. Crabtree, *J. Am. Chem. Soc.*, 2005, **127**, 16299–16311.
[13] S. Hohloch, D. Scheiffele and B. Sarkar, *Eur. J. Inorg. Chem.*, 2013, 3956–3965.
[14] T. Karthikeyan and S. Sankararaman, *Tetrahedron Lett.*, 2009, **50**, 5834–5837.
[15] T. Nakamura, K. Ogata, S.-i. Fukuzawa, *Chem. Lett.* 2010, ***39***, 920.
[16] K. J. Kilpin, U. S. D. Paul, A.-L. Lee, J. D. Crowley, *Chem. Commun. (Camb.)* 2010, ***47***, 328.
[17] T. Nakamura, T. Terashima, K. Ogata, S.-i. Fukuzawa, *Org. Lett.* 2011, ***13***, 620.
[18] S. Dı´ez-Gonza´lez, A. Correa, L. Cavallo, S. P. Nolan, *Chemistry* 2006, ***12***, 7558.
[19] R. Lalrempuia, N. D. McDaniel, H. Mueller-Bunz, S. Bernhard, M. Albrecht, *Angew. Chem. Int. Ed.* 2010, ***49***, 9765.
[20] D. Aucamp, T. Witteler, F. Dielmann, S. Siangwata, D. C. Liles, G. S. Smith and D. I. Bezuidenhout, *Eur. J. Inorg. Chem.*, 2017, **2017**, 1227-1236.
[21] M. van der Meer, E. Glais, I. Siewert and B. Sarkar, *Angewandte Chemie*, 2015, **127**, 13997–14000.
[22] (a) M. Baltrun, F. A. Watt, R. Schoch, C. Wölper, A. G. Neubba, S. Hohloch, S. *Dalton Trans.*, 2019, **48**, 14611–14625.
[23] P. L. Arnold and S. Pearson, *Coord. Chem. Rev.*, 2007, 251, 596–609.
[24] A. R. Chianese, A. Kovacevic, B. M. Zeglis, J. W. Faller and R. H. Crabtree, 2004, 2461–2468.
[25] *(a)* J. Arduengo, H. V. R. Dias, J. C. Calabrese and F. Davidson, *Homoleptic Carbene-Silver(1) and Carbene-Copper(1) Complexes*, 1993, vol. 12. *(b)* H. M. J. Wang and I. J. B. Lin, *Facile Synthesis of Silver(I)-Carbene Complexes. Useful Carbene Transfer Agents*, 1998. *(c)* M. Iglesias, D. J. Beetstra, J. C. Knight, L. L. Ooi, A. Stasch, S. Coles, L. Male, M. B. Hursthouse, K. J. Cavell, A. Dervisi and I. A. Fallis, *Organometallics*, 2008, **27**, 3279–3289.
[26] Wei Zhua and Dawei Ma. *Chem. Commun.,* 2004, 888–889.
[27] D. Canseco-Gonzalez, A. Gniewek, M. Szulmanowicz, H. Müller-Bunz, A. M. Trzeciak, M. Albrecht, *Chem. Eur. J.* **2012**, *18*, 6055.
[28] D. Aucamp, T. Witteler, F. Dielmann, S. Siangwata, D. C. Liles, G. S. Smith and D. I. Bezuidenhout, *Eur. J. Inorg. Chem.*, 2017, **2017**, 1227-1236.
[29] E. C. Keske, O. V. Zenkina, R. Wang, C. M. Crudden, *Organometallics*, 2012, **31**, 456 – 461.
[30] D. Aucamp, MSc Chemistry, University of Pretoria, 2016.
[31] G. Kleinhans, MSc Chemistry, University of Pretoria, 2014.
[32] A. F. Dupont and A. Foris, On ^{19}F NMR Spectra of BF_2 and BF Complexes and Related Compounds, DOI:10.13140/RG.2.2.30488.60160.
[33] A. Poulain, D. Canseco-Gonzalez, R. Hynes-Roche, H. Müller-Bunz, O. Schuster, H. Stoeckli-Evans, A. Neels and M. Albrecht, *Organometallics*, 2011, **30**, 1021–1029.
[34] a) A. R. Chianese, X. Li, M. C. Janzen, J. W. Faller, R. H. Crabtree and W. A., *J. Organomet*., 2003, 1663–1667. (b) R. A. K. Iii, H. Clavier, S. Giudice, N. M. Scott, E. D. Stevens, J. Bordner, I. Samardjiev, C. D. Hoff, L. Cavallo and S. P. Nolan, *Organometallics*., 2008, 202–210.

[35] H. K.-W. Hul and H. Shechter, *Thermolysis and photolysis of 4-diazo-1,2,3-triazoles in benzenoid solvents, systems which reveal decomposition of diazo compounds to carbenes to diazo compounds to carbenes*, 1982, vol. 23.
[36] I. Strydom, G. Guisado-Barrios, I. Fernández, D. C. Liles, E. Peris and D. I. Bezuidenhout, *Chem. Eur.*, 2017, **23**, 1393–1401.

Chapter 4: The preparation and characterisation of 1,3-Diarylated mesoionic carbene complexes of Rh(I) and Ir(I)

4.1. Background

Although N-heterocyclic carbene (NHC) complexes have been known for decades prior, the isolation of the free carbene was unheard of until Arduengo and co-workers isolated and unequivocally characterized the imidazole-2-ylidene in 1991[1] A few years later, enthused by the work of Albrecht, Bertrand and co-workers began the work of isolating the first free *a*NHC (Figure 4.1), which was then termed mesoionic as all its resonance structures cannot be drawn without a charge. Following on the success of this isolation, 1,2,3-triazolylidenes began to attract attention about a decade after the discovery of the first *abnormal* N-heterocyclic carbene (*a*NHC).[2] Not only were they regarded as superior to phosphines as tunable ligands on transition metals for catalytic reactions,[3] they were also found to be better σ-donors than their counterparts, the Arduengo-type NHC ligands.

Conversely to the finding of increased basicity, the absence of a second heteroatom adjacent to the carbene carbon atom was found to reduce the stability of the free carbene. The inclusion of more heteroatoms in the heterocycle at remote positions lead to the birth of the triazolylidene.[4] However, an increase in the number of heteroatoms occasions a decrease in donor strength, due to the inductive effect of the nitrogen atoms pulling electron density away from the carbene carbon.[5] Although inferior donors compared to imidazol-5-ylidene ligands, 1,2,3-triazol-5-ylidene ligands remain superior to imidazole-2-ylidenes in donor strength. [4]

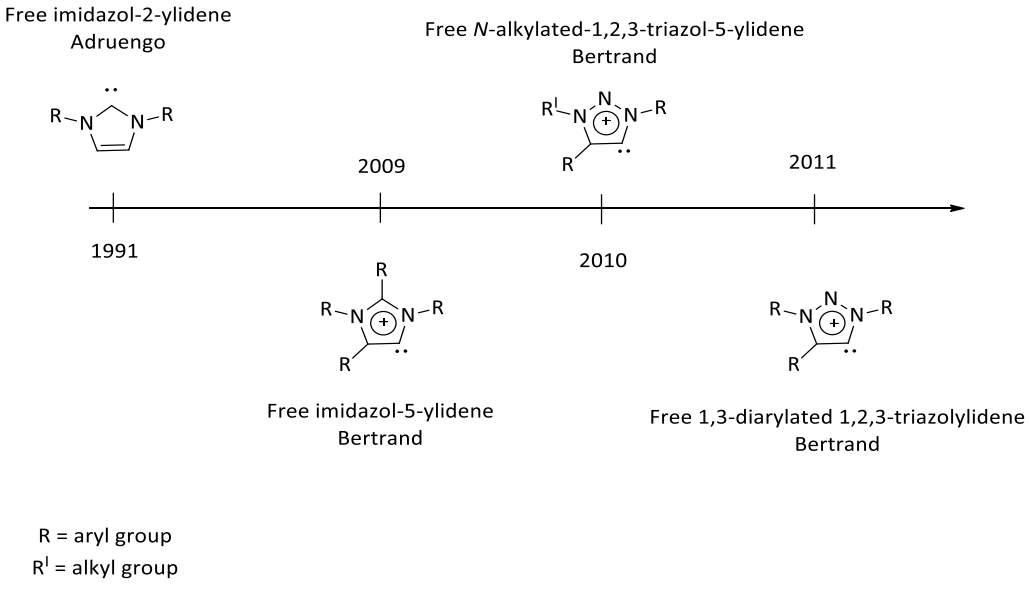

Figure 4. 1: A timeline of the isolation of the first type I, III and V free carbenes (see chapter 3 for carbene types).

For the past decade, free 1,2,3-triazol-5-ylidene ligands were known to decompose under thermal conditions in benzene as a solvent, into α-diazonitriles and ultimately into α-cyanocarbenes.[6] To circumvent this, and to exploit the regioselectivity of the copper-catalyzed click reaction, together with prior knowledge of steric bulk as a way to stabilize the intended free carbene, Bertrand designed an N3-alkylated ligand with aryl groups at the N1 and the C4 position. Furthermore, the substitution of the C2 carbon with a third heteroatom, eliminates the need to protect this position, and directs deprotonation to C5. With the aid of a non-nucleophilic base, the first free 1,2,3-triazol-5-ylidene was isolated and found to remain stable under inert conditions at a temperature of -30°C for numerous days. Upon heating in benzene, migration of the methyl group from position N3 to C5 was observed, but not in the case for the bulkier, more nucleophilic isopropyl analogue.[7] This limited the stability of these free mesoionic carbenes (MICs), and was speculated to be the pretext for failed attempts of earlier coordination reactions of the alkylated MIC to ruthenium. This prompted an investigation into the preparation and isolation of the free 1,3,4-triarylated-1,2,3-triazol-5-ylidene.[2]

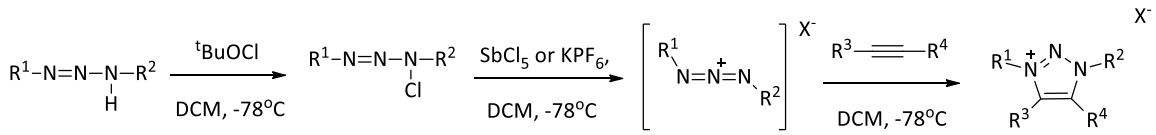

a **b** **c** **d**

R^1, R^2 = aryl
R^3, R^4 = H, alkyl or aryl
X^- = PF_6, $SbCl_6$

Scheme 4. 1: The stepwise formation of 1,3-diarylated triazolium salt as reported by Jochims et al.[9]

The copper-catalysed "click" reaction is high yielding, versatile and offers a range 1,4-disubstituted triazoles, provided the aim is to selectively alkylate the N3 position.[8] However, this synthetic route does not facilitate arylation at N3, therefore prompting the search for an alternative route. Bertrand and co-workers investigated this cycloaddition reaction (Scheme 4.1),[9] preparing **a** from an amalgamation of literature procedures[10] prior to the one-pot cycloaddition reaction. It was confirmed that a wide range of 1,3-diarylated triazolium salts can be accessed with yields ranging from 95-22% (depending the identity of the R^1-R^4 substituent) without the use of a copper catalyst, with an electron rich or poor alkyne (or enzymes) fulfilling the desired steric demands.[2]

Deprotonation reactions were carried out on the 1,3-diaryalated triazolium salts obtained from cycloaddition reactions with terminal alkynes using a potassium base to yield the corresponding free MIC (Scheme 4.2). The additional aryl group eliminates several decomposition pathways, including the migration of the N3 substituent at 50°C in benzene. Moreover, **e** is kinetically stable under air and moisture free conditions, with a lifespan of a number of weeks. This marked the isolation and unequivocal characterisation of the first free 1,3-diarylated1,2,3-triazol-5-yidene, which was successfully coordinated to iridium, to examine the ligands' donor ability, as well as to ruthenium to examine catalytic activity.[6]

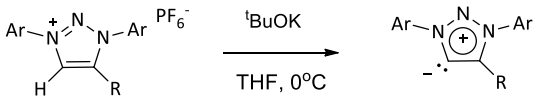

d **e**

Ar = Dipp, Mes
R = Dipp, Mes, Ph, Tipp, ^{t}Bu, Cy, OEt

*Scheme 4. 2: Preparation of free 1,3-diarylated-1,2,3-triazol-5-ylidenes, **e** from **d**.*[2]

Following the coordination of the triazol-5-ylidene to the ruthenium metal centre, the significance of the precatalyst ligands' sterics to the initiation of the olefin metathesis reactions as suggested previously by Grubbs was identified,[11] however a qualitative model illustrating this could not be obtained.[2] Although stable in the solid state, upon exposure to oxygen the decomposition of these ruthenium complexes was observed in solution. Nonetheless, these complexes were observed to be active at room temperature in ring-opening metathesis reactions.[5] To further understand the ligand effects of the triarylated triazolylidene, in 2015 Bertrand coordinated this free carbene to gold(I) resulting in catalysts with excellent activity in hydroamination reactions[12]

In 2017, our laboratory prepared the C4 ferrocenyl-substituted triarylated triazolylidene from the cycloaddition of 1,3-diisopropylphenyl-2-azoniaallene salt and the ferrocenyl alkyne. This transition metal-containing carbene was coordinated to rhodium, and the catalytic activity of this ligand in hydroformylation reactions was examined and compared to its N3-alkylated counterpart. Better conversions were observed for the N3-alkylated triazolylidene complex, however the bulkier N3-arylated complex displayed better selectivity towards the more industrially relevant linear aldehyde formation. Furthermore, the ferrocenyl moiety was subjected to chemical oxidation, resulting in enhanced conversions and reduced selectivity, thus corroborating the effect of the ligand's steric and electronic properties on the activity of the catalyst precursor and paving the way towards redox-switchable catalysts.[13]

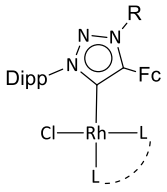

f

Dipp = 2,6-diisopropylphenyl
R = Dipp, Ethyl
Fc = ferrocenyl
LL = cod, CO

Figure 4. 2: 1,3-Diarylated ferrocenyl substituted 1,2,3-triazolylidene rhodium(I) complexes.[13]

4.2. Aim and objectives

4.2.1. Aim

Bertrand *et al*. prepared a series of protic triarylated triazolium salts for subsequent deprotonation by a non-nucleophilic base to access the corresponding free carbene. Although the copper-catalysed azide alkyne cycloaddition (CuAAC) or the "click" reaction displayed versatility and selectivity towards to the 1,4-disubstituted isomer of the triazole, limitations regarding the N3 functionalisation prompted Bertrand to consider alternative cycloaddition reactions. N3-alrylation became accessible through a modified rendition of the click reaction, whereby a 1,3-arylated 2-azoniaallene salt was reacted with a terminal aryl alkyne in the absence of a copper catalyst at low temperatures.[9] One of the triazolium salts prepared, was the cationic 1,3-bis(2,6-diisopropylphenyl)-4-phenyl-1,2,3-triazolium salt stabilized by a PF_6^- counterion, with an impressive yield of between 94 and 95%. The salt was treated with a base resulting in the corresponding free carbene at a 90% yield.[2]

To study the effect of the additional steric bulk, and the electronic effect of the additional aryl group, a diarylated ligand will be prepared following the method proposed by Bertrand. This will be followed by coordination to a transition group metals, for comparison to their N-alkylated counterparts in hydroformylation reactions.

4.2.2. Objectives

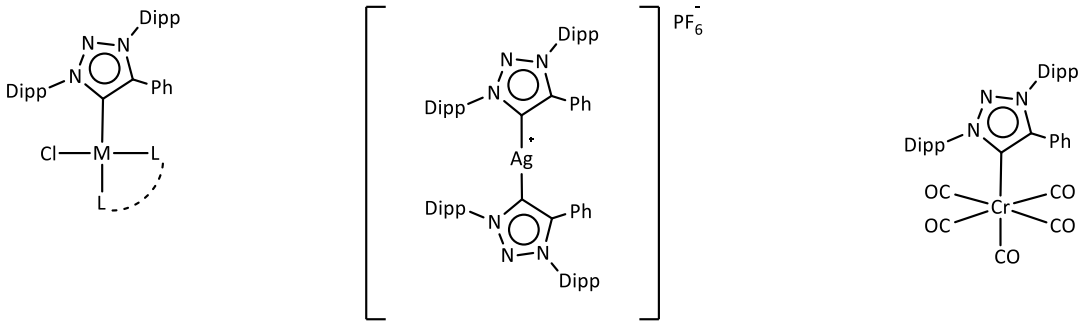

9 M = Rh, LL = cod
10 M = Rh, LL = $(CO)_2$
11 M = Ir, LL = cod
12 M = Ir, LL = $(CO)_2$
cod = 1,5-cyclooctadiene
Dipp = 2,6-diisopropylphenyl

S3

S4

*Figure 4. 3: Complexes **S3-S4, 9-12** to be prepared from a 1,3,4-triarylated-1,2,3-triazolium salt.*

As aforementioned, the free carbene was previously coordinated to ruthenium for application in olefin metathesis reactions, as well as to gold for hydroamination reactions. To further study its coordination versatility, and ultimately, its utility in molecular catalytic applications, this ligand will be coordinated to rhodium(I), silver(I), iridium(I) and chromium(0). The free carbene route will be examined for coordination to rhodium as well as to chromium, where *in situ* deprotonation and complexation will occur with regards to the rhodium and separate deprotonation will commence in the case of the chromium. Direct metalation of the salt will be carried out using Ag_2O to yield complex **S3,** a carbene

transfer agent which will participate in a transmetalation reaction with iridium. Once more, the donor properties of this ligand will be assessed using Tolman's Electronic Parameter (TEP) values obtained from the FT-IR carbonyl stretching frequencies of the metal complex. For this reason, complexes **9** and **11** will be subjected to ligand substitution reactions, where the 1,5-cyclooctadiene (cod) ligand will be replaced with carbonyl ligands to yield **10** and **12** (Figure 4.3).

4.3. Results and discussion

Herein, the preparation of metal complexes **S3-S4, 9-12** will be described following metalation techniques previously considered in chapter 3, from the triazolium salt **L3** as detailed in the experimental section (section 4.5). These complexes are to be spectroscopically characterised to draw informed conclusions regarding the electronic and steric properties of this ligand. To substantiate the resultant findings, the molecular structures obtained for complexes **S3-S4**, **9-12** will be evaluated against data obtained in the previous chapter, as well as in literature.

4.3.1. Preparation of compounds L3, S3-S4, 9-12

Following the method described by Jochims, a DCM solution of **A**, ^{t}BuOCl, KPF_6 and phenylacetylene was cooled to -78°C in the dark and left to stir overnight while warming up to room temperature. The resultant precipitate was washed with Et_2O followed by hexane to yield 69% of **L3** (Scheme 4.3)**.**[6,9] Under inert conditions, **L3** was treated with KHMDS in the presence $[Rh(cod)Cl]_2$ at a temperature of -78°C, left to stir overnight while warming up to room temperature and the volatiles removed under *vacuo*. The residue was washed with hexanes and **13** was extracted in toluene with a yield of 62%. The same precursor salt **L3**, AgO_2 and KCl were cooled to 0°C and dissolved in CH_3CN in the absence of light and left to stir incessantly overnight, while warming up to room temperature. The residue was washed with Et_2O and extracted in DCM yielding 43% of **S3.** Target complex **11** was isolated with a 67% yield from a transmetalation reaction between **S3** and $[Ir(cod)Cl]_2$ in DCM in the dark, and the product subsequently extracted from the reaction residue in hexanes.

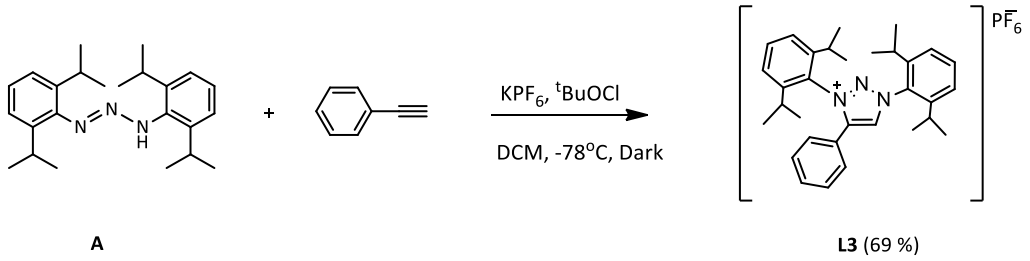

*Scheme 4. 3: The [3+2] cycloaddition reaction to yield the diarylated triazolium salt, **L3.***

The donor strength of a ligand is typically determined by the displacement of the labile bidentate cod ligand with more π-acidic CO ligands to be used as FT-IR probes.[14] Therefore complexes **9** and **11** were individually dissolved in DCM at room temperature, before allowing CO(g) to pass through each

solution for 20 minutes. Both solutions underwent solvent removal under reduced pressure, before washing with hexanes, affording **10** and **12** with yields of 92% and 87% respectively (Scheme 4.4).

The preparation of **S4** proceeded as previously reported by Herrmann and co-workers.[15] $Cr(CO)_6$ was suspended in THF at room temperature and photolyzed overnight while stirring. Separately, **L3** and KHMDS were dissolved in THF at -10°C and allowed to warm up to room temperature. The photolyzed chromium complex was transferred into the free carbene reaction mixture and left to stir overnight. Once the volatiles were removed, **S4** was extracted in hexanes and isolated with a yield of 41% (Scheme 4.5).

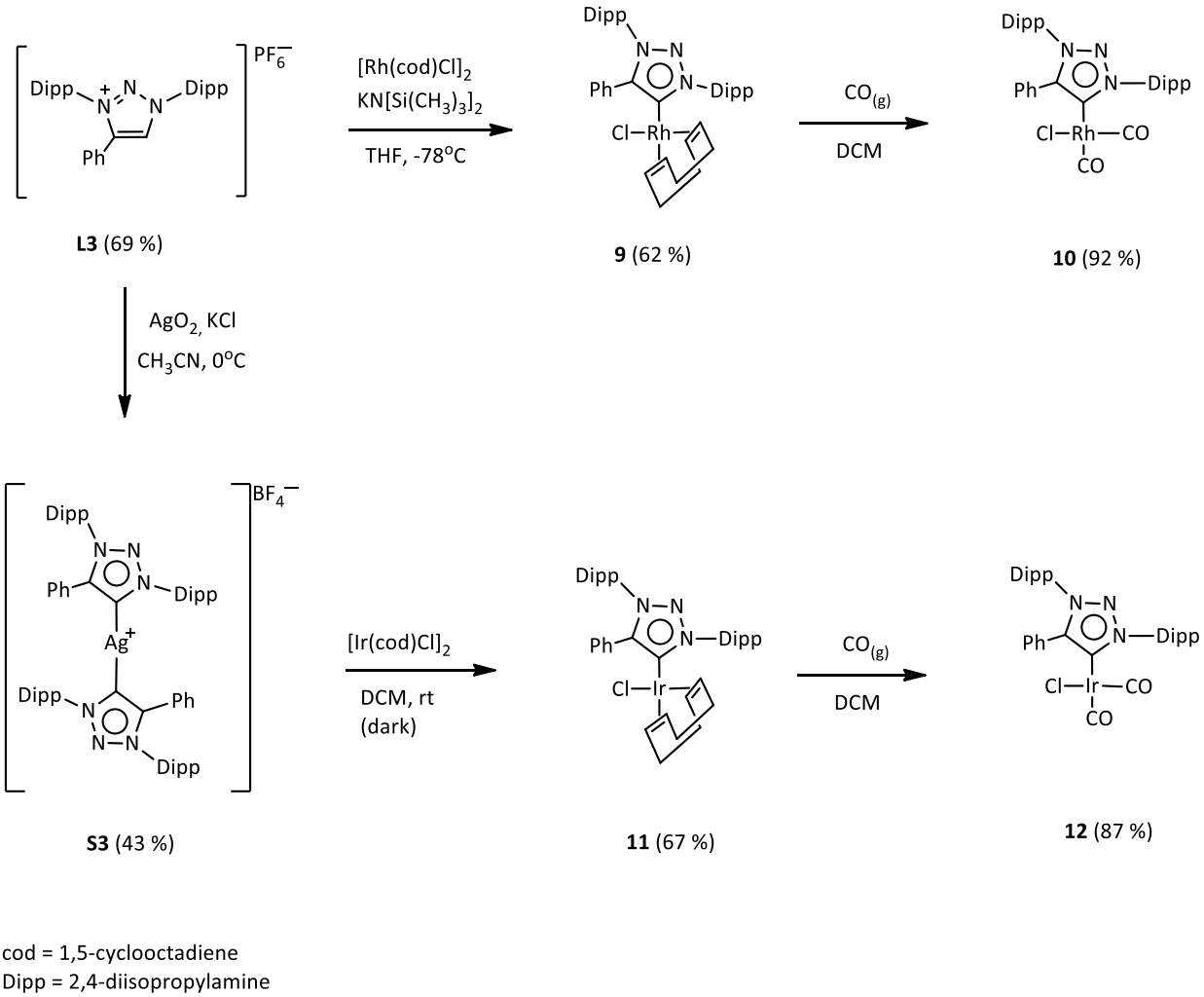

cod = 1,5-cyclooctadiene
Dipp = 2,4-diisopropylamine

*Scheme 4. 4: The Synthetic approach employed for the preparation of complexes **S3, 9-12.***

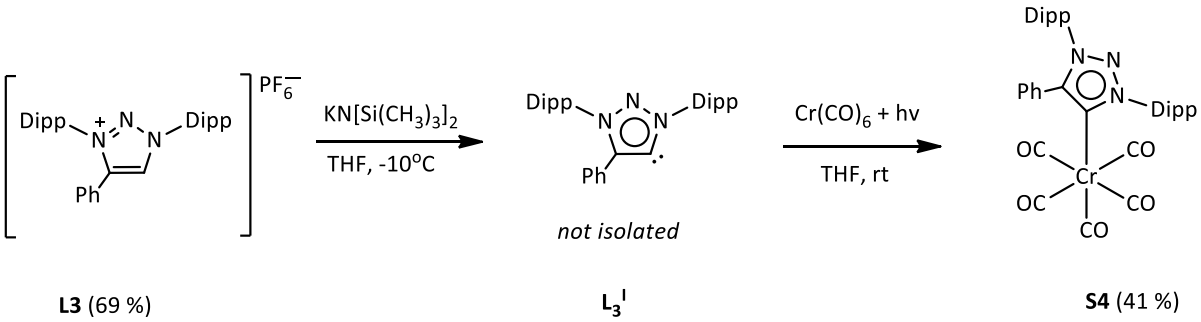

L3 (69 %) L_3^I **S4** (41 %)

Dipp = 2,6-diisopropylphenyl

*Scheme 4. 5: Synthesis of complex **S4** by coordination of the free carbene to the THF-substituted chromium pentacarbonyl.*

4.3.2. Spectroscopic analysis of compounds L3, S3-S4 and 9-12

4.3.2.1. Confirmation of the formation of L3, S3-S4 and 9-12 by ^{1}H-NMR

The triazolium salt **L3** formation was confirmed by ^{1}H, ^{13}C, ^{19}F and ^{31}P NMR spectroscopy (Figure 4.4 – 4.5). The ^{1}H NMR spectrum of **L3** shows the acidic triazol-CH proton is observed at 9.38 ppm. The presence of the counterion is confirmed by ^{19}F and ^{31}P NMR, where a doublet is observed in the ^{19}F due to the equivalent fluorine atoms coupling with the NMR active phosphorous. Similarly, the ^{31}P NMR spectrum splits into a septet, where the phosphorous couples with each NMR active fluorine nucleus.

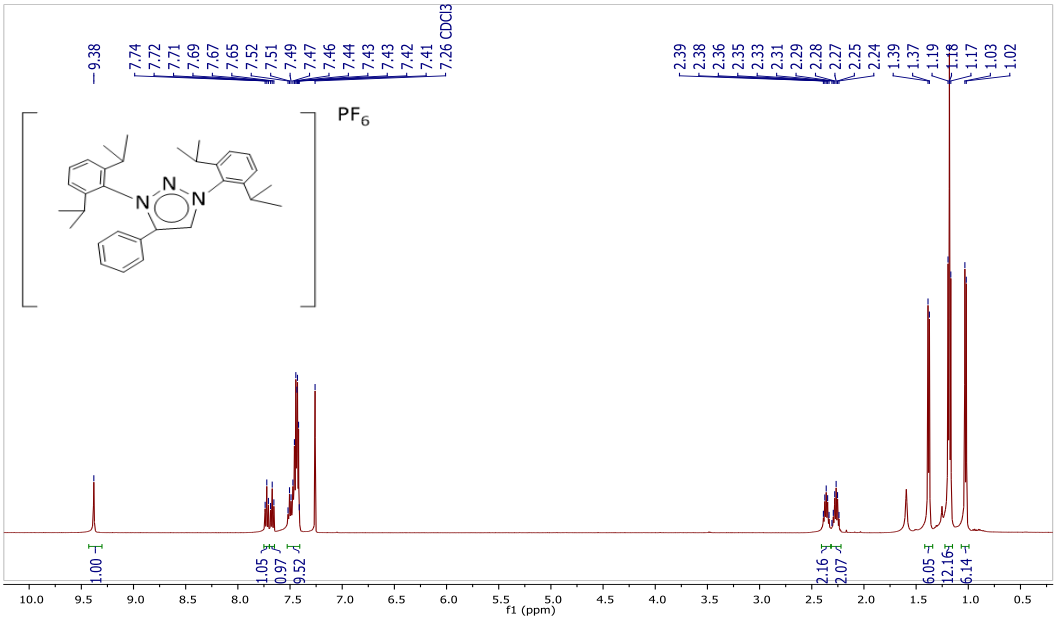

*Figure 4. 4: ^{1}H NMR spectrum of **L3** in solvent $CDCl_3$*

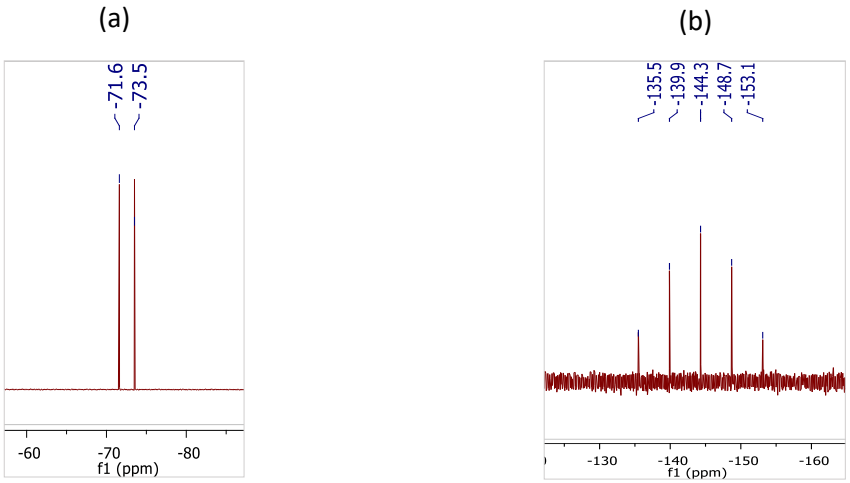

*Figure 4. 5: (a) ^{19}F NMR spectrum of **L3** in $CDCl_3$. (b) ^{31}P NMR spectrum of **L3** in $CDCl_3$.*

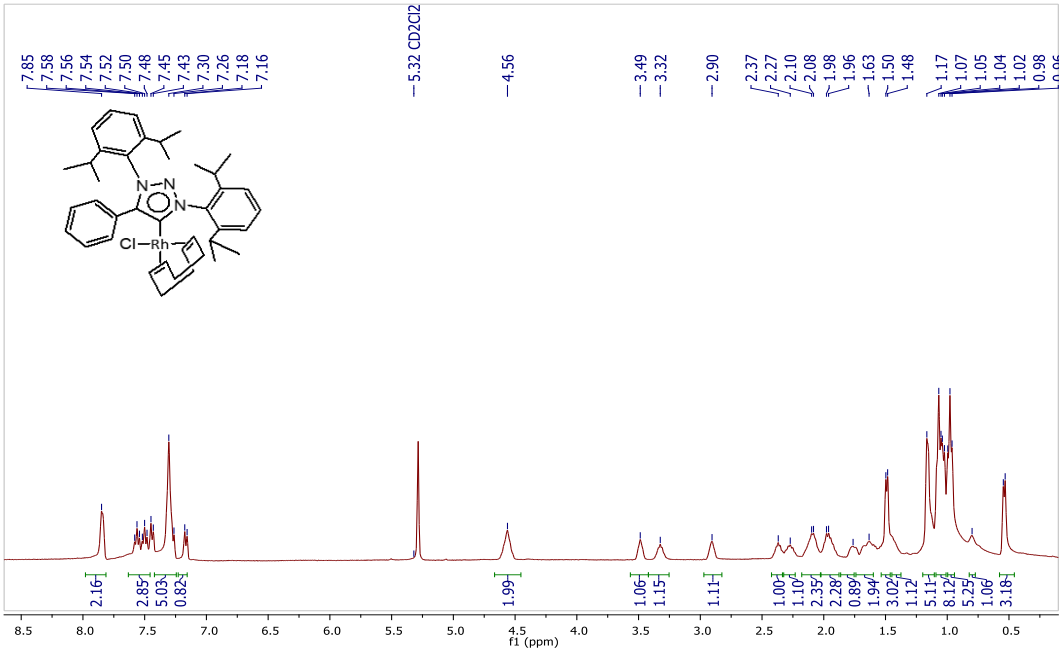

*Figure 4. 6: ^{1}H NMR Spectrum of **9** in solvent CD_2Cl_2*

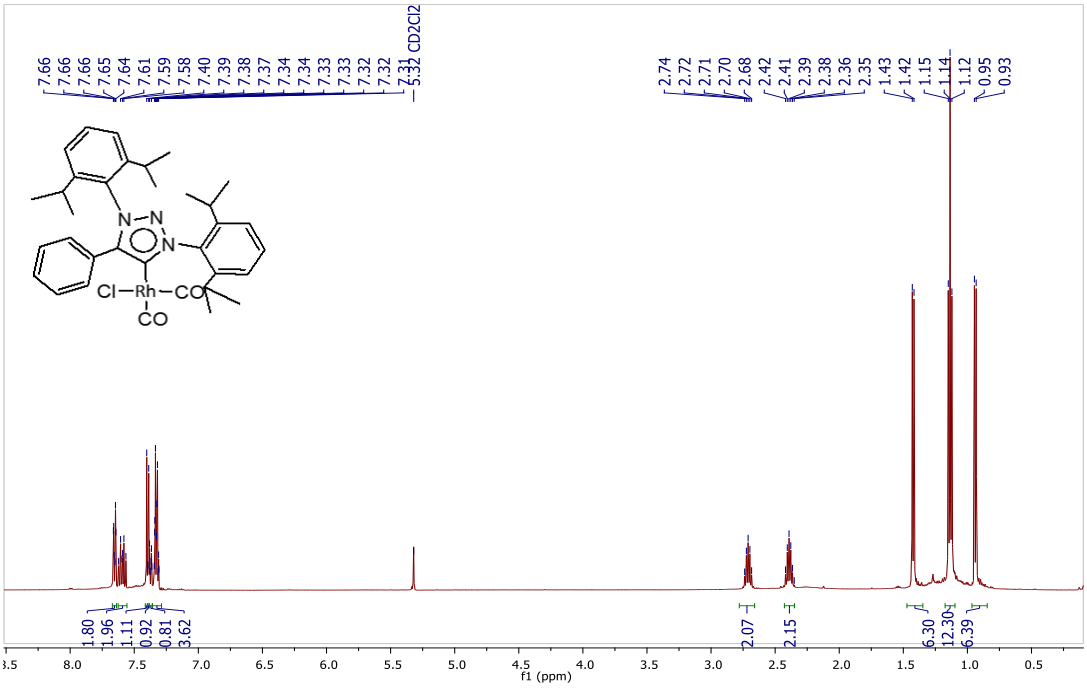

*Figure 4. 7 : ^{1}H NMR spectrum of **10** in solvent CD_2Cl_2*

The clean disappearance of the most downfield signal at 9.38 ppm in figure 4.5 corroborates the coordination of **L3^{I}**, as observed in the ^{1}H NMR spectra of **S3-S4, 9-12** in Figures 4.6-4.8 and 4.12. The ^{1}H NMR spectra of complexes bearing the labile cod ligand (Figures 4.6 and 4.10) display peak broadening as a result of dynamic processes. Substitution of the cod with the π-acidic carbonyl ligands, results in a decrease in the spread of the aromatic region as seen from complex **9** (7.16 ppm-7.85 ppm, Figure 4.6) to complex **10** (7.31 ppm-7.66 ppm, Figure 4.7). This is an indication of the change in the electron density donated from the carbene to the metal centre. A larger range of the aryl resonances over the aromatic region of the ^{1}H NMR spectrum of **11** (6.87 – 8.16 ppm), corroborates the coordination of **L3^{I}** to the iridium. The loss of symmetry about the coordination sphere of the metal centres rhodium (Figure 4.9 – 4.10) and iridium (Figure 4.16 – 4.17), is marked by the individual peaks of each carbon and corresponding proton in the ^{13}C and the ^{1}H NMR spectra is additionally observed.

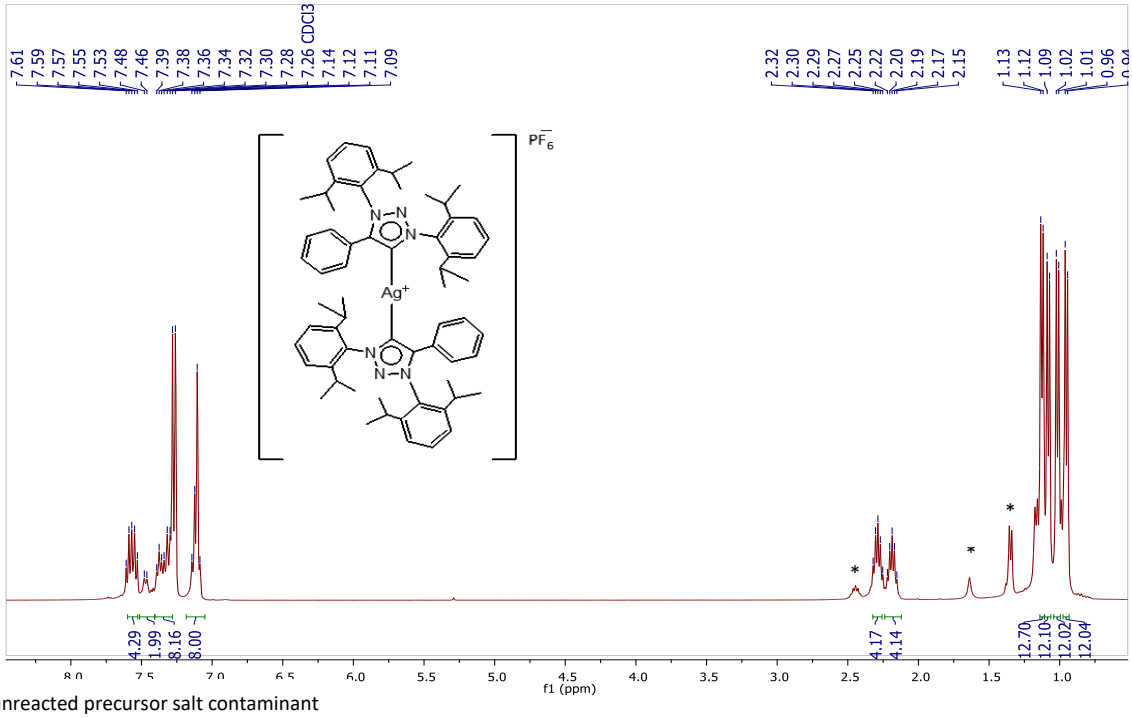

* unreacted precursor salt contaminant

*Figure 4. 8: ^{1}H NMR spectrum of **S3** in solvent $CDCl_3$*

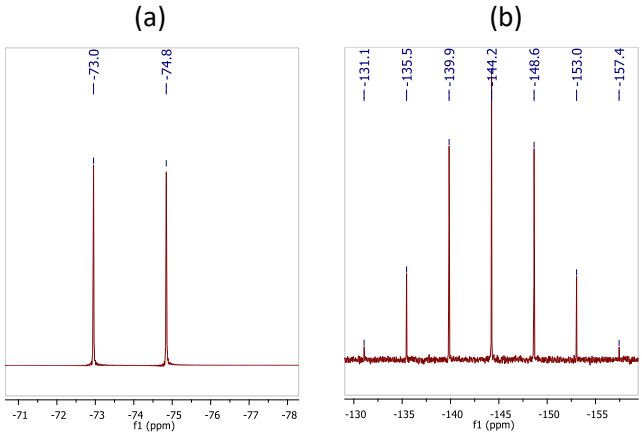

*Figure 4. 9: (a) ^{19}F NMR spectrum of **S3** in solvent $CDCl_3$. (b) ^{31}P NMR spectrum of **S3** in solvent $CDCl_3$.*

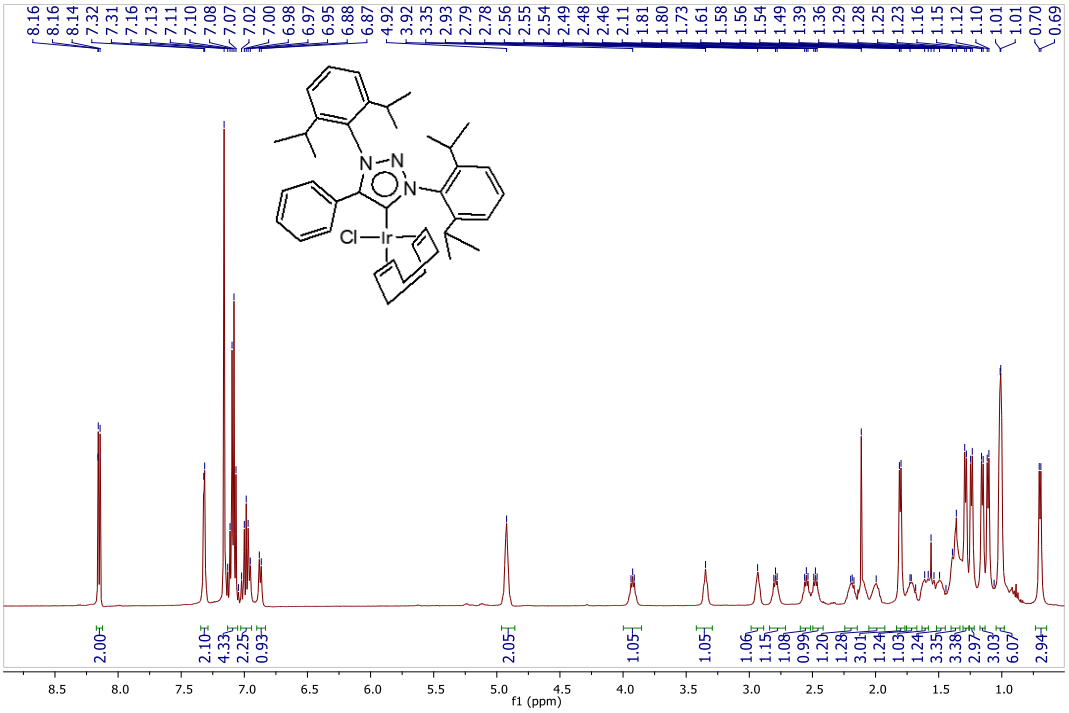

*Figure 4. 10: ^{1}H NMR spectrum of **11** in solvent C_6D_6*

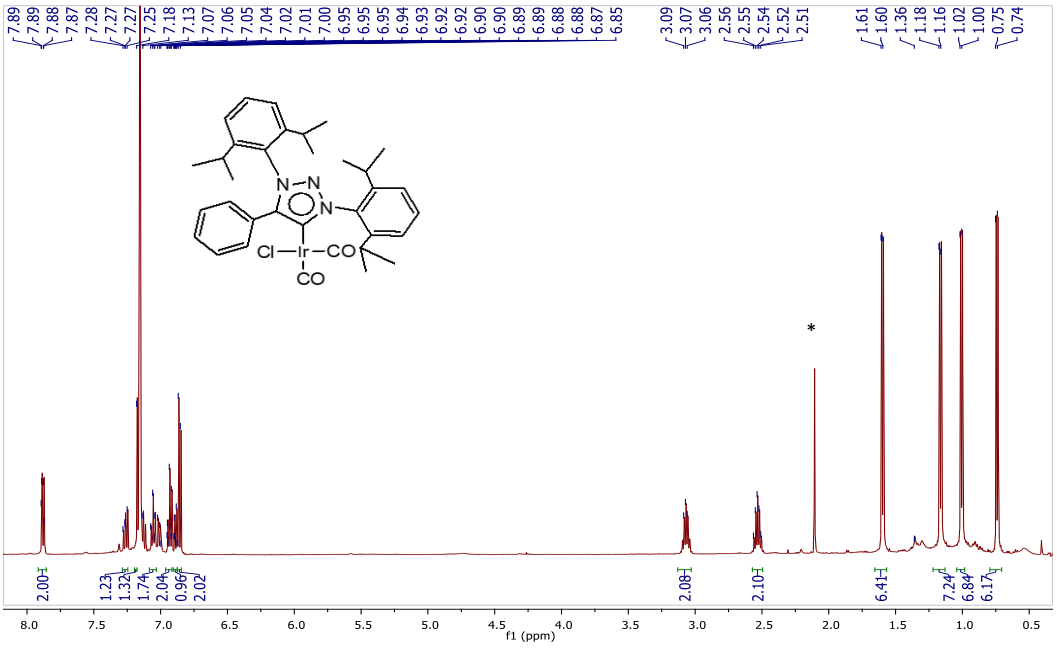

*toluene contaminant

*Figure 4. 11: ^{1}H NMR spectrum of **12** in solvent C_6D_6*

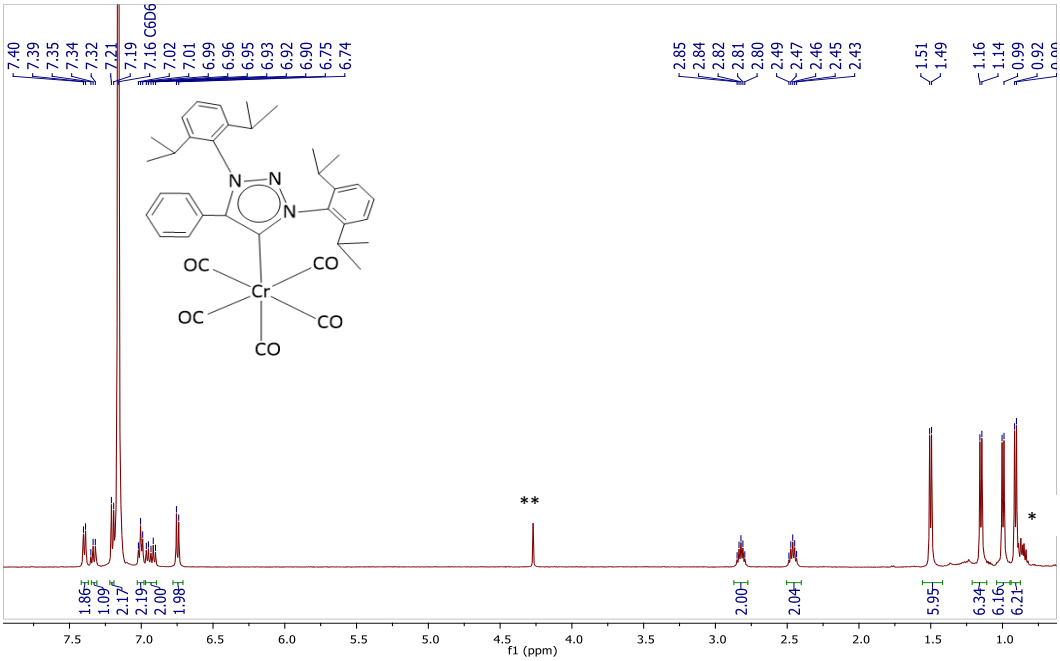

* *n*-hexane contaminant
** DCM contaminant

*Figure 4. 12: ^{1}H NMR spectrum of **S4** in solvent C_6D_6*

4.3.2.2. Evaluation of the ^{13}C NMR spectra obtained for S3-S4, 9-12

The formation of **9** is evidenced by the appearance of a carbene doublet signal at 172.3 ppm (*J*(RhC) = 47.3 Hz) in Figure 4.14, comparable to that of **5** (chapter 3, table 3.1) resonating at 171.6 ppm (*J*(RhC) = 47.4 Hz), characteristic of rhodium(I) triazol-5-ylidene complexes.[7,16] In contrast to less donating NHCs,[16] these MIC carbene signals resonated further downfield, suggesting a significant increase in the shielding of these carbene carbons. However, the effect of the triazol-substituents on the donor ability of the ligand appear to be negligible, based on the insignificant differences between the carbene chemical shifts of **9** versus **5**, and their corresponding coupling constants. Similarly, **f** (Figure 4.2) where LL = cod, and R = Dipp (171.9 ppm, *J*(RhC) = 46.6 Hz) compared to where LL = cod, and R = Et (172.3 ppm, *J*(RhC) = 47.1 Hz) displays no significant differences based on the ^{13}C NMR spectra.[16]

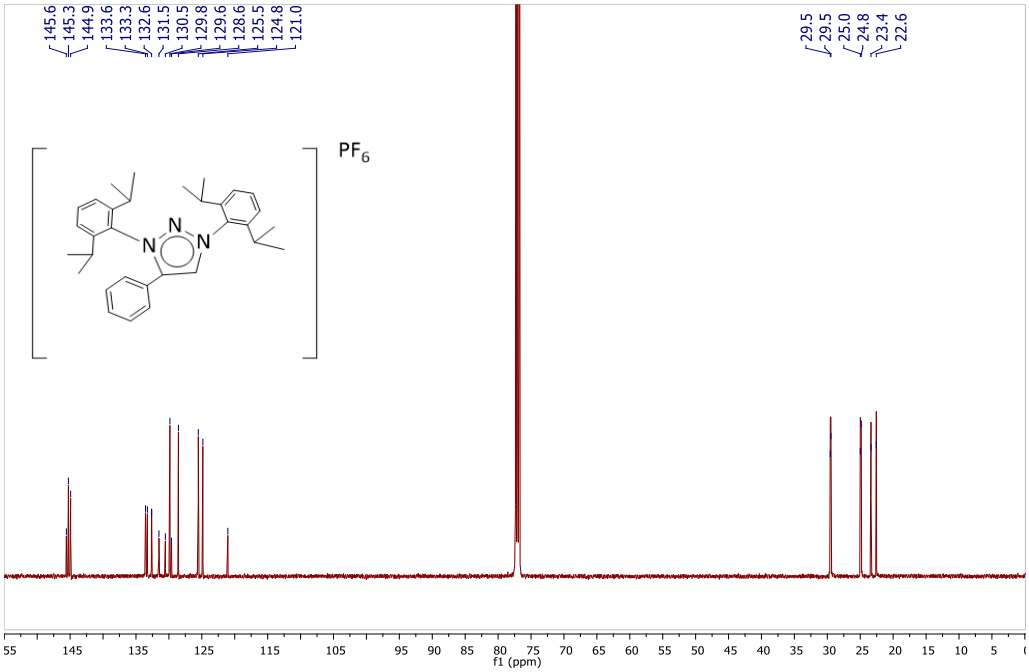

*Figure 4. 13: ^{13}C NMR of **L3** in solvent $CDCl_3$*

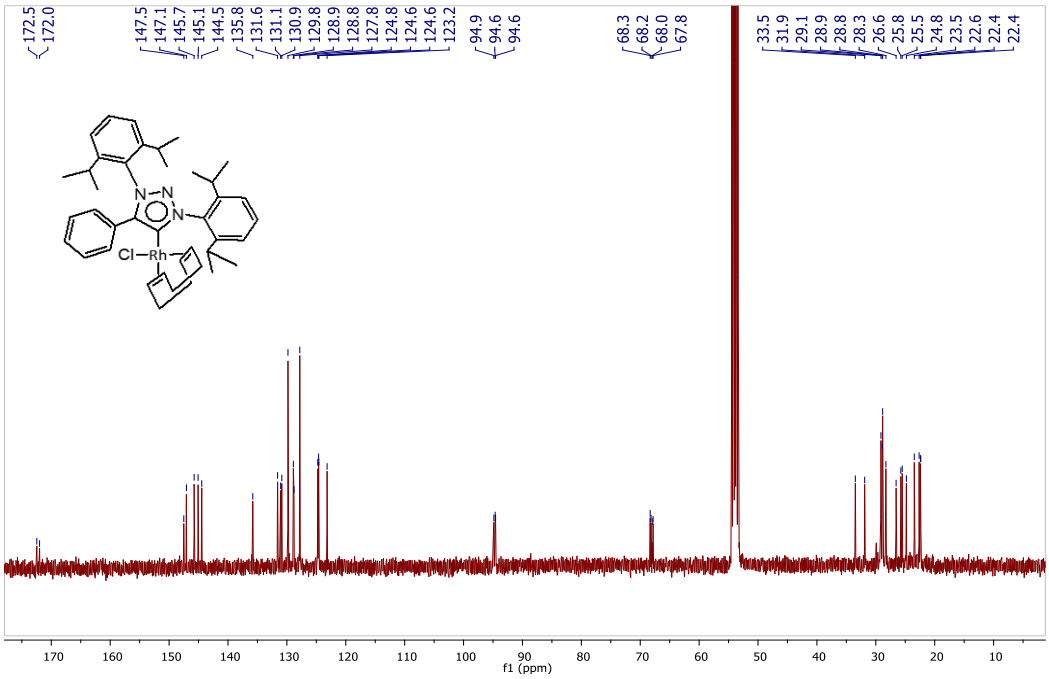

*Figure 4. 14: ^{13}C NMR spectrum of **9** in solvent CD_2Cl_2*

Formation of **S3** is evidenced by a doublet of doublets in the corresponding ^{13}C NMR spectrum (Figure 4.16) at 168.4 ppm (*J*(AgC) = 181, 13 Hz), in accordance to what is observed for **S2** (167.7 ppm, dd, *J*(AgC) = 177.6, 12.7 Hz) in chapter 3. The disappearance of this doublet of doublets, and the appearance of a downfield singlet at 173.5 ppm (complex **11**, figure 4.17), indicates a carbene transfer from silver to iridium. This characteristic iridium(I) carbene signal is also observed in chapter 3 for complex **7** (173.3 ppm).

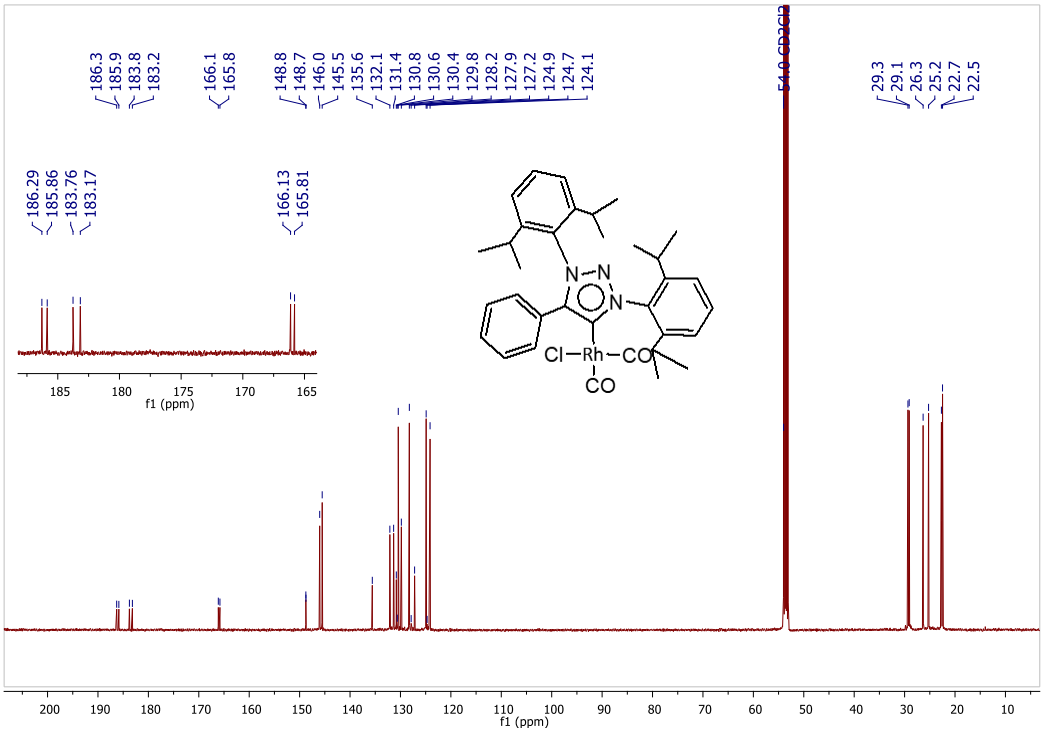

*Figure 4. 15: ^{13}C NMR spectrum of **10** in solvent CD_2Cl_2*

Ligand substitution of cod for carbonyls is confirmed by the appearance of a pair of downfield doublet signals in the ^{13}C NMR spectrum of **10** (Figure 4.15) at 186.5 ppm (*J*(RhC) = 54.5 Hz) and 183.9 ppm (*J*(RhC) = 74.5 Hz); also seen for **6** (185.6 ppm (*J*(RhC) = 54.5 Hz) and 183.5 ppm (*J*(RhC) = 75.4 Hz)), in chapter 3 (Table 3.1). These resemble what has been previously reported with regards to **f** (186.1 ppm, *J(*RhC) = 54.5 Hz; and 184.5 ppm, *J(*RhC) = 74.9 Hz) where R = Dipp. Once more it can be concluded that the CO *trans* to the carbene resonates the furthest downfield. Therefore, the larger the coupling constant, *J(*RhC), the more donating the trans ligand.[17] The carbene carbon chemical shift reported for **f** (where R = Dipp), is a doublet at 165.8 ppm (*J(*RhC) = 44.8 Hz). This is analogous to that obtained for **10** (166.4 ppm, *J(*RhC) = 40.8 Hz) – a substantial shift from the carbene carbon resonance of **9** (172.3 ppm, (*J(*RhC) = 47.3 Hz)).

As observed in chapter 3 for complex **8** (182.3 and 170.3 ppm for the CO ligands), two singlet peaks resonating at 181.6 and 169.8 ppm for complex **12** (Figure 4.18) represent the two new carbonyl ligands, following the substitution of the labile cod ligand. Once more, no significant differences are observed between the N3-alkylated and N3-diarylated carbene complexes. The carbene carbon of complex **8** resonates at 166.8 ppm while that of **12** resonates at 167.6 ppm, a marked shift from the corresponding precursors, **7** (173.3 ppm) and **11** (173.5 ppm), as consequence of the better π-accepting CO ligands compared to cod. As mentioned in the previous chapter, this unconventional upfield shift is a consequence of the increased electron density around the central metal caused by the σ-donor, π-acceptor nature of the CO, which is in contrast to the weaker π-donor olefinic cod.

The formation of complex **S4** is confirmed by the carbene carbon chemical shift at 182.9 ppm (Figure 4.19), upfield from the reported carbene resonances of known $[Cr(CO)_5(NHC)]$ complexes, which typically resonate between 210 – 225 ppm.[18] The notable donor ability of the triazolylidene ligand is confirmed by this upfield signal, which can be interpreted as an increase in π-electron density around the carbene carbon.[19] However, the strength of the electrostatic contribution to the bond between the carbene and the chromium is speculated to be inferior to that of a late group transition metal and a triazolylidene carbene, as these carbenes typically resonate further upfield as seen for the rhodium, iridium and silver complexes.

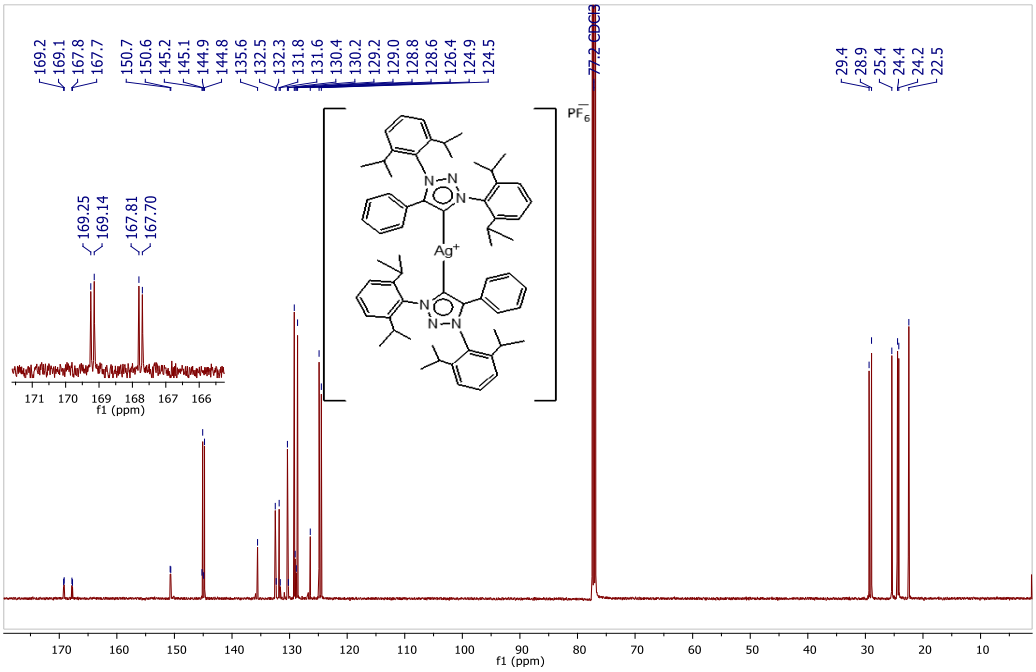

*Figure 4. 16: ^{13}C NMR spectrum of **S3** in solvent $CDCl_3$*

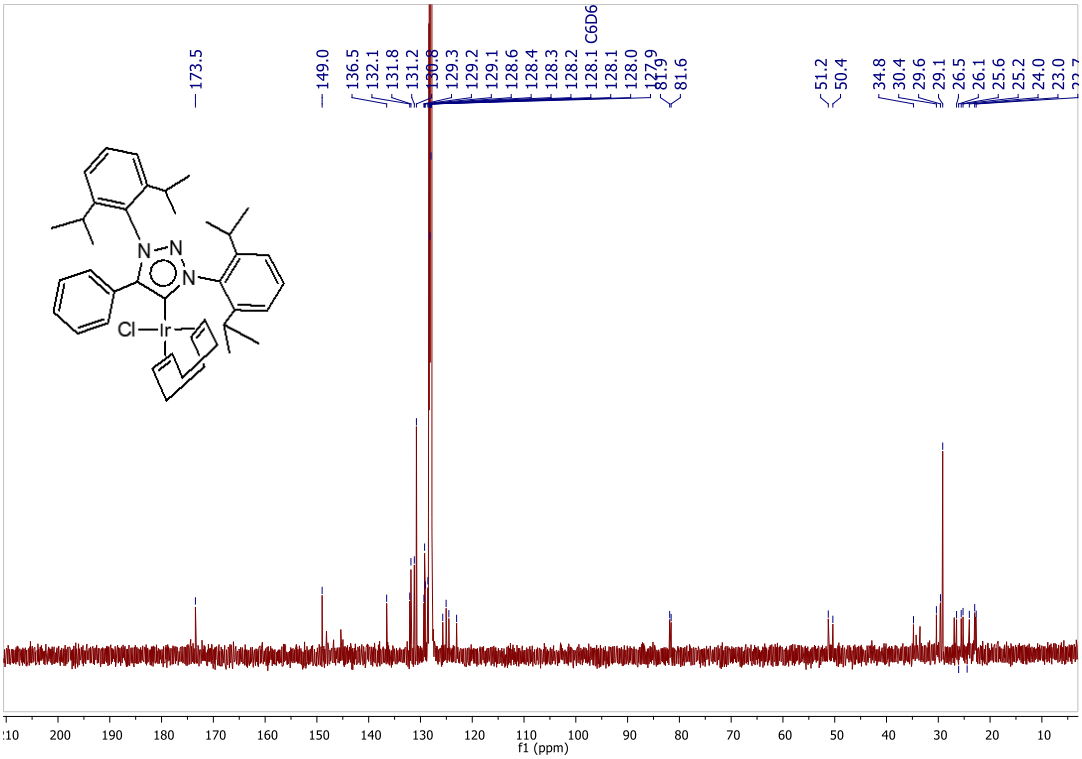

*Figure 4. 17: ^{13}C NMR spectrum of **11** in solvent C_6D_6*

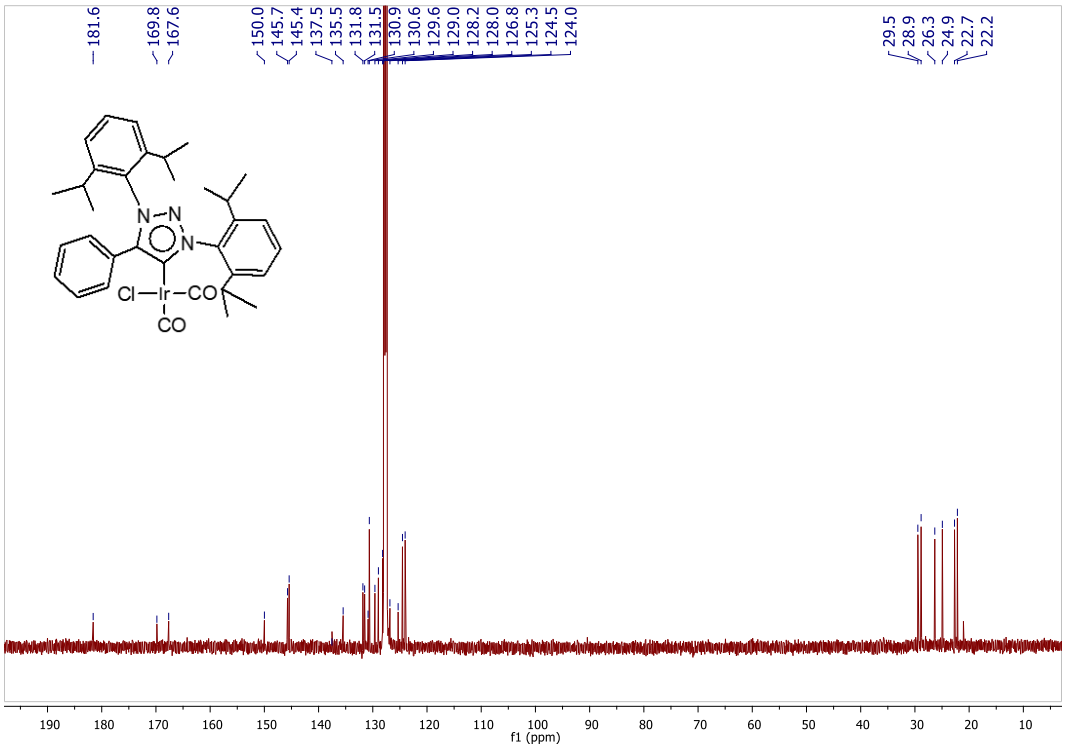

*Figure 4. 18: ^{13}C NMR spectrum of **12** in solvent C_6D_6*

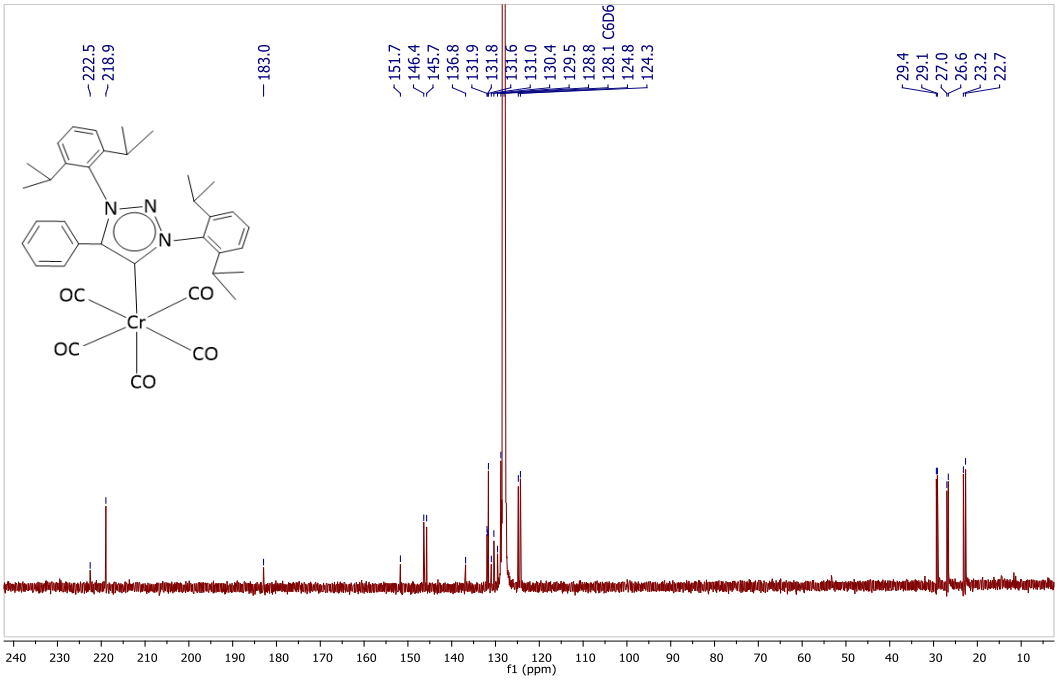

*Figure 4. 19: ^{13}C NMR spectrum of **S4** in solvent C_6D_6*

*Table 4. 1: Spectroscopic data of complexes **S3-S4, 9-12***

Complex	$^{13}C\delta(C_{carbene})$, ($^1J(M^eC)$)(Hz)	^{13}C δ(CO), (^1J(RhC))	IR[a] ν(CO), (cm^{-1})	IR[a] ν_{av}(CO), TEP, (cm^{-1})
9	172.3 (d, 47.3)	-	-	-
10	166.4 (d, 40.8)	186.5 (d, 54.5)[b] 183.9 (d, 74.5)[c]	2076[c] 1996[b]	2036 2049[f]
S3	168.4 (dd, 180.3, 13.0)	-	-	-
11	173.5	-	-	-
12	167.6	181.6[b] 169.8[c]	2062[c] 1977[b]	2019 2047[g]
S4	182.9	218.9[b] 222.5[d]	2050[d] 1965[d] 1920[d] 1889[b]	-

[a]Recorded in CH_2Cl_2. [b]CO-ligand trans to carbene. [c]CO-ligand trans to Cl. [d]CO-ligand trans to CO. [e]M = Cr, Rh, Ag, Ir. [f]Calculated using the linear regression model TEP = 0.8001ν_{av}(CO)Rh + 420 cm^{-1}.[19] [g]Calculated using the linear regression model TEP = 0.8475ν_{av}(CO)**Ir** + 336.2 cm^{-1}.[21]

4.3.2.3. Exploration of the donor properties of the ligand L3^{I}

Infrared (IR) spectroscopy is the conventional tool for the investigation of the donor strength of a ligand, enabling the calculation of TEP values from the stretching frequencies of carbonyl co-ligands on a metal complex.[20] The TEP values obtained for complexes **10** (2049 cm^{-1}) and **12** (2047 cm^{-1}) in Table 4.1 and Figure 4.4, (a) and (b), are almost identical to those obtained in the previous chapter for complexes **6** (2047 cm^{-1}) and **8** (2048 cm^{-1}) (See Section 3.3.2, Table 3.1, vide infra). This suggests limited sensitivity to the tenuous effect of the substituents on the ligand's triazole ring. This statement is further consolidated by previously obtained data from the ferrocenyl substituted analogue **f** (Figure 4.2) with a TEP of 2047 cm^{-1}.[16]

Additionally, complex **S4** was considered (Figure 4.20), and the stretching frequency of the carbonyl ligand *trans* to the carbene ligand gives rise to the vibration mode, the $A_1^{(1)}$ [30] band, with a frequency of 1889 cm^{-1}. Comparison of this IR band with the NHC type chromium carbene complex (1899.9 cm^{-1}) reported by Hermann and co-workers in 2006, leads to the conclusion that the higher frequency of the $A_1^{(1)}$ band for an octahedral group 6 metal pentacarbonyl complex is indicative of a less donating carbene ligand coordinated.[21] By this premise, it is confirmed that ligand **L3^{I}** is a better donor than the reported NHC ligands.

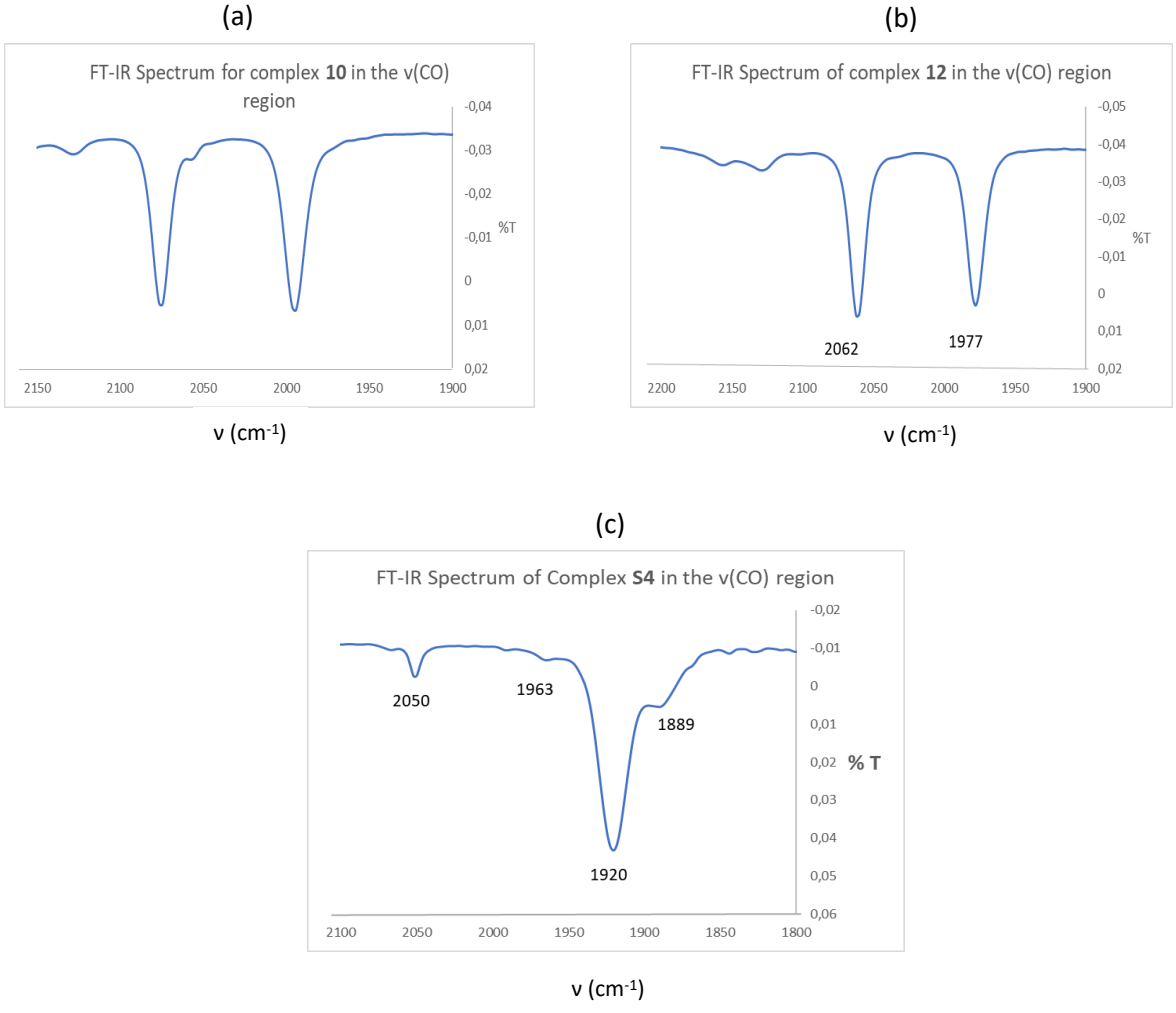

*Figure 4. 20: FT-IR spectrum of complexes (a) **10**, (b) **12** and (c) **S4** dissolved in DCM.*

4.3.3. Solid-state molecular structures of complexes S3, 9 – 12.

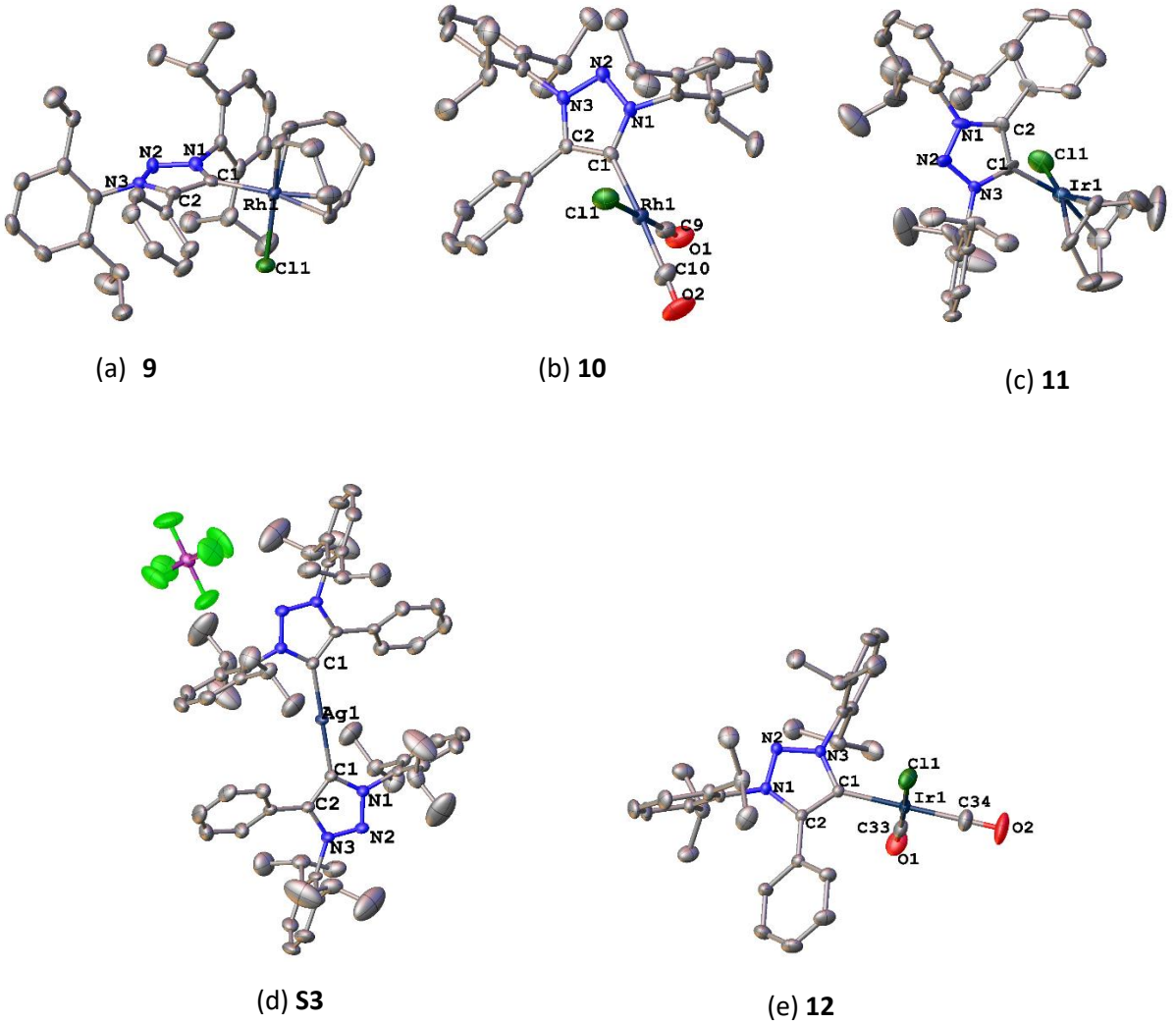

*Figure 4. 21: Solid-state molecular structures of (a) **9**, (b) **10**, (c) **11**, (d) **S3** and (e) **12** showing thermal ellipsoids at 50 % probability. Hydrogen atoms are omitted for clarity, and a partial atom numbering scheme is included.*

The molecular structures of complexes **S3, 9-12** (Figure 4.21) were obtained from hexane-layered DCM solutions of each complex. These were stored at 4°C overnight to obtain single crystals of each complex suitable for X-ray diffraction (XRD). The complexes **9**-**10** , and **11**-**12** display a pseudo-square planar geometry around the metal centre, with bond angles ranging from 87.30° to 89.03° (Table 4.2) for the $C_{carbene}$–M–Cl angle (where M = Rh, Ir).The iridium complexes **11** (87.30(2)°) and **12** (88.02(3)°) display more acute bond angles than their rhodium counterparts **9** (89.05(12)°) and **10** (89.07(7)°), moreover the cod complexes **9** and **11** are more acute compared to their corresponding CO complexes **10** and **12** due to the larger steric bulk occupied by the cod ligands compared to the carbonyl analogues.

Near-perfect linear geometry is observed for complex **S3** with a $C_{carbene}$–Ag–$C_{carbene}$ bond angle of 180.10(14)°. The opposite orientation of the coordinated triazolylidene ligands minimizes steric strain, so that the Dipp group of the one ligand is on the same side as the phenyl group of the other, contrary to what is observed for complex **S2** in Figure 3.4 (chapter 3).

*Table 4. 2: Selected bond lengths and bond angles of complexes **S3, 9-12***

Complex	9	10	S3	11	12
Bond Lengths (Å)					
M–$C_{carbene}$	2.053(4)	2.059(2)	2.080(3)	2.046(9)	2.0699(12)
$C_{carbene}$–N1/3	1.366(5)	1.367(3)	1.365(4)	1.381(11)	1.3692(15)
$C_{carbene}$–C_q	1.395(6)	1.389(3)	1.385(4)	1.417(12)	1.3929(16)
N1–N2	1.339(5)	1.337(3)	1.335(3)	1.322(9)	1.3226(14)
N2–N3	1.327(5)	1.326(3)	1.327(3)	1.335(9)	1.3330(14)
N1/3–C_q	1.375(5)	1.368(3)	1.368(4)	1.365(11)	1.3685(15)
M–Cl ($C_{carbene}^{I}$)	2.3846(12)	2.3537(8)	2.080(3)	2.353(3)	2.3492(4)
M–Y^a or M–CO_{trans}	2.1875(4)	1.907(3)	-	2.183(10)	1.8903(15)
M–Y^b or M–CO_{cis}	2.094(4)	1.852(4)	-	2.1025(9)	1.8314(17)
Bond Angles(^{O})					
$C_{carbene}$–M–Cl ($C_{carbene}$)	89.05(12)	89.07(7)	180.00(14)	87.30(2)	88.02(3)
$C_{carbene}$-C_q-N3	107.0(4)	106.6(2)	107.3(2)	106.1(7)	106.61(10)

^{a}Y = midpoint of C(33)-C(34). ^{b}Y = midpoint of C(37)-C(38). M = Rh, Ir, Ag.

Planarity of the ring is observed in Figure 4.5, with bond lengths intermediate between single and double bonds, suggesting the delocalisation of electrons within the ring for complexes **S3**, **9**-**12** (Table 4.2). The Rh–$C_{carbene}$ bond lengths of **9** and **10** are 2.053(4) Å and 2.059(2) Å respectively, in congruence with what was reported by Albrecht to be the average bond length (2.048 Å) of these types of bonds.[2] Due to the better accepting CO ligands in **10**, the Rh–$C_{carbene}$ bond is longer than that of **9**. Comparably, the bond Ir– $C_{carbene}$ bond of **12** is considerably longer than that of **11**. Additionally, the iridium complexes **11** and **12** display shorter M–$C_{carbene}$ bond lengths than the rhodium complexes **9** and **10**, not unlike what Albrecht *et al.* reported (average Ir–$C_{carbene}$ bond length = 2.037 Å).[2] A markedly shorter bond length of 2.029(4) Å was obtained for complex **5** in contrast to that of **9**, however this is not surprising considering the a similar trend was observed for **f** (figure 4.2) where the N3-alkylated had a

Rh–$C_{carbene}$ bond length of 2.053(3) Å and the diarylated analogue had a Rh–$C_{carbene}$ bond length of 2.059(2) Å.[16]

The Ag–$C_{carbene}$ bond lengths obtained for **S3** is 2.080(3) Å, not significantly longer than those obtained for **S2** (2.076(3) Å), which are comparable to the average reported by Albrecht *et al.* 2.071 Å in 2013. It can therefore be postulated that the N3-alkylated carbene complexes exhibit similar electronic properties as the 1,3-diarylated carbenes, although varying intramolecular steric hindrance is observed, likely caused by repulsions of π interactions between the aromatic substituents on the triazolylidene ligands.

4.4. Conclusion

The 1,3-diarylated-1,2,3-triazolium salt reported by Bertrand *et al*. in 2011 was accessed through the cycloaddition of a 1,3-diisopropylphenyl-2-azoniaallene salt and the phenyl alkyne reaction. This reaction involved the oxidation of this salt in the presence of KPF_6 at low temperatures, forming the desired triarylated triazolium salt. The metalation techniques used to obtain the metal complexes **9**, **S3, 11** and **S4** include deprotonation and *in situ* metalation; direct metalation; and transmetalation; all signalled by the absence of the acidic proton at C5 and with molecular structures confirmed by single crystal X-ray diffraction studies.

NMR spectroscopy shows subtle differences between the N3-alkylated triazolylidene complexes obtained in chapter 3 and the 1,3-diarylated triazolylidene complexes, however these are not sufficient to draw informed conclusions regarding the donor strength of **L3^{I}** compared to **L2^{I}**. Similarities were observed between the rhodium and the iridium metal complexes, such as the loss of symmetry about the coordination sphere of the metal centre. Furthermore, the carbene carbon chemical shifts resonate in the same region of ~172-173 ppm for the cod-substituted complexes, and further upfield for the CO complexes **10** and **12** in the region of 167pm**.** The complex **S4** carbene peak resonated at 182.9 ppm, more upfield compared to similar NHC chromium complexes, which is expected for triazolylidene ligands.

Complexes **9** and **11** underwent ligand substitution reactions where the cod ligand was substituted for CO ligands, to use these as probes in infrared spectroscopy as a means to measure the donor strength of the 1,3-diarylated triazolylidene ligand. It was established that the obtained TEP values of complex **10** (2049 cm^{-1}) and **12** (2047 cm^{-1}) are similar to those obtained in chapter 3 for complexes **6** and **8**, and those obtained for the previously reported ferrocenyl substituted 1,2,3-triazol-5-ylidene ligand. Complex **S4** displayed the expected four IR-active bands expected for an octahedral pentacarbonyl metal complex. The $A_1^{(1)}$ band (representing the CO stretching frequency of the carbonyl ligand *trans* to the carbene) gave relevant information regarding the donor strength of the carbene with a frequency of 1889 cm^{-1}.

4.5. Experimental

4.5.1. The detailed preparation of compound L3 and complexes S3-S4, 9-12

4.5.1.1. Synthesis of 1,3-bis(2,6-diisopropylphenyl)-4-phenyl-1H-1,2,3-triazolium hexafluorophosphate, **L3.**[12]

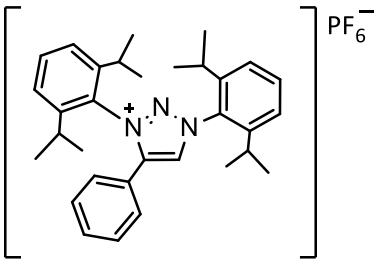

In a Schlenk tube, KPF_6 (4.72 g, 25.65 mmol), 1,3-bis(2,6-diisopropylphenyl) triazene (7.50 g, 20.51 mmol), and phenylacetylene (1.12 mL, 10.26 mmol) were dissolved in dried DCM (50mL) followed by cooling to -78°C in the absence of light. ^{t}BuOCl (2.37 mL, 20.51 mmol) was added dropwise while the solution stirred continuously. The reaction was left to stir overnight, while warming up to room temperature. The reaction was then cooled to 0°C before vacuum filtration. The precipitate was washed with *n*-hexane, followed by Et_2O to afford a white solid. The product was dried at 80°C overnight, under reduced pressure. Yield 69%.^{1}H NMR 500 MHz, $CDCl_3$ δ9.38 (s, 1H, trz-CH), 7.72 (t, ^{3}J(HH) = 7.9 Hz, 1H, Dipp-CH_{Ar}), 7.67 (t, ^{3}J(HH) = 7.9 Hz, 1H, Dipp-CH_{Ar}), 7.52-7.41(m, 9H, Dipp-CH_{Ar}, Ph-CH), 2.36(sept, ^{3}J(HH) =6.8 Hz, 2H, Dipp-CH_{iso}), 2.27(sept, ^{3}J(HH) =6.8 Hz, 2H, Dipp-CH_{iso}), 1.38(d, ^{3}J(HH) = 6.7 Hz, 6H, Dipp-CH_3), 1.18(t, ^{3}J(HH) = 6.7 Hz, 12H, Dipp-CH_3), 1.03(d, ^{3}J(HH) = 6.7 Hz, 6H, Dipp-CH_3). ^{13}C NMR (125 MHz, $CDCl_3$): δ145.6(trz-C_q), 145.3(Dipp-C_q), 144.9(Dipp-C_q), 133.6(Dipp-C_q), 133.3(Dipp-C_q), 132.6(trz-CH), 131.5(Ph-C_q), 130.5 (Dipp-CH_{Ar}), 129.9 (Dipp-CH_{Ar}), 129.6 (Ph-CH), 128.6(Ph-CH), 125.5 (Dipp-CH_{Ar}), 124.8 (Dipp-CH_{Ar}), 121.1 (Ph-CH), 29.6 (Dipp-CH_{iso}), 29.5 (Dipp-CH_{iso}), 25.0 (Dipp-CH_3), 24.9 (Dipp-CH_3), 23.4 (Dipp-CH_3), 22.6(Dipp-CH_3). 19F NMR (CDCl3, 470.59 MHz) δ_F: -72.6(d, ^{1}J(FP) = 713.1 Hz). ^{31}P NMR (CDCl3, 202.46 MHz) δ_P: -144.3 (sept, ^{1}J(PF) = 712.2 Hz).

4.5.1.2. Synthesis of 1,3-bis(2,6-diisopropylphenyl)-4-phenyl-1,2,3-triazol-5-ylidene chlorido-η4-1,5-cyclooctadienerhodium(I), **9.**[22]

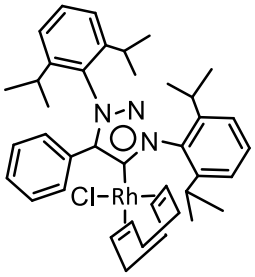

An $Ar_{(g)}$ purged, oven dried Schlenk tube was charged with **L3** (1.00 g, 1.68 mmol), $[Rh(C_8H_{12})Cl]_2$ (0.50 g, 1.01 mmol), and $KN[Si(CH_3)_3]_2$ (0.50 g, 2.52 mmol) before cooling to -75°C. THF(40 mL) was transferred to the reaction vessel, and the solution was left to stir overnight while warming up to room temperature. Volatiles were removed, and the residue was washed with *n*-hexane before extracting the product in toluene. The solvent was once again removed, and the product dried overnight under reduced pressure, to afford a yellow solid. M.P.(decomp): 220-223°C. ^{1}H NMR (400 MHz, CD_2Cl_2) δ 7.88 (d, ^{3}J = 5.4 Hz, 2H, Ph-CH), 7.54 (ddd, ^{3}J(HH) = 36.1, 18.1, 7.9 Hz, 3H, Dipp-CH_{Ar}), 7.33 (q, ^{3}J(HH) = 11.8, 9.1 Hz, 5H, Dipp-CH_{Ar}, Ph-CH), 7.20 (d, ^{3}J(HH) = 7.9 Hz, 1H, Dipp-CH_{Ar}), 4.60 (sept, ^{3}J = 8.7, 7.9 Hz, 2H, cod-CH), 3.51 (d, ^{3}J(HH) = 7.4 Hz, 1H, cod-CH), 3.36 (p, ^{3}J(HH) = 6.8 Hz, 1H, cod-CH), 2.93 (d, ^{3}J(HH) = 9.2 Hz, 1H, cod-CH_2), 2.40 (q, ^{3}J(HH) = 7.6 Hz, 1H, cod-CH_2), 2.35 – 2.26 (m, 1H, cod-CH_2), 2.22 – 2.07 (m, 2H, Dipp-CH_{iso}), 1.99 (dq, ^{3}J(HH) = 15.8, 8.0, 7.6 Hz, 2H, Dipp-CH_{iso}), 1.87 – 1.56 (m,

1H, cod-$\underline{CH_2}$), 1.53 (d, ^2J(HH) = 6.6 Hz, 3H, Dipp-$\underline{CH_3}$), 1.49(s, br, 1H, cod-$\underline{CH_2}$) 1.20 (d, ^2J(HH) = 5.9 Hz, 5H, Dipp-$\underline{CH_3}$), 1.15 – 1.05 (m, 8H, Dipp-$\underline{CH_3}$), 1.02 (t, ^2J(HH) = 7.6 Hz, 6H, Dipp-$\underline{CH_3}$), 0.84(s, br, 1H, cod-$\underline{CH_2}$) 0.57 (d, ^2J(HH) = 6.6 Hz, 3H, Dipp-$\underline{CH_3}$). ^{13}C NMR (101 MHz,CD_2Cl_2) δ 172.3 (d, ^1J(RhC) = 47.3 Hz), 147.6 (trz-$\underline{C}$), 147.1(Dipp-$\underline{C_q}$), 145.8 (Dipp-$\underline{C_q}$), 145.2(Dipp-$\underline{C_q}$), 144.5 (Dipp-$\underline{C_q}$), 135.9 (Dipp-$\underline{C_q}$), 131.7 (Dipp-CH_{Ar}), 131.1(Dipp-$\underline{C_q}$), 130.9 (Dipp-$\underline{CH_{Ar}}$), 129.9 (Ph-$\underline{CH}$), 129.0 (Ph-$\underline{C_q}$), 128.9 (Ph-$\underline{CH}$), 127.9 (Dipp-$\underline{CH_{Ar}}$), 124.8 (Dipp-$\underline{CH_{Ar}}$), 124.7(Dipp-$\underline{CH_{Ar}}$), 124.6(Dipp-$\underline{CH_{Ar}}$), 123.2(Ph-$\underline{CH}$), 95.0 (d, ^1J (RhC) = 7.3 Hz, cod-$\underline{CH}$), 94.7 (d, ^1J(RhC) = 7.4 Hz, cod-$\underline{CH}$), 68.3 (d,^{1} J(RhC) = 14.4 Hz, cod-$\underline{CH}$), 68.0 (d, ^1J (RhC)= 14.3 Hz, cod-$\underline{CH}$), 33.6(Dipp-$\underline{CH_3}$), 32.0 (Dipp-$\underline{CH_3}$), 30.0 (Dipp-$\underline{CH_3}$), 29.2(Dipp-$\underline{CH_{iso}}$), 29.0(Dipp-$\underline{CH_{iso}}$), 28.9 (Dipp-$\underline{CH_{iso}}$), 28.4 (Dipp-CH_3), 26.6 (Dipp-$\underline{CH_3}$), 25.8 (cod-$\underline{CH_2}$), 25.6 (cod-$\underline{CH_2}$), 24.9 (cod-$\underline{CH_2}$), 23.5 (Dipp-CH_3), 22.7 (Dipp-CH_3), 22.5(Dipp-CH_3),22.4(Dipp-CH_3). ESI-HRMS (15 V, positive mode, m/z): calcd for $[M+Na]^+$: 713.2430 Found: 713.2977.

4.5.1.3. Synthesis of 1,3-bis(2,6-diisopropylphenyl)-4-phenyl-1,2,3-triazol-5-ylidene chloridodicarbonyl rhodium(I), **10.**[24]

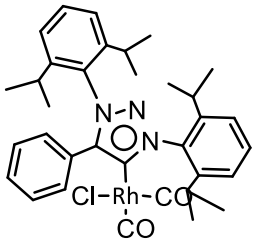

9 (0.50 g, 0.70 mmol) was dissolved in DCM (40 mL) in an oven dried Schlenk tube. The solution was purged with CO (g) for 15 minutes, followed by the removal of DCM under reduced pressure. The resulting residue was washed with hexane, and dried overnight at 80°C under reduced pressure, yielding a dark yellow solid. Yield 79%. M.P.(decomp): 185-189°C. ^{1}H NMR (500 MHz, CD_2Cl_2) δ 7.67 – 7.64 (m, 2H, Ph-$\underline{CH}$), 7.60 (dt, ^3J(HH) = 12.9, 7.8 Hz, 2H, Dipp-$\underline{CH_{Ar}}$), 7.40 (s, 1H, Dipp-$\underline{CH_{Ar}}$), 7.39 (s, 1H, Dipp-$\underline{CH_{Ar}}$), 7.39 – 7.36 (m, 1H, Ph-$\underline{CH}$), 7.35 – 7.30 (m, 4H, Dipp-$\underline{CH_{Ar}}$,Ph-$\underline{CH}$), 2.71 (sept, ^3J (HH)= 6.7 Hz, 2H, Dipp-CH_{iso}), 2.39 (sept, ^3J (RhC) = 6.8 Hz, 2H, Dipp-$\underline{CH_{iso}}$), 1.43 (d, ^2J (HH) = 6.7 Hz, 6H, Dipp-$\underline{CH_3}$), 1.14 (t, ^2J(HH) = 7.0 Hz, 12H, Dipp-$\underline{CH_3}$), 0.94 (d,^{2} J(HH) = 6.8 Hz, 6H, Dipp-$\underline{CH_3}$). ^{13}C NMR (126 MHz, CD_2Cl_2) δ 186.5 (d, ^1J(RhC) = 54.5 Hz, $\underline{CO}$), 183.9 (d, ^1J (RhC)= 74.5 Hz, $\underline{CO}$), 166.4 (d, J(RhC) = 40.8 Hz, $\underline{C_{Carbene}}$), 149.2 (trz-$\underline{C}$) , 146.5 (Dipp-$\underline{C_q}$) , 146.0 (Dipp-$\underline{C_q}$) , 136.0 (Dipp-$\underline{C_q}$), 132.6 (Ph-$\underline{CH}$) , 131.8 (Ph-$\underline{CH}$) , 131.3 (Ph-$\underline{C_q}$), 130.9 (Dipp-$\underline{CH_{Ar}}$) , 130.3 (Ph-$\underline{CH}$) , 128.7 (Dipp-$\underline{CH_{Ar}}$) , 127.6 (Dipp-$\underline{C_q}$) , 125.4 (Dipp-$\underline{CH_{Ar}}$), 124.6 (Dipp-$\underline{CH_{Ar}}$), 29.8 (Dipp-$\underline{CH_{iso}}$) , 29.5 (Dipp-$\underline{CH_{iso}}$), 26.8 (Dipp-$\underline{CH_3}$), 25.7 (Dipp-$\underline{CH_3}$), 23.1 (Dipp-$\underline{CH_3}$), 22.9 (Dipp-$\underline{CH_3}$). (CH_2Cl_2, ν(CO), cm^{-1}):1953, 1992. ESI-HRMS (15 V, positive mode, m/z): calcd for $[M+MeCN+H]^+$: 612.2793 Found: 612.1880.

4.5.1.4. Synthesis of 1,3-bis(2,6-diisopropylphenyl)-4-phenyl-1,2,3-triazol-5-ylidene chlorido-η4-1,5-cyclooctadieneiridium(I), **11.**[24]

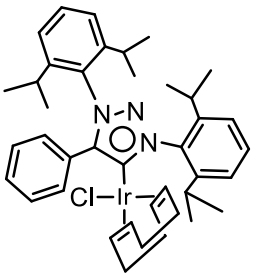

S3 (0.30 g, 0.27 mmol) and $[Ir(C_8H_{12})Cl]_2$ (0.22 g, 0.11 mmol) were transferred to an oven dried, argon gas purged Schlenk tube in the absence of light. DCM (40ml) was degassed and transferred into the reaction vessel, and the solution was left to stir for 4 days or until a precipitate was observed. After the removal of the solvent under reduced pressure, the product was extracted in *n*-hexane. The volatiles were evaporated, yielding a yellow solid. Yield: 67%. M.P. (decomp): 193-197°C. ^{1}H NMR (500 MHz, C_6D_6) δ 8.15 (dd, ^3J(HH) = 3.3, 5.2 Hz, 2H, Ph-CH), 7.32 (d, ^3J(HH) = 3.5 Hz, 3H, Dipp-CH_{Ar}), 7.13-7.05 (m, 4H, Dipp-CH_{Ar}, Ph-CH), 7.03-6.94 (m, 2H, Dipp-CH_{Ar}), 6.87 (d, ^3J(HH) = 7.7 Hz, 1H, Dipp-CH_{Ar}), 4.92 (br s, 2H, cod-CH), 3.92 (dp, ^3J(HH) = 6.7, 13.1 Hz, 1H, cod-CH), 3.35 (br s, 1H, cod-CH), 2.93 (br s, 1H, cod-CH_2), 2.85-2.74 (m, 1H, Dipp-CH_{iso}), 2.55 (td, ^2J(HH) = 7.0, 13.3 Hz, 1H, Dipp-CH_{iso}), 2.51 – 2.43 (m, 2H, Dipp-CH_{iso}), 2.25-2.14 (m, 1H, Dipp-CH_{iso}), 2.05-1.95 (m, 1H, cod-CH_2), 1.80 (d, ^2J(HH) = 6.3 Hz, 3H, Dipp-CH_3), 1.76-1.67 (m, 1H, cod-CH_2), 1.65-1.57 (m, 1H, cod-CH_2), 1.53-1.44 (m, 1H, cod-CH_2), 1.46-1.32 (m, 3H, cod-CH_2), 1.29 (d, ^2J(HH) = 6.6 Hz, 3H, Dipp-CH_3), 1.24 (d, ^2J(HH) = 6.7 Hz, 3H, Dipp-CH_3), 1.15 (d, ^2J(HH) = 6.5 Hz, 3H, Dipp-CH_3), 1.11 (d, ^2J(HH) = 6.6 Hz, 3H, Dipp-CH_3), 1.01 (d, ^2J(HH) = 2.3 Hz, 6H, Dipp-CH_3), 0.70 (d, ^2J(HH) = 6.6 Hz, 3H, Dipp-CH_3). ^{13}C NMR (126 MHz, C_6D_6) δ 173.5 ($C_{carbene}$), 149.9 (trz-C_q), 148.2(Dipp-C_q), 136.5 (Dipp-C_q), 132.1 (Dipp-C_q), 131.8 (Dipp-C_q), 131.2(Dipp-C_q), 130.8 (Dipp-C_q), 129.3 (Ph-CH), 129.2 (Ph-C_q), 129.1 (Ph-CH), 128.6 (Ph-CH), 128.4 (Dipp-CH_{Ar}), 128.2 (Dipp-CH_{Ar}), 128.1 (Dipp-CH_{Ar}), 125.7 (Dipp-CH_{Ar}), 125.1 (Ph-CH), 124.5 (Dipp-CH_{Ar}), 123.0 (Dipp-CH_{Ar}). 81.9 (cod-CH), 81.6 (cod-CH), 51.3 (cod-CH), 50.4 (cod-CH), 34.8(Dipp-CH_{iso}), 34.3 (Dipp-CH_{iso}), 33.6 (cod-CH_2), 30.4 (Dipp-CH_{iso}), 30.2 (Dipp-CH_{iso}), 29.6 (cod-CH_2), 29.1 (cod-CH_2), 26.9 (Dipp-CH_3), 26.8 (Dipp-CH_3), 26.5 (cod-CH_2), 25.6 (cod-CH_2), 25.2 (cod-CH_2), 24.0 (cod-CH_2), 23.0 (Dipp-CH_3), 22.8(Dipp-CH_3),22.7(Dipp-CH_3). ESI-HRMS (15 V, positive mode, m/z): calcd for $[M+Na-Cl]^+$: 807.3978 Found: 807.3988.

4.5.1.5. Synthesis of 1,3-bis(2,6-diisopropylphenyl)-4-phenyl-1,2,3-triazol-5-ylidene chloridodicarbonyl iridium(I), **12**[24]

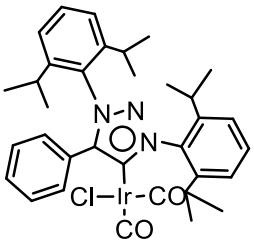

11 (0.50 g, 0.67 mmol) was dissolved in DCM(40 mL) in an oven dried Schlenk tube. The solution was purged with CO gas for 15 minutes, followed by the removal of DCM under reduced pressure. The resulting residue was washed with hexane, and dried overnight at 80°C under reduced pressure, yielding a yellow solid. . Yield 87%. M.P. (decomp): 210-214°C. ^{1}H NMR (500 MHz, C_6D_6) δ7.88(dt, ^3J(HH) =3.64, 1.61, 0.89 Hz, 2H, Ph-CH), 7.27(dd, ^3J(HH) = 8.37, 7.17 Hz, 1H, Dipp-CH_{Ar}), 7.18(d, ^3J(HH) =6.78 Hz, Dipp-CH_{Ar}), 7.06(t, ^3J(HH) =7.79 Hz, 2H, Dipp-CH_{Ar}), 6.93(tt, ^3J(HH) =5.19, 1.99, 1.20 Hz, 2H, Ph-CH), 6.89(dd, ^3J=4.35, 2.68 Hz, Ph-CH), 6.86(d, ^3J=7.88 Hz, 2H, Dipp-CH_{Ar}), 3.07(sept, ^3J=6.98, 6.87, 6.44, 6.57, 0.54 Hz, 2H, Dipp-CH_{iso}), 2.54(sept, $^{4,3,2}J$(HH) 6.81, 6.40 Hz, 2H, Dipp-CH_{iso}), 1.60(d, ^3J(HH) = 6.68 Hz, 6H, Dipp-CH_3), 1.17(d, ^3J(HH) =6.86 Hz, 6H, Dipp-CH_3), 1.01(d, ^3J(HH) =6.83 Hz, 6H, Dipp-CH_3), 0.74(d, ^3J=6.81 Hz, 6H, Dipp-CH_3). ^{13}C NMR (126

MHz, C_6D_6): δ181.94 (CO), 170.2(CO), 168.0($C_{carbene}$), 150.3(trz-C), 146.1(Dipp-C_q), 145.8(Dipp-C_q), 137.9(Dipp-C_q), 135.8(Dipp-C_q), 132.2(Dipp-CH_{Ar}), 131.8(Dipp-CH_{Ar}), 131.2(Dipp-C_q), 131.0(Ph-CH), 129.9(Ph-C_q), 129.3(Ph-CH), 128.3(Dipp-C_q), 128.5(Ph-CH), 127.2(Dipp-CH_{Ar}), 125.7(Dipp-CH_{Ar}), 124.9(Dipp-CH_{Ar}), 124.4(Dipp-CH_{Ar}), 29.8(Dipp-CH_{iso}), 29.2(Dipp-CH_{iso}), 26.7(Dipp-CH_3), 25.3(Dipp-CH_3), 23.0(Dipp-CH_3), 22.5(Dipp-CH_3). ESI-HRMS (15 V, positive mode, m/z): calcd for $[M+K]^+$: 806.2860 Found: 806.5470.

4.5.1.6. Synthesis of 1,3-bis(2,6-diisopropylphenyl)-4-phenyl-1,2,3-triazol-5-ylidene pentacarbonyl chromium(0), **S4.**[17]

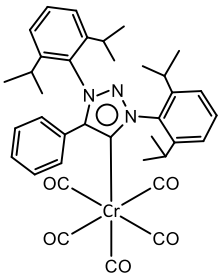

In an argon gas purged, flame dried Schlenk tube, $Cr(CO)_6$ was dissolved in 40 ml dry THF, and photolyzed for 24hr while stirring continuously. In a separate argon gas purged, flame dried Schlenk tube, **L3** (0.50 g, 0.84 mmol) and $KN[Si(CH_3)_3]_2$ (0.25 g, 1.26 mmol) were cooled to -10ºC and dissolved in dry THF (20 mL) subsequently. After 30 min, the reaction mixture was removed from the cold and allowed to warm up to room temperature while stirring continuously. The contents of the first Schlenk tube were then transferred into the **L3** deprotonation reaction and allowed to stir overnight at room temperature. The volatiles were removed under reduced pressure, and the product extracted with hexane. The solvent was removed to yield an off-white solid. Yield: 41%. M.P.(decomp): 165-169ºC. ^{1}H NMR (300 MHz, C6D6) δ 7.39 (d, ^3J(HH) =7.9 Hz, 2H, Ph CH), 7.34(t, ^3J(HH) = 8.3, 7.26 Hz, 1H, Dipp CH_{Ar}), 7.20 (d, ^3J(HH) =7.8 Hz, 2H, Dipp-CH_{Ar}), 7.01(dd, ^3J=8.4, 6.5 Hz, 2H, Ph-CH), 6.95 (t, ^3J=7.3 Hz, 1H, Dipp-CH_{Ar}), 6.92 (t, ^3J(HH) =8.0 Hz, 1H, Ph-CH), 6.74 (d, ^3J(HH) =7.86 Hz, 2H, Dipp-CH_{Ar}), 2.82(sept, ^3J(HH) =6.78 Hz, 2H, Dipp-CH_{iso}), 2.46(sept, ^3J=6.79 Hz, 2H, Dipp-CH_{Ar}), 1.50(d, ^3J(HH) =6.68 Hz, 6H, Dipp-CH_3), 1.15(d, ^3J(HH) =6.83 Hz, 6H, Dipp-CH_3), 1.00(d, ^3J(HH) = 6.80 Hz, 6H, Dipp-CH_3), 0.91(d, ^3J= 6.78 Hz, 6H, Dipp-CH_3). ^{13}C NMR (75MHz, C_6D_6)δ 222.5(CO_{trans}), 218.9(CO_{cis}), 182.9($C_{carbene}$), 151.7(trz-C), 146.4(Dipp-CH_{Ar}), 145.7(Dipp-CH_{Ar}), 136.8(Dipp-C_q), 131.9(Dipp-CH_{Ar}), 131.7(Dipp CH_{Ar}), 131.6(Ph-CH), 130.9(Dipp-C_q), 130.3(Ph-CH), 129.5(Ph-C_q), 128.7(Ph-CH), 124.7(Dipp CH_{Ar}), 124.3(Dipp CH_{Ar}), 29.3(Dipp-CH_{iso}), 29.1(Dipp-CH_{iso}), 26.8(Dipp-CH_3), 26.6(Dipp-CH_3), 23.2(Dipp-CH_3), 22.7(Dipp-CH_3). (CH_2Cl_2, ν(CO), cm^{-1}):1887, 1920, 1976, 2049. ESI-HRMS (15 V, positive mode, m/z): calcd for $[M+H-CO]^+$: 634.2737 Found: 634.2121.

4.5.2. Single-crystal X-ray diffraction

Crystal Data for **9**: $C_{40}H_{51}ClN_3Rh$ (M =712.20 g/mol): monoclinic, space group $P2_1/n$ (no. 14), a = 18.5347(9) Å, b = 10.3075(5) Å, c = 19.6524(11) Å, β = 107.574(3)°, V = 3579.3(3) Å^3, Z = 4, T = 173.15 K, μ(MoKα) = 0.583 mm^{-1}, *Dcalc* = 1.322 g/cm^3, 32741 reflections measured (3.614° ≤ 2Θ ≤ 51.998°), 7037 unique (R_{int} = 0.1124, R_{sigma} = 0.1064) which were used in all calculations. The final R_1 was 0.0530 (I > 2σ(I)) and wR_2 was 0.1323 (all data).

Crystal Data for **10**: $C_{34}H_{39}ClN_3O_2Rh$ (*M* =660.04 g/mol): triclinic, space group P-1 (no. 2), *a* = 10.5904(2) Å, *b* = 10.8731(3) Å, *c* = 15.2113(3) Å, *α* = 97.9085(12)°, *β* = 97.3841(12)°, *γ* = 110.0498(11)°, *V* = 1600.47(6) Å^3, *Z* = 2, *T* = 173.15 K, μ(MoKα) = 0.651 mm^{-1}, *Dcalc* = 1.370 g/cm^3, 22804 reflections measured (4.066° ≤ 2Θ ≤ 56.538°), 7795 unique (R_{int} = 0.0343, R_{sigma} = 0.0604) which were used in all calculations. The final R_1 was 0.0394 (I > 2σ(I)) and wR_2 was 0.1077 (all data).

Crystal Data for **S3**: $C_{67}H_{84}AgCl_6F_6N_6P$ (*M* =1438.94 g/mol): monoclinic, space group C2/c (no. 15), *a* = 18.4506(11) Å, *b* = 18.6525(10) Å, *c* = 22.9936(13) Å, *β* = 111.365(3)°, *V* = 7369.5(7) Å^3, *Z* = 4, *T* = 173.15 K, μ(MoKα) = 0.569 mm^{-1}, *Dcalc* = 1.297 g/cm^3, 31958 reflections measured (3.222° ≤ 2Θ ≤ 56.776°), 9182 unique (R_{int} = 0.0677, R_{sigma} = 0.0850) which were used in all calculations. The final R_1 was 0.0526 (I > 2σ(I)) and wR_2 was 0.1359 (all data).

Crystal Data for **11**: $C_{40}H_{51}ClIrN_3$ (*M* =267.16 g/mol): monoclinic, space group $P2_1/n$ (no. 14), *a* = 10.4226(12) Å, *b* = 18.528(2) Å, *c* = 20.536(3) Å, *β* = 91.978(4)°, *V* = 3963.4(8) Å^3, *Z* = 12, *T* = 296.15 K, μ(MoKα) = 3.465 mm^{-1}, *Dcalc* = 1.343 g/cm^3, 36307 reflections measured (5.886° ≤ 2Θ ≤ 52.974°), 8131 unique (R_{int} = 0.0927, R_{sigma} = 0.0942) which were used in all calculations. The final R_1 was 0.0818 (I > 2σ(I)) and wR_2 was 0.2319 (all data).

Crystal Data for **12**: $C_{34}H_{39}ClIrN_3O_2$ (*M* =749.33 g/mol): triclinic, space group P-1 (no. 2), *a* = 10.5527(5) Å, *b* = 10.9468(4) Å, *c* = 15.1683(7) Å, *α* = 97.9998(16)°, *β* = 96.8932(17)°, *γ* = 110.3337(15)°, *V* = 1600.06(12) Å^3, *Z* = 2, *T* = 173.15 K, μ(MoKα) = 4.289 mm^{-1}, *Dcalc* = 1.555 g/cm^3, 60672 reflections measured (6.174° ≤ 2Θ ≤ 61.052°), 9753 unique (R_{int} = 0.0221, R_{sigma} = 0.0136) which were used in all calculations. The final R_1 was 0.0139 (I > 2σ(I)) and wR_2 was 0.0332 (all data).

4.5. References

[1] A. J. Arduengo, M. Kline, J. C. Calabrese, F. Davidson and N. M. R. Hi, *J. Am. Chem. Soc.*, 1991, **113**, 9704–9705.
[2] J. Bouffard, B. K. Keitz, R. Tonner, G. Guisado-barrios, G. Frenking, R. H. Grubbs and G. Bertrand, *Organometallics,* 2011, **30**, 2617–2627.
[3] P. Mathew, A. Neels and M. Albrecht, *J. Am. Chem. Soc.*, 2008, **130**, 13534–13535.
[4] K. F. Donnelly, A. Petronilho and M. Albrecht, *Chem. Commun.*, 2013, **49**, 1145–1159.
[5] J. D. Crowley, A. L. Lee and K. J. Kilpin, *Aust. J. Chem.*, 2011, 64, 1118–1132.
[6] H. K.-W. Hul and H. Shechter, *Thermolysis and photolysis of 4-diazo-1,2,3-triazoles in benzenoid solvents, systems which reveal decomposition of diazo compounds to carbenes to diazo compounds to carbenes*, 1982, vol. 23.
[7] G. Guisado-Barrios, M. Soleilhavoup and G. Bertrand, *Acc. Chem. Res.*, 2018, **51**, 3236–3244.
[8] A. Poulain, D. Canseco-Gonzalez, R. Hynes-Roche, H. Müller-Bunz, O. Schuster, H. Stoeckli-Evans, A. Neels and M. Albrecht, *Organometallics*, 2011, **30**, 1021–1029.
[9] W. Wirschun, M. Winkler, K. Lutz and J. C. Jochims, *J. Chem. Soc., Perkin Trans. **1***,1998, 1755-1762.
[10] (a) Vernin, G.; Siv, C.; Metzger, *J. Synthesis* 1977, 691–693.(b) Nimitsiriwat, N.; Gibson, V. C.; Marshall, E. L.; Takolpockdee, P.; Tomov, A. K.; White, A. J. P.; Williams, D. J.; Elsegood, M. R. J.; Dale, S. H. *Inorg. Chem*. 2007, **46**, 9988–9997. (c) Barrett, A. G.; Crimmin, M. R.; Hill, M. S.; Hitchcock, P. B.; Kociok-K€ohn, G.; Procopiou, P. A. *Inorg. Chem*. 2008, 47, 7366–7376. (d) Hartman, W. W.; Dickey, J. B. *Org. Synth*. 1934, **14**, 163. (e) Hauber, S.-O.; Lissner, F.;Deacon,G. B.;Niemeyer,M. *Angew. Chem., Int. Ed*. 2005, **44**, 5871–5875. (f) Alexander, S. G.; Cole, M. L.; Forsyth, C. M.; Furfari, S.; Konstas, K. *Dalton Trans*. 2009, 2326–2336.
[11]Sanford, M. S.; Love, J. A.; Grubbs, R. H. *J. Am. Chem. Soc.* 2001, **123**, 6543–6554.
[12] D. R. Tolentino, L. Jin, M. Melaimi and G. Bertrand, *Chem.: Asian J.*, 2015, **10**, 2139–2142.
[13] D. Aucamp, T. Witteler, F. Dielmann, S. Siangwata, D. C. Liles, G. S. Smith and D. I. Bezuidenhout, *Eur. J. Inorg. Chem.*, 2017, **2017**, 1227–1236.
[14] M. Albrecht, Chem. Commun., 2008, 3601–3610.
[15] G. D. Frey, E. Herdtweck and W. A. Herrmann, *J. Organomet. Chem.*, 2006, **691**, 2465–2478.
[16] S. Burling, L. D. Field, H. L. Li, B. A. Messerle, P. Turner, *Eur. J. Inorg. Chem.* 2003, 3179‑3184
[17] D. Aucamp, MSc Chemistry, University of Pretoria, 2016.
[18] M. Nonnenmacher, D. Kunz, F. Rominger and T. Oeser, *J. Organomet. Chem*., 2005, **690**, 5647–5653.
[19] (a) A. R. Chianese, X. Li, M. C. Janzen, J. W. Faller, R. H. Crabtree and W. A. *J. Organomet*., 2003, 1663–1667. (b) R. A. K. Iii, H. Clavier, S. Giudice, N. M. Scott, E. D. Stevens, J. Bordner, I. Samardjiev, C. D. Hoff, L. Cavallo and S. P. Nolan, *Organometallics*., 2008, 202–210.
[20] R. A. K. Iii, H. Clavier, S. Giudice, N. M. Scott, E. D. Stevens, J. Bordner, I. Samardjiev, C. D. Hoff, L. Cavallo and S. P. Nolan, *Organometallics*., 2008, 202–210
[21] G. D. Frey, E. Herdtweck and W. A. Herrmann, *J. Organomet. Chem.*, 2006, **691**, 2465–2478.
[22] *(a)* J. Arduengo, H. V. R. Dias, J. C. Calabrese and F. Davidson, *Homoleptic Carbene-Silver(1) and Carbene-Copper(1) Complexes*, 1993, vol. 12. *(b)* H. M. J. Wang and I. J. B. Lin, *Facile Synthesis of Silver(I)-Carbene Complexes. Useful Carbene Transfer Agents*, 1998. *(c)* M. Iglesias, D. J. Beetstra, J. C. Knight, L. L. Ooi, A. Stasch, S. Coles, L. Male, M. B. Hursthouse, K. J. Cavell, A. Dervisi and I. A. Fallis, *Organometallics*, 2008, **27**, 3279–3289. (e) K. J. Kilpin, U. S. D. Paul, A. L. Lee and J. D. Crowley, *Chem. Commun.*, 2011, **47**, 328–330.

Chapter 5: Synthesis and characterisation of rhodium(I) biscarbene complexes

5.1. Background

One of the most widely explored chelate systems,[1] the complexation of the 2,2'-bipyridine ligand, gained popularity following its first report in 1889.[2] Its redox stability and ease of tunability, enthused the exploration of carbenes as systems with similar topology but better ligand functionalization as a result of the difference in electronic properties.

In the past decade, Bertrand and co-workers have been instrumental in the isolation of a range of free aNHCs, namely the first examples of a crystalline imidazole-4-ylidene[3] and a 1,2,3-triazol-5-ylidene.[3,4] This is due to the superiority in donor strength of the aNHC, as result of the mesoionic nature of the ligand as attested by experimental data.[5]

Inspired by the work of Crabtree, as well as their own previous success in the isolation of free abnormal NHCs , Bertrand and co-workers isolated the free 4,4'-bis(1,2,3-triazol-5-ylidene) (i-bitz) ligand before chelation to rhodium(I) resulting in a square planar mononuclear complex.[7] The synthetic procedure involved *in situ* azide formation,[6] systematically followed by a modified version of the classic "click" reaction. The bitriazole was subsequently alkylated and deprotonated with a non-nucleophilic base. The resulting free i-bitz was found to be stable in solid state under inert conditions with melting points ranging from 124°C for the less bulky mesityl wingtip group to 139°C for the 2,6-diisopropylphenyl substituent. Scheme 5.1 shows the preparation of i-bitz rhodium(I) complex **n** by deprotonation of precursor bis-triazolium **b,** followed by the exposure of **c** to CO in order to study the donor properties of the ligand **b**^{I} in complex **d**.[7]

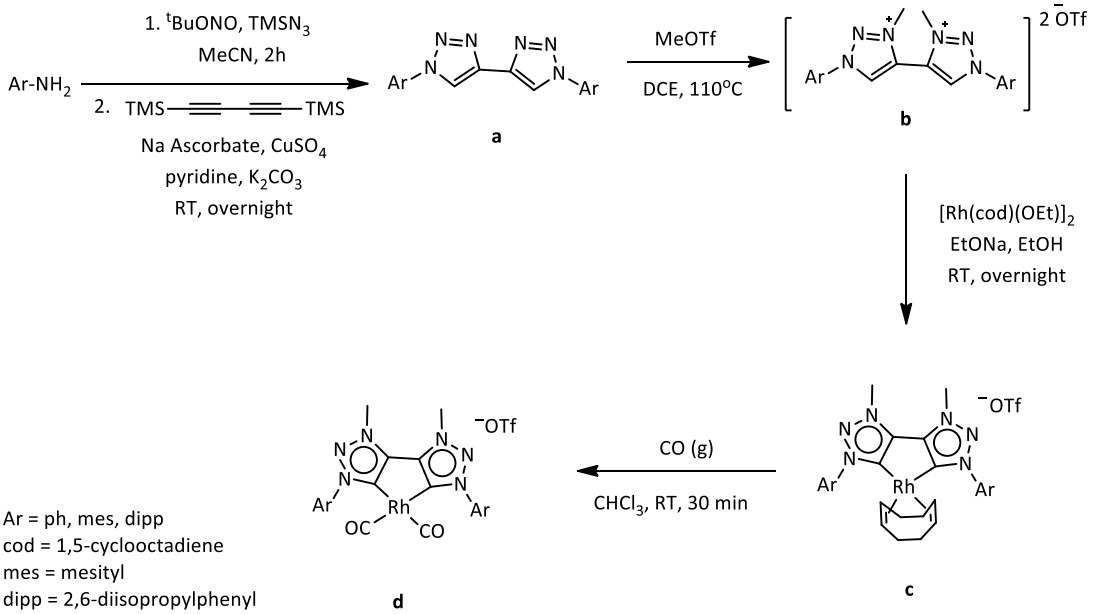

Scheme 5. 1: Preparation of the i-bitz salt for chelation to rhodium(I) in a square planar geometry about the metal centre[7]

Monodentate NHC and Fischer-type heterodicarbene complexes have been previously considered by Barluenga and co-workers.[8] In 2006, there had been limited reports of biscarbene complexes containing both the NHC and the Fischer type carbene ligands coordinated to the metal centre, prompting Barluenga's work on NHC rhodium Fischer carbene complexes.[8] The earliest reported mixed biscarbene complexes bearing an NHC and a Fischer carbene (FC) were of group 6 transition metals chromium, tungsten and molybdenum.[9] Fischer carbene complexes of group 6 metals were employed as carbene sources in late group transition metal-catalysed reactions. However, Sierra and co-workers showed that the driving force of these reactions is the transfer of the carbene ligand to palladium, forming and intermediate palladium Fischer carbene complex (see chapter 2).[10] A year later in 1999, Aumann reported rhodium-catalysed alkyne condensation reactions to generate aminocyclopentadienes, from group 6 Fischer carbene complexes based on the same transmetalation principle reported by Sierra.[19,11] Rhodium NHC complexes gained traction as a result of excellent conversions of up to 90% in hydroformylation reactions.[12] Thus, taking advantage of the high reactivity of rhodium NHCs in catalytic reactions, Barluenga began the work of isolating the first NHC-based rhodium Fischer carbene complex using the transmetalation principle[13] used to isolate the cationic rhodium Fischer carbene complex.[13] The rhodium NHC complex (Chapter 2, Scheme 2.3) was reacted with a chromium(methoxy) Fischer carbene complex to transfer this Fischer carbene (as well as a CO co-ligand) to the rhodium NHC. Reactions with the Fischer aminocarbene analogue required longer reactions time[8] as a result of the added stabilisation from the amino group to the carbene carbon, increasing C-N bond order.[14] However, both types of reactions resulted in yields of between 35% and 50%.[8,13]

Upon heating at 60°C in toluene, the mixed carbene complex dimerised into an alkene product **g,** as well as a chloride bridged rhodium(I) NHC dimer **f** (Scheme 5.2).[8] The rhodium complexes of type **e** were used to catalyse cyclization reactions and displayed no activity. Subsequently, a chloride abstractor $AgSbF_6$ was added to the catalytic reaction along with **e** revealing that the catalyst is only active in its cationic form,[8] in congruence with the previously reported $[(cod)(CO)RhC(OMe)R]^+$ complex.[12]

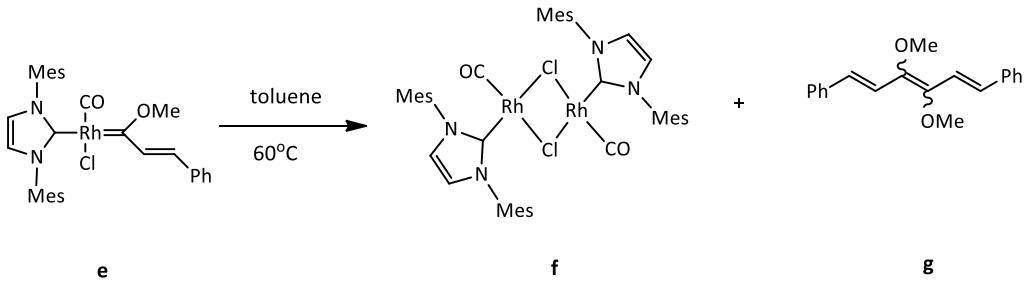

*Scheme 5. 2: The dimerization reaction of the mixed biscarbene complex **e** at 60°C.[8]*

5.2. Aim

In this chapter, the two main objectives include (i) the preparation of a chelating bis-mesoionic carbene rhodium(I) complex, (ii) as well as a hybrid rhodium(I) carbene complex containing both a MIC and a FC ligand.

As aforementioned, two modes of coordination for bidentate NHC ligands are possible. These ligands can chelate to a central metal, forming a mononuclear complex, or each carbene can coordinate to a metal, forming a bridged dinuclear complex. To predict the outcome of coordination, Crabtree and co-workers highlighted the importance of the length of the linker, performing experiments on bidentate NHC ligands with chain lengths ranging from n = 1-4. Furthermore, the steric bulk of both the wingtip groups on the NHC along with the ensuing co-ligands play a major role in the coordination of the ligand as well as the spatial arrangement of the heterocycles with respect to the rest of the complex. Ultimately, the presence of a halide in the reaction solution often results in a bridged bimetallic complex.[3, 5,6,10]

Following Crabree's work on the bitriazole (bitz) ligand (the first of its kind), Bertrand isolated the first free bis(1,2,3-triazol-5-ylidene) (i-bitz).[15] The i-bitz ligand is predictably a better donating ligand than the bitz since normal NHCs are less donating than abnormal NHCs (see chapter 3, Figure 3.19). The bitz is more unstable than the i-bitz as a result of the bitz being linked directly by the N – N bond between the two rings. The free bitz undergoes spontaneous rearrangement, while the free i-bitz remains stable under inert conditions, and only decomposes at temperatures of up to 139°C.[5,9,15]

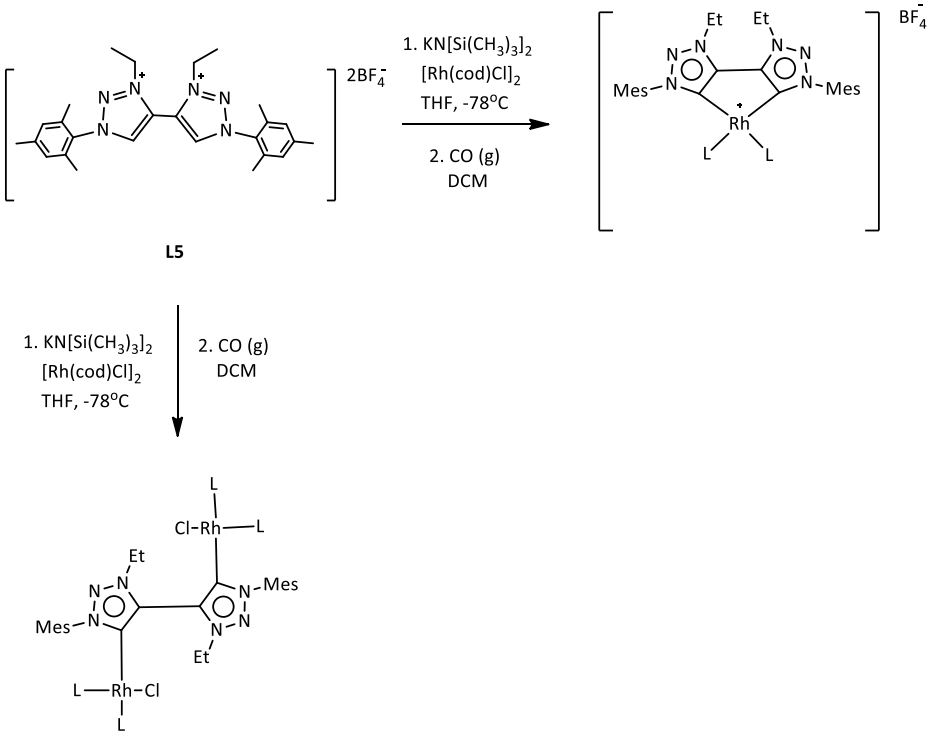

*Scheme 5. 3 Target compounds illustrating the chelation and bridging coordination modes of **L5** as a ligand on a rhodium(I) metal centre.*

Employing the same synthetic strategy as Bertrand, the i-bitz ligand will be prepared using the copper-catalyzed "click" reaction.[15] Instead of MeOTf, Et_3OBF_4 is the alkylating agent to be used so as to afford the bis(1,2,3-triazolium) salt, **L5**. The resultant salt will be deprotonated and metalated *in situ*, with the intention of isolating the chelated ethyl analogue of **c**, without neglecting the possibility of isolating the corresponding binuclear rhodium complex (Scheme 5.1).

In terms of the second objective of this study, the effect of two monodentate carbene ligands on a central metal where one of the carbene ligands is a Fischer carbene, is under-explored.[6] To investigate the possibility of introducing a 'push-pull' electronic effect with the introduction of a donating and electron withdrawing carbene ligand, respectively, the preparation of a rhodium(I) biscarbene complex bearing a 1,3,4-trisubstituted 1,2,3-triazol-5-ylidene concurrently with a Fischer carbene will be attempted. The five synthetic routes highlighted in Scheme 5.4 will be examined. The free carbene routes, **A** and **B**; the transmetalation routes **C** and **D**; and lastly the transmetalation route, **E**.

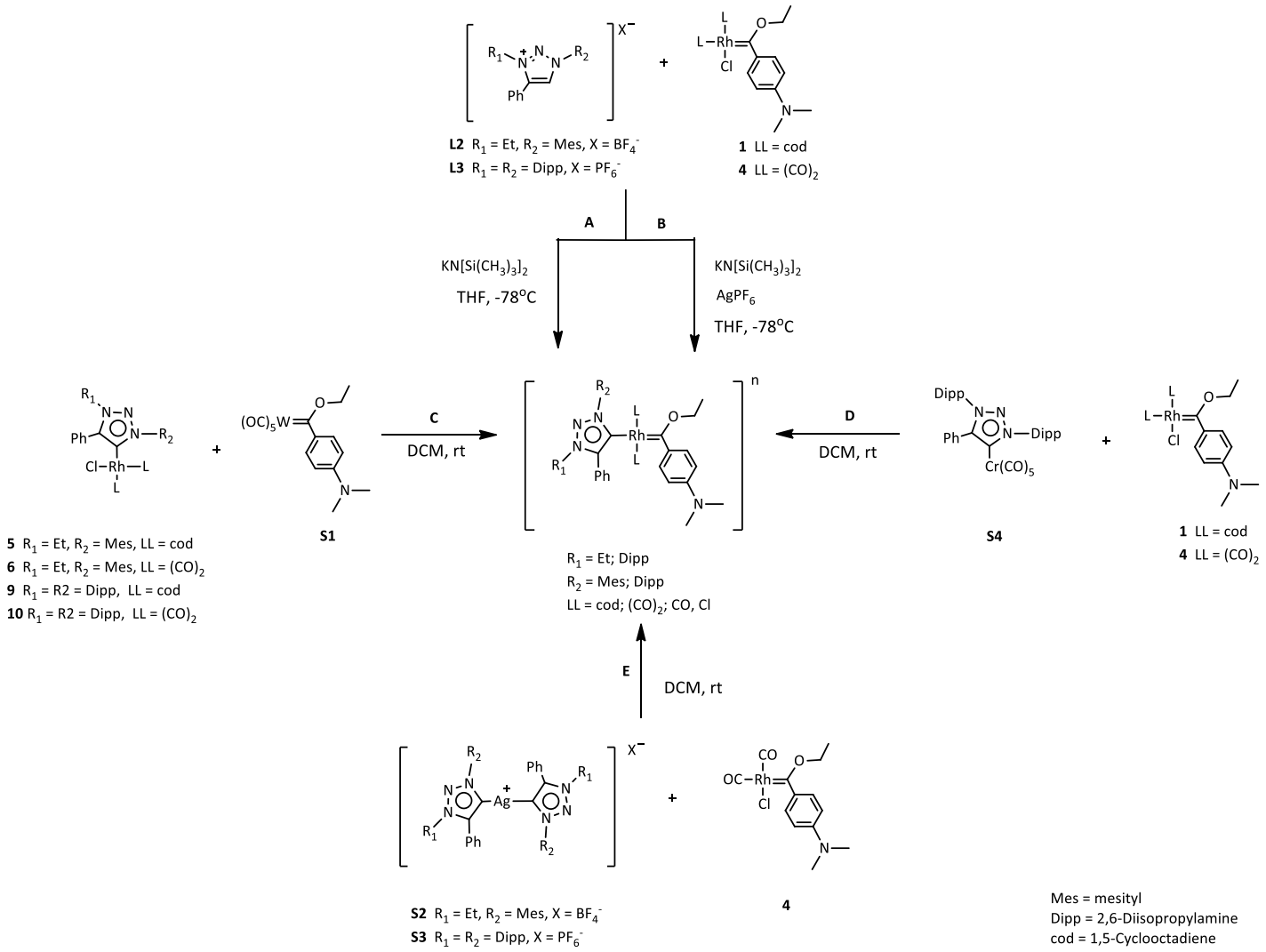

Scheme 5. 4: Proposed reaction routes to access the rhodium(I) mixed biscarbene complex

5.3. Results and discussion

Herein, the preparation of the precursors **L4** and **L5** is described following a modified version of the classical copper-catalysed "click" method described in chapter 3, succeeded by alkylation. The chelation of **13** to rhodium(I) will be reported, along with the synthesis of the dinuclear rhodium(I) complex, **14**. The obtained spectroscopic and molecular structural data will be reviewed and compared to the previously reported data of related complexes.

5.3.1. Preparation of compounds L4-L5 and complexes 13-14

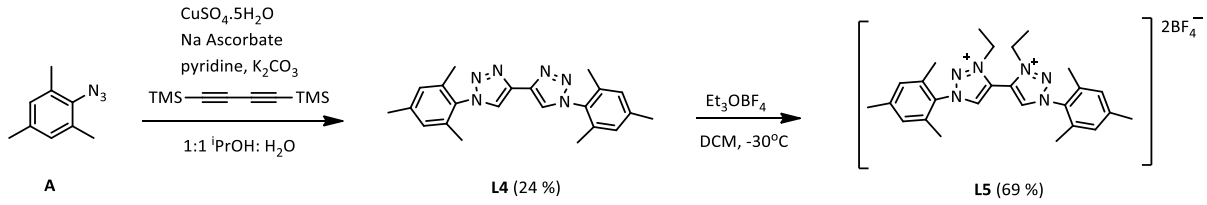

TMS = trimethylsilane
^{i}PrOH = isopropanol

Scheme 5. 5: Copper-catalyzed "click" cycloaddition reaction for i-bitz precursor preparation.[15]

The preparation of precursor compounds **L4** and **L5** follows a modified version of the copper-catalysed cycloaddition reaction of 1,4-bis(trimethylsilane)-butadiyne with 2 equivalents of mesitylazide in the presence of $CuSO_4.5H_2O$, sodium ascorbate, pyridine and K_2CO_3 (Scheme 5.3).[15] The reaction mixture was allowed to stir overnight in 1:1 ^{i}PrOH:H_2O at room temperature and **L4** was extracted in DCM and isolated with a 24% yield. The yield obtained is significantly less than that reported by Bertrand, whose yields were between 51% and 81%. Seemingly, isolation of the azide results in poor yields, the only marked difference between the synthetic approach used here and that employed by Bertrand.[7] The alkylation of **L4** proceeded under inert conditions at -30°C over a period of 3-5 days, while warming up to room temperature followed by the recrystallization, affording complex **L5** (69%).

Compound **L5** was treated with KHMDS in the presence of $[Rh(cod)Cl]_2$ at -78°C, washed with diethyl ether and **13** (49%) was extracted in DCM, instead of the expected ethyl analogue of **n**.[7] Astoundingly, a bimetallic complex with a bridging chloride, comparable to the previously reported 1,2-dihapto 1,2,3-triazol-4,5-diylidene complex (52%) was isolated, with analogous yields.[15] It is speculated that the combined effect of the steric bulk of the substituents on the ligand and of the cod co-ligand; a short linker,[19] together with an increase in temperature during the early stages of the reaction stimulates dihapto bridging of the ligand.[15]

A similar procedure was followed to obtain **14**, with excess $NaBF_4$ included in the initial reaction mixture, however the reaction was left in the cold overnight. Gaseous CO was passed through the resultant crude mixture and **14** was extracted in DCM with a yield of 42%.

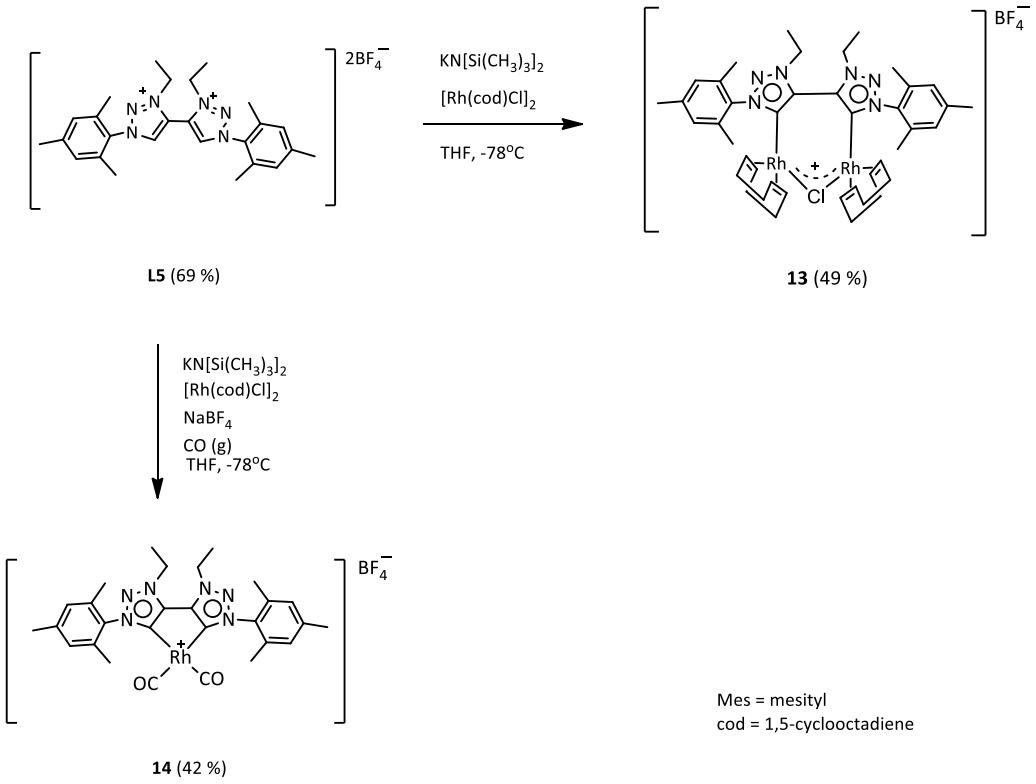

*Scheme 5. 6: The preparation of complexes **14** and **15** from compound **L5***

5.3.2. Spectroscopic analysis of compounds L4-L5, 13-14.

5.3.2.1. Evaluation of the ^{1}H NMR spectra of compounds L4-L5, 13-14.

The NMR spectra of compounds **L4-L5**, **13-14** are given in the experimental section. The alkylation of **L4** is evidenced in the proton spectrum of complex **L5** (Figure 5.2), indicated by the increase in acidity of the triazole proton shifting from 8.10 ppm (Figure 5.1) to 9.15 ppm. The appearance of a quartet integrating for 4 protons resonating at 4.74 ppm is seen, along with the corresponding triplet at 1.74 ppm, integrating for 6 protons. The presence of the BF_4^- counterion is corroborated by ^{19}F NMR, showing two isotopologue signals in Figure 5.3 resonating at 151.7 ppm. These are a consequence of the coupling of fluorine with two boron isotopes ^{10}B (natural abundance of 19.9%) and ^{11}B (natural abundance of 80.1%).[16]

The clean disappearance of the acidic proton at 9.15 ppm in the ^{1}H NMR spectrum of **13** at together with broadened peaks indicate an alteration to the structure of the precursor **L5**.[14] Broadening is also attributed to dynamic processes within the complex, inter-coordination sphere, as well as intra-coordination sphere. Asymmetric coordination about the rhodium centre is substantiated by the splitting pattern of the proton signals of **13**. The signals on the aromatic region have split into doublets from a singlets compared to the uncoordinated salt in Figure 5.2.[17] The proton NMR spectrum of complex **14** (Figure 5.6) shows the disappearance of the acidic peak, signifying coordination to the

rhodium metal centre. Dissimilar to complex **13,** perfect symmetry is observed about the coordination sphere of the metal.

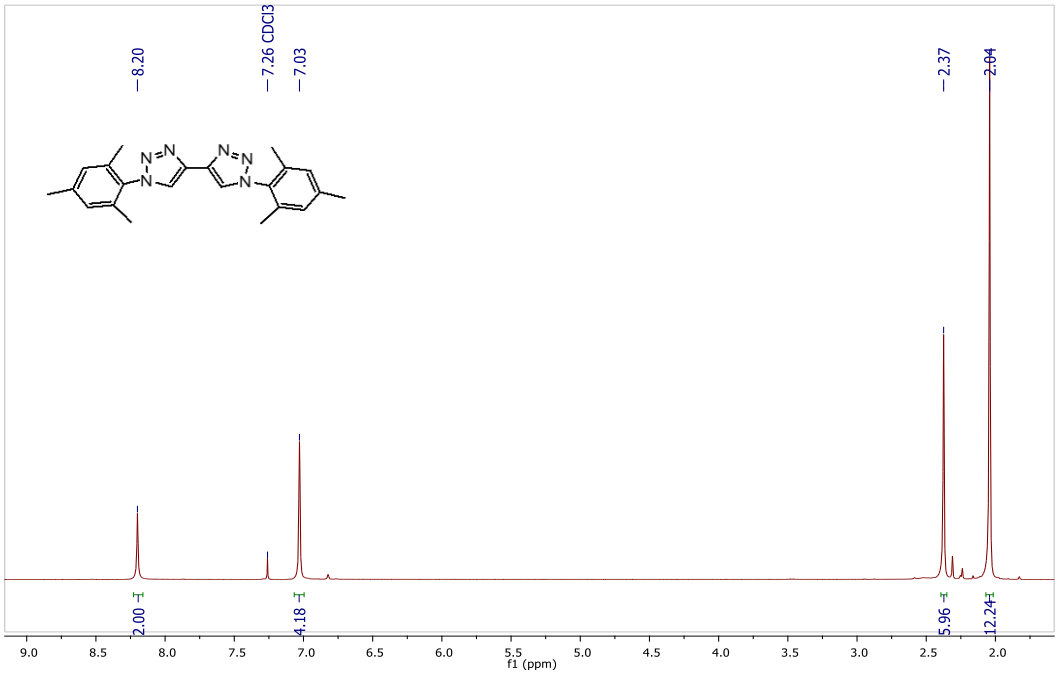

*Figure 5. 1: ^{1}H NMR spectrum of compound **L4** in $CDCl_3$*

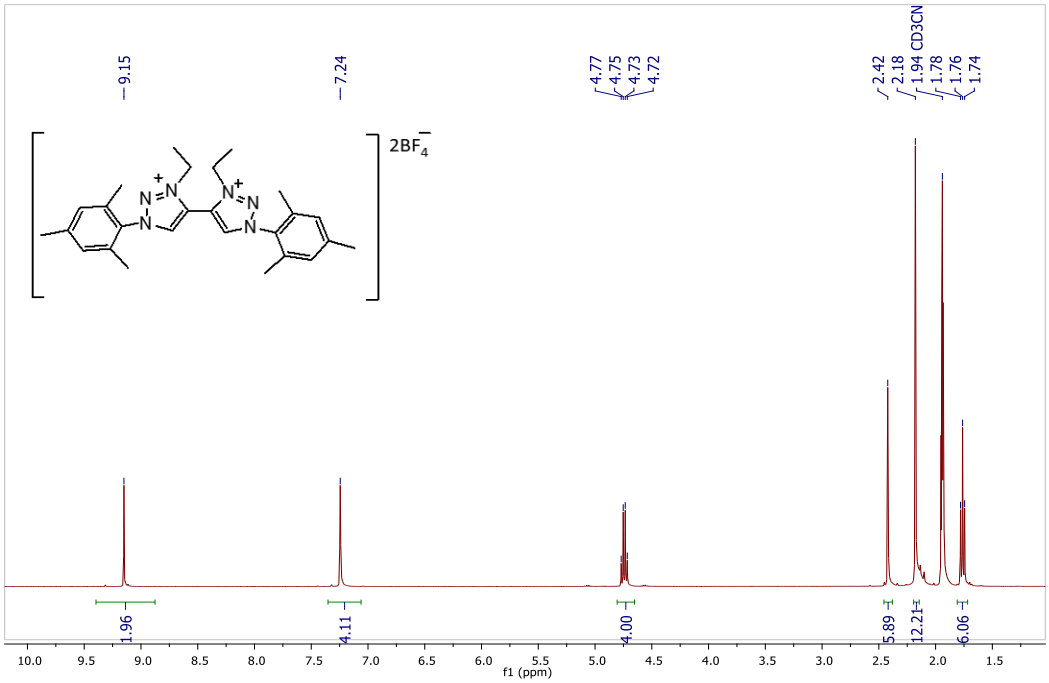

*Figure 5. 2: ^{1}H NMR spectrum of compound **L5** in $CDCN_3$*

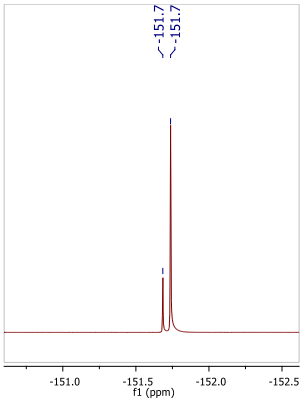

*Figure 5. 3: ^{19}F NMR spectrum of compound **L5** in solvent $CDCN_3$*

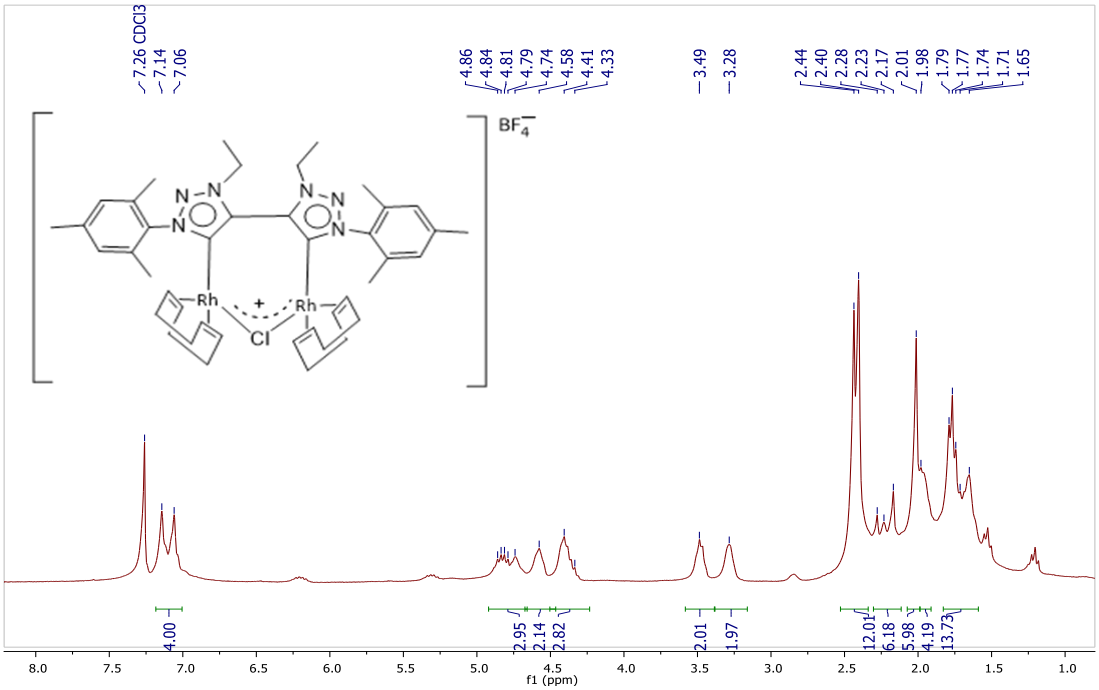

*Figure 5. 4: ^{1}H NMR spectrum of complex **13** in solvent $CDCl_3$*

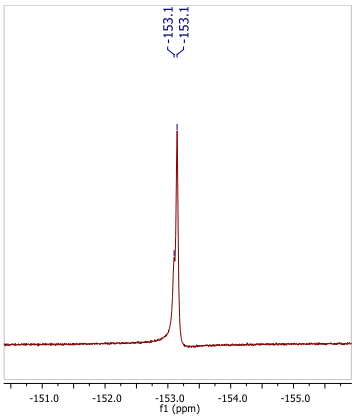

*Figure 5. 5: ^{19}F NMR of complex **13** in solvent $CDCl_3$*

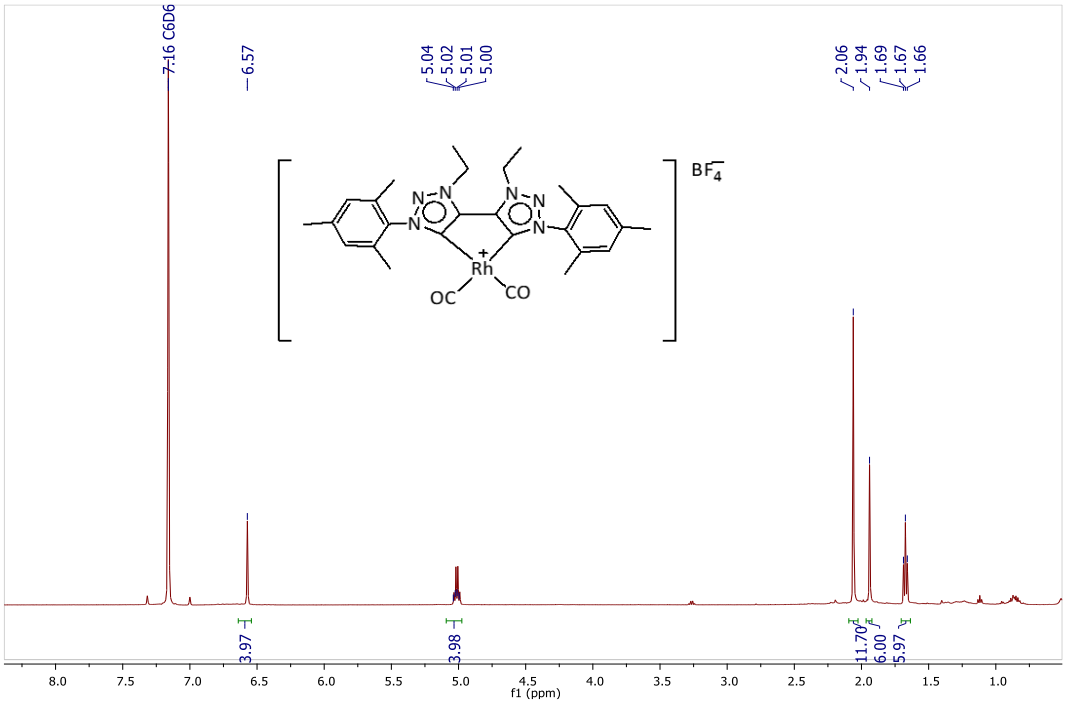

*Figure 5. 6: ^{1}H NMR spectrum of complex **14** in solvent C_6D_6*

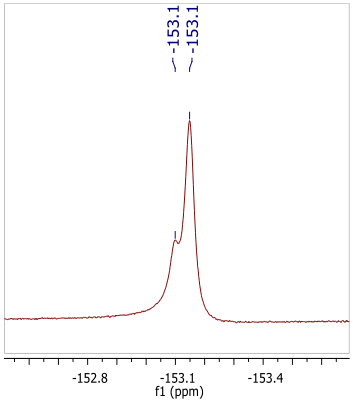

*Figure 5. 7 : ^{19}F NMR spectrum of complex **14** in solvent C_6D_6*

5.3.2.2. Evaluation of the ^{13}C NMR spectra of compounds L4-L5, 13-14.

*Table 5. 1: Spectroscopic data of complexes **13** and **14***

Complex	$^{13}C\delta(C_{carbene})$, ($^{1}J$(RhC))(Hz)	^{13}C δ(CO)	IR[a] ν(CO), (cm^{-1})
13	172.8 (d, 47.0)	-	-
14	172.9 (d, 44.1)	Not observed (n.o.)	2056[b]

[a]Recorded in CH_2Cl_2. [b]CO-ligand trans to carbene.

From the ^{13}C NMR spectrum of **13** (Figure 5.13), a low-field doublet representing the carbene carbon atom resonance is seen at 172.8 ppm (*J*(RhC) = 47.0 Hz) (Table 5.1). The carbene carbon of the methyl analogue of the mononuclear rhodium complex reportedly resonates at 172.9 ppm (*J*(RhC) = 40 Hz), corresponding to that obtained for **13**.[7] Additionally, the carbene carbon chemical shifts of the monodentate rhodium 1,2,3-triazol-5-ylidene complexes **5** (Chapter 3) and **9** (Chapter 4) resonate as doublets at 171.6 ppm (*J*(RhC) = 47.4 Hz) and 172.3 ppm (*J*(RhC) = 47.3 Hz) respectively. Therefore, it is deduced that the carbene peak of cod bearing rhodium(I) 1,2,3-triazol-5-ylidene complexes resonate as a doublet signal in the region of ~170 ppm, irrespective of the mode of coordination. The coupling constant (*J)* of the carbene carbon in **13** is similar to those obtained for monodentate complexes **5** and **9,** and markedly deviates from the mononuclear complex reported by Bertrand. A smaller coupling constant implies a better σ-donation.[18] This signifies the enhanced donor effect of a pair of 1,2,3-triazol-5-ylidene donors to a central metal, compared to a single donor as in monodentate or bridged complexes.

The ^{13}C NMR spectrum of **14** shows the appearance of a doublet signal corresponding to the carbene carbon at 172.9 ppm with a coupling constant *J*(RhC) = 44.1 Hz. As aforementioned, this coupling constant is expected to be smaller than that of complex **13** (*J*(RhC) = 47.0 Hz, Table 5.1) as a result of the amplified donor ability of this ligand as a chelating bidentate ligand, in comparison to that of the bridged ligand which is synonymous with monodentate ligands. **14** is directly comparable to its methyl analogue prepared by Bertrand, with a carbene doublet at 173.6 ppm and a coupling constant *J*(RhC) = 44.0 Hz.[7] However, unlike the methyl analogue, the CO singlet of **14** was not observed at the expected 187.3 ppm.

The cationic nature of both complex **13** and **14** is supported by ^{19}F NMR spectra confirming the presence of a BF_4^- counterion with overlapping isotopologue peaks resonating at -153 ppm.

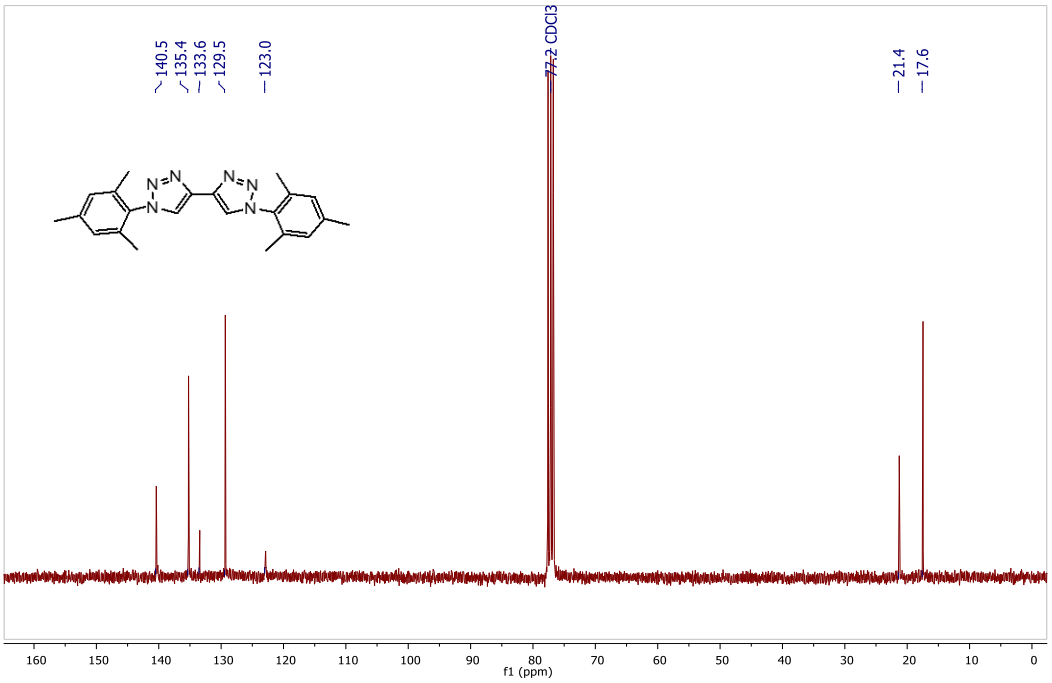

*Figure 5. 8: ^{13}C NMR spectrum of compound **L4** in $CDCl_3$*

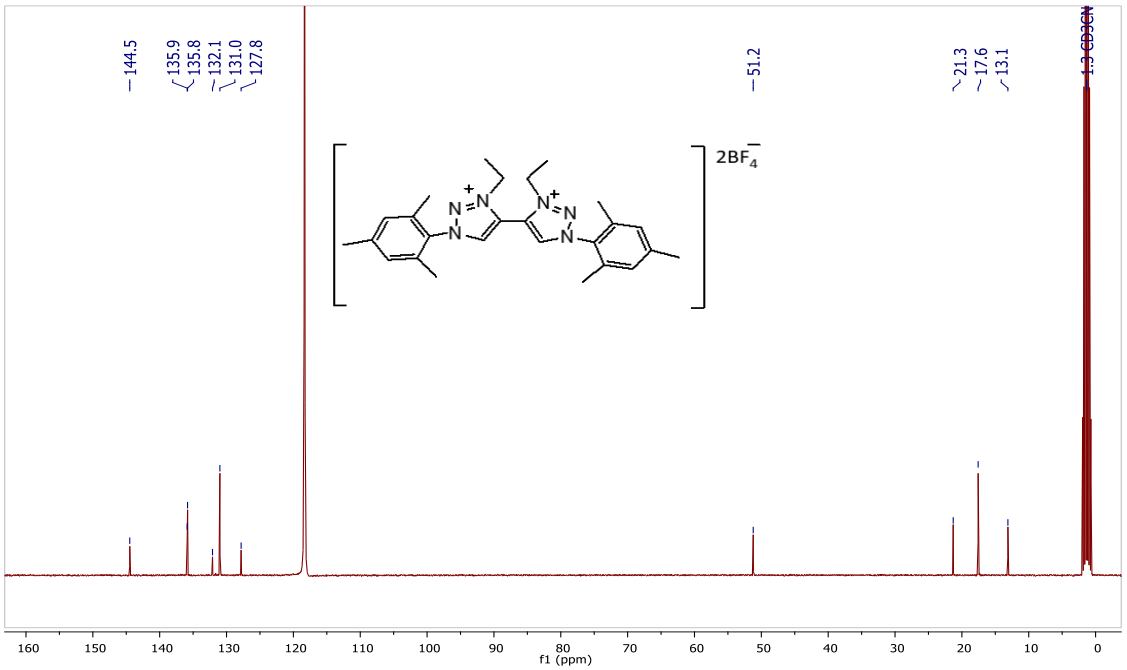

*Figure 5. 9: ^{13}C NMR spectrum of compound **L5** in $CDCN_3$*

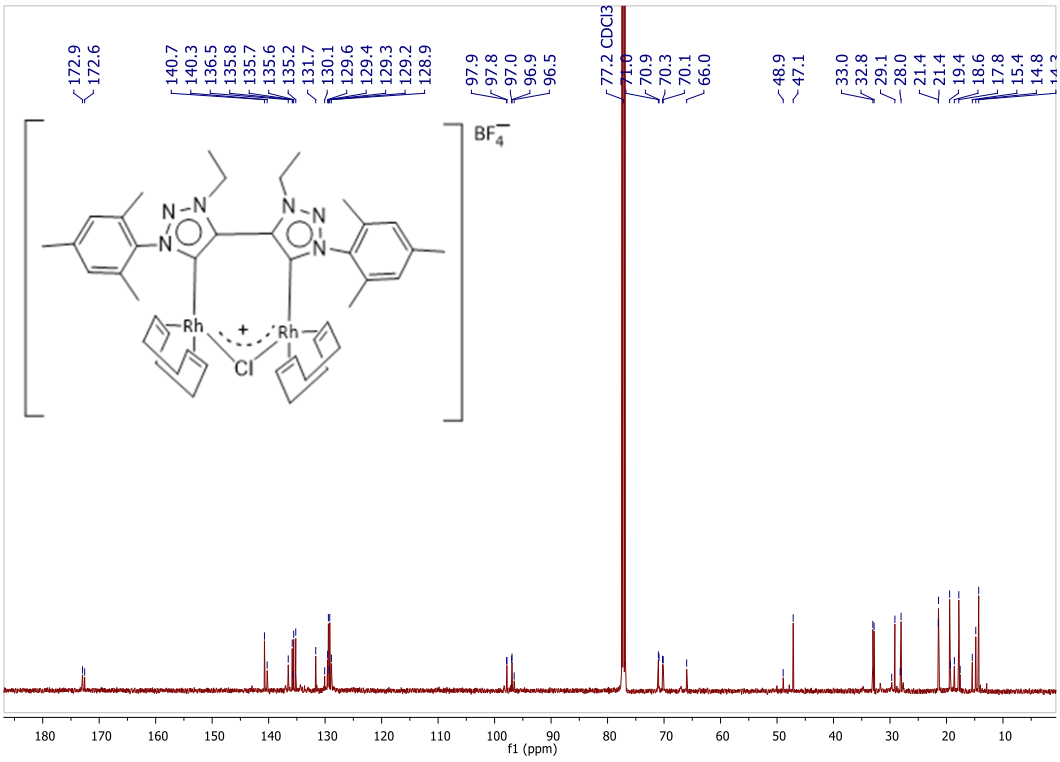

*Figure 5. 10: ^{13}C NMR spectrum of complex **13** in solvent $CDCl_3$*

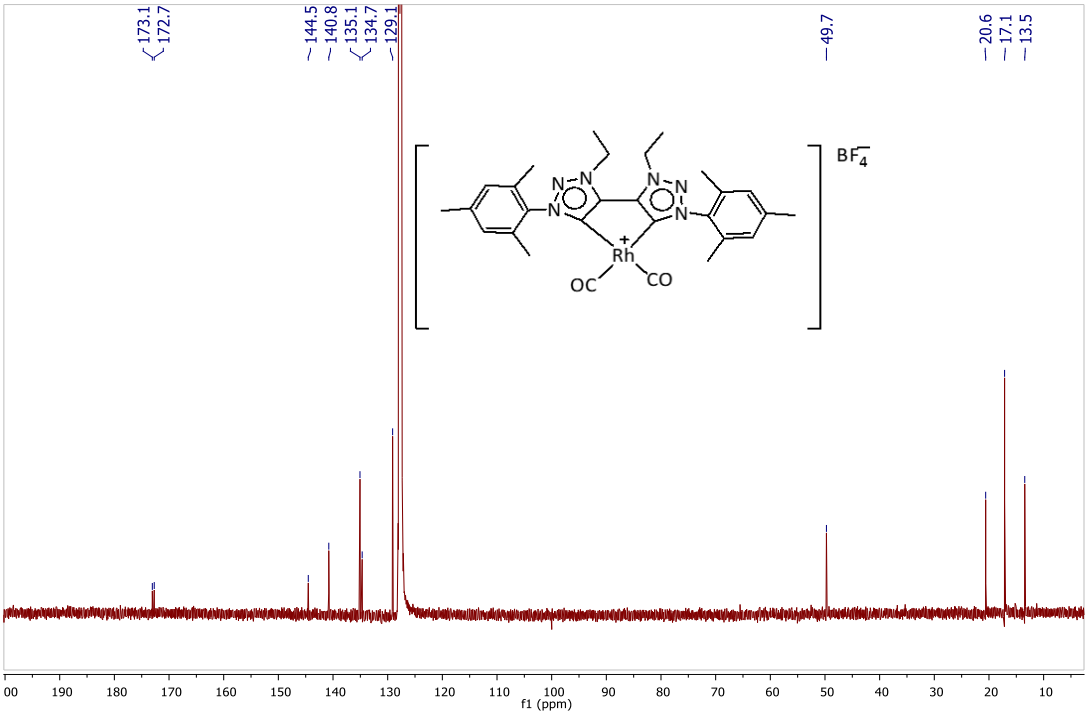

*Figure 5. 11: ^{13}C NMR spectrum of complex **14** in solvent C_6D_6*

5.3.2.2. Inspection of the donor strength of ligand L5^{I}.

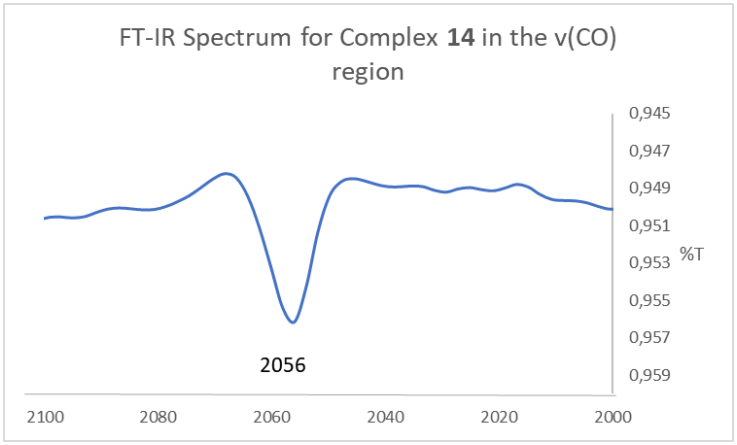

*Figure 5. 12: FT-IR spectrum of complex **14** in CH_2Cl_2*

Upon investigation, the infrared (FT-IR) spectrum of **14** showed a single peak at 2056 cm^{-1} which is presumably as a result of the symmetry of the complex (Figure 5.4), as both CO ligands are coordinated *trans* to a carbene. ligand. The positive mode ESI-HRMS (15 V, m/z) $[M]^+$ found is 587.1577 for the calculated $[M]^+$ value of 587.1641, confirming the presence of two carbonyl groups.

5.3.3. Molecular structure of complex 13

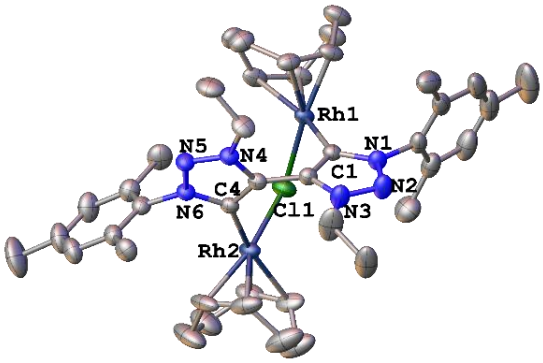

*Figure 5. 13 The solid-state molecular structure of **13** with ellipsoids of 50% probability, with the omission of hydrogens and tetrafluoroborate counterion for clarity. Selected bond lengths (Å) and angles (°): C1–Rh1 2.023(3); C4–Rh2 2.028(3); C1–C2 1.380(4); C2–C3 1.467(4); C3–C4 1.381(4); C2–N31.361(4); C3-N4 1.363(4); N2–N3 1.316(4); N5–N6 1.344(3); N1–N2 1.335(3); N4–N5 1.305(3); C1– N1 1.366(4); C4– N6 1.373(4); N1– C1– C2*

Suitable single crystals of **13** were obtained from the slow diffusion of *n*-hexane into a concentrated DCM solution of the complex and stored overnight at 4°C. A pseudo-square planar geometry is observed about each rhodium centre with a Cl1–Rh1–C1 bond angle of 89.98(8)°, and a Cl1–Rh2–C4 bond angle of 92.55(8)° (Figure 5.13). Both triazol- rings are planar,[15] however to circumvent steric repulsions between the two cod ligands, the rings are oriented perpendicularly with respect to each other, with dihedral angle of 66.3(4)°. For mononuclear i-bitz complexes with carbonyl co-ligands, these triazoles are in the same plane to induce a square planar geometry about the metal centre,[19] with a recorded bite angle of 77.01(15)°.[7] Each mesityl group is also oriented in an antiperiplanar fashion with respect to its corresponding heterocycle. The bond angles N1–C1–C2 (102.1(3)°) and N6–C4– C3 (101.6(2)°) are comparable to that of coordinated monodentate 1,2,3-triazol-5-ylidene complexes **5** (100.6(4)°) and **9** (107.0(4)°) of chapter 3 and 4 respectively. The $C1_{carbene}$–Rh1, and the $C4_{carbene}$–Rh2 bond lengths were found to be 2.023(3) Å and 2.028(3) Å, which are analogous to monodentate complexes **5** (2.029(3) Å) and **9** (2.053(4) Å). These are shorter than the corresponding bond lengths in chelated i-bitz dicarbonyl rhodium(I) complexes (2.069(4)-2.071(4) Å), as reported by Bertrand.[7] In general, square planar 1,2,3-triazolylidene complexes with cod co-ligands exhibit shorter bond lengths than their CO counterparts[15] as can be observed in chapter 4 between complexes **9** (2.053(4) Å) and **10** (2.059(2) Å); and between **11** (2.046(9) Å)and **12** (2.0699(12) Å). Moreover, the obtained structural data illustrates an intermediate structure where the bridging chloride coordinates to one of the metal centres as an X-type ligand resulting in a neutral moiety, and the other as an L-type ligand resulting in a charged moiety, thus delocalising the electron density between the two metal centres through the chloride ligand.

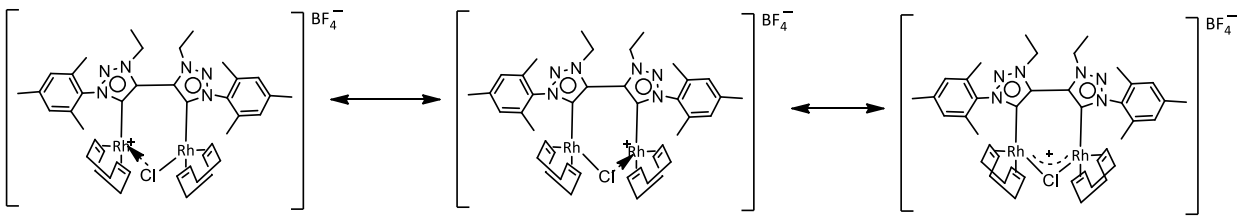

*Figure 5. 14: The resonance structure illustrating the delocalisation of charge in the complex **14***

5.3.4. Attempted preparation of a hybrid carbene complex

A variety of synthetic routes to access the targeted 1,2,3-triazol-5-ylidene rhodium(I) Fischer carbene complex will be described, along with the serendipitous isolation of complex **15**. A selection of the compounds described and isolated in chapters 2-4 will be used as precursors in reactions of the ensuing mixed carbene complex.

5.3.4.1. The free carbene routes

The free carbene route is a useful technique to obtain 1,2,3-triazolylidene complexes of transition metals. This can proceed by deprotonation with a non-nucleophilic base in the presence of a metal, or by isolation of the free carbene following deprotonation, before metalation with the desired metal. Scheme 5.7 is a representation of the free carbene reactions performed in preparation of the hybrid biscarbene complex.

Compound **L2** or **L3**, KHMDS and complex **1** were added to an argon-purged Schlenk tube and cooled to -78ºC before transferring dried THF. The reaction was left to stir overnight while warming up to room temperature before removing volatiles under reduced pressure. N-hexane, Et_2O and DCM were used to extract the ensuing product however this reaction proved to be unsuccessful. The reaction was repeated with complex **4**, this proved to be a futile exercise. Both reactions yielded a mixture of unreacted starting material **L2** or **L3** as well as unidentifiable decomposition products of **1** or **4**. Although KHMDS is a weak nucleophile, the Fischer carbene carbon is highly electrophilic and may be susceptible to even the weakest nucleophilic attack, which is speculated to be the cause of the unsuccessful reactions.

To remedy this aforementioned situation, compound **L2** or **L3** was treated with excess KHMDS in Et_2O where the base is partially soluble in one Schlenk tube at -78ºC and allowed to warm up to -10ºC, before canular filtering into a cold THF solution of **1** or **4**, allowing a solution of the free carbene to pass through the canular. This reaction did not work presumably due to insufficient solubility of the salt and the base as in one case, the trace amounts of the starting material was isolated; the instability of the resulting free triazolylidene in the case of compound **L2** the indeterminable decomposition product of the triazolylidene salt was isolated; as well as inadequate activation of the Fischer carbene **1** or **4.** The reaction was repeated with the more stable salt **L3,** and the free carbene was transferred to a solution of **1** or **4** with a chloride abstractor, $AgPF_6$. These reactions were unsuccessful.

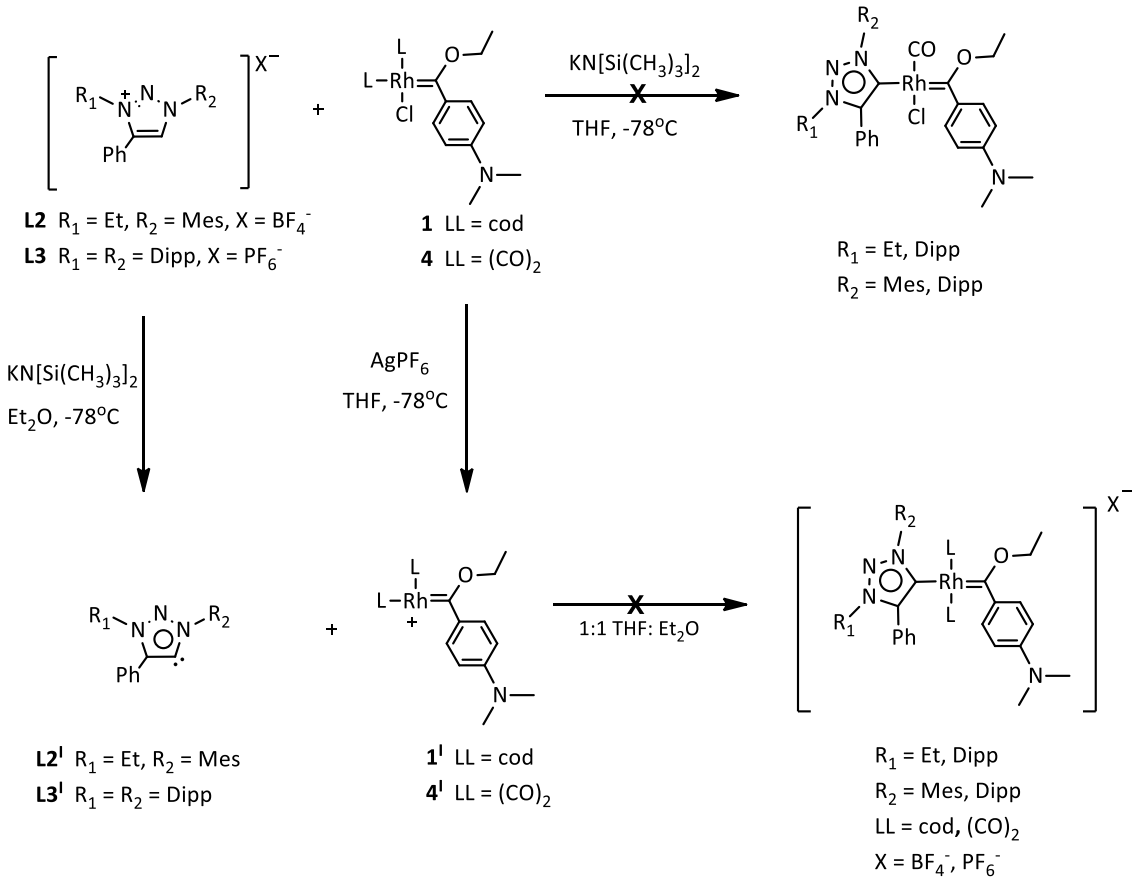

Scheme 5. 7: The attempted free carbene approach for the preparation of the mixed biscarbene complex

5.3.4.2. The transmetalation routes

Since the 1970s,[20] the transmetalation of carbenes from group 6 transition metals to late group transition metals have been utilised in countless reactions, and gained popularity after Sierra and co-workers established the effectiveness of late-group transition metal catalyst in comparison to group 6 complexes.[19] Using Barluenga's facile approach,[8,13] complex **5** or **9** was reacted with **S1** in DCM at room temperature and allowed to stir for 1-7 days (Scheme 5.8). The aim was to transfer the Fischer carbene along with a carbonyl,[13] to access the mixed carbene complex. This reaction route proved ineffective, also when repeated with complex **6** or **10.** This is speculated to be due to the better donating ability of the of the 1,2,3-triazolylidene compared to the NHC complex used by Barluenga, causing complexes **5, 6, 9** and **10** to be more inert and resistant to carbene transfer/ transmetalation reactions. Barluenga experienced similar repercussions when transmetalating from a group 6 amino Fischer carbene which required longer reaction times due to the increased stability of the amino carbene compared to the ethoxy analogue.[13]

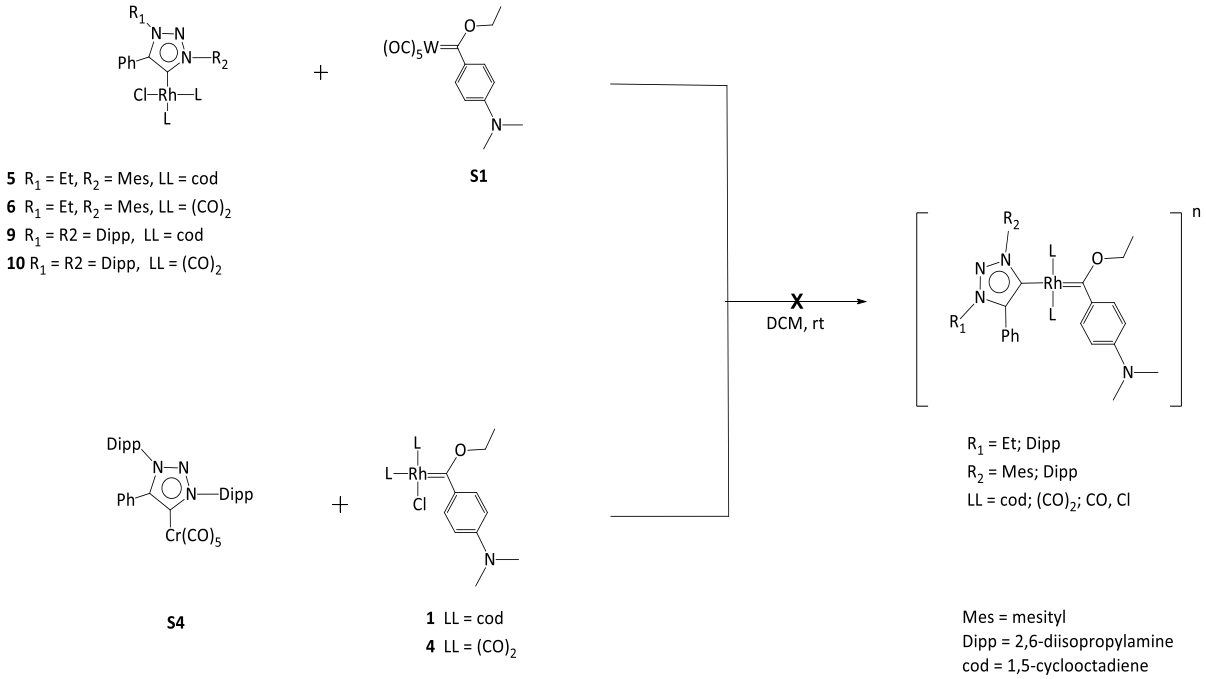

Scheme 5. 8: The attempted synthesis of the rhodium(I) mixed carbene complex following the transmetalation approach.

Complex **S4** was reacted with **1** or **4** in DCM at room temperature and left to stir for 1-7 days, resulting in a mixture of unreacted starting material **1** or **4** and the protonated compound **L3** in the DCM fraction. This reaction was repeated once more in toluene, refluxing at 50°C, resulting in complete decomposition signalled by a colour change from orange to black.

Silver(I) NHC complexes are well-known carbene transfer agents (see Chapters 3 and 4).[21] Using this approach, complex **S2** or **S3** was reacted with the Fischer carbene complex **4** in DCM at room temperature in the absence of light, for 1-7 days or until a precipitate was observed in the reaction vessel. The crude product was washed with hexane, and an orange product extracted in toluene. The products were dissolved in DCM and layered in hexane resulting in single crystals suitable for X-ray diffraction from the reaction of complex **S2** with **4** (Figure 5.6). However, complex **15** was not isolated or characterised spectroscopically, only a single crystal could be extracted from the reaction mixture during recrystallization. When washed with a less polar solvent such as Et_2O and *n*-hexane, the crystals remain intact. When dissolved in DCM or $CDCl_3$ for NMR, a mixture of products is observed. (Figure 5.19). No suitable crystals were obtained from the reaction of **S3** with **4**. It is speculated that during the carbene transfer from **S2**, the resulting silver monocarbene abstracts a chloride from complex **4** (or from the chlorinated solvent DCM) affording complex **15** instead of the target hybrid carbene complex**.**

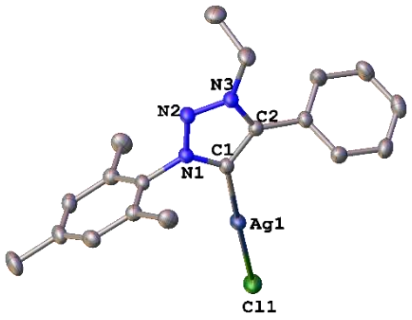

*Figure 5. 15: Molecular structure of **15** with ellipsoids of 50% probability, with the omission of hydrogens and tetrafluoroborate counterion for clarity. Selected bond lengths (Å) and angles (°): Ag– C1 2.0704(16); Ag– Cl 2.3273(4); C1– C2 1.391(2); C1–N1 1.363(2); N1–N2 1.3367(18); N2-N3 1.3221(19); C2– N3 1.362(2); C1– Ag1– Cl1 178.66(4); N1–C1–C2 102.10(13).*

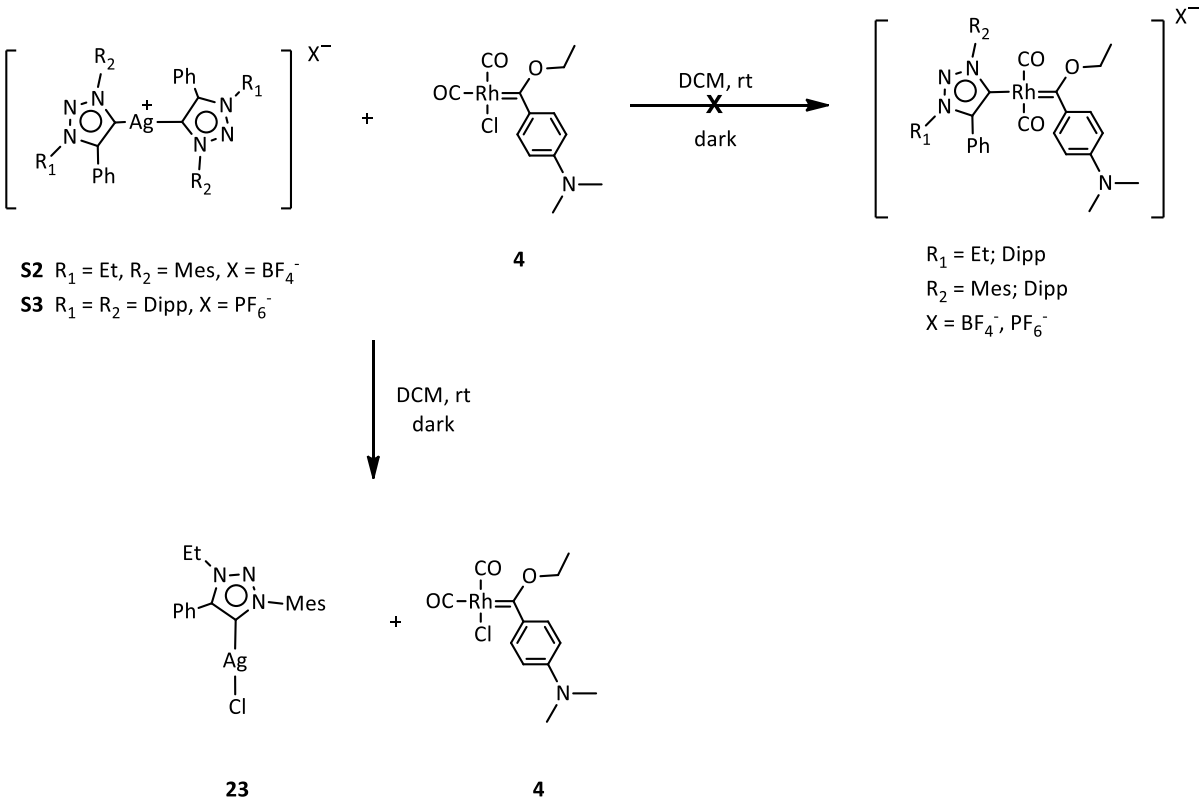

*Scheme 5. 9: The attempted preparation of the rhodium(I) hybrid biscarbene complex using carbene transfer agents **S2** and **S3** resulting in the serendipitous.*

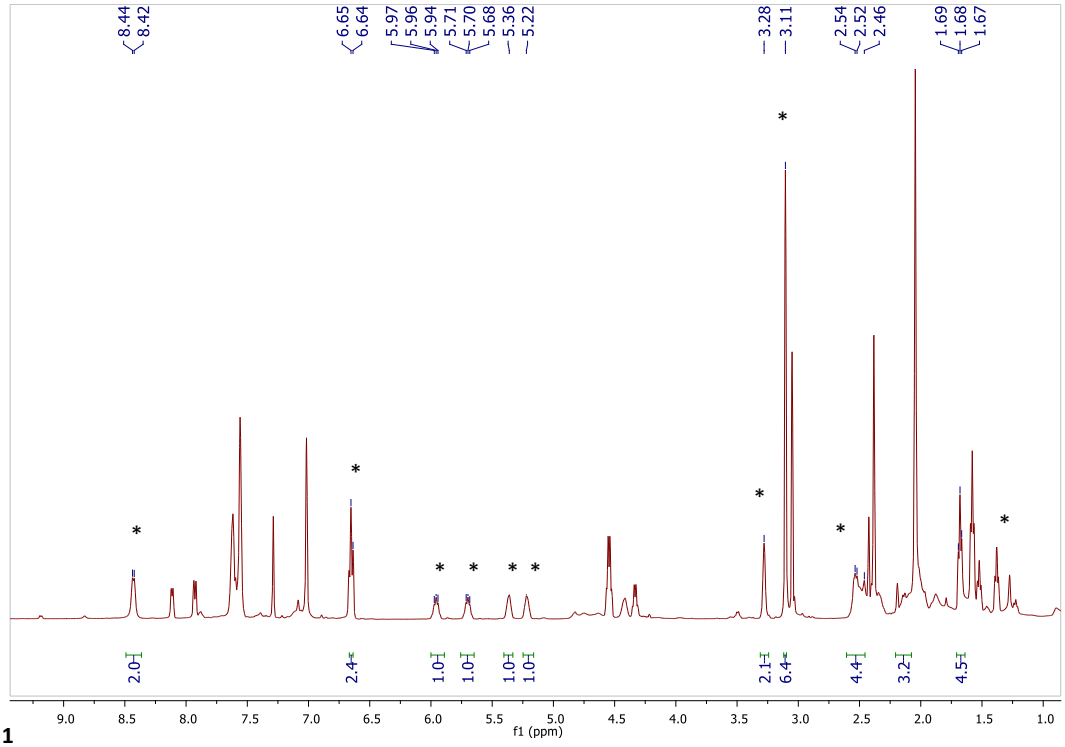

* complex **1**

*Figure 5. 16: ^{1}H NMR spectrum of complex **15** in $CDCl_3$ displaying a mixture of **15** and complex **1.***

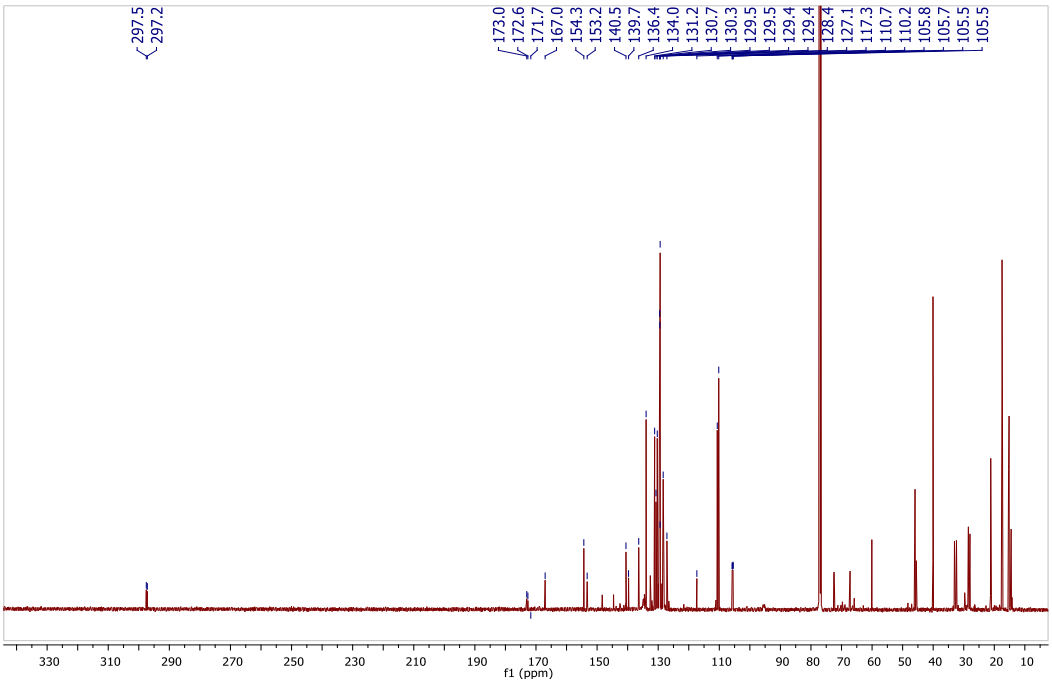

*Figure 5. 17: ^{13}C NMR spectrum of **15** in $CDCl_3$ displaying a mixture of **15** and complex **1***

5.4. Conclusion

The ethyl analogue (compound **L5**) of the known methylated i-bitz salt was isolated from the corresponding bitz **L4**,[7] by alkylation with Meerwein's triethyloxonium salt. Coordination to a rhodium(cod) chloride dimer yielded complexes with two different geometries: if **L5** was deprotonated *in situ* and reacted with the rhodium precursor, the triazolylidene ligand acts as a bridging ligand to the rhodium dimer $[Rh(cod)Cl]_2$; forming the dinuclear complex **13**, with a similar topology to Bertrand's 1,2-dihapto-1,2,3-triazol-4,5-ylidene rhodium(I) complex,[15] If however, the same route is followed with subsequent treatment with CO (g) prior to purification, the expected mononuclear chelated complex **14** is obtained. Thus, **13** is similar to Bertrand's dihapto bimetallic ligand with a bridging chloride, and **14** corresponds to Bertrand's i-bitz rhodium complex. Broadening of the ^{1}H NMR signals in figure 5.12 is observed, congruent to the previously reported 1,2-dihapto-1,2,3-triazol-4,5-ylidene rhodium(I) complex.[15] Dissimilar to this complex, the carbene doublet of **13** in the corresponding ^{13}C NMR spectrum resonates at 172.8 ppm (J(RhC) = 47.0 Hz) consistent with what has been previously reported for monodentate and chelated 1,2,3-triazol-5-ylidene rhodium complexes, with a cod co-ligand.[7,15]

The molecular structure of **13** confirmed the unexpected bridging dinuclear structure of the complexes. The bond lengths $C1_{carbene}$–Rh1 (2.023(3) Å), and $C4_{carbene}$–Rh2 (2.028(3) Å) were attained, and found to be analogous to those of monodentate rhodium 1,2,3-triazol-5-ylidene complexes.[25] The ^{1}H NMR spectrum of **14** is completely symmetrical with well resolved peaks in contrast to that of **13**. A carbene doublet is observed at 172.9 ppm (J(RhC) = 44.1 Hz) of the ^{13}C NMR spectrum which corresponds to that obtained by Bertrand for the methyl analogue of **14**.[7] The differences in coupling constants between **13** and **14** are expected, as the metal centre in the chelated complex experiences enhanced σ-donation compared to the individual metal centres of the bridged complex. Therefore, it can be deduced that each metal in bridged complexes behaves analogously to monodentate complexes. Conversely, chelated complexes are superior σ-donors. Thus, the first objective in the aim of this study was successfully accomplished.

A number of synthetic routes were employed for the isolation of the hybrid 1,2,3-triazol-5-ylidene rhodium(I) Fischer carbene complex including free carbene routes where the triazolium salt was deprotonated and reacted a rhodium Fischer carbene complex. Two types of transmetalation reactions were performed, including the transmetalation from a group 6 carbene (Fischer or mesoionic) to a rhodium carbene (Fischer or mesoionic) (Scheme 5.11); and transmetalation from a carbene transfer agent to a rhodium Fischer carbene complex. None of these reactions were successful, however the latter reaction resulted in the isolation of complex **15** (Scheme 5.12), which was only characterised in solid state. In a solution, a mixture of **15** and the starting material **1** or **2** is observed on the obtained ^{1}H and ^{13}C NMR spectra (Figure 5.18 and 5.19).

The second objective of this study, namely the incorporation of two different types of singlet carbene ligands (strong σ-donor vs strong π-acceptor for MIC vs FC, respectively) could not be exploited in the unsuccessful synthesis of mixed biscarbene complexes of rhodium(I).

5.5. Experimental data

5.5.1. Comprehensive synthetic routes of compounds 19-22

5.5.1.1. Synthesis of 4,4'-bis(1-mesityl-1,2,3-triazole), **L4**[5]

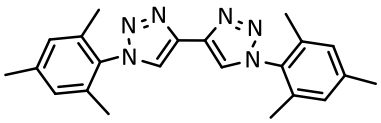

Bis(trimethylsilane)-butadiyne was dissolved in 1:1 ^{i}PrOH: H_2O at room temperature. To that, $CuSO_4.5H_2O$, K_2CO_3, mesityl azide, pyridine and sodium ascorbate were added and left to stir overnight. The reaction mixture was added to a large conical flask containing 1:1 DCM:NH_4OH and left to stir overnight at room temperature. The reaction was left to separate into an aqueous and organic layer, and the aqueous layer washed with DCM. The organic fractions were combined and dried over $MgSO_4$. The solution was filtered and concentrated and then dried under vacuum at 80^{o}C, yielding an off-white solid. Yield: 24%. M.P(dec): 310-313°C. ^{1}H NMR (300 MHz, $CDCl_3$) δ8.20 (s, 2H, trz-H), 7.03(s, 4H, mes-CH), 2.37(s, 6H, mes-CH_3), 2.04(s, 12H, mes-CH_3). ^{13}C NMR (75MHz, $CDCl_3$) δ140.3 (trz-CH)140.1(mes-C_q) , 135.2(mes-C_q), 133.4(trz-C_q), 129.3(mes-CH), 122.8(mes-C_q).

5.5.1.2. Synthesis of 4,4'-bis(3-ethyl-1-mesityl-1,2,3-triazolium tetrafluoroborate), **L5**[22]

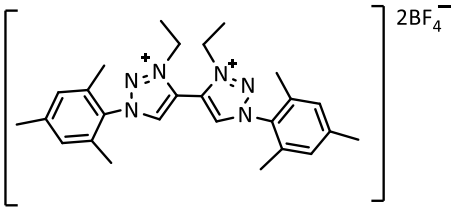

L4 was charged to a flame-dried, $Ar_{(g)}$ purged Schlenk tube, and dissolved in degassed DCM (15 mL) before cooling to -30°C. In a separate Schlenk tube, triethyloxonium tetrafluoroborate was dried and dissolved in DCM (5mL), before transferring to the cooled solution. The reaction mixture is left to stir for 4 days then quenched with MeOH, followed by the removal of volatiles under reduced pressure. The residue was filtered through an ALOX plug, flushed with 1:1 DCM: MeCN, and allowed to crystalize overnight. The crystals were washed with hexane and diethyl ether; then dried overnight under vacuum at 80°C. Yield: 69%. M.P. (decomp): 269-272°C. 1H NMR (400 MHz, CD_3CN) δ 9.15 (s, 2H, trz-CH), 7.24 (s, 4H, mes-CH), 4.74 (q, ^{3}J(HH) = 7.2 Hz, 4H, NCH_2CH_3), 2.42 (s, 6H, mes-CH_3), 2.18 (s, 12H, mes-CH_3), 1.76 (t, J = 7.2 Hz, 1H). ^{13}C NMR (101 MHz, CD_3CN) δ 144.40 (mes-C_q), 135.8 (trz-C_q), 135.7(trz-CH), 132.0(mes-C_q), 130.9(mes-CH), 127.8(mes-C_q), 51.2(NCH_2CH_3), 21.2(mes-CH_3), 17.5(mes-CH_3), 13.1(NCH_2CH_3). ^{19}F NMR (376 MHz, CD_3CN) δ -151.73 (d, ^{2}J(BF) = 19.6 Hz). ESI-HRMS (15 V, positive mode, m/z): calcd for $[M]^{2+}$: 430.2844 Found: 430.2992.

5.5.1.3. Synthesis of μ-bis(3-ethyl-1-mesityl-1,2,3-triazol-5-ylidene)-μ-chlorido-bis(η4-1,5-cyclooctadienerhodium(I)) tetrafluoroborate, **13**[15]

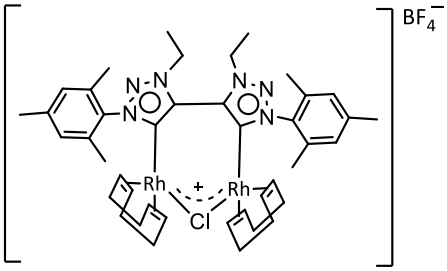

L5 (0.30 g, 0.34 mmol), $[Rh(cod)Cl]_2$ (0.17 g, 0.34 mmol), and $KN[Si(CH_3)_3]_2$ (0.20 g, 1.01 mmol) were added to a flame-dried, $Ar_{(g)}$ purged Schlenk tube and cooled to -78°C, before transferring dried THF (40 ml). The reaction mixture was left to stir for 48hr while the temperature increased to room temperature. The volatiles were removed under reduced pressure, and the residue was washed with diethyl ether. The product was extracted in DCM, and the solvent removed under vacuum, yielding a dark yellow solid. Yield 49 %. M.P. (decomp): 218-222°C. ^{1}H NMR (500 MHz, $CDCl_3$) δ 7.20 – 6.98 (m, 4H, mes-CH), 4.96-4.67 (m, 3H, NCH_2CH_3, cod-CH), 4.58 (br s, 2H, cod-CH), 4.49-4.29 (m, 3H, NCH_2CH_3, cod-CH), 3.55-3.41 (m, 2H, cod-CH), 3.28 (br s, 2H cod-CH), 2.42 (d, ^2J(HH) = 9.5 Hz, 12H, mes-CH_3), 2.30-2.14 (m, 6H, cod-CH), 2.01 (s, 6H, mes-CH_3), 1.97-1.90 (m, 4H, cod-CH), 1.84-1.59 (m, 12H, cod-CH, NCH_2CH_3). ^{13}C NMR (126 MHz, $CDCl_3$) δ 172.76 (d, ^1J(RhC) = 47.0 Hz, $C_{Carbene}$), 140.7 (trz-C_q), 140.2 (trz-C_q), 136.5 (mes-C_q), 135.8 (mes-C_q), 135.7 (mes-C_q), 135.6(mes-C_q), 135.2(mes-C_q), 131.7(mes-C_q), 130.1(mes-C_q), 129.6 (mes-CH), 129.4 (mes-CH), 129.3 (mes-CH), 129.2 (mes-CH), 128.9(mes-C_q), 97.9 (d, ^1J(RhC) = 7.0 Hz, cod-CH), 96.9 (d, ^1J(RhC) = 7.0 Hz, cod-CH), 70.9 (d, ^1J(RhC) = 14.9 Hz, cod-CH), 70.2 (d, ^1J(RhC) = 15.1 Hz, cod-CH), 66.0 (cod-CH), 48.9 (NCH_2CH_3), 47.1 (NCH_2CH_3), 33.0 (cod-CH), 32.8 (cod-CH), 29.1 (cod-CH), 28.1 (cod-CH), 21.4 (mes-CH_3), 19.4 (mes-CH_3), 18.6 (mes-CH_3), 17.8 (mes-CH_3), 17.6 (mes-CH_3), 15.4 (cod-CH), 14.8 (NCH_2CH_3), 14.3(NCH_2CH_3). ^{19}F NMR (471 MHz, $CDCl_3$) δ -153.1 (d, ^1J(BF) = 21.3 Hz). ESI-HRMS (15 V, positive mode, m/z): calcd for $[M\text{-}Cl\text{-}cod]^{2+}$: 741.2236 Found: 714.241

5.5.1.4. Synthesis of 4,4'-bis(3-ethyl-1-mesityl-1,2,3-triazol-5-ylidene)) rhodium(I) dicarbonyl tetrafluoroborate, **14**[7]

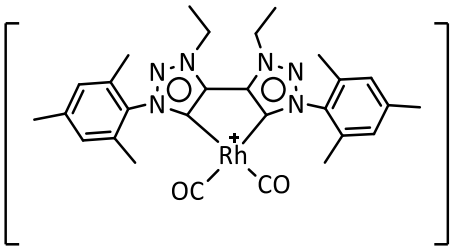

L5 (0.30 g, 0.34 mmol), $[Rh(C_8H_{12})Cl]_2$ (0.17 g, 0.34 mmol), and $KN[Si(CH_3)_3]_2$ (0.20 g, 1.01 mmol) were added to a flame-dried, $Ar_{(g)}$ purged Schlenk tube and cooled to -78°C, before transferring dried THF (40 ml). The reaction mixture was left to stir for 48hr while the temperature increased to room temperature. The volatiles were removed under reduced pressure, and the residue washed with hexane. Diethyl ether was used to extract the product before $CO_{(g)}$ was purged through the solution. The volatiles were removed, the residue was washed with hexanes once more, followed by extraction of the product with DCM. The solvent was removed under reduced pressure, yielding a yellow solid. Yield 42%. M.P.(decomp): 218-222°C ^{1}H NMR (500 MHz, C_6D_6) δ 6.57 (s, 4H, mes-CH_3), 5.01 (q, ^3J(HH) = 7.1 Hz, 4H, NCH_2CH_3), 2.05 (s, 12H, mes-CH_3), 1.93 (s, 6H, mes-CH_3), 1.67 (t, ^3J(HH) = 7.1 Hz, 6H, NCH_2CH_3). ^{13}C NMR (126 MHz, C_6D_6) δ (CO n.o.), 172.88 (d, ^1J(RhC) = 44.1 Hz, $C_{carbene}$), 144.5 (trz-C_q), 140.8 (mes-C_q), 135.1 (mes-C_q), 134.7 (mes-C_q), 128.1 (mes-CH), 49.7

(N<u>CH$_2$</u>CH$_3$), 20.6 (Mes-CH$_3$), 17.2 (mes-<u>CH$_3$</u>), 13.5 (NCH$_2$<u>CH$_3$</u>). ^{19}F NMR (471 MHz, $CDCl_3$) δ -153.1 (d, ^1J(BF) = 22.0 Hz). ESI-HRMS (15 V, positive mode, m/z): calcd for $[M]^+$: 587.1641 Found: 587.1577.

5.5.2. Molecular structural data of complex 13 and 15

Crystal Data for **13**: $C_{42}H_{56}BClF_4N_6Rh_2$ (*M* =973.00 g/mol): monoclinic, space group C2/c (no. 15), *a* = 35.3141(7) Å, *b* = 13.6968(3) Å, *c* = 25.8483(9) Å, *β* = 126.9258(8)°, *V* = 9994.7(5) Å^3, *Z* = 8, *T* = 173.15 K, μ(MoKα) = 0.761 mm^{-1}, *Dcalc* = 1.293 g/cm^3, 82374 reflections measured (2.886° ≤ 2Θ ≤ 56.764°), 12505 unique (R_{int} = 0.0588, R_{sigma} = 0.0458) which were used in all calculations. The final R_1 was 0.0367 (I > 2σ(I)) and wR_2 was 0.0913 (all data).

Crystal Data for **15**: $C_{20}H_{23}AgCl_3N_3$ (*M* =519.63 g/mol): triclinic, space group P-1 (no. 2), *a* = 9.1406(3) Å, *b* = 10.8797(4) Å, *c* = 12.1339(4) Å, *α* = 65.6446(14)°, *β* = 89.5099(16)°, *γ* = 82.4997(16)°, *V* = 1088.52(7) Å^3, *Z* = 2, *T* = 173.15 K, μ(MoKα) = 1.304 mm^{-1}, *Dcalc* = 1.585 g/cm^3, 23183 reflections measured (3.69° ≤ 2Θ ≤ 56.828°), 5472 unique (R_{int} = 0.0222, R_{sigma} = 0.0182) which were used in all calculations. The final R_1 was 0.0214 (I > 2σ(I)) and wR_2 was 0.0552 (all data).

5.6. References

[1] C. Kaes, A. Katz and M. W. Hosseini, *Chem. Rev.*, 2000, **100**, 3553–3590.
[2] Blau, F. *Monatsh. Chem.* 1889, ***10***, 375-388.
[3] Guisado-Barrios, G.; Bouffard, J.; Donnadieu, B.; Bertrand, G. *Angew. Chem., Int. Ed*. 2010, **49**, 4759–4762.
[4] Guisado-Barrios, G.; Bouffard, J.; Donnadieu, B.; Bertrand, G. *Angew. Chem., Int. Ed*. 2010, **49**, 4759–4762.
[5] E. Aldeco-Perez, A. J. Rosenthal, B. Donnadieu, P. Parameswaran, G. Frenking and G. Bertrand, *Science*, 2009, **326**, 556–559.
[6] K. Barral, A. D. Moorhouse and J. E. Moses, *Org. Lett.* 2007, 3567–3569.
[7] G. Guisado-Barrios, J. Bouffard, B. Donnadieu and G. Bertrand, Organometallics, 2011, **30**, 6017–6021.
[8] J. Barluenga, R. Vicente, L. A. López and M. Tomás, *J. Organomet. Chem.*, 2006, **691**, 5642–5647.
[9] M. F. Lappert and P. l. Pye, *Daltons Trans.*, 1977, **21**, 1272-1280.
[10] M. A. Sierra, M. J. Mancheño, E. Sáez and J. C. del Amo, *J. Am. Chem. Soc.*, 1998, **120**, 6812-6813.
[11] R. Aumann, I. Göttker-Schnetmann, R. Fröhlich and O. Meyer,. *Eur. J. Org. chem*., 1999, **10**, 2545-2561.
[12] W. Gil and A. M. Trzeciak, *Coord. Chem. Rev.*, 2011, **255**, 473-483.
[13] J. Barluenga, R. Vicente, L. A. López, E. Rubio, M. Tomás and C. Álvarez-Rúa, *J. Am. Chem. Soc.*, 2004, **126**, 470–471.
[14] R. A. Kelly III, H. Clavier, S. Giudice, N. M. Scott, E. D. Stevens, J. Bordner, I. Samardjiev, C. D. Hoff, L. Cavallo, S. P. Nolan, *Organometallics* 2008, ***27***, 202-210
[15] X. Yan, J. Bouffard, G. Guisado-Barrios, B. Donnadieu and G. Bertrand, *Chem. Eur. J.,* 2012, 18, 14627–14631.
[16] Steven A. Hardinger*, Illustrated Glossary of Organic Chemistry*, http://www.chem.ucla.edu/~harding/IGOC/D/doublet.html#:~:text=Doublet%3A%20In%20NMR%20spectroscopy%2C%20a,to%20the%20indicated%20methyl%20group. (Accessed 10 August 2020).
[17] *See chapter 3 and 4 of this thesis.* (a) D. Aucamp, T. Witteler, F. Dielmann, S. Siangwata, D. C. Liles, G. S. Smith and D. I. Bezuidenhout, *Eur. J. Inorg. Chem.*, 2017, **2017**, 1227–1236. (b) P. Mathew, A. Neels and M. Albrecht, *J.Am.Chem.Soc.*, 2008, **130**, 13534-13535. (c) G. Guisado-Barrios, M. Soleilhavoup and G. Bertrand, *Acc. Chem. Res.*, 2018, **51**, 3236–3244. (d) J. Bouffard, B. K. Keitz, R. Tonner, G. Guisado-barrios, G. Frenking, R. H. Grubbs and G. Bertrand, *Organometallics,* 2011, **30**, 2617–2627.
[18] D. Aucamp, MSc Chemistry, University of Pretoria, 2016
[19] A. Mata, A. R. Chianese, J. R. Miecznikowski, M. Poyatos, E. Peris, J. W. Faller and R. H. Crabtree, *Organometallics,* 2004, **23**, 1253-1263.
[20] E. Fischer and H. J. Beck, *Angew. Chem. Int. Ed. Engl.*, 1970, **9**, 72-73
[21] *(a)* J. Arduengo, H. V. R. Dias, J. C. Calabrese and F. Davidson, *Homoleptic Carbene-Silver(1) and Carbene-Copper(1) Complexes*, 1993, vol. 12. *(b)* H. M. J. Wang and I. J. B. Lin, *Facile Synthesis of Silver(I)-Carbene Complexes. Useful Carbene Transfer Agents*, 1998. *(c)* M. Iglesias, D. J. Beetstra, J. C. Knight, L. L. Ooi, A. Stasch, S. Coles, L. Male, M. B. Hursthouse, K. J. Cavell, A. Dervisi and I. A. Fallis, *Organometallics*, 2008, **27**, 3279–3289.
[22] S. Hohloch, D. Scheiffele and B. Sarkar, *Eur. J. Inorg. Chem.*, 2013, 3956–3965

Chapter 6: Hydroformylation of 1-octene

6.1. Background

The hydroformylation reaction was serendipitously discovered in 1948 during the reintroduction of ethylene into a Fischer-Tropsch reaction.[1] Otto Roelen observed the formation of propanal from the reaction of ethylene, ammonia and a Fischer-Tropsch catalyst (an amalgamation of cobalt, magnesium and iron oxide) at a temperature of 170°C.[2] Since then the development of this process has seen substantial growth in industry,[2] reputable as one of the largest transformations in homogeneous catalysis.[1]

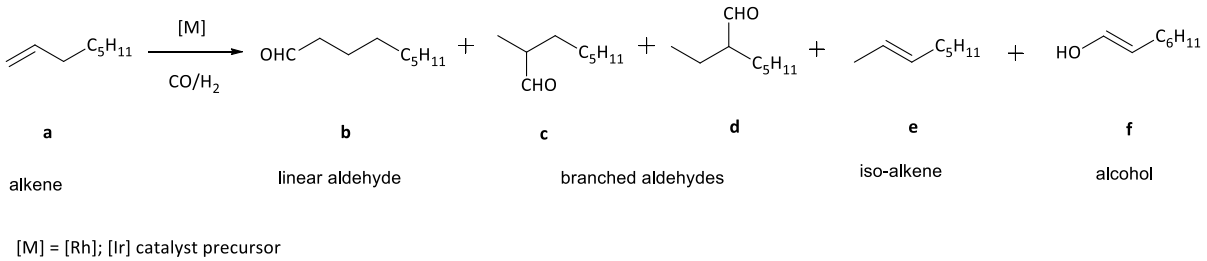

Scheme 6. *1*: Hydroformylation reaction of 1-octene with a catalyst precursor in the presence of syngas, and the possible products.

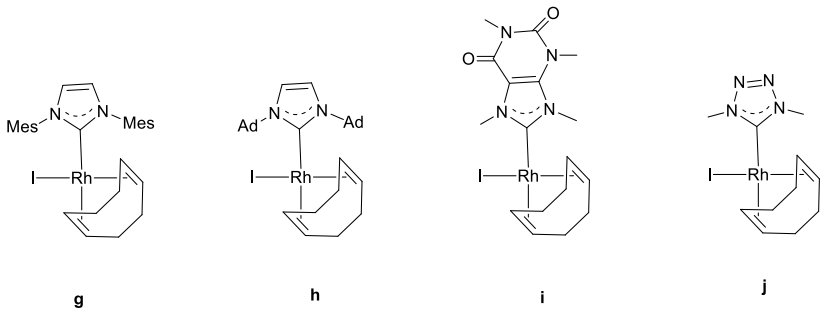

Figure 6. 1: Rhodium-NHC complexes employed as catalyst precursors for the hydroformylation of 1-octene.[3]

Hydroformylation reactions were performed in 2005 on 1-octene using phosphine-free rhodium NHC complexes, **g-j** (Figure 6.2).[3] It was concluded that the 1,5-cyclooctadiene (cod) ligand does not take part in the reaction as it is replaced by CO ligands, similarly the halide is replaced by a hydride to form the active species [HRh(NHC)$(CO)_2$]. The NHC does not undergo substitution due to the donor strength of the ligand, which forges a strong σ-bond with rhodium, dissimilar to the phosphine ligand.[18,4] The obtained results revealed conversions between 19.1% (complex **h,** TOF = 1150 h^{-1}) and 50.4% (complex **j,** TOF = 3540 h^{-1}) after an hour at 100°C (where TOF is turnover frequency) and a syngas (1:1 H_2/CO) pressure of 50 bar.[3] Comparable n/iso ratios were obtained for all complexes, however as the conversion increased, a rapid decline is observed in the selectivity, which is presumed to be due to the isomerisation products undergoing hydroformylation.[3] Therefore it was concluded that the less donating the ligand, like in the case of complex **j,** the better the activity of the catalyst, moreover, steric bulk did not have an influence on the n/iso ratios.[3]

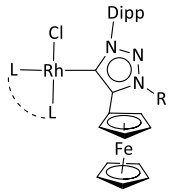

k

R = Dipp, Ethyl
LL = cod, CO
Dipp = 2,6-diisopropylphenyl

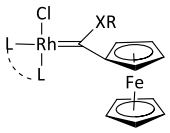

l

XR = OEt; ^{n}PrNH
LL= cod; $(CO)_2$; CO,PR_3; CO, $AsPh_3$

cod = 1,5-cyclooctadiene

Figure 6. 2: Rhodium(I) complexes bearing (k) 1,3,4 trisubstituted 1,2,3-triazol-5-ylidene and (l) ferrocenyl Fischer carbene ligands used as catalyst precursors for hydroformylation reactions.

Abnormal NHCs (*a*NHCs) as ligands are scarcely explored in hydroformylation reactions which is expected based on the premise that the more donating the ligand, less conversion will be observed in these transformations.[5,6,] 1,2,3-triazol-5-ylidenes are the least donating of the aNHCs (see Chapter 3, Figure 3.19). Taking advantage of their ease of access and their tunability, 1,3,4-trisubstituted 1,2,3-triazolylidenes, **k** were employed as catalyst precursors in the hydroformylation of 1-octene (Figure 6.3). Conversions were observed to be between 95.83% and 99.9% at 75°C, under a syngas pressure of 40 bars for 8 hours resulting in n/iso ratios of between 1.60 and 2.83.[7] Prior to this, the less donating Fischer carbene was explored as a ligand for hydroformylation precatalysts **l** (Figure 6.3). After 4 hours at a temperature of 80°C, and syngas pressure of 40 bars conversions were observed to be between 99% and 100%. However, n/iso ratios ranged between 0.79-1.33 which was much less than the bulkier, more donating complexes, **k**.[8] Therefore, the reduced activity of the precatalysts **k** is compensated by its enhanced regioselectivity while the limited regioselectivity of precatalysts **l** is counteracted by its improved activity.

Rhodium is among the rarest metals with widespread demand in industrial chemistry for its catalytic applications like hydroformylation, as well as in the automotive industry for use in catalytic converters, accounting for almost 80% of the world's rhodium produce.[11] This prompting the use of alternative metals for hydroformylation reactions. Based on the following order of activity in hydroformylation reactions of unmodified metal centres : Rh >> Co > Ir, Ru > Os > Pt > Pd > Fe > Ni; Pino and co-workers began studies in modifying iridium for use as a hydroformylation catalyst precursor.[9] The competing hydrogenation reaction was previously identified as the cause for the limited exploration of this metal, prompting Haukka to explore methods of suppressing hydrogenation products under hydroformylation conditions. The complexes $IrCl_3$, $[IrCl(CO)_3]_n$ and $[Ir_4(CO)_{12}]$ were found to be marginally active with TOFs of <0.5 h^{-1}, and increased pressures were found to reduced chemoselectivity.[10] Furthermore, the chemoselectivity increased with the addition of a salt, however the size of the cation and anion of the salt played significant role in whether hydrogenation is suppressed or not. Therefore, the best performing additives were LiCl and $CaCl_2$.[10,17] Altering solvent systems as well as ligands, Beller found that $[HIr(CO)(PPh_3)_3]$ resulted in 80% yields of aldehyde in THF at 100°C after 20 hours at syngas (2:1, CO/H_2) pressures of 20bars with n/iso ratios of 3.17 and TOFs of 163 h^{-1}.[11] Although the iridium complexes proved to be up to 1000 fold less active than its

corresponding rhodium counterparts, ligand modifications and the adjustment of reaction conditions may result in improved activity and selectivity in hydroformylation reactions.[10-19]

6.2. Aim

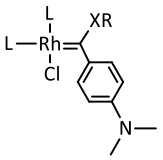

1. LL = cod, XR = OEt
2. LL = cod, XR = ^{n}PrNH
3. LL = $(CO)_2$, XR = ^{n}PrNH
4. LL = $(CO)_2$, XR = OEt

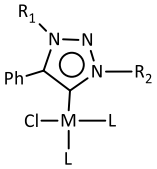

5. M = Rh, LL = cod, R_1 = Mes, R_2 = Et
6. M = Rh, LL = $(CO)_2$, R_1 = Mes, R_2 = Et
7. M = Ir, LL = cod, R_1 = Mes, R_2 = Et
8. M = Ir, LL = $(CO)_2$, R_1 = Mes, R_2 = Et
9. M = Rh, LL = cod, R_1 = R_2 = Dipp
10. M = Rh, LL = $(CO)_2$, R_1 = R_2 = Dipp
11. M = Ir, LL = cod, R_1 = R_2 = Dipp
12. M = Ir, LL = $(CO)_2$, R_1 = R_2 = Dipp

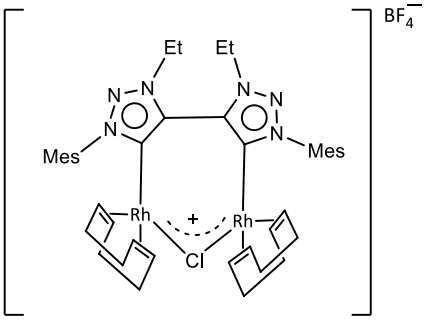

13

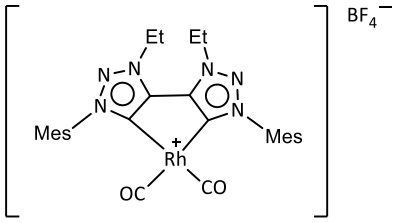

14

Mes = mesityl
Dipp = 2,6-diisopropylphenyl
cod = 1,5-cyclooctadiene

Figure 6. 3: Catalyst precursors to be examined for activity in hydroformylation reactions of 1-octene.

Catalyst-mediated hydroformylation transformations have been extensively explored since their discovery in the mid 1960's.[1,2,17] The effect of the central metal was determined a substantial role player in the chemoselectivity of these reactions, thus resulting in rhodium as a the metal of choice due to its increased activity under milder conditions.[12] The regioselectivity was found to be influenced greatly by the steric properties of the ligands coordinated to the catalyst precursor necessitating a range of ligand modification studies, to compliment the atom economy of this reaction.[13,14] Furthermore, the donor properties of these ligands influence the activity of the catalyst precursor.[3]

These properties regarding the performance of the catalysts will be reported in a table. The headings of the table include:

- % Conversion. This is a measure of how much of the substrate (1-octene) has been converted to another species, specifically aldehydes or iso-octenes.
- % Aldehydes refers to how much of the converted species are aldehydes. This is a measure of chemoselectivity (selectivity towards aldehydes instead of iso-octenes).
- TOF (Turn over Frequency) is a measure of the quantity of aldehydes produced per hour.

- n/iso is a ratio of the quantity of linear aldehydes produced compared to branched aldehydes. This is a measure of regioselectivity.

All these properties are influenced by the reaction time, the syngas pressure, the temperature of the reaction and most importantly by the steric and electronic properties of the catalyst precursor.

Thus, the purpose of this study is to investigate the catalytic activity of the carbene complexes **1 – 14** (Figure 6.4) in hydroformylation reactions. The activity of rhodium diarylated 1,2,3- triazol-5-ylidene complexes will be studied alongside their alkylated counterparts to better understand the effect of sterically hindered wingtip substituents compared to the less bulky alkyl group. This chapter will also focus on rhodium(I) Fischer carbene complexes and how their electron withdrawing properties affect activity and in turn, selectivity in comparison to the electron donating effects of the rhodium(I) triazolylidene. Conclusively, iridium complexes will be examined for activity in hydroformylation reactions, with the objective of finding an affordable alternative to rhodium.

6.3. Results and discussion

6.3.1. Rhodium Fischer carbene complexes as catalyst precursors

The hydroformylation of the substrate 1-octene was carried out at 75°C with syngas pressures of 40 bar to obtain results comparable to those reported by us for the ferrocenyl analogues of the catalyst precursors **1-4** (Table 6.1).[8] After 4 hours these complexes resulted in >99% conversion with 82%-99% aldehydes illustrating chemoselectivity towards aldehydes, while reduced conversions and selectivity were observed for complex **4** (79% conversion, 64% aldehydes). These results are comparable to those observed for the previously reported ferrocenyl analogues (>99% conversions, 85% -99% aldehydes)[8] apart from **4**.

TOFs were recorded to be between 318 h^{-1}-543 h^{-1}, higher than what was recorded for the more donating ferrocenyl analogues with TOFs ranging from 204 h^{-1}-418 h^{-1}. This confirms that the higher the electron density around the metal centre, the less active the catalyst precursor.[14] Similar trends are observed between the amino and the ethoxycarbenes, where the more donating amino carbene **2** has a lower TOF (512 h^{-1}) than the more withdrawing ethoxy analogue **1** with a TOF of 543 h^{-1}. Additionally, entries 2 and 5 displayed identical conversions (>99%) with the same catalyst loading (5.096 x 10^{-3} mmol) and different TOFs (Entry 2 TOF(512 h^{-1}), Entry 5 TOF(528 h^{-1})). This can be attributed to the differences in the catalysts' behaviour during the reaction, where catalyst **2** produces less aldehydes (82%) than catalyst **3** (85%). Considering the cod analogue (catalyst **2**) undergoes ligand exchange prior to hydroformylation transformation, and by definition, TOF is the mmol of aldehydes produced per mmol of rhodium per unit time, this would be expected.

The n/iso ratios of complexes **1-3** are between 0.89 and 1.25, however these are comparable to those obtained for the ferrocenyl analogues (0.79-1.33)[8]. The more π-donating (and slightly larger) amino analogues **2** and **3** are more regioselective than the less donating ethoxy complex **1**, corroborating the effect of steric repulsion on regioselectivity.[15,16] This means selectivity is usually compromised by high conversions. For FCCs that result in high % conversion, lower regioselectivity is apparently obtained. Thus the % conversions correlate to isomerisation of the double bond rather that aldehyde yield in such instances.

Complex **2** (Entry 4) was run for 2 hours under the same conditions and an increase in regioselectivity (n/iso = 1.95) was observed along with a decrease in total aldehydes (70%). Presumably, 2 hours into the reaction, the isomerisation products (30%) are yet to undergo hydroformylation thus validating Herrmann's findings.[3,14] Furthermore with an increase in the total number of aldehydes, a notable decrease in regioselectivity is observed.[7,8] Comparison of the complexes' catalytic performance at maximum conversion does not allow for deduction of CO ligand structure-reactivity correlation. Indeed, a kinetic profile at lower conversions would be more informative in this regard. A mercury drop test was performed on complex **2** to verify the homogeneity of all the prepared rhodium catalyst precursors. The results obtained for **2** with and without the mercury drop were analogous, indicative of a homogeneous mode-of-action for the catalysts.[17]

*[a]Table 6. 1: Hydroformylation data of rhodium Fischer carbene complexes **1-4**.*

Entry	Complex	Conversion (%)	Aldehydes (%)			Iso-octenes (%)	[c]TOF (h^{-1})	n/iso
			[b]Total aldehydes	Nonanal	Branched			
Rhodium Fischer carbene complexes								
1	**1**[18]	99(1.1)	99(0.7)	47(1.1)	53(1.1)	1(0.7)	543(2.6)	0.89(0.035)
2	**2**	>99(0.3)	82(4.0)	57(3.0)	43(3.0)	18(4.0)	512(26.2)	1.32(0.160)
3	**2** + Hg	>99(0.1)	81(0.9)	57(0.2)	43(0.2)	19(0.9)	449(4.8)	1.31(0.014)
4	[d]**2**	>99(0.2)	70(2.8)	66(4.3)	34(4.3)	30(2.8)	386(14.5)	1.95(0.368)
5	**3**	>99(0.3)	85(4.0)	56(3.0)	44(3.0)	15(4.0)	528(26.2)	1.25(0.162)
6	**4**[24]	79(10.2)	64(3.9)	71(1.1)	29(1.1)	36(3.9)	318(21.9)	2.44(0.127)

Hydroformylation of 1-octene in toluene (5 mL) at a temperature of 75°C, with syngas (1:1 $CO:H_2$) at a pressure of 40 bar, a reaction time of 4 hours, and catalyst loading of 5.096 x 10^{-3} mmol. [a]All reactions are performed in triplicates or duplicates, and the average is reported with the standard deviation in parenthesis. Conversions were monitored by gas chromatography, using *n*-decane as an internal standard. [b]Total aldehydes are a composition of linear and branched aldehydes in a mixture with a percentage sum of 100 %. [c]TOF = (mmol aldehydes per mmol Rh)/ time. [d]Reaction conditions: temperature of 75°C. syngas pressure of 40 bar, a reaction time of 2 hours, and catalyst loading of 5.096 x 10^{-3} mmol.

6.3.2. Rhodium 1,2,3-triazol-5-ylidene complexes as catalyst precursors.

Entries 1 – 3, and entry 6 (Table 6.2), complexes **5, 6, 9** and **14** displayed conversions of 64% - 76% after heating for 4 hours at 75°C at pressure of 40 bars. Complex **10** displayed a significantly higher conversion of 97% deviating significantly from **5, 6**, and **9**. However, comparable to what has been previously reported for rhodium 1,2,3-triazol-5-ylidene complexes after 8 hours of heating at 75°C (95.3% - 99.9%).[7] Total aldehydes produced are between 63% and 70% with n/iso ratios of between 2.26-2.38 for entries 1-4. TOFs obtained are between 244 h^{-1} and 399 h^{-1}, with the CO analogues

producing the highest number of aldehydes per hour compared to their cod counterparts. The bulkier diarylated precatalysts (Entries 3 and 4) result in slightly higher TOFs than the less sterically hindered ethyl analogues. This is a consequence of the favouring of anti-Markovnikov substrate addition, stimulated by bulkier ligands of the catalyst, during the hydroformylation catalytic cycle.[19] Due to longer reaction times, the previously obtained data from the ferrocenyl analogues of entries 1-4 resulted in lower n/iso ratios (2.43-1.75)[7] as a result of the isomers undergoing hydroformylation. However, after 4 hours, the ferrocenyl analogue of entry 3 resulted in a TOF of 305 h^{-1} (n/iso 2.3) and 70% conversion as well as aldehydes.[6]

*[a]Table 6. 2: Hydroformylation data of rhodium 1,2,3-triazol-5-ylidene complexes **5 – 6**, **9 – 10**, and **13 – 14.***

Entry	Complex	Conversion (%)	Aldehydes (%)			Iso-octenes (%)	[c]TOF (h^{-1})	n/iso
			[b]Total aldehydes	Nonanal	Branched			
Rhodium (1.2.3-triazol-5-ylidene) complexes								
1	**5**	70(14.2)	63(1.2)	70(0.3)	30(0.3)	37(1.2)	244(46.1)	2.38(0.035)
2	**6**	64(5.0)	70(7.4)	73(1.6)	27(1.6)	30(7.4)	277(11.9)	2.67(0.204)
3	**9**	76(6.7)	63(1.9)	71(0.2)	29(0.2)	37(1.9)	251(60.6)	2.46(0.031)
4	**10**	97(1.1)	66(5.4)	69(0.8)	30(0.8)	34(5.4)	399(35.6)	2.26(0.083)
5	[e]**13**	93(3.7)	93(3.2)	66(2.0)	34(2.0)	26(3.2)	133(7.8)	1.99(0.174)
6	**14**	69(7.8)	62(3.8)	70(0.5)	30(0.5)	38(3.8)	271(25.4)	2.36(0.056)
7	[d]**14**	90(5.7)	64(0.4)	70(0.2)	30(0.2)	36(0.4)	316(18.3)	2.34(0.021)

Hydroformylation of 1-octene in toluene (5 mL) at a temperature of 75°C, with syngas (1:1 $CO:H_2$) at a pressure of 40 bar, a reaction time of 4 hours, and catalyst loading of 5.096 x 10^{-3} mmol. [a]All reactions are performed in triplicates or duplicates, and the average is reported with the standard deviation in parenthesis. Conversions were monitored by gas chromatography, using *n*-decane as an internal standard. [b]Total aldehydes are a composition of linear and branched aldehydes in a mixture with a percentage sum of 100 %. [c]TOF = (mmol aldehydes per mmol Rh)/ time. [d]Reaction conditions: temperature of 75°C, syngas pressure of 40 bar, a reaction time of 8 hours, and catalyst loading of 5.096 x 10^{-3} mmol. [e]Reaction conditions: temperature of 75°C, syngas pressure of 40 bar, a reaction time of 4 hours, and catalyst loading of 2.548 x 10^{-3} mmol.

Due to its bimetallic nature, 2.548 x 10^{-3} mmol catalyst loading of complex **13** was added to the reaction instead of 5.096 x 10^{-3} mmol to obtain comparable data. Significantly higher conversions were obtained for the bridged complex **13** (93% conversion and 93% aldehydes) in comparison to the chelated complex **14** (69% conversion, 62% aldehydes). This can be attributed to the better donor ability i-bitz as chelated ligand, which is not favourable for hydroformylation reactions according to Herrmann and co-workers.[14] The n/iso ratios are significantly lower for the bimetallic complex **13** (1.99), compared to the monometallic complex **14** (2.36) which is comparable to those obtained for entries 1-4, 7 as well as the previously reported ferrocenyl analogues of entries 1-4.[6,7] To examine the

behaviour of the rhodium 1,2,3-triazol-5-ylidene complexes at longer reaction times, complex **14** was reacted under the same conditions for 8 hours resulting in 90% conversion, an improvement from the 69% obtained after 4 hours, 64% aldehydes and n/iso ratios of 2.34 which are comparable to those obtained in entry 6. Therefore, TOFs improve (along with conversion) over extended periods, however the n/iso ratios remain consistent.

Rhodium 1,2,3-triazol-5-ylidene complexes result in 64%-97% conversions and n/iso ratios 2.26-2.67, except for entry 5 (1.99). This is comparable to the n/iso ratio obtained for rhodium Fischer carbene complexes in table 6.1 which ranges from 0.89-1.95. Table 6.1 shows conversions of >99%. Fischer carbenes are more withdrawing and less sterically hindered therefore, better conversions and TOFs are observed however this is as the cost of selectivity. Additionally, 1,2,3-triazol-5-ylidenes are more donating and bulkier thus, better selectivity is observed at the cost of conversion. This is due to more isomerisation products undergoing hydroformylation over time.

6.3.3. Iridium 1,2,3-triazol-5-ylidene complexes as catalyst precursors.

The iridium analogues of the complexes reported in Table 6.2 were employed as catalyst precursors under the same conditions as the rhodium analogues. Trivial amounts of aldehydes were produced (Table 6.3), even in the presence of a LiCl salt (see entries 4-7, Table 6.3) which was meant to supress the competing hydrogenation reaction pathway.[10-11,19-22] The less bulky ethyl analogues complexes **7** and **8** had conversions of 11% and 16% respectively with comparable TOFs of 8 h^{-1}. Entries 4 and 6, the diarylated analogues has similar conversions of 35% and 33% respectively. However, the TOF of complex **12** (45 h^{-1}) is significantly higher than that of complex **11** (19 h^{-1}).

Despite the poor conversions, the n/iso ratios obtained for these iridium complexes (1.08-2.04) were analogous with those obtained for the rhodium Fischer carbene complexes (0.89-1.95), and significantly less than those obtained the corresponding rhodium catalyst precursor (1.99-2.67). The activity of complex **12** is noteworthy, with the highest number of aldehydes (51%), the largest n/iso ratio of 2.04, and the largest TOF. A similar trend is observed for the rhodium analogue of complex **12** with the largest TOF of 399 h^{-1}

Wilkinson and co-workers observed the same trends regardless of additive to suppress the competing reaction, consolidating the requirement of harsher reaction conditions.[20] It was reasoned that following Heck and Breslow's mechanism, the rate determining step is the oxidative addition of the hydride to the square planar complex, thus changing the oxidation state and the geometry of the complex.[22] Therefore, oxidation occurs more readily for rhodium compared to iridium.[22] Furthermore, once the pentacoordinate iridium species forms, it is more stable than the corresponding rhodium counterpart, therefore requiring harsher conditions to facilitate dissociation and thus formation of the aldehyde product.[22]

A mercury drop test was performed for the iridium complexes (Table 6.3, entry 3) to serve as a preliminary indicator to confirm homogeneity of the transformation, No conversion was observed after addition of excess mercury to the catalytic reactions. This implies that the observed conversions are due to nanoparticles and once the mercury drop was added to the reactor, the catalyst was deactivated.[21] Although this method has been used for almost a century, it is not definitive and presents only one possible explanation for catalyst mode-of-action.[17]

*[a]Table 6. 3: Hydroformylation data of iridium 1,2,3-triazol-5-ylidene complexes **7 – 8** and **11 –12**.*

Entry	Complex	Conversion (%)	Aldehydes (%)			Iso-octenes (%)	[c]TOF (h^{-1})	n/iso
			[b]Total aldehydes	Nonanal	Branched			
Iridium (1.2.3-triazol-5-ylidene) complexes								
1	**7**	11(0.3)	24(0.0)	55(0.6)	45(0.6)	76(0.0)	8(0.2)	1.21(0.029)
2	**8**	16(0.1)	17(0.4)	53(0.0)	47(0.0)	83(0.4)	8(0.1)	1.12(0.002)
3	**8** + Hg	0	0	0	0	0	0	N/A
4	**11**	35(4.1)	23(6.1)	53(0.4)	47(0.4)	77(6.1)	19(3.0)	1.11(0.017)
5	[d]**11**	33(0.5)	17(1.4)	52(0.1)	48(0.1)	83(1.4)	14(1.3)	1.08(0.005)
6	**12**	33(2.8)	51(0.6)	67(0.2)	33(0.2)	49(0.6)	45(3.3)	2.04(0.019)
7	[d]**12**	25(1.4)	46(0.6)	65(1.0)	35(1.0)	54(0.6)	30(2.1)	1.87(0.085)

Hydroformylation of 1-octene in toluene (5 mL) at a temperature of 75°C, with syngas (1:1 $CO:H_2$) at a pressure of 40 bar, a reaction time of 4 hours, and catalyst loading of 5.096 x 10^{-3} mmol. [a]All reactions are performed in triplicates or duplicates, and the average is reported with the standard deviation in parenthesis. Conversions were monitored by gas chromatography, using *n*-decane as an internal standard. [b]Total aldehydes are a composition of linear and branched aldehydes in a mixture with a percentage sum of 100 %. [c]TOF = (mmol aldehydes per mmol Rh)/ time. [d]Addition of LiCl (2:1 LiCl:[Ir]).[22,23]

6.3. Conclusion

Various classes of rhodium(I) carbene complexes, namely: rhodium Fischer carbene complexes (ethoxy and amino); rhodium 1,2,3-triazol-5-ylidene complexes (N3 alkylated and diarylated); as well as rhodium i-bitz complexes (mono- and bimetallic). These complexes along with the iridium analogues of the 1,2,3-triazol-5-ylidene complexes, were screened for catalytic activity in hydroformylation reactions at 75°C and 40 bars of syngas pressure for 4 hours, and were found to be active under these conditions with a catalyst loading of 0.08% towards the substrate 1-octene. *N*-decane was used as an internal standard.

The Fischer carbene complexes **1-4** displayed the highest activity with conversions of >99%, these complexes displayed excellent chemoselectivity towards aldehydes (85%-99%) however their draw back was the moderate regioselectivity with n/iso aldehydes of 0.89-1.32. The regioselectivity was improved at shortened reaction times observed when complex **2**(1.95) was reacted for 2 hours instead of 4, conversely total aldehydes dropped to 70%.

The rhodium 1,2,3-triazol-5-ylidene complexes **5, 6, 9**, and **10** exhibited superior regioselectivity towards linear aldehydes with n/iso ratios of 2.26-2.67. Contrariwise, lower chemoselectivity towards aldehydes was observed ranging between 63% and 70%. Confirming that the better the regioselectivity, the worse the conversion and chemoselectivity. These complexes were more selective towards linear aldehydes due to the steric bulk of the 1,2,3-triazol-5-ylidene ligands. The i-

bitz ligand is a linker-free bidentate 1,2,3-triazol-5-ylidene, therefore the n/iso ratios obtained from reactions with the corresponding rhodium complexes were in agreement with those of the monodentate rhodium 1,2,3-triazol-5-ylidene complexes (1.99-2.36). Complex **13** produced the highest number of aldehydes (93%) comparable to those obtained for the rhodium Fischer carbene complex, thus predictably, decreased regioselectivity is observed. Notably, extended reaction times result in higher conversions and TOFs, yet no significant differences are observed in the n/iso ratios.

*[a]Table 6. 4: Hydroformylation data of the best performing catalyst (complex **2, 10, 14**) from each class of complexes.*

Entry	Complex	Conversion (%)	Aldehydes (%)			Iso-octenes (%)	[c]TOF (h^{-1})	n/iso
			[b]Total aldehydes	Nonanal	Branched			
1	**2**	>99(0.3)	82(4.0)	57(3.0)	43(3.0)	18(4.0)	512(26.2)	1.32(0.160)
2	**10**	97(1.1)	66(5.4)	69(0.8)	30(0.8)	34(5.4)	399(35.6)	2.26(0.083)
3	**14**	69(7.8)	62(3.8)	70(0.5)	30(0.5)	38(3.8)	271(25.4)	2.36(0.056)

Hydroformylation of 1-octene in toluene (5 mL) at a temperature of 75°C, with syngas (1:1 $CO:H_2$) at a pressure of 40 bar, a reaction time of 4 hours, and catalyst loading of 5.096 x 10^{-3} mmol. [a]All reactions are performed in triplicates or duplicates, and the average is reported with the standard deviation in parenthesis. Conversions were monitored by gas chromatography, using *n*-decane as an internal standard. [b]Total aldehydes are a composition of linear and branched aldehydes in a mixture with a percentage sum of 100 %. [c]TOF = (mmol aldehydes per mmol Rh)/ time.

Complexes **2, 10,** and **14** were identified as the best performing catalyst precursors from each section 6.3.1.-6.3.3. based on % conversion, total aldehydes, TOFs and n/iso ratios (Table 6.4). Complex **2** is the best performing catalyst with >99% conversion and 82% aldehydes. The electron withdrawing nature of the Fischer carbene ligand translates to superior activities, resulting in the highest TOF reported for this series (512(26.1) h^{-1}). Good selectivity towards aldehydes is observed, however, complex **2** has the lowest regioselectivity based on the obtained n/iso presumably due to the limited steric bulk of this complex. Compared to complex **3,** the carbonyl analogue of **2,** slightly better TOFs are observed (528(26.1) h^{-1}) as a combined effect of the better π-accepting carbonyls reducing electron density around the central metal; as well as the circumvention of the first step in hydroformylation (carbonyl substitution) allowing for more time to produce more aldehydes. This catalyst was however less selective than complex **2**, consolidating the influence of steric bulk as the cod analogue is bulkier than the carbonyl complex.

Complex **14** is the most regioselective, with n/iso ratio of 2.36, which is expected considering the steric bulk of the i-bitz ligand. This catalyst is the least active**,** with conversion of 69% and 62% aldehydes which corroborates the statement: with higher activity, selectivity is compromised. The low selectivity is an expected consequence of the amplified donor ability of the bidentate ligand, increasing electron density around the metal centre. This effect is countered by the carbonyl ligands' electron withdrawing ability as well as the cationic nature of the of complex **14** resulting in reasonable activity with TOF of (271(25.4) h^{-1}).

The overall best performing catalyst is complex **10**, this complex results in high activity analogous with that of complex **2** due to the inductive σ-withdrawing effect of the 3 aromatic substituents on the heterocycle, with n/iso selectivity comparable to that of complex **14** due to the steric bulk offered by the same substituents**.** The total aldehydes produced are significantly less than those produced by **2**, as a result of the better σ-donating ability of the 1,2,3-triazol-5-ylidene ligand of **10,** increasing electron density around the metal centre and thus reducing the ease of oxidation required for aldehyde formation during the reaction. However, it should be noted that all the aldehydes produced by complex **2** are an equal composition of branched and linear aldehydes, thus making complex **10** superior in that regard.

The iridium 1,2,3-triazol-5-ylidene complexes **7, 8, 11**, and **12** displayed limited conversions regardless of the additive LiCl, with n/iso ratios of between (1.08-2.04). The mercury drop test revealed that the observed activity is a result of nanoparticles in solution, thus revealing the presumed heterogeneity of this catalyst. Despite this, the best performing iridium precatalyst is the sterically hindered complex **12** with n/iso ratio of 2.04 and total aldehydes of 51%.

6.4. Experimental

6.4.1. General technique for hydroformylation experiments

90mL high-pressure stainless-steel reactors were used to carry out the said hydroformylation reactions. These reactions were executed in triplicates or duplicates, using 5mL of toluene as a solvent, 1-octene (0.715 g, 6.37 mmol) as the substrate, and *n*-decane (0.204 g, 1.45 mmol) as an internal standard. 0.08 mol% of the catalyst precursor was added to this reaction mixture, before sealing and purging three times with $N_{2(g)}$; and twice with syngas (CO/H_2, 1:1). The reactors were then heated to the desired temperature under the desired syngas pressure for a specified amount of time after which they were allowed to cool down to room temperature. The cooled off reaction mixtures were then decanted into glass vials. For GC analysis and quantification of the catalytic products, a 1µL syringe was used to inject 0.1 µL of the cooled reaction mixture into a Perkin Elmer Clarus 580 GC instrument equipped with a flame ionisation detector and a 30 m capillary column.

For the confirmation of the products afforded, authenticated iso-octene and aldehyde standards were utilised. Figure 6.5 shows 1-octene as well as all the possible isomerisation products that maybe formed, with 2-octene forming more readily than the other isomers. Although these isomers were not separated and quantified, it can be speculated that the most abundant iso-octene is 2-octene, while the least abundant is 4-octene. From these isomers, branched aldehydes are formed at extended reaction times which is observed when complex **2** is left to react for 2 hours compared to when it is allowed to react for 4 hours. Thus, the most abundant branched aldehyde is 2-methyl-octanal, as this is speculated to form from 1-octene (substrate) as well as from 2-octene (the most abundant iso-octene). The least abundant of the branched aldehydes is the 2-propyl-hexanal.

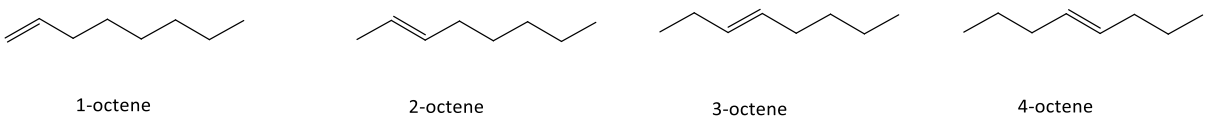

Figure 6. 4: 1-octene and all possible iso-octene products of the hydroformylation reactions.

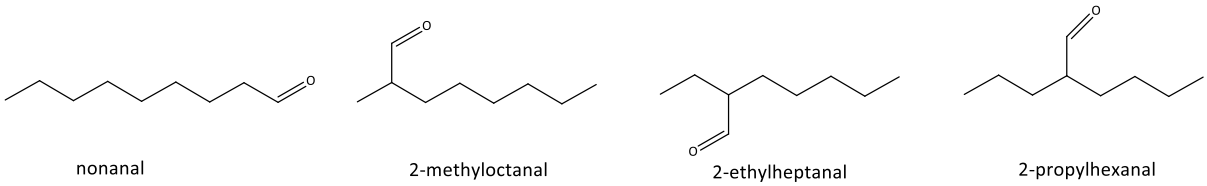

Figure 6. 5: Nonanal and all the possible branched aldehyde products of the hydroformylation reactions.

6.4. References

[1] R. Franke, D. Selent and A. Börner, *Chem. Rev.*, 2012, **112**, 5675–5732.
[2] G. D. Frey, *J. Organomet. Chem.*, 2014, **754,** 5–7.
[3] M. Bortenschlager, J. Schütz, D. Von Preysing, O. Nuyken, W. A. Herrmann and R. Weberskirch, *J. Organomet. Chem.*, 2005, **690**, 6233–6237.
[4] M. Bortenschlager, M. Mayr, O. Nuyken and M. R. Buchmeiser, *J. Mol. Catal. A-Chem.*, 2005, **233**, 67–71.
[5] W. Gil and A. M. Trzeciak, *Coord. Chem. Rev.*, 2011, **255**, 473–483.
[6] D. Aucamp, MSc Chemistry, University of Pretoria, 2016.
[7] D. Aucamp, T. Witteler, F. Dielmann, S. Siangwata, D. C. Liles, G. S. Smith and D. I. Bezuidenhout, *Eur. J. Inorg. Chem.*, 2017, **2017**, 1227–1236.
[8]G. K. Ramollo, M. J. López-Gómez, D. C. Liles, L. C. Matsinha, G. S. Smith and D. I. Bezuidenhout, *Organometallics*, 2015, **34**, 5745-5753.
[9] P. Pino, F. Piacenti, M. Bianchi, in: I. Wender, P. Pino (Eds.), Organic Synthesis via Metal Carbonyl, Vol. 2,Wiley & Sons, New York, 1977, 44–231
[10] M. A. Moreno, M. Haukka and T. A. Pakkanen, *J. Catal.*, 2003, **215**, 326–331.
[11] I. Piras, R. Jennerjahn, R. Jackstell, A. Spannenberg, R. Franke and M. Beller, *Angew. Chem. Intl. Ed.*, 2011, **50**, 280–284.
[12] L. H. Slaugh and R. D. Mui, *United States Patent Office HYDROFORMYLATION OF OLEFENS*, 1966.
[13] W. Herrmann, M. Elison, J. Fischer, C. Kocher and G. R. Artus, *Angew. Chem. Int.*, 1995, **34**, 2371–2375.
[14] W. A. Herrmann and C. Kocher. *Angen. Chem. Int. Ed. Engi.* 1997,**36**, 2162-2187.
[15] L. A. Van Der Veen, *New ligands for selective hydroformylation Unraveling the bite angle effect*, 1999.
[16] C. A. Tolman, *Chem. Rev.* 1977, **77**, 313-348.
[17] R. H. Crabtree, Chemical Reviews, 2012, **112**, 1536–1554.
[18] T. L. Mashabane, G. K. Ramollo, G. Kleinhans, S. De Doncker, S. Siangwata, M. A. Fernandes, A. Lemmerer, G. S. Smith and D. I. Bezuidenhout, *J. Organomet. Chem.*, DOI:10.1016/j.jorganchem.2020.121341.
[19] Heck, R. F., Breslow, D. S., *J. Am. Chem. Soc.* 1961, **83**, 4023.
[20] B. D. Evans, J. A. Osborn and G. Wilkinson, *J. Am. Chem. Soc.*, 1968, **62**, 3133-3142
[21] (a) M. D. Argyle and C. H. Bartholomew, *Catalysts*, 2015, 5, 145–269. (b) J. A. Widegren and R. G. Finke, *J. Mol. Catal. A-Chem.*, 2003, **198**, 317–341.
[22] Behr A, Kämper A, Nickel M, Franke R. *Appl. Catal. A-Gen*., 2015, **505**, 243-248.
[23] A. Kämper, S. J. Warrelmann, K. Reiswich, R. Kuhlmann, R. Franke and A. Behr, *Chem. Eng. Sci.*, 2016, **144**, 346-371.

Chapter 7: Conclusion and future perspectives

7.1. Conclusion and future perspectives

Rhodium Fischer carbene complexes **1-4** were prepared by transmetalation from the corresponding tungsten complex. Dimethylaniline was selected as the aryl α-carbene substituent due to its π-donating ability, stabilizing the π-accepting Fischer carbene carbon following transmetalation to rhodium, a less π-basic transition metal. The product was aminolyzed, reducing the double bond character of the metal-carbene bond, by increasing the π-character of the amino-carbene carbon bond. The steric bulk of both products (ethoxy and amino), along with the respective electron density at the metal centres was reduced by substitution of the 1,5-cyclooctadiene ligand with π-acidic carbonyl ligands (Scheme 7.1).

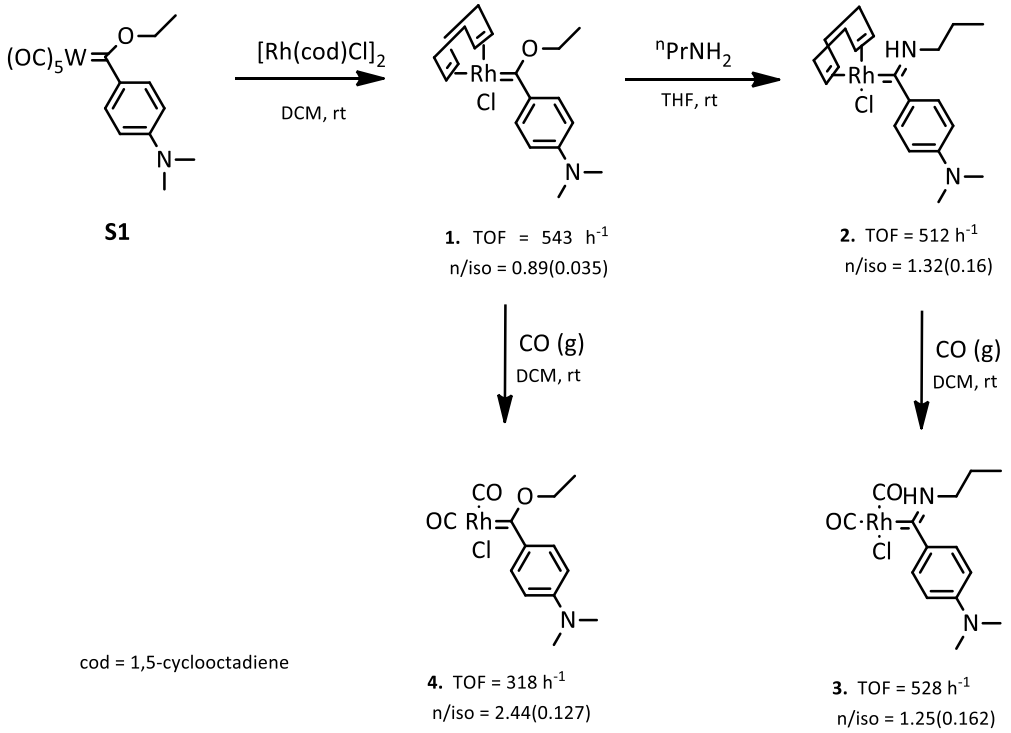

Scheme 7. 1: The alteration of the electronic and steric properties of the rhodium catalyst precursor and the resultant activity and selectivity in hydroformylation reactions.

As an extension of our previous work on metallocenyl Fischer carbene complexes of Rh(I) as hydroformylation catalyst precursors, these mononuclear Fischer carbene complexes were screened in the catalytic hydroformylation of 1-octene. High activities in hydroformylation reactions were observed for these Fischer carbene complexes, with TOF of between 512 h^{-1} and 543 h^{-1}, superior to those previously reported for the ferrocenyl analogues (343 h^{-1}-418 h^{-1}) of complexes **1**-**4**.[1] These signify reduced electron density around the metal centre as a result of the π-accepting nature of this carbene ligand. Comparable to the ferrocenyl analogues, moderate regioselectivity with *n*/iso ratios of 0.89-1.32 is observed, a consequence of the steric bulk deficiency of the Fisher carbene complexes. An increase in regioselectivity is observed at shorter reaction times, consolidating the aldehyde

formation from the isomerisation products at extended periods, which in turn affects the chemoselectivity observed. This is seen when complex **2** resulted in an n/iso ratio of 1.95(0.368) after a reaction time of 2 hours, and 1.32(0.16) in 4 hours under the same reaction conditions with the exception of varied time periods.

Future considerations to increase the regioselectivity rhodium Fischer carbene ligands produce, include increasing the steric bulk of the α-substituent of the Fischer carbene such as a triphenylamine, or related amine dendrimers to the metal centre. This will result in increased steric hinderance without drastically affecting the electronics of the π-accepting Fischer carbene complex. This would presumably result in improved selectivity, without compromising the activity of the catalyst precursor. Furthermore, a time study can be conducted to determine and compare the performances of the catalyst precursors at 30-minute intervals. From the obtained data, a better understanding of the behaviour of the catalyst precursor at varied stages throughout the reactions can be obtained. Moreover, the effects of temperature and pressure can be studied by varying each component to perform kinetic studies of the catalyst precursors.

Contrary to Fischer carbene ligands, 1,2,3-triazolylidene ligands are electron donating and require negligible π-back donation from the metal centre, resulting in a single bond between the carbene and the central metal. The preceding salts were prepared by two methods to achieve varied steric repulsions. The "click" route was employed to obtain the *N*3-alkylated 1,2,3-triazolylidene ligand, and the 1,3-dipolar cycloaddition reaction was used to acquire the diarylated salt. The ensuing rhodium complexes were attained from deprotonation reactions with the non-nucleophilic base, KHMDS. The iridium complexes were obtained from transmetalations reactions with the corresponding silver biscarbene salt, a well-known carbene transfer agent. Both the iridium and the rhodium complexes underwent ligand substitution reactions, resulting in 4 new carbonyl complexes (Scheme 7.2).

Hydroformylation reactions were performed with the rhodium and the iridium complexes as precatalysts. The rhodium complexes displayed moderate activity compared to the Fischer carbene complexes, with TOFs between 244 h^{-1}- 399 h^{-1}, inferior to previously reported rhodium imidazole-2-ylidene complexes with TOF of up to 3540 h^{-1}.[2] However, this is an improvement on the previously reported results for the ferrocenyl substituted rhodium 1,2,3-triazol-5-ylidene complexes (116.83 h^{-1}-99.73 h^{-1})[3]. In addition, the carbonyl complexes are more active than their cod counterparts. Contrariwise, selectivity towards the formation of linear aldehydes is increased as a result of the steric bulk of the 1,2,3-triazol-5-ylidene ligand (n/iso between 2.26(0.083) – 2.67(0.204)) for the rhodium complexes, disparate to the less sterically hindered Fischer carbene ligand.

The iridium complexes showed little to no activity in the hydroformylation reactions, despite the addition of the lithium salts as hydrogenation suppressant. The decrease in activity was attributed to the increased electron density around the central metal, increasing the difficulty of CO insertion following the oxidative addition of the H_2 during the catalytic cycle. The combined effect of increased syngas ratio to 2:1 CO/H_2, decreased pressures and increased temperatures was reported to suppress hydrogenation while increasing activity for iridium(I) complexes bearing phosphine ligands.[4] Thus, for

future considerations, for iridium catalysed hydroformylation reactions, higher temperatures and CO/H_2 ratios should be applied.

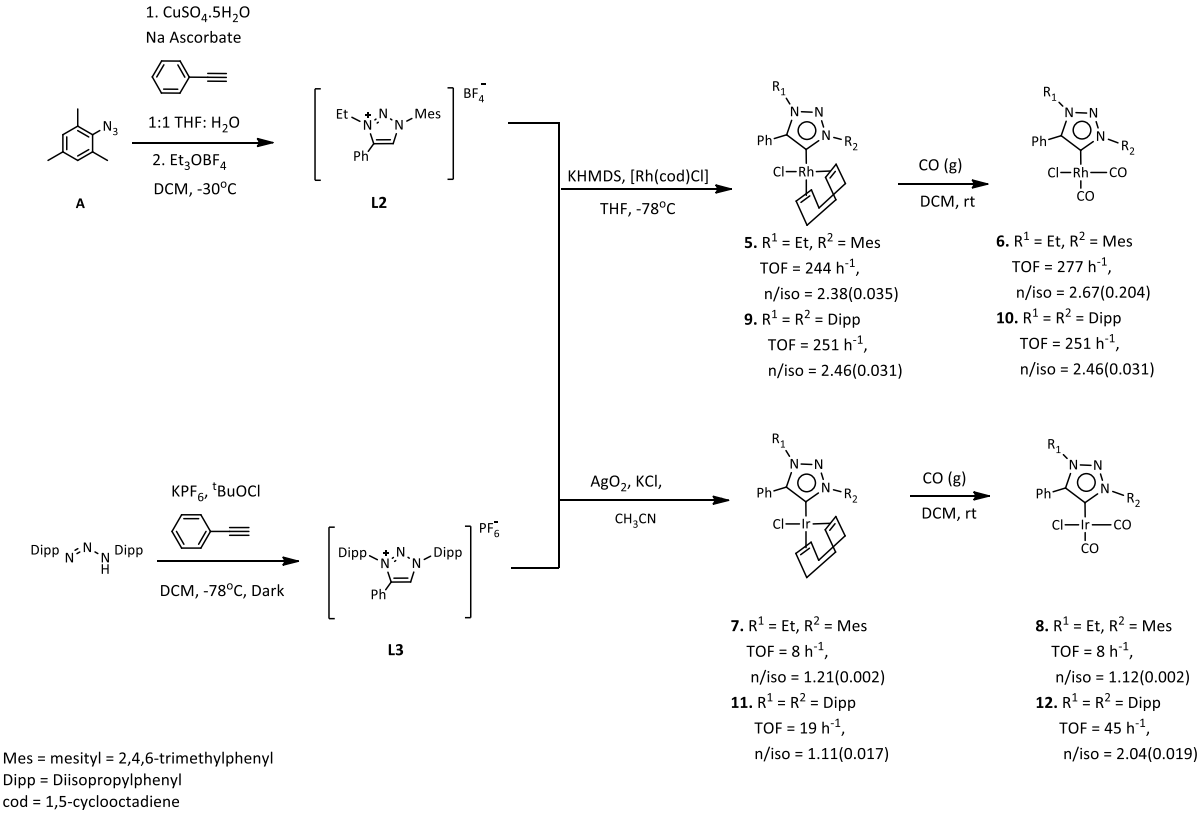

Scheme 7. 2: Variation of the steric and electronic parameters around the rhodium precatalyst and the resulting activity and regioselectivity in hydroformylation reactions.

Cationic rhodium 1,2,3-triazol-5-ylidene complexes **5, 6, 9** and **10** can be prepared and studied under the same conditions, presenting the opportunity to alter the electronic properties of the catalyst precursor, by removing the halido co-ligands from the central metal's coordination sphere. This would circumvent replacement of these ligands as one of the steps in the catalytic cycle, as anticipated in the mechanism for rhodium-catalysed hydroformylation reactions. Possible benefits include increasing the TOFs by increasing chemoselectivity towards aldehydes. Furthermore, bulkier R1 and R2 substituents (Scheme 7.2) can be employed to increase regioselectivity.

The 4,4'-bis(1,2,3-triazol-5-ylidene) or i-bitz ligand was chelated to rhodium cod dimer precursor but was not isolated. Instead, in situ treatment with carbon monoxide yielded the complex **14**. An attempt to isolate the cod complex serendipitously resulted in the formation of a bridged dinuclear rhodium complex **13**. The bridged complex is charged, with a chloride ligand bridging between the two rhodium(I) metal centres, bonding with one metal centre as an X-type ligand, and with the other as an L-type ligand. This results in a positive charge, delocalised between the two metal centres. These cationic complexes were found to be active as hydroformylation precatalyst resulting in TOF (271(25.4) h^{-1}) and n/iso ratio (2.36(0.056)) comparable with those of monodentate 1,2,3-triazol-5-

ylidene complexes for the chelated complex **14**. However, the dihapto dinuclear complex **13** performed poorly, with a TOF of 133(7.8) $h^{-1}$and n/iso of 1.99(0.174) h^{-1} due to the steric bulk of the metal complex (Scheme 7.3).

One of the aims of the project included the preparation of a biscarbene rhodium(I) complex, containing both a donating triazolylidene and an electron withdrawing mono-heteroatom stabilized Fischer carbene ligand, as a hydroformylation catalyst. A range of synthetic approaches were employed for the preparation of the hybrid 1,2,3-triazol-5-ylidene rhodium(I) Fischer carbene complex, however the heteroleptic biscarbene complex was not isolated. The preparative routes employing free carbene generation failed, even in the presence of a chloride abstractor to activate the Fischer carbene complex. This is due to insufficient stability of the free 1,2,3-triazol-5-ylidene in the case of the *N*-alkylated moiety, and presumably due to the decomposition of the Fischer carbene complex in the presence of trace amounts of base remaining after triazolium deprotonation. Transmetalation strategies ((i) from a group 6 1,2,3-triazol-5-ylidene complex to a rhodium Fischer carbene complex, (ii) from a group 6 Fischer carbene complex to a rhodium 1,2,3-triazol-5-ylidene was ineffective, and (iii) the transmetalation from a silver bis 1,2,3-triazol-5-ylidene to the rhodium Fischer carbene complex) also proved unsuccessful.

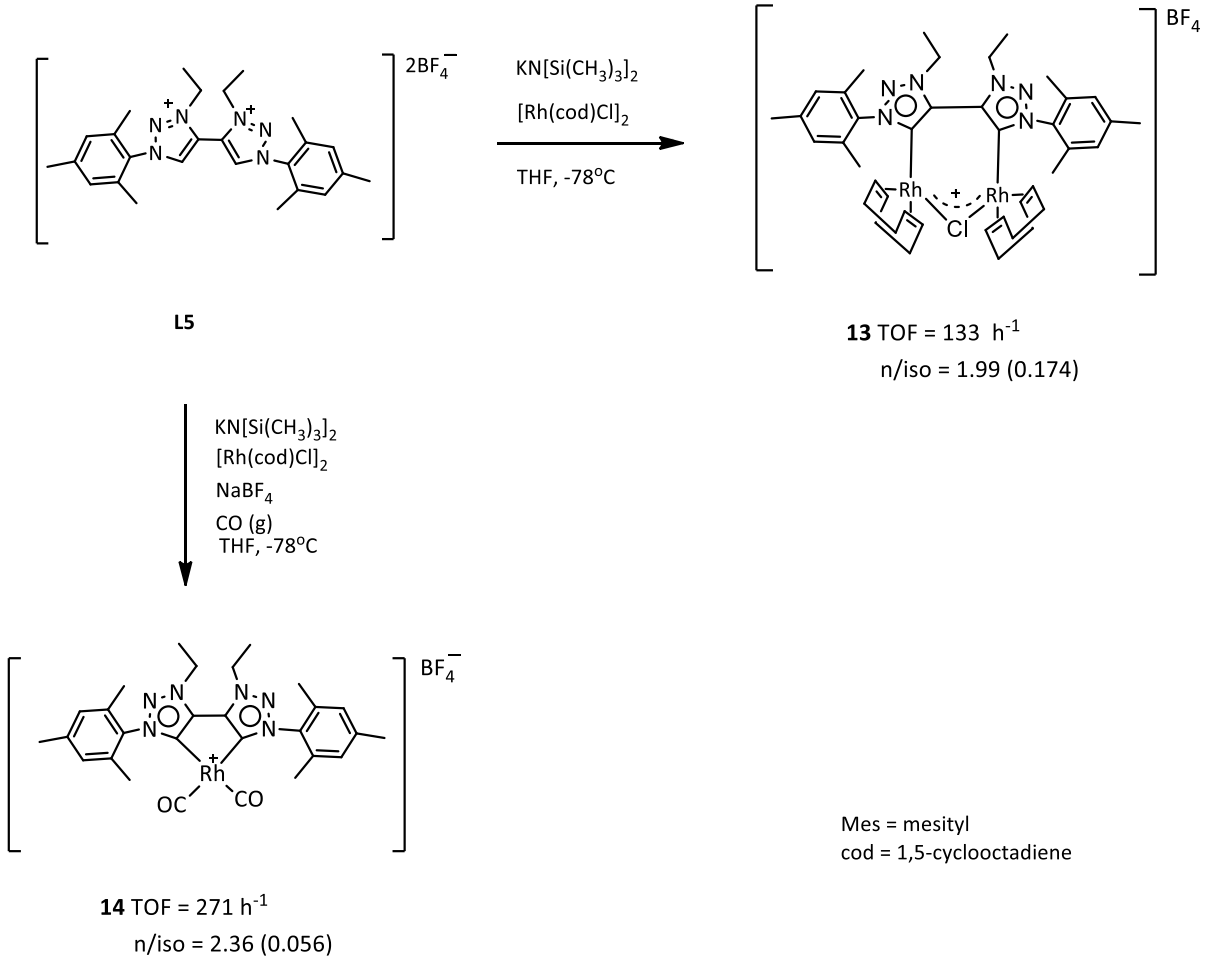

Scheme 7. 3: The effect of chelation compared to bridging of a bidentate ligand on hydroformylation reactions.

Alternative routes towards isolating the hybrid 1,2,3-triazol-5-ylidene rhodium Fischer carbene complex can be attempted, for instance by preparing unprecedented silver Fischer carbene complexes for transmetalation to rhodium(I) 1,2,3-triazol-5-ylidene complexes. Additionally, the preparation of cationic rhodium(I) 1,2,3-triazolylidene complexes can aid in easing the transmetalation of a Fischer carbene ligand to the said rhodium complex. This approach may be successful based on the data obtained from Barluenga and co-workers when isolating a hybrid rhodium(I) carbene complex.[5]

Overall, the rhodium Fischer carbene complexes displayed the best activity due to the electron withdrawing nature of these carbenes and the rhodium 1,2,3-triazol-5-ylidene complexes displayed the best regioselectivity towards formation of linear aldehydes as a result of their steric bulk. The iridium 1,2,3-triazol-5-ylidene complexes were marginally active under the same reaction conditions employed for their rhodium counterparts, even with the addition of salt to suppress the competing hydroformylation reaction. Catalytic activities of the rhodium i-bitz complexes, mono- and dinuclear, varied vastly with better activity and selectivity observed for the mononuclear complex due to the steric bulk around the coordination sphere of the metal centre, comparable to the data obtained for the monodentate rhodium 1,2,3-triazol-5-ylidene complexes.

7.2. References

[1] G. K. Ramollo, M. J. López-Gómez, D. C. Liles, L. C. Matsinha, G. S. Smith and D. I. Bezuidenhout, *Organometallics*, 2015, **34**, 5745-5753.
[2]W. Gil, A. M. Trzeciak and J. J. Ziółkowski, *Organometallics*, 2008, **27**, 4131–4138.
[3] D. Aucamp, T. Witteler, F. Dielmann, S. Siangwata, D. C. Liles, G. S. Smith and D. I. Bezuidenhout, *Eur. J. Inorg. Chem.*, 2017, **2017**, 1227–1236.
[4] A. Kämper, S. J. Warrelmann, K. Reiswich, R. Kuhlmann, R. Franke and A. Behr, *Chem. Eng. Sci.*, 2016, **144**, 346-371.
[5] J. Barluenga, R. Vicente, L. A. López, E. Rubio, M. Tomás and C. Álvarez-Rúa, *J. Am. Chem. Soc.*, 2004, **126**, 470–471.

Chapter 8: General experimental methods

8.1. Standard operating procedures

8.1.1. Method

All synthetic procedures were performed in flame or oven dried glassware, under an N_2 (g) or Ar (g) atmosphere, unless otherwise specified. Standard Schlenk or vacuum line techniques were employed. A PureLab HE glove box under N_2 (g) or constant vacuum was used for the storage and handling of air and moisture sensitive solids, as well as anhydrous deuterated solvents. NMR samples that require inert conditions during preparation, were also prepared in the glove box. All reactions were stirred mechanically.

8.1.2. Materials

All the solvents utilized for reactions were dehydrated by distillation under inert N_2 (g) atmosphere. Toluene and hexane were distilled over sodium metal under an inert atmosphere , whereas THF and Et_2O were distilled over sodium together with benzophenone under the same conditions. The distillation of CH_2Cl_2 (DCM) and CH_3CN (MeCN) was carried out over CaH under $N_{2(g)}$ atmosphere. All solvents were deaerated for a minimum of 20 minutes under N_2 (g) or Ar (g) preceding utilization. $CDCl_3$, CD_2Cl_2, and CD_3CN were dried over CaH under Ar (g) atmosphere, while C_6D_6 was dried over sodium metal under the same inert conditions.

The following reagents were prepared using previously reported procedures: $[Rh(cod)Cl]_2$,[1] $[Ir(cod)Cl]_2$,[2] $[W(CO)_5C\{(OEt)(p\text{-DMA})\}]$,[3] mesitylazide,[4] 1,3-bis(2,6-diisopropylphenyl)triaz-1-ene (triazene),[5] *tert*-butylhypochlorite,[6] triethyloxonium tetrafluoroborate,[7] compounds **1, 4,**[8] **5,**[9] and **12**. All the other precursors were used as purchased, without additional purification.

8.2. Characterisation Techniques

8.2.1. Nuclear magnetic resonance spectroscopy

A variety of nuclear magnetic resonance (NMR) spectrometers were used to acquire the NMR spectra, specifically a Bruker AVANCE-III-300 running at 300.13 MHz, 75.47 MHz, 121.49 MHz, and 282.40 for ^1H, ^{13}C, ^{31}P, and ^{19}F respectively; a Bruker AVANCE-III-400 running at 400.21 MHz, 100.64 MHz, 162.01 MHz, and 376.57 MHz for ^1H, ^{13}C, ^{31}P, and ^{19}F respectively; and a Bruker AVANCE-III-500 running at 500.13 MHz, 125.78 MHz, 162 MHz and 376.46 MHz for ^1H, ^{13}C, ^{31}P, and ^{19}F respectively. Deuterated solvents used include $CDCl_3$, C_6D_6, CD_2Cl_2, and CD_3CN referenced to 7.26 ppm, 7.16 ppm, 5.32 ppm, and 1.94 ppm for ^1H chemical shifts respectively; and 77.16 ppm, 128.06 ppm, 54.00 ppm, 1.32 ppm for ^{13}C chemical shifts, respectively. Spectral splitting patterns are assigned as follows: s - singlet; br s - broad singlet; d – doublet; t – triplet; q – quartet; sept – septet; dt – doublet of triplets; td – triplet of doublets; dq – doublet of quartets; m – multiplet.

8.2.2. Fourier-transform Infrared spectroscopy

A Bruker AILPHA Fourier-transform Infrared (FT-IR) spectrometer was used together with a NaCl or a CsCl cell to perform solution IR spectroscopy with an absorption range of between 4000-600 cm^{-1}. All solids were dissolved in anhydrous DCM.

8.2.3. High Resolution Mass spectrometry

All mass spectra were recorded on a Bruker Compact Q-TOF mass spectrometer (Bruker Daltonics, Bremen, Germany), using the mass range of 50-1300, after the direct infusion of 5 µL of the complex (dissolved in HPLC grade CH_3CN) into a Dionex Ultimate 3000 UHPLC (Thermoscientific, Dionex, Sunnyvale, California, USA). The sample passed through a loop with the flowrate of 0.3 ml/min prior to undergoing positive ionization by the Electrospray ionization (ESI) technique.

8.2.4. Melting Point

The melting point data for the compounds were recorded using the SMP10 melting point apparatus or the Büchi 540 melting point apparatus.

8.4. References

[1] G. Giordano and R. H. Crabtree, *Inorganic Syntheses: Reagents for Transition Metal Complex and Organometallic Syntheses*, J. Wiley & Sons, Hoboken, Vol 28., 1991.
[2] J. Choudhury, S. Podder and S. Roy, *J. Am. Chem. Soc.*, 2005, **127**, 6162–6163.
[3] S. Lotz, M. van den Berg and J. L. Dillen, *Transition Metal Chemistry*, 1988, **13**, 170-175
[4] W. Zhu and D. Ma, *Chemical Communications*, 2004, **10**, 888–889.
[5] (a) N. Nimitsiriwat, V. C. Gibson, E. L. Marshall, P. Takolpuckdee, A. K. Tomov, A. J. P. White, D. J. Williams, M. R. J. Elsegood and S. H. Dale, *Inorg. Chem.*, 2007, **46**, 9988–9997. (b) A. G. M. Barrett, M. R. Crimmin, M. S. Hill, P. B. Hitchcock, G. Kociok-Köhn and P. A. Procopiou, *Inorg. Chem.*, 2008, **47**, 7366–7376.
[6] C. Mintz, M. J. Walling, *Org. Synth.*, 1969, **49**, 9.
[7] H. Meerwein, Org. Synth., 1966, **46**, 113
[8] G. K. Ramollo, Ph.D. Chemistry Thesis, University of the Witwatersrand, 2020.
[9] D. Canseco-Gonzalez, A. Gniewek, M. Szulmanowicz, H. Müller-Bunz, A. M. Trzeciak, M. Albrecht, *Chem. Eur. J.* **2012**, *18*, 6055

Appendix A: FT-IR Spectra of selected complexes

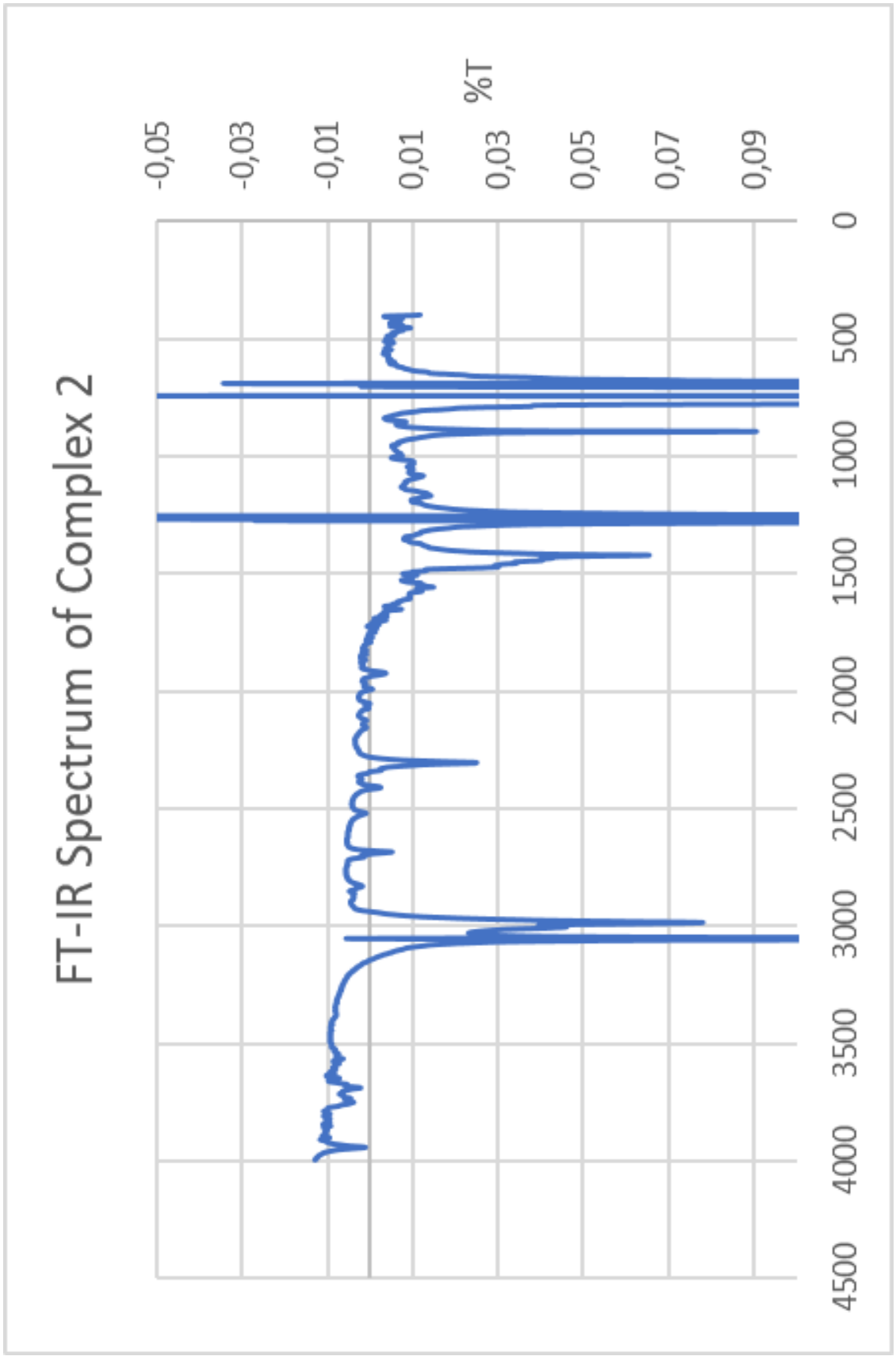

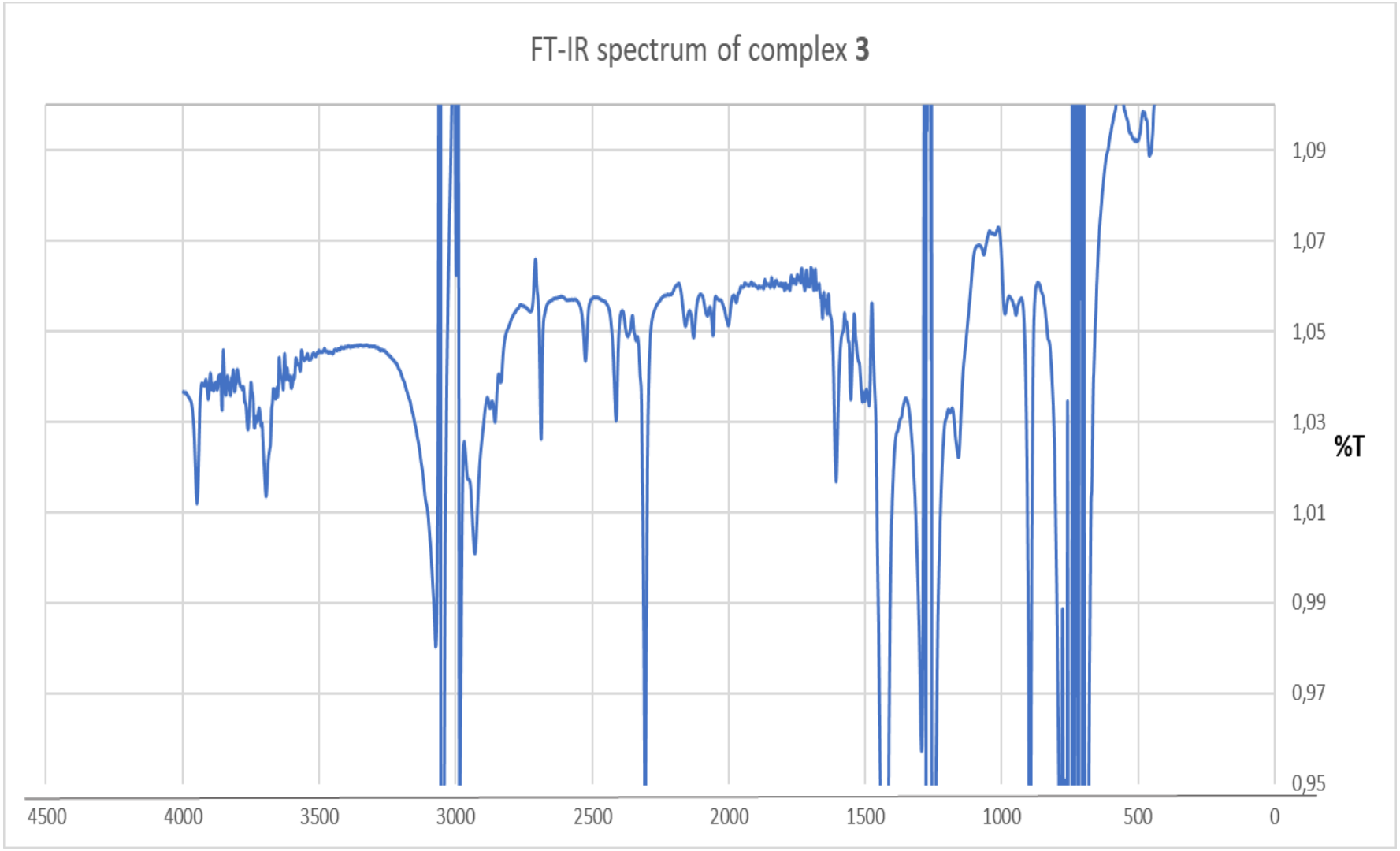
FT-IR spectrum of complex 3
1,09
1,07
1,05
1,03
1,01
0,99
0,97
0,95
%T
4500
4000
3500
3000
2500
2000
1500
1000
500
0
ν (cm)-1

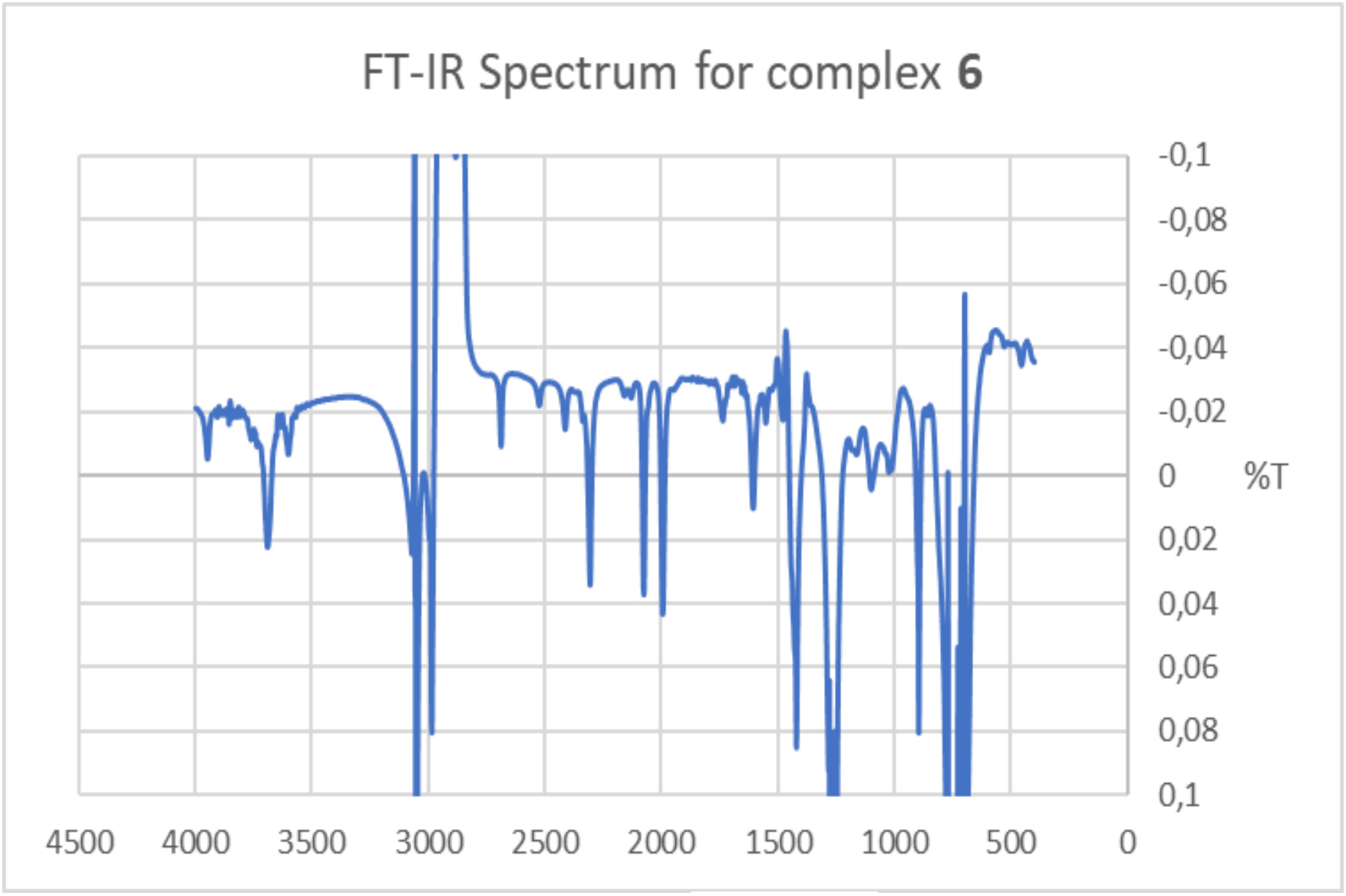
FT-IR Spectrum for complex 6
-0,1
-0,08
-0,06
-0,04
-0,02
0
%T
0,02
0,04
0,06
0,08
0,1
4500
4000
3500
3000
2500
2000
1500
1000
500
0
ν (cm)-1

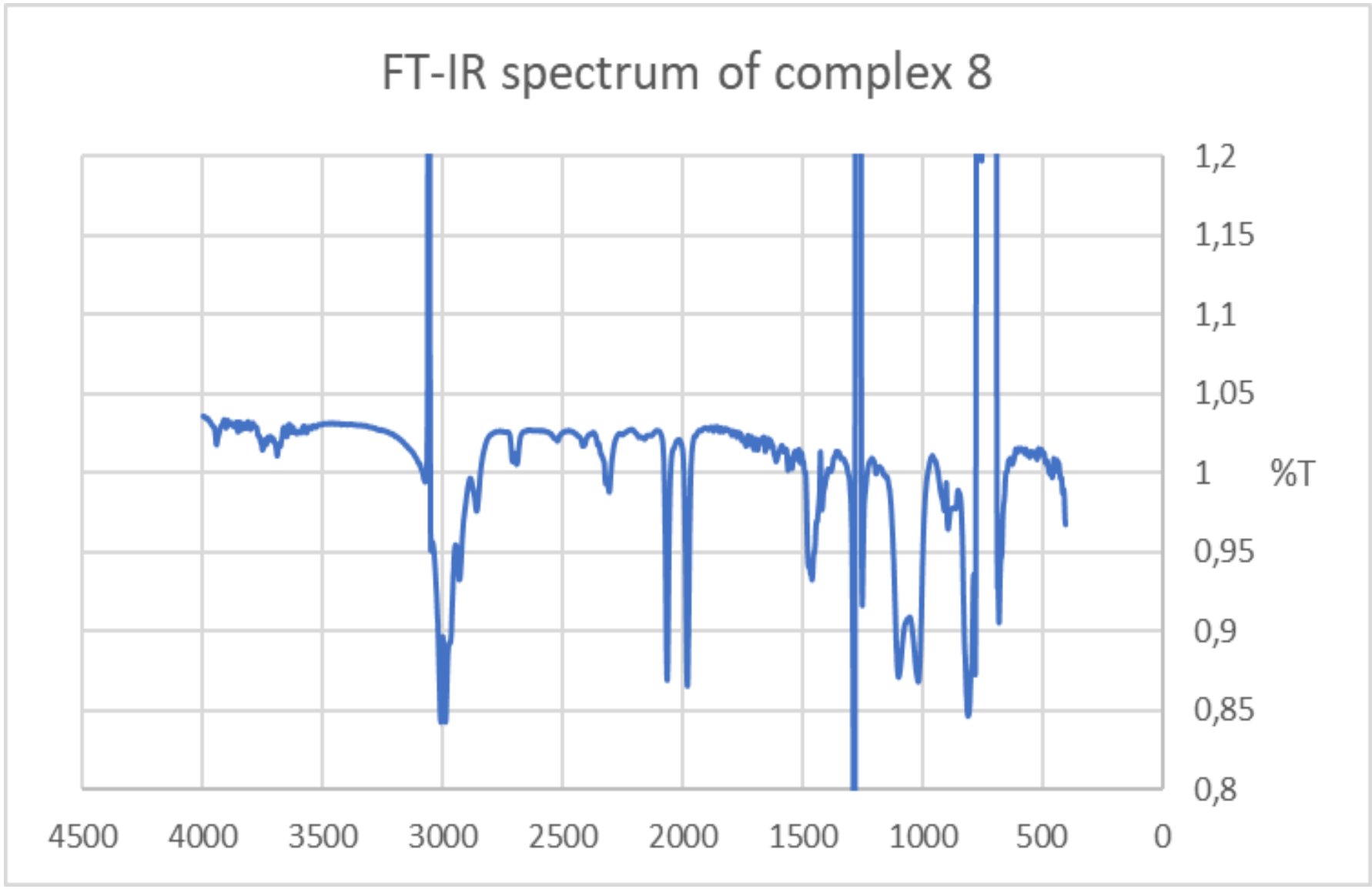
FT-IR spectrum of complex 8
1,2
1,15
1,1
1,05
1
0,95
0,9
0,85
0,8
%T
4500
4000
3500
3000
2500
2000
1500
1000
500
0
ν (cm)-1

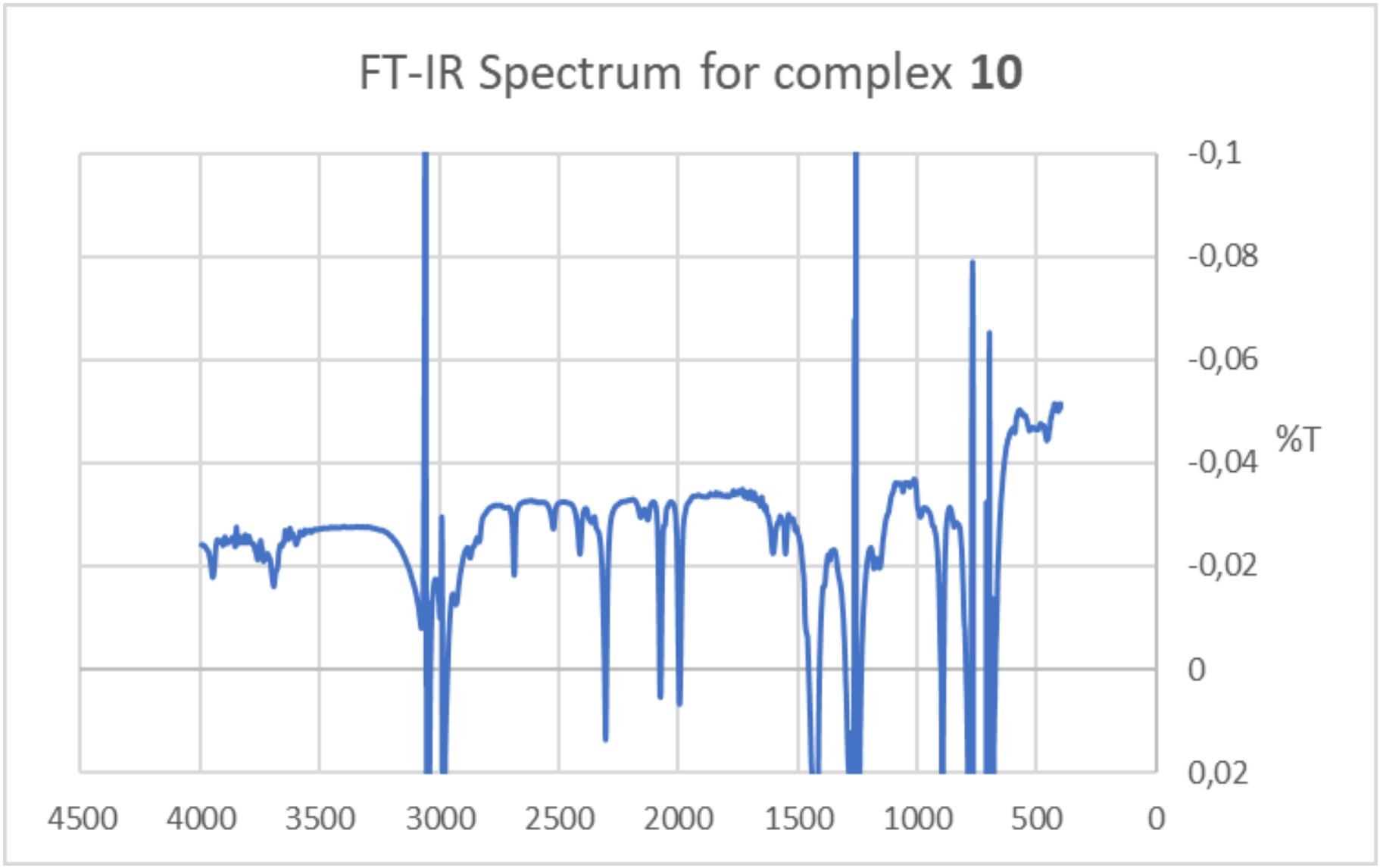
FT-IR Spectrum for complex 10
-0,1
-0,08
-0,06
-0,04
-0,02
0
0,02
%T
4500
4000
3500
3000
2500
2000
1500
1000
500
0
ν (cm)-1

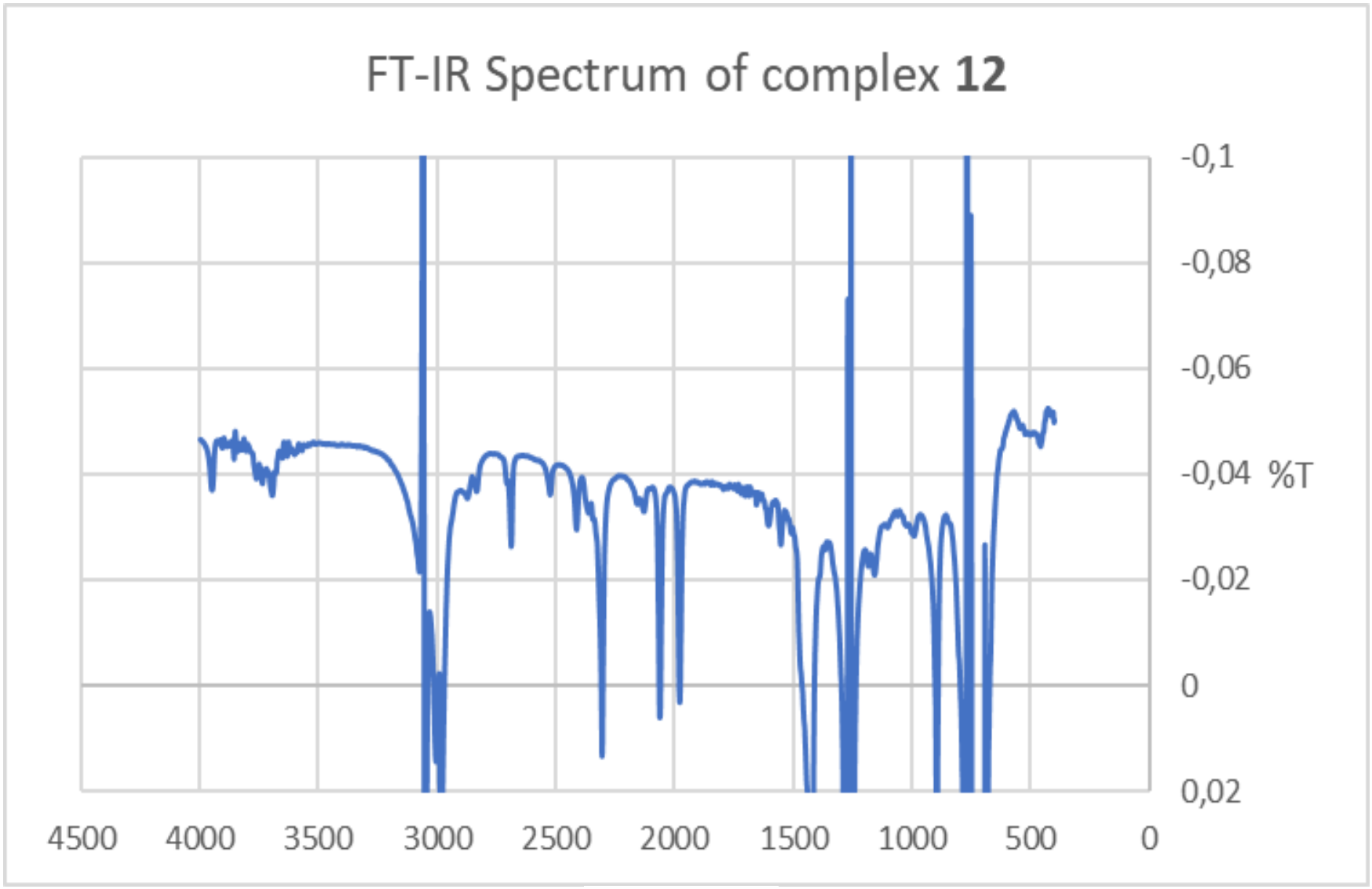
FT-IR Spectrum of complex **12**
-0,1
-0,08
-0,06
-0,04
-0,02
0
0,02
%T
4500
4000
3500
3000
2500
2000
1500
1000
500
0
ν (cm)-1

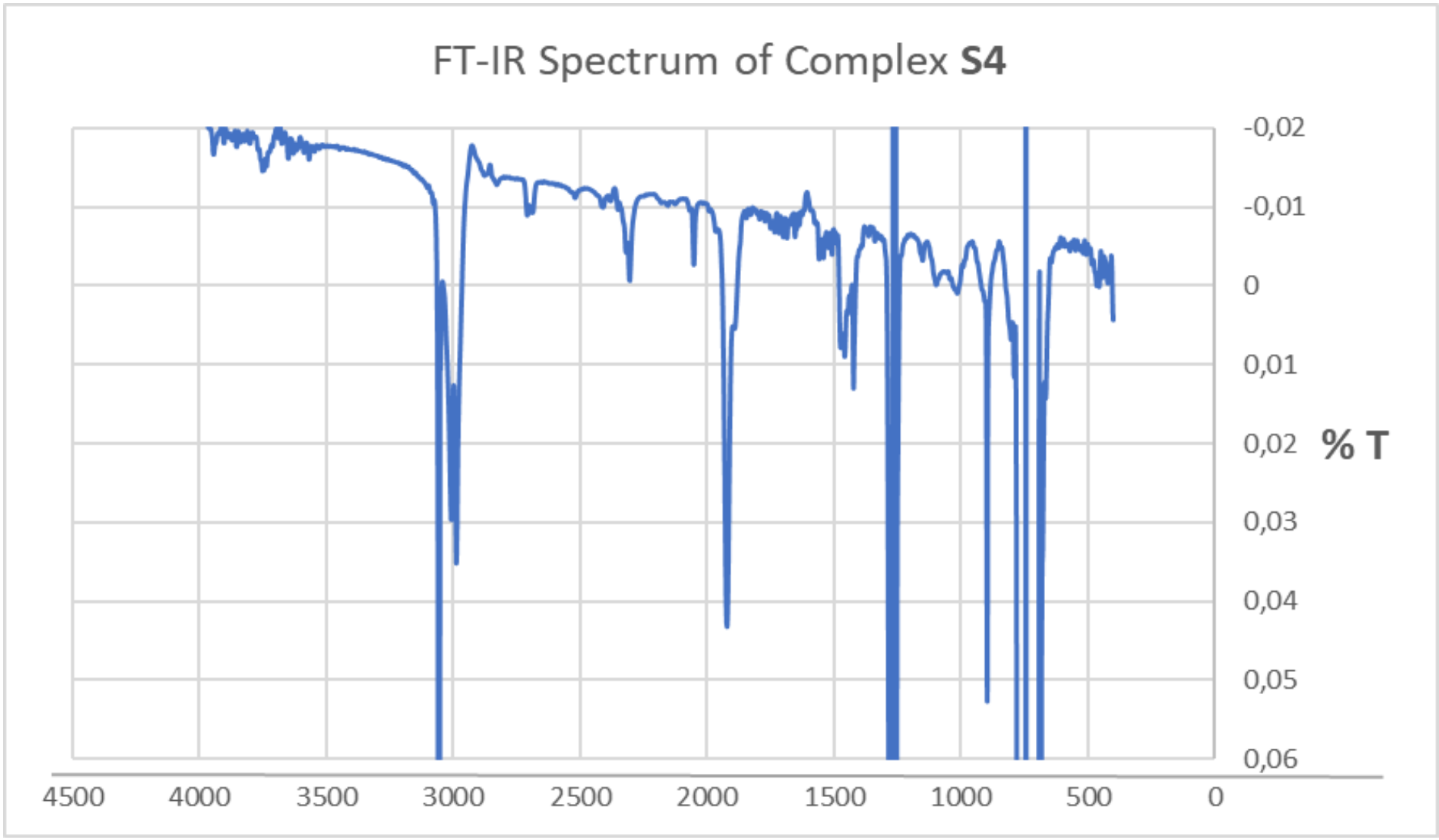
FT-IR Spectrum of Complex **S4**
-0,02
-0,01
0
0,01
0,02
0,03
0,04
0,05
0,06
% T
4500
4000
3500
3000
2500
2000
1500
1000
500
0
ν (cm)-1

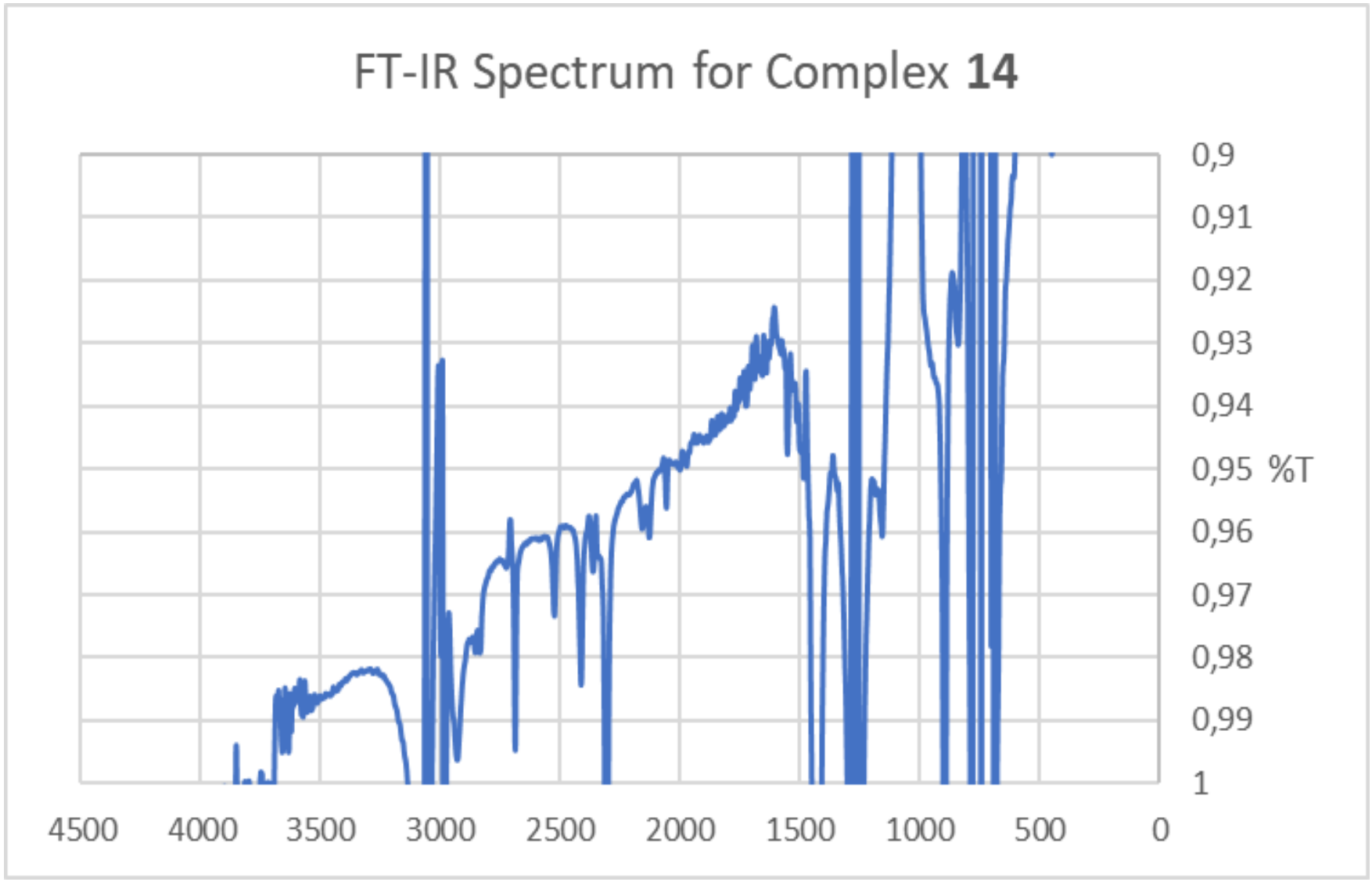
FT-IR Spectrum for Complex 14
0,9
0,91
0,92
0,93
0,94
0,95
%T
0,96
0,97
0,98
0,99
1
4500
4000
3500
3000
2500
2000
1500
1000
500
0
ν (cm)-1

Appendix B: Mass Spectra of selected compounds and complexes

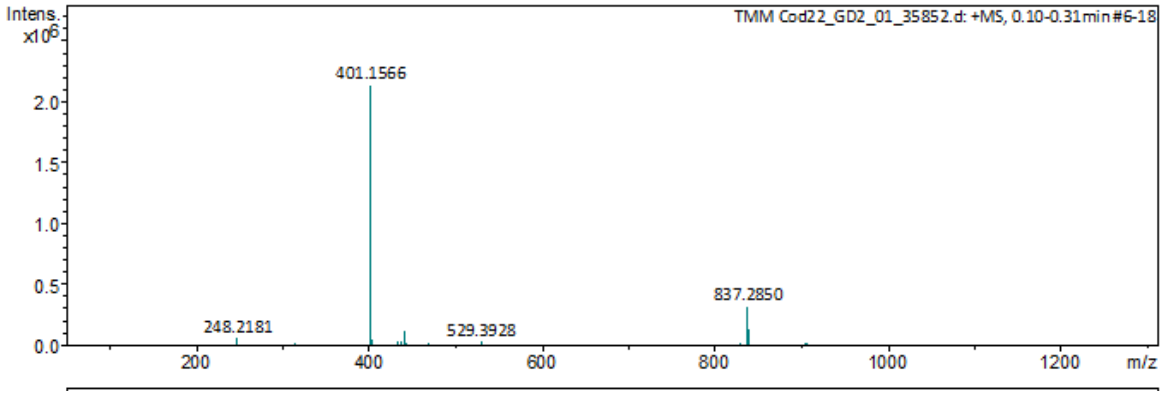

*Figure 1: MS spectrum of complex **2***

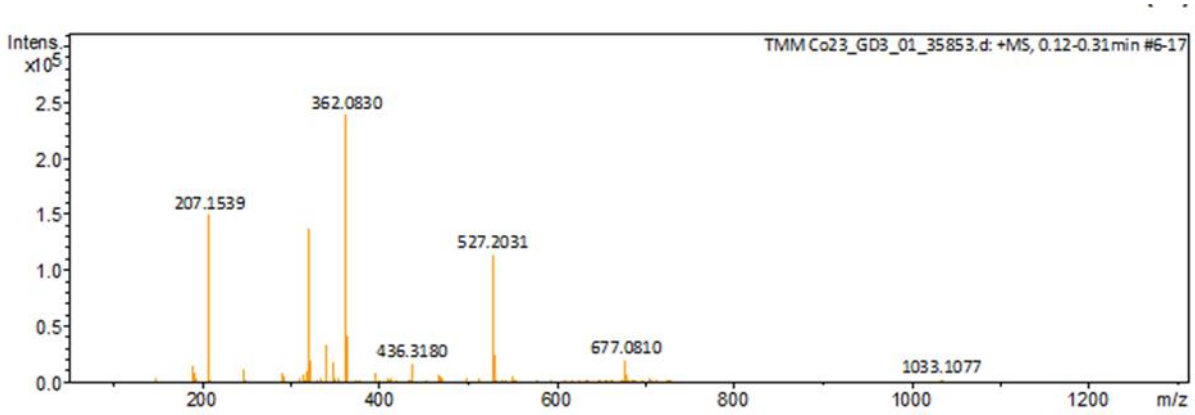

*Figure 2: MS Spectrum of complex **3***

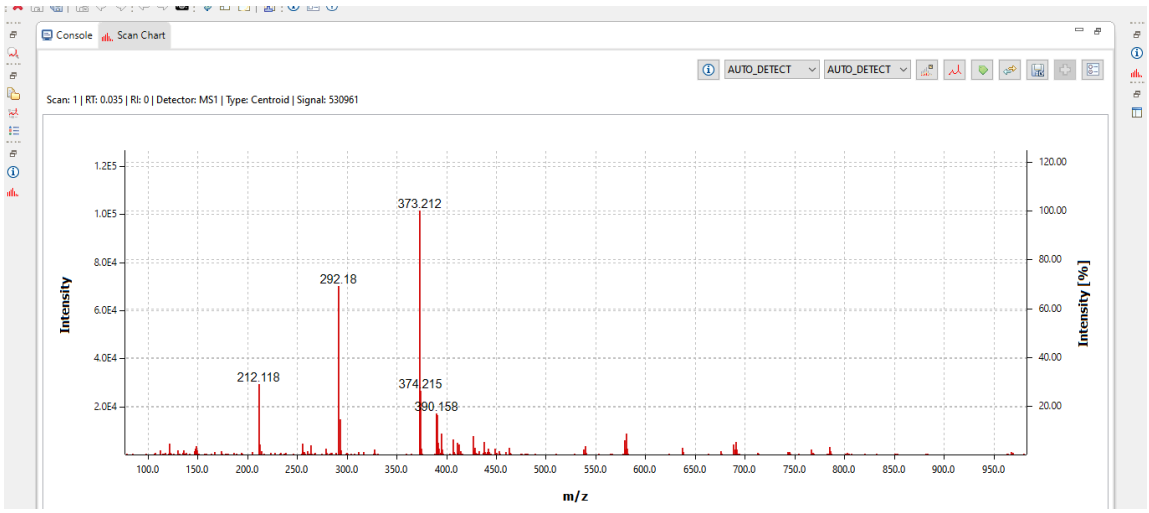

*Figure 3: MS spectrum of **L2***

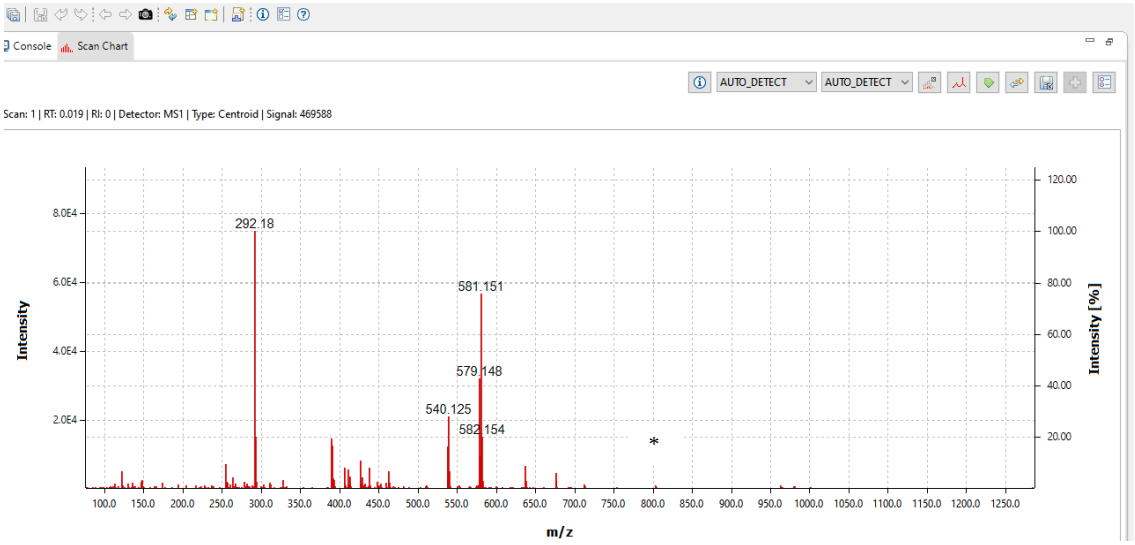

*Figure 4: MS spectrum of **S2***

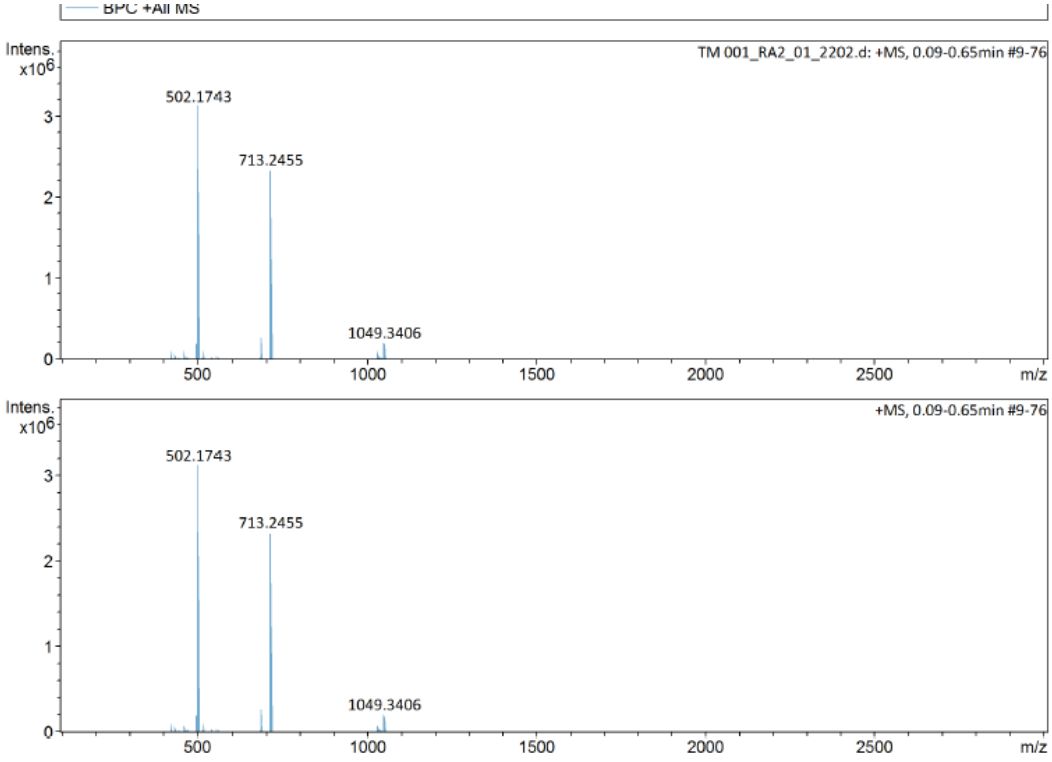

*Figure 5: MS Spectrum for complex **5***

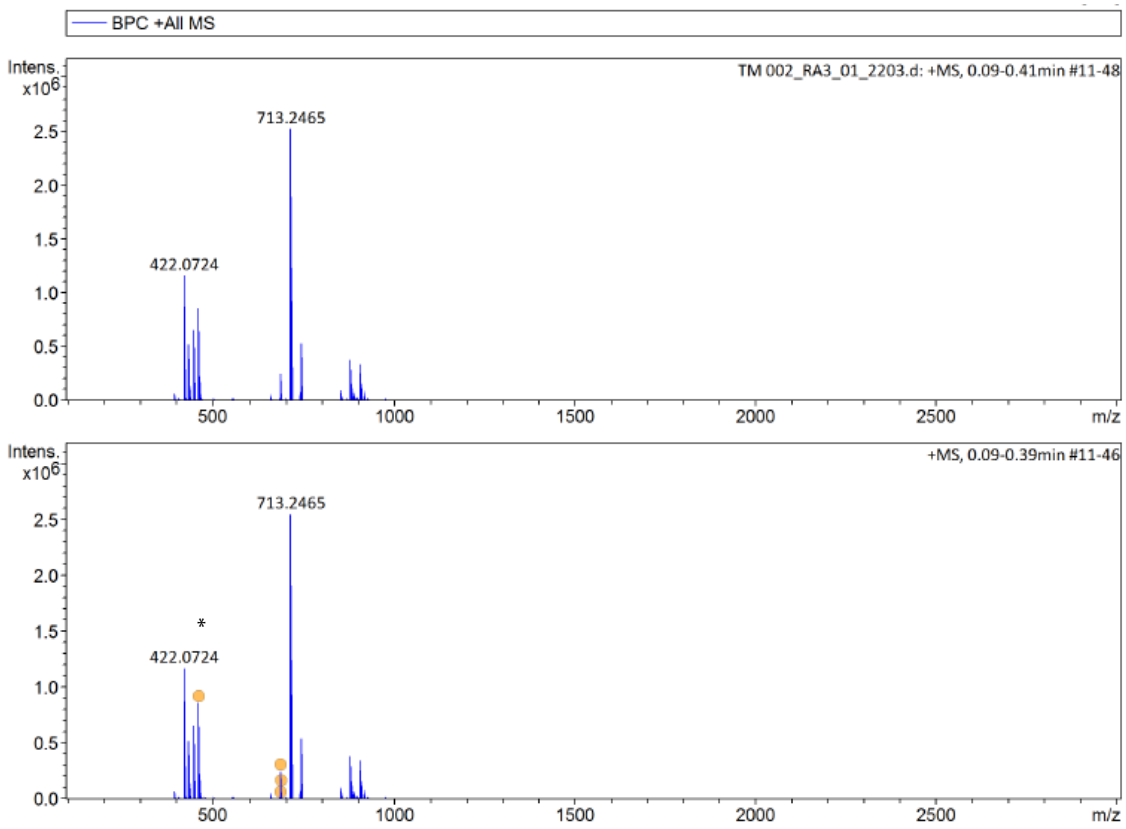

*Figure 6: MS spectrum for complex **6***

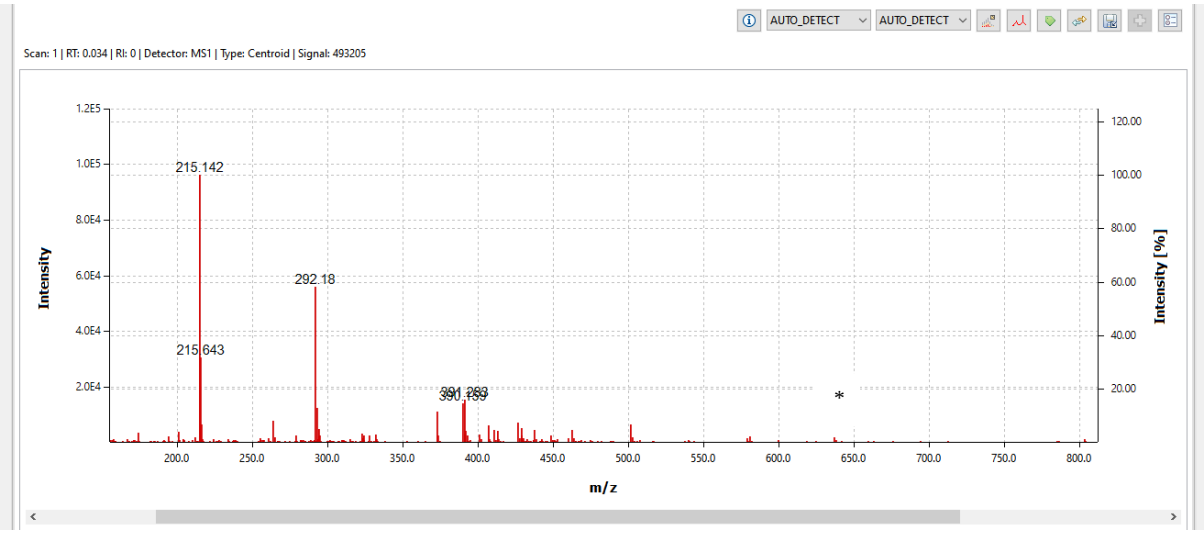

*Figure 7: MS spectrum of complex **7***

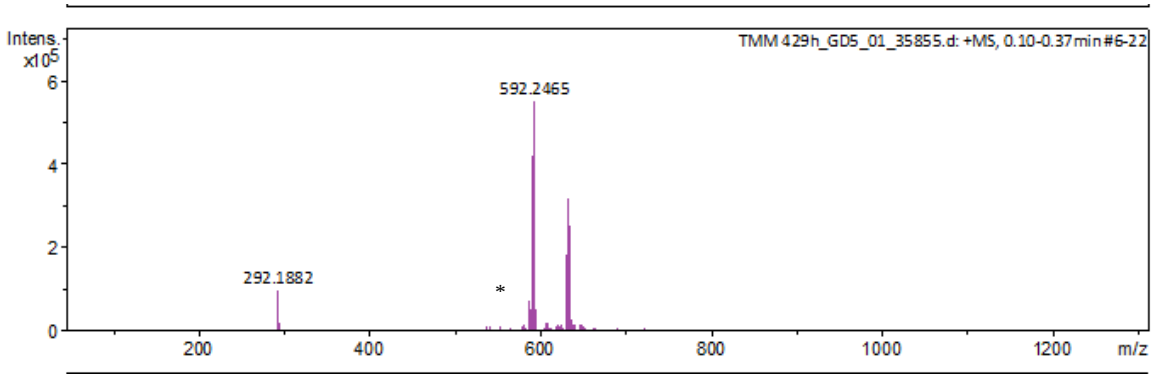

*Figure 8: MS spectrum of complex **8***

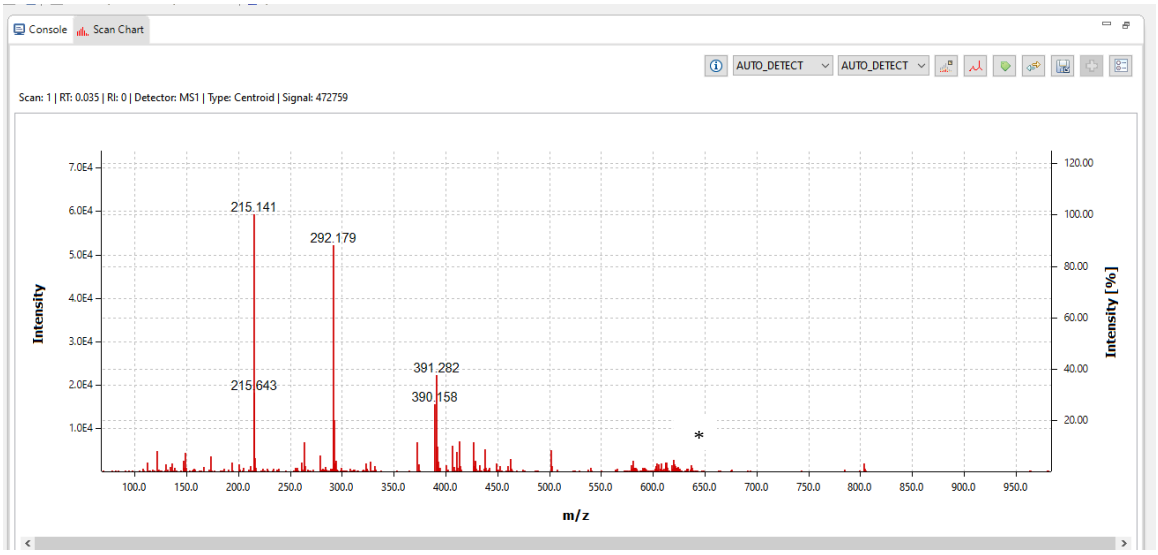

*Figure 9: MS spectrum for **S4***

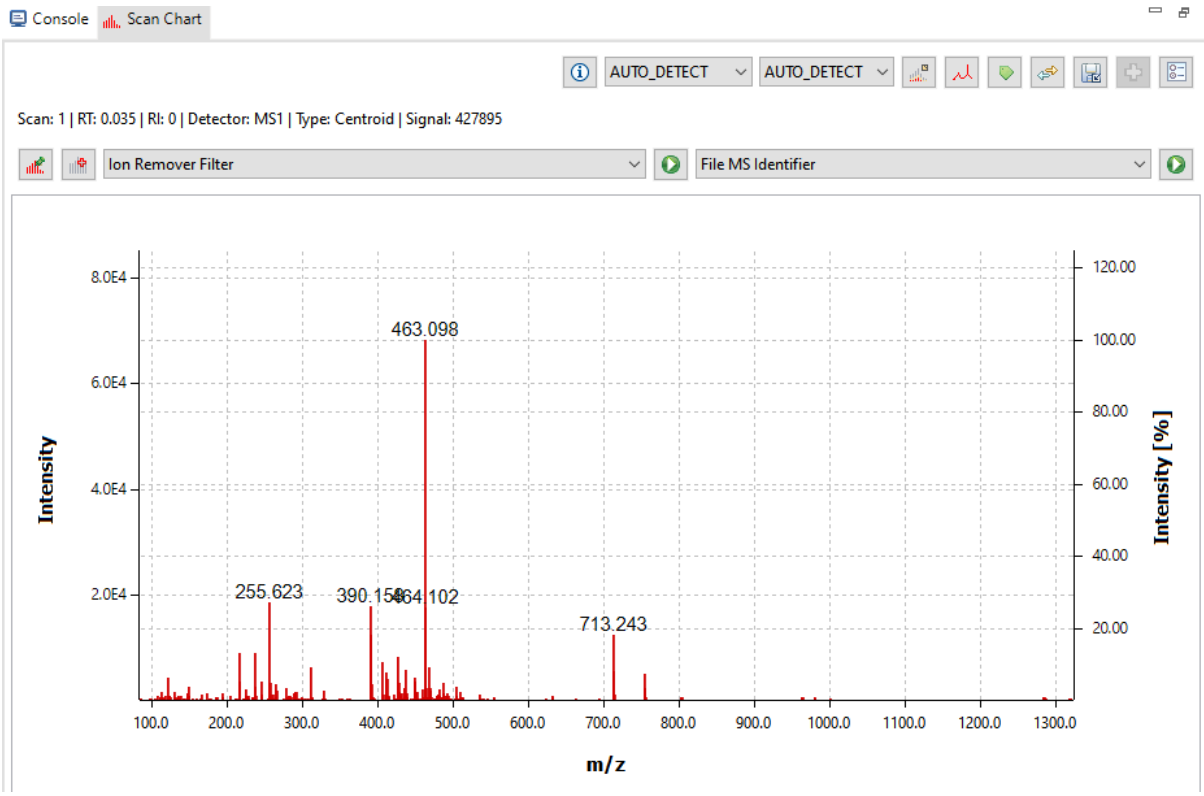

*Figure 10: MS spectrum of complex **9***

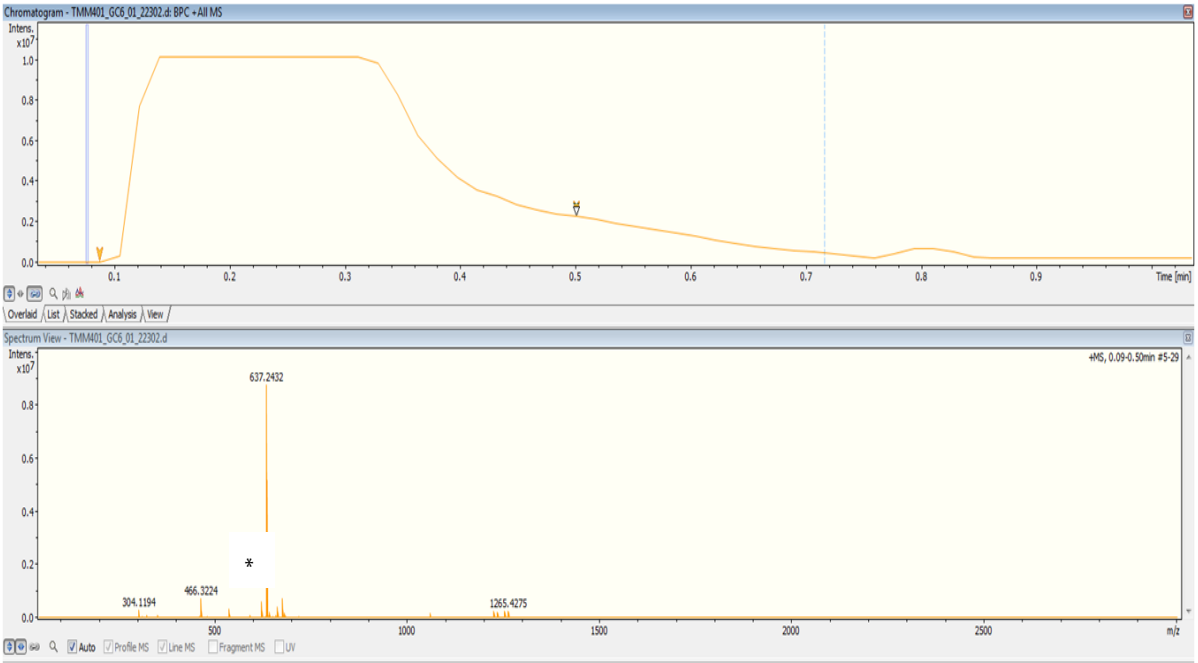

*Figure 11: MS spectrum for complex **10***

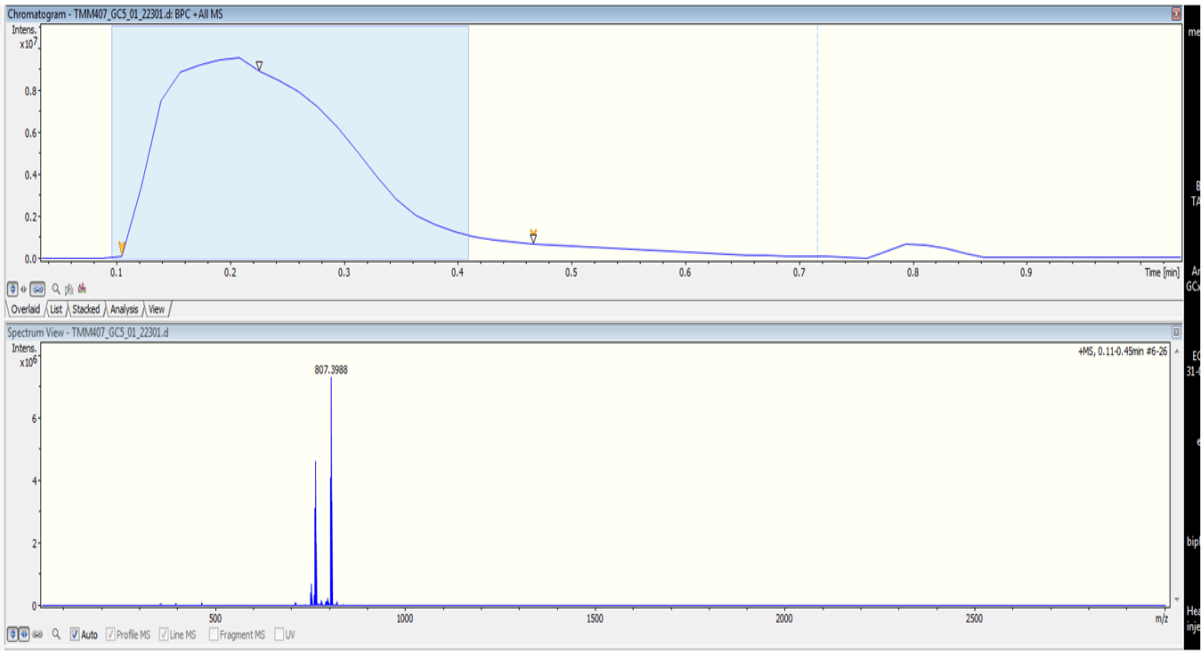

*Figure 12: MS spectrum for complex **11***

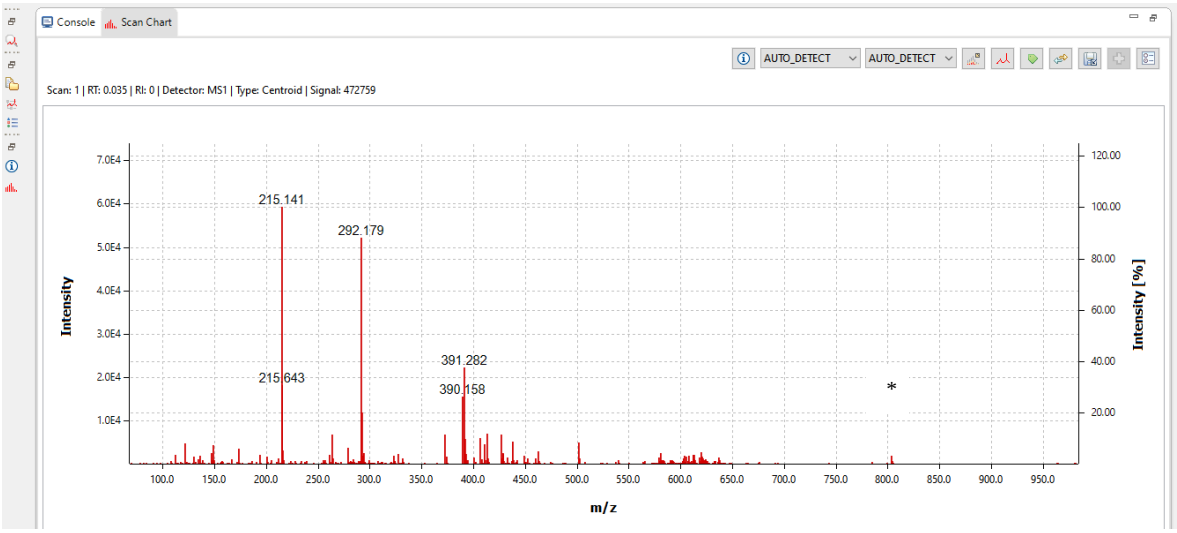

*Figure 13: MS spectrum of complex **12***

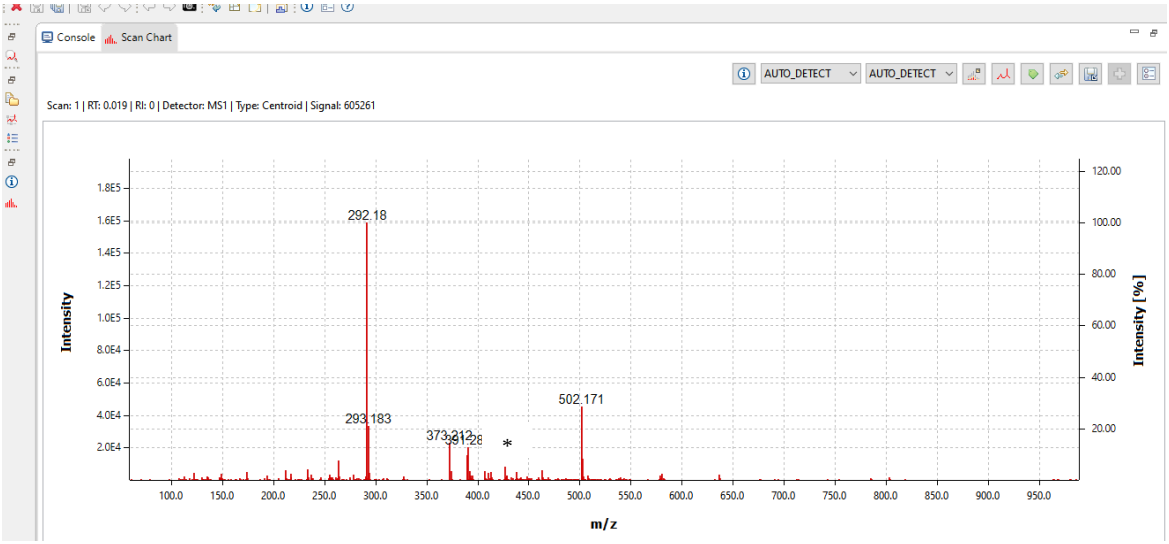

*Figure 14: MS spectrum of **L5***

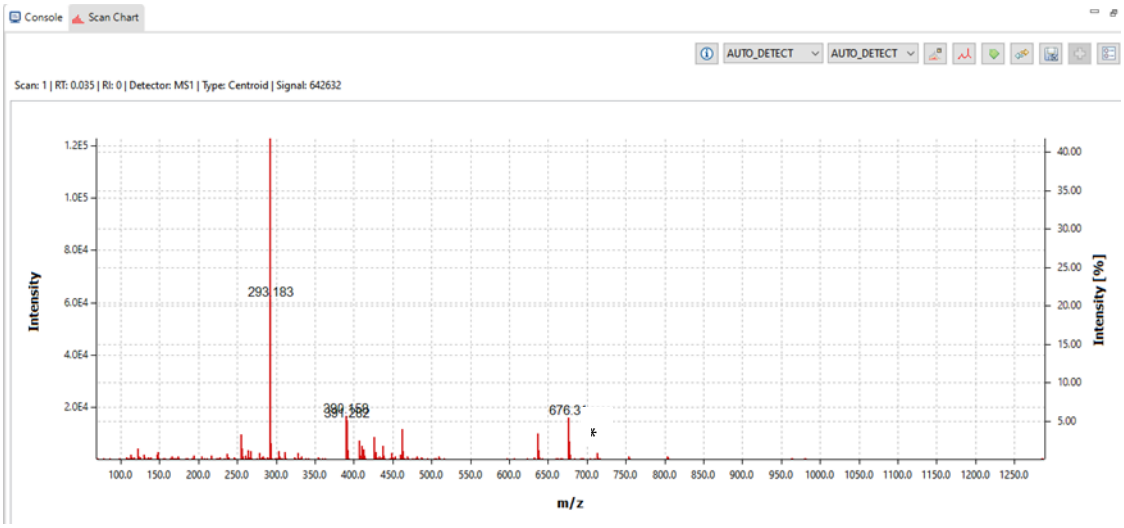

*Figure 15: MS Spectrum of **13***

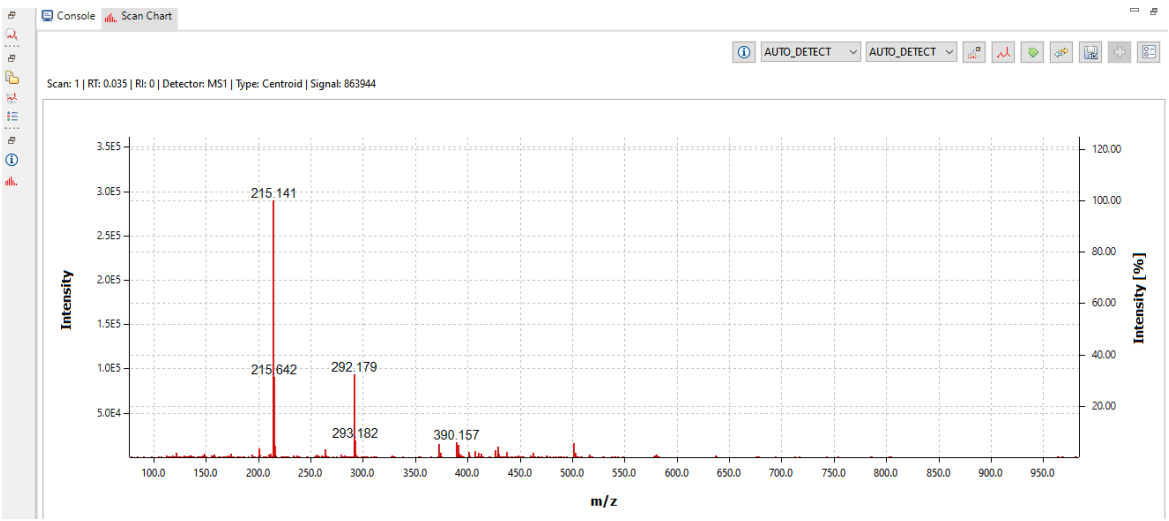

*Figure 16: MS spectrum of **14***

Appendix C: Crystallographic data for complex **2**

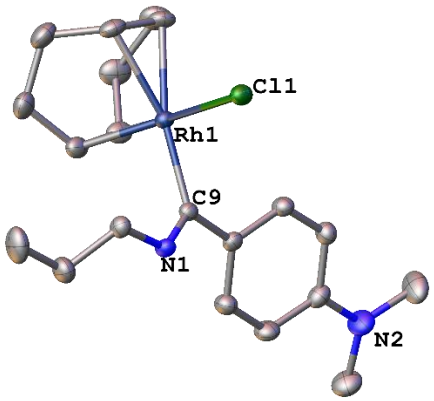

Table 1 Crystal data and structure refinement.

Empirical formula	$C_{20}H_{30}ClN_2Rh$
Formula weight	436.82
Temperature/K	173.15
Crystal system	monoclinic
Space group	$P2_1/n$
a/Å	12.0275(3)
b/Å	11.6854(3)
c/Å	16.7976(4)
α/°	90
β/°	99.2027(11)
γ/°	90
Volume/Å^3	2330.45(10)
Z	4
ρ_{calc}g/cm^3	1.487
μ/mm^{-1}	1.086
F(000)	1072.0
Crystal size/mm^3	0.34 × 0.172 × 0.084
Radiation	MoKα (λ = 0.71073)
2Θ range for data collection/°	3.886 to 61.146
Index ranges	-17 ≤ h ≤ 17, -16 ≤ k ≤ 16, -24 ≤ l ≤ 23
Reflections collected	59021
Independent reflections	7133 [R_{int} = 0.0423, R_{sigma} = 0.0261]
Data/restraints/parameters	7133/0/247
Goodness-of-fit on F^2	1.054

Final R indexes [I>=2σ (I)]	R_1 = 0.0259, wR_2 = 0.0576
Final R indexes [all data]	R_1 = 0.0360, wR_2 = 0.0616
Largest diff. peak/hole / e Å^{-3}	0.68/-0.62

Table 2 Fractional Atomic Coordinates (×10^4) and Equivalent Isotropic Displacement Parameters (Å^2×10^3). U_{eq} is defined as 1/3 of the trace of the orthogonalised U_{IJ} tensor.

Atom	*x*	*y*	*z*	U(eq)
C1	4850.6(16)	3149.1(15)	7913.2(10)	27.3(4)
C2	5538.3(16)	3998.2(15)	8281.1(10)	26.4(4)
C3	5239.0(19)	4822.9(18)	8900.7(12)	36.3(5)
C4	4065.2(19)	5352.6(18)	8668.8(12)	35.6(4)
C5	3725.6(15)	5494.8(15)	7760.5(11)	26.1(4)
C6	3110.0(15)	4671.3(15)	7258.0(11)	25.5(4)
C7	2755.2(17)	3507.5(18)	7520.2(13)	34.6(4)
C8	3687.0(18)	2881.8(17)	8092.5(13)	36.0(5)
C9	4382.0(13)	5665.1(13)	6118.7(10)	18.3(3)
C10	4642.4(14)	6894.6(13)	6155.9(9)	19.0(3)
C11	5626.3(14)	7287.4(14)	6635.6(10)	22.6(3)
C12	5912.2(15)	8433.9(14)	6679.4(11)	24.1(3)
C13	5185.2(16)	9262.9(14)	6269.1(11)	25.0(4)
C14	4176.3(16)	8872.8(15)	5808.4(11)	27.8(4)
C15	3927.6(15)	7720.3(15)	5741.9(11)	25.1(4)
C16	3513.8(14)	4090.1(14)	5279.5(10)	22.0(3)
C17	2299.1(16)	3974.9(17)	4899.8(12)	32.9(4)
C18	1973.0(19)	2723.7(19)	4779.7(14)	43.4(5)
C19	6513.1(19)	10782.4(17)	6765.9(16)	45.0(6)
C20	4619.5(19)	11252.6(16)	6009.4(13)	37.4(5)
Cl1	6429.5(3)	4028.0(4)	6532.6(2)	23.77(8)
N1	3857.4(12)	5279.0(11)	5429.7(8)	20.4(3)
N2	5456.5(15)	10403.6(13)	6315.7(11)	34.6(4)
Rh1	4798.7(2)	4639.0(2)	7077.1(2)	16.76(4)
C21	5686(2)	8456(2)	8670.5(14)	51.0(6)
Cl2	5889.4(6)	8003.6(7)	9684.7(4)	59.80(17)
Cl3	4914.5(6)	9733.7(7)	8523.7(5)	68.7(2)

Table 3 Anisotropic Displacement Parameters (Å^2×10^3). The Anisotropic displacement factor exponent takes the form: -2π^2[h^{2}a*^{2}U$_{11}$+2hka*b*U$_{12}$+…].

Atom	U_{11}	U_{22}	U_{33}	U_{23}	U_{13}	U_{12}
C1	35.7(10)	22.9(8)	23.5(8)	8.5(7)	5.8(7)	5.9(7)
C2	31.3(9)	29.7(9)	17.0(8)	5.1(7)	0.6(7)	8.0(7)

C3	45.7(12)	41.0(11)	20.2(9)	-3.5(8)	-1.0(8)	6.3(9)
C4	45.7(12)	38.9(11)	23.8(9)	-4.7(8)	10.5(8)	9.2(9)
C5	28.4(9)	26.4(9)	25.1(8)	1.2(7)	9.3(7)	9.5(7)
C6	21.7(8)	31.1(9)	25.0(8)	5.2(7)	7.8(7)	4.7(7)
C7	31.0(10)	40.4(11)	34.5(10)	6.0(8)	11.0(8)	-7.2(8)
C8	42.6(12)	31.4(10)	36.0(11)	10.2(8)	12.7(9)	-3.4(9)
C9	16.7(7)	18.9(7)	19.4(7)	1.9(6)	3.4(6)	1.7(6)
C10	22.0(8)	18.4(7)	17.2(7)	1.1(6)	4.5(6)	-0.1(6)
C11	24.9(9)	18.4(7)	23.3(8)	1.6(6)	0.5(7)	0.7(6)
C12	23.1(8)	20.8(8)	27.9(9)	-1.6(7)	2.2(7)	-2.0(6)
C13	31.2(10)	17.6(7)	27.5(9)	0.2(6)	9.0(7)	-0.5(7)
C14	30.1(10)	20.1(8)	32.0(9)	4.1(7)	1.5(7)	5.6(7)
C15	24.7(9)	23.2(8)	26.2(8)	1.4(7)	-0.1(7)	1.0(7)
C16	24.3(9)	19.1(8)	22.0(8)	-2.1(6)	2.4(6)	-2.8(6)
C17	26.4(10)	33.6(10)	36.4(10)	-1.0(8)	-1.5(8)	-6.1(8)
C18	36.5(12)	44.1(12)	49.8(13)	-17.0(10)	7.8(10)	-17.7(10)
C19	38.4(12)	19.3(9)	75.4(17)	-2.6(10)	3.5(11)	-4.8(8)
C20	47.6(13)	20.3(9)	44.2(12)	1.6(8)	7.2(10)	5.0(8)
Cl1	22.2(2)	26.2(2)	23.61(19)	3.29(15)	5.95(15)	3.98(15)
N1	22.5(7)	19.7(6)	18.1(6)	2.8(5)	0.5(5)	-1.6(5)
N2	38.9(10)	17.2(7)	46.3(10)	1.8(7)	2.4(8)	0.2(7)
Rh1	19.07(7)	15.69(6)	15.45(6)	1.09(4)	2.58(4)	0.97(5)
C21	40.1(13)	74.7(17)	39.1(12)	-6.5(12)	8.5(10)	-9.7(12)
Cl2	54.6(4)	78.6(5)	45.4(3)	2.7(3)	5.7(3)	-14.9(3)
Cl3	38.7(3)	94.1(6)	68.6(5)	1.6(4)	-5.4(3)	8.6(3)

Table 4 Bond Lengths.

Atom	Atom	Length/Å	Atom	Atom	Length/Å
C1	C2	1.374(3)	C10	C11	1.398(2)
C1	C8	1.511(3)	C10	C15	1.401(2)
C1	Rh1	2.2315(16)	C11	C12	1.382(2)
C2	C3	1.504(3)	C12	C13	1.409(2)
C2	Rh1	2.2061(16)	C13	C14	1.407(3)
C3	C4	1.534(3)	C13	N2	1.372(2)
C4	C5	1.524(3)	C14	C15	1.380(2)
C5	C6	1.410(3)	C16	C17	1.504(2)
C5	Rh1	2.1113(17)	C16	N1	1.460(2)
C6	C7	1.512(3)	C17	C18	1.519(3)
C6	Rh1	2.1016(17)	C19	N2	1.441(3)
C7	C8	1.539(3)	C20	N2	1.448(2)
C9	C10	1.470(2)	Cl1	Rh1	2.4015(4)

C9	N1	1.307(2)	C21	Cl2	1.763(2)
C9	Rh1	2.0056(16)	C21	Cl3	1.755(3)

Table 5 Bond Angles.

Atom	Atom	Atom	Angle/˚	Atom	Atom	Atom	Angle/˚
C2	C1	C8	124.75(17)	N2	C13	C14	121.52(17)
C2	C1	Rh1	70.96(10)	C15	C14	C13	121.16(16)
C8	C1	Rh1	110.69(12)	C14	C15	C10	121.60(17)
C1	C2	C3	125.50(18)	N1	C16	C17	112.79(14)
C1	C2	Rh1	72.98(10)	C16	C17	C18	110.81(17)
C3	C2	Rh1	108.12(12)	C9	N1	C16	124.39(14)
C2	C3	C4	113.29(16)	C13	N2	C19	120.69(16)
C5	C4	C3	112.75(15)	C13	N2	C20	120.00(17)
C4	C5	Rh1	113.79(12)	C19	N2	C20	118.74(16)
C6	C5	C4	123.78(17)	C1	Rh1	Cl1	93.75(5)
C6	C5	Rh1	70.08(10)	C2	Rh1	C1	36.06(7)
C5	C6	C7	125.83(17)	C2	Rh1	Cl1	90.81(5)
C5	C6	Rh1	70.82(10)	C5	Rh1	C1	89.16(7)
C7	C6	Rh1	110.51(12)	C5	Rh1	C2	81.62(7)
C6	C7	C8	113.44(16)	C5	Rh1	Cl1	162.83(5)
C1	C8	C7	112.49(15)	C6	Rh1	C1	81.57(7)
C10	C9	Rh1	121.74(11)	C6	Rh1	C2	97.52(7)
N1	C9	C10	116.40(14)	C6	Rh1	C5	39.09(7)
N1	C9	Rh1	121.86(12)	C6	Rh1	Cl1	158.05(5)
C11	C10	C9	120.02(14)	C9	Rh1	C1	161.78(7)
C11	C10	C15	117.10(15)	C9	Rh1	C2	162.02(7)
C15	C10	C9	122.85(15)	C9	Rh1	C5	93.28(7)
C12	C11	C10	121.95(16)	C9	Rh1	C6	88.97(7)
C11	C12	C13	120.71(16)	C9	Rh1	Cl1	89.23(5)
C14	C13	C12	117.36(15)	Cl3	C21	Cl2	112.28(14)
N2	C13	C12	121.12(17)				

Table 6 Torsion Angles.

A	B	C	D	Angle/˚	A	B	C	D	Angle/˚
C1	C2	C3	C4	-46.4(3)	C12	C13	N2	C19	2.1(3)
C2	C1	C8	C7	93.4(2)	C12	C13	N2	C20	-169.20(18)
C2	C3	C4	C5	-31.7(3)	C13	C14	C15	C10	2.8(3)
C3	C4	C5	C6	92.7(2)	C14	C13	N2	C19	-177.6(2)
C3	C4	C5	Rh1	11.5(2)	C14	C13	N2	C20	11.1(3)
C4	C5	C6	C7	-4.0(3)	C15	C10	C11	C12	-2.5(3)
C4	C5	C6	Rh1	-105.89(17)	C17	C16	N1	C9	129.76(18)

C5	C6	C7	C8	-43.1(3)	N1	C9	C10	C11	-146.34(16)
C6	C7	C8	C1	-33.1(2)	N1	C9	C10	C15	35.3(2)
C8	C1	C2	C3	-2.0(3)	N1	C16	C17	C18	-178.24(16)
C8	C1	C2	Rh1	-102.44(17)	N2	C13	C14	C15	177.72(18)
C9	C10	C11	C12	179.05(16)	Rh1	C1	C2	C3	100.43(17)
C9	C10	C15	C14	177.89(17)	Rh1	C1	C8	C7	12.8(2)
C10	C9	N1	C16	-179.08(14)	Rh1	C2	C3	C4	35.3(2)
C10	C11	C12	C13	3.3(3)	Rh1	C5	C6	C7	101.91(18)
C11	C10	C15	C14	-0.5(3)	Rh1	C6	C7	C8	37.5(2)
C11	C12	C13	C14	-1.0(3)	Rh1	C9	C10	C11	34.2(2)
C11	C12	C13	N2	179.31(17)	Rh1	C9	C10	C15	-144.22(14)
C12	C13	C14	C15	-2.0(3)	Rh1	C9	N1	C16	0.4(2)

Table 7 Hydrogen Atom Coordinates (Å×10^4) and Isotropic Displacement Parameters (Å^2×10^3).

Atom	*x*	*y*	*z*	U(eq)
H1	5263.66	2469.37	7746.92	33
H2	6360.49	3819.64	8339.52	32
H3A	5805.94	5443.93	8977.81	44
H3B	5273.35	4417.44	9421.55	44
H4A	3505.47	4859.93	8875.61	43
H4B	4053.52	6110.69	8930.47	43
H5	3552.89	6302.65	7586.73	31
H6	2581.63	5006.62	6796.87	31
H7A	2526.41	3028.25	7035.68	42
H7B	2090.16	3599.99	7793.73	42
H8A	3644.2	3105.23	8655.29	43
H8B	3556.61	2046.41	8044.26	43
H11	6112.65	6750.33	6940.5	27
H12	6606.45	8665.46	6989.41	29
H14	3656.87	9412.1	5538.4	33
H15	3255.38	7481.14	5407.22	30
H16A	3636.82	3666.24	5796.47	26
H16B	3994.05	3736.3	4920.32	26
H17A	2176.29	4371.61	4372.24	39
H17B	1814.5	4343.33	5249.68	39
H18A	2467.62	2353.55	4446.61	65
H18B	1189.82	2668.64	4509.86	65
H18C	2051.32	2341.68	5305.04	65
H19A	6531.52	10613.46	7339.28	67
H19B	6593	11608.83	6693.4	67
H19C	7133.63	10382.55	6571.13	67

H20A	4380.19	11134.02	5429.74	56
H20B	4944.24	12019.47	6102.04	56
H20C	3967.75	11178.78	6289	56
H1A	3700.63	5768.57	5029.36	24
H21A	6428.93	8567.76	8499.43	61
H21B	5282.56	7849.48	8327.16	61

Appendix D: Crystallographic data for complex **3**.

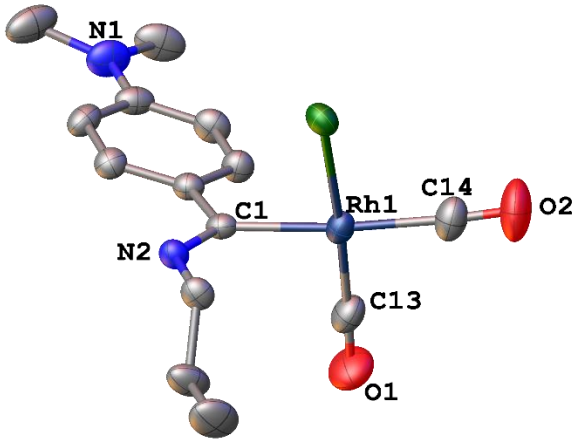

Table 1 Crystal data and structure refinement.

Empirical formula	$C_{14}H_{18}ClN_2O_2Rh$
Formula weight	384.66
Temperature/K	173.15
Crystal system	triclinic
Space group	P-1
a/Å	8.5569(5)
b/Å	10.4188(6)
c/Å	10.5705(6)
α/°	71.6988(18)
β/°	66.4054(18)
γ/°	77.0938(19)
Volume/Å^3	814.74(8)
Z	2
ρ_{calc}g/cm^3	1.568
μ/mm^{-1}	1.214
F(000)	388.0
Crystal size/mm^3	0.313 × 0.177 × 0.122
Radiation	MoKα (λ = 0.71073)
2Θ range for data collection/°	6.298 to 56.684
Index ranges	-11 ≤ h ≤ 11, -13 ≤ k ≤ 13, -14 ≤ l ≤ 14
Reflections collected	28474
Independent reflections	4026 [R_{int} = 0.0328, R_{sigma} = 0.0219]
Data/restraints/parameters	4026/0/184
Goodness-of-fit on F^2	1.037
Final R indexes [I>=2σ (I)]	R_1 = 0.0236, wR_2 = 0.0495

Final R indexes [all data]	R_1 = 0.0307, wR_2 = 0.0519
Largest diff. peak/hole / e Å^{-3}	0.55/-0.41

Table 2 Fractional Atomic Coordinates (×10^4) and Equivalent Isotropic Displacement Parameters (Å^2×10^3). U_{eq} is defined as 1/3 of the trace of the 154rthogonalized U_{IJ} tensor.

Atom	*x*	*y*	*z*	U(eq)
C1	4592(2)	7938.6(17)	6767.4(18)	25.1(4)
C2	5550(2)	6895.3(17)	6000.6(19)	26.3(4)
C3	6484(2)	5780.5(19)	6638(2)	32.1(4)
C4	7476(3)	4789(2)	5963(2)	36.1(4)
C5	7643(2)	4873.8(19)	4566(2)	34.1(4)
C6	6714(3)	5990.0(19)	3911(2)	34.2(4)
C7	5679(2)	6951.0(18)	4623(2)	30.4(4)
C8	9534(3)	2749(2)	4582(3)	53.0(6)
C9	8997(4)	4116(3)	2367(3)	58.8(7)
C10	2529(2)	9999.2(18)	6875(2)	31.1(4)
C11	681(3)	9781(2)	7679(3)	46.6(6)
C12	-318(3)	10990(3)	8297(3)	62.1(7)
C13	3567(3)	6834(2)	9652(2)	42.4(5)
C14	5750(3)	8156(2)	9980(2)	46.8(5)
Cl1	6897.7(6)	9742.1(5)	6873.4(5)	35.39(11)
N1	8663(2)	3920.7(18)	3862(2)	46.2(5)
N2	3543.7(19)	8868.3(15)	6260.4(16)	27.8(3)
O1	2595(3)	6084(2)	10360.5(19)	65.3(5)
O2	6226(3)	8186(2)	10816(2)	79.0(6)
Rh1	5077.9(2)	8063.2(2)	8481.5(2)	29.57(5)

Table 3 Anisotropic Displacement Parameters (Å^2×10^3). The Anisotropic displacement factor exponent takes the form: -2π^2[h^{2}a*^{2}U$_{11}$+2hka*b*U$_{12}$+…].

Atom	U_{11}	U_{22}	U_{33}	U_{23}	U_{13}	U_{12}
C1	22.0(8)	22.0(8)	26.6(9)	-4.0(7)	-5.8(7)	-2.0(7)
C2	23.6(9)	22.6(8)	29.7(9)	-5.7(7)	-8.2(7)	-1.0(7)
C3	32.0(10)	28.9(9)	34.4(10)	-9.8(8)	-13.0(8)	3.3(8)
C4	32.8(10)	27.4(9)	47.1(12)	-11.9(9)	-16.2(9)	6.1(8)
C5	27.2(10)	27.5(9)	43.5(11)	-14.6(8)	-3.8(8)	-3.6(7)
C6	39.9(11)	31.4(10)	27.5(9)	-8.9(8)	-4.9(8)	-8.2(8)
C7	33.3(10)	24.1(9)	31.9(10)	-5.5(7)	-10.7(8)	-3.4(7)
C8	38.6(12)	36.2(12)	82.4(18)	-32.0(12)	-13.7(12)	8.5(10)
C9	61.8(16)	48.5(14)	53.6(15)	-29.5(12)	8.8(12)	-14.2(12)
C10	29.4(10)	24.4(9)	40.0(10)	-11.4(8)	-15.1(8)	5.8(7)

C11	28.1(11)	52.3(13)	64.4(15)	-35.2(12)	-10.0(10)	2.9(9)
C12	39.7(13)	69.3(17)	78.5(19)	-47.5(15)	-10.8(13)	13.5(12)
C13	49.1(13)	42.1(12)	30.4(10)	-6.0(9)	-13.5(10)	-0.1(10)
C14	60.8(15)	43.5(12)	38.2(12)	-13.7(10)	-23.7(11)	6.3(11)
Cl1	31.0(2)	36.5(2)	41.5(3)	-7.6(2)	-18.1(2)	-2.58(19)
N1	43.0(11)	38.8(10)	54.1(11)	-27.1(9)	-7.2(9)	3.8(8)
N2	25.0(8)	27.9(8)	31.4(8)	-10.4(6)	-11.3(6)	2.2(6)
O1	73.9(13)	62.7(12)	46.8(10)	7.4(9)	-15.4(9)	-25.9(10)
O2	118.8(19)	81.6(14)	61.2(12)	-24.6(11)	-59.6(13)	3.4(13)
Rh1	32.38(9)	28.50(8)	25.92(8)	-7.93(6)	-11.58(6)	4.09(6)

Table 4 Bond Lengths.

Atom	Atom	Length/Å	Atom	Atom	Length/Å
C1	C2	1.461(2)	C8	N1	1.445(3)
C1	N2	1.304(2)	C9	N1	1.444(3)
C1	Rh1	2.0608(18)	C10	C11	1.495(3)
C2	C3	1.403(2)	C10	N2	1.462(2)
C2	C7	1.399(3)	C11	C12	1.527(3)
C3	C4	1.373(3)	C13	O1	1.135(3)
C4	C5	1.401(3)	C13	Rh1	1.819(2)
C5	C6	1.409(3)	C14	O2	1.122(3)
C5	N1	1.363(2)	C14	Rh1	1.924(2)
C6	C7	1.377(3)	Cl1	Rh1	2.3674(5)

Table 5 Bond Angles.

Atom	Atom	Atom	Angle/˚	Atom	Atom	Atom	Angle/˚
C2	C1	Rh1	120.74(12)	C10	C11	C12	110.64(19)
N2	C1	C2	118.42(16)	O1	C13	Rh1	178.0(2)
N2	C1	Rh1	120.51(13)	O2	C14	Rh1	176.5(2)
C3	C2	C1	118.96(17)	C5	N1	C8	120.0(2)
C7	C2	C1	124.61(16)	C5	N1	C9	120.8(2)
C7	C2	C3	116.36(17)	C9	N1	C8	119.02(19)
C4	C3	C2	122.54(18)	C1	N2	C10	125.25(16)
C3	C4	C5	120.77(18)	C1	Rh1	Cl1	87.35(5)
C4	C5	C6	117.29(17)	C13	Rh1	C1	89.57(8)
N1	C5	C4	121.64(19)	C13	Rh1	C14	93.84(10)
N1	C5	C6	121.07(19)	C13	Rh1	Cl1	175.79(7)
C7	C6	C5	121.13(18)	C14	Rh1	C1	174.77(9)
C6	C7	C2	121.84(18)	C14	Rh1	Cl1	89.44(8)
N2	C10	C11	112.79(16)				

Table 6 Torsion Angles.

A	B	C	D	Angle/˚	A	B	C	D	Angle/˚
C1	C2	C3	C4	-177.08(18)	C6	C5	N1	C8	-176.85(19)
C1	C2	C7	C6	174.65(17)	C6	C5	N1	C9	8.0(3)
C2	C1	N2	C10	-178.31(16)	C7	C2	C3	C4	0.0(3)
C2	C3	C4	C5	2.1(3)	C11	C10	N2	C1	-103.4(2)
C3	C2	C7	C6	-2.2(3)	N1	C5	C6	C7	179.81(19)
C3	C4	C5	C6	-1.8(3)	N2	C1	C2	C3	-170.72(17)
C3	C4	C5	N1	177.99(19)	N2	C1	C2	C7	12.5(3)
C4	C5	C6	C7	-0.4(3)	N2	C10	C11	C12	-179.9(2)
C4	C5	N1	C8	3.3(3)	Rh1	C1	C2	C3	15.8(2)
C4	C5	N1	C9	-171.8(2)	Rh1	C1	C2	C7	-160.94(15)
C5	C6	C7	C2	2.4(3)	Rh1	C1	N2	C10	-4.8(2)

Table 7 Hydrogen Atom Coordinates (Å×10^4) and Isotropic Displacement Parameters (Å^2×10^3).

Atom	*x*	*y*	*z*	U(eq)
H3	6427.76	5708.93	7573.24	38
H4	8056.99	4036.01	6448.01	43
H6	6803.51	6081.04	2962.62	41
H7	5035.11	7672.2	4164.87	36
H8A	10350.14	3047.49	4838.95	79
H8B	10151.6	2143.13	3947.79	79
H8C	8689.74	2260.94	5448.35	79
H9A	7937.76	4074.66	2239.53	88
H9B	9872.75	3399.61	2011.54	88
H9C	9407.89	5006.45	1833.76	88
H10A	2607.98	10844.23	6100.36	37
H10B	3019.69	10123.15	7527.43	37
H11A	590.75	8941.9	8462.04	56
H11B	178.65	9662.98	7032.11	56
H12A	-245.29	11817.53	7519.53	93
H12B	172.43	11100.14	8944.9	93
H12C	-1522.92	10827.48	8821.52	93
H2	3438.75	8810.22	5485.88	33

Appendix E: Crystallographic data for complex **L2.**

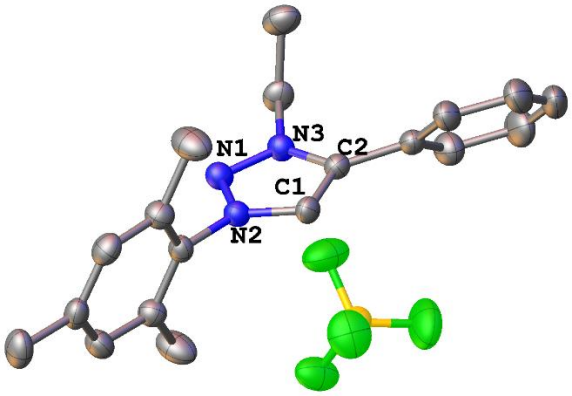

Table 1 Crystal data and structure refinement for 6

Empirical formula	$C_{19}H_{22}BF_4N_3$
Formula weight	379.20
Temperature/K	173.15
Crystal system	monoclinic
Space group	$P2_1/c$
a/Å	20.3243(6)
b/Å	7.0742(3)
c/Å	13.9627(5)
α/°	90
β/°	104.390(2)
γ/°	90
Volume/Å^3	1944.55(12)
Z	4
ρ_{calc}g/cm^3	1.295
μ/mm^{-1}	0.104
F(000)	792.0
Crystal size/mm^3	0.273 × 0.078 × 0.074
Radiation	MoKα (λ = 0.71073)
2Θ range for data collection/°	2.068 to 51.998
Index ranges	-24 ≤ h ≤ 25, -8 ≤ k ≤ 8, -17 ≤ l ≤ 17
Reflections collected	15193
Independent reflections	3823 [R_{int} = 0.0634, R_{sigma} = 0.0692]
Data/restraints/parameters	3823/0/248
Goodness-of-fit on F^2	1.009
Final R indexes [I>=2σ (I)]	R_1 = 0.0488, wR_2 = 0.0982
Final R indexes [all data]	R_1 = 0.1184, wR_2 = 0.1225
Largest diff. peak/hole / e Å^{-3}	0.17/-0.19

Table 2 Fractional Atomic Coordinates ($\times 10^4$) and Equivalent Isotropic Displacement Parameters ($Å^2 \times 10^3$). U_{eq} is defined as 1/3 of the trace of the orthogonalised U_{IJ} tensor.

Atom	*x*	*y*	*z*	U(eq)
B1	2254.5(15)	3377(4)	3712(2)	37.4(7)
F1	2521.4(8)	5126(2)	3598.3(13)	65.7(5)
F2	2110.8(9)	3302(2)	4638.5(12)	65.8(5)
F3	1674.3(8)	3083(3)	2993.8(14)	77.9(6)
F4	2719.0(8)	1969(2)	3669.4(12)	54.7(5)
C1	2482.5(11)	8657(3)	5053.1(16)	28.1(6)
C2	1923.7(10)	7724(3)	5193.1(16)	27.7(6)
C3	1206.7(11)	7926(4)	4645.5(17)	30.8(6)
C4	941.0(12)	9724(4)	4472.1(18)	38.7(7)
C5	281.6(13)	9975(5)	3921(2)	53.8(8)
C6	-109.8(14)	8446(6)	3553(2)	58.6(9)
C7	151.1(13)	6645(5)	3724(2)	56.1(9)
C8	810.0(12)	6377(4)	4265.0(19)	44.9(7)
C9	3713.6(11)	8637(3)	5986.0(17)	27.4(6)
C10	3850.1(11)	10364(3)	6458.5(18)	33.4(6)
C11	4520.2(12)	10989(4)	6657.1(18)	36.3(6)
C12	5027.1(11)	9953(4)	6401.3(17)	33.3(6)
C13	4856.2(11)	8228(4)	5943.5(18)	36.5(6)
C14	4197.7(11)	7511(3)	5719.3(18)	30.7(6)
C15	3303.9(13)	11511(4)	6753(2)	54.1(8)
C17	4027.0(13)	5635(4)	5222(2)	50.7(8)
C18	1796.0(12)	5354(4)	6524.1(18)	34.4(6)

C19	1456.1(13)	6536(4)	7156.3(19)	47.0(7)
N1	3014.3(8)	7996(3)	5763.6(14)	27.0(5)
N2	2831.9(9)	6719(3)	6337.3(14)	28.7(5)
N3	2167.3(9)	6562(3)	5977.9(14)	27.6(5)
C16	5746.5(12)	10693(4)	6635(2)	47.1(7)

Table 3 Anisotropic Displacement Parameters ($Å^2×10^3$). The Anisotropic displacement factor exponent takes the form: $-2\pi^2[h^2a^{*2}U_{11}+2hka^*b^*U_{12}+\ldots]$.

Atom	U_{11}	U_{22}	U_{33}	U_{23}	U_{13}	U_{12}
B1	48.1(19)	28.9(18)	34.9(18)	-1.1(14)	10.1(14)	3.5(16)
F1	74.1(12)	36.0(10)	84.2(13)	5.5(9)	14.1(10)	-3.3(8)
F2	91.7(13)	62.1(12)	51.7(11)	-0.3(9)	33.0(9)	17.0(10)
F3	61.9(11)	83.8(15)	70.5(13)	-25.0(11)	-16.4(9)	3.3(10)
F4	65.8(10)	42.6(10)	64.2(11)	13.5(9)	32.2(8)	17.5(9)
C1	27.4(12)	32.3(14)	23.5(13)	5.1(11)	4.6(10)	3.8(11)
C2	27.1(13)	32.3(14)	23.8(13)	0.8(11)	6.6(10)	1.6(11)
C3	25.5(12)	43.7(16)	23.8(13)	0.2(12)	7.4(10)	1.2(12)
C4	32.6(14)	49.6(18)	33.5(15)	6.3(13)	7.2(11)	9.4(13)
C5	38.5(17)	76(2)	44.7(18)	11.1(17)	6.9(14)	20.3(17)
C6	28.9(15)	109(3)	35.1(17)	4.5(19)	2.7(12)	9.0(19)
C7	30.7(16)	83(3)	50.1(19)	-10.2(18)	1.5(13)	-11.6(16)
C8	35.0(15)	54.4(19)	43.5(17)	-6.3(14)	6.4(12)	-1.3(14)
C9	23.4(12)	32.2(14)	26.2(13)	2.9(11)	5.1(10)	-1.7(11)
C10	33.2(14)	33.2(15)	34.1(15)	-0.6(12)	9.1(11)	2.0(12)
C11	40.3(15)	36.1(15)	30.1(15)	-3.8(12)	4.4(11)	-6.6(13)
C12	29.1(13)	41.9(17)	26.1(14)	5.2(12)	1.7(10)	-3.3(12)
C13	27.0(13)	44.6(17)	38.8(15)	3.0(13)	9.9(11)	3.6(12)
C14	30.3(13)	31.0(15)	31.4(14)	0.5(11)	8.9(11)	0.2(12)

C15	47.1(17)	51.0(19)	67(2)	-22.2(17)	18.6(15)	-1.2(15)
C17	41.9(16)	39.5(17)	74(2)	-16.0(16)	21.5(15)	-0.4(14)
C18	35.2(14)	36.2(15)	33.2(14)	7.2(12)	11.1(11)	-8.8(12)
C19	49.8(17)	57(2)	39.3(16)	-3.3(15)	21.1(13)	-11.5(15)
N1	25.3(10)	28.8(12)	27.6(11)	1.1(9)	7.8(8)	0.1(9)
N2	27.5(11)	28.2(12)	31.2(11)	2.7(10)	8.6(9)	0.5(9)
N3	25.1(11)	28.4(12)	29.6(11)	1.3(9)	7.7(8)	-2.0(9)
C16	33.3(14)	58.4(19)	44.0(17)	4.5(15)	-1.2(12)	-9.7(14)

Table 4 Bond Lengths.

Atom	Atom	Length/Å	Atom	Atom	Length/Å
B1	F1	1.376(3)	C9	C10	1.383(3)
B1	F2	1.396(3)	C9	C14	1.387(3)
B1	F3	1.361(3)	C9	N1	1.450(3)
B1	F4	1.384(3)	C10	C11	1.393(3)
C1	C2	1.369(3)	C10	C15	1.512(3)
C1	N1	1.356(3)	C11	C12	1.382(3)
C2	C3	1.475(3)	C12	C13	1.381(3)
C2	N3	1.361(3)	C12	C16	1.510(3)
C3	C4	1.379(3)	C13	C14	1.392(3)
C3	C8	1.386(3)	C14	C17	1.498(3)
C4	C5	1.381(3)	C18	C19	1.503(3)
C5	C6	1.365(4)	C18	N3	1.472(3)
C6	C7	1.377(4)	N1	N2	1.320(2)
C7	C8	1.377(4)	N2	N3	1.323(2)

Table 5 Bond Angles.

Atom	Atom	Atom	Angle/˚	Atom	Atom	Atom	Angle/˚
F1	B1	F2	108.7(2)	C14	C9	N1	119.1(2)
F1	B1	F4	110.4(2)	C9	C10	C11	116.5(2)
F3	B1	F1	110.2(2)	C9	C10	C15	122.0(2)
F3	B1	F2	109.6(2)	C11	C10	C15	121.5(2)
F3	B1	F4	109.5(2)	C12	C11	C10	122.3(2)
F4	B1	F2	108.4(2)	C11	C12	C16	120.3(2)
N1	C1	C2	105.6(2)	C13	C12	C11	118.1(2)
C1	C2	C3	128.8(2)	C13	C12	C16	121.6(2)
N3	C2	C1	104.92(19)	C12	C13	C14	122.9(2)
N3	C2	C3	126.2(2)	C9	C14	C13	115.9(2)
C4	C3	C2	118.3(2)	C9	C14	C17	122.4(2)
C4	C3	C8	119.8(2)	C13	C14	C17	121.7(2)
C8	C3	C2	121.9(2)	N3	C18	C19	110.6(2)
C3	C4	C5	120.0(3)	C1	N1	C9	127.59(19)
C6	C5	C4	120.1(3)	N2	N1	C1	112.75(17)
C5	C6	C7	120.3(3)	N2	N1	C9	119.47(18)
C8	C7	C6	120.2(3)	N1	N2	N3	103.98(17)
C7	C8	C3	119.7(3)	C2	N3	C18	129.57(19)
C10	C9	C14	124.3(2)	N2	N3	C2	112.78(17)
C10	C9	N1	116.6(2)	N2	N3	C18	117.30(18)

Table 6 Torsion Angles.

A	B	C	D	Angle/˚	A	B	C	D	Angle/˚
C1	C2	C3	C4	-47.4(3)	C10	C11	C12	C13	-0.8(4)
C1	C2	C3	C8	129.4(3)	C10	C11	C12	C16	-179.9(2)
C1	C2	N3	C18	173.5(2)	C11	C12	C13	C14	0.9(4)

C1	C2	N3	N2	0.6(3)	C12	C13	C14	C9	-0.1(4)
C1	N1	N2	N3	0.2(2)	C12	C13	C14	C17	-180.0(2)
C2	C1	N1	C9	-174.8(2)	C14	C9	C10	C11	1.0(4)
C2	C1	N1	N2	0.1(3)	C14	C9	C10	C15	-178.6(2)
C2	C3	C4	C5	176.9(2)	C14	C9	N1	C1	-106.3(3)
C2	C3	C8	C7	-177.4(2)	C14	C9	N1	N2	79.1(3)
C3	C2	N3	C18	-5.3(4)	C15	C10	C11	C12	179.5(2)
C3	C2	N3	N2	-178.2(2)	C19	C18	N3	C2	-72.7(3)
C3	C4	C5	C6	0.4(4)	C19	C18	N3	N2	100.0(2)
C4	C3	C8	C7	-0.6(4)	N1	C1	C2	C3	178.3(2)
C4	C5	C6	C7	-0.3(4)	N1	C1	C2	N3	-0.4(2)
C5	C6	C7	C8	-0.3(4)	N1	C9	C10	C11	-179.0(2)
C6	C7	C8	C3	0.7(4)	N1	C9	C10	C15	1.4(3)
C8	C3	C4	C5	0.0(4)	N1	C9	C14	C13	179.1(2)
C9	C10	C11	C12	-0.1(4)	N1	C9	C14	C17	-1.0(3)
C9	N1	N2	N3	175.60(19)	N1	N2	N3	C2	-0.5(2)
C10	C9	C14	C13	-0.9(4)	N1	N2	N3	C18	-174.36(18)
C10	C9	C14	C17	179.0(2)	N3	C2	C3	C4	131.1(3)
C10	C9	N1	C1	73.6(3)	N3	C2	C3	C8	-52.1(3)
C10	C9	N1	N2	-101.0(2)	C16	C12	C13	C14	180.0(2)

Table 7 Hydrogen Atom Coordinates (Å×10^4) and Isotropic Displacement Parameters (Å^2×10^3).

Atom	***x***	***y***	***z***	**U(eq)**
H1	2494.98	9574.44	4561.16	34
H4	1211.63	10788.76	4731.41	46
H5	99.92	11213.68	3798.43	65
H6	-563.97	8623.95	3177.55	70
H7	-124.13	5586	3468.91	67

H8	991.69	5136.07	4376.53	54
H11	4632.82	12170.56	6979.83	44
H13	5203.33	7499.46	5774.04	44
H15A	3002.91	12067.51	6160.99	81
H15B	3515.24	12520.9	7206.04	81
H15C	3039.64	10688.66	7081.44	81
H17A	3864.08	4775.89	5664.08	76
H17B	4433.48	5098.97	5068.6	76
H17C	3671.79	5801.34	4609.52	76
H18A	2115.86	4460.37	6947	41
H18B	1449.59	4607.95	6050.5	41
H19A	1799.04	7280.6	7621.57	70
H19B	1219.8	5709.15	7524.97	70
H19C	1127.71	7388.38	6734.71	70
H16A	5958.12	10517.83	7341	71
H16B	5741.5	12040.52	6471.93	71
H16C	6006.57	9999.07	6245.01	71

Appendix F: Crystallographic data for complex **5.**

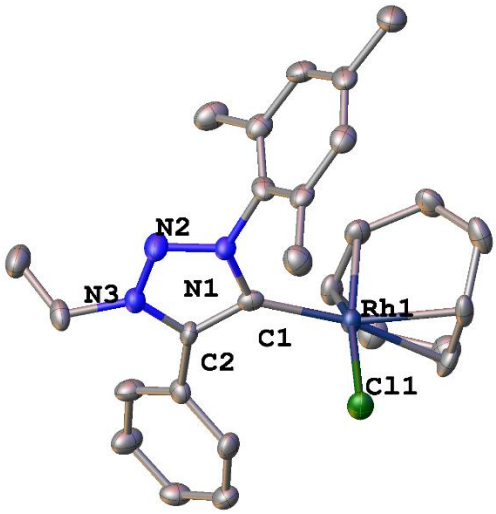

Table 1 Crystal data and structure refinement.

Empirical formula	$C_{27}H_{33}ClN_3Rh$
Formula weight	537.92
Temperature/K	173.15
Crystal system	monoclinic
Space group	$P2_1/c$
a/Å	7.8416(7)
b/Å	15.8217(13)
c/Å	19.8844(18)
α/°	90
β/°	94.644(3)
γ/°	90
Volume/Å^3	2458.9(4)
Z	4
ρ_{calc}g/cm^3	1.453
μ/mm^{-1}	0.823
F(000)	1112.0
Crystal size/mm^3	0.197 × 0.038 × 0.033
Radiation	MoKα (λ = 0.71073)
2Θ range for data collection/°	3.294 to 52
Index ranges	-9 ≤ h ≤ 9, -19 ≤ k ≤ 19, -24 ≤ l ≤ 24
Reflections collected	23085
Independent reflections	4841 [R_{int} = 0.1029, R_{sigma} = 0.0916]
Data/restraints/parameters	4841/0/293
Goodness-of-fit on F^2	1.006
Final R indexes [I>=2σ (I)]	R_1 = 0.0464, wR_2 = 0.0859
Final R indexes [all data]	R_1 = 0.0887, wR_2 = 0.0997

Largest diff. peak/hole / e Å^{-3}	0.54/-0.57

Table 2 Fractional Atomic Coordinates (×10^4) and Equivalent Isotropic Displacement Parameters (Å^2×10^3). U_{eq} is defined as 1/3 of the trace of the orthogonalised U_{IJ} tensor.

Atom	*x*	*y*	*z*	U(eq)
C1	5409(6)	7119(3)	3851(2)	21.0(10)
C2	6556(6)	6543(3)	4170(2)	20.1(10)
C3	6644(6)	5616(3)	4055(2)	21.8(10)
C4	6434(6)	5310(3)	3392(2)	25.8(11)
C5	6349(6)	4448(3)	3273(2)	30.5(12)
C6	6446(6)	3887(3)	3806(2)	30.6(12)
C7	6684(7)	4186(3)	4461(2)	36.1(13)
C8	6779(6)	5046(3)	4579(2)	30.3(12)
C9	4913(6)	8642(3)	4191(2)	25.1(11)
C10	3792(6)	8777(3)	4681(2)	28.0(12)
C11	2780(6)	9509(3)	4621(2)	32.5(13)
C12	2916(6)	10082(3)	4098(2)	31.2(12)
C13	4132(6)	9945(3)	3655(2)	30.3(12)
C14	5198(6)	9231(3)	3684(2)	25.5(11)
C15	3640(7)	8197(3)	5273(2)	37.1(13)
C16	1748(7)	10841(3)	4033(3)	41.6(14)
C17	6595(6)	9118(3)	3221(2)	36.1(13)
C18	9002(6)	6678(3)	5118(2)	30.0(12)
C19	8565(7)	6640(3)	5845(2)	42.4(14)
C20	1601(6)	7091(3)	3723(2)	28.2(11)
C21	2151(6)	6246(3)	3697(2)	28.3(12)
C22	1208(7)	5537(3)	3308(2)	34.5(13)
C23	512(6)	5807(3)	2599(2)	36.0(13)
C24	1698(6)	6434(3)	2293(2)	29.8(12)
C25	1514(6)	7300(3)	2319(2)	27.5(12)
C26	209(6)	7786(3)	2675(3)	37.7(13)
C27	-40(6)	7437(3)	3385(2)	35.3(13)
Cl1	5625.2(15)	7156.7(7)	2260.3(6)	28.5(3)
N1	5849(5)	7844(2)	4209.8(18)	20.7(9)
N2	7123(5)	7767(2)	4695.4(19)	28.9(10)
N3	7549(4)	6957(2)	4658.9(17)	23.2(8)
Rh1	3583.0(5)	6967.5(2)	3078.3(2)	20.84(12)

Table 3 Anisotropic Displacement Parameters (Å^2×10^3). The Anisotropic displacement factor exponent takes the form: $-2\pi^2[h^2a^{*2}U_{11}+2hka^*b^*U_{12}+\ldots]$.

Atom	U_{11}	U_{22}	U_{33}	U_{23}	U_{13}	U_{12}
C1	25(3)	19(3)	20(2)	-1(2)	8(2)	-2(2)
C2	20(3)	23(2)	16(2)	0.3(19)	-4(2)	-1(2)
C3	17(3)	23(3)	25(3)	0(2)	-2(2)	0(2)
C4	31(3)	29(3)	17(2)	4(2)	-1(2)	1(2)
C5	34(3)	31(3)	27(3)	-8(2)	-1(2)	3(2)
C6	38(3)	21(3)	34(3)	-3(2)	9(2)	3(2)
C7	56(4)	27(3)	26(3)	1(2)	6(3)	4(3)
C8	42(3)	23(3)	27(3)	-5(2)	7(2)	3(2)
C9	30(3)	14(2)	30(3)	-3(2)	-5(2)	2(2)
C10	37(3)	22(3)	25(3)	-1(2)	1(2)	-3(2)
C11	39(3)	30(3)	29(3)	-11(2)	5(2)	3(2)
C12	38(3)	22(3)	32(3)	-10(2)	-7(2)	5(2)
C13	40(3)	21(3)	29(3)	1(2)	-2(2)	-2(2)
C14	35(3)	18(2)	23(3)	-4(2)	-3(2)	-2(2)
C15	53(4)	31(3)	29(3)	0(2)	11(3)	-5(3)
C16	48(4)	37(3)	39(3)	-8(3)	-2(3)	13(3)
C17	37(3)	35(3)	37(3)	6(2)	3(3)	3(2)
C18	26(3)	26(3)	35(3)	3(2)	-12(2)	0(2)
C19	55(4)	40(3)	30(3)	0(2)	-12(3)	6(3)
C20	29(3)	35(3)	21(2)	2(2)	6(2)	0(2)
C21	26(3)	38(3)	21(3)	10(2)	1(2)	-1(2)
C22	37(3)	32(3)	35(3)	4(2)	3(2)	-8(2)
C23	33(3)	38(3)	36(3)	-4(3)	1(2)	-6(2)
C24	27(3)	44(3)	18(3)	-3(2)	-5(2)	-9(2)
C25	20(3)	43(3)	19(3)	12(2)	-2(2)	0(2)
C26	22(3)	46(3)	45(3)	16(3)	-3(2)	4(2)
C27	24(3)	45(3)	37(3)	4(3)	8(2)	7(2)
Cl1	24.2(7)	35.9(7)	25.9(6)	2.9(5)	5.5(5)	-1.6(5)
N1	25(2)	16(2)	19.9(19)	0.8(16)	-1.8(17)	0.2(17)
N2	37(3)	20(2)	29(2)	-0.8(18)	-8(2)	-0.1(18)
N3	23(2)	24(2)	21.8(19)	1.6(18)	-2.1(16)	1.5(19)
Rh1	19.5(2)	24.1(2)	18.68(18)	2.86(18)	-0.08(13)	-0.23(19)

Table 4 Bond Lengths for.

Atom	Atom	Length/Å	Atom	Atom	Length/Å
C1	C2	1.396(6)	C13	C14	1.403(6)
C1	N1	1.380(5)	C14	C17	1.497(6)
C1	Rh1	2.029(4)	C18	C19	1.514(6)
C2	C3	1.487(6)	C18	N3	1.469(5)
C2	N3	1.363(5)	C20	C21	1.407(6)

C3	C4	1.403(6)	C20	C27	1.506(6)
C3	C8	1.375(6)	C20	Rh1	2.102(5)
C4	C5	1.384(6)	C21	C22	1.520(6)
C5	C6	1.379(6)	C21	Rh1	2.074(4)
C6	C7	1.385(6)	C22	C23	1.531(6)
C7	C8	1.381(6)	C23	C24	1.519(6)
C9	C10	1.381(6)	C24	C25	1.379(6)
C9	C14	1.404(6)	C24	Rh1	2.228(4)
C9	N1	1.459(5)	C25	C26	1.503(7)
C10	C11	1.403(6)	C25	Rh1	2.189(4)
C10	C15	1.505(6)	C26	C27	1.542(6)
C11	C12	1.390(6)	Cl1	Rh1	2.3919(12)
C12	C13	1.367(6)	N1	N2	1.338(5)
C12	C16	1.510(6)	N2	N3	1.328(5)

Table 5 Bond Angles.

Atom	Atom	Atom	Angle/˚	Atom	Atom	Atom	Angle/˚
C2	C1	Rh1	131.0(3)	C22	C21	Rh1	111.6(3)
N1	C1	C2	100.6(4)	C21	C22	C23	112.6(4)
N1	C1	Rh1	128.4(3)	C24	C23	C22	111.5(4)
C1	C2	C3	127.7(4)	C23	C24	Rh1	111.0(3)
N3	C2	C1	108.6(4)	C25	C24	C23	124.3(5)
N3	C2	C3	123.5(4)	C25	C24	Rh1	70.3(3)
C4	C3	C2	118.8(4)	C24	C25	C26	127.2(5)
C8	C3	C2	122.1(4)	C24	C25	Rh1	73.4(3)
C8	C3	C4	118.8(4)	C26	C25	Rh1	107.0(3)
C5	C4	C3	120.0(4)	C25	C26	C27	112.9(4)
C6	C5	C4	120.3(4)	C20	C27	C26	111.8(4)
C5	C6	C7	119.8(4)	C1	N1	C9	127.0(4)
C8	C7	C6	119.9(5)	N2	N1	C1	116.0(3)
C3	C8	C7	121.1(4)	N2	N1	C9	116.3(3)
C10	C9	C14	123.4(4)	N3	N2	N1	103.0(3)
C10	C9	N1	117.7(4)	C2	N3	C18	131.9(4)
C14	C9	N1	118.9(4)	N2	N3	C2	111.8(4)
C9	C10	C11	117.1(4)	N2	N3	C18	116.2(4)
C9	C10	C15	123.5(4)	C1	Rh1	C20	92.20(18)
C11	C10	C15	119.3(4)	C1	Rh1	C21	89.91(17)
C12	C11	C10	121.6(5)	C1	Rh1	C24	164.52(17)
C11	C12	C16	120.0(5)	C1	Rh1	C25	158.84(18)
C13	C12	C11	118.5(4)	C1	Rh1	Cl1	91.72(12)
C13	C12	C16	121.5(5)	C20	Rh1	C24	88.94(18)

C12	C13	C14	123.1(5)	C20	Rh1	C25	81.65(18)
C9	C14	C17	122.0(4)	C20	Rh1	Cl1	166.32(13)
C13	C14	C9	115.8(4)	C21	Rh1	C20	39.38(17)
C13	C14	C17	122.2(4)	C21	Rh1	C24	81.21(18)
N3	C18	C19	112.4(4)	C21	Rh1	C25	97.74(18)
C21	C20	C27	125.7(4)	C21	Rh1	Cl1	153.74(14)
C21	C20	Rh1	69.2(3)	C24	Rh1	Cl1	90.77(13)
C27	C20	Rh1	114.2(3)	C25	Rh1	C24	36.38(17)
C20	C21	C22	125.6(4)	C25	Rh1	Cl1	90.04(13)
C20	C21	Rh1	71.4(3)				

Table 6 Torsion Angles.

A	B	C	D	Angle/˚	A	B	C	D	Angle/˚
C1	C2	C3	C4	41.7(7)	C16	C12	C13	C14	-177.6(4)
C1	C2	C3	C8	-132.7(5)	C19	C18	N3	C2	-111.0(5)
C1	C2	N3	C18	-176.2(4)	C19	C18	N3	N2	71.7(5)
C1	C2	N3	N2	1.1(5)	C20	C21	C22	C23	43.6(7)
C1	N1	N2	N3	0.0(5)	C21	C20	C27	C26	-92.2(6)
C2	C1	N1	C9	-168.8(4)	C21	C22	C23	C24	34.6(6)
C2	C1	N1	N2	0.6(5)	C22	C23	C24	C25	-94.9(6)
C2	C3	C4	C5	-173.9(4)	C22	C23	C24	Rh1	-15.1(5)
C2	C3	C8	C7	173.3(5)	C23	C24	C25	C26	3.5(8)
C3	C2	N3	C18	8.1(7)	C23	C24	C25	Rh1	102.5(4)
C3	C2	N3	N2	-174.6(4)	C24	C25	C26	C27	43.2(7)
C3	C4	C5	C6	0.9(7)	C25	C26	C27	C20	33.8(6)
C4	C3	C8	C7	-1.0(7)	C27	C20	C21	C22	1.8(7)
C4	C5	C6	C7	-2.0(8)	C27	C20	C21	Rh1	105.5(5)
C5	C6	C7	C8	1.6(8)	N1	C1	C2	C3	174.4(4)
C6	C7	C8	C3	-0.1(8)	N1	C1	C2	N3	-1.0(5)
C8	C3	C4	C5	0.6(7)	N1	C9	C10	C11	-174.1(4)
C9	C10	C11	C12	-1.0(7)	N1	C9	C10	C15	7.4(7)
C9	N1	N2	N3	170.6(4)	N1	C9	C14	C13	173.8(4)
C10	C9	C14	C13	-6.5(7)	N1	C9	C14	C17	-8.4(7)
C10	C9	C14	C17	171.2(4)	N1	N2	N3	C2	-0.7(5)
C10	C9	N1	C1	95.4(5)	N1	N2	N3	C18	177.1(4)
C10	C9	N1	N2	-74.0(5)	N3	C2	C3	C4	-143.5(4)
C10	C11	C12	C13	-3.5(7)	N3	C2	C3	C8	42.1(7)
C10	C11	C12	C16	177.2(4)	Rh1	C1	C2	C3	-5.5(7)
C11	C12	C13	C14	3.1(7)	Rh1	C1	C2	N3	179.1(3)
C12	C13	C14	C9	1.7(7)	Rh1	C1	N1	C9	11.1(6)
C12	C13	C14	C17	-176.1(4)	Rh1	C1	N1	N2	-179.5(3)

C14	C9	C10	C11	6.2(7)	Rh1	C20	C21	C22	-103.7(4)
C14	C9	C10	C15	-172.3(4)	Rh1	C20	C27	C26	-11.2(5)
C14	C9	N1	C1	-84.9(6)	Rh1	C21	C22	C23	-38.4(5)
C14	C9	N1	N2	105.7(5)	Rh1	C24	C25	C26	-99.0(5)
C15	C10	C11	C12	177.6(4)	Rh1	C25	C26	C27	-38.5(5)

Table 7 Hydrogen Atom Coordinates (Å×10^4) and Isotropic Displacement Parameters (Å^2×10^3).

Atom	*x*	*y*	*z*	U(eq)
H4	6349.5	5693.9	3023.16	31
H5	6222.39	4242.36	2823.4	37
H6	6350.71	3297.05	3723.12	37
H7	6781.51	3801.21	4828.7	43
H8	6940.37	5247.38	5029.89	36
H11	1982.67	9616	4945.88	39
H13	4262.45	10351.26	3311.5	36
H15A	3800.9	7611.11	5132.31	56
H15B	2503.45	8259.87	5438.98	56
H15C	4516.83	8343.45	5633.69	56
H16A	1744.69	11124.76	4471.32	62
H16B	584.16	10657.71	3885.13	62
H16C	2156.56	11234.76	3700.98	62
H17A	7706.58	9130.66	3484.45	54
H17B	6540.91	9576.78	2888.84	54
H17C	6450.68	8574.46	2988.08	54
H18A	9971.18	7072.03	5082.24	36
H18B	9372.23	6110.8	4977.33	36
H19A	7574.27	6269.43	5879.89	64
H19B	8292.56	7208.92	5998.78	64
H19C	9545.01	6416.49	6127.18	64
H20	1966.9	7378.95	4158.76	34
H21	2811.25	6052.64	4120.76	34
H22A	245.74	5344.43	3562.42	41
H22B	1996.94	5053.56	3271.74	41
H23A	375.55	5302.49	2305.51	43
H23B	-628.92	6068.6	2621.57	43
H24	2212.44	6223.43	1880.17	36
H25	1913.15	7600.36	1918.25	33
H26A	-899.54	7768.58	2399.86	45
H26B	572.36	8384.67	2715.48	45
H27A	-467.73	7894.89	3666.69	42
H27B	-912.48	6983.98	3348.33	42

Appendix G: Crystallographic data for complex **S2.**

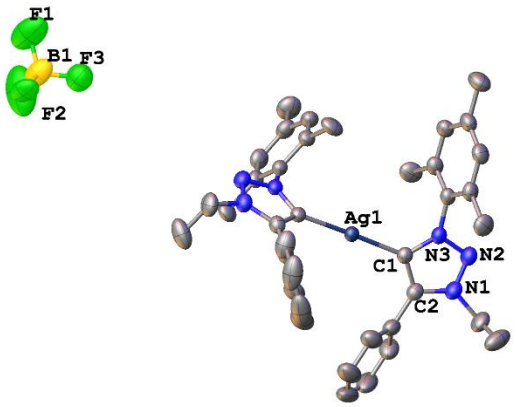

Table 1 Crystal data and structure refinement.

Empirical formula	$C_{40}H_{46}AgBCl_4F_4N_6$
Formula weight	947.31
Temperature/K	173(2)
Crystal system	monoclinic
Space group	C2/c
a/Å	17.6372(4)
b/Å	15.8542(4)
c/Å	15.9115(3)
α/°	90
β/°	91.4780(10)
γ/°	90
Volume/Å^3	4447.75(17)
Z	4
ρ_{calc}g/cm^3	1.415
μ/mm^{-1}	0.746
F(000)	1936.0
Crystal size/mm^3	0.437 × 0.261 × 0.212
Radiation	MoKα (λ = 0.71073)
2Θ range for data collection/°	3.454 to 56.822
Index ranges	-23 ≤ h ≤ 23, -21 ≤ k ≤ 21, -21 ≤ l ≤ 20
Reflections collected	29630
Independent reflections	5572 [R_{int} = 0.0387, R_{sigma} = 0.0283]
Data/restraints/parameters	5572/51/271
Goodness-of-fit on F^2	1.041
Final R indexes [I>=2σ (I)]	R_1 = 0.0471, wR_2 = 0.1326
Final R indexes [all data]	R_1 = 0.0557, wR_2 = 0.1390

Largest diff. peak/hole / e Å^{-3}	0.99/-0.83

Table 2 Fractional Atomic Coordinates (×10^4) and Equivalent Isotropic Displacement Parameters (Å^2×10^3). U_{eq} is defined as 1/3 of the trace of the orthogonalised U_{IJ} tensor.

Atom	*x*	*y*	*z*	U(eq)
Ag1	10000	6050.6(2)	2500	31.42(11)
C1	8883.0(16)	6072.0(16)	2880.9(17)	33.4(5)
C2	8305.3(16)	6636.1(19)	2690.4(18)	38.3(6)
C3	8321.4(19)	7422(2)	2193(2)	46.0(7)
C4	7808(2)	7570(3)	1540(3)	67.1(11)
C5	7832(3)	8323(4)	1091(3)	89.2(18)
C6	8370(4)	8913(3)	1288(4)	92(2)
C7	8894(4)	8766(3)	1931(3)	80.2(15)
C8	8871(3)	8016(2)	2390(3)	59.5(9)
C9	6931.5(19)	6760(3)	3185(2)	56.7(9)
C10	6939(3)	7335(3)	3921(3)	78.3(14)
C11	8848.1(16)	4789.5(17)	3833.1(17)	34.8(6)
C12	9026.3(19)	4059.5(18)	3402(2)	40.4(6)
C13	9308.8(18)	3381.7(19)	3865(2)	45.1(7)
C14	9397.8(19)	3423(2)	4737(2)	48.9(7)
C15	9219(2)	4165(2)	5142(2)	48.7(7)
C16	8942.3(18)	4866(2)	4701.9(18)	40.9(6)
C17	8757(2)	5673(2)	5156(2)	54.3(8)
C18	8907(3)	3996(2)	2463(2)	55.8(9)
C19	9698(3)	2673(3)	5223(3)	70.5(11)
N1	7675.6(14)	6354.9(18)	3092.5(17)	42.1(5)
N2	7799.6(14)	5659.2(17)	3517.4(17)	41.9(6)
N3	8530.1(13)	5499.5(14)	3382.8(14)	34.5(5)
C20	6144(6)	4937(6)	5972(5)	154(3)
Cl1	6022(3)	5804(2)	5379(2)	246(2)
Cl2	7087.9(15)	4701.2(19)	6156.5(16)	166.0(10)
B1	5091(2)	6246(3)	2434(3)	86(3)
F1	4640(3)	6986(3)	2418(6)	153(3)
F2	4650(3)	5552(2)	2142(3)	87.2(18)
F3	5720(2)	6357(3)	1908(4)	93.2(17)
F4	5354(4)	6087(5)	3269(3)	189(5)

Table 3 Anisotropic Displacement Parameters (Å^2×10^3). The Anisotropic displacement factor exponent takes the form: $-2\pi^2[h^2a^{*2}U_{11}+2hka^*b^*U_{12}+\ldots]$.

Atom	U_{11}	U_{22}	U_{33}	U_{23}	U_{13}	U_{12}
Ag1	32.50(17)	30.22(16)	31.72(16)	0	4.38(10)	0

C1	34.2(13)	33.3(12)	32.8(13)	-3.5(10)	1.9(10)	-2.2(10)
C2	35.5(14)	43.2(15)	36.1(14)	-3.1(11)	0.9(11)	2.8(11)
C3	50.4(17)	43.8(16)	44.2(16)	3.4(13)	10.0(13)	13.6(13)
C4	52(2)	88(3)	61(2)	26(2)	6.2(17)	20(2)
C5	79(3)	111(4)	80(3)	47(3)	26(2)	52(3)
C6	131(5)	61(3)	87(4)	35(2)	52(4)	50(3)
C7	123(4)	37.5(18)	82(3)	2.2(19)	31(3)	5(2)
C8	84(3)	37.9(16)	57(2)	-2.0(15)	11.0(19)	5.3(17)
C9	36.0(16)	71(2)	63(2)	4.1(18)	7.3(14)	13.5(15)
C10	84(3)	94(3)	57(2)	-6(2)	5(2)	46(3)
C11	37.5(14)	33.6(12)	33.6(13)	-2.1(10)	5.9(11)	-4.5(10)
C12	46.1(16)	38.3(15)	37.3(15)	-6.2(11)	6.4(12)	-6.3(12)
C13	49.5(17)	33.8(14)	52.5(18)	0.6(13)	10.8(14)	-3.2(12)
C14	47.3(17)	47.2(17)	52.4(18)	11.6(14)	9.1(14)	-4.1(14)
C15	55.5(19)	56.9(18)	33.9(15)	5.9(13)	6.1(13)	-3.0(15)
C16	44.8(16)	46.5(16)	31.9(13)	-5.0(12)	8.0(12)	-4.6(12)
C17	69(2)	57(2)	36.8(16)	-14.4(15)	7.5(15)	2.2(17)
C18	83(3)	44.4(18)	39.7(17)	-12.9(13)	-1.1(17)	-0.2(16)
C19	79(3)	58(2)	75(3)	26(2)	6(2)	4(2)
N1	33.0(12)	48.2(14)	45.1(14)	-1.1(11)	2.3(10)	3.3(10)
N2	34.0(12)	45.1(14)	46.8(14)	-2.5(11)	3.8(10)	-2.7(10)
N3	33.3(11)	35.6(11)	34.7(11)	-4.4(9)	3.9(9)	-2.7(9)
C20	176(9)	153(7)	135(7)	18(6)	49(6)	58(6)
Cl1	395(6)	155(2)	191(3)	54(2)	59(3)	141(3)
Cl2	144.1(19)	200(3)	154(2)	61.2(18)	3.7(15)	-26.4(17)
B1	48(5)	86(5)	123(6)	-53(5)	-7(4)	-17(4)
F1	102(4)	91(4)	266(10)	-80(5)	17(6)	-26(3)
F2	76(3)	44(2)	142(5)	-32(3)	3(3)	-12(2)
F3	83(4)	84(3)	113(4)	-16(3)	5(3)	-15(3)
F4	124(7)	295(13)	146(7)	6(6)	-11(5)	-100(7)

Table 4 Bond Lengths

Atom	Atom	Length/Å	Atom	Atom	Length/Å
Ag1	C1[1]	2.076(3)	C11	N3	1.440(4)
Ag1	C1	2.076(3)	C12	C13	1.388(4)
C1	N3	1.369(3)	C12	C18	1.507(5)
C1	C2	1.384(4)	C13	C14	1.393(5)
C2	N1	1.370(4)	C14	C15	1.383(5)
C2	C3	1.477(4)	C14	C19	1.507(5)
C3	C8	1.380(5)	C15	C16	1.394(5)
C3	C4	1.380(5)	C16	C17	1.511(4)

C4	C5	1.393(6)	N1	N2	1.309(4)
C5	C6	1.363(9)	N2	N3	1.336(3)
C6	C7	1.381(9)	C20	Cl1	1.679(9)
C7	C8	1.397(5)	C20	Cl2	1.723(9)
C9	N1	1.472(4)	B1	F1	1.4179
C9	C10	1.482(6)	B1	F3	1.4180
C11	C12	1.386(4)	B1	F2	1.4181
C11	C16	1.393(4)	B1	F4	1.4185

[1]2-X,+Y,1/2-Z

Table 5 Bond Angles

Atom	Atom	Atom	Angle/˚	Atom	Atom	Atom	Angle/˚
C1[1]	Ag1	C1	178.13(14)	C12	C13	C14	121.5(3)
N3	C1	C2	102.3(2)	C15	C14	C13	118.8(3)
N3	C1	Ag1	127.5(2)	C15	C14	C19	120.9(3)
C2	C1	Ag1	130.2(2)	C13	C14	C19	120.2(3)
N1	C2	C1	106.8(3)	C14	C15	C16	121.7(3)
N1	C2	C3	123.5(3)	C11	C16	C15	117.4(3)
C1	C2	C3	129.7(3)	C11	C16	C17	121.7(3)
C8	C3	C4	119.9(4)	C15	C16	C17	120.8(3)
C8	C3	C2	118.5(3)	N2	N1	C2	112.9(2)
C4	C3	C2	121.6(3)	N2	N1	C9	117.0(3)
C3	C4	C5	120.2(5)	C2	N1	C9	129.8(3)
C6	C5	C4	120.0(5)	N1	N2	N3	103.1(2)
C5	C6	C7	120.2(4)	N2	N3	C1	115.0(2)
C6	C7	C8	120.2(5)	N2	N3	C11	115.7(2)
C3	C8	C7	119.4(4)	C1	N3	C11	129.1(2)
N1	C9	C10	111.0(3)	Cl1	C20	Cl2	112.5(6)
C12	C11	C16	122.7(3)	F1	B1	F3	109.5
C12	C11	N3	119.8(3)	F1	B1	F2	109.5
C16	C11	N3	117.4(2)	F3	B1	F2	109.5
C11	C12	C13	117.8(3)	F1	B1	F4	109.5
C11	C12	C18	121.3(3)	F3	B1	F4	109.5
C13	C12	C18	120.9(3)	F2	B1	F4	109.5

[1]2-X,+Y,1/2-Z

Table 6 Torsion Angles

A	B	C	D	Angle/˚	A	B	C	D	Angle/˚
N3	C1	C2	N1	0.3(3)	C19	C14	C15	C16	179.8(3)
Ag1	C1	C2	N1	179.0(2)	C12	C11	C16	C15	-0.9(5)
N3	C1	C2	C3	177.5(3)	N3	C11	C16	C15	177.2(3)

Ag1	C1	C2	C3	-3.8(5)	C12	C11	C16	C17	178.9(3)
N1	C2	C3	C8	125.5(3)	N3	C11	C16	C17	-3.0(4)
C1	C2	C3	C8	-51.3(5)	C14	C15	C16	C11	0.3(5)
N1	C2	C3	C4	-55.1(5)	C14	C15	C16	C17	-179.5(3)
C1	C2	C3	C4	128.1(4)	C1	C2	N1	N2	-0.4(4)
C8	C3	C4	C5	-1.4(6)	C3	C2	N1	N2	-177.9(3)
C2	C3	C4	C5	179.1(4)	C1	C2	N1	C9	172.3(3)
C3	C4	C5	C6	0.9(7)	C3	C2	N1	C9	-5.1(5)
C4	C5	C6	C7	0.2(7)	C10	C9	N1	N2	86.5(4)
C5	C6	C7	C8	-0.8(7)	C10	C9	N1	C2	-85.9(5)
C4	C3	C8	C7	0.8(6)	C2	N1	N2	N3	0.3(3)
C2	C3	C8	C7	-179.7(3)	C9	N1	N2	N3	-173.4(3)
C6	C7	C8	C3	0.3(6)	N1	N2	N3	C1	-0.1(3)
C16	C11	C12	C13	0.1(5)	N1	N2	N3	C11	175.5(2)
N3	C11	C12	C13	-178.0(3)	C2	C1	N3	N2	-0.1(3)
C16	C11	C12	C18	179.2(3)	Ag1	C1	N3	N2	-178.89(19)
N3	C11	C12	C18	1.1(5)	C2	C1	N3	C11	-175.0(3)
C11	C12	C13	C14	1.3(5)	Ag1	C1	N3	C11	6.2(4)
C18	C12	C13	C14	-177.8(3)	C12	C11	N3	N2	109.0(3)
C12	C13	C14	C15	-1.8(5)	C16	C11	N3	N2	-69.2(3)
C12	C13	C14	C19	179.4(3)	C12	C11	N3	C1	-76.2(4)
C13	C14	C15	C16	1.0(5)	C16	C11	N3	C1	105.7(3)

Table 7 Hydrogen Atom Coordinates (Å×10^4) and Isotropic Displacement Parameters (Å^2×10^3)

Atom	***x***	***y***	***z***	**U(eq)**
H4	7437	7156	1397	81
H5	7473	8425	647	107
H6	8384	9427	982	111
H7	9272	9176	2061	96
H8	9230	7914	2834	71
H9A	6539	6322	3257	68
H9B	6800	7084	2670	68
H10A	7294	7799	3827	117
H10B	7099	7022	4426	117
H10C	6429	7564	3995	117
H13	9444	2879	3581	54
H15	9286	4199	5735	58
H17A	8934	6156	4830	81
H17B	9008	5674	5712	81
H17C	8207	5715	5219	81
H18A	8363	4016	2323	84

H18B	9118	3462	2264	84
H18C	9162	4468	2190	84
H19A	9834	2225	4830	106
H19B	9308	2466	5598	106
H19C	10148	2840	5556	106
H20A	5894	4453	5686	185
H20B	5896	5022	6517	185

Table 8 Atomic Occupancy

Atom	***Occupancy***	**Atom**	***Occupancy***	**Atom**	***Occupancy***
B1	0.5	F1	0.5	F2	0.5
F3	0.5	F4	0.5		

Appendix H: Crystallographic data for complex **9**:

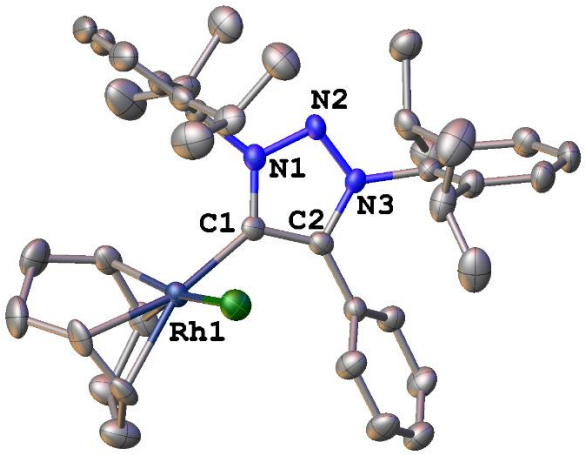

Table 1 Crystal data and structure refinement.

Empirical formula	$C_{40}H_{51}ClN_3Rh$
Formula weight	712.20
Temperature/K	173.15
Crystal system	monoclinic
Space group	$P2_1/n$
a/Å	18.5347(9)
b/Å	10.3075(5)
c/Å	19.6524(11)
α/°	90
β/°	107.574(3)
γ/°	90
Volume/Å^3	3579.3(3)
Z	4
ρ_{calc}g/cm^3	1.322
μ/mm^{-1}	0.583
F(000)	1496.0
Crystal size/mm^3	0.388 × 0.08 × 0.044
Radiation	MoKα (λ = 0.71073)
2Θ range for data collection/°	3.614 to 51.998
Index ranges	-22 ≤ h ≤ 22, -12 ≤ k ≤ 12, -24 ≤ l ≤ 24
Reflections collected	32741
Independent reflections	7037 [R_{int} = 0.1124, R_{sigma} = 0.1064]
Data/restraints/parameters	7037/0/414
Goodness-of-fit on F^2	0.981
Final R indexes [I>=2σ (I)]	R_1 = 0.0530, wR_2 = 0.1098

Final R indexes [all data]	R_1 = 0.1055, wR_2 = 0.1323
Largest diff. peak/hole / e Å^{-3}	1.42/-0.71

Table 2 Fractional Atomic Coordinates (×10^4) and Equivalent Isotropic Displacement Parameters (Å^2×10^3). U_{eq} is defined as 1/3 of the trace of the orthogonalised U_{IJ} tensor.

Atom	*x*	*y*	*z*	U(eq)
C1	7043(2)	3097(4)	4947(2)	22.4(10)
C2	6352(3)	3392(4)	4443(2)	24.3(10)
C3	5574(2)	3070(4)	4415(2)	24.9(10)
C4	5020(3)	4021(4)	4300(2)	30.0(11)
C5	4292(3)	3704(5)	4288(3)	35.8(12)
C6	4098(3)	2448(5)	4377(3)	37.1(13)
C7	4648(3)	1484(5)	4492(3)	39.5(13)
C8	5376(3)	1793(4)	4517(3)	34.7(12)
C9	8364(2)	3798(4)	4991(2)	26.3(11)
C10	8808(3)	2791(5)	4879(3)	31.3(12)
C11	9590(3)	2890(5)	5222(3)	42.1(14)
C12	9882(3)	3951(6)	5636(3)	46.5(15)
C13	9422(3)	4954(5)	5716(3)	39.0(13)
C14	8641(3)	4911(5)	5380(2)	31.2(12)
C15	8500(3)	1710(4)	4350(3)	36.4(12)
C16	8875(3)	391(5)	4567(4)	59.2(17)
C17	8573(3)	2114(5)	3624(3)	51.8(16)
C18	8158(3)	6091(5)	5401(3)	36.7(13)
C19	8238(3)	7044(5)	4843(3)	48.0(15)
C20	8344(4)	6759(5)	6126(3)	65.8(19)
C21	5999(2)	4458(4)	3222(2)	26.0(11)
C22	5785(3)	3468(4)	2725(3)	30.2(12)
C23	5261(3)	3786(5)	2072(3)	36.3(12)
C24	4983(3)	5025(5)	1943(3)	41.4(14)
C25	5217(3)	5990(5)	2443(3)	36.0(13)
C26	5747(2)	5736(4)	3105(2)	27.5(11)
C27	6121(3)	2106(5)	2845(3)	41.6(14)
C28	6619(3)	1880(6)	2367(4)	68(2)
C29	5500(3)	1075(5)	2722(3)	53.8(16)
C30	6054(3)	6830(4)	3620(3)	33.0(11)
C31	6614(3)	7621(5)	3358(3)	43.0(14)
C32	5436(3)	7717(5)	3733(3)	45.5(14)
C33	7077(3)	459(4)	6561(2)	32.8(12)
C34	7844(3)	615(4)	6716(2)	36.0(13)
C35	8316(3)	1411(5)	7340(3)	47.4(15)

C36	8424(3)	2797(5)	7110(3)	47.5(15)
C37	7765(3)	3296(4)	6522(3)	34.0(12)
C38	7000(3)	3173(4)	6484(3)	33.6(12)
C39	6739(3)	2562(5)	7071(3)	46.7(14)
C40	6578(3)	1101(5)	6935(3)	50.1(15)
Cl1	7134.3(7)	73.0(11)	4978.5(6)	34.7(3)
N1	7546(2)	3700(3)	4668.1(19)	24.3(9)
N2	7248(2)	4304(3)	4043.2(19)	23.9(9)
N3	6511.2(19)	4117(3)	3919.0(18)	20.4(8)
Rh1	7273.1(2)	1835.2(3)	5794.2(2)	23.47(13)

Table 3 Anisotropic Displacement Parameters ($Å^2×10^3$). The Anisotropic displacement factor exponent takes the form: $-2\pi^2[h^2a^{*2}U_{11}+2hka^*b^*U_{12}+\ldots]$.

Atom	U_{11}	U_{22}	U_{33}	U_{23}	U_{13}	U_{12}
C1	28(3)	21(2)	19(2)	-7(2)	8.0(19)	-3(2)
C2	30(3)	21(2)	23(2)	-1(2)	9(2)	-3(2)
C3	26(3)	25(2)	22(2)	1(2)	5(2)	0(2)
C4	30(3)	25(3)	34(3)	0(2)	8(2)	-4(2)
C5	26(3)	34(3)	46(3)	2(3)	8(2)	6(2)
C6	29(3)	37(3)	44(3)	-2(3)	9(3)	-5(3)
C7	35(3)	24(3)	56(4)	7(2)	10(3)	-5(2)
C8	29(3)	26(3)	47(3)	3(2)	9(2)	1(2)
C9	22(3)	27(3)	27(3)	9(2)	2(2)	0(2)
C10	28(3)	34(3)	31(3)	15(2)	8(2)	5(2)
C11	30(3)	48(3)	46(3)	19(3)	7(3)	7(3)
C12	29(3)	63(4)	39(3)	27(3)	-3(3)	-7(3)
C13	37(3)	40(3)	32(3)	13(2)	0(2)	-12(3)
C14	33(3)	36(3)	23(3)	4(2)	5(2)	-10(2)
C15	31(3)	30(3)	48(3)	5(3)	12(2)	9(2)
C16	61(4)	39(3)	80(5)	9(3)	24(4)	11(3)
C17	65(4)	47(3)	48(4)	0(3)	24(3)	9(3)
C18	40(3)	32(3)	40(3)	-8(2)	14(3)	-12(2)
C19	51(4)	39(3)	53(4)	8(3)	14(3)	14(3)
C20	104(5)	46(4)	48(4)	-15(3)	24(4)	-19(4)
C21	24(3)	30(3)	23(3)	1(2)	6(2)	-4(2)
C22	29(3)	28(3)	31(3)	1(2)	5(2)	0(2)
C23	36(3)	38(3)	28(3)	-3(2)	0(2)	-6(3)
C24	36(3)	50(3)	29(3)	10(3)	-3(2)	-5(3)
C25	38(3)	30(3)	37(3)	8(2)	6(2)	0(2)
C26	25(3)	29(3)	27(3)	6(2)	6(2)	-1(2)
C27	37(3)	39(3)	39(3)	-10(3)	-2(3)	8(3)

C28	55(4)	76(5)	69(5)	-32(4)	14(3)	7(3)
C29	67(4)	28(3)	54(4)	-6(3)	-1(3)	5(3)
C30	43(3)	26(3)	27(3)	4(2)	6(2)	3(2)
C31	41(3)	34(3)	50(4)	-1(3)	8(3)	-6(3)
C32	56(4)	35(3)	51(4)	0(3)	24(3)	4(3)
C33	56(4)	20(2)	22(3)	5(2)	12(2)	-6(2)
C34	56(4)	20(3)	25(3)	9(2)	2(3)	12(3)
C35	45(3)	53(4)	32(3)	4(3)	-7(3)	14(3)
C36	46(3)	44(3)	44(4)	-17(3)	0(3)	-11(3)
C37	50(3)	21(3)	28(3)	-2(2)	8(2)	-9(2)
C38	50(3)	16(2)	33(3)	-2(2)	11(2)	10(2)
C39	64(4)	39(3)	47(4)	-7(3)	32(3)	-2(3)
C40	67(4)	43(3)	51(4)	-7(3)	33(3)	-13(3)
Cl1	43.6(8)	26.7(6)	34.7(7)	-6.7(5)	13.3(6)	-1.2(6)
N1	26(2)	24(2)	21(2)	-0.7(17)	4.2(17)	1.5(18)
N2	24(2)	25(2)	20(2)	4.6(17)	2.3(17)	1.8(17)
N3	20(2)	18.6(19)	21(2)	-2.9(16)	2.5(16)	-0.5(16)
Rh1	28.0(2)	18.05(19)	23.0(2)	1.25(17)	5.61(15)	0.05(18)

Table 4 Bond Lengths.

Atom	Atom	Length/Å	Atom	Atom	Length/Å
C1	C2	1.395(6)	C21	N3	1.455(5)
C1	N1	1.366(5)	C22	C23	1.395(6)
C1	Rh1	2.053(4)	C22	C27	1.526(6)
C2	C3	1.464(6)	C23	C24	1.371(7)
C2	N3	1.375(5)	C24	C25	1.374(7)
C3	C4	1.388(6)	C25	C26	1.397(6)
C3	C8	1.397(6)	C26	C30	1.507(6)
C4	C5	1.381(6)	C27	C28	1.520(8)
C5	C6	1.369(7)	C27	C29	1.531(7)
C6	C7	1.392(7)	C30	C31	1.526(7)
C7	C8	1.374(7)	C30	C32	1.532(7)
C9	C10	1.382(6)	C33	C34	1.371(7)
C9	C14	1.389(6)	C33	C40	1.499(7)
C9	N1	1.460(5)	C33	Rh1	2.178(4)
C10	C11	1.406(7)	C34	C35	1.515(7)
C10	C15	1.514(7)	C34	Rh1	2.197(4)
C11	C12	1.373(7)	C35	C36	1.530(7)
C12	C13	1.378(7)	C36	C37	1.495(7)
C13	C14	1.399(6)	C37	C38	1.403(7)
C14	C18	1.518(7)	C37	Rh1	2.088(4)

C15	C16	1.528(7)	C38	C39	1.516(7)
C15	C17	1.529(7)	C38	Rh1	2.100(4)
C18	C19	1.513(7)	C39	C40	1.542(7)
C18	C20	1.525(7)	Cl1	Rh1	2.3846(12)
C21	C22	1.384(6)	N1	N2	1.339(5)
C21	C26	1.393(6)	N2	N3	1.327(5)

Table 5 Bond Angles.

Atom	Atom	Atom	Angle/˚	Atom	Atom	Atom	Angle/˚
C2	C1	Rh1	129.4(3)	C22	C27	C29	111.2(4)
N1	C1	C2	102.0(4)	C28	C27	C22	110.0(5)
N1	C1	Rh1	127.9(3)	C28	C27	C29	111.4(4)
C1	C2	C3	131.3(4)	C26	C30	C31	109.3(4)
N3	C2	C1	107.0(4)	C26	C30	C32	113.4(4)
N3	C2	C3	121.7(4)	C31	C30	C32	110.1(4)
C4	C3	C2	121.2(4)	C34	C33	C40	126.2(5)
C4	C3	C8	118.4(4)	C34	C33	Rh1	72.5(3)
C8	C3	C2	120.4(4)	C40	C33	Rh1	108.0(3)
C5	C4	C3	120.4(4)	C33	C34	C35	123.4(5)
C6	C5	C4	121.0(5)	C33	C34	Rh1	71.0(3)
C5	C6	C7	119.2(5)	C35	C34	Rh1	112.0(3)
C8	C7	C6	120.2(4)	C34	C35	C36	111.1(4)
C7	C8	C3	120.7(4)	C37	C36	C35	113.6(4)
C10	C9	C14	124.7(4)	C36	C37	Rh1	111.5(3)
C10	C9	N1	118.0(4)	C38	C37	C36	125.9(5)
C14	C9	N1	117.4(4)	C38	C37	Rh1	70.9(3)
C9	C10	C11	116.5(5)	C37	C38	C39	123.1(5)
C9	C10	C15	122.9(4)	C37	C38	Rh1	70.0(3)
C11	C10	C15	120.2(4)	C39	C38	Rh1	114.4(3)
C12	C11	C10	120.4(5)	C38	C39	C40	111.3(4)
C11	C12	C13	121.3(5)	C33	C40	C39	113.6(4)
C12	C13	C14	120.6(5)	C1	N1	C9	127.1(4)
C9	C14	C13	116.4(5)	N2	N1	C1	115.9(3)
C9	C14	C18	123.6(4)	N2	N1	C9	117.0(4)
C13	C14	C18	119.8(4)	N3	N2	N1	102.6(3)
C10	C15	C16	114.7(4)	C2	N3	C21	127.6(4)
C10	C15	C17	108.7(4)	N2	N3	C2	112.5(3)
C16	C15	C17	110.0(5)	N2	N3	C21	118.7(3)
C14	C18	C20	114.7(5)	C1	Rh1	C33	159.38(19)
C19	C18	C14	108.2(4)	C1	Rh1	C34	164.07(19)
C19	C18	C20	109.9(4)	C1	Rh1	C37	92.27(18)

C22	C21	C26	124.7(4)	C1	Rh1	C38	94.36(17)
C22	C21	N3	116.9(4)	C1	Rh1	Cl1	89.05(12)
C26	C21	N3	118.4(4)	C33	Rh1	C34	36.54(17)
C21	C22	C23	116.6(4)	C33	Rh1	Cl1	87.84(13)
C21	C22	C27	123.6(4)	C34	Rh1	Cl1	92.62(13)
C23	C22	C27	119.8(4)	C37	Rh1	C33	97.21(18)
C24	C23	C22	120.5(5)	C37	Rh1	C34	81.12(18)
C23	C24	C25	121.5(5)	C37	Rh1	C38	39.15(18)
C24	C25	C26	120.7(5)	C37	Rh1	Cl1	161.12(15)
C21	C26	C25	115.9(4)	C38	Rh1	C33	81.84(18)
C21	C26	C30	123.8(4)	C38	Rh1	C34	89.62(19)
C25	C26	C30	120.1(4)	C38	Rh1	Cl1	159.42(15)

Table 6 Torsion Angles.

A	B	C	D	Angle/˚	A	B	C	D	Angle/˚
C1	C2	C3	C4	128.8(5)	C22	C21	N3	N2	95.9(5)
C1	C2	C3	C8	-49.8(7)	C22	C23	C24	C25	1.0(8)
C1	C2	N3	C21	168.0(4)	C23	C22	C27	C28	67.1(6)
C1	C2	N3	N2	0.3(5)	C23	C22	C27	C29	-56.9(7)
C1	N1	N2	N3	1.8(5)	C23	C24	C25	C26	-0.2(8)
C2	C1	N1	C9	175.8(4)	C24	C25	C26	C21	-1.5(7)
C2	C1	N1	N2	-1.6(5)	C24	C25	C26	C30	174.1(4)
C2	C3	C4	C5	-178.8(4)	C25	C26	C30	C31	-74.3(6)
C2	C3	C8	C7	179.9(5)	C25	C26	C30	C32	48.9(6)
C3	C2	N3	C21	-12.5(6)	C26	C21	C22	C23	-2.1(7)
C3	C2	N3	N2	179.9(4)	C26	C21	C22	C27	174.5(5)
C3	C4	C5	C6	-1.0(8)	C26	C21	N3	C2	107.6(5)
C4	C3	C8	C7	1.2(7)	C26	C21	N3	N2	-85.5(5)
C4	C5	C6	C7	1.0(8)	C27	C22	C23	C24	-176.6(5)
C5	C6	C7	C8	0.1(8)	C33	C34	C35	C36	-94.8(6)
C6	C7	C8	C3	-1.2(8)	C34	C33	C40	C39	44.9(7)
C8	C3	C4	C5	-0.1(7)	C34	C35	C36	C37	32.6(7)
C9	C10	C11	C12	-0.7(7)	C35	C36	C37	C38	45.0(7)
C9	C10	C15	C16	-146.8(5)	C35	C36	C37	Rh1	-36.4(6)
C9	C10	C15	C17	89.6(6)	C36	C37	C38	C39	3.5(7)
C9	C14	C18	C19	-94.6(5)	C36	C37	C38	Rh1	-103.2(5)
C9	C14	C18	C20	142.2(5)	C37	C38	C39	C40	-92.9(6)
C9	N1	N2	N3	-175.8(3)	C38	C39	C40	C33	32.3(7)
C10	C9	C14	C13	-4.3(7)	C40	C33	C34	C35	4.5(7)
C10	C9	C14	C18	170.2(5)	C40	C33	C34	Rh1	-99.8(5)
C10	C9	N1	C1	85.9(6)	N1	C1	C2	C3	-178.8(4)

C10	C9	N1	N2	-96.7(5)	N1	C1	C2	N3	0.7(4)
C10	C11	C12	C13	-1.3(8)	N1	C9	C10	C11	-177.4(4)
C11	C10	C15	C16	40.8(6)	N1	C9	C10	C15	10.0(7)
C11	C10	C15	C17	-82.8(5)	N1	C9	C14	C13	176.7(4)
C11	C12	C13	C14	0.6(8)	N1	C9	C14	C18	-8.8(7)
C12	C13	C14	C9	2.1(7)	N1	N2	N3	C2	-1.2(4)
C12	C13	C14	C18	-172.6(5)	N1	N2	N3	C21	-170.1(3)
C13	C14	C18	C19	79.6(6)	N3	C2	C3	C4	-50.6(6)
C13	C14	C18	C20	-43.5(6)	N3	C2	C3	C8	130.8(5)
C14	C9	C10	C11	3.6(7)	N3	C21	C22	C23	176.5(4)
C14	C9	C10	C15	-169.0(4)	N3	C21	C22	C27	-6.9(7)
C14	C9	N1	C1	-95.0(5)	N3	C21	C26	C25	-175.8(4)
C14	C9	N1	N2	82.4(5)	N3	C21	C26	C30	8.7(7)
C15	C10	C11	C12	172.2(5)	Rh1	C1	C2	C3	10.6(7)
C21	C22	C23	C24	0.1(7)	Rh1	C1	C2	N3	-169.9(3)
C21	C22	C27	C28	-109.4(5)	Rh1	C1	N1	C9	-13.4(6)
C21	C22	C27	C29	126.7(5)	Rh1	C1	N1	N2	169.2(3)
C21	C26	C30	C31	100.9(5)	Rh1	C33	C34	C35	104.3(4)
C21	C26	C30	C32	-135.8(5)	Rh1	C33	C40	C39	-36.2(6)
C22	C21	C26	C25	2.7(7)	Rh1	C34	C35	C36	-13.7(6)
C22	C21	C26	C30	-172.7(4)	Rh1	C37	C38	C39	106.7(4)
C22	C21	N3	C2	-71.1(6)	Rh1	C38	C39	C40	-11.7(6)

Table 7 Hydrogen Atom Coordinates (Å×10^4) and Isotropic Displacement Parameters (Å^2×10^3).

Atom	*x*	*y*	*z*	U(eq)
H4	5142.15	4895.55	4229	36
H5	3921.16	4367.62	4216.07	43
H6	3593.66	2237.55	4360.23	45
H7	4518.56	609.04	4553.77	47
H8	5750.14	1131.43	4605.83	42
H11	9919.15	2218.97	5166.52	51
H12	10410.19	3994.78	5871.96	56
H13	9638.18	5681.75	6002.16	47
H15	7949.08	1614.69	4296.6	44
H16A	9401.18	425.65	4561.66	89
H16B	8600.52	-273.3	4231.16	89
H16C	8862.46	172.96	5049.3	89
H17A	8297.34	2926.31	3471.53	78
H17B	8360.4	1433.81	3272.4	78
H17C	9108.53	2239.61	3664.44	78
H18	7617.82	5804.45	5265.37	44

H19A	8759.56	7367.33	4975.04	72
H19B	7890.34	7771.91	4813.06	72
H19C	8117.18	6608.7	4378.34	72
H20A	8331.89	6120.11	6491.85	99
H20B	7969.67	7439.32	6108.87	99
H20C	8849.58	7145.94	6243.07	99
H23	5095.07	3139.97	1713.96	44
H24	4620.56	5219.67	1497.52	50
H25	5016.22	6840.33	2338.17	43
H27	6446.5	2041.89	3352.18	50
H28A	6312.07	1940.89	1866.07	101
H28B	6848.26	1015.61	2460.55	101
H28C	7019.48	2538.18	2468.06	101
H29A	5180.78	1260.41	3027.3	81
H29B	5732.41	217.69	2840.82	81
H29C	5190.08	1088.22	2220.69	81
H30	6335.36	6441.38	4091.31	40
H31A	7024.22	7055.98	3318.11	64
H31B	6823.45	8319.95	3698.03	64
H31C	6352.58	7994.25	2889.63	64
H32A	5172.55	8151.71	3283.08	68
H32B	5667.61	8368.06	4096.45	68
H32C	5074.21	7197.16	3891.19	68
H33	6888.5	-405.75	6350.81	39
H34	8113.21	-153.25	6597.7	43
H35A	8816.61	995.81	7542.73	57
H35B	8062.71	1436.06	7717.61	57
H36A	8511.57	3378.82	7527.43	57
H36B	8881.54	2824.89	6949.59	57
H37	7879.85	4104.51	6292.81	41
H38	6675.39	3908.04	6233.64	40
H39A	6274.15	3003.55	7097.16	56
H39B	7134.65	2681.15	7534.84	56
H40A	6646.21	661.87	7398.41	60
H40B	6043.21	987.61	6644.66	60

Appendix I: Crystallographic data for complex **10**.

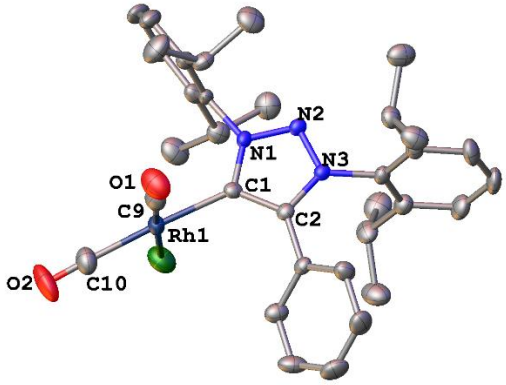

Table 1 Crystal data and structure refinement.

Empirical formula	$C_{34}H_{39}ClN_3O_2Rh$
Formula weight	660.04
Temperature/K	173.15
Crystal system	triclinic
Space group	P-1
a/Å	10.5904(2)
b/Å	10.8731(3)
c/Å	15.2113(3)
α/°	97.9085(12)
β/°	97.3841(12)
γ/°	110.0498(11)
Volume/Å^3	1600.47(6)
Z	2
ρ_{calc}g/cm^3	1.370
μ/mm^{-1}	0.651
F(000)	684.0
Crystal size/mm^3	0.346 × 0.129 × 0.098
Radiation	MoKα (λ = 0.71073)
2Θ range for data collection/°	4.066 to 56.538
Index ranges	-14 ≤ h ≤ 14, -14 ≤ k ≤ 14, -20 ≤ l ≤ 20
Reflections collected	22804
Independent reflections	7795 [R_{int} = 0.0343, R_{sigma} = 0.0604]
Data/restraints/parameters	7795/0/378
Goodness-of-fit on F^2	1.050
Final R indexes [I>=2σ (I)]	R_1 = 0.0394, wR_2 = 0.0928
Final R indexes [all data]	R_1 = 0.0650, wR_2 = 0.1077
Largest diff. peak/hole / e Å^{-3}	1.02/-0.78

Table 2 Fractional Atomic Coordinates (×10^4) and Equivalent Isotropic Displacement Parameters (Å^2×10^3). U_{eq} is defined as 1/3 of the trace of the orthogonalised U_{IJ} tensor.

Atom	*x*	*y*	*z*	U(eq)
C1	3597(2)	6203(2)	7751.9(16)	20.0(5)

C2	3353(2)	4940(2)	7946.6(16)	19.0(5)
C3	2541(2)	4256(2)	8569.6(16)	20.6(5)
C4	3023(3)	3544(3)	9133.2(18)	30.6(6)
C5	2227(3)	2895(3)	9708(2)	39.4(7)
C6	953(3)	2967(3)	9732(2)	40.4(8)
C7	488(3)	3691(3)	9191(2)	37.5(7)
C8	1269(3)	4335(3)	8611.8(18)	29.9(6)
C9	4418(3)	8349(3)	9157(2)	35.6(7)
C10	2154(3)	8957(3)	8651(2)	41.5(8)
C11	4959(2)	7300(2)	6622.3(16)	20.3(5)
C12	6221(3)	8296(3)	7025.1(18)	25.8(6)
C13	6765(3)	9277(3)	6531(2)	33.5(7)
C14	6102(3)	9229(3)	5677(2)	36.9(7)
C15	4874(3)	8223(3)	5300.6(19)	35.5(7)
C16	4244(3)	7232(3)	5769.3(17)	26.7(6)
C17	7047(3)	8271(3)	7909.1(18)	28.0(6)
C18	8068(3)	7606(3)	7702(2)	45.1(8)
C19	7784(3)	9650(3)	8508(2)	46.7(8)
C20	2892(3)	6121(3)	5337.1(18)	30.4(6)
C21	1867(3)	6654(4)	4866(2)	44.8(8)
C22	3133(3)	5074(3)	4670(2)	41.8(8)
C23	3947(3)	2972(2)	7251.2(17)	22.3(6)
C24	2764(3)	1993(3)	6728.9(18)	27.2(6)
C25	2730(3)	691(3)	6596(2)	35.2(7)
C26	3839(3)	408(3)	6960(2)	37.3(7)
C27	4989(3)	1407(3)	7467.7(19)	34.7(7)
C28	5082(3)	2725(3)	7640.5(17)	25.2(6)
C29	1554(3)	2293(3)	6290(2)	34.0(7)
C30	267(3)	1594(3)	6649(2)	48.2(8)
C31	1317(3)	1902(3)	5259(2)	46.5(8)
C32	6360(3)	3801(3)	8213.8(18)	29.6(6)
C33	7576(3)	4036(3)	7731(2)	41.2(8)
C34	6711(3)	3462(3)	9137.7(19)	40.1(7)
Cl1	964.4(8)	6704.5(9)	7062.2(6)	46.5(2)
N1	4381(2)	6233.4(19)	7102.2(13)	18.7(4)
N2	4635(2)	5122(2)	6869.4(13)	19.9(4)
N3	3992(2)	4344(2)	7397.6(13)	18.3(4)
O1	5307(3)	8730(3)	9698.6(17)	56.4(6)
O2	1683(3)	9687(3)	8894.1(19)	71.2(8)
Rh1	2902.1(2)	7670.0(2)	8229.7(2)	25.84(9)

Table 3 Anisotropic Displacement Parameters ($Å^2×10^3$). The Anisotropic displacement factor exponent takes the form: $-2π^2[h^2a^{*2}U_{11}+2hka*b*U_{12}+…]$.

Atom	U_{11}	U_{22}	U_{33}	U_{23}	U_{13}	U_{12}
C1	15.4(13)	23.5(13)	21.7(12)	6.5(11)	2.7(10)	7.3(10)
C2	16.8(13)	18.2(12)	18.8(12)	2.0(10)	0.8(10)	4.0(10)
C3	21.0(13)	16.3(12)	21.5(12)	3.0(10)	3.5(10)	3.4(10)
C4	33.3(16)	35.1(16)	31.7(15)	12.9(13)	13.3(13)	17.9(13)
C5	53(2)	38.3(18)	38.3(17)	22.1(14)	18.7(15)	21.5(15)
C6	41.6(19)	44.6(19)	33.9(17)	18.3(15)	16.5(14)	7.0(15)
C7	22.7(15)	54(2)	35.7(16)	12.3(15)	10.5(13)	10.1(14)
C8	25.4(15)	35.5(16)	27.8(15)	10.4(12)	4.4(12)	8.7(12)
C9	44(2)	31.0(17)	36.1(17)	3.8(14)	16.1(16)	17.1(15)
C10	42.0(19)	32.4(17)	50(2)	1.6(15)	4.2(15)	17.8(15)
C11	22.7(14)	18.1(13)	26.5(13)	9.9(11)	11.6(11)	10.9(11)
C12	27.2(15)	25.1(14)	31.7(15)	12.3(12)	12.5(12)	12.6(12)
C13	27.3(15)	29.3(16)	47.0(18)	18.6(14)	12.7(13)	7.9(13)
C14	40.0(18)	36.7(17)	47.4(18)	30.7(15)	22.1(15)	17.4(15)
C15	43.9(19)	45.0(18)	31.0(16)	23.4(14)	12.0(14)	24.9(16)
C16	30.8(15)	33.0(15)	25.5(14)	12.3(12)	10.1(12)	19.0(13)
C17	23.2(14)	25.7(14)	31.1(15)	9.4(12)	4.9(12)	2.7(11)
C18	35.7(18)	58(2)	46.7(19)	12.9(17)	2.2(15)	24.9(16)
C19	51(2)	30.7(18)	44.4(19)	6.2(15)	2.0(16)	0.2(15)
C20	32.2(16)	36.5(16)	24.1(14)	8.7(12)	3.6(12)	14.0(13)
C21	41.9(19)	61(2)	39.2(18)	13.5(16)	1.4(15)	28.5(17)
C22	45(2)	43.4(19)	33.0(17)	3.5(14)	0.8(14)	15.8(16)
C23	26.9(14)	17.9(13)	24.6(13)	7.0(11)	8.2(11)	9.0(11)
C24	28.1(15)	22.4(14)	28.7(14)	3.3(12)	6.1(12)	6.7(12)
C25	42.3(18)	19.6(14)	37.7(16)	-0.1(12)	6.6(14)	6.5(13)
C26	56(2)	18.6(14)	42.5(18)	6.4(13)	14.9(16)	18.2(14)
C27	49.1(19)	31.8(16)	34.6(16)	9.4(13)	7.3(14)	27.9(15)
C28	32.3(15)	25.4(14)	22.6(13)	7.0(11)	7.0(11)	14.7(12)
C29	23.4(15)	24.5(15)	44.9(18)	-2.2(13)	-0.7(13)	3.2(12)
C30	30.4(18)	48(2)	57(2)	-2.7(17)	10.0(16)	7.1(15)
C31	37.9(19)	43.8(19)	46.9(19)	6.0(16)	-6.8(15)	7.8(15)
C32	28.3(15)	29.2(15)	33.5(15)	7.0(12)	1.9(12)	14.2(12)
C33	35.7(18)	54(2)	38.3(17)	21.3(15)	7.5(14)	16.8(15)
C34	35.5(18)	55(2)	33.5(16)	10.9(15)	5.0(14)	21.6(16)
Cl1	38.2(5)	59.0(5)	45.9(5)	4.6(4)	4.0(4)	25.7(4)
N1	17.6(11)	16.1(10)	24.0(11)	6.8(9)	3.8(9)	7.0(9)
N2	20.0(11)	20.1(11)	20.8(11)	7.8(9)	4.2(9)	7.3(9)
N3	16.8(11)	18.2(11)	20.5(10)	6.2(9)	3.5(8)	6.2(9)

O1	53.1(16)	58.0(16)	54.1(16)	-8.9(13)	4.5(13)	24.8(13)
O2	69.0(19)	60.8(18)	90(2)	-17.1(15)	7.2(16)	46.7(16)
Rh1	29.19(14)	20.92(13)	30.90(13)	5.61(9)	9.15(9)	12.07(10)

Table 4 Bond Lengths.

Atom	Atom	Length/Å	Atom	Atom	Length/Å
C1	C2	1.389(3)	C15	C16	1.399(4)
C1	N1	1.367(3)	C16	C20	1.515(4)
C1	Rh1	2.059(2)	C17	C18	1.534(4)
C2	C3	1.469(3)	C17	C19	1.524(4)
C2	N3	1.368(3)	C20	C21	1.541(4)
C3	C4	1.391(3)	C20	C22	1.529(4)
C3	C8	1.388(4)	C23	C24	1.389(4)
C4	C5	1.387(4)	C23	C28	1.397(4)
C5	C6	1.383(4)	C23	N3	1.461(3)
C6	C7	1.371(4)	C24	C25	1.390(4)
C7	C8	1.382(4)	C24	C29	1.523(4)
C9	O1	1.084(4)	C25	C26	1.381(4)
C9	Rh1	1.852(4)	C26	C27	1.371(4)
C10	O2	1.121(4)	C27	C28	1.388(4)
C10	Rh1	1.907(3)	C28	C32	1.513(4)
C11	C12	1.396(4)	C29	C30	1.526(4)
C11	C16	1.395(4)	C29	C31	1.532(4)
C11	N1	1.453(3)	C32	C33	1.528(4)
C12	C13	1.394(4)	C32	C34	1.534(4)
C12	C17	1.516(4)	Cl1	Rh1	2.3537(8)
C13	C14	1.380(4)	N1	N2	1.337(3)
C14	C15	1.370(4)	N2	N3	1.326(3)

Table 5 Bond Angles.

Atom	Atom	Atom	Angle/˚	Atom	Atom	Atom	Angle/˚
C2	C1	Rh1	130.75(19)	C22	C20	C21	110.7(2)
N1	C1	C2	102.5(2)	C24	C23	C28	124.2(2)
N1	C1	Rh1	126.66(17)	C24	C23	N3	117.3(2)
C1	C2	C3	130.6(2)	C28	C23	N3	118.5(2)
N3	C2	C1	106.6(2)	C23	C24	C25	116.8(3)
N3	C2	C3	122.7(2)	C23	C24	C29	123.3(2)
C4	C3	C2	121.6(2)	C25	C24	C29	119.9(3)
C8	C3	C2	119.5(2)	C26	C25	C24	120.7(3)
C8	C3	C4	118.8(2)	C27	C26	C25	120.5(3)
C5	C4	C3	120.4(3)	C26	C27	C28	121.8(3)

C6	C5	C4	120.0(3)	C23	C28	C32	123.6(2)
C7	C6	C5	119.6(3)	C27	C28	C23	115.9(3)
C6	C7	C8	120.8(3)	C27	C28	C32	120.4(2)
C7	C8	C3	120.2(3)	C24	C29	C30	111.0(3)
O1	C9	Rh1	179.0(3)	C24	C29	C31	110.7(2)
O2	C10	Rh1	178.2(3)	C30	C29	C31	111.2(2)
C12	C11	N1	118.1(2)	C28	C32	C33	111.2(2)
C16	C11	C12	124.0(2)	C28	C32	C34	111.5(2)
C16	C11	N1	117.8(2)	C33	C32	C34	110.0(2)
C11	C12	C17	123.0(2)	C1	N1	C11	128.9(2)
C13	C12	C11	116.5(2)	N2	N1	C1	115.39(19)
C13	C12	C17	120.3(2)	N2	N1	C11	115.71(19)
C14	C13	C12	121.2(3)	N3	N2	N1	102.52(18)
C15	C14	C13	120.4(3)	C2	N3	C23	129.8(2)
C14	C15	C16	121.5(3)	N2	N3	C2	112.95(19)
C11	C16	C15	116.3(3)	N2	N3	C23	116.95(19)
C11	C16	C20	123.0(2)	C1	Rh1	Cl1	89.07(7)
C15	C16	C20	120.6(2)	C9	Rh1	C1	88.95(11)
C12	C17	C18	108.8(2)	C9	Rh1	C10	93.71(13)
C12	C17	C19	113.3(2)	C9	Rh1	Cl1	177.28(9)
C19	C17	C18	110.8(3)	C10	Rh1	C1	176.74(11)
C16	C20	C21	111.9(2)	C10	Rh1	Cl1	88.22(10)
C16	C20	C22	109.8(2)				

Table 6 Torsion Angles.

A	B	C	D	Angle/˚	A	B	C	D	Angle/˚
C1	C2	C3	C4	-136.1(3)	C23	C24	C25	C26	-1.0(4)
C1	C2	C3	C8	42.8(4)	C23	C24	C29	C30	-118.4(3)
C1	C2	N3	C23	-172.7(2)	C23	C24	C29	C31	117.6(3)
C1	C2	N3	N2	0.5(3)	C23	C28	C32	C33	-111.2(3)
C1	N1	N2	N3	-0.4(2)	C23	C28	C32	C34	125.6(3)
C2	C1	N1	C11	179.7(2)	C24	C23	C28	C27	0.9(4)
C2	C1	N1	N2	0.6(3)	C24	C23	C28	C32	-179.5(2)
C2	C3	C4	C5	-179.3(3)	C24	C23	N3	C2	74.8(3)
C2	C3	C8	C7	179.6(3)	C24	C23	N3	N2	-98.1(3)
C3	C2	N3	C23	4.9(4)	C24	C25	C26	C27	0.7(4)
C3	C2	N3	N2	178.1(2)	C25	C24	C29	C30	63.2(3)
C3	C4	C5	C6	-0.8(5)	C25	C24	C29	C31	-60.7(3)
C4	C3	C8	C7	-1.5(4)	C25	C26	C27	C28	0.5(5)
C4	C5	C6	C7	-0.6(5)	C26	C27	C28	C23	-1.2(4)
C5	C6	C7	C8	1.0(5)	C26	C27	C28	C32	179.2(3)

C6	C7	C8	C3	0.1(5)	C27	C28	C32 C33 68.3(3)
C8	C3	C4	C5	1.8(4)	C27	C28	C32 C34 -54.9(3)
C11	C12	C13	C14	-2.1(4)	C28	C23	C24 C25 0.2(4)
C11	C12	C17	C18	93.3(3)	C28	C23	C24 C29 -178.2(2)
C11	C12	C17	C19	-143.0(3)	C28	C23	N3 C2 -105.2(3)
C11	C16	C20	C21	137.9(3)	C28	C23	N3 N2 81.9(3)
C11	C16	C20	C22	-98.7(3)	C29	C24	C25 C26 177.5(3)
C11	N1	N2	N3	-179.54(19)	N1	C1	C2 C3 -178.0(2)
C12	C11	C16	C15	1.3(4)	N1	C1	C2 N3 -0.6(2)
C12	C11	C16	C20	178.5(2)	N1	C11	C12 C13 177.9(2)
C12	C11	N1	C1	85.7(3)	N1	C11	C12 C17 3.7(4)
C12	C11	N1	N2	-95.3(3)	N1	C11	C16 C15 -175.8(2)
C12	C13	C14	C15	1.3(5)	N1	C11	C16 C20 1.4(4)
C13	C12	C17	C18	-80.7(3)	N1	N2	N3 C2 -0.1(2)
C13	C12	C17	C19	43.0(4)	N1	N2	N3 C23 174.03(19)
C13	C14	C15	C16	1.0(5)	N3	C2	C3 C4 47.0(4)
C14	C15	C16	C11	-2.2(4)	N3	C2	C3 C8 -134.2(3)
C14	C15	C16	C20	-179.4(3)	N3	C23	C24 C25 -179.8(2)
C15	C16	C20	C21	-45.1(3)	N3	C23	C24 C29 1.8(4)
C15	C16	C20	C22	78.4(3)	N3	C23	C28 C27 -179.1(2)
C16	C11	C12	C13	0.7(4)	N3	C23	C28 C32 0.4(4)
C16	C11	C12	C17	-173.5(2)	Rh1	C1	C2 C3 -1.3(4)
C16	C11	N1	C1	-97.0(3)	Rh1	C1	C2 N3 176.05(17)
C16	C11	N1	N2	82.0(3)	Rh1	C1	N1 C11 2.8(4)
C17	C12	C13	C14	172.3(3)	Rh1	C1	N1 N2 -176.21(15)

Table 7 Hydrogen Atom Coordinates (Å×10^4) and Isotropic Displacement Parameters (Å^2×10^3).

Atom	*x*	*y*	*z*	U(eq)
H4	3902.91	3502.99	9124.49	37
H5	2557.81	2401.6	10085.51	47
H6	402.12	2516.26	10120.75	49
H7	-382.04	3751.08	9214.14	45
H8	934.41	4834.75	8241.42	36
H13	7606.74	9990.74	6786.62	40
H14	6500.97	9898.14	5347.4	44
H15	4440.32	8198.74	4708.18	43
H17	6402.81	7706.48	8248.45	34
H18A	7570.55	6707.17	7339.58	68
H18B	8578.06	7547.04	8269.3	68
H18C	8707.23	8138.66	7363.92	68
H19A	8472.09	10202.39	8208.15	70

H19B	8232.79	9562.06	9087.6	70
H19C	7118.95	10071.49	8611.75	70
H20	2488	5682.91	5824.97	37
H21A	1740.31	7335.53	5300.52	67
H21B	986.41	5917.69	4633.42	67
H21C	2220.93	7046.96	4363.71	67
H22A	3659.54	5509.48	4240.89	63
H22B	2249.76	4413.95	4341.63	63
H22C	3643.3	4626.49	5001.74	63
H25	1935.58	-11.95	6251.07	42
H26	3804.2	-486.19	6857.46	45
H27	5742.42	1190.55	7707.72	42
H29	1780.18	3276.8	6451.67	41
H30A	10.12	625.36	6483.53	72
H30B	-481.05	1845.65	6385.47	72
H30C	446.59	1863.99	7308.47	72
H31A	2152.79	2376.52	5045.87	70
H31B	565.55	2143.19	4987.85	70
H31C	1081.75	937.59	5082.59	70
H32	6181.31	4650.15	8318.04	36
H33A	7797.42	3228.61	7645.86	62
H33B	8369.5	4781.41	8096.6	62
H33C	7342.67	4249.88	7141	62
H34A	5922.1	3301.59	9439.44	60
H34B	7496.06	4209.18	9509.69	60
H34C	6940.48	2658.94	9054.35	60

Appendix J: Crystallographic data for complex **S3**.

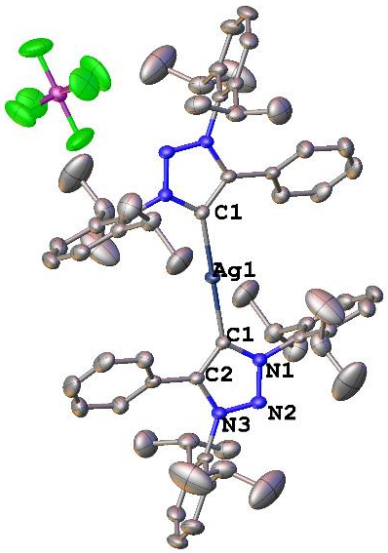

Table 1 Crystal data and structure refinement.

Empirical formula	$C_{67}H_{84}AgCl_6F_6N_6P$
Formula weight	1438.94
Temperature/K	173.15
Crystal system	monoclinic
Space group	C2/c
a/Å	18.4506(11)
b/Å	18.6525(10)
c/Å	22.9936(13)
α/°	90
β/°	111.365(3)
γ/°	90
Volume/Å^3	7369.5(7)
Z	4
ρ_{calc}g/cm^3	1.297
μ/mm^{-1}	0.569
F(000)	2984.0
Crystal size/mm^3	0.411 × 0.149 × 0.106
Radiation	MoKα (λ = 0.71073)
2Θ range for data collection/°	3.222 to 56.776
Index ranges	-20 ≤ h ≤ 24, -24 ≤ k ≤ 24, -30 ≤ l ≤ 28
Reflections collected	31958
Independent reflections	9182 [R_{int} = 0.0677, R_{sigma} = 0.0850]
Data/restraints/parameters	9182/70/429

Goodness-of-fit on F^2	1.018
Final R indexes [I>=2σ (I)]	R_1 = 0.0526, wR_2 = 0.1168
Final R indexes [all data]	R_1 = 0.1048, wR_2 = 0.1359
Largest diff. peak/hole / e $Å^{-3}$	0.82/-0.65

Table 2 Fractional Atomic Coordinates (×10^4) and Equivalent Isotropic Displacement Parameters (Å²×10^3). U_{eq} is defined as 1/3 of the trace of the orthogonalised U_{IJ} tensor.

Atom	*x*	*y*	*z*	U(eq)
Ag1	5000	5000	5000	24.94(10)
C1	5977.5(18)	4617.6(15)	4851.4(14)	24.3(6)
N1	6434.2(14)	4052.3(12)	5145.9(11)	23.8(5)
C2	6323.4(17)	4832.4(15)	4437.1(14)	24.4(7)
N2	7023.0(15)	3899.2(13)	4960.0(12)	25.4(6)
C3	6129.6(18)	5442.1(16)	4002.0(15)	27.7(7)
N3	6942.6(14)	4387.3(13)	4521.0(11)	24.7(6)
C4	5950(2)	6095.1(17)	4205.5(17)	35.9(8)
C5	5774(2)	6687.4(18)	3814.5(19)	46.4(10)
C6	5765(2)	6625(2)	3213(2)	53.0(11)
C7	5924(2)	5980(2)	3004.5(18)	51.2(10)
C8	6112(2)	5386.1(19)	3396.1(16)	39.7(9)
C9	6353.0(18)	3620.6(15)	5646.4(14)	26.1(7)
C10	5977.3(19)	2959.2(16)	5490.8(15)	30.8(7)
C11	5908(2)	2571.2(19)	5987.3(18)	41.9(9)
C12	6205(2)	2820(2)	6585.5(18)	45.6(10)
C13	6582(2)	3466(2)	6718.2(17)	43.6(9)
C14	6664(2)	3895.1(18)	6248.9(15)	33.9(8)
C15	5648(2)	2684.5(18)	4826.4(17)	39.1(8)
C16	4780(3)	2838(3)	4531(2)	72.5(14)
C17	5807(3)	1885(2)	4782(2)	61.8(12)
C18	7086(2)	4606.5(19)	6403.3(17)	47.3(10)
C19	7935(3)	4502(3)	6732(4)	122(3)
C20	6738(5)	5090(3)	6775(3)	116(3)
C21	7480.9(18)	4370.7(16)	4188.2(15)	27.4(7)
C22	8102(2)	4855.3(17)	4371.2(17)	36.2(8)
C23	8592(2)	4830(2)	4030(2)	48.3(10)
C24	8464(2)	4356(2)	3548.2(19)	51.1(11)
C25	7842(2)	3892(2)	3380.9(17)	42.8(9)
C26	7324(2)	3887.9(18)	3700.2(15)	33.1(8)
C27	8252(2)	5377.2(19)	4906.0(19)	47.4(10)
C28	8963(4)	5161(4)	5456(3)	133(3)

C29	8322(4)	6136(3)	4694(3)	125(3)
C30	6645(2)	3367.1(19)	3514.8(17)	40.5(9)
C31	6917(2)	2625(2)	3784(2)	54.5(11)
C32	6199(3)	3334(3)	2807.8(19)	68.6(13)
Cl1	7228.5(10)	6537.9(12)	5751.8(10)	140.7(8)
Cl2	7296.3(10)	7481.4(9)	6751.2(6)	98.2(5)
C33	7780(3)	7048(3)	6325(3)	106(2)
P1	10021.3(16)	6179.3(7)	7579.6(13)	29.9(5)
F1	10867.7(18)	5897.4(18)	7702(2)	97(2)
F2	9864(2)	5508.4(14)	7931(2)	78(2)
F3	9174.6(18)	6460.8(18)	7457(2)	94(2)
F4	10179(3)	6850.0(14)	7228.2(17)	102(2)
F5	10332(3)	6606.0(17)	8212.8(14)	85.6(19)
F6	9710(3)	5753.0(18)	6946.2(17)	88(2)
C34	10070(10)	4081(3)	7318(6)	103(6)
Cl3	9849(3)	3552(3)	7869(3)	141(2)
Cl4	10547(3)	3534(3)	6941(3)	146(3)

Table 3 Anisotropic Displacement Parameters ($Å^2×10^3$). The Anisotropic displacement factor exponent takes the form: $-2\pi^2[h^2a^{*2}U_{11}+2hka^*b^*U_{12}+\ldots]$.

Atom	U_{11}	U_{22}	U_{33}	U_{23}	U_{13}	U_{12}
Ag1	24.74(17)	23.42(15)	32.63(18)	5.66(16)	17.56(13)	7.50(16)
C1	24.5(16)	21.7(15)	28.3(16)	1.9(13)	11.4(13)	5.6(13)
N1	23.9(14)	24.6(12)	25.6(13)	2.3(10)	12.2(11)	5.6(11)
C2	22.1(15)	24.9(16)	29.0(16)	0.1(11)	12.8(13)	4.8(12)
N2	24.0(14)	24.4(12)	32.0(14)	2.6(11)	15.0(12)	5.7(11)
C3	21.8(16)	28.0(16)	37.4(19)	8.7(14)	15.6(14)	5.6(13)
N3	24.3(14)	24.8(13)	30.2(14)	5.3(11)	16.0(12)	7.0(11)
C4	37(2)	30.3(17)	44(2)	6.7(15)	19.0(17)	5.6(15)
C5	39(2)	27.1(18)	73(3)	12.6(18)	20(2)	7.7(16)
C6	48(3)	46(2)	65(3)	34(2)	21(2)	9.8(19)
C7	52(3)	63(3)	44(2)	23(2)	24(2)	13(2)
C8	42(2)	39(2)	42(2)	10.7(17)	21.1(17)	13.9(17)
C9	25.2(17)	24.9(15)	32.3(17)	8.5(13)	15.4(14)	11.5(13)
C10	26.0(18)	27.1(16)	41(2)	6.3(14)	14.4(15)	5.5(14)
C11	37(2)	35.8(19)	60(3)	14.4(18)	26.3(19)	7.2(16)
C12	51(2)	49(2)	50(2)	23.2(19)	34(2)	17(2)
C13	53(2)	48(2)	37(2)	7.6(17)	25.1(19)	16.2(19)
C14	38(2)	37.1(18)	32.1(18)	5.8(15)	18.9(16)	11.4(16)
C15	34(2)	29.9(17)	49(2)	2.1(16)	10.8(17)	-0.4(15)
C16	48(3)	75(3)	72(3)	-14(3)	-4(2)	9(3)

C17	74(3)	37(2)	69(3)	-8(2)	19(3)	8(2)
C18	66(3)	39(2)	38(2)	-6.0(17)	20(2)	-5(2)
C19	65(4)	78(4)	172(7)	11(4)	-18(4)	-23(3)
C20	217(8)	56(3)	124(5)	-37(3)	119(6)	-22(4)
C21	23.5(17)	29.4(16)	36.5(18)	8.0(14)	19.4(14)	11.4(14)
C22	30.9(18)	36(2)	48(2)	9.8(15)	21.9(16)	7.6(15)
C23	38(2)	52(2)	67(3)	8.6(19)	33(2)	-0.3(17)
C24	50(3)	64(3)	59(3)	19(2)	42(2)	19(2)
C25	47(2)	52(2)	38(2)	4.4(17)	26.3(18)	17(2)
C26	31.2(19)	37.6(18)	35.1(19)	5.1(15)	17.5(15)	14.1(15)
C27	44(2)	40(2)	67(3)	-9.6(19)	29(2)	-5.1(18)
C28	103(5)	154(6)	92(4)	-69(4)	-22(4)	44(5)
C29	197(8)	51(3)	183(7)	-28(4)	138(6)	-42(4)
C30	38(2)	46(2)	43(2)	-7.2(17)	20.9(17)	7.2(17)
C31	48(3)	40(2)	85(3)	-2(2)	34(2)	3.0(19)
C32	71(3)	79(3)	47(3)	-15(2)	11(2)	-5(3)
Cl1	79.4(12)	178.4(19)	147.9(16)	-84.5(15)	22.1(11)	8.9(12)
Cl2	97.3(12)	135.5(13)	59.7(8)	-18.2(8)	25.9(8)	-24.9(10)
C33	67(4)	102(5)	144(6)	-29(4)	31(4)	-16(3)
P1	36.5(8)	23.9(6)	34.3(16)	-2.0(10)	18.8(9)	0.1(14)
F1	54(3)	119(5)	133(6)	6(5)	52(4)	27(4)
F2	134(6)	39(3)	102(5)	6(3)	90(5)	-3(3)
F3	54(4)	139(6)	85(4)	7(4)	20(3)	52(4)
F4	189(8)	38(3)	117(6)	23(3)	101(6)	-8(4)
F5	105(5)	82(4)	71(4)	-37(3)	34(3)	-24(4)
F6	114(6)	98(5)	47(3)	-43(4)	24(4)	-24(4)
C34	85(9)	51(5)	125(18)	-6(6)	-18(10)	20(7)
Cl3	120(5)	89(3)	175(6)	32(3)	6(3)	10(3)
Cl4	162(6)	114(3)	102(3)	-45(3)	-23(3)	45(4)

Table 4 Bond Lengths.

Atom	Atom	Length/Å	Atom	Atom	Length/Å
Ag1	C1[1]	2.080(3)	C15	C17	1.531(5)
Ag1	C1	2.080(3)	C18	C19	1.483(6)
C1	N1	1.365(4)	C18	C20	1.534(6)
C1	C2	1.385(4)	C21	C22	1.398(5)
N1	N2	1.335(3)	C21	C26	1.384(4)
N1	C9	1.456(4)	C22	C23	1.399(5)
C2	C3	1.470(4)	C22	C27	1.513(5)
C2	N3	1.368(4)	C23	C24	1.368(5)
N2	N3	1.327(3)	C24	C25	1.375(5)

C3	C4	1.388(4)	C25	C26	1.403(4)
C3	C8	1.385(4)	C26	C30	1.518(5)
N3	C21	1.458(4)	C27	C28	1.508(7)
C4	C5	1.386(4)	C27	C29	1.518(6)
C5	C6	1.381(5)	C30	C31	1.525(5)
C6	C7	1.368(6)	C30	C32	1.532(5)
C7	C8	1.389(5)	Cl1	C33	1.645(6)
C9	C10	1.396(4)	Cl2	C33	1.745(6)
C9	C14	1.390(4)	P1	F1	1.5731
C10	C11	1.396(4)	P1	F2	1.5728
C10	C15	1.513(5)	P1	F3	1.5732
C11	C12	1.363(5)	P1	F4	1.5728
C12	C13	1.369(5)	P1	F5	1.5728
C13	C14	1.395(5)	P1	F6	1.5728
C14	C18	1.514(5)	C34	Cl3	1.7668
C15	C16	1.521(5)	C34	Cl4	1.7665

[1]1-X,1-Y,1-Z

Table 5 Bond Angles.

Atom	Atom	Atom	Angle/˚	Atom	Atom	Atom	Angle/˚
C1[1]	Ag1	C1	180.00(14)	C19	C18	C14	111.2(4)
N1	C1	Ag1	126.8(2)	C19	C18	C20	111.8(5)
N1	C1	C2	102.0(2)	C22	C21	N3	117.9(3)
C2	C1	Ag1	131.2(2)	C26	C21	N3	117.2(3)
C1	N1	C9	126.6(2)	C26	C21	C22	124.9(3)
N2	N1	C1	115.7(2)	C21	C22	C23	115.8(3)
N2	N1	C9	117.7(2)	C21	C22	C27	123.2(3)
C1	C2	C3	129.3(3)	C23	C22	C27	120.9(3)
N3	C2	C1	107.3(2)	C24	C23	C22	121.3(4)
N3	C2	C3	123.3(3)	C23	C24	C25	120.9(3)
N3	N2	N1	102.6(2)	C24	C25	C26	121.0(3)
C4	C3	C2	118.6(3)	C21	C26	C25	116.0(3)
C8	C3	C2	122.5(3)	C21	C26	C30	123.5(3)
C8	C3	C4	119.0(3)	C25	C26	C30	120.5(3)
C2	N3	C21	129.2(2)	C22	C27	C29	110.5(4)
N2	N3	C2	112.3(2)	C28	C27	C22	110.8(3)
N2	N3	C21	118.4(2)	C28	C27	C29	111.6(5)
C5	C4	C3	120.6(3)	C26	C30	C31	110.5(3)
C6	C5	C4	119.8(3)	C26	C30	C32	113.1(3)
C7	C6	C5	120.0(3)	C31	C30	C32	111.4(3)
C6	C7	C8	120.6(4)	Cl1	C33	Cl2	115.1(3)

C3	C8	C7	120.1(3)	F1	P1	F3	180.0
C10	C9	N1	118.1(3)	F2	P1	F1	90.0
C14	C9	N1	117.4(3)	F2	P1	F3	90.0
C14	C9	C10	124.5(3)	F2	P1	F5	90.0
C9	C10	C15	122.5(3)	F4	P1	F1	90.0
C11	C10	C9	115.7(3)	F4	P1	F2	180.0
C11	C10	C15	121.8(3)	F4	P1	F3	90.0
C12	C11	C10	121.7(3)	F4	P1	F5	90.0
C11	C12	C13	120.6(3)	F4	P1	F6	90.0
C12	C13	C14	121.5(4)	F5	P1	F1	90.0
C9	C14	C13	116.0(3)	F5	P1	F3	90.0
C9	C14	C18	123.2(3)	F6	P1	F1	90.0
C13	C14	C18	120.9(3)	F6	P1	F2	90.0
C10	C15	C16	110.9(3)	F6	P1	F3	90.0
C10	C15	C17	112.4(3)	F6	P1	F5	180.0
C16	C15	C17	110.5(3)	Cl4	C34	Cl3	108.3
C14	C18	C20	111.3(4)				

[1]1-X,1-Y,1-Z

Table 6 Torsion Angles.

A	B	C	D	Angle/˚	A	B	C	D	Angle/˚
Ag1	C1	N1	N2	178.6(2)	C5	C6	C7	C8	-1.3(6)
Ag1	C1	N1	C9	-3.1(4)	C6	C7	C8	C3	0.7(6)
Ag1	C1	C2	C3	5.1(5)	C8	C3	C4	C5	-1.6(5)
Ag1	C1	C2	N3	-178.4(2)	C9	N1	N2	N3	-178.7(2)
C1	N1	N2	N3	-0.3(3)	C9	C10	C11	C12	-1.4(5)
C1	N1	C9	C10	99.4(4)	C9	C10	C15	C16	-97.3(4)
C1	N1	C9	C14	-81.3(4)	C9	C10	C15	C17	138.5(3)
C1	C2	C3	C4	41.7(5)	C9	C14	C18	C19	-107.7(5)
C1	C2	C3	C8	-137.6(4)	C9	C14	C18	C20	126.9(4)
C1	C2	N3	N2	0.0(3)	C10	C9	C14	C13	-0.2(5)
C1	C2	N3	C21	177.8(3)	C10	C9	C14	C18	178.4(3)
N1	C1	C2	C3	-176.7(3)	C10	C11	C12	C13	0.3(5)
N1	C1	C2	N3	-0.2(3)	C11	C10	C15	C16	81.2(4)
N1	N2	N3	C2	0.2(3)	C11	C10	C15	C17	-43.0(5)
N1	N2	N3	C21	-177.9(3)	C11	C12	C13	C14	1.0(6)
N1	C9	C10	C11	-179.3(3)	C12	C13	C14	C9	-1.0(5)
N1	C9	C10	C15	-0.8(4)	C12	C13	C14	C18	-179.7(3)
N1	C9	C14	C13	-179.5(3)	C13	C14	C18	C19	70.9(5)
N1	C9	C14	C18	-0.9(5)	C13	C14	C18	C20	-54.5(5)
C2	C1	N1	N2	0.3(3)	C14	C9	C10	C11	1.4(5)

C2	C1	N1	C9	178.6(3)	C14	C9	C10	C15	179.9(3)
C2	C3	C4	C5	179.1(3)	C15	C10	C11	C12	-180.0(3)
C2	C3	C8	C7	179.9(3)	C21	C22	C23	C24	-0.1(5)
C2	N3	C21	C22	82.0(4)	C21	C22	C27	C28	108.8(5)
C2	N3	C21	C26	-96.1(4)	C21	C22	C27	C29	-126.9(4)
N2	N1	C9	C10	-82.4(3)	C21	C26	C30	C31	-99.4(4)
N2	N1	C9	C14	97.0(3)	C21	C26	C30	C32	135.0(4)
N2	N3	C21	C22	-100.4(3)	C22	C21	C26	C25	0.9(5)
N2	N3	C21	C26	81.5(4)	C22	C21	C26	C30	179.8(3)
C3	C2	N3	N2	176.8(3)	C22	C23	C24	C25	0.5(6)
C3	C2	N3	C21	-5.4(5)	C23	C22	C27	C28	-70.8(6)
C3	C4	C5	C6	1.1(6)	C23	C22	C27	C29	53.5(5)
N3	C2	C3	C4	-134.3(3)	C23	C24	C25	C26	-0.2(6)
N3	C2	C3	C8	46.4(5)	C24	C25	C26	C21	-0.4(5)
N3	C21	C22	C23	-178.6(3)	C24	C25	C26	C30	-179.4(3)
N3	C21	C22	C27	1.8(5)	C25	C26	C30	C31	79.5(4)
N3	C21	C26	C25	178.9(3)	C25	C26	C30	C32	-46.1(5)
N3	C21	C26	C30	-2.2(5)	C26	C21	C22	C23	-0.7(5)
C4	C3	C8	C7	0.7(5)	C26	C21	C22	C27	179.7(3)
C4	C5	C6	C7	0.3(6)	C27	C22	C23	C24	179.5(4)

Table 7 Hydrogen Atom Coordinates (Å×10^4) and Isotropic Displacement Parameters (Å^2×10^3).

Atom	*x*	*y*	*z*	U(eq)
H4	5946.87	6136.58	4616.46	43
H5	5660.37	7134.7	3959.67	56
H6	5647.07	7030.67	2945.1	64
H7	5906.96	5937.02	2587.88	61
H8	6227.99	4941.39	3248.32	48
H11	5647.15	2122.2	5906.14	50
H12	6150.44	2542.12	6913.34	55
H13	6791.74	3625.94	7139.08	52
H15	5910.37	2951.08	4580.96	47
H16A	4501.9	2555.26	4743	109
H16B	4592.19	2708.45	4087.92	109
H16C	4686.69	3349.43	4572.76	109
H17A	6366.65	1793.19	4982.56	93
H17B	5631.98	1742.45	4342	93
H17C	5525.05	1606.37	4993.26	93
H18	7008.77	4853.82	5999.26	57
H19A	8028.36	4232.08	7117.9	183

H19B	8191.83	4969.87	6832.1	183
H19C	8145.27	4234.54	6461.59	183
H20A	6178.12	5144.31	6545.06	175
H20B	6988.93	5561.63	6833.82	175
H20C	6826.51	4872.73	7183.04	175
H23	9022.7	5148.27	4133.85	58
H24	8808.53	4348.12	3326.18	61
H25	7763.35	3568.73	3043.98	51
H27	7793.87	5361.37	5040.5	57
H28A	8844.2	4734.05	5653.72	199
H28B	9115.51	5554.17	5759.34	199
H28C	9390.3	5053.92	5312.83	199
H29A	7839.24	6268.7	4353.27	187
H29B	8758.05	6161.98	4547.85	187
H29C	8413.95	6467.12	5044.77	187
H30	6272.23	3542.91	3708.2	49
H31A	7287.74	2436.64	3606.77	82
H31B	6468.72	2302.69	3680.42	82
H31C	7171.42	2659.5	4239.23	82
H32A	6019.07	3815.34	2650.44	103
H32B	5750.41	3013.85	2718.07	103
H32C	6543.73	3151.18	2602.8	103
H33A	8029.78	7415.59	6149.73	127
H33B	8199.7	6748.43	6615.68	127
H34A	9585.8	4279.49	7007.58	123
H34B	10411.07	4485.44	7530.71	123

Table 8 Atomic Occupancy.

Atom	***Occupancy***	**Atom**	***Occupancy***	**Atom**	***Occupancy***
P1	0.5	F1	0.5	F2	0.5
F3	0.5	F4	0.5	F5	0.5
F6	0.5	C34	0.5	H34A	0.5
H34B	0.5	Cl3	0.5	Cl4	0.5

Appendix K: Crystallographic data for complex **11.**

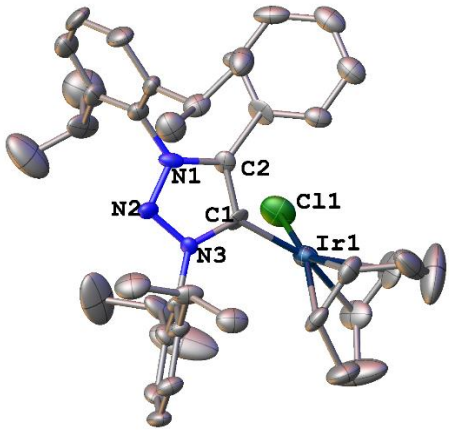

Table 1 Crystal data.

Empirical formula	$C_{40}H_{51}ClIrN_3$
Formula weight	801.48
Temperature/K	173.15
Crystal system	monoclinic
Space group	$P2_1/n$
a/Å	10.4226(12)
b/Å	18.528(2)
c/Å	20.536(3)
α/°	90
β/°	91.978(4)
γ/°	90
Volume/Å^3	3963.4(8)
Z	4
ρ_{calc}g/cm^3	1.343
μ/mm^{-1}	3.465
F(000)	1624.0
Crystal size/mm^3	0.29 × 0.183 × 0.07
Radiation	MoKα (λ = 0.71073)
2Θ range for data collection/°	5.886 to 51.998
Index ranges	-12 ≤ h ≤ 11, -22 ≤ k ≤ 22, -25 ≤ l ≤ 25
Reflections collected	35174
Independent reflections	7769 [R_{int} = 0.0899, R_{sigma} = 0.0892]
Data/restraints/parameters	7769/12/414
Goodness-of-fit on F^2	1.054
Final R indexes [I>=2σ (I)]	R_1 = 0.0683, wR_2 = 0.1372
Final R indexes [all data]	R_1 = 0.1128, wR_2 = 0.1544

Largest diff. peak/hole / e $Å^{-3}$	2.87/-1.78

Table 2 Fractional Atomic Coordinates ($\times 10^4$) and Equivalent Isotropic Displacement Parameters ($Å^2 \times 10^3$). U_{eq} is defined as 1/3 of the trace of the orthogonalised U_{IJ} tensor.

Atom	*x*	*y*	*z*	U(eq)
C1	4162(8)	2395(5)	1960(4)	26.3(14)
C2	4630(7)	2837(5)	1458(4)	27.4(12)
C3	5715(8)	3354(5)	1488(4)	28.5(14)
C4	5958(9)	3722(5)	2069(5)	33(2)
C5	6917(9)	4238(5)	2100(6)	43(3)
C6	7622(10)	4390(5)	1561(6)	48(3)
C7	7379(9)	4027(5)	989(5)	41(3)
C8	6442(9)	3503(5)	949(5)	36(2)
C9	3903(9)	3031(5)	272(4)	32(2)
C10	3436(9)	3729(5)	198(4)	30(2)
C11	3563(10)	4024(6)	-424(4)	43(3)
C12	4071(11)	3640(6)	-920(5)	49(3)
C13	4514(11)	2952(6)	-821(5)	49(3)
C14	4414(10)	2612(5)	-222(5)	43(3)
C15	2876(9)	4160(5)	735(4)	33(2)
C16	3569(11)	4867(5)	864(5)	48(3)
C17	1445(10)	4282(6)	582(6)	53(3)
C18	4904(12)	1836(6)	-98(6)	57(4)
C19	6274(14)	1706(8)	-287(8)	90(5)
C20	4010(14)	1301(8)	-435(10)	107(6)
C21	2227(8)	1546(4)	1912(4)	23.6(18)
C22	1011(8)	1808(5)	2043(4)	27(2)
C23	170(9)	1332(5)	2320(4)	34(2)
C24	530(10)	630(5)	2464(4)	37(2)
C25	1734(10)	388(5)	2307(5)	36(2)
C26	2633(9)	842(4)	2034(4)	28(2)
C27	593(9)	2569(5)	1870(5)	35(2)
C28	-71(10)	2951(5)	2430(5)	45(3)
C29	-297(11)	2556(6)	1260(6)	55(3)
C30	3898(10)	554(5)	1835(5)	45(3)
C31	3746(14)	183(9)	1181(8)	108(7)
C32	4552(15)	63(8)	2343(10)	113(7)
C33	5457(11)	1627(7)	3772(5)	57(3)
C34	6001(13)	2316(8)	3800(5)	69(4)
C35	5470(20)	2934(10)	4204(8)	119(7)

C36	4398(14)	3332(7)	3898(7)	78(4)
C37	3749(10)	2964(6)	3330(5)	44(3)
C38	3151(9)	2273(6)	3343(4)	37(2)
C39	3126(13)	1811(7)	3966(6)	63(3)
C40	4271(14)	1402(10)	4115(8)	110(7)
Cl1	6709(2)	1702.3(16)	2379.4(15)	55.5(7)
Ir1	4910.3(4)	2198.0(2)	2877.5(2)	33.77(14)
N1	3863(7)	2703(3)	919(3)	25.0(16)
N2	2948(7)	2225(4)	1018(3)	27.0(16)
N3	3136(6)	2056(3)	1646(3)	21.4(15)

Table 3 Anisotropic Displacement Parameters ($Å^2×10^3$). The Anisotropic displacement factor exponent takes the form: $-2\pi^2[h^2a^{*2}U_{11}+2hka^*b^*U_{12}+…]$.

Atom	U_{11}	U_{22}	U_{33}	U_{23}	U_{13}	U_{12}
C1	12(3)	37(3)	31(3)	-4(3)	10(2)	9(3)
C2	11(2)	38(3)	34(3)	-3(3)	6(2)	8(2)
C3	11(3)	38(3)	36(3)	-3(3)	3(2)	7(3)
C4	23(5)	31(5)	46(6)	7(4)	7(4)	4(4)
C5	31(6)	35(5)	63(7)	1(5)	-1(5)	0(5)
C6	36(6)	23(5)	84(9)	7(5)	-5(6)	0(5)
C7	28(6)	38(5)	58(7)	22(5)	12(5)	3(5)
C8	32(5)	29(5)	47(6)	5(4)	13(4)	3(4)
C9	30(5)	38(5)	29(5)	0(4)	14(4)	-7(4)
C10	28(5)	42(5)	22(5)	-4(4)	2(4)	-10(4)
C11	51(7)	52(6)	28(5)	10(5)	8(5)	-10(5)
C12	56(7)	72(8)	19(5)	7(5)	5(5)	-13(6)
C13	50(7)	61(8)	37(6)	-17(5)	20(5)	-13(6)
C14	48(7)	48(7)	35(6)	-15(5)	19(5)	-12(5)
C15	36(6)	31(5)	30(5)	7(4)	4(4)	9(4)
C16	67(8)	37(6)	38(6)	-6(5)	3(5)	-4(5)
C17	40(7)	53(7)	66(8)	-10(6)	11(5)	5(5)
C18	77(9)	39(6)	59(7)	-21(5)	50(7)	-8(6)
C19	73(10)	89(11)	111(12)	0(9)	24(9)	19(9)
C20	67(10)	63(9)	191(19)	-48(11)	11(11)	2(8)
C21	20(5)	28(4)	24(4)	-1(4)	8(3)	-3(4)
C22	23(5)	37(5)	21(4)	7(4)	5(4)	-1(4)
C23	32(5)	38(5)	33(5)	9(4)	11(4)	1(4)
C24	45(6)	40(6)	28(5)	10(4)	3(4)	-17(5)
C25	48(7)	18(4)	44(6)	8(4)	4(5)	0(4)
C26	28(5)	22(4)	35(5)	-4(4)	2(4)	0(4)
C27	24(5)	32(5)	49(6)	12(4)	15(5)	8(4)

C28	46(7)	30(6)	61(7)	4(5)	13(5)	7(5)
C29	56(8)	51(6)	57(7)	20(6)	3(6)	14(6)
C30	34(6)	25(5)	78(8)	-14(5)	15(5)	1(4)
C31	55(9)	122(13)	149(15)	-92(12)	30(9)	4(9)
C32	71(11)	59(9)	210(20)	60(11)	16(12)	29(8)
C33	42(7)	76(8)	52(7)	22(6)	-24(5)	-1(6)
C34	69(9)	102(11)	34(6)	8(7)	-36(6)	0(8)
C35	159(19)	116(15)	78(11)	-39(10)	-54(12)	26(14)
C36	80(10)	66(8)	88(10)	-30(8)	30(8)	-34(8)
C37	53(7)	51(7)	29(5)	-7(5)	13(5)	13(5)
C38	29(5)	60(7)	22(4)	6(5)	2(4)	2(5)
C39	74(9)	69(8)	45(7)	21(6)	9(6)	-10(7)
C40	71(11)	139(15)	119(14)	92(12)	14(9)	8(10)
Cl1	23.7(14)	60.0(17)	83(2)	0.8(15)	6.0(13)	10.9(13)
Ir1	25.8(2)	35.4(2)	40.0(2)	5.6(2)	-0.67(13)	-0.9(2)
N1	23(4)	17(4)	36(4)	4(3)	11(3)	-1(3)
N2	30(4)	29(4)	23(4)	-2(3)	13(3)	-4(4)
N3	16(4)	26(4)	23(4)	-2(3)	4(3)	-1(3)

Table 4 Bond Lengths.

Atom	Atom	Length/Å	Atom	Atom	Length/Å
C1	C2	1.417(12)	C21	N3	1.457(10)
C1	Ir1	2.046(9)	C22	C23	1.379(12)
C1	N3	1.381(11)	C22	C27	1.515(12)
C2	C3	1.482(12)	C23	C24	1.384(13)
C2	N1	1.365(11)	C24	C25	1.381(13)
C3	C4	1.389(13)	C25	C26	1.391(12)
C3	C8	1.391(12)	C26	C30	1.493(12)
C4	C5	1.383(13)	C27	C28	1.535(13)
C5	C6	1.379(15)	C27	C29	1.534(15)
C6	C7	1.371(15)	C30	C31	1.512(17)
C7	C8	1.376(13)	C30	C32	1.527(18)
C9	C10	1.387(13)	C33	C34	1.396(17)
C9	C14	1.397(13)	C33	C40	1.503(17)
C9	N1	1.464(11)	C33	Ir1	2.179(10)
C10	C11	1.400(12)	C34	C35	1.53(2)
C10	C15	1.496(12)	C34	Ir1	2.187(10)
C11	C12	1.363(14)	C35	C36	1.46(2)
C12	C13	1.369(15)	C36	C37	1.493(16)
C13	C14	1.389(15)	C37	C38	1.426(14)
C14	C18	1.543(15)	C37	Ir1	2.103(9)

C15	C16	1.514(13)	C38	C39	1.539(13)
C15	C17	1.530(14)	C38	Ir1	2.102(9)
C18	C19	1.511(17)	C39	C40	1.438(18)
C18	C20	1.511(18)	Cl1	Ir1	2.353(3)
C21	C22	1.392(11)	N1	N2	1.322(9)
C21	C26	1.392(12)	N2	N3	1.335(9)

Table 5 Bond Angles.

Atom	Atom	Atom	Angle/˚	Atom	Atom	Atom	Angle/˚
C2	C1	Ir1	130.0(6)	C22	C27	C28	112.7(8)
N3	C1	C2	101.7(7)	C22	C27	C29	109.7(8)
N3	C1	Ir1	127.9(6)	C29	C27	C28	110.1(8)
C1	C2	C3	128.7(8)	C26	C30	C31	109.8(9)
N1	C2	C1	106.1(7)	C26	C30	C32	113.8(10)
N1	C2	C3	125.2(8)	C31	C30	C32	111.5(12)
C4	C3	C2	118.0(7)	C34	C33	C40	125.0(14)
C4	C3	C8	119.8(9)	C34	C33	Ir1	71.7(6)
C8	C3	C2	122.1(8)	C40	C33	Ir1	109.5(8)
C5	C4	C3	119.3(9)	C33	C34	C35	123.7(15)
C6	C5	C4	120.5(10)	C33	C34	Ir1	71.0(6)
C7	C6	C5	120.0(10)	C35	C34	Ir1	111.0(9)
C6	C7	C8	120.4(9)	C36	C35	C34	115.5(12)
C7	C8	C3	119.9(9)	C35	C36	C37	115.1(11)
C10	C9	C14	125.5(9)	C36	C37	Ir1	113.6(8)
C10	C9	N1	117.7(7)	C38	C37	C36	125.6(10)
C14	C9	N1	116.8(8)	C38	C37	Ir1	70.1(5)
C9	C10	C11	114.8(8)	C37	C38	C39	122.4(9)
C9	C10	C15	124.2(8)	C37	C38	Ir1	70.2(5)
C11	C10	C15	121.0(9)	C39	C38	Ir1	112.4(7)
C12	C11	C10	122.0(10)	C40	C39	C38	115.6(10)
C11	C12	C13	120.8(9)	C39	C40	C33	116.3(11)
C12	C13	C14	121.2(9)	C1	Ir1	C33	160.5(4)
C9	C14	C18	122.1(9)	C1	Ir1	C34	161.8(4)
C13	C14	C9	115.6(9)	C1	Ir1	C37	94.5(4)
C13	C14	C18	122.2(9)	C1	Ir1	C38	95.5(3)
C10	C15	C16	113.3(8)	C1	Ir1	Cl1	87.3(2)
C10	C15	C17	109.3(8)	C33	Ir1	C34	37.3(4)
C16	C15	C17	111.4(8)	C33	Ir1	Cl1	89.3(3)
C19	C18	C14	114.6(10)	C34	Ir1	Cl1	91.0(4)
C20	C18	C14	109.9(11)	C37	Ir1	C33	95.4(5)
C20	C18	C19	110.6(10)	C37	Ir1	C34	80.8(5)

C22	C21	C26	124.3(8)	C37	Ir1	Cl1	159.2(3)
C22	C21	N3	117.1(7)	C38	Ir1	C33	81.7(4)
C26	C21	N3	118.6(7)	C38	Ir1	C34	92.0(5)
C21	C22	C27	122.3(7)	C38	Ir1	C37	39.6(4)
C23	C22	C21	117.0(8)	C38	Ir1	Cl1	160.8(3)
C23	C22	C27	120.7(8)	C2	N1	C9	128.8(7)
C22	C23	C24	121.2(9)	N2	N1	C2	113.8(7)
C25	C24	C23	119.9(8)	N2	N1	C9	117.4(7)
C24	C25	C26	121.8(8)	N1	N2	N3	102.9(6)
C21	C26	C30	123.4(8)	C1	N3	C21	128.5(7)
C25	C26	C21	115.8(8)	N2	N3	C1	115.5(6)
C25	C26	C30	120.5(8)	N2	N3	C21	116.0(6)

Table 6 Torsion Angles.

A	B	C	D	Angle/˚	A	B	C	D	Angle/˚
C1	C2	C3	C4	-33.3(13)	C22	C21	N3	N2	-75.6(9)
C1	C2	C3	C8	150.0(9)	C22	C23	C24	C25	-2.3(14)
C1	C2	N1	C9	178.0(7)	C23	C22	C27	C28	48.9(12)
C1	C2	N1	N2	0.4(9)	C23	C22	C27	C29	-74.2(11)
C2	C1	N3	C21	-177.7(7)	C23	C24	C25	C26	3.1(15)
C2	C1	N3	N2	1.5(9)	C24	C25	C26	C21	-1.8(14)
C2	C3	C4	C5	-176.3(8)	C24	C25	C26	C30	-176.4(9)
C2	C3	C8	C7	175.1(8)	C25	C26	C30	C31	80.0(13)
C2	N1	N2	N3	0.5(8)	C25	C26	C30	C32	-45.7(14)
C3	C2	N1	C9	-1.5(13)	C26	C21	C22	C23	0.9(13)
C3	C2	N1	N2	-179.1(7)	C26	C21	C22	C27	-176.9(8)
C3	C4	C5	C6	0.4(14)	C26	C21	N3	C1	-74.7(10)
C4	C3	C8	C7	-1.5(13)	C26	C21	N3	N2	106.1(9)
C4	C5	C6	C7	-0.3(15)	C27	C22	C23	C24	178.2(9)
C5	C6	C7	C8	-0.8(15)	C33	C34	C35	C36	-82.4(19)
C6	C7	C8	C3	1.6(14)	C34	C33	C40	C39	57(2)
C8	C3	C4	C5	0.4(13)	C34	C35	C36	C37	16(2)
C9	C10	C11	C12	2.0(14)	C35	C36	C37	C38	59.0(17)
C9	C10	C15	C16	121.8(10)	C35	C36	C37	Ir1	-22.8(16)
C9	C10	C15	C17	-113.4(10)	C36	C37	C38	C39	-0.8(16)
C9	C14	C18	C19	-124.8(12)	C36	C37	C38	Ir1	-105.4(11)
C9	C14	C18	C20	109.9(13)	C37	C38	C39	C40	-81.4(16)
C9	N1	N2	N3	-177.4(6)	C38	C39	C40	C33	17(2)
C10	C9	C14	C13	3.7(15)	C40	C33	C34	C35	1.7(18)
C10	C9	C14	C18	-179.5(10)	C40	C33	C34	Ir1	-101.4(11)
C10	C9	N1	C2	-74.9(11)	Ir1	C1	C2	C3	-8.4(13)

C10	C9	N1	N2	102.7(9)	Ir1	C1	C2	N1	172.1(6)
C10	C11	C12	C13	-1.9(17)	Ir1	C1	N3	C21	8.9(11)
C11	C10	C15	C16	-56.0(12)	Ir1	C1	N3	N2	-171.8(5)
C11	C10	C15	C17	68.8(11)	Ir1	C33	C34	C35	103.1(12)
C11	C12	C13	C14	2.6(17)	Ir1	C33	C40	C39	-23.4(19)
C12	C13	C14	C9	-3.3(16)	Ir1	C34	C35	C36	-2(2)
C12	C13	C14	C18	180.0(11)	Ir1	C37	C38	C39	104.6(9)
C13	C14	C18	C19	51.7(16)	Ir1	C38	C39	C40	-1.3(16)
C13	C14	C18	C20	-73.5(14)	N1	C2	C3	C4	146.1(8)
C14	C9	C10	C11	-3.1(14)	N1	C2	C3	C8	-30.6(13)
C14	C9	C10	C15	179.0(9)	N1	C9	C10	C11	176.8(8)
C14	C9	N1	C2	105.0(10)	N1	C9	C10	C15	-1.1(13)
C14	C9	N1	N2	-77.4(10)	N1	C9	C14	C13	-176.2(9)
C15	C10	C11	C12	180.0(10)	N1	C9	C14	C18	0.6(14)
C21	C22	C23	C24	0.4(13)	N1	N2	N3	C1	-1.3(8)
C21	C22	C27	C28	-133.4(9)	N1	N2	N3	C21	178.0(6)
C21	C22	C27	C29	103.5(10)	N3	C1	C2	C3	178.4(8)
C21	C26	C30	C31	-94.2(12)	N3	C1	C2	N1	-1.1(8)
C21	C26	C30	C32	140.1(11)	N3	C21	C22	C23	-177.4(8)
C22	C21	C26	C25	-0.2(13)	N3	C21	C22	C27	4.8(12)
C22	C21	C26	C30	174.2(9)	N3	C21	C26	C25	178.0(8)
C22	C21	N3	C1	103.7(10)	N3	C21	C26	C30	-7.6(13)

Table 7 Hydrogen Atom Coordinates (Å×10^4) and Isotropic Displacement Parameters (Å^2×10^3).

Atom	*x*	*y*	*z*	U(eq)
H4	5469.75	3620.92	2440.11	40
H5	7091.18	4489.36	2496.71	52
H6	8276.87	4746.84	1586.7	57
H7	7859.61	4137.11	616.67	49
H8	6292.99	3244.66	554.42	43
H11	3287.33	4505.7	-503	52
H12	4119.14	3853.59	-1338.81	59
H13	4895.94	2701.91	-1168.26	59
H15	2952.44	3865.61	1141.98	39
H16A	4469.57	4769.31	986.28	71
H16B	3161.95	5123.22	1219.12	71
H16C	3524.78	5164.37	469.15	71
H17A	1340.14	4597.64	200.39	79
H17B	1051.99	4510.02	956.7	79
H17C	1027.14	3817.94	490.2	79
H18	4866.36	1744.76	380.45	69

H19A	6347.58	1789.19	-755.6	136
H19B	6516.66	1207.35	-183.13	136
H19C	6845.86	2038.1	-44.75	136
H20A	3120.65	1418.06	-336.77	161
H20B	4214.56	812.96	-280.76	161
H20C	4115.82	1326.25	-907.23	161
H23	-670.61	1490.18	2413.57	41
H24	-50.42	314.83	2669.1	45
H25	1955.46	-102.3	2388.89	44
H27	1376.42	2853.12	1766.22	42
H28A	-852.81	2686.97	2533.69	68
H28B	-295.26	3444.64	2298.5	68
H28C	511.03	2964.24	2814.78	68
H29A	154.61	2338.8	897.72	82
H29B	-551.01	3050.28	1144.41	82
H29C	-1063.79	2270.61	1347.08	82
H30	4476.37	977.95	1775.85	54
H31A	3197.51	-243.22	1222.77	162
H31B	4590.58	34.41	1034.46	162
H31C	3350.6	516.78	863.43	162
H32A	4731.32	336.44	2743.87	170
H32B	5358.18	-119.92	2174.63	170
H32C	3984.75	-343.79	2435.47	170
H33	6091.05	1229.06	3712.7	69
H34	6953.6	2323.97	3757.49	83
H35A	5193.04	2735.49	4623.13	143
H35B	6179.34	3278.35	4302.58	143
H36A	4717.12	3806.49	3752.42	93
H36B	3753.33	3422.52	4231.1	93
H37	3318.12	3306.79	3015.79	53
H38	2374.7	2222.26	3046.84	44
H39A	2964.49	2133.1	4338.63	75
H39B	2394.19	1471.51	3923.49	75
H40A	4095.21	889.11	4008.85	132
H40B	4455.47	1430.95	4590.53	132

Table 8 Solvent masks information.

Number	X	Y	Z	Volume	Electron count	Content
1	0.000	0.000	0.000	237	89	
2	0.500	0.500	0.500	237	89	

Appendix L: Crystallographic data for complex **12**.

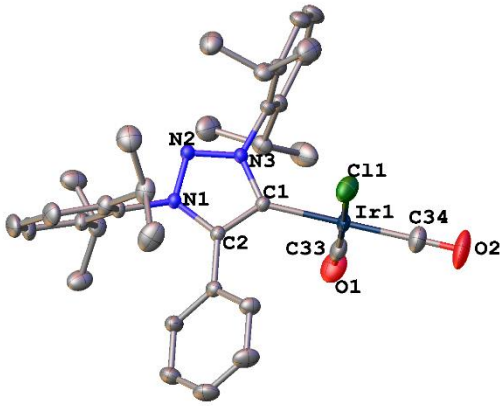

Table 1 Crystal data and structure refinement.

Empirical formula	$C_{34}H_{39}ClIrN_3O_2$
Formula weight	749.33
Temperature/K	173.15
Crystal system	triclinic
Space group	P-1
a/Å	10.5527(5)
b/Å	10.9468(4)
c/Å	15.1683(7)
α/°	97.9998(16)
β/°	96.8932(17)
γ/°	110.3337(15)
Volume/Å^3	1600.06(12)
Z	2
ρ_{calc}g/cm^3	1.555
μ/mm^{-1}	4.289
F(000)	748.0
Crystal size/mm^3	0.37 × 0.298 × 0.118
Radiation	MoKα (λ = 0.71073)
2Θ range for data collection/°	6.174 to 61.052
Index ranges	-15 ≤ h ≤ 15, -15 ≤ k ≤ 15, -21 ≤ l ≤ 21
Reflections collected	60672
Independent reflections	9753 [R_{int} = 0.0221, R_{sigma} = 0.0136]
Data/restraints/parameters	9753/0/378
Goodness-of-fit on F^2	1.086
Final R indexes [I>=2σ (I)]	R_1 = 0.0139, wR_2 = 0.0325
Final R indexes [all data]	R_1 = 0.0158, wR_2 = 0.0332
Largest diff. peak/hole / e Å^{-3}	0.60/-0.55

Table 2 Fractional Atomic Coordinates ($\times 10^4$) and Equivalent Isotropic Displacement Parameters ($Å^2 \times 10^3$). U_{eq} is defined as 1/3 of the trace of the orthogonalised U_{IJ} tensor.

Atom	*x*	*y*	*z*	U(eq)
C1	3557.7(12)	6191.7(12)	7755.2(8)	16.7(2)
C2	3317.3(12)	4929.9(11)	7945.2(8)	16.1(2)
C3	2496.2(13)	4244.6(12)	8574.7(8)	19.0(2)
C4	1220.1(13)	4324.7(14)	8622.2(9)	25.1(3)
C5	428.1(15)	3666.0(17)	9205.3(11)	33.8(3)
C6	899.7(17)	2927.0(17)	9735.3(11)	36.0(3)
C7	2169.8(18)	2854.9(16)	9697.3(11)	35.4(3)
C8	2974.3(15)	3511.6(14)	9118.5(10)	27.3(3)
C9	3943.6(12)	3007.4(11)	7250.1(8)	17.9(2)
C10	5086.0(14)	2775.1(13)	7640.2(9)	22.1(2)
C11	5010.7(17)	1464.5(15)	7470.1(10)	31.9(3)
C12	3855.7(18)	454.5(14)	6958.5(11)	34.8(3)
C13	2745.3(17)	725.1(14)	6593.5(11)	32.3(3)
C14	2762.2(14)	2018.8(13)	6716.6(9)	23.7(2)
C15	6353.4(14)	3857.6(14)	8221.5(10)	26.5(3)
C16	7590.3(17)	4109.1(19)	7744.7(11)	37.9(4)
C17	6688.8(16)	3520.2(19)	9146.3(10)	36.1(3)
C18	1551.3(14)	2299.4(14)	6277.8(11)	30.4(3)
C19	254.4(17)	1593.5(19)	6641.4(14)	45.2(4)
C20	1321.1(18)	1897.6(18)	5246.7(12)	41.4(4)
C21	4931.5(13)	7308.7(12)	6627.3(8)	19.3(2)
C22	6195.8(13)	8310.4(13)	7032.2(9)	22.6(2)
C23	6745.9(15)	9294.1(15)	6539.7(11)	30.5(3)
C24	6086.9(17)	9237.7(16)	5680.9(12)	35.1(3)
C25	4859.5(17)	8225.4(16)	5299.5(10)	32.1(3)
C26	4226.3(14)	7233.3(14)	5767.9(9)	23.6(2)
C27	7012.4(14)	8292.9(14)	7918.6(10)	25.8(3)
C28	7730(2)	9667.4(17)	8522.1(13)	46.6(4)
C29	8053.7(18)	7657(2)	7714.9(13)	43.4(4)
C30	2876.5(15)	6120.3(15)	5333.5(9)	27.6(3)
C31	3139.3(19)	5081.4(18)	4670.5(11)	38.7(4)
C32	1858.6(18)	6629(2)	4852.7(12)	41.6(4)
C33	4372.4(17)	8344.5(15)	9177.9(11)	31.6(3)
C34	2168.3(18)	8960.9(16)	8670.0(12)	36.8(3)
Cl1	967.9(4)	6723.4(5)	7075.4(3)	39.19(9)
Ir1	2883.4(2)	7669.4(2)	8254.5(2)	21.44(2)

N1	3973.4(10)	4354.3(9)	7393.2(7)	15.48(18)
N2	4617.8(10)	5142.6(10)	6870.0(7)	16.73(18)
N3	4356.2(10)	6238.8(10)	7103.3(7)	16.11(18)
O1	5303.9(14)	8734.1(14)	9750.7(9)	49.8(3)
O2	1704.6(17)	9712.4(15)	8908.2(12)	63.7(4)

Table 3 Anisotropic Displacement Parameters ($Å^2×10^3$). The Anisotropic displacement factor exponent takes the form: $-2\pi^2[h^2a^{*2}U_{11}+2hka^*b^*U_{12}+\ldots]$.

Atom	U_{11}	U_{22}	U_{33}	U_{23}	U_{13}	U_{12}
C1	17.0(5)	17.4(5)	16.5(5)	2.7(4)	3.8(4)	7.4(4)
C2	15.8(5)	16.4(5)	16.1(5)	2.1(4)	2.9(4)	6.5(4)
C3	21.1(5)	17.4(5)	18.2(5)	2.7(4)	4.7(4)	6.7(4)
C4	19.8(6)	31.7(7)	24.6(6)	8.2(5)	5.3(5)	9.0(5)
C5	20.2(6)	49.2(9)	31.1(7)	11.5(7)	9.5(5)	8.9(6)
C6	36.9(8)	39.2(8)	31.4(8)	14.9(6)	15.5(6)	7.2(7)
C7	47.7(9)	37.0(8)	32.7(8)	19.5(6)	17.6(7)	21.3(7)
C8	33.0(7)	32.2(7)	26.9(7)	13.4(5)	13.4(5)	19.1(6)
C9	21.5(5)	14.1(5)	20.0(5)	2.7(4)	5.9(4)	8.6(4)
C10	26.8(6)	22.7(6)	20.6(6)	3.6(5)	3.5(5)	14.4(5)
C11	44.4(8)	29.1(7)	31.5(7)	6.0(6)	4.3(6)	25.9(7)
C12	53.0(9)	19.3(6)	36.3(8)	3.7(6)	9.6(7)	18.7(6)
C13	37.9(8)	16.6(6)	37.5(8)	-1.5(5)	5.9(6)	7.0(5)
C14	23.6(6)	18.7(6)	26.1(6)	-0.1(5)	4.0(5)	6.2(5)
C15	25.3(6)	29.8(7)	26.6(7)	3.9(5)	-0.6(5)	15.3(5)
C16	31.2(7)	52.4(10)	33.7(8)	17.1(7)	5.7(6)	16.5(7)
C17	30.5(7)	54.7(10)	25.1(7)	7.9(7)	2.2(6)	19.1(7)
C18	20.0(6)	24.0(6)	39.3(8)	-4.2(6)	-2.7(5)	4.9(5)
C19	24.1(7)	43.8(9)	55.9(11)	-5.4(8)	6.2(7)	4.1(7)
C20	35.3(8)	41.5(9)	39.3(9)	0.8(7)	-6.3(7)	11.2(7)
C21	22.2(5)	19.2(5)	21.7(6)	8.9(4)	8.6(4)	10.6(5)
C22	23.0(6)	21.0(6)	27.3(6)	8.8(5)	8.4(5)	9.6(5)
C23	27.9(7)	26.1(7)	41.1(8)	15.9(6)	13.6(6)	8.4(5)
C24	39.0(8)	36.7(8)	42.3(9)	26.1(7)	20.5(7)	18.1(7)
C25	40.1(8)	40.2(8)	27.4(7)	19.6(6)	11.9(6)	21.9(7)
C26	27.7(6)	28.4(6)	21.9(6)	9.2(5)	7.8(5)	16.5(5)
C27	23.0(6)	23.4(6)	27.6(7)	7.0(5)	2.7(5)	4.2(5)
C28	57.0(11)	28.1(8)	38.1(9)	2.9(7)	0.0(8)	-0.4(7)
C29	35.0(8)	61.4(11)	42.5(9)	14.3(8)	3.7(7)	27.8(8)
C30	27.9(6)	35.9(7)	21.2(6)	7.3(5)	2.3(5)	14.4(6)
C31	44.7(9)	42.5(9)	28.1(8)	0.6(6)	0.5(6)	19.6(7)
C32	36.6(8)	59.8(11)	36.3(9)	11.2(8)	1.4(7)	28.2(8)

C33	37.2(8)	26.1(7)	33.5(8)	-1.2(6)	11.0(6)	15.2(6)
C34	39.0(8)	31.7(7)	42.4(9)	-1.1(6)	6.9(7)	19.6(7)
Cl1	32.73(18)	52.2(2)	35.74(19)	-0.61(17)	0.06(15)	25.06(17)
Ir1	25.64(3)	17.61(2)	24.75(3)	2.87(2)	8.12(2)	11.82(2)
N1	16.0(4)	14.2(4)	16.8(4)	2.6(3)	3.5(3)	6.3(4)
N2	18.1(4)	16.4(4)	17.1(5)	3.6(4)	4.0(4)	7.9(4)
N3	17.4(4)	15.5(4)	17.4(5)	4.5(4)	4.1(4)	7.8(4)
O1	44.4(7)	51.2(8)	44.8(7)	-11.2(6)	-3.7(6)	18.1(6)
O2	65.4(9)	54.3(9)	79.3(11)	-15.2(8)	5.7(8)	44.7(8)

Table 4 Bond Lengths.

Atom	Atom	Length/Å	Atom	Atom	Length/Å
C1	C2	1.3929(16)	C18	C19	1.529(2)
C1	Ir1	2.0699(12)	C18	C20	1.530(2)
C1	N3	1.3692(15)	C21	C22	1.3995(18)
C2	C3	1.4736(16)	C21	C26	1.3980(18)
C2	N1	1.3685(15)	C21	N3	1.4518(15)
C3	C4	1.3892(18)	C22	C23	1.3958(18)
C3	C8	1.3945(18)	C22	C27	1.5137(19)
C4	C5	1.3918(19)	C23	C24	1.384(2)
C5	C6	1.383(2)	C24	C25	1.373(2)
C6	C7	1.377(2)	C25	C26	1.3983(19)
C7	C8	1.392(2)	C26	C30	1.514(2)
C9	C10	1.3972(17)	C27	C28	1.528(2)
C9	C14	1.3987(18)	C27	C29	1.530(2)
C9	N1	1.4489(15)	C30	C31	1.533(2)
C10	C11	1.3943(18)	C30	C32	1.528(2)
C10	C15	1.5150(19)	C33	Ir1	1.8314(17)
C11	C12	1.381(2)	C33	O1	1.142(2)
C12	C13	1.378(2)	C34	Ir1	1.8903(15)
C13	C14	1.3960(19)	C34	O2	1.134(2)
C14	C18	1.515(2)	Cl1	Ir1	2.3492(4)
C15	C16	1.528(2)	N1	N2	1.3226(14)
C15	C17	1.532(2)	N2	N3	1.3330(14)

Table 5 Bond Angles.

Atom	Atom	Atom	Angle/˚	Atom	Atom	Atom	Angle/˚
C2	C1	Ir1	131.39(9)	C26	C21	C22	123.95(12)
N3	C1	C2	102.49(10)	C26	C21	N3	117.83(11)
N3	C1	Ir1	126.10(8)	C21	C22	C27	122.96(11)
C1	C2	C3	130.09(11)	C23	C22	C21	116.61(13)

N1	C2	C1	106.61(10)	C23	C22	C27	120.21(12)
N1	C2	C3	123.27(10)	C24	C23	C22	120.93(14)
C4	C3	C2	119.33(11)	C25	C24	C23	120.73(13)
C4	C3	C8	119.52(12)	C24	C25	C26	121.32(14)
C8	C3	C2	121.15(11)	C21	C26	C25	116.40(13)
C3	C4	C5	119.79(13)	C21	C26	C30	123.02(12)
C6	C5	C4	120.47(14)	C25	C26	C30	120.54(13)
C7	C6	C5	119.97(14)	C22	C27	C28	113.25(13)
C6	C7	C8	120.16(14)	C22	C27	C29	108.76(12)
C7	C8	C3	120.09(13)	C28	C27	C29	110.79(14)
C10	C9	C14	124.16(12)	C26	C30	C31	109.72(12)
C10	C9	N1	118.66(11)	C26	C30	C32	112.10(13)
C14	C9	N1	117.17(11)	C32	C30	C31	110.45(13)
C9	C10	C15	123.41(11)	O1	C33	Ir1	178.22(14)
C11	C10	C9	116.27(12)	O2	C34	Ir1	178.14(17)
C11	C10	C15	120.32(12)	C1	Ir1	Cl1	88.02(3)
C12	C11	C10	121.47(14)	C33	Ir1	C1	90.32(5)
C13	C12	C11	120.37(13)	C33	Ir1	C34	92.79(7)
C12	C13	C14	121.29(14)	C33	Ir1	Cl1	177.87(5)
C9	C14	C18	123.26(12)	C34	Ir1	C1	176.75(6)
C13	C14	C9	116.41(13)	C34	Ir1	Cl1	88.85(5)
C13	C14	C18	120.33(12)	C2	N1	C9	129.48(10)
C10	C15	C16	111.07(12)	N2	N1	C2	112.69(9)
C10	C15	C17	111.48(13)	N2	N1	C9	117.53(9)
C16	C15	C17	110.00(12)	N1	N2	N3	103.15(9)
C14	C18	C19	110.92(14)	C1	N3	C21	128.73(10)
C14	C18	C20	110.55(13)	N2	N3	C1	115.06(10)
C19	C18	C20	111.03(13)	N2	N3	C21	116.21(10)
C22	C21	N3	118.11(11)				

Table 6 Torsion Angles.

A	B	C	D	Angle/˚	A	B	C	D	Angle/˚
C1	C2	C3	C4	42.68(19)	C21	C22	C23	C24	-2.4(2)
C1	C2	C3	C8	-137.72(14)	C21	C22	C27	C28	-142.42(15)
C1	C2	N1	C9	-173.19(11)	C21	C22	C27	C29	93.94(16)
C1	C2	N1	N2	0.31(13)	C21	C26	C30	C31	-98.64(15)
C2	C1	N3	C21	179.50(11)	C21	C26	C30	C32	138.25(14)
C2	C1	N3	N2	0.57(13)	C22	C21	C26	C25	0.8(2)
C2	C3	C4	C5	179.11(13)	C22	C21	C26	C30	178.39(12)
C2	C3	C8	C7	-178.95(13)	C22	C21	N3	C1	85.92(16)
C2	N1	N2	N3	0.04(12)	C22	C21	N3	N2	-95.16(13)

C3	C2	N1	C9	4.85(19)	C22	C23	C24	C25	1.3(2)
C3	C2	N1	N2	178.35(10)	C23	C22	C27	C28	43.11(19)
C3	C4	C5	C6	-0.3(2)	C23	C22	C27	C29	-80.53(17)
C4	C3	C8	C7	0.6(2)	C23	C24	C25	C26	1.0(2)
C4	C5	C6	C7	0.9(3)	C24	C25	C26	C21	-2.0(2)
C5	C6	C7	C8	-0.8(3)	C24	C25	C26	C30	-179.65(14)
C6	C7	C8	C3	0.0(2)	C25	C26	C30	C31	78.87(17)
C8	C3	C4	C5	-0.5(2)	C25	C26	C30	C32	-44.24(18)
C9	C10	C11	C12	-1.2(2)	C26	C21	C22	C23	1.4(2)
C9	C10	C15	C16	-111.77(15)	C26	C21	C22	C27	-173.29(12)
C9	C10	C15	C17	125.16(14)	C26	C21	N3	C1	-97.73(15)
C9	C14	C18	C19	-117.57(15)	C26	C21	N3	N2	81.19(14)
C9	C14	C18	C20	118.82(15)	C27	C22	C23	C24	172.39(14)
C9	N1	N2	N3	174.38(10)	Ir1	C1	C2	C3	-0.2(2)
C10	C9	C14	C13	1.3(2)	Ir1	C1	C2	N1	177.64(9)
C10	C9	C14	C18	-178.18(13)	Ir1	C1	N3	C21	1.23(18)
C10	C9	N1	C2	-105.02(15)	Ir1	C1	N3	N2	-177.70(8)
C10	C9	N1	N2	81.74(14)	N1	C2	C3	C4	-134.87(13)
C10	C11	C12	C13	0.6(2)	N1	C2	C3	C8	44.73(18)
C11	C10	C15	C16	68.39(17)	N1	C9	C10	C11	-179.09(12)
C11	C10	C15	C17	-54.67(18)	N1	C9	C10	C15	1.07(19)
C11	C12	C13	C14	1.0(3)	N1	C9	C14	C13	-179.37(12)
C12	C13	C14	C9	-1.9(2)	N1	C9	C14	C18	1.18(19)
C12	C13	C14	C18	177.57(15)	N1	N2	N3	C1	-0.40(13)
C13	C14	C18	C19	62.99(18)	N1	N2	N3	C21	-179.46(10)
C13	C14	C18	C20	-60.62(19)	N3	C1	C2	C3	-178.36(12)
C14	C9	C10	C11	0.3(2)	N3	C1	C2	N1	-0.50(12)
C14	C9	C10	C15	-179.58(13)	N3	C21	C22	C23	177.46(12)
C14	C9	N1	C2	75.58(16)	N3	C21	C22	C27	2.81(19)
C14	C9	N1	N2	-97.65(13)	N3	C21	C26	C25	-175.32(12)
C15	C10	C11	C12	178.61(14)	N3	C21	C26	C30	2.28(19)

Table 7 Hydrogen Atom Coordinates (Å×10^4) and Isotropic Displacement Parameters (Å^2×10^3).

Atom	*x*	*y*	*z*	U(eq)
H4	889.09	4827.51	8257.7	30
H5	-442.7	3724.4	9239.57	41
H6	347.84	2469.36	10125.31	43
H7	2497.87	2355.93	10066.92	42
H8	3850.11	3460.13	9093.99	33
H11	5770.71	1261.6	7711.38	38
H12	3826.8	-431.72	6857.63	42

H13	1952.69	17.49	6251.47	39
H15	6163.24	4694.89	8323.62	32
H16A	7809.06	3306.14	7650.23	57
H16B	8382.56	4843.59	8119.77	57
H16C	7372.55	4338.92	7158.42	57
H17A	5894.41	3370.58	9450.28	54
H17B	7481.55	4258.93	9517.02	54
H17C	6904.9	2715.02	9063.51	54
H18	1770.32	3277.4	6434.3	37
H19A	-5.52	630.25	6469.56	68
H19B	-495.42	1844.9	6384.92	68
H19C	433.11	1853.03	7302.66	68
H20A	2169.08	2351.54	5031.56	62
H20B	582.47	2149.39	4972.06	62
H20C	1064.35	934.61	5076.25	62
H23	7584.65	10012.51	6797.77	37
H24	6488.23	9907.01	5351.7	42
H25	4431.8	8198.23	4705.27	39
H27	6361.6	7719.39	8255.05	31
H28A	8418.18	10231.43	8222.94	70
H28B	8181.35	9584.46	9101.84	70
H28C	7049.59	10068.04	8628.69	70
H29A	7568.75	6760.19	7352.34	65
H29B	8562.32	7605.85	8284.59	65
H29C	8696.98	8195.93	7377.5	65
H30	2460.01	5683.52	5821.41	33
H31A	3652.01	5513.45	4229.75	58
H31B	2259.26	4402.35	4352.85	58
H31C	3674.77	4664.23	5005.13	58
H32A	1708.3	7297.57	5283.56	62
H32B	983.95	5887.16	4611.9	62
H32C	2231.03	7028.16	4354.52	62

Appendix M: Crystallographic data for complex **13**.

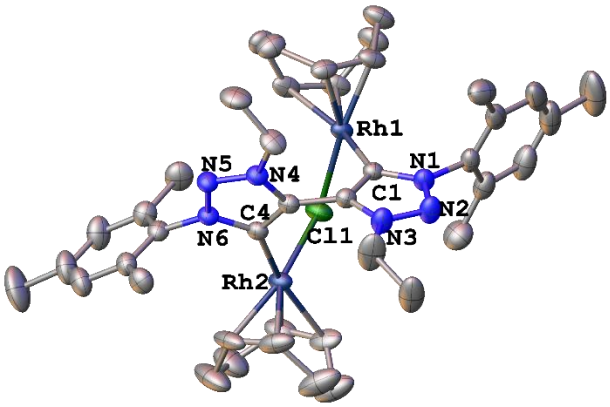

Table 1 Crystal data and structure refinement.

Empirical formula	$C_{42}H_{56}BClF_4N_6Rh_2$
Formula weight	973.00
Temperature/K	173.15
Crystal system	monoclinic
Space group	C2/c
a/Å	35.3141(7)
b/Å	13.6968(3)
c/Å	25.8483(9)
α/°	90
β/°	126.9258(8)
γ/°	90
Volume/Å^3	9994.7(5)
Z	8
ρ_{calc}g/cm^3	1.293
μ/mm^{-1}	0.761
F(000)	3984.0
Crystal size/mm^3	0.361 × 0.222 × 0.135
Radiation	MoKα (λ = 0.71073)
2Θ range for data collection/°	2.886 to 56.764
Index ranges	-35 ≤ h ≤ 47, -18 ≤ k ≤ 18, -34 ≤ l ≤ 34
Reflections collected	82374
Independent reflections	12505 [R_{int} = 0.0588, R_{sigma} = 0.0458]
Data/restraints/parameters	12505/100/570
Goodness-of-fit on F^2	1.024
Final R indexes [I>=2σ (I)]	R_1 = 0.0367, wR_2 = 0.0806
Final R indexes [all data]	R_1 = 0.0651, wR_2 = 0.0913

Largest diff. peak/hole / e Å^{-3}	0.64/-0.39

Table 2 Fractional Atomic Coordinates (×10^4) and Equivalent Isotropic Displacement Parameters (Å^2×10^3). U_{eq} is defined as 1/3 of the trace of the orthogonalised U_{IJ} tensor.

Atom	*x*	*y*	*z*	U(eq)
C1	5939.1(9)	7239(2)	6576.6(12)	26.8(6)
C2	5929.2(9)	7113.6(19)	7098.1(13)	28.1(6)
C3	6139.2(9)	6287.6(19)	7549.7(12)	26.5(6)
C4	6614.3(9)	6065.5(19)	7980.4(12)	26.2(6)
C5	5637.0(11)	8625(2)	5785.2(14)	35.6(7)
C6	6023.5(13)	9086(2)	5871.2(17)	45.2(8)
C7	5950.2(16)	9465(3)	5314(2)	59.1(10)
C8	5519.0(18)	9405(3)	4716(2)	65.3(12)
C9	5145.4(16)	8987(3)	4665.4(18)	60.6(11)
C10	5190.6(13)	8581(2)	5198.3(15)	45.1(8)
C11	6492.3(13)	9187(3)	6525.1(19)	58.3(10)
C12	5460(2)	9801(4)	4119(2)	102.6(19)
C13	4774.7(12)	8133(3)	5127.1(18)	56.8(10)
C14	5617.2(16)	8100(3)	7603(2)	65.0(11)
C15	5651(7)	9160(4)	7780(8)	81(4)
C15A	5921(8)	8952(12)	8041(9)	110(6)
C16	6990.2(9)	4524(2)	8646.8(13)	30.8(6)
C17	7266.4(11)	4123(2)	8481.6(15)	39.0(7)
C18	7661.4(12)	3594(3)	8958.6(18)	51.6(9)
C19	7783.2(12)	3462(3)	9570.0(19)	53.7(9)
C20	7485.1(11)	3853(2)	9702.5(16)	47.3(8)
C21	7085.3(10)	4386(2)	9248.9(14)	34.0(6)
C22	7145.4(13)	4249(3)	7819.2(16)	51.4(9)
C23	8227.2(15)	2911(4)	10084(2)	87.7(16)
C24	6772.5(11)	4810(2)	9407.6(15)	41.6(7)
C25	5366.0(10)	5433(2)	7152.5(15)	40.7(7)
C26	5195.7(11)	4408(3)	6972.5(16)	52.0(9)
C27	5552.8(10)	6047(2)	5387.4(13)	37.0(7)
C28	5617.5(10)	5425(2)	5861.7(14)	35.3(7)
C29	5758.3(11)	4362(2)	5965.3(17)	46.2(8)
C30	6151.3(11)	4148(2)	5893.2(16)	42.3(7)
C31	6497.8(10)	4978(2)	6129.5(14)	37.7(7)
C32	6466.0(10)	5717(2)	5743.9(14)	39.0(7)
C33	6072.3(11)	5831(3)	5025.7(14)	48.3(8)

C34	5579.0(11)	5708(3)	4850.9(15)	50.5(9)
C35	7491.7(13)	6753(3)	9237.1(14)	54.0(10)
C36	7171.5(14)	7520(3)	8990.2(17)	54.2(10)
C37	7298.9(18)	8585(3)	9081(2)	78.0(14)
C38	7646.2(17)	8853(3)	8954(2)	72.5(13)
C39	7622.9(12)	8202(3)	8462.8(17)	47.5(9)
C40	7889.8(11)	7381(3)	8618.1(15)	46.2(8)
C41	8227.4(13)	6961(4)	9292.2(18)	71.7(12)
C42	8027.6(14)	6855(4)	9660.8(18)	81.6(15)
Cl1	7004.7(3)	6775.6(6)	7186.8(3)	38.71(17)
N1	5722.8(8)	8124.8(16)	6341.7(11)	30.8(5)
N2	5587.9(10)	8547.3(18)	6673.0(13)	41.7(6)
N3	5718.7(9)	7913.9(18)	7136.0(12)	37.5(6)
N4	5886.6(7)	5514.2(17)	7527.5(10)	27.8(5)
N5	6160.3(8)	4809.3(17)	7914.7(11)	30.0(5)
N6	6598.7(7)	5152.0(16)	8185.8(10)	26.7(5)
Rh1	6215.9(2)	6308.0(2)	6276.8(2)	26.23(6)
Rh2	7174.9(2)	6914.6(2)	8244.7(2)	30.08(7)
B1	5724(2)	6845(5)	8883(3)	59.9(16)
F1	6109.2(19)	7285(6)	9026(3)	166(3)
F2	5659(3)	6018(6)	8527(4)	109(2)
F3	5324.8(16)	7397(3)	8496(2)	86.5(16)
F4	5769(3)	6537(5)	9411(3)	143(3)
B1A	5721(3)	6814(6)	8999(4)	48.8(19)
F1A	6122(2)	6458(5)	9520(3)	75(2)
F2A	5630(4)	6365(5)	8452(4)	69(2)
F3A	5773(3)	7796(4)	8963(4)	91(3)
F4A	5378(2)	6614(6)	9066(3)	83(2)

Table 3 Anisotropic Displacement Parameters ($Å^2×10^3$). The Anisotropic displacement factor exponent takes the form: $-2\pi^2[h^2a^{*2}U_{11}+2hka^*b^*U_{12}+\ldots]$.

Atom	U_{11}	U_{22}	U_{33}	U_{23}	U_{13}	U_{12}
C1	23.2(13)	30.7(14)	25.3(13)	-2.5(11)	14.0(11)	-1.5(11)
C2	27.2(14)	31.7(15)	29.1(14)	-1.4(11)	18.9(12)	1.7(12)
C3	26.3(14)	32.6(14)	26.2(13)	-1.6(11)	18.8(12)	-2.3(12)
C4	27.3(14)	32.2(15)	23.5(13)	-2.6(11)	17.6(12)	-3.2(11)
C5	50.2(19)	30.7(15)	34.1(15)	4.5(13)	29.7(15)	9.4(14)
C6	66(2)	32.8(16)	56(2)	4.1(15)	47(2)	6.2(16)
C7	92(3)	42(2)	82(3)	14.6(19)	73(3)	15(2)
C8	108(4)	50(2)	62(3)	20.0(19)	64(3)	30(2)
C9	84(3)	49(2)	42(2)	12.1(17)	34(2)	30(2)

C10	60(2)	35.1(17)	40.3(17)	5.6(14)	30.1(17)	17.1(16)
C11	57(2)	56(2)	72(3)	-1(2)	44(2)	-9.8(19)
C12	177(6)	93(4)	87(3)	45(3)	105(4)	57(4)
C13	44(2)	54(2)	55(2)	-5.6(18)	19.9(18)	10.2(17)
C14	106(3)	62(2)	79(3)	15.8(19)	83(3)	30(2)
C15	151(12)	63(3)	87(8)	15(4)	101(9)	37(5)
C15A	252(16)	38(6)	133(10)	-12(6)	165(11)	-3(8)
C16	24.3(14)	32.3(15)	35.0(15)	0.1(12)	17.4(12)	-2.3(12)
C17	37.1(17)	41.3(17)	47.5(18)	2.7(14)	30.2(15)	2.8(14)
C18	46(2)	54(2)	71(2)	18.6(18)	43(2)	17.8(17)
C19	39.2(19)	56(2)	64(2)	26.8(18)	29.8(18)	15.7(17)
C20	40.3(19)	54(2)	43.3(18)	17.7(16)	22.9(16)	6.2(16)
C21	29.2(15)	36.0(16)	37.3(15)	5.6(13)	20.1(13)	-0.1(13)
C22	61(2)	57(2)	56(2)	-1.1(17)	46(2)	9.2(18)
C23	56(3)	110(4)	94(3)	59(3)	44(3)	43(3)
C24	43.9(18)	51(2)	38.9(16)	4.9(15)	29.9(15)	1.4(15)
C25	19.5(14)	58(2)	42.6(17)	2.2(15)	17.8(13)	-3.3(14)
C26	30.6(17)	72(2)	44.9(19)	-11.9(18)	18.2(15)	-19.4(17)
C27	21.2(14)	54.6(19)	28.5(14)	-10.0(14)	11.3(12)	3.5(13)
C28	22.5(14)	41.2(17)	40.4(16)	-12.7(14)	18.0(13)	-4.5(13)
C29	39.0(18)	44.7(19)	58(2)	-9.9(16)	31.0(17)	-6.5(15)
C30	44.1(19)	40.5(17)	48.3(18)	-7.4(15)	31.0(16)	6.2(15)
C31	27.2(15)	54.6(19)	34.2(15)	-10.3(14)	20.0(13)	9.7(14)
C32	30.9(16)	61(2)	36.2(16)	-11.7(15)	25.8(14)	-1.0(15)
C33	47(2)	74(2)	32.5(16)	-4.8(16)	28.1(16)	-6.0(18)
C34	40.4(19)	77(3)	30.6(16)	-8.6(17)	19.6(15)	1.5(18)
C35	54(2)	77(3)	24.2(15)	-10.7(16)	19.9(16)	-41(2)
C36	73(3)	63(2)	52(2)	-27.8(19)	51(2)	-38(2)
C37	115(4)	68(3)	104(3)	-44(2)	94(3)	-48(3)
C38	105(3)	62(2)	96(3)	-36(2)	84(3)	-45(2)
C39	55(2)	53(2)	54(2)	-19.1(17)	43.5(19)	-33.4(18)
C40	29.6(17)	72(2)	37.2(17)	-10.8(17)	19.9(14)	-22.0(17)
C41	41(2)	110(4)	48(2)	2(2)	17.6(18)	-11(2)
C42	57(3)	120(4)	37(2)	5(2)	11.4(19)	-42(3)
Cl1	30.1(4)	56.4(5)	28.6(3)	-7.0(3)	17.1(3)	-9.0(3)
N1	36.6(13)	32.1(13)	32.4(12)	1.3(10)	25.5(11)	5.4(11)
N2	58.5(18)	37.4(14)	47.3(15)	5.4(12)	41.5(15)	11.9(13)
N3	51.1(16)	35.7(14)	42.7(14)	4.0(11)	37.2(13)	9.3(12)
N4	22.2(11)	34.8(13)	30.2(12)	-2.0(10)	17.7(10)	-2.3(10)
N5	23.2(12)	33.4(13)	32.5(12)	0.2(10)	16.2(10)	-3.5(10)
N6	20.9(11)	33.1(12)	27.7(11)	-1.6(10)	15.6(10)	-3.0(10)

Rh1	21.84(11)	35.17(12)	23.97(10)	-5.62(9)	14.97(9)	-0.58(9)
Rh2	27.57(12)	38.81(13)	26.38(11)	-5.93(9)	17.54(10)	-11.95(10)
B1	53(3)	93(4)	25(3)	1(2)	19(3)	-22(2)
F1	72(3)	238(7)	105(4)	36(4)	9(3)	-83(4)
F2	53(3)	157(5)	97(4)	-49(4)	35(3)	3(3)
F3	81(3)	95(3)	86(3)	22(2)	51(2)	4(2)
F4	260(9)	124(4)	107(4)	59(4)	144(6)	50(6)
B1A	49(4)	54(3)	40(3)	-10(3)	25(3)	-9(3)
F1A	60(3)	90(4)	49(3)	-7(3)	19(3)	-1(3)
F2A	118(7)	60(4)	52(3)	-5(3)	63(4)	-21(4)
F3A	138(8)	50(3)	112(6)	-3(3)	91(6)	-2(3)
F4A	66(3)	126(6)	69(4)	-42(4)	47(3)	-36(4)

Table 4 Bond Lengths.

Atom	Atom	Length/Å	Atom	Atom	Length/Å
C1	C2	1.380(4)	C27	Rh1	2.104(3)
C1	N1	1.366(3)	C28	C29	1.510(4)
C1	Rh1	2.023(3)	C28	Rh1	2.087(3)
C2	C3	1.467(4)	C29	C30	1.535(4)
C2	N3	1.361(3)	C30	C31	1.505(4)
C3	C4	1.379(4)	C31	C32	1.377(4)
C3	N4	1.364(3)	C31	Rh1	2.215(3)
C4	N6	1.373(3)	C32	C33	1.517(4)
C4	Rh2	2.028(3)	C32	Rh1	2.189(3)
C5	C6	1.395(5)	C33	C34	1.524(4)
C5	C10	1.384(4)	C35	C36	1.387(5)
C5	N1	1.452(3)	C35	C42	1.520(5)
C6	C7	1.400(5)	C35	Rh2	2.105(3)
C6	C11	1.501(5)	C36	C37	1.504(5)
C7	C8	1.374(6)	C36	Rh2	2.104(3)
C8	C9	1.371(6)	C37	C38	1.494(5)
C8	C12	1.527(5)	C38	C39	1.512(5)
C9	C10	1.403(5)	C39	C40	1.363(5)
C10	C13	1.497(5)	C39	Rh2	2.204(3)
C14	C15	1.505(5)	C40	C41	1.514(5)
C14	C15A	1.528(5)	C40	Rh2	2.188(3)
C14	N3	1.473(4)	C41	C42	1.495(6)
C16	C17	1.392(4)	Cl1	Rh1	2.4144(7)
C16	C21	1.394(4)	Cl1	Rh2	2.4290(7)
C16	N6	1.446(3)	N1	N2	1.336(3)
C17	C18	1.388(4)	N2	N3	1.317(3)

C17	C22	1.505(4)	N4	N5	1.306(3)
C18	C19	1.378(5)	N5	N6	1.343(3)
C19	C20	1.395(5)	B1	F1	1.322(7)
C19	C23	1.513(5)	B1	F2	1.389(7)
C20	C21	1.383(4)	B1	F3	1.366(7)
C21	C24	1.506(4)	B1	F4	1.344(7)
C25	C26	1.487(5)	B1A	F1A	1.328(7)
C25	N4	1.480(3)	B1A	F2A	1.391(7)
C27	C28	1.394(4)	B1A	F3A	1.369(8)
C27	C34	1.517(4)	B1A	F4A	1.350(8)

Table 5 Bond Angles.

Atom	Atom	Atom	Angle/˚	Atom	Atom	Atom	Angle/˚
C2	C1	Rh1	126.7(2)	C37	C38	C39	113.7(3)
N1	C1	C2	102.1(2)	C38	C39	Rh2	110.8(2)
N1	C1	Rh1	131.26(19)	C40	C39	C38	124.0(4)
C1	C2	C3	125.2(2)	C40	C39	Rh2	71.27(18)
N3	C2	C1	107.8(2)	C39	C40	C41	125.4(3)
N3	C2	C3	126.9(2)	C39	C40	Rh2	72.56(18)
C4	C3	C2	126.9(2)	C41	C40	Rh2	107.4(2)
N4	C3	C2	124.1(2)	C42	C41	C40	115.1(3)
N4	C3	C4	108.1(2)	C41	C42	C35	114.2(3)
C3	C4	Rh2	127.8(2)	Rh1	Cl1	Rh2	118.55(3)
N6	C4	C3	101.6(2)	C1	N1	C5	126.0(2)
N6	C4	Rh2	130.55(19)	N2	N1	C1	114.8(2)
C6	C5	N1	117.0(3)	N2	N1	C5	119.2(2)
C10	C5	C6	123.8(3)	N3	N2	N1	103.4(2)
C10	C5	N1	119.2(3)	C2	N3	C14	127.7(3)
C5	C6	C7	116.4(3)	N2	N3	C2	111.9(2)
C5	C6	C11	122.2(3)	N2	N3	C14	120.4(2)
C7	C6	C11	121.4(3)	C3	N4	C25	127.6(2)
C8	C7	C6	122.1(4)	N5	N4	C3	112.2(2)
C7	C8	C12	120.2(4)	N5	N4	C25	120.2(2)
C9	C8	C7	119.0(3)	N4	N5	N6	103.4(2)
C9	C8	C12	120.9(4)	C4	N6	C16	128.3(2)
C8	C9	C10	122.5(4)	N5	N6	C4	114.7(2)
C5	C10	C9	116.2(3)	N5	N6	C16	117.0(2)
C5	C10	C13	122.7(3)	C1	Rh1	C27	92.81(11)
C9	C10	C13	121.1(3)	C1	Rh1	C28	89.39(11)
N3	C14	C15	113.8(6)	C1	Rh1	C31	162.64(11)
N3	C14	C15A	109.3(6)	C1	Rh1	C32	160.79(12)

C17	C16	C21	123.1(3)	C1	Rh1	Cl1	89.99(8)
C17	C16	N6	118.8(2)	C27	Rh1	C31	89.57(11)
C21	C16	N6	118.1(2)	C27	Rh1	C32	81.64(11)
C16	C17	C22	122.1(3)	C27	Rh1	Cl1	169.98(9)
C18	C17	C16	116.7(3)	C28	Rh1	C27	38.86(12)
C18	C17	C22	121.2(3)	C28	Rh1	C31	81.71(11)
C19	C18	C17	122.8(3)	C28	Rh1	C32	97.41(11)
C18	C19	C20	118.0(3)	C28	Rh1	Cl1	150.90(9)
C18	C19	C23	121.2(4)	C31	Rh1	Cl1	90.63(8)
C20	C19	C23	120.8(4)	C32	Rh1	C31	36.43(11)
C21	C20	C19	122.1(3)	C32	Rh1	Cl1	92.62(8)
C16	C21	C24	121.8(3)	C4	Rh2	C35	92.68(11)
C20	C21	C16	117.2(3)	C4	Rh2	C36	89.60(11)
C20	C21	C24	121.0(3)	C4	Rh2	C39	161.86(13)
N4	C25	C26	112.7(3)	C4	Rh2	C40	161.86(13)
C28	C27	C34	123.3(3)	C4	Rh2	Cl1	92.55(7)
C28	C27	Rh1	69.90(16)	C35	Rh2	C39	89.90(13)
C34	C27	Rh1	114.3(2)	C35	Rh2	C40	82.28(12)
C27	C28	C29	127.4(3)	C35	Rh2	Cl1	162.61(12)
C27	C28	Rh1	71.24(17)	C36	Rh2	C35	38.46(15)
C29	C28	Rh1	110.1(2)	C36	Rh2	C39	81.31(12)
C28	C29	C30	112.8(3)	C36	Rh2	C40	96.94(13)
C31	C30	C29	112.4(2)	C36	Rh2	Cl1	158.14(12)
C30	C31	Rh1	110.56(18)	C39	Rh2	Cl1	90.27(9)
C32	C31	C30	124.7(3)	C40	Rh2	C39	36.16(13)
C32	C31	Rh1	70.76(17)	C40	Rh2	Cl1	87.65(8)
C31	C32	C33	125.3(3)	F1	B1	F2	106.8(7)
C31	C32	Rh1	72.82(16)	F1	B1	F3	112.8(6)
C33	C32	Rh1	108.2(2)	F1	B1	F4	112.6(7)
C32	C33	C34	113.3(3)	F3	B1	F2	106.3(6)
C27	C34	C33	112.4(3)	F4	B1	F2	106.8(7)
C36	C35	C42	125.4(4)	F4	B1	F3	111.1(6)
C36	C35	Rh2	70.72(18)	F1A	B1A	F2A	108.7(8)
C42	C35	Rh2	112.9(2)	F1A	B1A	F3A	109.0(8)
C35	C36	C37	125.4(4)	F1A	B1A	F4A	106.8(8)
C35	C36	Rh2	70.81(19)	F3A	B1A	F2A	108.8(7)
C37	C36	Rh2	111.1(2)	F4A	B1A	F2A	111.3(8)
C38	C37	C36	114.3(3)	F4A	B1A	F3A	112.1(8)

Table 6 Torsion Angles.

A	**B**	**C**	**D**	**Angle/˚**	**A**	**B**	**C**	**D**	**Angle/˚**

C1	C2	C3	C4	66.3(4)
C1	C2	C3	N4	-101.3(3)
C1	C2	N3	C14	178.2(3)
C1	C2	N3	N2	0.5(3)
C1	N1	N2	N3	-0.3(3)
C2	C1	N1	C5	179.9(3)
C2	C1	N1	N2	0.6(3)
C2	C3	C4	N6	-169.9(2)
C2	C3	C4	Rh2	11.9(4)
C2	C3	N4	C25	-12.9(4)
C2	C3	N4	N5	170.2(2)
C3	C2	N3	C14	-5.5(5)
C3	C2	N3	N2	176.7(3)
C3	C4	N6	C16	-180.0(2)
C3	C4	N6	N5	0.5(3)
C3	N4	N5	N6	-0.3(3)
C4	C3	N4	C25	177.5(2)
C4	C3	N4	N5	0.6(3)
C5	C6	C7	C8	1.3(5)
C5	N1	N2	N3	-179.7(3)
C6	C5	C10	C9	3.4(4)
C6	C5	C10	C13	-176.3(3)
C6	C5	N1	C1	-76.5(4)
C6	C5	N1	N2	102.8(3)
C6	C7	C8	C9	1.9(5)
C6	C7	C8	C12	-178.2(3)
C7	C8	C9	C10	-2.6(5)
C8	C9	C10	C5	0.1(5)
C8	C9	C10	C13	179.8(3)
C10	C5	C6	C7	-4.0(4)
C10	C5	C6	C11	175.2(3)
C10	C5	N1	C1	100.3(3)
C10	C5	N1	N2	-80.5(3)
C11	C6	C7	C8	-177.9(3)
C12	C8	C9	C10	177.5(3)
C15	C14	N3	C2	146.8(9)
C15	C14	N3	N2	-35.6(9)
C15A	C14	N3	C2	113.3(12)
C15A	C14	N3	N2	-69.1(11)
C16	C17	C18	C19	-0.1(5)
C17	C16	C21	C20	2.5(4)
C26	C25	N4	N5	-31.9(4)
C27	C28	C29	C30	42.1(4)
C28	C27	C34	C33	-93.2(4)
C28	C29	C30	C31	34.4(4)
C29	C30	C31	C32	-93.4(3)
C29	C30	C31	Rh1	-13.1(3)
C30	C31	C32	C33	1.7(4)
C30	C31	C32	Rh1	102.2(3)
C31	C32	C33	C34	46.8(4)
C32	C33	C34	C27	31.5(4)
C34	C27	C28	C29	5.1(5)
C34	C27	C28	Rh1	106.5(3)
C35	C36	C37	C38	47.6(6)
C36	C35	C42	C41	-87.0(5)
C36	C37	C38	C39	29.0(6)
C37	C38	C39	C40	-91.6(5)
C37	C38	C39	Rh2	-10.7(5)
C38	C39	C40	C41	3.6(5)
C38	C39	C40	Rh2	102.9(3)
C39	C40	C41	C42	48.9(5)
C40	C41	C42	C35	25.3(6)
C42	C35	C36	C37	2.1(5)
C42	C35	C36	Rh2	104.8(3)
N1	C1	C2	C3	-176.9(3)
N1	C1	C2	N3	-0.6(3)
N1	C5	C6	C7	172.6(3)
N1	C5	C6	C11	-8.2(4)
N1	C5	C10	C9	-173.2(3)
N1	C5	C10	C13	7.1(4)
N1	N2	N3	C2	-0.1(3)
N1	N2	N3	C14	-178.1(3)
N3	C2	C3	C4	-109.3(3)
N3	C2	C3	N4	83.1(4)
N4	C3	C4	N6	-0.6(3)
N4	C3	C4	Rh2	-178.82(17)
N4	N5	N6	C4	-0.1(3)
N4	N5	N6	C16	-179.7(2)
N6	C16	C17	C18	174.7(3)
N6	C16	C17	C22	-5.5(4)
N6	C16	C21	C20	-174.6(3)
N6	C16	C21	C24	4.5(4)

C17	C16	C21	C24	-178.5(3)	Rh1	C1	C2	C3	2.7(4)
C17	C16	N6	C4	-68.2(4)	Rh1	C1	C2	N3	179.1(2)
C17	C16	N6	N5	111.3(3)	Rh1	C1	N1	C5	0.2(4)
C17	C18	C19	C20	2.2(6)	Rh1	C1	N1	N2	-179.1(2)
C17	C18	C19	C23	-177.7(4)	Rh1	C27	C28	C29	-101.4(3)
C18	C19	C20	C21	-2.0(5)	Rh1	C27	C34	C33	-12.1(4)
C19	C20	C21	C16	-0.2(5)	Rh1	C28	C29	C30	-39.2(3)
C19	C20	C21	C24	-179.3(3)	Rh1	C31	C32	C33	-100.5(3)
C21	C16	C17	C18	-2.3(5)	Rh1	C32	C33	C34	-34.7(4)
C21	C16	C17	C22	177.5(3)	Rh2	C4	N6	C16	-1.8(4)
C21	C16	N6	C4	109.0(3)	Rh2	C4	N6	N5	178.62(18)
C21	C16	N6	N5	-71.5(3)	Rh2	C35	C36	C37	-102.7(3)
C22	C17	C18	C19	-179.9(3)	Rh2	C35	C42	C41	-5.1(5)
C23	C19	C20	C21	177.9(4)	Rh2	C36	C37	C38	-33.3(5)
C25	N4	N5	N6	-177.4(2)	Rh2	C39	C40	C41	-99.3(3)
C26	C25	N4	C3	151.5(3)	Rh2	C40	C41	C42	-31.7(5)

Table 7 Hydrogen Atom Coordinates (Å×10^4) and Isotropic Displacement Parameters (Å^2×10^3).

Atom	***x***	***y***	***z***	**U(eq)**
H7	6206.66	9772.31	5351.54	71
H9	4844.58	8971.3	4254.05	73
H11A	6442.43	9443.91	6833.67	87
H11B	6695.01	9635.34	6496.08	87
H11C	6645.54	8545.75	6672.36	87
H12A	5676.24	10352.69	4244.5	154
H12B	5132.79	10020.33	3800.64	154
H12C	5533.54	9285.59	3929.15	154
H13A	4880.54	7568.49	5416.37	85
H13B	4541.06	7920.74	4678.37	85
H13C	4630.48	8615.67	5239.8	85
H14A	5842.74	7721.06	8001.43	78
H14B	5294.21	7861.88	7417.08	78
H14C	5688.1	7509.18	7867.27	78
H14D	5277.55	8259.52	7368.54	78
H15A	5608.27	9224.39	8120.03	122
H15B	5402.85	9530.68	7397.68	122
H15C	5962.1	9415.3	7937.43	122
H15D	5872.44	9516.57	7774.01	164
H15E	6255.93	8762.06	8307.97	164
H15F	5830.51	9122.56	8320.66	164
H18	7856.27	3309.84	8859.38	62

H20	7559.03	3749.65	10117.58	57
H22A	6800.37	4264.03	7494.77	77
H22B	7275.87	3701.29	7727.92	77
H22C	7281.02	4861.88	7803.38	77
H23A	8250.46	2879.38	10481.45	131
H23B	8505.11	3250.28	10173.41	131
H23C	8213.47	2248.37	9931.58	131
H24A	6726.26	5508.46	9305.39	62
H24B	6922.76	4718.64	9869.29	62
H24C	6465.01	4477.82	9151.38	62
H25A	5213.03	5829	6753.7	49
H25B	5269.29	5703.49	7412.21	49
H26A	4848.7	4399.21	6696.34	78
H26B	5319.9	4027.04	7365.21	78
H26C	5306.37	4123.02	6737.24	78
H27	5315.25	6575.59	5254.11	44
H28	5416.52	5598.74	6001.62	42
H29A	5476.76	3962.46	5648.39	55
H29B	5868.36	4165.42	6404.08	55
H30A	6323.56	3551.24	6140.91	51
H30B	6006.14	4021.32	5431.9	51
H31	6829.34	4808.6	6503.89	45
H32	6778.81	5982.42	5885.65	47
H33A	6117.02	5340.67	4785.23	58
H33B	6095.8	6486.13	4885.39	58
H34A	5349.45	6085.84	4453.35	61
H34B	5487.15	5011.23	4757.27	61
H35	7381.55	6159.86	9337.89	65
H36	6877.71	7373.64	8950.9	65
H37A	7005.94	8970.26	8788.71	94
H37B	7432.62	8771.17	9531.17	94
H38A	7969.9	8821.1	9365.88	87
H38B	7587.34	9535.55	8797.73	87
H39	7547.36	8553.02	8071.83	57
H40	7978.15	7239.57	8323.56	55
H41A	8333.26	6311.3	9257.94	86
H41B	8510.4	7386.68	9543.05	86
H42A	8119.88	7432.13	9943.73	98
H42B	8170.82	6272.9	9943.18	98

Table 8 Atomic Occupancy.

Atom	***Occupancy***	**Atom**	***Occupancy***	**Atom**	***Occupancy***
H14A	0.52(3)	H14B	0.52(3)	H14C	0.48(3)
H14D	0.48(3)	C15	0.52(3)	H15A	0.52(3)
H15B	0.52(3)	H15C	0.52(3)	C15A	0.48(3)
H15D	0.48(3)	H15E	0.48(3)	H15F	0.48(3)
B1	0.610(5)	F1	0.610(5)	F2	0.610(5)
F3	0.610(5)	F4	0.610(5)	B1A	0.390(5)
F1A	0.390(5)	F2A	0.390(5)	F3A	0.390(5)
F4A	0.390(5)				

Appendix N: Crystallographic data for complex **15**.

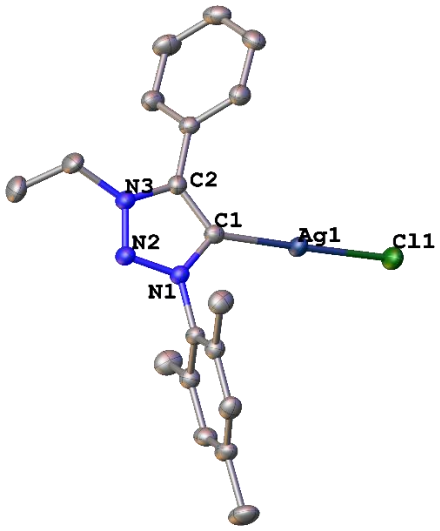

Table 1 Crystal data and structure refinement

Identification code	18m_db19_TMM324A_0fa
Empirical formula	$C_{20}H_{23}AgCl_3N_3$
Formula weight	519.63
Temperature/K	173.15
Crystal system	triclinic
Space group	P-1
a/Å	9.1406(3)
b/Å	10.8797(4)
c/Å	12.1339(4)
α/°	65.6446(14)
β/°	89.5099(16)
γ/°	82.4997(16)
Volume/Å^3	1088.52(7)
Z	2
ρ_{calc}g/cm^3	1.585
μ/mm^{-1}	1.304
F(000)	524.0
Crystal size/mm^3	0.432 × 0.302 × 0.176
Radiation	MoKα (λ = 0.71073)
2Θ range for data collection/°	3.69 to 56.828
Index ranges	-12 ≤ h ≤ 12, -14 ≤ k ≤ 14, -16 ≤ l ≤ 16
Reflections collected	23183
Independent reflections	5472 [R_{int} = 0.0222, R_{sigma} = 0.0182]

Data/restraints/parameters	5472/0/248
Goodness-of-fit on F^2	1.041
Final R indexes [I>=2σ (I)]	R_1 = 0.0214, wR_2 = 0.0534
Final R indexes [all data]	R_1 = 0.0247, wR_2 = 0.0552
Largest diff. peak/hole / e $Å^{-3}$	0.62/-0.56

Table 2 Fractional Atomic Coordinates (×10^4) and Equivalent Isotropic Displacement Parameters (Å^2×10^3) for 18m_db19_TMM324A_0fa. U_{eq} is defined as 1/3 of the trace of the orthogonalised U_{IJ} tensor.

Atom	*x*	*y*	*z*	U(eq)
Ag1	5773.1(2)	6278.6(2)	5730.6(2)	25.37(4)
C1	4457.5(17)	7534.8(16)	4197.6(14)	21.8(3)
C2	4745.6(17)	7919.4(16)	2981.1(14)	22.2(3)
C3	6122.7(18)	7608.9(16)	2443.2(14)	22.6(3)
C4	7434.0(19)	7921.3(18)	2768.0(15)	27.5(3)
C5	8757(2)	7604.5(19)	2311.4(16)	32.2(4)
C6	8773(2)	6979.4(19)	1521.9(17)	34.3(4)
C7	7473(2)	6662(2)	1197.6(17)	35.7(4)
C8	6145(2)	6966.9(19)	1657.2(16)	30.2(4)
C9	2130.1(17)	8058.1(16)	5143.2(13)	21.5(3)
C10	1986.8(18)	9141.6(16)	5482.3(14)	23.5(3)
C11	1125.8(19)	9023.3(18)	6470.0(15)	28.3(3)
C12	444.4(19)	7882.8(19)	7089.4(15)	29.2(3)
C13	607.5(19)	6835.8(18)	6704.9(15)	28.3(3)
C14	1453.4(18)	6899.3(16)	5727.0(14)	24.5(3)
C15	2734(2)	10386.7(18)	4843.0(17)	32.6(4)
C16	-462(2)	7763(2)	8168.2(18)	42.8(5)
C17	1636(2)	5748.0(19)	5334.7(18)	35.4(4)
C18	3238(2)	9424(2)	996.2(15)	33.0(4)
C19	1938(2)	9032(2)	537.4(17)	39.4(4)
Cl1	7294.1(5)	4857.2(5)	7424.9(4)	34.78(10)
N1	3032.0(15)	8124.8(13)	4133.9(11)	21.5(3)
N2	2415.6(15)	8824.1(15)	3015.8(12)	25.6(3)
N3	3493.8(15)	8683.8(15)	2325.6(12)	25.2(3)
C20	4310(2)	6903(2)	8236.6(17)	39.1(4)
Cl2	3401.0(6)	6268.0(5)	9599.2(4)	41.00(11)
Cl3	4841.2(8)	8512.1(7)	7961.1(6)	63.15(17)

Table 3 Anisotropic Displacement Parameters ($Å^2×10^3$). The Anisotropic displacement factor exponent takes the form: $-2π^2[h^2a^{*2}U_{11}+2hka^*b^*U_{12}+…]$.

Atom	U_{11}	U_{22}	U_{33}	U_{23}	U_{13}	U_{12}
Ag1	23.49(7)	29.12(7)	18.90(6)	-6.77(5)	0.55(4)	1.14(5)
C1	21.1(7)	23.0(7)	22.2(7)	-10.1(6)	3.0(6)	-3.7(6)
C2	21.2(7)	24.1(7)	20.5(7)	-8.0(6)	1.2(6)	-4.9(6)
C3	22.9(8)	23.1(7)	20.0(7)	-7.0(6)	4.2(6)	-4.1(6)
C4	26.6(8)	31.7(8)	25.6(8)	-12.3(7)	3.2(6)	-7.9(7)
C5	22.7(8)	37.9(10)	31.6(9)	-9.1(7)	4.1(7)	-8.1(7)
C6	30.3(9)	33.7(9)	32.7(9)	-8.6(7)	12.5(7)	-1.5(7)
C7	42.0(11)	38.3(10)	33.2(9)	-20.6(8)	12.9(8)	-8.0(8)
C8	30.0(9)	37.7(9)	28.1(8)	-17.3(7)	6.1(7)	-10.8(7)
C9	19.3(7)	24.2(7)	18.8(7)	-7.4(6)	1.6(5)	-0.8(6)
C10	23.4(8)	22.7(7)	22.2(7)	-7.5(6)	0.0(6)	-1.9(6)
C11	29.9(9)	29.0(8)	26.9(8)	-14.1(7)	1.6(7)	1.5(7)
C12	23.5(8)	35.2(9)	23.6(8)	-8.9(7)	4.8(6)	2.2(7)
C13	24.2(8)	28.6(8)	27.0(8)	-6.0(7)	5.8(6)	-5.2(6)
C14	23.8(8)	23.7(7)	24.1(7)	-8.3(6)	1.0(6)	-2.4(6)
C15	39.8(10)	28.1(8)	31.6(9)	-12.5(7)	3.9(7)	-10.3(7)
C16	39.5(11)	50.8(12)	33.1(10)	-14.8(9)	16.1(8)	0.8(9)
C17	46.0(11)	27.1(9)	36.7(10)	-15.2(8)	7.6(8)	-11.0(8)
C18	30.5(9)	39.4(10)	19.0(7)	-1.9(7)	2.3(6)	-5.2(7)
C19	39.4(11)	46.4(11)	24.8(8)	-7.0(8)	-5.3(8)	-5.9(9)
Cl1	28.4(2)	41.0(2)	23.39(19)	-3.50(17)	-1.80(16)	1.23(18)
N1	21.7(6)	22.6(6)	18.1(6)	-6.6(5)	1.6(5)	-2.6(5)
N2	22.5(7)	30.3(7)	19.2(6)	-5.8(5)	1.9(5)	-2.7(5)
N3	22.5(7)	30.1(7)	19.0(6)	-5.8(5)	2.1(5)	-4.9(5)
C20	45.1(11)	43.0(11)	25.0(8)	-12.9(8)	-0.5(8)	4.2(9)
Cl2	46.1(3)	42.4(3)	31.5(2)	-12.90(19)	4.36(19)	-4.6(2)
Cl3	65.5(4)	64.1(4)	53.2(3)	-11.4(3)	2.8(3)	-30.3(3)

Table 4 Bond Lengths.

Atom	Atom	Length/Å	Atom	Atom	Length/Å
Ag1	C1	2.0704(16)	C9	N1	1.4526(19)
Ag1	Cl1	2.3273(4)	C10	C11	1.398(2)
C1	C2	1.391(2)	C10	C15	1.506(2)
C1	N1	1.363(2)	C11	C12	1.385(3)
C2	C3	1.477(2)	C12	C13	1.389(3)
C2	N3	1.362(2)	C12	C16	1.512(2)
C3	C4	1.390(2)	C13	C14	1.393(2)

C3	C8	1.394(2)	C14	C17	1.503(2)
C4	C5	1.388(2)	C18	C19	1.498(3)
C5	C6	1.384(3)	C18	N3	1.480(2)
C6	C7	1.383(3)	N1	N2	1.3367(18)
C7	C8	1.389(3)	N2	N3	1.3221(19)
C9	C10	1.391(2)	C20	Cl2	1.757(2)
C9	C14	1.390(2)	C20	Cl3	1.774(2)

Table 5 Bond Angles.

Atom	Atom	Atom	Angle/˚	Atom	Atom	Atom	Angle/˚
C1	Ag1	Cl1	178.66(4)	C9	C10	C15	122.52(15)
C2	C1	Ag1	129.70(12)	C11	C10	C15	120.51(15)
N1	C1	Ag1	128.07(11)	C12	C11	C10	121.93(16)
N1	C1	C2	102.10(13)	C11	C12	C13	118.83(15)
C1	C2	C3	128.76(14)	C11	C12	C16	121.17(17)
N3	C2	C1	107.05(14)	C13	C12	C16	120.00(17)
N3	C2	C3	124.18(14)	C12	C13	C14	121.66(16)
C4	C3	C2	118.85(14)	C9	C14	C13	117.37(15)
C4	C3	C8	119.50(15)	C9	C14	C17	121.67(15)
C8	C3	C2	121.60(15)	C13	C14	C17	120.95(15)
C5	C4	C3	120.49(16)	N3	C18	C19	112.16(15)
C6	C5	C4	119.84(17)	C1	N1	C9	126.93(13)
C7	C6	C5	119.98(17)	N2	N1	C1	115.45(13)
C6	C7	C8	120.57(17)	N2	N1	C9	117.62(13)
C7	C8	C3	119.62(16)	N3	N2	N1	102.72(12)
C10	C9	N1	119.00(14)	C2	N3	C18	129.21(14)
C14	C9	C10	123.23(14)	N2	N3	C2	112.68(13)
C14	C9	N1	117.77(14)	N2	N3	C18	117.95(14)
C9	C10	C11	116.97(15)	Cl2	C20	Cl3	110.69(11)

Table 6 Torsion Angles.

A	B	C	D	Angle/˚	A	B	C	D	Angle/˚
Ag1	C1	C2	C3	-4.7(3)	C10	C9	N1	C1	98.61(19)
Ag1	C1	C2	N3	176.05(11)	C10	C9	N1	N2	-82.03(18)
Ag1	C1	N1	C9	3.4(2)	C10	C11	C12	C13	-0.9(3)
Ag1	C1	N1	N2	-175.98(11)	C10	C11	C12	C16	178.99(17)
C1	C2	C3	C4	-53.6(2)	C11	C12	C13	C14	0.9(3)
C1	C2	C3	C8	123.97(19)	C12	C13	C14	C9	-0.2(3)
C1	C2	N3	C18	175.15(16)	C12	C13	C14	C17	179.09(17)
C1	C2	N3	N2	-0.18(19)	C14	C9	C10	C11	0.7(2)

C1	N1	N2	N3	-0.24(18)	C14	C9	C10	C15	179.69(16)
C2	C1	N1	C9	179.50(14)	C14	C9	N1	C1	-81.2(2)
C2	C1	N1	N2	0.13(18)	C14	C9	N1	N2	98.19(17)
C2	C3	C4	C5	177.92(16)	C15	C10	C11	C12	-178.91(16)
C2	C3	C8	C7	-178.31(16)	C16	C12	C13	C14	-178.95(17)
C3	C2	N3	C18	-4.2(3)	C19	C18	N3	C2	125.91(19)
C3	C2	N3	N2	-179.49(15)	C19	C18	N3	N2	-59.0(2)
C3	C4	C5	C6	0.3(3)	N1	C1	C2	C3	179.30(15)
C4	C3	C8	C7	-0.8(3)	N1	C1	C2	N3	0.03(17)
C4	C5	C6	C7	-0.5(3)	N1	C9	C10	C11	-179.07(14)
C5	C6	C7	C8	0.0(3)	N1	C9	C10	C15	-0.1(2)
C6	C7	C8	C3	0.6(3)	N1	C9	C14	C13	179.11(14)
C8	C3	C4	C5	0.3(3)	N1	C9	C14	C17	-0.2(2)
C9	C10	C11	C12	0.1(2)	N1	N2	N3	C2	0.25(18)
C9	N1	N2	N3	-179.67(13)	N1	N2	N3	C18	-175.66(14)
C10	C9	C14	C13	-0.7(2)	N3	C2	C3	C4	125.57(18)
C10	C9	C14	C17	-179.93(16)	N3	C2	C3	C8	-56.9(2)

Table 7 Hydrogen Atom Coordinates (Å×10^4) and Isotropic Displacement Parameters (Å^2×10^3).

Atom	*x*	*y*	*z*	U(eq)
H4	7424.2	8354.87	3306.52	33
H5	9650.6	7816.26	2540.27	39
H6	9675.78	6768.22	1202.83	41
H7	7488.38	6232.61	655.85	43
H8	5256.96	6738.83	1437.1	36
H11	1004.92	9746.68	6723.46	34
H13	130.25	6056.94	7119.28	34
H15A	3641.68	10307.36	5306.24	49
H15B	2068.44	11199.86	4775.54	49
H15C	2979.3	10462.88	4031.5	49
H16A	-1431.3	7525.5	8057.81	64
H16B	-591.46	8635.19	8240.18	64
H16C	49.52	7051.54	8905.96	64
H17A	1493.09	6115.81	4451.62	53
H17B	902.95	5138.02	5714.16	53
H17C	2631.59	5239.53	5582.43	53
H18A	4131.64	9227.66	597.27	40
H18B	3070.79	10416.32	777.14	40
H19A	1868.34	9473.31	-349.83	59

H19B 1032.47	9325.89	853.47	59
H19C 2061.4	8040.85	808.41	59
H20A 3646	6994.93	7558.74	47
H20B 5197.56	6253.82	8280.22	47